COALTECH 2020

Task 1.3.1b

Detection of old workings, sinkholes, underground fires and acid mine pollution using geophysics and airborne thermal infrared imagery

by

Michael van Schoor

March 2002

?

EXECUTIVE SUMMARY

During Year 1 (2000/2001) of this project an audit of various geophysical techniques was conducted to assess their applicability to solving typical coal related problems such as the detection of old workings, sinkholes, underground fires and acid mine pollution. A number of promising techniques were identified and Year 2 (2001/2002) of Task 1.3.1b was set aside to test these techniques in the field.

Geophysical trials were conducted at Kromdraai, New Largo, Arthur Taylor and Bank collieries during 2001/2002. These surveys resulted in the compilation of a collection of case studies and a geophysical applications guideline for the Witbank-Highveld collieries.

The following ground geophysical techniques were tested: micro-gravity, electrical resistivity methods (including resistivity tomography), magnetics, ground penetrating radar, and frequency domain and time domain electromagnetics (FDEM and TDEM). An airborne geophysical technique was also tested, namely the thermal infrared imaging (TIR) method.

The results from the various surveys were discussed in detail in several interim reports and memos (Hallbauer-Zadarozhnaya, 2001; Lowe et al., 2001; Van Schoor, 2001b). In this, the final project report, only the key results will be discussed.

Micro-gravity, electrical resistivity and TDEM proved to be the most promising ground geophysical techniques in terms of locating the edge of old workings and cavity detection. The accurate mapping of individual bords and pillars, however, does not seem possible with any of the conventional techniques tested. Although it was not demonstrated as part of Task 1.3.1b, the electrical resistivity and TDEM techniques are also known to be well suited to mapping pollution plumes.

The TIR method is a very versatile yet cost effective tool for regional and mine-scale mapping. Despite a relatively high mobilisation cost, the overall cost per square metre is only a fraction of the cost of applying other conventional geophysical methods. The TIR surveys yielded some promising results. It appears to be the ideal reconnaissance tool for the regional detection of shallow sinkholes, fires and possible pollution plumes. The TIR technique does, however, appear incapable of accurately mapping the exact positions of individual bords and pillars.

Seismic techniques were evaluated by a couple of experts and the end result was that seismic methods are not well suited to applications such as the detection of cavities and workings in the South African coal environment. Limited experimentation with, for example, fan shooting refraction techniques was proposed.

Novel and unconventional techniques were also investigated. One such technique involves the surface tracking of a miniature “submarine-like” electromagnetic tag that is deployed in flooded workings. Techniques such as this may be regarded as impractical, but a need for some new, innovative ideas to solving age-old problems were definitely highlighted in the process.

TABLE OF CONTENTS

LIST OF TABLES AND FIGURES

1 BACKGROUND

The aim of Coaltech 2020 Task 1.3.1b was to find geophysical solutions to a variety of mining related problems and to provide the mining industry with general guidelines for the application of geophysical techniques. These mining problems include the following:

1) pillars and voids of old mine workings,
2) shallow sinkholes developed in overburden above old mine workings,
3) underground fires, and
4) acid mine pollution plumes.

Task 1.3.1b was a two-year project that started in April 2000 and ended in March 2002. During the first year various geophysical techniques were evaluated on a theoretical level and the applicability of the different techniques was predicted. Of those considered, a performance prediction analysis indicated that the most promising techniques were Thermal Infrared Imagery (TIR), micro-gravity and electrical resistivity (Van Schoor, 2001a). It was recommended to test these, and a few other techniques at a minimum of two sites during Year 2 (2001/2002).

Ground geophysical trials were conducted at four different sites. The sites with the primary geophysical targets indicated in brackets were:

? Kromdraai (individual bord-and-pillars, edge of workings and near surface cavities),
? New Largo (near surface cavities),
? Arthur Taylor (edge of workings) and
? Bank Colliery (edge of workings and dyke).

In addition to the ground geophysics, an airborne TIR survey was flown over the Kromdraai, New Largo and Tavistock (Arthur Taylor) collieries during July 2001.

Task 1.3.1b can be seen as a pre-cursor to a current Coaltech 2020 project entitled *'High-resolution remote sensing and dynamic monitoring of coal mines'* (Task 1.3.5). Whereas Task 1.3.1b was aimed at providing geophysical solutions on a mine-scale, Task 1.3.5 focuses on 'the bigger picture', in other words, regional geophysical solutions. The successful and effective integration of Task 1.3.1b and 1.3.5 outcomes is the ultimate combined goal. Ideally geoscientists on the coal mines should be aware of what remote sensing skills are available for assessing and identifying problem areas and to assist in mine planning. If more detail is required, follow-up (mostly ground) geophysical methods may be employed. The concept behind Task 1.3.1b was to provide mining personnel with a geophysical applications guide to ensure knowledgeable and effective utilisation of geophysical techniques in the coal environment.

2 PROBLEM DEFINITION

A detailed overview of the mining problems mentioned in Section 1 was given in the Year 1 Final Report (Van Schoor, 2001a – 2001-0124). The discussion is not repeated here; instead a schematic summary of the various problems is presented in the figures in Appendix A. A brief explanation of the schematics is presented below.

Old bord-and-pillar mine workings is the root of most of the problems on which the Task 1.3.1b research is focussed. Figure A1 shows a schematic plan and cross-sectional view of a typical bord-and-pillar mine. The size of the typical pillar is approximately 6 m x 6 m and the mining height is approximately 2-4 m. The depth to the mined-out seam can vary from as shallow as a few metres to more than 60 m, but it is typically 20-40 m in the Witbank area. Figure A1 highlights two of the most common challenges to geophysics. It is sometimes critical for current and future mining operations to know where the boundary between previously mined and unmined areas is located. On some mines, for example, a safety barrier is required to prevent old water-filled workings from flooding current developments. In other cases mining personnel require more detailed information – for example, the knowledge of the exact location of individual pillars may be required for blasting purposes.

Figure A2 illustrates that old workings are sometimes partially or completely water-filled. Another challenge to the geophysicist is to discriminate between flooded and void workings.

Figure A3 depicts one of the most dangerous hazards resulting from the deterioration of old bords and pillars. This deterioration may eventually, sometimes even decades later, result in the failure or collapse of old workings and associated subsidence or caving above the workings. In some cases such caving may break through to surface, or it could lead to the formation of undetected, subsurface cavities that can lead to unpredictable disasters. Loss of life and equipment can be reduced if advanced knowledge of subsidence and subsurface sinkholes could be gained.

Pollution from acidic mine water and underground fires are the other principle problems associated with old mine workings. The underground fires are mostly the result of spontaneous combustion; while the in-mine oxidation of pyrites results in the high sulphate levels and acidification of excess mine water. This acidic water often affects the surrounding groundwater system (Figure A4). Leakage from evaporation/treatment dams is another source of such pollution.

3 TASK 1.3.1b METHODOLOGY

The combined work programme for Task 1.3.1b (Years 1 and 2) can be divided into two phases. The first phase (Year 1) involved a theoretical assessment of various geophysical techniques and their application to the problem scenarios listed in Section 2. The outcome of this phase was an applicability and performance prediction analysis of the various techniques. The ratings were based on a combination of information gathered in an international literature review and some computer simulations. Details of these studies can be found in Van Schoor, 2001a.

The analysis indicated that, of those considered, the most promising techniques were the TIR and electrical methods as well as the micro-gravity method. Techniques that were given a poor rating included the controlled source audio-magnetotelluric (CSAMT) method.

The second phase of the project involved the practical application or testing of the most promising techniques.

The role of the TIR surveys in Task 1.3.1b must also be clarified. As was stated earlier, the focus of Task 1.3.1b was on ground / mine scale geophysical solutions. The airborne TIR technique is better suited to the scope of Task 1.3.5 (Remote Sensing project), but is part of Task 1.3.1b as a result of the manner in which the various Coaltech 2020 geophysics projects evolved. It would, from a strategic point of view, also have made more sense to conduct any proposed airborne surveys at the beginning of Task 1.3.1b and to use the results to help design ground surveys. The TIR surveys were, in fact planned for Year 1, but due to a combination of poor weather and the limited availability of the scanner system the surveys could only take place during Year 2 (July 2001). The TIR results will still be used as input to the Remote Sensing project, Task 1.3.5. Consequently, the TIR will be evaluated as a stand-alone technique. The target areas that were selected for the TIR surveys are the same properties on which ground geophysical trials were conducted. Where possible, the TIR results were therefore used to verify or compliment the ground geophysical surveys results.

The final product of this project is a summarised geophysical applications guide, which is aimed at assisting geology and mining personnel in making more informed decisions regarding the selection of the most appropriate geophysical solution(s) for a given scenario.

A number of recommendations for future research are also provided in the closing section.

4 TEST SITE SELECTION AND TRIAL SURVEYS

4.1 Kromdraai

The first test site was on the Kromdraai Colliery property. This site was selected on the basis that a small-scale micro-gravity survey had already been conducted on the property, shortly before Task 1.3.1b commenced in April 2000. The purpose of the micro-gravity survey was to map the boundary between old #1 Seam workings and unmined areas, and to detect subsurface sinkholes. As this survey is well suited to the project definition of Task 1.3.1b, the same survey area was targeted with other ground geophysical techniques. Unfortunately, when the site was revisited to conduct these follow-up surveys, the overburden removal for the next phase of surface mining had already commenced and this affected part of the planned survey area. Consequently, it was decided to focus the follow-up surveys on the south-eastern side of the original micro-gravity grid on the problem of detecting the edge of old workings. Details of the micro-gravity survey can be found in Lowe et al., 2001, while details of the other ground geophysical techniques are given in van Schoor, 2001b. Kromdraai was considered an ideal test site as the old #1 Seam workings are relatively shallow (~12-15 m) compared to other Witbank-Highveld collieries. The Kromdraai site can therefore be regarded as an example of a "best-case-scenario" for evaluating the applicability of geophysical techniques to mapping the edge of old workings. Besides micro-gravity, the following geophysical techniques were tested at Kromdraai: total field magnetics (TFM), frequency domain electromagnetics (FDEM), ground penetrating radar (GPR) and resistivity imaging/tomography (RESTOM).

4.2 New Largo

The New Largo test site served as a substitute for Middelburg Steam & Station, one of the preferred test sites for Task 1.3.1b. Unfortunately, the latter was considered to be an unsafe area and members of the Coaltech 2020 committee proposed New Largo as an alternative. The primary target at New Largo is, however, the same as at Middelburg Steam & Station, namely near-surface cavities. The depth to the old workings at the survey site is approximately 30 m below surface, which is not necessarily beyond the probing range of geophysics, however, it was decided to focus on the detection of sinkholes.

During a site visit to the New Largo property, a small area was selected to serve as a tests site for various ground geophysical techniques. The chosen site was one with a low safety factor (< 1.0), that is, high risk. Part of the area subsided in 1999 due to the collapse of old bord-and-pillar workings and a relatively large sinkhole (diameter approximately 20 m) is present in the area. For more details on the New Largo surveys, refer to van Schoor, 2001b. Geophysical, techniques tested at New Largo included TFM, resistivity mapping, GPR and FDEM.

4.3 Arthur Taylor Colliery (ATC)

The Arthur Taylor site was chosen for the same reason as Kromdraai - a small-scale micro-gravity survey had been conducted there prior to the start of Task 1.3.1b. The purpose of the micro-gravity survey was to map the boundary between old #2 Seam workings and unmined areas. The main difference between the Kromdraai target workings and those at ATC is that the Kromdraai workings were void, while the ATC workings were flooded with acid mine water. Furthermore, the ATC workings occur at a greater depth of approximately 30 m below surface.

The nature of the geophysical problem at the ATC site made the successful application of time domain electromagnetics a strong possibility, as the water-filled mined-out cavities constituted a good TDEM target (relatively conductive). Besides the TDEM method some TFM tests were also conducted. Although resistivity imaging trials were also planned the onset of the rainy season made this virtually impossible as the site is located in a marshy terrain.

4.4 Bank Colliery

During the last couple of months of Task 1.3.1b some RESTOM and TFM surveys were carried out at an optional site, Bank Colliery. Again, a site was chosen where a boundary between old workings (in this case void) and virgin ground occurred at a depth of approximately 30 m. This site was different, in that a known dyke occurs on the virgin ground side. The occurrence of burnt coal dictated the termination of mining, and hence the location of the boundary in that area. The aim of the survey was to determine how the presence of the dyke would affect the performance of geophysical surveys aimed at detecting the boundary.

4.5 Airborne Thermal Infrared (TIR) Survey

As was explained in Section 3, the TIR survey was originally planned for Year 1 of the project, but could only be conducted in July 2001. A regional map showing the areas covered by the TIR survey is shown in Figure A5. Some more details of the TIR survey and results can be found in Ferraz, 2002.

5 GENERAL DISCUSSION OF GROUND GEOPHYSICAL RESULTS

5.1 Site by Site

The geophysical results from the three test sites are discussed in detail in the various interim reports – Lowe et al., 2001, van Schoor, 2001a, b & c, Hallbauer-Zadarozhnaya, 2001, Ferraz, 2002.

In this report only a general overview of the successes, failures and recommendations etc. is presented. For reference purposes, the presentation is given in both a site by site and a technique by technique format.

5.1.1 Kromdraai

As predicted by modelling experiments, the edge of workings was successfully identified using the micro-gravity technique. A gravity low was observed over the un-flooded workings and a gravity high over the unmined area, with the edge being located at the inflection point between the high and the low. Individual bords and pillars could not be discriminated and modelling has shown that this discrimination would only be possible for ultra-shallow (< 6 m) workings. The practical application of the micro-gravity technique would therefore be limited to detecting the edge of old workings. During the course of the project it was not possible to test the performance limits of the technique fully, but modelling results suggests that it should be possible to map old workings to a depth of 150 m for air-filled and 50 m for water-filled. The main disadvantage of the micro-gravity technique is the speed of data acquisition and thus the cost of surveys.

The TFM survey result was not convincing. A trend in the data did, however, suggest a lower total field strength over the mined-out areas, due to the presence of the air-filled voids, as one would expect. Removing this trend from the data resulted in a low field strength anomalous zone that correlates well with the location of the known edge of workings. It was recommended that the response of sub-surface voids on TFM responses be modelled to gain a better understanding of magnetic data over mined-out areas. Unfortunately. this was not possible due to time constraints and the unavailability of suitable modelling software.

The FDEM technique failed to discriminate the individual bords and pillars and, as with the TFM technique, it was unconvincing in detecting the edge of workings. Little more than a subtle trend, suggesting a cross-over from unmined (more conductive) to mined-out (more rersistive) areas, was evident in the data.

GPR penetration could only be achieved down to a few metres at this site. Even over an area where the overburden removal had already taken place, GPR penetration was no better than approximately 6 m.

Finally, the RESTOM technique was tested. The survey was designed to determine if the technique could discriminate between the unmined and mined-out areas. The survey was reasonably successful in that a distinct crossover from a higher to a lower bulk resistivity is evident in the output image. The higher bulk resistivity is mainly the result of the contribution from the air-filled mining voids. In terms of locating the edge of workings, the mapping accuracy of the survey was approximately 2-5 m.

5.1.2 New Largo

The site at New Largo was chosen on the potential occurrence of near-surface cavities. The depth to the old workings at the survey site is approximately 30 m below surface. This is not necessarily beyond the probing range of conventional geophysics, however, it was decided to focus on the detection of unknown sinkholes. Unfortunately the ground geophysics was conducted 'blindly', that is, without prior knowledge of possible sinkhole occurrences. This is not an ideal situation as it would have made more sense to have-done follow-up groundwork based on, for example, the TIR results. The methodology was, however, dictated by circumstances beyond our control.

A small-scale (65 m x 60 m) magnetic survey yielded no more than a dominant positive-negative anomaly. The cause of this anomaly was later established to be an old buried steel borehole casing. Apart from this anomaly, there was nothing in the data that suggested possible presence of sinkholes or other prominent geological features.

A gradient array electrical resistivity survey over approximately the same area yielded interesting results. Circular cracked zones resulting from nearby subsidence / sinkhole manifested on the resistivity map as a high resistive zone. A conductive anomaly was correlated with the above-mentioned old borehole location and similar correlations with other old borehole locations were made. No further prominent resistive anomalies indicative of potential subsurface cavities were evident in the data.

A FDEM survey was conducted and only a single significant EM anomaly was identified, which was again correlated with the previously mentioned borehole collar.

As was the case at Kromdraai, the GPR technique yielded poor penetration of possibly only a few metres and the only possible anomalies corresponded with the borehole anomalies detected with the EM and electrical methods.

Finally, a RESTOM profile was conducted at New Largo. It was located such that it traversed the cracked zone with the aim of determining the depth extent of the cracks and to probe for potential larger cavities at depth. The only indication of potential subsurface voids in the RESTOM image was a single deeper zone (refer to Van Schoor 2001b). The near surface resistivity shows reasonable correlation with the resistivity values depicted on the gradient array contour map. The cracked zone is also manifest on the image. To add value to RESTOM results in future surveys, a pseudo-3D RESTOM approach is recommended. That is, a grid of closely spaced lines needs to be acquired. This will ensure greater confidence in the data and allow correlation and interpolation between adjacent profiles.

5.1.3 Arthur Taylor Colliery

The third test site presented an ideal opportunity for testing of the time domain electromagnetic (TDEM) technique. This technique was not given a good rating in the first phases of the project, but after considering the nature of the problem at ATC, it was decided to test TDEM. The survey was successful in that the boundary between the water-filled mined-out areas at a depth of approximately 30 m and the virgin ground was mapped with reasonable accuracy. The presence of conductive acid mine water in the mining cavities is an ideal electromagnetic target.

Resistivity profiling or imaging surveys were also scheduled for ATC, but the onset of the rainy season prevented this work from being conducted. The ATC site lies in a marshy area that was flooded and overgrown with reeds following the first few weeks of rain.

The other geophysical technique tested at ATC was the magnetic method. Two closely spaced profiles that traversed the edge of workings gave no indication that the technique has the capability of detecting this feature.

5.1.4 Bank Colliery

A RESTOM survey aimed at detecting the boundary between old #5 seam workings at a depth of approximately 30 m and virgin ground was conducted (Van Schoor, 2002). The presence of a known dyke running parallel to the boundary on the virgin side affected the RESTOM survey. Computer simulations conducted prior to the survey indicated that RESTOM is capable of detecting the boundary provided a dyke is not present. The boundary was, however, not evident on the field output image; only the dyke manifested on the image. This effect was confirmed through computer simulations.

A few TFM profiles were run across the dyke and it was found that conventional TFM could not unequivocally map the dyke. The results of the Bank survey are valuable in that they illustrate how a geophysical technique that is perceived to be correct may not be the correct approach. In this case the detection of dykes using magnetics.

5.2 Technique by Technique

5.2.1 Micro-gravity

The micro-gravity technique exploits density contrasts in rocks to detect subsurface features with anomalous gravity responses such as air- or water-filled cavities. The micro-gravity technique has great potential for mapping sinkholes, and delineating old workings. During trial surveys at Kromdraai and Arthur Taylor Collieries the boundaries between old workings and virgin ground were successful mapped. At Kromdraai the workings were air-filled and at a depth of approximately 14 m, while at ATC the 30 m deep workings were flooded. Modelling results carried out during the technology audit phase suggested that the technique has a depth of investigation of well beyond the average depth of 30-40 m for old Witbank-Highveld workings. The current drawback of the micro-gravity technique is the speed of data acquisition, the availability of expertise and the cost of surveying. Unless the instrumentation and skills are made locally available the technique is too costly. The speed of data acquisition remains a weakness that could prevent the technique from becoming a routinely applied tool.

5.2.2 Resistivity (gradient array)

Resistivity mapping techniques, of which the gradient array is an example, can be very effective in delineating high resistivitity zones in a sinkhole prone area. The survey at New Largo is an example of the application of this technique. The technique can also be used as an alternative to EM methods for delineating pollution plumes. The advantage that electrical (DC) resistivity mapping methods have over most EM techniques is that DC methods are more sensitive to subtle resistivity variations.

5.2.3 Resistivity profiling (conventional)

Resistivity profiling is usually applied in reconnaissance mode and focuses on a pre-defined depth of investigation. The output is similar to magnetic or FDEM results in that single profiles are correlated to a specific depth of investigation. This technique may be well suited to mapping features that have resistivity contrast with their surroundings, for example, sinkholes, pollution plumes and dykes. It is also often used to map variations in the bedrock topography or the depth of weathering profile.

5.2.4 Resistivity tomography (RESTOM)

RESTOM uses conventional resistivity profiling principles, however, a lot more data is acquired per profile so that a tomographic image of the subsurface can be reconstructed. The speed of RESTOM data acquisition tends to be slower than that for conventional resistivity profiling. RESTOM appears to be best suited to follow-up work where an anomaly detected using another technique can be investigated in more detail. A typical application would be to survey potential sinkhole sites (e.g., as identified from airborne geophysical data) to determine the geometry and extent of such features. Another useful application is the 3D characterisation of pollution plumes that have been delineated using other exploration techniques.

5.2.5 Total field magnetics (TFM)

It is unfortunate that the magnetic technique is incapable of solving at least one of the specified mining related problems as the technique is a fast and inexpensive reconnaissance tool. The technique probably only has value in cases where magnetic structural features, such as dykes and sills, need to be delineated or where there is a need to locate buried man made features such as mining machinery. The technique should, however, not be discarded completely as it may be applicable to delineating certain types of pollution plumes. This application was not tested in the Task 1.3.1b work programme.

5.2.6 Frequency domain electromagnetics (FDEM)

The performance of FDEM at two different sites was unconvincing. It must be noted that in one of these cases, namely New Largo, a ‘blind’ approach was adopted and no primary targets, such as sinkholes, were present at the site. FDEM is a relatively inexpensive ground geophysical technique and may still be useful for reconnaissance work aimed at detecting near surface cavities and pollution plumes. The technique’s depth of investigation is limited to approximately 10-15 m due to the conductive nature of the Karoo overburden.

5.2.7 Time domain electromagnetics (TDEM)

Even though TDEM was not considered a promising technique during the initial technology audit, it was tested at Arthur Taylor Colliery and performed reasonably well. The technique was used to successfully map the contact between un-mined ground and flooded workings located at a depth of approximately 30 m. Acid mine water is a good EM target in that it is relatively conductive. The TDEM technique has the potential to become a routine tool for delineating flooded old workings in situations where a barrier between such old workings and current mining operations is required.

Although it was not demonstrated as part of Task 1.3.1b, the TDEM technique is well suited to mapping pollution plumes and the technique could therefore be used routinely for this application. The technology is locally available and is a relatively inexpensive ground exploration technique.

5.2.8 Ground penetrating radar (GPR)

Prior to the commencement of Task 1.3.1b, GPR was viewed with scepticism by the coal mining industry as the technique has performed poorly on previous occasions. GPR was tested at two different locations during the course of Task 1.3.1b and in both cases the same limitation, depth penetration, was evident. The Karoo overburden of the Witbank-Highveld area is simply too conductive for GPR to penetrate beyond a few metres. The only potential application for GPR, in terms of the Task 1.3.1b project definition, would be the detection of very-near surface cavities say, in the upper 4 metes. Unfortunately, no test data is available to support this. Both shallow air and water-filled cavities should manifest clearly on radargrams provided they are sufficiently large; at least of the order of a wavelength, that is, tens of centimetres in diameter.

6 AIRBORNE THERMAL INFRARED IMAGING (TIR) SURVEYS

The complete final report on the TIR campaign is available as an electronic Appendix to this document and as separate Coaltech 2020 report (Ferraz, 2002). Ferraz's report includes full details of the TIR survey planning, data acquisition, data quality control and pre-processing. A brief, qualitative overview is presented here.

The Coaltech TIR surveys focused on three areas of specific interest, namely:

- New Largo: ground geophysical surveys aimed at sinkhole detection had been conducted at the site previously (van Schoor, 2001b).
- Arthur Taylor Colliery: Anglo American had previously conducted a microgravity survey at this site (Lowe et al., 2001).
- Kromdraai: also coinciding with an Anglo American microgravity test site (Lowe et al., 2001).

Although the areas covered during the TIR surveys were large, smaller target areas were selected for detailed interpretation. Areas of approximately 1 km x 1 km were chosen to include the sites where other geophysical techniques had been tested during the Task 1.3.1b work programme (Van Schoor, 2001b).

Temperature calibration and interpretations were carried out over these selected sub-areas of interest (Ferraz, 2002). The interpretation of these subsets involved detailed image processing using a combination of colour tables with different image enhancement techniques. The thermal data sets were used in conjunction with topographic map data. The two datasets are complementary; topographic data provides surface information while thermal data provides sub-surface information. The integration of these data contributed to the identification and delineation of problem areas.

6.1 Site 1 - New Largo

The New Largo site covers old workings at a depth of approximately 30 m. These workings, however, were not the primary target at this site. Rather, the site shows some clear surface expressions related to subsidence and sinkhole occurrences. It was anticipated that further potential sinkholes would be identified using the TIR technique. The 998 m x 1346 m TIR images clearly show features related to sinkholes and subsidence. A number of *probable* and *possible* subsurface sinkholes were identified. These features range in diameter from 11 m to 145 m. A couple of man-made features, the one probably an inclined shaft and the other possibly a trench or excavation, are also visible on the TIR images. Other smaller features such as a man-made fire and a fence can also be discriminated.

6.2 Site 2 - Tavistock (Arthur Taylor)

The Arthur Taylor site straddles the boundary between water-filled old workings and virgin ground at a depth of approximately 30 m. The target at this site was the boundary. Man-made features are prominent in the TIR images, and include a trench with surface water as well as some infrastructure. It is not obvious from the image that the TIR technique was capable of discriminating between mined out areas and virgin ground. Although two distinct zones were identified, one possibly related to water-filled workings, the other with dry workings. The boundary of the mined out area is not mapped very accurately. Additional image processing may be required to achieve this although the workings occur at a depth of 30 m or more and may be too deep for the TIR technique to detect. Areas where water appears to be accumulating and surface water occurrences such as dams were easily discriminated. A single *probable* sinkhole was also identified.

6.3 Site 3 - Kromdraai

At Kromdraai an area overlying relatively shallow old workings that had been analysed using other geophysical techniques such as microgravity, was targeted. There was a known boundary between air-filled workings at a depth of 12-15 m and virgin ground at this site. The resulting TIR image shows locations of *probable* underground fires ranging in diameter from 4.5 to 35 m. A number of *possible* underground fires are also identified. Areas thought to be bord-and-pillar structures, both water-filled and dry workings, are mapped. Comparison with known maps of the area (Lowe et al., 2001) shows that the mined out area is significantly larger than the aforementioned anomalous areas. Also, the area where most of the interpreted fires occur, is not undermined. These findings thus cast some doubt over the performance of the TIR technique.

6.4 Conclusions Following from Discussion of the TIR Results

The following key points can be highlighted:

?? It would have been preferable for the TIR surveys to have been conducted earlier in the work schedule of Task 1.3.1b, as originally planned. This would have allowed sufficient time to do follow-up ground referencing and ground geophysics to confirm the various interpreted TIR anomalies.

?? There is sufficient evidence to suggest that the TIR technique can detect old workings, provided the workings are relatively shallow, for example at Kromdraai.

?? In order to quantitatively assess the mapping accuracy of the technique, it may be necessary to focus on areas of say, 100 m x 100 m. Overlaying such an image on a reliable workings plan should give an indication of how accurately the boundary between mined-out and virgin ground can be detected.

?? The TIR technique appears to be unsuited to mapping individual bords and pillars. It is believed that this may only be possible for ultra-shallow workings, which is not the norm in the Witbank coalfield.

?? The TIR technique seems well suited to the regional mapping of potential hazardous sites such as underground fires and sinkholes. It is probably also well suited to environmental mapping of pollution plumes.

7 COST AND SKILLS ANALYSIS

The estimated cost of applying all the geophysical techniques tested during the course of the project is listed below. The cost provided is for data acquisition and data processing.

Table 1: Cost and skills analysis of relevant geophysical techniques.

Technique	**Local technology?**	**Estimated survey time (1 ha at 5 m line spacings, unless stated otherwise)**	**Estimated cost (per hectare) processing *included***	**Required processing time**
Micro-gravity	NO	15-20 days	R 100 000	~ 1 week
Resistivity (gradient array)	YES	1-2 days	R 4000 - 8000	1 day
Resistivity Tomography (RESTOM)	YES	6 days	R 25000	2 days
Resistivity profiling (conventional)	YES	1-2 days	R 4000 – 8000	1-2 days
Magnetics	YES	1 day	R 2500	1 day
Frequency domain electromagnetics (FDEM)	YES	1 day	R3500	1 day
Time domain electromagnetics (TDEM)	YES	1-2 days	R 10 000	1 week
Ground Penetrating Radar (GPR)	YES	1-2 days	R8000	1 day
Airborne thermal infrared imaging (TIR)	NO	1 night = 330 km^2 (at 1 m pixels)	R2.50[A]	1-2 months

Note that, despite a relatively costly mobilization component, some airborne geophysical techniques such as TIR, tend to be more cost effective than ground geophysics. It is therefore strongly recommended that all possible information be extracted from existing airborne data, or alternatively, to conduct a reconnaissance airborne survey(s) if appropriate prior to conducting follow-up with ground surveys.

[A] Note that although the cost per hectare is extremely low the minimum cost of a survey is in the order of R50000 – R100 000, because of the high mobilization component.

8 ALTERNATIVE TECHNIQUES

8.1 Seismic Methods

Initially, seismic methods were not considered as a potential technique for solving the typical coal mining problems addressed in the Task 1.3.1b research programme. This was a because Coaltech project, Task 1.3.1a, was focussed on seismic methods. However, due to several rescoping iterations of the seismic related activities, a new Task 1.3.1b subtask was created to accommodate the remaining seismic related work.

A technology audit, aimed at assessing seismic methodologies for detecting buried cavities or tunnels, was conducted by Professor Cedric Wright, Wits University. His report is available as an electronic Appendix to this document and as a separate report (Wright, 2002). A summary of his key findings follow:

A literature review by Wright indicated that, despite extensive theoretical studies in this regard, the applications of seismology to detecting shallow coal mine workings have not been particularly successful, or that the methodology has not been adequately developed. Successes have been focussed on detecting cavities or sinkholes in limestone or in civil engineering / geotechnical problems.

A major obstacle for the successful application of seismic techniques to the coal mining areas, is the fact that the dimensions of cavities / tunnels are often less than the wavelengths of the highest frequency seismic signals that can be generated by seismic sources near the surface or in boreholes.

Wright further reports that it is challenging to theoretically deriving exact synthetic seismograms showing all wave types generated by an explosive source in a layered elastic medium containing an inclusion or cavity. Consequently, further work on the use of synthetic seismograms to test the feasibility of detecting old mine workings is therefore not recommended at present.

An experiment, based on the results of laboratory modelling reported on in the literature, was proposed by Professor Wright. The principle involves the detection of cavities using diffracted or scattered P waves. However, the masking effect of the Rayleigh waves needs to be addressed and can be achieved by placing a trench between the source and geophones. The Rayleigh waves themselves may be used to detect shallow cavities by measuring fluctuations in phase velocity as a function of frequency.

A trial experiment is recommended in which seismic waves are recorded over a shallow cavity (< 10 m deep) and over a deeper cavity (10-30 m below the surface). Recording should be undertaken both with and without trenching, enabling the Rayleigh waves to be used in detecting the shallow cavity, and the body waves can be analysed to locate the deeper cavity without interference from the Rayleigh waves. Further survey design specification were also proposed by Professor Wright.

Finally, Professor Wright emphasized that the present seismic study is incomplete since critical evaluation of both relatively obscure publications and fairly recent articles in journals not available in South Africa needs to be undertaken.

Chris Van Dam (2002) made the following comments about Professor Wrights's contribution: He suggested that the blocking the Raleigh waves was not a practical or realistic solution. He regarded Professor Wright's conclusion that seismic wavelengths are normally much longer than the dimension of mine cavities, thereby excluding the use of seismic P wave reflection of any kind in mapping old mine workings and subsidence, as important.

Van Dam further stated that geophysicists are often at a disadvantage in that problems needing to be resolved are not always clearly specified. Mapping in-tact mining tunnels at 30 m depth is a completely different problem to mapping a 20 m deep mine tunnel with roof caving up to close to surface; the latter being of potential or eminent danger to industrial and domestic surface users. It also stands to reason that such caving will start and be at it's most severe, at the intersection of two tunnels, forming a dome-shaped rubble filled cavity. The top of such a cavity will, in all likelihood, be partially collapsed and ring cracks or joints will have developed, i.e. the bedrock refraction horizon will be locally seismically disturbed.

Van Dam proposes the use of a seismic refraction technique, known as fan shooting, be investigated. Fan shooting can be used to map areas of slowness and this approach may be applicable to mapping disturbed ground, e.g., cavings that form above mined out tunnels. The technique, which is described in detail in the Attachment, is based on tomographic reconstruction principles.

8.2 Novel Techniques

Dr Kononov (CSIR, Miningtek) conducted an audit of some novel techniques with the potential to detect cavities. Some of his ideas had already been addressed in Task 1.3.1b, however two techniques, not discussed elsewhere, are briefly mentioned here. Dr. Kononov's report is attached to this document (Kononov, 2002).

8.2.1 Laser surveying

Dr Kononov firstly proposed the use of laser surveying as is applied at Kalgoorlie Gold Mine in Australia. A laser scanning system is lowered down a borehole and measurements are then taken of the inside of the mined out cavity. By taking measurements in various directions a plan of the cavity can be reconstructed from the data.

This technology may be applicability to the mapping of subsurface sinkholes and other cavities although its routine application is unlikely as application requires a borehole intersecting the cavity.

8.2.2 Random oriented, self-propelled electromagnetic tag

Dr Kononov also proposed the use of a random oriented, self-propelled electromagnetic tag. The method requires flooded underground workings intersected by at least one access borehole. A disposable, submersible, self-propelled, randomly oriented electromagnetic (EM) tag and surface location receiver could then be used to map workings.

A person equipped with a searching receiver and a loop antenna would follow and record the tag movement on surface. Each time the tag is deflected off the sidewall the position is recorded using either a GPS or by placing a marker in the ground corresponding to the position of the sidewall. Through the random movement of the tag it will be possible to map old workings. The anticipated location accuracy for old workings located at a depth of 40 m is approximately 10 cm.

This method may prove to be very time consuming and is limited to flooded workings.

9 SUMMARY – GEOPHYSICAL APPLICATIONS GUIDELINE

Following evaluation of all the results and findings in the technical audits and field surveys, as well as considering inputs from various technical experts, a geophysical applications guideline was compiled. For easy reference purposes this information is contained in a single table, Table 2. On the vertical axis of Table 2 the problem scenarios are listed including some sub-classifications, for example, the delineation of old workings is sub-divided into two distinct cases, flooded and air-filled workings. Another sub-division incorporates target depth information, arguably the most crucial factor in determining the probing limits of a geophysical technique. On the horizontal axis of Table 2 the various geophysical methods considered in Task 1.3.1b are listed. Techniques are rated according to four different categories:

1) First choice technique for regional or first phase exploration
2) First choice technique for follow-up ground-geophysics
3) Second choice technique for solving given problem
4) Alternative technique that may also be applicable to the given problem

Table 2: Geophysical applications guidelines summarised.

Type of problem		Technique / Target Depth	TIR	GPR	TDEM	FDEM	MAG	RES	RESTOM	MGRAV	CSAMT
Delineation of old workings	Water-filled	10-25 m									
		25-40 m									
		40-100 m									
	Air-filled	10-25 m									
		25-40 m									
		40-100 m									
Sinkholes	Water-filled	0-10 m									
		10-40 m									
	Air-filled	0-10 m									
		10-40 m									
Pollution plumes	Conductive										
	Resistive										
Underground fires		10-25 m									
		25-40 m									
		40-100 m									

First choice technique for regional or first phase exploration

First choice technique for follow-up ground-geophysics

Second choice technique for solving given problem

Alternative technique that may also be applicable to the given problem

10 CONCLUSION AND RECOMMENDATIONS

The main conclusions and recommendations that follow from the Task 1.3.1b research are listed below. The first point given below is taken from the interim report on the surveys at Kromdraai and New Largo. It is repeated here as this is a key issue:

? The practical evaluation of geophysical techniques that formed part of Task 1.3.1b was complicated through surveying 'blind' and the lack of sufficient 'ground truthing' data. For example, although it is relatively easy to design a survey to cover an area of old workings or the edge of old workings, sinkholes and pollution occurrences are more difficult to target because their location is usually unknown. Furthermore, sufficient ground truthing data, for example through drilling, is often not possible unless the drilling can be motivated, for example, in the event of the safety risk posed by a possible sinkhole.

For similar future research activities, it is recommended that test sites be more carefully selected to enable evaluation of interpretations using existing boreholes or accurate mine plans. Provision should also be made for limited additional drilling. A further solution would be to limit future ground geophysical surveys to investigating anomalies identified using airborne or satellite-based sensors. This approach will reduce costs and is thus recommended for the remainder of the Remote Sensing project (Task 1.3.5).

? Most old bord-and-pillar workings occur at a depth of more than 12 m, with an average depth of between 25 and 40 m. The typical dimensions of bord-and-pillar structures are of the order of 4-6 m. To date, no ground geophysical method has been found that is capable of resolving the individual pillars. This would only be possible under exceptional circumstances where the workings are very close to surface (<~ 6 m).

? Under favourable conditions, airborne thermal infrared (TIR) surveys can successfully map the grid-like pattern of bord-and-pillar workings. An example of a successful survey was reported on in Van Schoor (2001a) and is also documented in Brink (1980). The typical Witbank-Highveld bord-and-pillar scenario is, however, not conducive to successful TIR mapping of individual pillars for the reasons described in the previous point.

? There are at least three ground-geophysical techniques capable of mapping the boundary between old workings and virgin ground. These are the micro-gravity, TDEM and resistivity methods. The choice of technique depends on the parameters of the problem. From a cost point of view, the resistivity approach is the most cost effective, followed by the TDEM method, which is approximately twice as costly to apply. The micro-gravity technique is 10 times more costly than the resistivity method.

For relatively shallow workings (< 30 m) the resistivity method is the most suitable. The technique should be able to detect both water-filled and air-filled workings. For water-filled workings that lie in the depth range 20+ metres, the TDEM technique is more suitable. For air-filled workings at depths in excess of 20 - 30 m, micro-gravity is expected to outperform the former techniques. Modelling results suggest that the micro-gravity method is capable of detecting the edge of water-filled and air-filled workings at depths of 50 m and > 100 m, respectively.

? Shallow cavities such as developing sinkholes may be detectable on TIR images. Ground follow-up to confirm suspected sinkhole anomalies can be carried out with either the micro-gravity or resistivity techniques. Resistivity Tomography is probably the ideal technique for this application as it enables 3D geometric characterisation of such features.

? For regional detection of pollution plumes an airborne technique, such as TIR, can provide some useful information. As is the case with sinkholes, ground follow-up may be required to delineate / characterise the plume. For this application, TDEM is the most suitable technique, however, a combination of TDEM and electrical methods (RESTOM or resistivity profiling / mapping) is recommended.

? The TIR technique is well suited to the problem of delineating and monitoring underground fires. No ground techniques were tested on this problem during the course of Task 1.3.b, but there are techniques that have reportedly been used elsewhere to delineate fires. The controlled source audio magnetotelluric (CSAMT) is one such technique (Van Schoor, 2001a).

? Despite a poor rating during the technical audit stage of this project, the CSAMT method has received favourable comment from one of the geophysical representatives on the Geology & Geophysics Steering Group and its applicability needs to be investigated. The author of this report is, however, of the opinion that the CSAMT technique will, as suggested by computer simulations (Cole, 2000), not provide results of high enough resolution to outperform the other techniques discussed in this document.

? Applicability of the GPR technique is limited due to the conductive nature of the Karoo sediments. Radar penetration is usually limited to a few metres, thus GPR would only be applicable to the mapping of ultra-shallow (< 6 - 8 m) voids or workings.

? On a regional scale, the application of ground geophysical techniques is relatively expensive compared with airborne methods such as TIR or airborne magnetics. It can be concluded that ground geophysics is best suited to solving high-resolution, mine-scale problems where the area of interest is approximately 1 hectare or less. A key result expected from the integration of this project with Task 1.3.5 is that, wherever possible, geophysics should be applied in an integrated and site specific manner. It is often through the joint use of different techniques that a given geological problem can be solved. Finally, it must be emphasised that geophysical techniques are site specific; a technique that proves successful on one mine will not necessarily work at another mine and vice versa.

? The TIR results are promising. The technique has the ability to detect features such as near surface cavities and underground fires. As mentioned earlier, it may also play a key role in environmental mapping. A recommendation is that the mapping accuracy of the technique as well as the depth penetration be better quantified, specifically for the Witbank coal environment.

? Historically, seismic methods have not been successful in the South African coal context. It is recommended that the theoretical aspects and modelling of the application of seismic methods in this environment be addressed prior to further seismic experimentation.

? Although the novel techniques proposed by Kononov appear impractical. Unless conventional geophysics can be proven effective in the near future we may have to turn to novel and innovative ideas such as the self-propelled EM tag to enable the accurate mapping of old workings.

REFERENCES

Brink, A.B.A. 1983. Engineering Geology of Southern Africa, Volume 3 (Karoo Sequence).

Cole, J., 2000. CSAMT numerical modelling of coals seams. Coaltech Report, CSIR Report number 2002-0121

Ferraz, F.F., 2002. TIR Final Report, Coaltech Report, CSIR Report number 2002-0144

Geonics Limited. Technical Note TN-6: Electromagnetic terrain conductivity measurements at low induction numbers.

Hallbauer-Zadarozhnaya, V., 2001. Report on a TDEM survey at the Arthur Taylor Colliery. Coaltech 2020 report, CSIR Report number 2001-0649.

Kononov, V., 2002. Technology audit of other techniques that may be applicable to the detection of old workings Coaltech 2020 report, CSIR Report number 2002-0139.

Lowe, S.J., Muller, M., and Pretorius, C., 2001. The microgravity method for underground cavity detection in the coal mine environment. Coaltech 2020 report, CSIR Report number 2001-0120.

Van Dam, 2002. Fan shooting - a possible low cost hammer refraction seismic method to map near surface mining induced caving. Sub-contractor report.

Van Schoor, M., 2001a. Detection of old workings, sinkholes, underground fires and acid mine pollution using geophysics and airborne thermal infrared imagery. Coaltech 2020 report, CSIR Report number 2001-0124.

Van Schoor, M., 2001b. Geophysical trials at Kromdraai & New Largo Collieries. Preliminary results. Coaltech 2020 report, CSIR Report number 2001-0122.

Van Schoor, M., 2002. Geophysical trials at Bank Colliery. Coaltech 2020 report, CSIR Report number 2001-0143.

Van Zijl, J. S. V., 1985. A practical manual on the resistivity method (Revised edition). CSIR Report K79. Geophysics Division National Physical Research Laboratory, CSIR.

Vogt, D.R., 2001. Application of GPR in coal. Coaltech 2020 Report (part of Subtask 4, Task 1.3.1b).

Wright, C., 2002. An Assessment of The Use of Seismic Methodologies to Detect Buried Cavities or Tunnels. Coaltech 2020 subcontractor report.

APPENDIX A

FIGURES

7

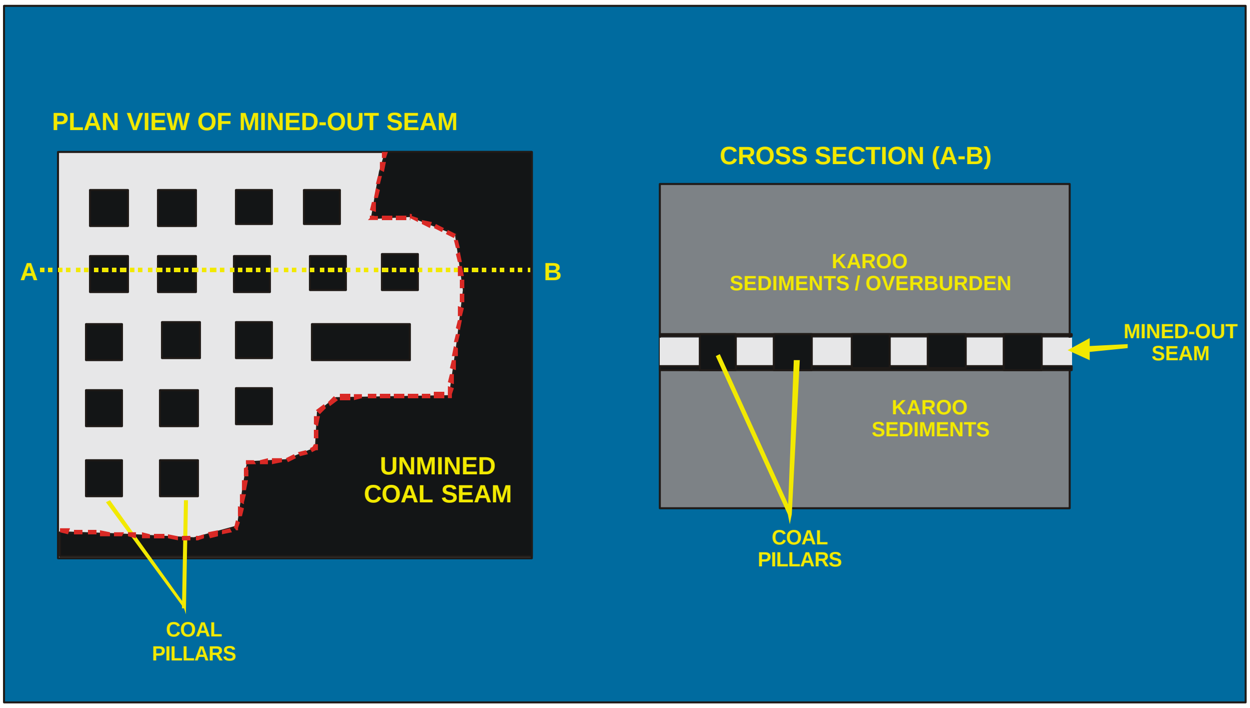

Figure A1: Schematic showing a typical old workings (bord-and-pillar) layout.

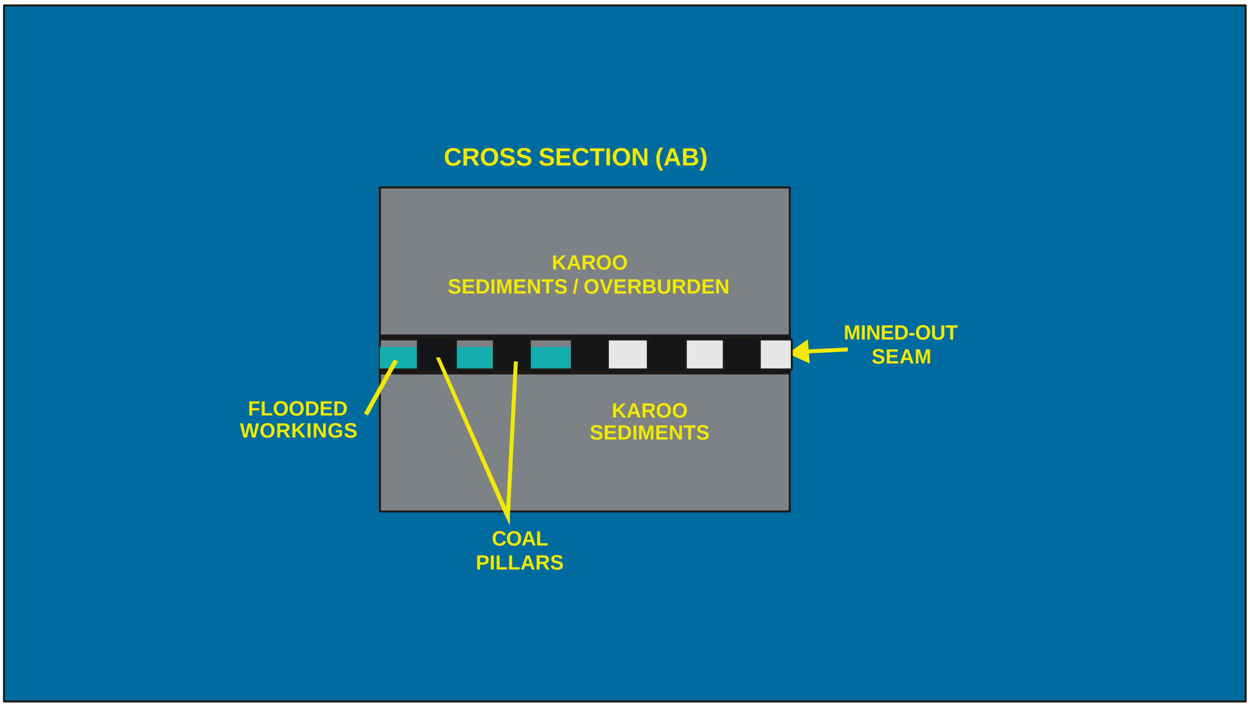

Figure A2: Schematic showing the partial flooding of old workings.

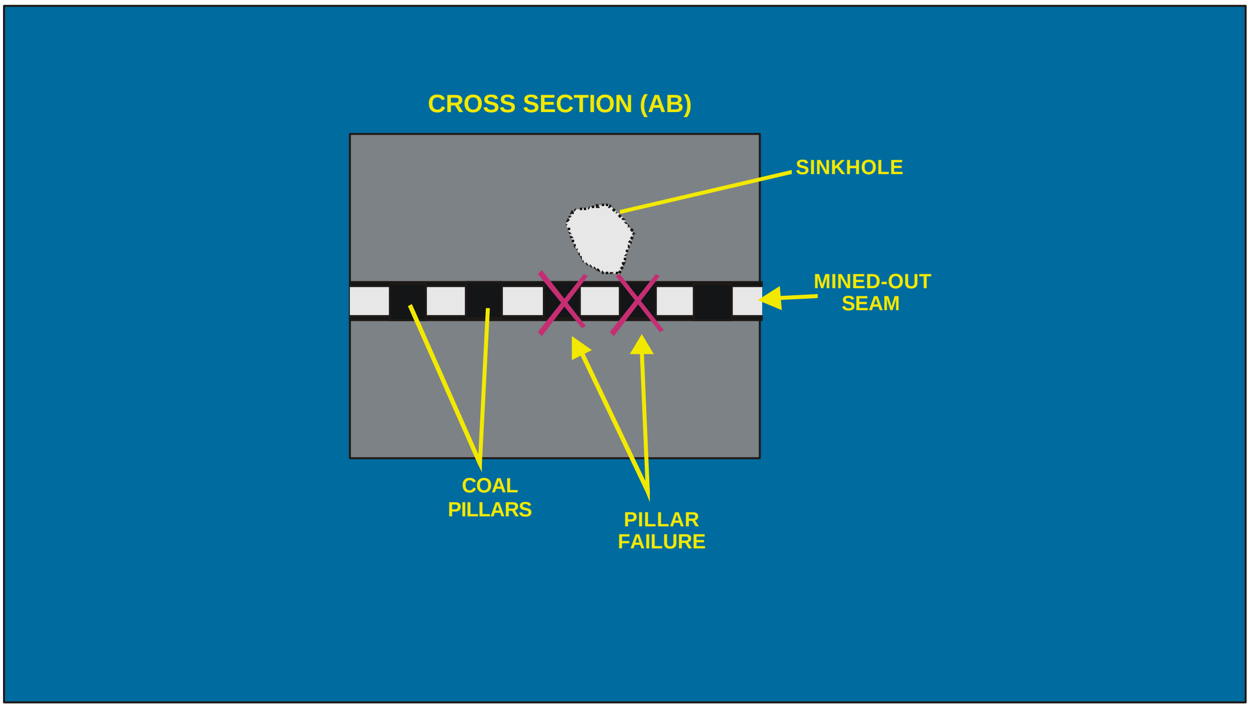

Figure A3: Schematic showing the development of a sinkhole above old workings.

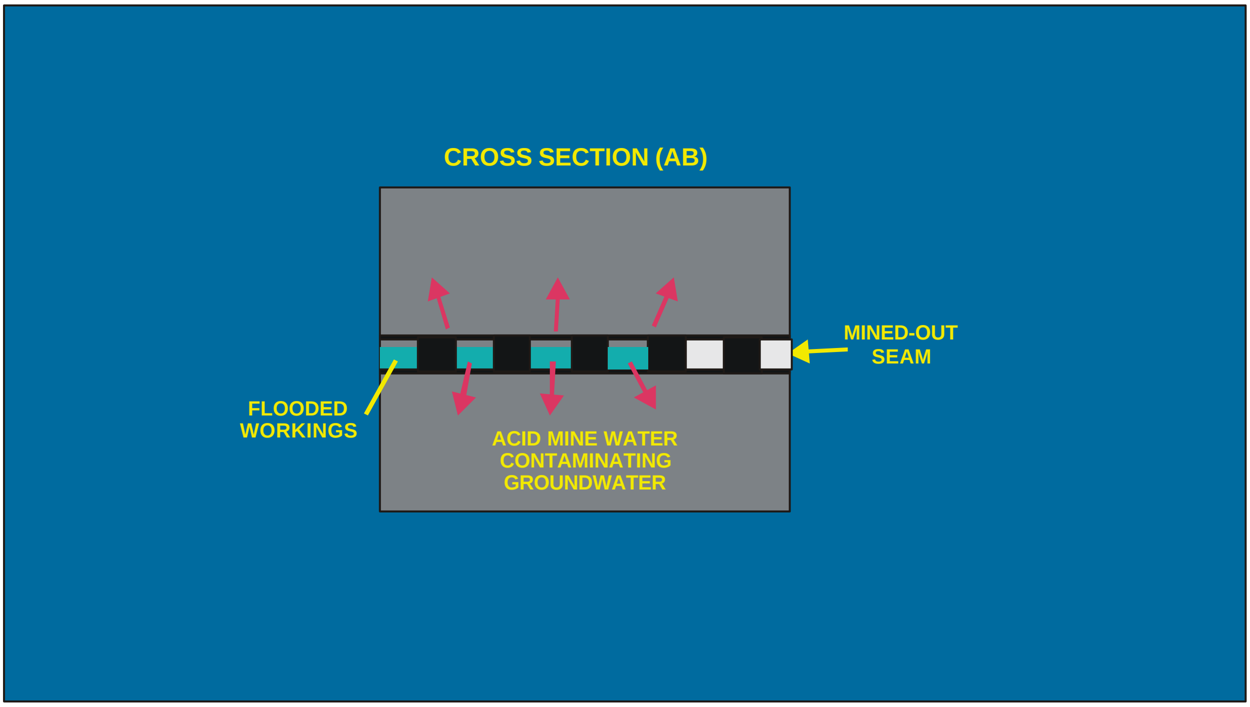

Figure A4: Schematic showing the contamination of groundwater from acid mine water.

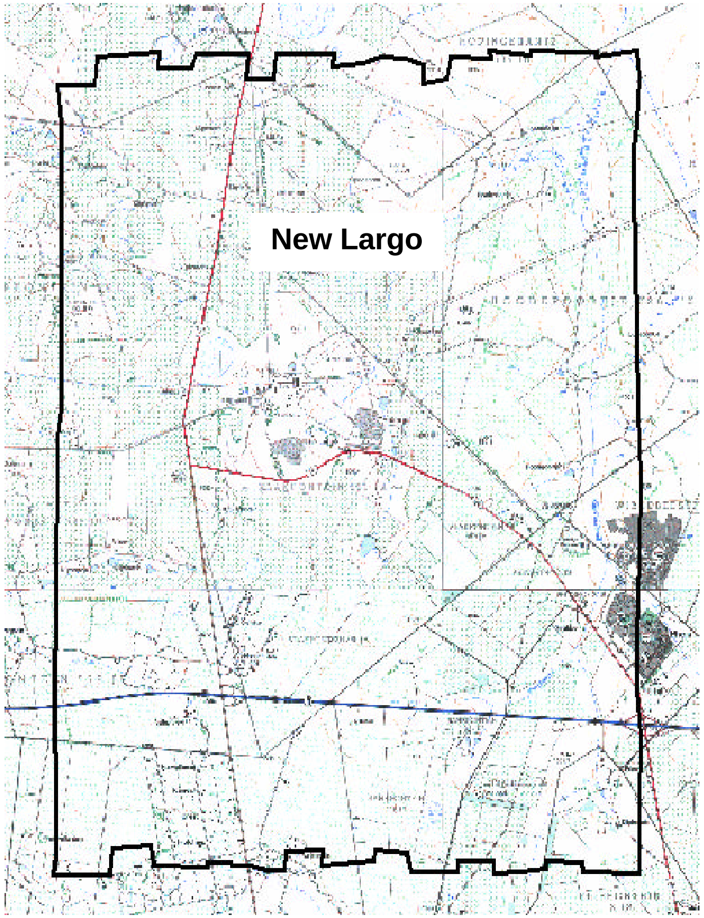

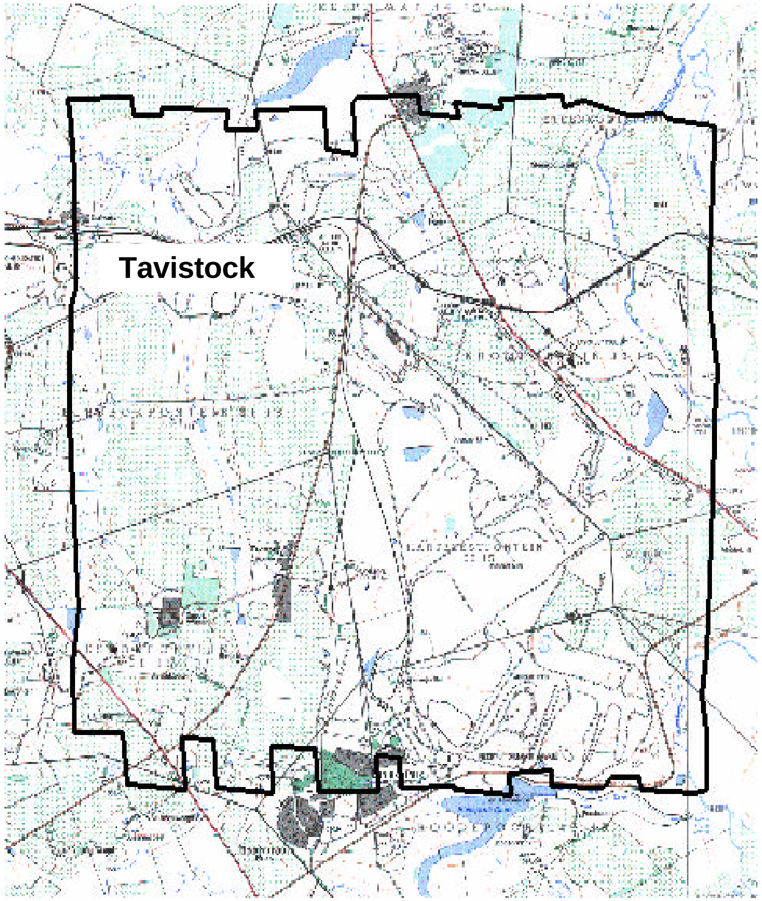

Figure A5: Maps showing the TIR surveys areas.

APPENDIX I

COALTECH 2020

Subtask Report

(part of Subtask 4)

CSAMT numerical modelling of coals seams

J. Cole

Council for Geoscience
Geological Survey

CSIR, Division of Mining Technology

Report number: 2001-0121

Task 1.3.1b

Detection of old workings, sinkholes, underground fires and acid mine pollution using geophysics and airborne thermal infrared imagery

October 2000

EXECUTIVE SUMMARY

Two dimensional magnetotelluric modelling was undertaken to study coal seams in old coal mines. The aim of the study was to determine whether Controlled Source Audio Magnetotellurics (CSAMT) could be used to detect seams and cavities within the seams. The frequency range of the Geometrics Stratagem was used. The modelling results show that the frequency range of this instrument is too low to resolve small features within the first 60m below the surface.

TABLE OF CONTENTS

LIST OF FIGURES AND TABLES

LIST OF ADDITIONAL FIGURES IN APPENDIX A

1 INTRODUCTION

The Geophysics Business Unit of the Council for Geoscience was approached by CSIR Miningtek to determine the applicability of controlled source audio frequency magnetotelluric (CSAMT) work in detecting old workings, sinkholes, underground fires and acid mine pollution in old coal mines. The specific task was to undertake numerical modelling to establish whether CSAMT can be used, and if that is the case to determine the optimum parameters for such surveys.

The first phase involved two-dimensional modelling of various 2-D earth models specified by the client. Once the success of two-dimensional modelling has been established, modelling in three dimensions can be considered.

2 SPECIFICATIONS PROVIDED BY CLIENT

2.1 2D coal model

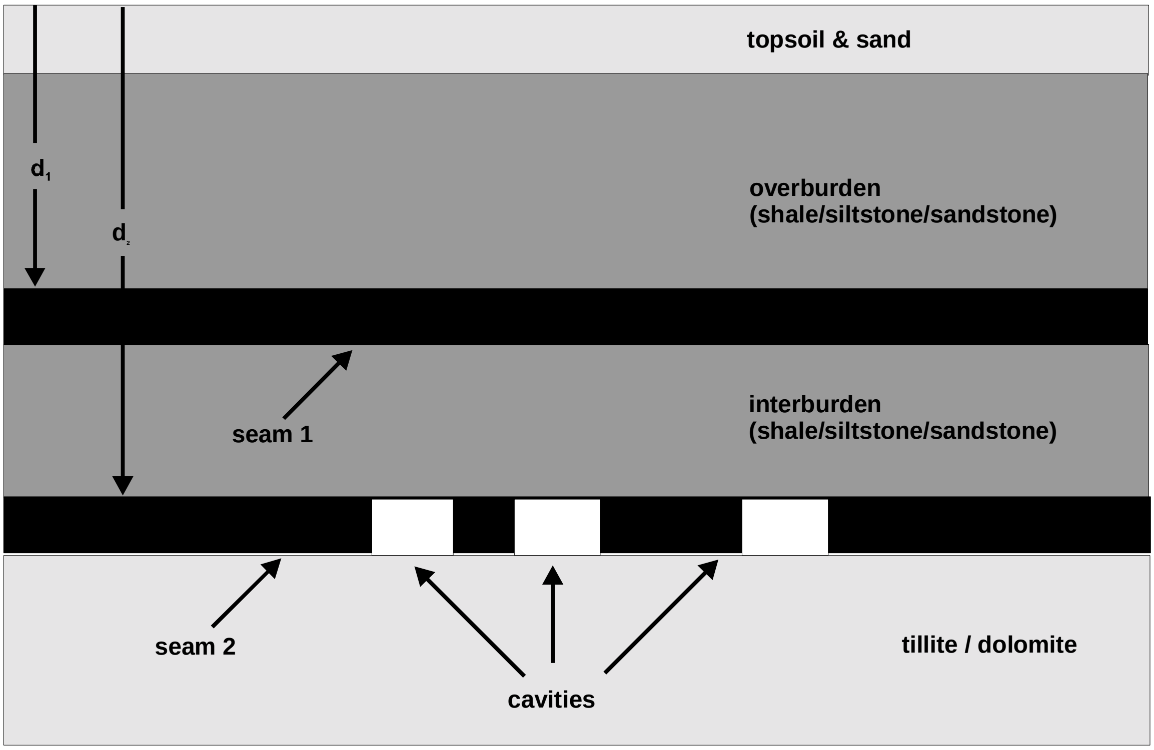

Figure 2.1: 2D coal model.

2.2 Background

The above 2D section (Figure 2.1) depicts the simplified coal scenario to be used as guide to design the input models for numerical modelling. The soft overburden (topsoil & sand) varies in thickness from a few metres to about 15 m. There may be several coal seams of which one or more may be partially mined out using the bord-and-pillar method. This typically leaves a series of coal pillars and bords/cavities. The latter are often filled with water/mud. The hard overburden and interburden consists of shale/siltstone/sandstone layers, while the floor (below the bottom seam) comprises Dwyka tillite/diamictite resting on Transvaal dolomites.

The thickness of the seams typically varies between 2 m and 8 m. The dimensions of the bord-and-pillar grid average about 6 m x 6 m (horizontally), while the vertical extent of these old workings are dictated by the seam thickness. The depth to the top seam can be as shallow as about 15 m, while the deepest seam can occur at depths of around 100 m.

2.3 Modelling specifications

For the purposes of the numerical modelling – consider the following estimates of electrical property ranges (at frequencies of a few MHz):

Table 2.3: Estimated electrical properties for numerical modelling.

Unit	Resistivity (Ωm)	Dielectric
Soft overburden	Tens to a few hundred	~10 – 20
Hard overburden	A few hundred	~10 – 20
Interburden	A few hundred	~10 – 20
Coal	Several thousand	~10 – 20
Floor	Similar to over/interburden	~10 – 20
Cavity	Insulator	~10 – 20
Flooded cavity	A few Ωms (~10)	~10 – 20

For the 2D modelling – make the following simplifications:

- Consider only a single overburden layer with a resistivity of ~ 200-500 Ωm
- Give the interburden and floor a similar resistivity value (~ 200-500 Ωm).
- Choose a resistivity value for the coal between say 5000 and 10 000 Ωm.
- Make the coal layers 5 m thick and consider at least 2 seams.
- Put the old workings in the lower seam – the dimensions of these cavities within the seam can be taken as 6 m wide x 4 m high.
- Cavities are either insulators (air-filled) or highly conductive when they are flooded (~ 10 Ωm).

The initial interest would be the following scenarios/problems:

1a. What is the shallowest depth at which CSAMT will be able to resolve features/layers and how does this depend on the overburden properties?
1b. How well can one resolve features and layers between this (shallowest) depth and say about 60 m?
1c. Through these simulations the optimum STRATAGEM parameters need to be determined (in order to achieve maximum resolution).

These questions could perhaps be investigated by just considering the two resistive coal seams in a uniform, more conductive background. Fix the separation between the seams at 15 m and vary the over/interburden resistivity between 200 and 500 Ωm. Also, vary the depths to the top of the seams between 15 and 30 m (seam 1) – i.e., 35 – 50 m for seam 2.

2. If the various layers can be resolved, what is the minimum distance between two coal seams that can be resolved (provided of course both seams lie below the minimum depth of investigation)?

3. Can a single cavity in the lower seam be detected? (I suspect it would only be possible – if at all – for a conductive, flooded cavity).

Place a single cavity in the lower seam. Consider the two extreme cases:

a) air-filled
b) flooded

4. If the above results are positive the minimum gap between two cavities that can be resolved can be determined.

3 TWO DIMENSIONAL MAGNETOTELLURIC MODELLING

The two dimensional models were created using the EMIXMT2D software package developed by Interpex. It uses a finite element routine to calculate the theoretical response of a given model (Wannamaker and Stodt, 1987). Models were calculated using a frequency range of 10 Hz to 70 000 Hz, similar to the range covered by the Geometrics Stratagem. The results calculated for the models are shown in the form of pseudosections. The x-axis shows the distance along the traverse, and the z-axis shows the frequency. The colours indicate resistivity in Ωm, ie red colours depict conductive units. For gridding purposes the log of the frequency had to be used. Frequency and depth are related via the skindepth:

$$\delta = \sqrt{\frac{2\rho}{\omega\mu}}$$

where δ = skindepth (m)
ω = angular frequency (s)
μ = magnetic permeability of free space (H/m)
ρ = resistivity (Ωm)

The first model consists of two coal seams 15m apart. The top of the first seam is at 15m. Each seam is 5m thick and has a resistivity of 10 000 Ωm. The host rock has a resistivity of 200 Ωm. Figure 1(a) shows the layout of the model. Results calculated for model 1 are shown in Figure 1(b). It is not possible to distinguish between the two coal seams. On the apparent resistivity versus frequency pseudosection they appear as one resistive layer. The impedance phase gives the phase difference between the electric and magnetic fields that are used to calculate the impedance tensor. In a uniform earth the electric field leads the magnetic field in-phase by 45º (Vozoff, 1972). Where there are variations in resistivity the impedance phase will deviate from 45º. On the impedance phase versus frequency pseudosection the two coal seams are also only seen as one anomalous feature.

In model 2 the seams were moved down to 30m and 50m respectively. Once again the two seams only cause a single feature.

Decreasing the resistivity of the coal seams to 5000 Ωm (Figures 3 and 4) does not improve the results. For the sake of completeness, the resistivity of the host rock was increased to 500 Ωm (Figures 5 and 6).

A layer of more conductive (20 Ωm) overburden was added to the model. Figure 7 shows the model and results. The highly conductive material has a large impact on the depth of penetration. In Figure 7(b) the effect of the resistive coal seam only starts to appear on the apparent resistivity pseudosection at frequencies just above 10Hz. The resistivity of the soft overburden was increased progressive, and although the resistive layer becomes more visible at higher frequencies, it is still not possible to separate the two layers.

Although it was not possible to distinguish between the two coal seams on the modelling results, it was decided to add a cavity in the lower seam to study the effect on the MT field. Figure 8(a) shows the case where the cavity is air filled. No effect of this cavity can be seen on the results (Figure 8(b)). When the cavity is flooded with conductive material, the effect is quite large (Figure 9(b)). It is not possible to obtain a clear delineation of the cavity's boundaries and it is concluded that the CSAMT method is not suited to solving this problem.

4 CONCLUSIONS

From the numerical modelling exercise it is deduced that the CSAMT is not suited to studying the worked out coal mine problem specified in this project. Electromagnetic methods are not well suited to distinguish between resistors in a more conductive terrain.

5 REFERENCES

Vozoff, K. 1972. The magnetotelluric method in the exploration of sedimentary basins. *Geophysics*, 37, 98 - 141.

Wannamaker, P.E., Stodt, J.A. 1987. A stable finite element solution for two dimensional magnetotelluric modelling. *Geophysical Journal of the Royal Astronomical Society*, 88, 277-296.

APPENDIX A

FIGURES – RESULTS OF 2D CSAMT MODELLING

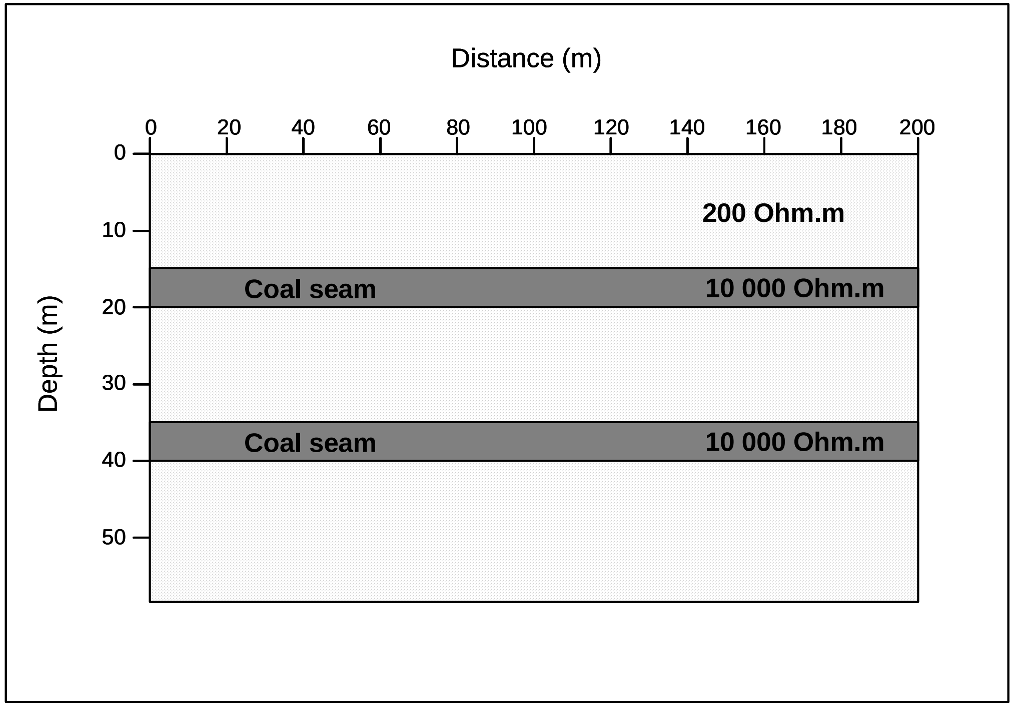

Figure 1(a): Model 1.

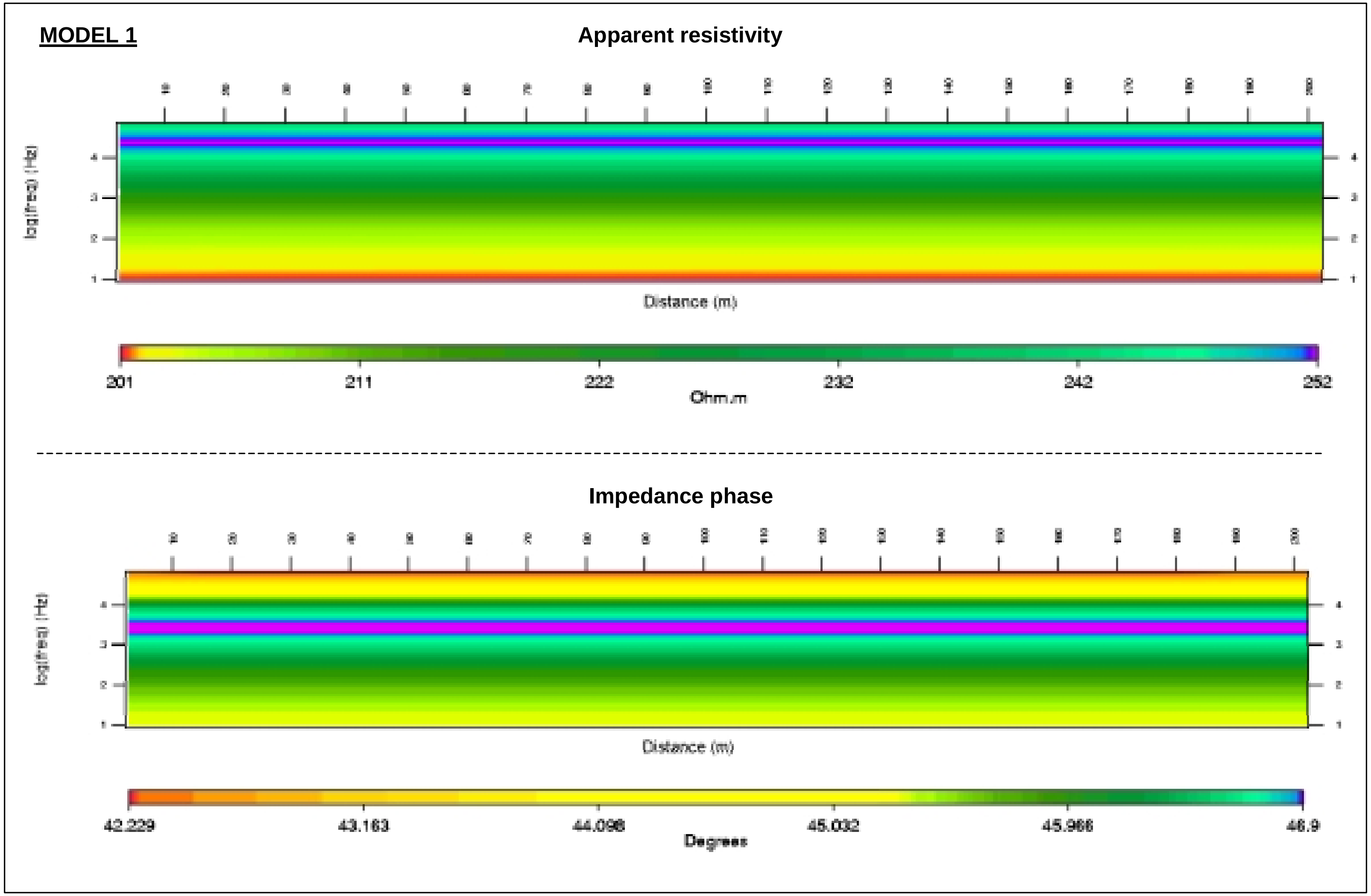

Figure 1(b): Results calculated for model 1.

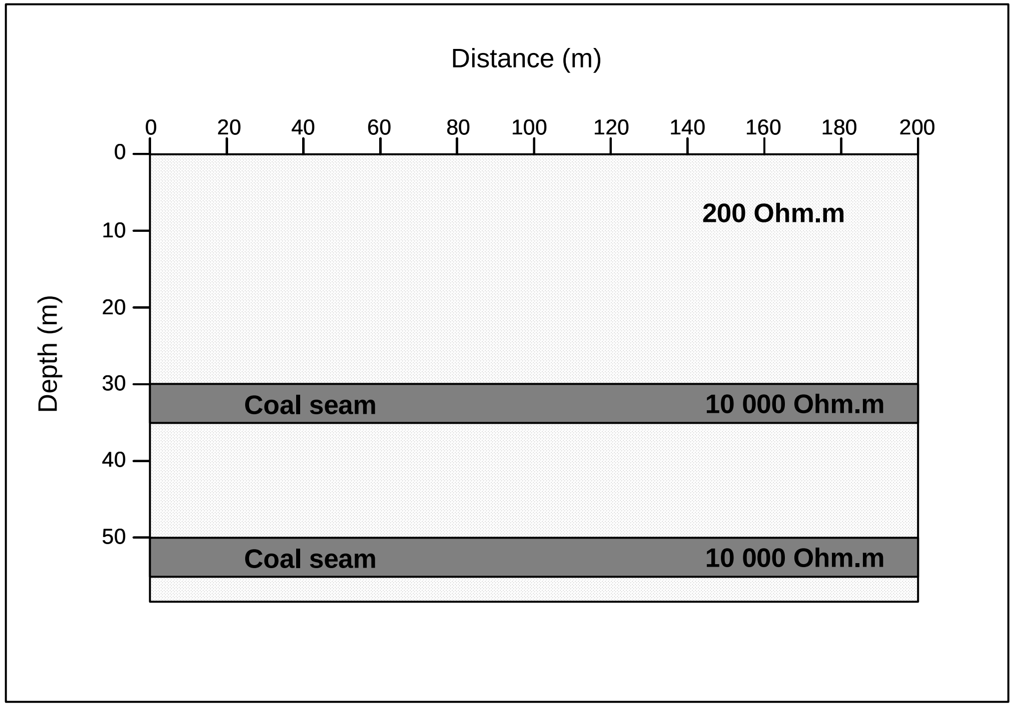

Figure 2(a): Model 2.

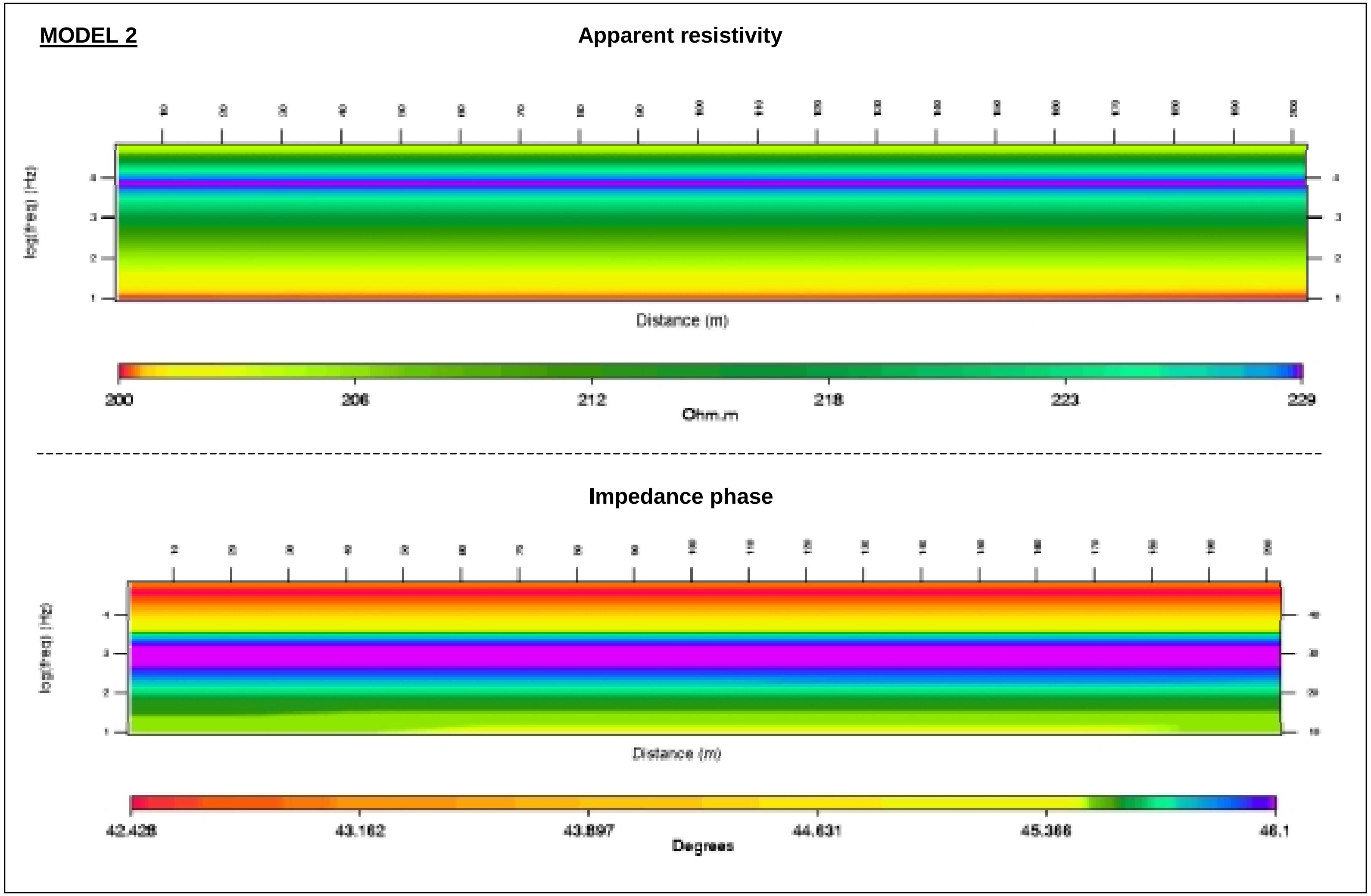

Figure 2(b): Results calculated for model 2.

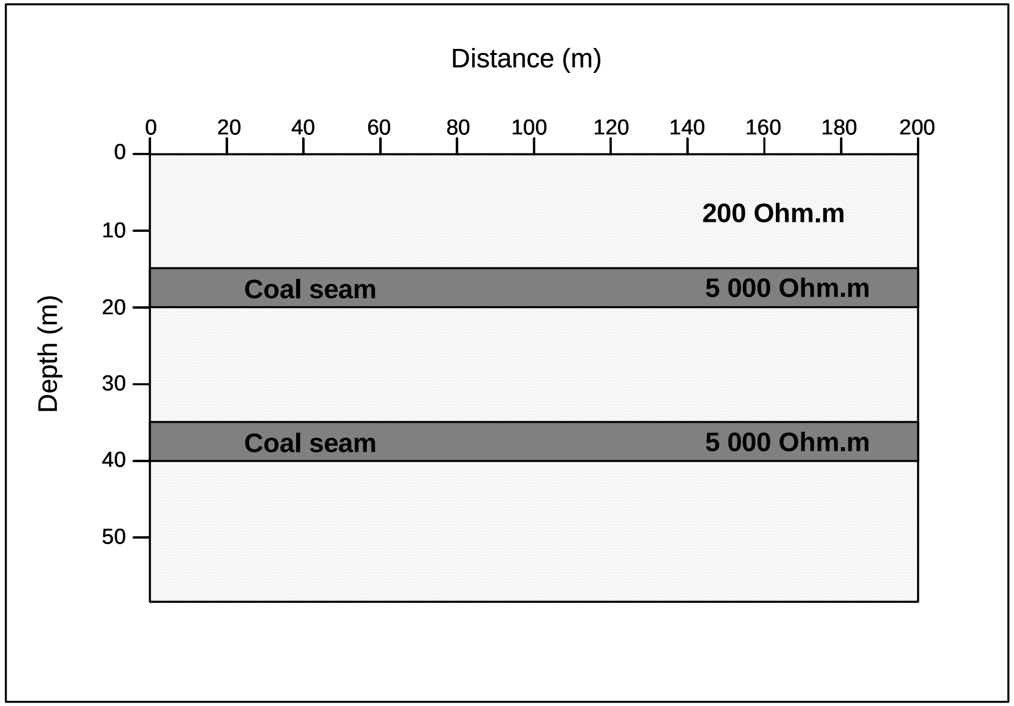

Figure 3(a): Model 3.

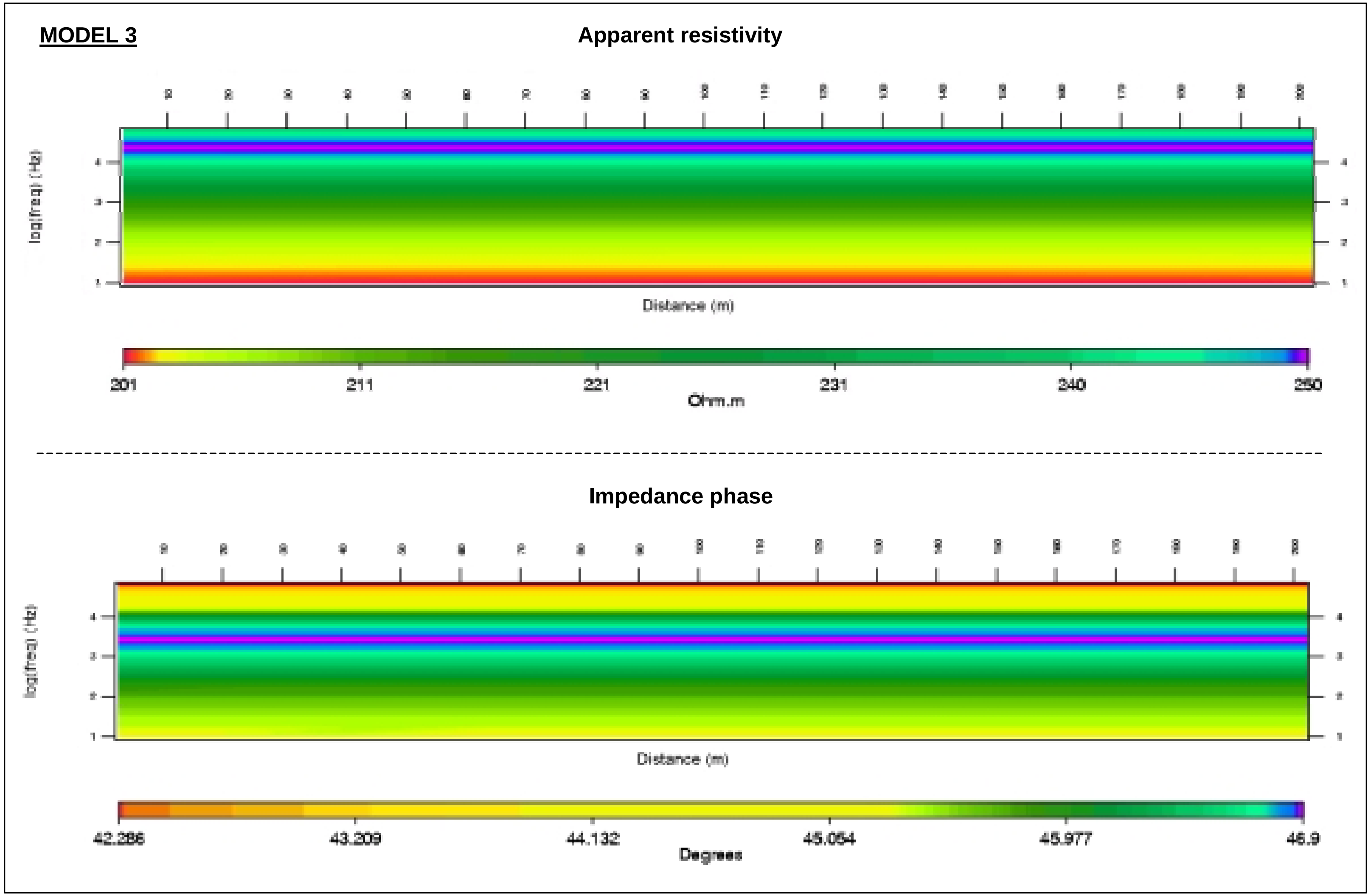

Figure 3(b): Results calculated for model 3.

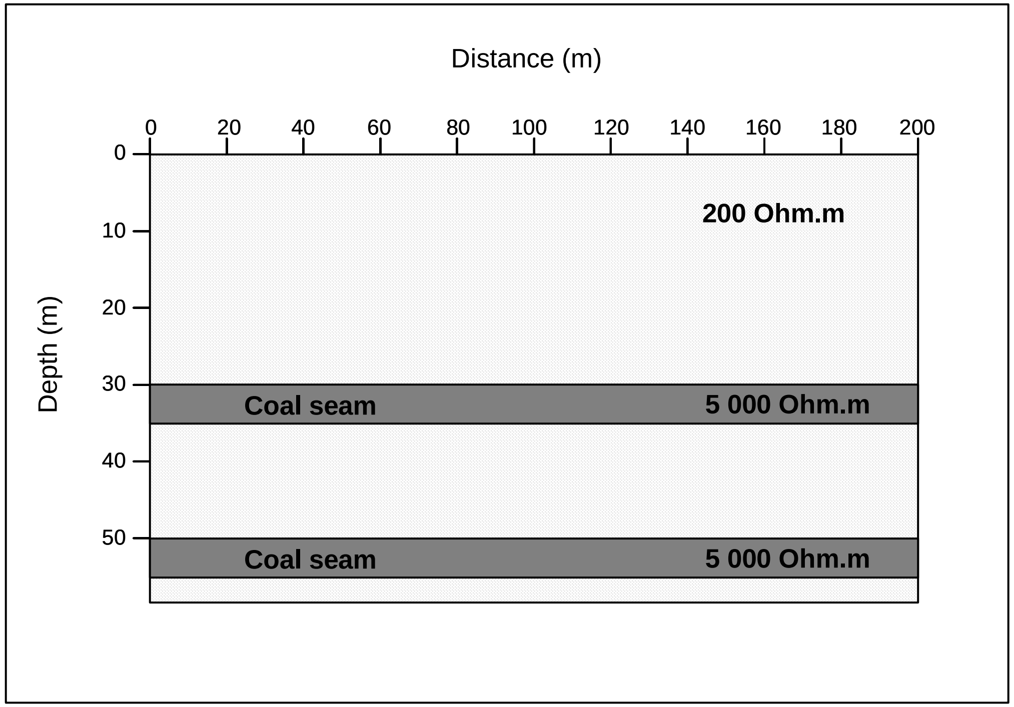

Figure 4(a): Model 4.

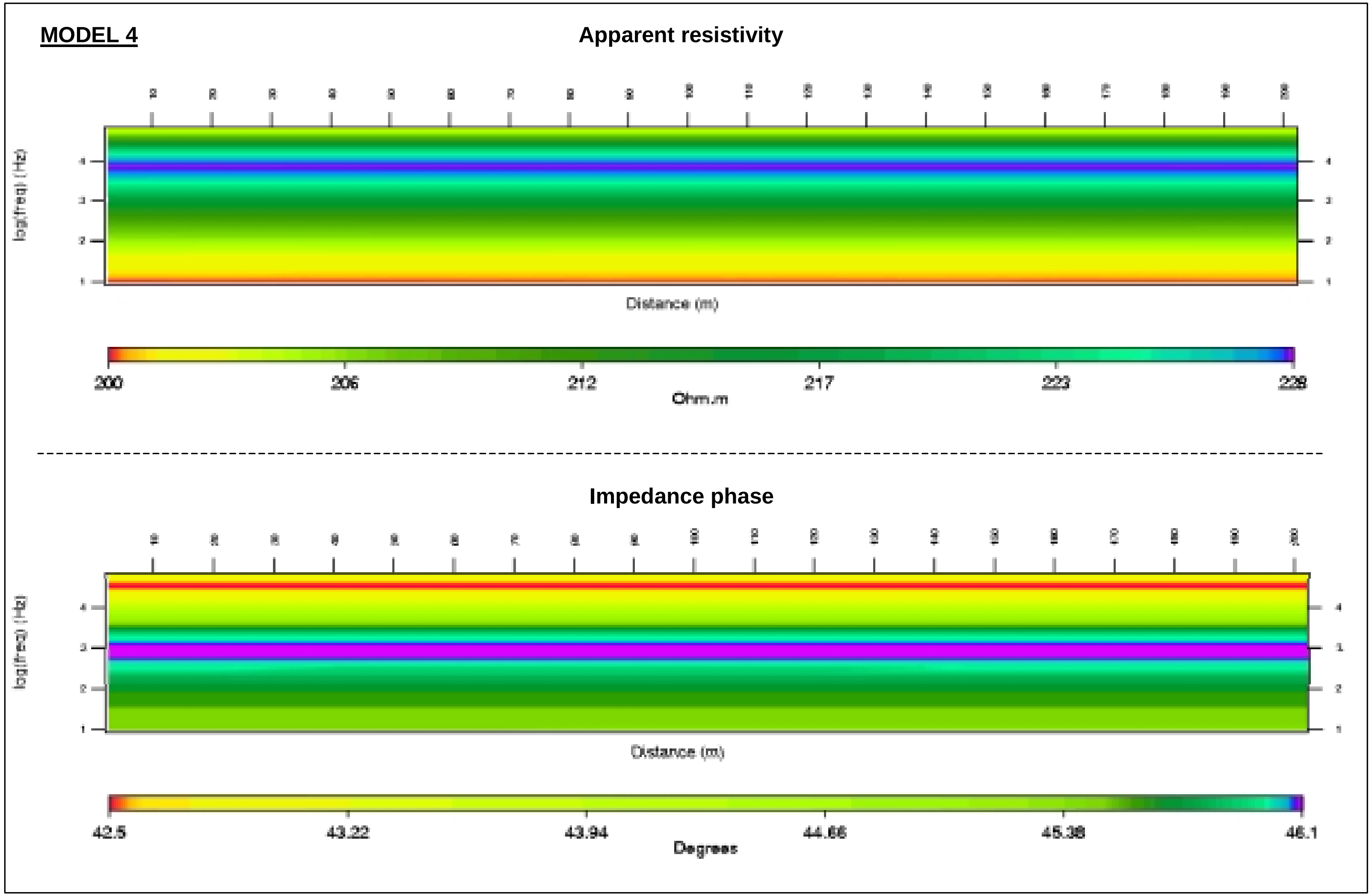

Figure 4(b): Results calculated for model 4.

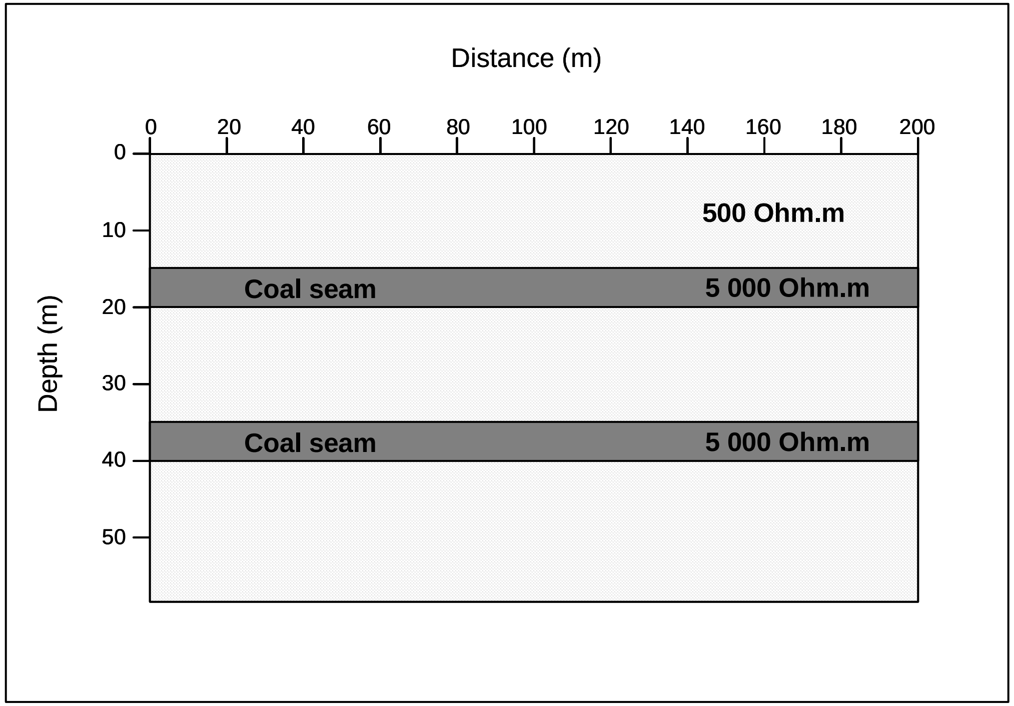

Figure 5(a): Model 5.

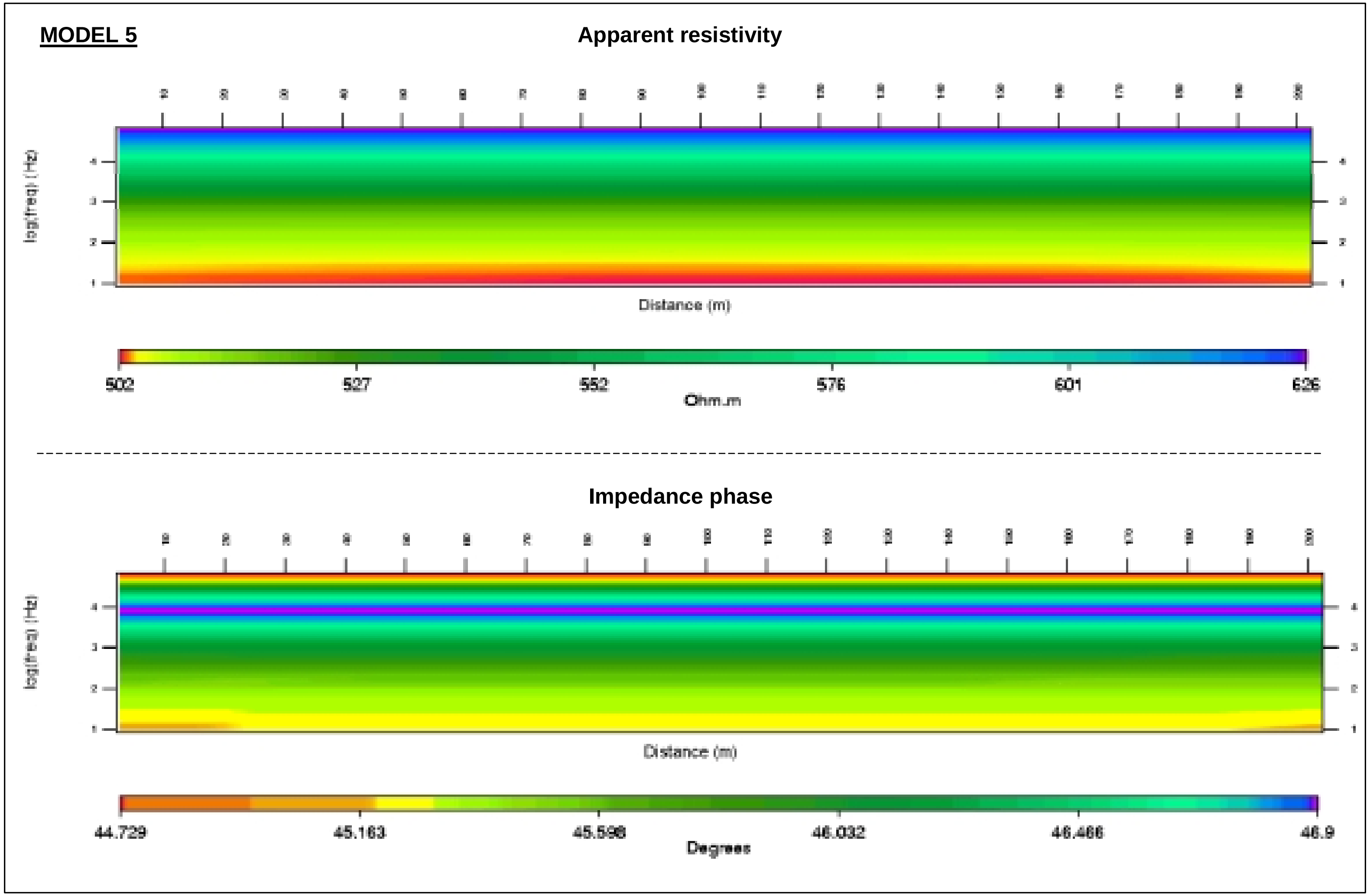

Figure 5(b): Results calculated for model 5.

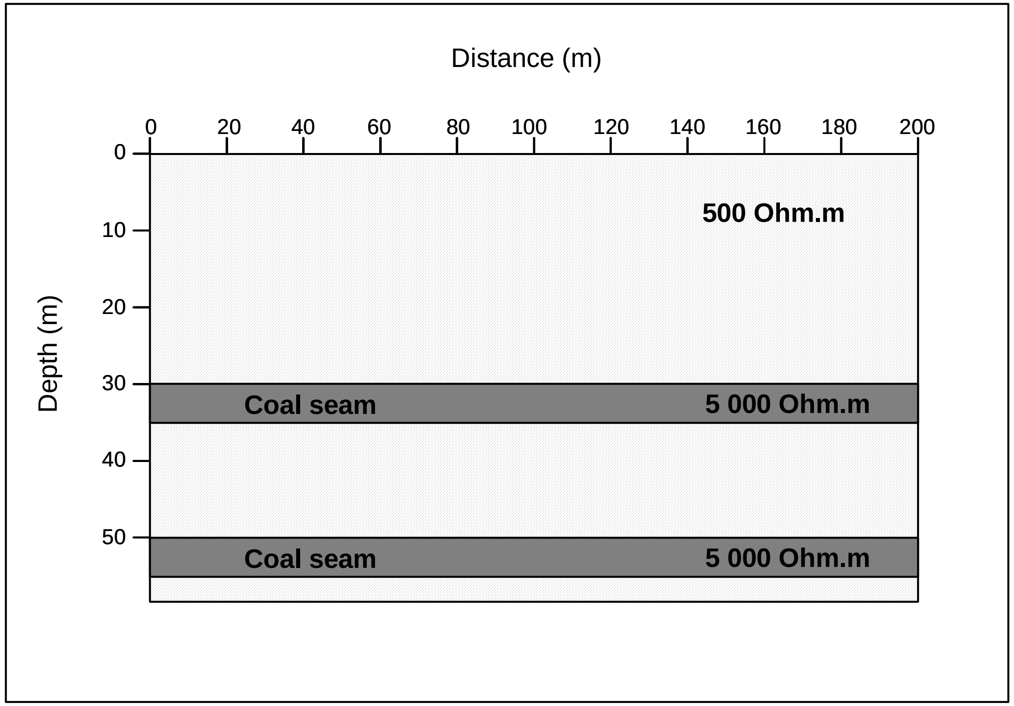

Figure 6(a): Model 6.

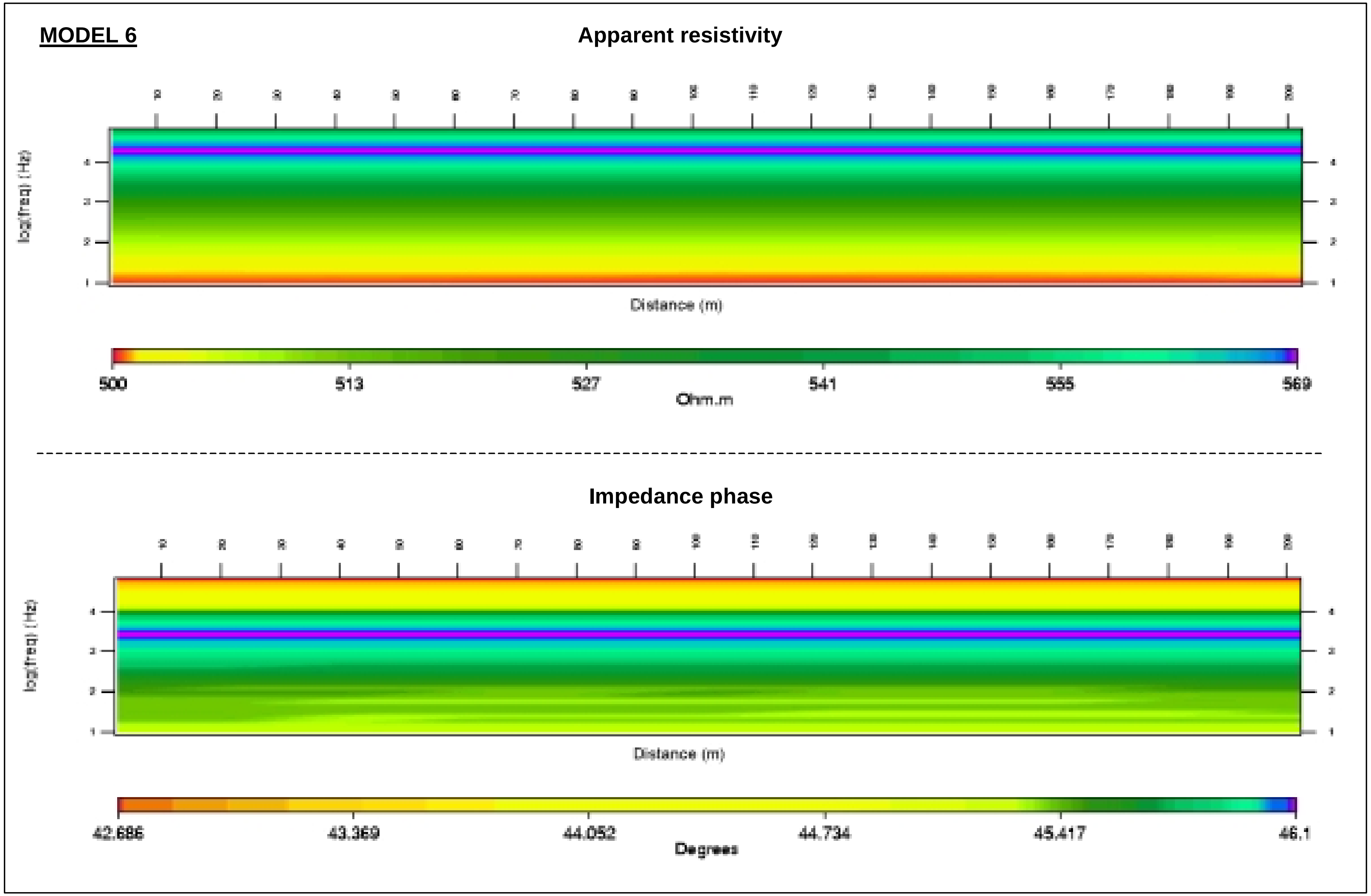

Figure 6(b): Results calculated for model 6.

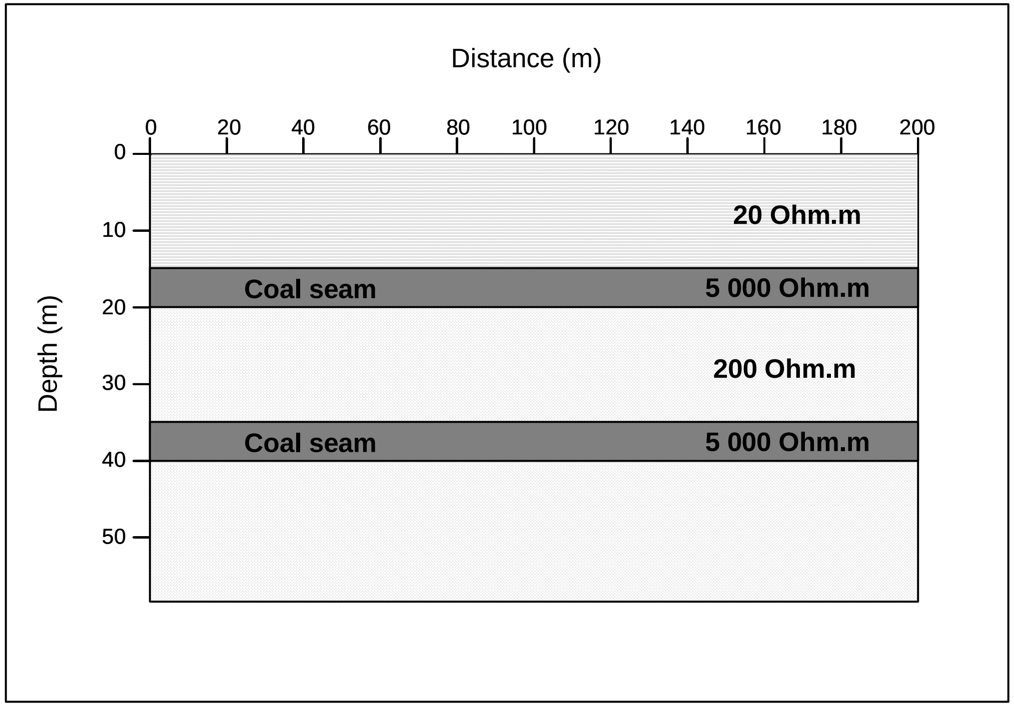

Figure 7(a): Model 7.

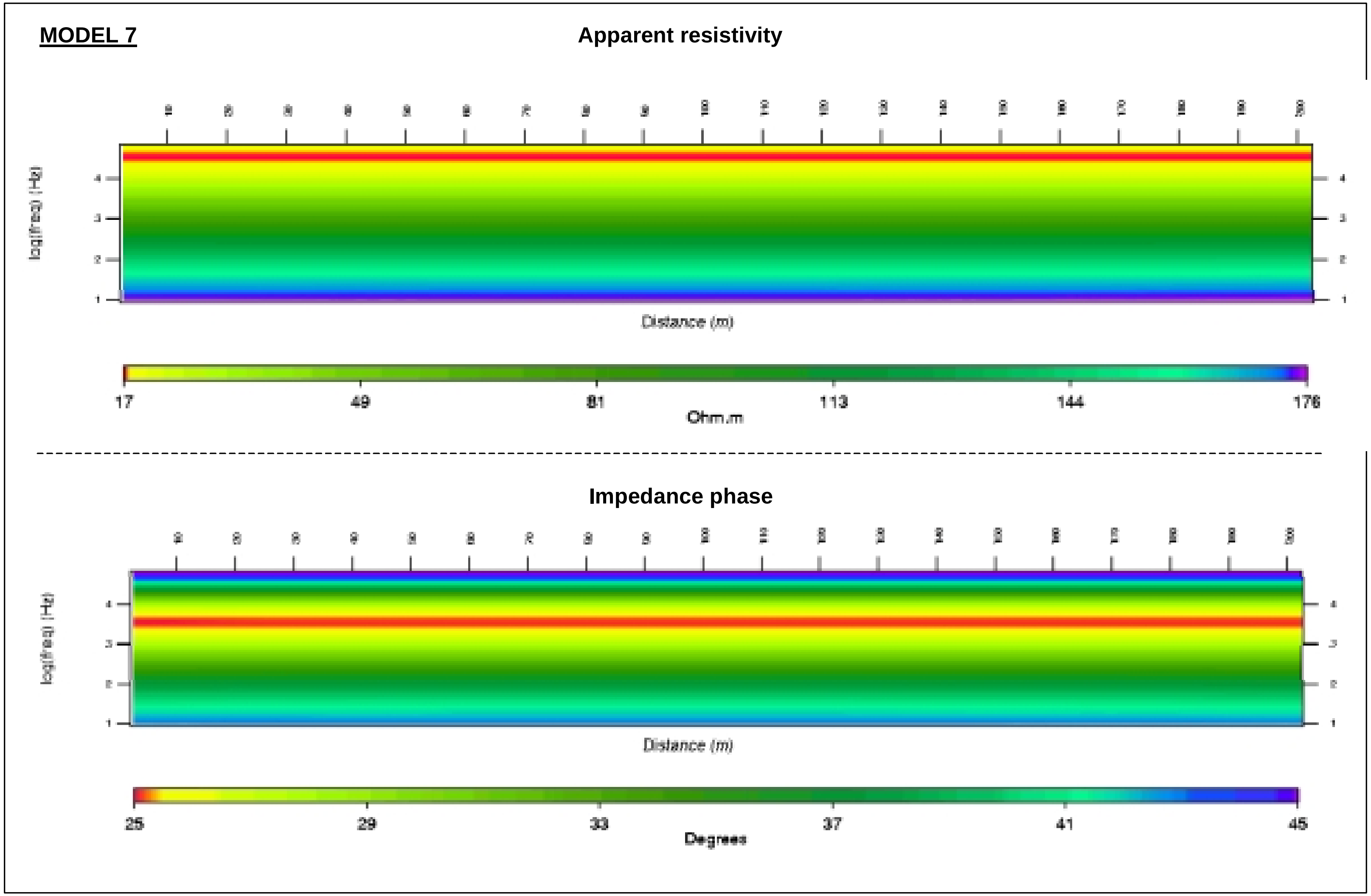

Figure 7(b): Results calculated for model 7.

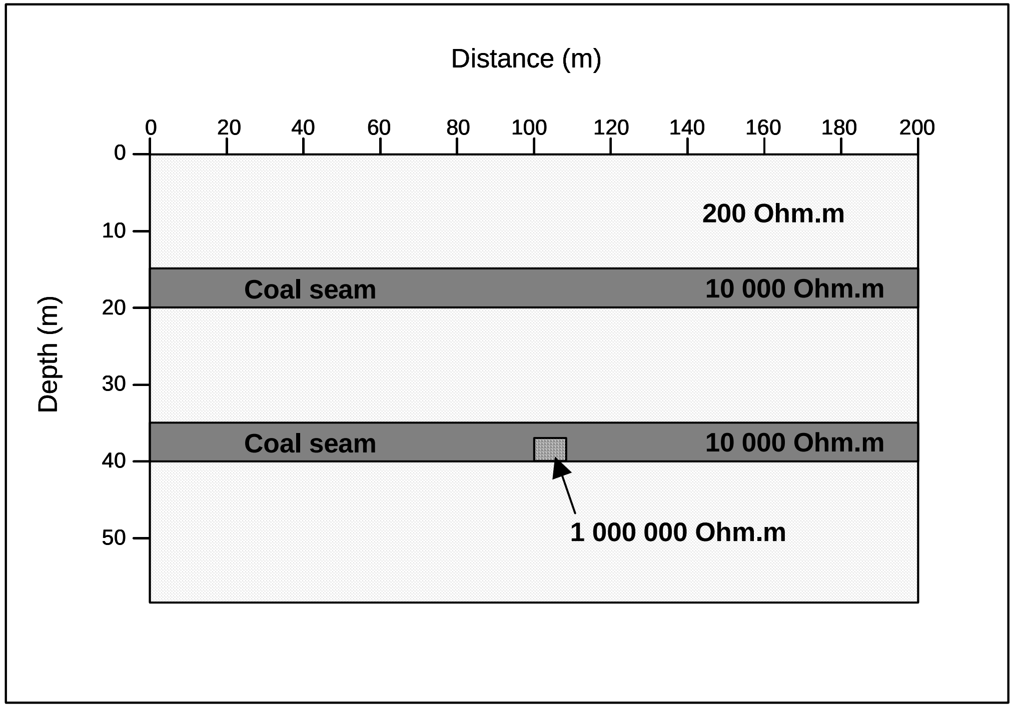

Figure 8(a): Model 8.

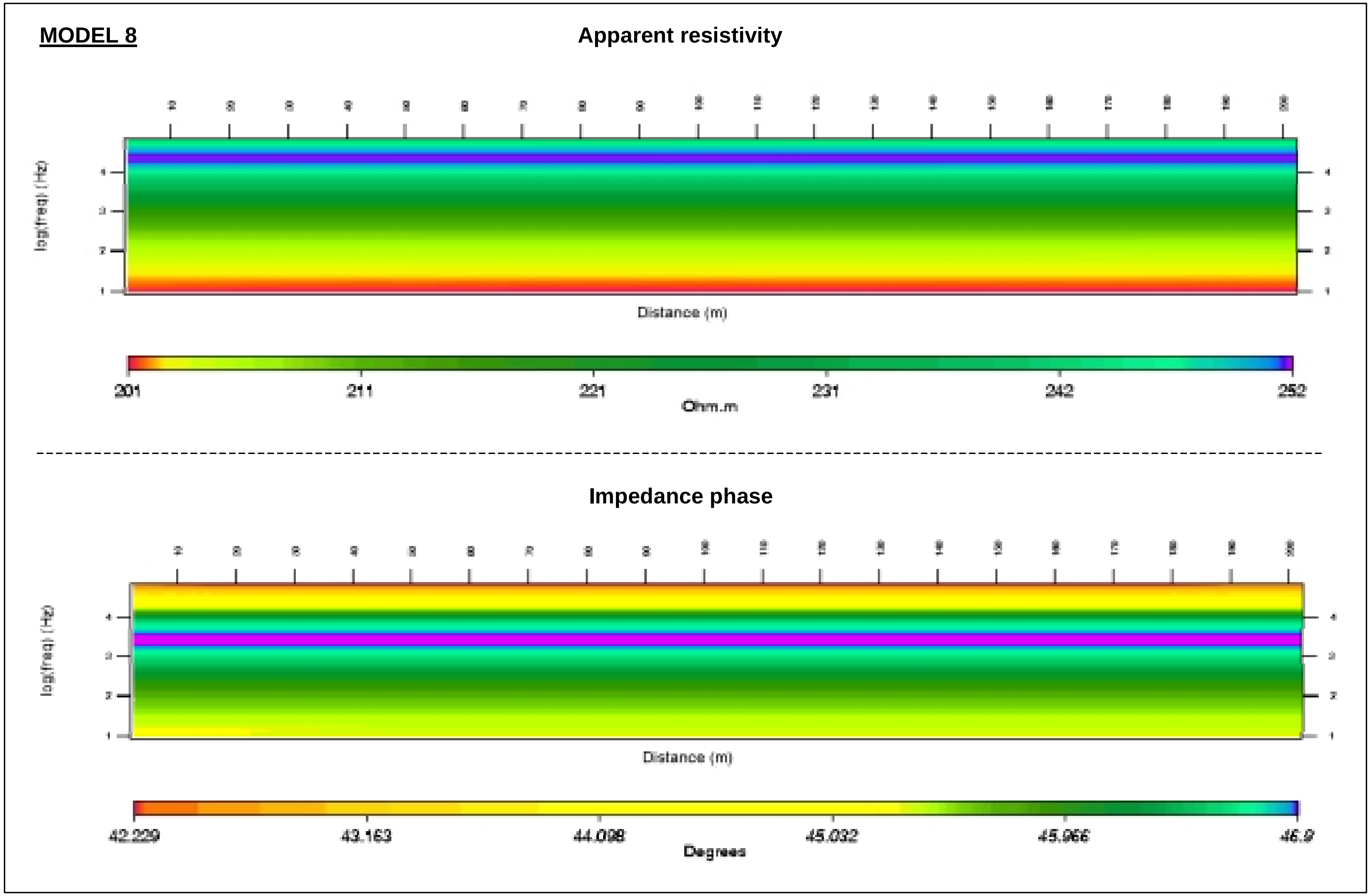

Figure 8(b): Results calculated for model 8.

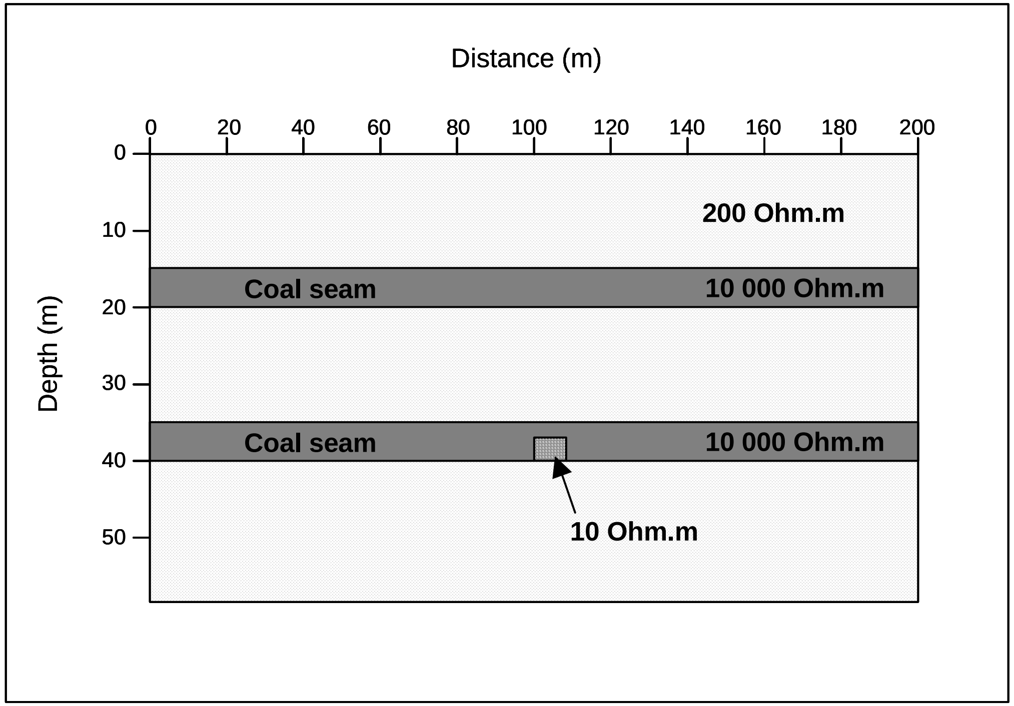

Figure 9(a): Model 9.

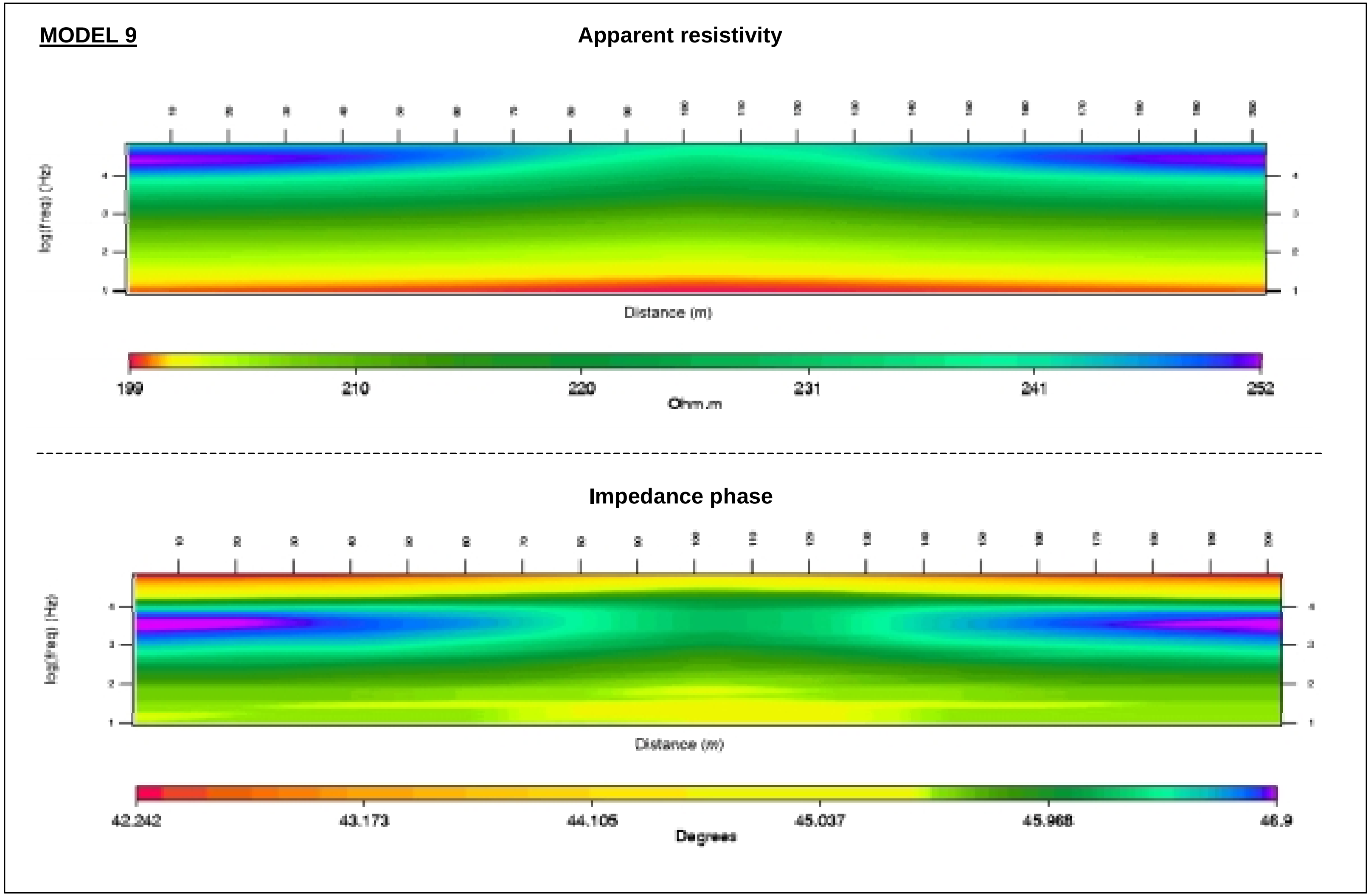

Figure 9(b): Results calculated for model 9.

APPENDIX II

COALTECH 2020
Subtask Report

Acquisition and interpretation of night-time airborne thermal imagery over New Largo and Tavistock.

M. F. F. Ferraz
Environmental Projects Manager, Geosciences Resource Group,
Anglo Technical Division

Report number: 2002-0144

Task 1.3.1b
Detection of old workings, sinkholes, underground fires and acid mine pollution using airborne thermal infrared imagery

February 2002

EXECUTIVE SUMMARY

The main objective of this study, a component of Task 1.3.1b, was to use night-time airborne thermal imagery to detect and map the aerial distribution of:

- bord and pillars of old mine workings;
- shallow sinkholes developed in overburden above mining bords;
- underground fires; and
- acid mine drainage pollution plumes.

The data acquisition, using the Tallytherm Airborne Thermal Scanner, was completed in July 2001. Data preparation, including geometric correction, was completed according to specifications.

Using the airborne thermal data subsets, it has been possible to detect and map selected features, namely, the presence of old workings, sinkholes and fires in the New Largo, Tavistock and Kromdraai imagery. The presence of acid mine drainage could not be conclusively established on the selected subsets from this imagery although the ponding of water within an ash dump at New Largo has been identified as a potential problem. This water could mobilise any existing fines and sulphides from within the slimes dam into the surrounding fields. This could lead to the contamination of the land by forming acid mine drainage during the chemical breakdown of sulphides. The absence of clearly identifiable acid mine drainage on these subsets can be interpreted as a positive result, indicating currently effective slimes control measures. Moisture and/or water, infrastructure as well as vegetation could also be recognised and delineated.

The 1m x 1m pixel resolution of the airborne thermal data was sufficient to identify the relevant features although sub-meter pixel resolution would provide more detail, particularly for old workings.

The interpretation of this thermal data is preliminary and only 1:50 000 topographic map data has been evaluated simultaneously. A detailed interpretation can extract more information from this data through the integration of other datasets, thus refining the interpretation. Field verification is required to establish the veracity of this preliminary interpretation and provide an assessment of the overall feature mapping accuracy.

This data should be integrated into management plans for monitoring and/or rehabilitation for these areas. Any airborne thermal data collected in the future, can be used with this data in change detection studies.

TABLE OF CONTENTS

LIST OF FIGURES

LIST OF TABLES

LIST OF APPENDICES

1. INTRODUCTION

A number of scenarios have been identified in the Witbank area as problematic from a mining as well as an environmental point of view. These problematic scenarios include not knowing the location or extents of various features such as old underground workings and pollution plumes. Four features have been selected as crucial to the planning of future mining and/or developments on surface and these include:

- bord and pillars of old mine workings;
- shallow sinkholes developed in overburden above mining bords;
- underground fires; and
- acid mine drainage pollution plumes.

The mining technique used underground was predominantly bord and pillar. The mining depth was shallow, typically varying from 15m to 30m although in some areas a depth of 70m was achieved. Over the years the surface has caved into the undermined cavities. However, in many instances the spatial distribution of these bord and pillar cave-ins is unknown. Such sinkholes would have a surface and/or a near-surface expression. Mining activities, both past and present, contribute to underground fires as well as groundwater pollution. These could have a surface and/or a near-surface expression. Further, the potential for monitoring using this data type particularly in the vicinity of slimes dams and rock dumps will also be discussed.

The main objective of this study, a component of Task 1.3.1b was thus to acquire and interpret night-time airborne thermal data to detect and map the aerial distribution of the listed features. *Van Schoor, 2000*, stated that 'The great challenge in detecting and mapping the four types of targets lies in the fact that they differ significantly in their anticipated geometry and physical characteristics. Furthermore, the varying depth and rock type in which they occur contribute to the challenge. It is however difficult to predict the applicability of a geophysical technique from one site to the next.'

The airborne thermal survey area flown is located west of Johannesburg over the lithologies of the coal-bearing Karoo Supergroup in the Mpumalanga Province of South Africa. The survey area, south-west of Witbank, is outlined below in *Figure 1.1*. Mining commenced in the early 1900's. Although mining continues in some areas, it has ceased in others at different dates across the coalfield. Airborne thermal data from the Tallytherm scanner was acquired across the 8.5 µm to 13.5 µm wavelength range.

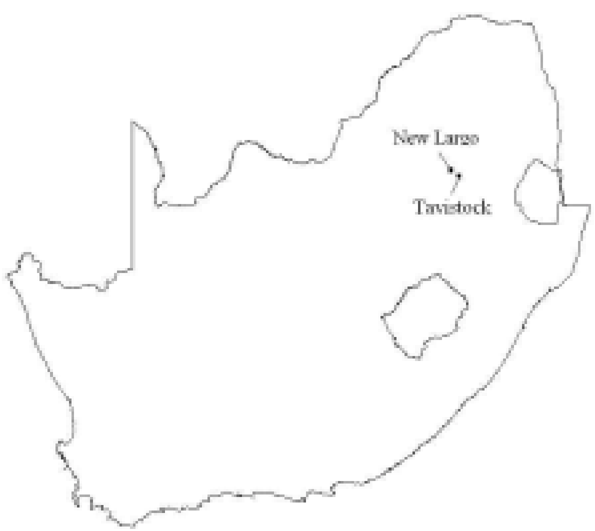

Figure 1.1. Locality Map of the 2001 Coaltech 2020 Airborne Thermal Survey Sites of New Largo and Tavistock.

1.1 Literature Survey

The literature survey portion of this has been reported on in report number 2001-0119, 'The application of airborne thermal imagery to the coal environment' prepared by A.J. Franzsen from Anglo Technical Division in October 2000. This document includes an introduction to airborne thermal remote sensing with selected references. A brief extract from this report follows.

Airborne Thermal Remote Sensing used for earth science applications comprises the 8 to 14 µm portion of the Electromagnetic Spectrum because it is in this spectral range where the earth radiates maximum thermal energy. This portion of the spectrum is known as Long Wave Thermal Infrared (LWTIR). In contrast, the Mid Wave Infrared (MWTIR), used in military applications to detect mainly the heat from engines, falls in the 3 – 5 µm portion of the Electromagnetic Spectrum. Most thermal camera systems use this latter spectral range, which is not suitable for earth science applications because of the short wavelength.

Apart from synthetic aperture radar, no imaging technique, other than Long Wavelength Thermal Imaging (LWTIR) is capable of depicting sub-surface features. Airborne LWTIR imagery has been used to map various sub-surface features. This includes the detection and/or mapping of:

- potentially mineralised palaeochannels;
- subsidence;
- old bord and pillar workings;
- geological and structural mapping;
- lithological mapping;
- sub-surface water; and
- pollution detection and geohydrology studies;

Such data has also been used for planning the siting of slimes dams and other structures.

1.2 Research Methodology

The features selected for study are:

- bord and pillars of old mine workings;
- shallow sinkholes developed in overburden above mining bords;
- underground fires; and
- acid mine drainage pollution plumes.

The resultant problem scenarios have been discussed in detail by *Van Schoor, 2000.* In the same report, there is also an evaluation of the geophysical criteria as well as techniques which can be used to identify the selected features. *Franzsen, 2000,* presented an overview of the ability of the thermal infrared imaging techniques to map the selected features of interest. Night-time airborne thermal imaging techniques appear to have the widest range of applicability although the performance of this tool is expected to deteriorate for targets beyond about 30 m depth. LWTIR seems like the only promising technique capable of directly detecting underground fires.

Thus remote sensing technologies will be used to acquire and subsequently interpret night-time airborne thermal infrared data for the selected features of concern.

2. DATA AND METHODOLOGY

The airborne thermal survey was requested in the year 2000, however, the survey was cancelled due to rainy weather. The acquisition campaign was re-scheduled for 2001 and data was successfully collected in July 2001 before the onset of any summer rain.

The required spatial mapping accuracy is approximately one to two metres as the typical bord-and-pillar structures have dimensions of about six by six metres. Surveys were planned to be flown using a long wave thermal infrared scanner with a ground pixel size of one metre so as to maximise the spatial informational content. At this resolution, the data strips would be about 860 metres wide, depending on undulations in the topography. All strips were planned with an intended overlap of 20% to allow for any undue yaw or roll of the aircraft. Post processing of the data would have compensated for roll as this would have been measured and recorded together with GPS information.

The survey plan provided for coverage of areas from all the major companies involved with coal mining in the Witbank area. At the same time, Anglo Coal and other interested parties had planned a separate survey over Witbank town and adjacent areas. The Coaltech 2020 survey sites, were planned around the Anglo Coal area to avoid repetition. These include an area around New Largo where old workings as well as dumps occur. In addition, a survey was planned to coincide with the ground geophysical work undertaken at Tavistock Colliery (Duiker), as well as several dumps and active workings. This area also has both water filled and dry older bord and pillar workings. A different thermal response would be expected from these two sub-surface areas.

A detailed methodology follows:

2.1 Data Acquisition

The survey area, acquired for Coaltech 2020, coincides with various collieries, mine dumps, residential as well as industrial sites in the Witbank coalfield. The geographic extents of the surveys are tabled below *(Table 2.1).*

Table 2.1. Geographic extents of the Coaltech 2020 Airborne Thermal Survey Sites of New Largo and Tavistock.

SURVEY	**New Largo**		**Tavistock**	
Corner	**Latitude**	**Longitude**	**Latitude**	**Longitude**
Upper Left	S 25° 54’ 47.2”	E 28° 55’ 35.3”	S 26° 04’ 10.6”	E 29° 08’ 51.2”
Upper Right	S 25° 54’ 47.2”	E 29° 02’ 27.5”	S 26° 04’ 10.1”	E 29° 15’ 21.5”
Lower Right	S 26° 02’ 45.1”	E 29° 02’ 27.7”	S 26° 10’ 15.2”	E 29° 15’ 11.3”
Lower Left	S 26° 02’ 45.0”	E 28° 55’ 35.0”	S 26° 10’ 15.7”	E 29° 08’ 51.6”

The study areas, outlined below in *Figure 2.1*, extend across part of the following 1:50 000 topographic map sheets: 2528DD, 2529CC, 2628BB, 2629AA.

The Tallytherm airborne thermal scanner instrument, operated by Infoterra, UK, was selected because of its’ ability to achieve a resolution of 1m x 1m on the ground.

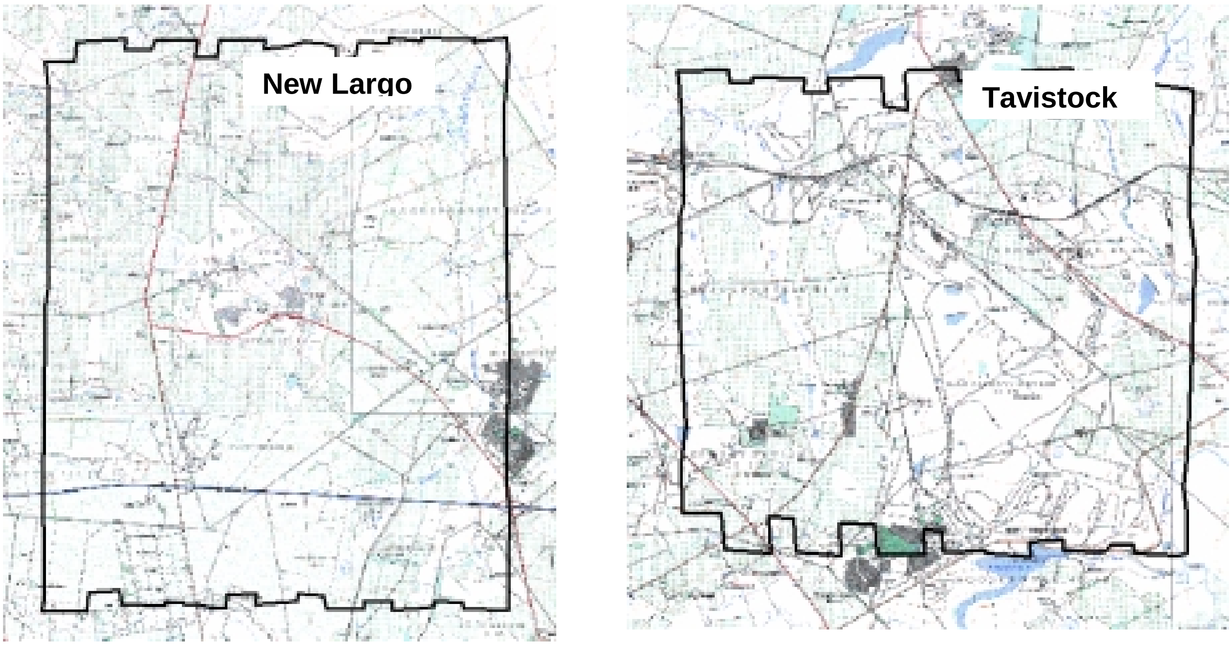

Figure 2.1. Detailed Survey Plans of the Study Sites, South West of Witbank.

The data sets used in this study are listed below in *Table 2.2.*

Table 2.2. List of data sets used in this study.

Data	**Date**	
Airborne Thermal	21-22nd, 24th July 2001	• Tallytherm Airborne Thermal Scanner • Data acquisition details below
Topographic Maps		• 2528DD, 2529CC, 2628BB, 2629AA 1:50 000

Stage	Results
1. Lease the Tallytherm Airborne Thermal Scanner from Infoterra in UK and an aircraft from FUGRO in South Africa during July 2001.	• Scanner specifications: ➢ One spectrometer, 8.0 µm to 14.0 µm wavelength range in the thermal infra-red, in one band. ➢ Spectral resolution (bandwidth) is 6 µm. ➢ Temperature resolution better than 0.1°C; does not have an internal temperature calibration source. ➢ Nitrogen gas cooled. ➢ 8 bit quantisation with operator controlled gain/offset adjustment. • Line scan mirror rotates at 19500 rpm or 1950 scans per second. Records a new line of data when the aircraft has moved forward sufficiently. Data recording rate is dependent on altitude above ground level and ground speed. At acquisition altitude, a new line of data was written every 26 scans. • The instrument payload is 16.4kg for the scanner head and 56kg for the equipment rack. • Lease agreement completed July 2001.
2. Carry out the survey planning.	• Flight altitude: 2446 ft or 746 m above ground level at a ground speed of ~120 knots for 1 m x 1 m pixel or ground resolution. • Completed July 2001.
3. Aircraft details	• Cessna 404 with available power of 28 V DC. • Typical sorties between 23:00 and 05:00.
4. Acquire the thermal data New Largo and Tavistock area.	• Acquired. • New Largo ➢ Acq date 24 July 2001 ➢ Acq time 01:13:19 – 02:18:15 ➢ 13 strips, each ~13.8 km long, ~860 m wide ➢ Covered ~140 km^2 or 140000 ha. • Tavistock ➢ Acq date 21 July 2001 (strips 09-13) ➢ Acq date 22 July 2001 (strips 01-08) ➢ Acq time 03:20:55 – 03:42:40 (strips 09-13) ➢ Acq time 22:55:29 – 23:33:00 (strips 01-08) ➢ 13 strips, each ~10 km long, ~860 m wide ➢ Covering ~110 km^2

2.2 Data Preparation

Stage	Results
1. Evaluate the thermal raw data in terms of: - dark current / black body temperature settings - data format - GPS co-ordinates per scan line - survey planning data	• Gains and offsets set by operator. Black body temperature settings done externally from ground temperatures over water bodies. • Format of the raw data is .BIL with 59 header bytes and 1312 columns; ➢ column 1-72 housekeeping data; ➢ column 73-1312 image data ➢ to get 1240 pixels per scan line ➢ number of image lines on bitmap file ➢ strips have to be mirrored • Non-differential GPS data of the aircraft location was acquired for each scan line, including speed and direction. However, these were insignificant as they were too inaccurate to be usable for georeferencing. • Check that correct number of strips were acquired over correct area.
2. Assess quality control and accuracy of the thermal data.	• Ground conditions were suited to good pre-dawn thermal IR data acquisition. There was little ground moisture (dew) to significantly diminish signal quality. The DN and temperature range of the pixels is thus not affected. • Bitmaps were created for on-line quality control.
3. Pre-processing of thermal data.	• The image data was corrected for roll but not for pitch and yaw.
4. Scan available topographic maps.	• Maps were scanned, ground control points were collected then warped to a common projection to enable the overlay of the different data sets. • 1:50 000 topographic maps were geometrically corrected and projected to ➢ Co-ordinate system: Gauss Conform LO29 ➢ Datum: Cape (Molodensky) ➢ Spheroid: Clarke 1880 (Africa) ➢ Central Scale: 1 ➢ Central Meridian: 29ºE ➢ Origin Latitude: 00ºN ➢ False Easting: 0.00m ➢ False Northing: 0.00m • Used piecewise affine and nearest neighbour algorithms; 5m x 5m pixel resolution.

Stage	Results
5. Georeference the thermal data.	• Import data into relevant software using an SML to ➢ Mirror the strips ➢ Rotate every second strip 180° in flight direction ➢ Remove speckle in null boundary area. • Geometrically corrected and projected to ➢ Co-ordinate system: Gauss Conform LO29 ➢ Datum: Cape (Molodensky) ➢ Spheroid: Clarke 1880 (Africa) ➢ Central Scale: 1 ➢ Central Meridian: 29ºE ➢ Origin Latitude: 00ºN ➢ False Easting: 0.00m ➢ False Northing: 0.00m • Used piecewise affine and nearest neighbour algorithms; 1m x 1m pixel resolution. • New Largo: ➢ 13 strips, each ~13.8 km long, ~860 m wide ➢ ~20% overlap • Tavistock: ➢ 13 strips, each ~10 km long, ~860 m wide ➢ ~20% overlap
6. Create thermal mosaics	• Georeferenced individual strips were edge matched using manual mosaicking to edge match features such as roads and rivers. • Once the strips were in place, these were then globally georeferenced and warped using piecewise affine. • Mosaic layouts were created and run. • New Largo **absolute georeferencing accuracy:** Pixels of the final mosaic are within 30m of their position according to the reference data while a few pixels are within 50m. • Tavistock **absolute georeferencing accuracy**: Pixels of the final mosaic are within 30m to 50m of their position according to the reference data while a few pixels are within 80m. Accuracy here is not as good as New Largo because a lot of development has taken place since the preparation of the topographic maps, making it difficult to find ground control points.
7. Overview image processing of the thermal georeferenced data.	• Thermal data was processed; contrast stretches, colour tables and edge enhancement filters were applied. • Grayscale prints (1:25000) and printfiles prepared. Delivered ref.: 15/173/713/01/115. • Interim report, ref.: 15/173/713/02/11.

3. PRELIMINARY INTERPRETATION

3.1 Introduction

Temperature calibration as well as an interpretation has been carried out over selected subsets of areas of interest:

- New Largo: site around the colliery
- Tavistock: sites around Arthur Taylor
- Kromdraai: in vicinity of microgravity test site

The co-ordinates of each subset are listed below in *Table 3.1*.

Table 3.1. Geographic extents of the selected subsets.

SURVEY	New Largo		Tavistock		Kromdraai	
Corner	**Northing**	**Easting**	**Northing**	**Easting**	**Northing**	**Easting**
Upper Left	-2871759.7N	-4000.5E	-2885999.5N	19799.6E	-2848299.5N	9299.5E
Upper Right	-2871759.7N	-3000.5E	-2885999.5N	20699.6E	-2848299.5N	10099.5E
Lower Right	-2873110.7N	-3000.5E	-2886700.5N	20699.6E	-2849100.5N	10099.5E
Lower Left	-2873110.7N	-4000.5E	-2886700.5N	19799.6E	-2849100.5N	9299.5E
SURVEY	**New Largo**	**Ash Dump**				
Corner	**Northing**	**Easting**				
Upper Left	-2870964.7	-2805.5				
Upper Right	-2870964.7	-1244.5				
Lower Right	-2871846.7	-1244.5				
Lower Left	-281846.7	-2805.5				

3.2 Detection and mapping of Selected Features

The New Largo site covers old workings and dumps (*Figure 3.2a & Figure 3.2d*). The Tavistock site coincides with both water filled and dry older bord and pillar workings, several dumps and active workings (*Figure 3.2b*). Kromdraai (*Figure 3.2c*) coincides with an area of old workings, which has been analysed using other geophysical techniques such as microgravity. Different thermal response would be expected to characterise these sub-surface areas.

On thermal infrared images, the brightest tones represent the warmest radiant temperatures, and the darkest tones represent the coolest ones. Materials that display cooler thermal responses have a low thermal conductivity, thermal inertia and thermal capacity. In contrast, materials that display warmer thermal responses have a high thermal conductivity, thermal inertia and thermal capacity. Water bodies have a cooler surface temperature than soils and rocks during day. At night, though, the relative surface temperatures are reversed, so that surface water is warmer than soils and rocks. Brighter tones are also associated with vegetation due to the insulating effect of the foliage as well as its' higher water content. When related to soil moisture, the cool anomalies in black to gray tones, develop as a result of evaporative cooling. Man-made features though, can also have warm and/or cool thermal responses which can confuse the interpretation.

Some of the warm (light tones) and cool (dark tones) thermal responses across the areas of interest are associated with lineament features. Such features are often indicative of lithology and/or of areas of structural concern. Additionally though, lineament features can be associated with man-made structures.

The interpretation of the selected subsets involved detailed image processing using a combination of colour tables with different image enhancement techniques. The thermal imagery was used together with topographic map data. The two datasets are complementary; topographic data provided surface information while thermal data provided near-surface and sub-surface information. The integration of these data contributed to the recognition and delineation of problem areas.

3.2.1 Workings

Possible bord and pillar workings have been demarcated in Tavistock, *Figure 3.2b* and in Kromdraai, *Figure 3.2c*. The thermal response associated with dry bord and pillar workings is warm, in light gray tones. This contrasts to the cool thermal response associated with water-filled bord and pillar workings, where the tones are dark gray to black.

3.2.2 Sinkholes

Probable as well as possible sinkholes, which trend north-east and range in diameter from 11m to 145m, have been identified in New Largo, *Figure 3.2a.* This north-east alignment of warm thermal anomalies appears to be structurally controlled. A sinkhole has also been interpreted in Tavistock, *Figure 3.2b.*

3.2.3 Fires

Surface and subsurface fires have been identified in the selected subsets. A surface fire, with a hot thermal response, has been identified in New Largo, *Figure 3.2a.* Further, a number of underground fires have been identified in Kromdraai, *Figure 3.2c*. These underground fires trend north-east, possibly following existing underground infrastructure or else, structural control. These fires have warm thermal signatures in gray to bright tones which range in diameter from diameter from 4.5m to 35m.

3.2.4 Acid Mine Drainage Pollution Plumes

The thermal infrared images over New Largo and Tavistock do not reveal any obvious acid mine drainage pollution plumes associated with slimes dams and waste rock dumps. Pollution seepages are generally characterised by warm thermal signatures and associated with subsurface water flowing away from slimes dams and waste rock dumps into plumes. Although there is no obvious acid mine drainage pollution plumes in the subset over the New Largo subset over the Wilge ash dump, the ponding of water could be problematic (*Figure 3.2d*). Near- and subsurface moisture and/or water appears to be ponding (dark to black tones) although largely contained within the area of the dump. This water could mobilise any existing sulphides from within the dump into the surrounding fields where it could contaminate the land by forming acid mine drainage during the chemical breakdown of sulphides. Usually, both surface and sub-surface lineament features and water saturated soils can be recognised. These can be significant as polluted water will migrate along zones of weakness and the delineation of lineaments and detailed structure can be used to monitor the movement of groundwater. Brighter tones are also associated with surface water and vegetation, which can complicate the interpretation of acid mine drainage.

3.2.5 Water

Near- and subsurface moisture and/or water can be seen to be ponding in the New Largo subsets, *Figures 3.2a and 3.2d* and in the Tavistock data, *Figure 3.2b*. Such moisture is characterised by cool thermal responses from dark gray to black tones. In contrast, surface moisture and/or water, also demarcated in these figures, is characterised by bright thermal signatures.

3.2.6 Man-made Features

Linear structures can be associated with man-made structures, e.g. underground piping and tunnels. Examples of such man-made features would be the possible inclined shaft, the trench as well as the fence line in New Largo, *Figure 3.2a* and the infrastructure in Tavistock, *Figure 3.2b.*

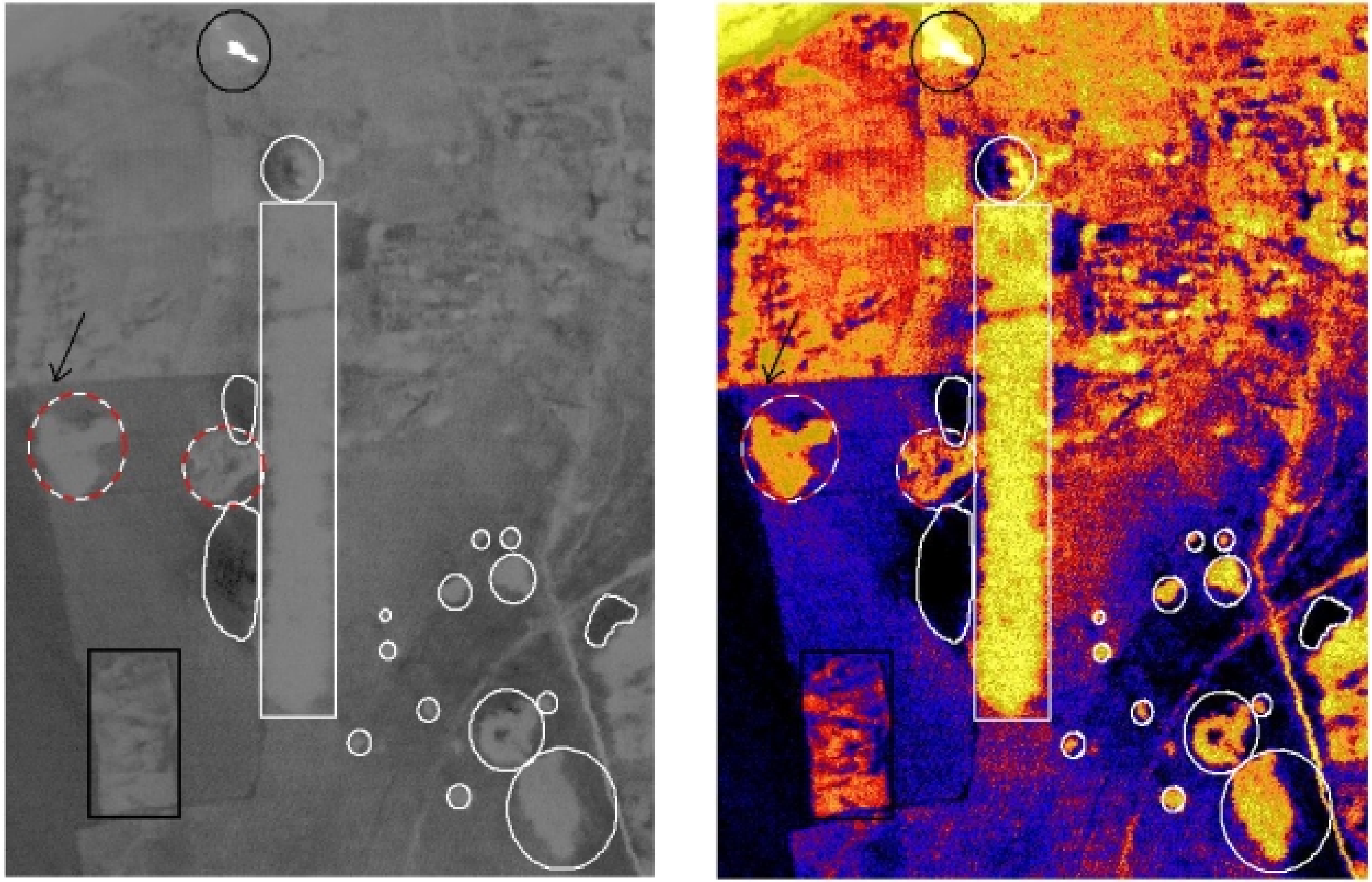

Figure 3.2a. New Largo subset.

The white circles outline sites of probable sinkholes, which trend north-east and range in diameter from 11m to 145m. Possible sinkholes are outlined in red and white circles. A black circle outlines a surficial fire. Man-made features are outlined in rectangles, white possibly an inclined shaft; black a trench or excavation site. White polygons demarcate areas where water appears to be ponding in the subsurface. Arrow points to a surface fence line. Image is 998m wide by 1346m long.

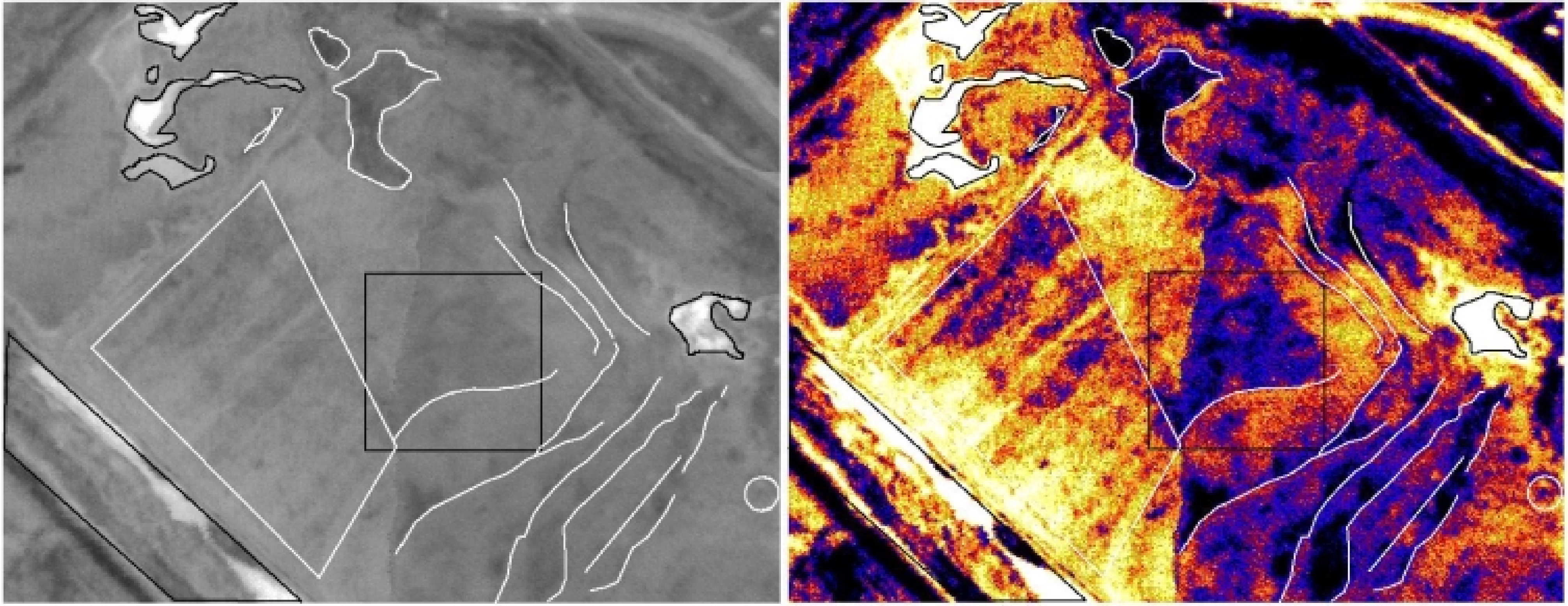

Figure 3.2b. Tavistock subset.

Man-made features are prominent in this image, outlined in black to the left, a trench with surficial water on the northern limb indicated in gray to white tones; with infrastructure in the top right of the image. NE-SW trending lineaments, in white, map probably the subsurface mine infrastructure although geological control is also suggested. The white rectangle demarcates an area of possible dry bord and pillar workings while the black square outlines one example of wet bord and pillar workings here. White polygons demarcate areas where water appears to be ponding while black polygons outline surface water, probably dams. The white circle outlines a site of a probable sinkhole. The obvious line down the center of the image is where two acquisition strips merge. Image is 898m wide by 696m long.

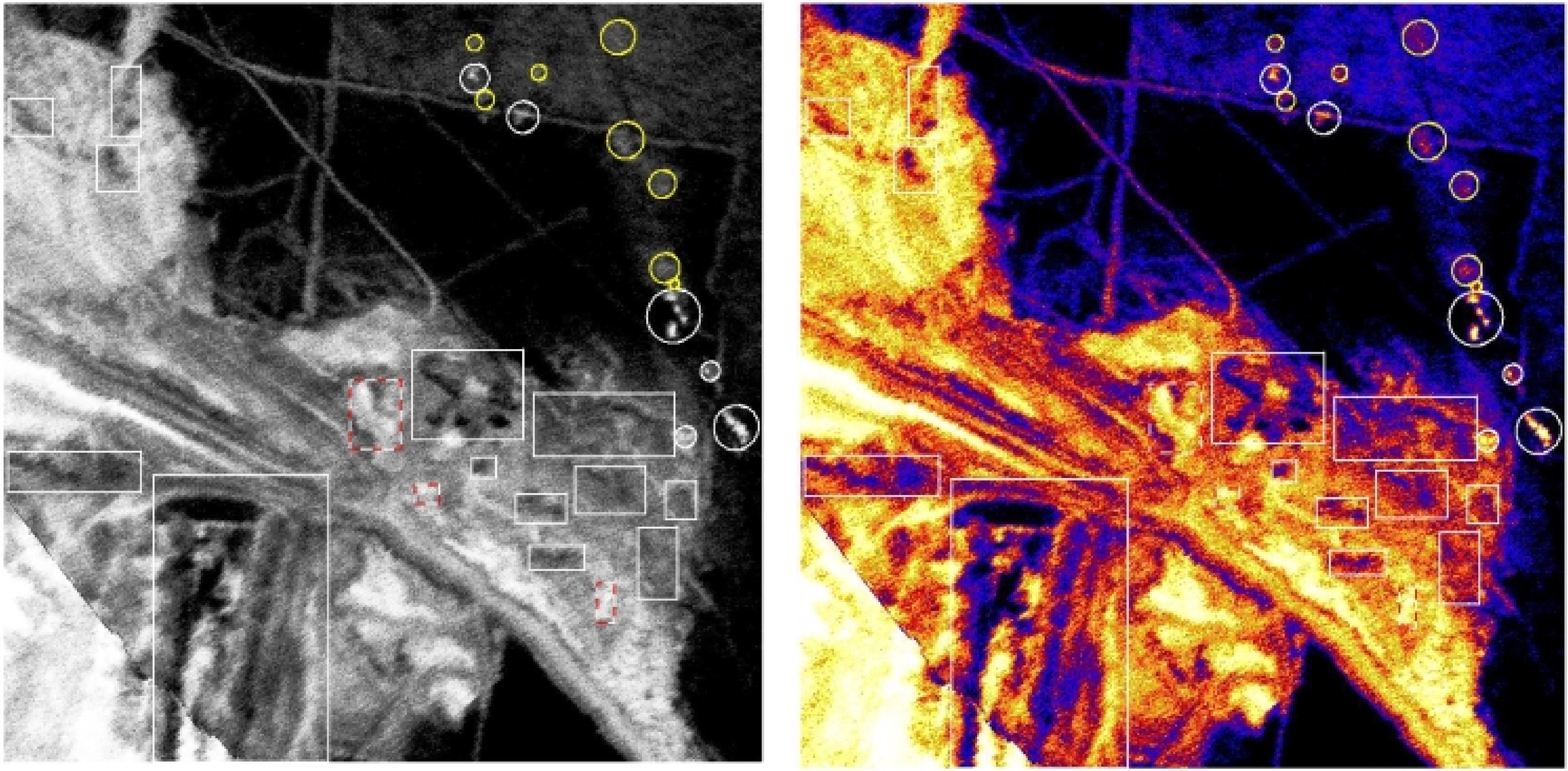

Figure 3.2c. Kromdraai subset.

The white circles outline sites of probable underground fires, trending north-east. These probable fire signatures range in diameter from 4.5m to 35m. Possible underground fires are outlined in yellow. Bord and pillar structures are outlined in rectangles, white possibly water-filled; red and white probably dry. The obvious line down the lower left of the image is where two acquisition strips merge. Image is 796m wide by 799m long.

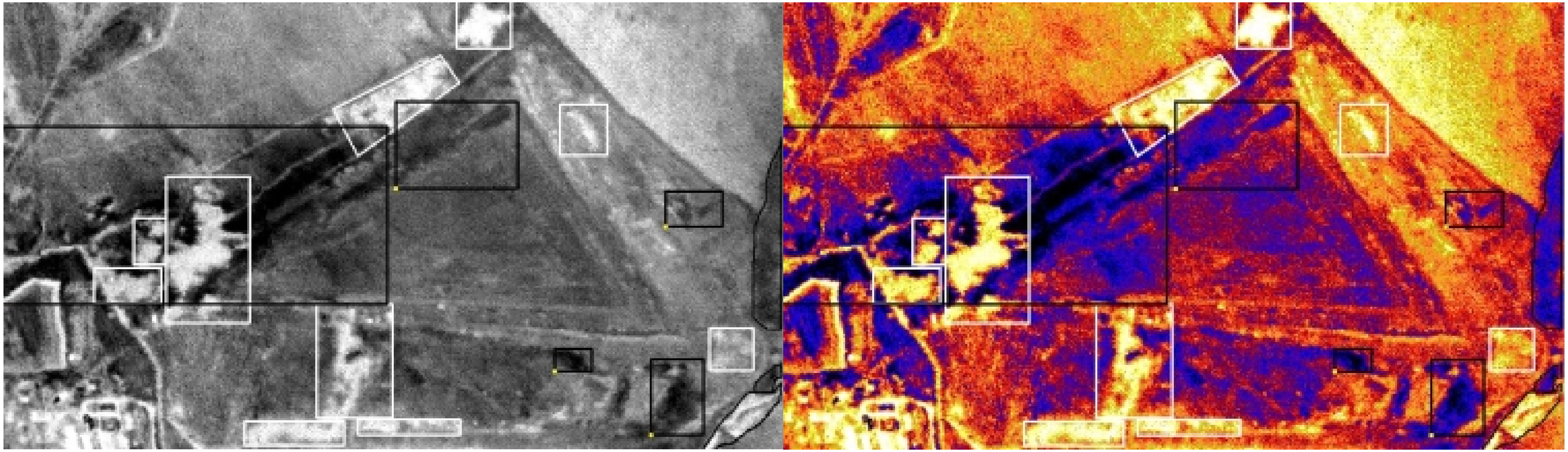

Figure 3.2d. New Largo: Wilge Ash Dump subset.

There is no clear evidence of acid mine drainage occurring at present in this image. Acid mine drainage would have a warm signature due to the chemical breakdown of sulphides. Although the black rectangles demarcate areas of near- and subsurface moisture and/or water, these appear largely contained within the area of the slimes dam. The white rectangles delineates sites of probable tree vegetation and not acid mine drainage. A stream or river with both surficial and subsurface water is outlined in black polygons to the lower right. The obvious line down the upper right of the image denotes a farm boundary. Image is 900m wide by 1500m long.

4. COMMENTS AND RECOMMENDATIONS

The principal objective of this report is to report on the effectiveness of using night-time airborne thermal data to assist in the management, monitoring and/or rehabilitation of the identified problem scenarios. These include the detection and mapping of the aerial distribution of bord and pillars of old mine workings, sinkholes, underground fires and acid mine drainage in the imagery which was acquired for this Coaltech2020 project Task 1.3.1b.

A series of comments follows.

- The data acquisition, using the Tallytherm Airborne Thermal Scanner from Infoterra in UK and an aircraft from FUGRO in South Africa, was completed to specifications in July 2001.

- Data preparation, including quality control, roll correction, geometric correction, overview image processing and printing, as well as data subsetting was completed to specification.

- The preliminary interpretation of the airborne thermal data subsets has yielded much information (see Section 3).

  - It has been possible to detect and map selected features, namely, the presence of old workings, sinkholes and fires in the New Largo, Tavistock and Kromdraai imagery.

  - The presence of acid mine drainage could not be conclusively established on the selected subsets from this imagery although the ponding of water within an ash dump at New Largo has been identified as a potential problem. This water could mobilise both fines and any existing sulphides from within the dump into the surrounding fields. This could lead to the contamination of the land by forming acid mine drainage during the chemical breakdown of sulphides. The absence of clearly identifiable acid mine drainage on these subsets can be interpreted as a positive result, indicating currently effective control measures.

  - Near- and subsurface moisture and/or water and infrastructure was readily identified from these datasets. Vegetation was also readily outlined.

- The 1m x 1m pixel resolution of the airborne thermal data was sufficient to identify the relevant features although sub-meter pixel resolution would provide more detail, particularly for old workings.

Recommendations follow.

- The interpretation of this thermal data is preliminary and only 1:50 000 topographic map data has been evaluated simultaneously. A detailed interpretation can extract more information from this data through the integration of other datasets. This can lead to a refinement of the processing techniques, colour tables used and ultimately, the interpretation.

- Field verification is required to establish the veracity of this preliminary interpretation. In addition, it will enable an assessment of overall feature mapping accuracy. The stated overall aim for mapping of bord and pillar old workings is to try and map these with an accuracy of 1-2 metres. These features typically occur between surface and about 25-30 m below surface, but in some cases old workings may, for example, be located between 30 and 60 m (*Van Schoor, 2000).*

- Any airborne thermal data collected in the future, can be used with this data in change detection studies.

- This data should be integrated into management plans for monitoring and/or rehabilitation of these areas.

5. REFERENCES

Franzsen, A.J. 2000. The application of airborne thermal imagery to the coal environment. Coaltech 2020 Report Number 2001-0119, 10pp.

Van Schoor, M. 2000. Detection of old workings, sinkholes, underground fires and acid mine pollution using geophysics and airborne thermal infrared imagery. Task 1.3.1b Subtask 2&3, Internal Coaltech 2020 Report, 17pp.

APPENDIX III

COALTECH 2020

Report on a TDEM survey at the Arthur Taylor Colliery

V. Hallbauer-Zadarozhnaya

Terra Sounding and Analytical (Pty) Ltd

CSIR, Division of Mining Technology
Report number: 2001-0649

Task 1.3.1b

Detection of old workings, sinkholes, underground fires and acid mine pollution using geophysics and airborne thermal infrared imagery

5 December 2001

TABLE OF CONTENTS

LIST OF FIGURES AND TABLES

1 INTRODUCTION

The field investigation had been invited by CSIR, Miningtek with an aim to study the possibility of detecting, from surface, the underlying, hidden boundary between the virgin coal seam and mined-out areas, using TDEM (time-domain electromagnetic) techniques. The selected survey area contained sections of both the coal seam and mined-out area. The map provided showed the border and helped to compare the geophysical data obtained against actual structures.

On the surface transmitter loops of a size 50x50 m were placed. The receiver loops of 1 m^2 in size were placed at selected positions inside of each transmitter loop. The distance between the receiver loops varied between 5 and 10 m. A plan showing the relative locations of the TDEM stations is given in Figure 1. For recording, an instrument of the type "Zikl-5" was employed.

2 INTERPRETATION OF MEASURED DATA

The full interpretation cycle included the analysis of the *emf* distribution at different times of the transient EM (electromagnetic) field, mathematical modelling and analysis of the apparent longitudinal conductivity in different time domains of the EM field propagation.

3 ANALYSIS OF EMF DISTRIBUTION

During a typical TDEM survey we register the *emf* during a large range of times (channels). The amplitude of the *emf* characterizes the electrical properties of each layer. As the EM field propagates into the subsurface media, the maximum of EM intensity also moves to depth. The EM intensity can be regarded as a function of depth and resistivity. It is therefore important to determine the time when the EM field propagates in coal. For a calculation of the depth of the EM field propagation we use the following formula:

$$H = \sqrt{\frac{t \cdot \rho}{2}} \qquad (1)$$

where,
t – time [microseconds],
ρ – resistivity [Ωm],
H – depth [m].

For a calculation of ρ Gummel's formula can be used:

$$\rho = \frac{H}{S}, \qquad (2)$$

where,

S – the sum of the conductivity of media contained in *i* layers with a total thickness of H or total longitudinal conductance.

Consequently,

$$S = \sum_{i}^{n} S_i , \qquad (3)$$

In the next part of this report the parameters of a cross-section will be obtained by mathematical modelling of TDEM. Here we calculate the total longitudinal conductance for the upper part of the cross-section, above the coal layer.

Type of layers	Resistivity, ρ [Ωm]	Thickness [m]	Conductivity [S]
1. Soil	8.0	1.4	0.175
2. Clay	40.0	4.0	0.1
3. Sandstone	1000	23	0.023

Table 1: Parameters for an average cross-section above a coal seam.

The total longitudinal conductance is 0.298 S. Using formula (2) the average resistivity for this part of the cross-section, up to the depth of 28.4 m, is 95.3 Ωm. Using formula (1) we can calculate the time of EM field penetration in the coal layer as

$$t = \frac{2H^2}{\rho} = \frac{2 \cdot 28.4 \cdot 28.4}{95.3} = 16.9\,\mu s \qquad (4)$$

Figures 2 to 8 show the contoured distribution of *emf* for the study area at times10.5, 12.5, 14.5, 18.0, 22.0, 26.0 and 30.0 µs. These indicate the edge between fresh coal and mined-out area to occur at the times 10.5, 12.5, 14.5 µs. It is, however, best seen at the time of 18 µs, close to the value determined above. A comparison of the results received by the TDEM survey and geological data supplied (see Figure 1) show good agreement. During later times of penetration (times 22, 26.0 and 30 µs) the EM field was concentrated in the low-conductivity areas – in the eastern part of the plot.

4 MATHEMATICAL MODELLING

Looking at Figures 6 - 8 the different intensities of *emf*, which characterize the same layer of coal, can be seen. Additionally to the results, described above, a study of the resistivity of the coal layer in the different parts of that area is presented. In this case mathematical modelling was done using the program ERA (Epov et al., 1990).

Figures 9 -14 show the parameters of cross-section for the TDEM stations № 11, 25, 59, 86, 133 and 159. All stations show the first layer having a thickness of 1.05-1.55 m. This is soil with a resistivity of 8 Ωm. The second layer, a clay with thickness of approximately 4 m (on the station 86 it was 6 m), had a resistivity of 40 Ωm. For the third layer – sandstone – a very high resistivity of about 1000 Ωm was obtained. The coal layer (the fourth layer) gave different resistivities for different parts of the area. Station 11, placed in the fresh coal area, showed a high resistivity for that layer, practically undistinguishable from the layer of upper sandstone. Stations 25 and 159 had been placed close to the boundary edge (in the mined-out area). The resistivity of the remaining layer there showed a value of 90 Ωm. This indicates the presence of water in those parts of the area. At station 133, placed in the south of the area, a resistivity of 65 Ωm was obtained for the coal-bearing layer. As this is low, in a position close to the border, we can assume an increase in the volume of water in that area.
More important is the northern (upper) part of the plot for this area. Here, the resistivity of coal-bearing strata decreases to 26 Ωm (TDEM 59) and 23 Ωm (TDEM 86), respectively. This could be interpreted as an occurrence of acidic water. Note, that the resistivity of fresh drinking water is approximately 20 Ωm. Here, within a water-bearing layer, oxidation of pyrite could have caused an increase in acidity and decrease in resistivity.

5 DISTRIBUTION OF APPARENT LONGITUDINAL CONDUCTIVITY

The S_T – version (Sidorov & Tikshaev, 1967) is a widespread type of transformation used in Russia for TDEM data. The S_T – version represents the TDEM data as the apparent longitudinal conductivity, equivalent to a plane with conductivity S at a given moment of time. The rise of the apparent longitudinal conductivity generally corresponds to low resistivity horizons. This algorithm uses the first derivative of *emf* and is very sensitive to changes in the geo-electrical parameters of the cross-section. Figures 15 - 18 show the distribution of S_T at the times 14.5, 18.0, 22.0 and 26.0. Figure 16 thus shows best the conductivity distribution in the coal-bearing strata. Also, Figures 16 - 18 show the most conductive part of the coal layer to be situated in the east of the study area. The coal-bearing layer is thus characterized by changes in conductivity for which no immediate explanation can be given without further geological information.

6 CONCLUSION

The aim of this preliminary investigation has been to apply TDEM to detect the boundary between virgin coal and mined-out areas in a shallow coal mine. The results show that the boundary between the fresh coal and mined out areas can be successfully distinguished using a TDEM survey.

Further mathematical modelling of the TDEM data showed that the resistivity of the coal-bearing strata is different in the both parts of that area - very high for fresh coal (~ 1000 Ωm) and decreases in the mined-out area to about 23-90 Ωm. This allows the use of TDEM to study the inhomogeneity of coal from a geo-electrical point of view.

Finally, the distribution of apparent longitudinal conductivity also indicates the inhomogeneity of the coal-bearing layer with the more conductive eastern part perhaps containing acidic water.

7 REFERENCES

Epov, M.I., Dashevsky, Yu.A and Eltsov I.N., 1990. Automatic interpretation of electromagnetic sounding. Novosibirsk, Institute of Geology and Geophysics, Sibirian Branch of Academy of Science of USSR, No3 (in Russian)

Sidorov, V.A. and Tikshaev V.V., 1967. Interpretation of TDEM curves. Razvedochnaya Geofizika, V.42 (in Russian)

APPENDIX A

Modelling of air-filled cavities

Additionally mathematical modelling has been done to investigate the influence of air-filled cavities on a TDEM record. We used TDEM station 86 as example. Here the resistivity of the coal layer, calculated by mathematical modelling, is the lowest (23 Ωm).
However, it is well known that the resistivity of air is very high, thousands of Ωm . We therefore calculated the theoretical TDEM curves using another resistivity for the fourth layer (coal), consequently, 1000, 500, 250, 100, 50 and 35 Ωm and compared it with transformed field data (Figures A1-A6).
Figure A1 shows the comparison of the field curve with mathematical modelling when the resisitivity of fourth layer is 1000 Ωm. That resisitivity can correspond to air or fresh coal. The difference between the theoretical and field curves can be seen.
Figures A2-A6 show the comparison of theoretical data with field data when the resisitivity decreases. Even if the resistivity of the coal layer is 50-35 Ωm, which is very low and corresponds to wet sediments, we cannot obtain the good fit between field data and mathematical modelling. We therefore have to deduce that the coal layer in that area contains a certain amount of water.
Finally, to answer the question whether an air-filled cavity can be distinguished by TDEM: If the wall of the cavity is wet and conducting, the cavity can be detected (indirectly) by its conducting wall.

FIGURES

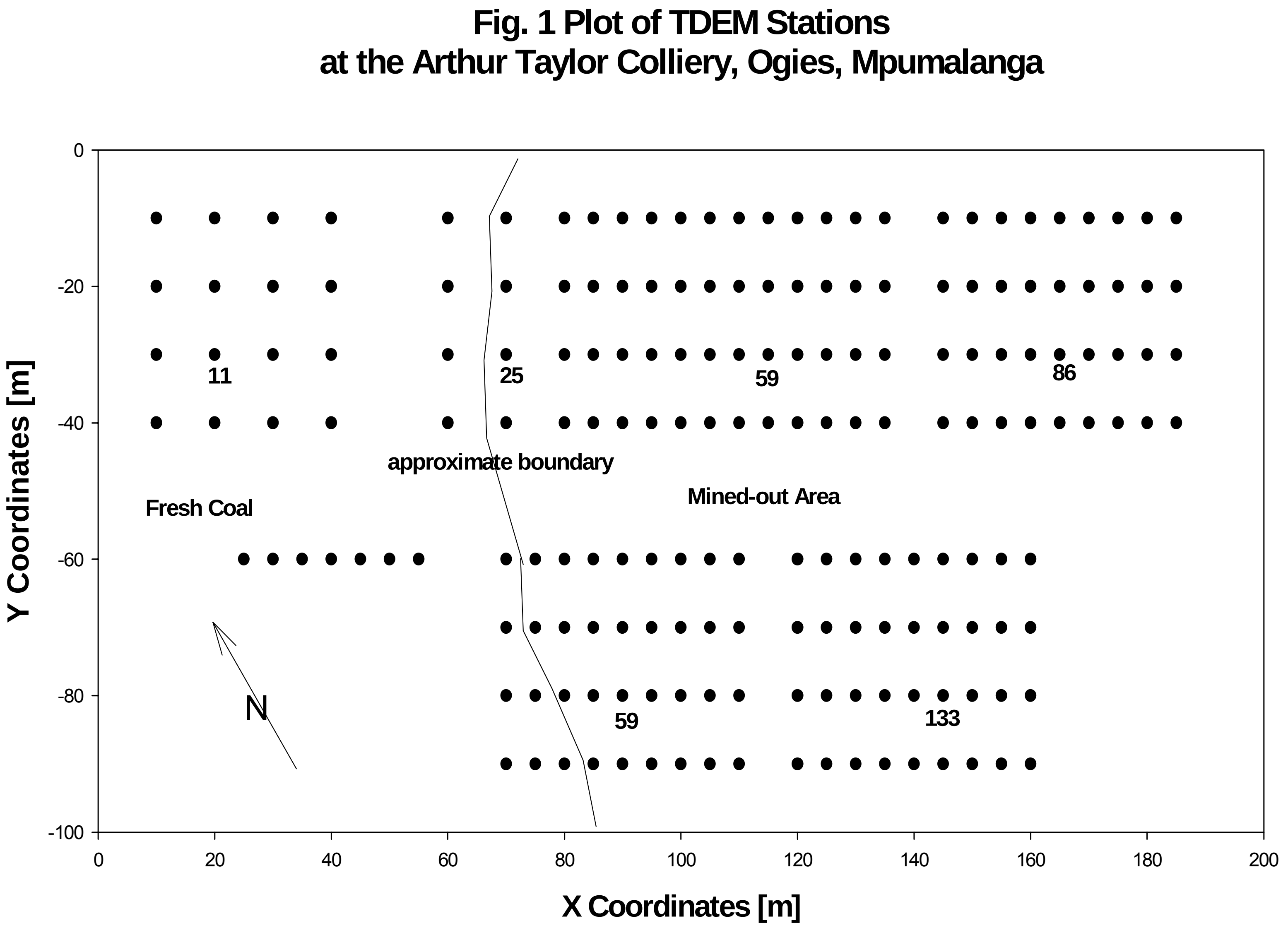

Figure 1: Plot of TDEM stations.

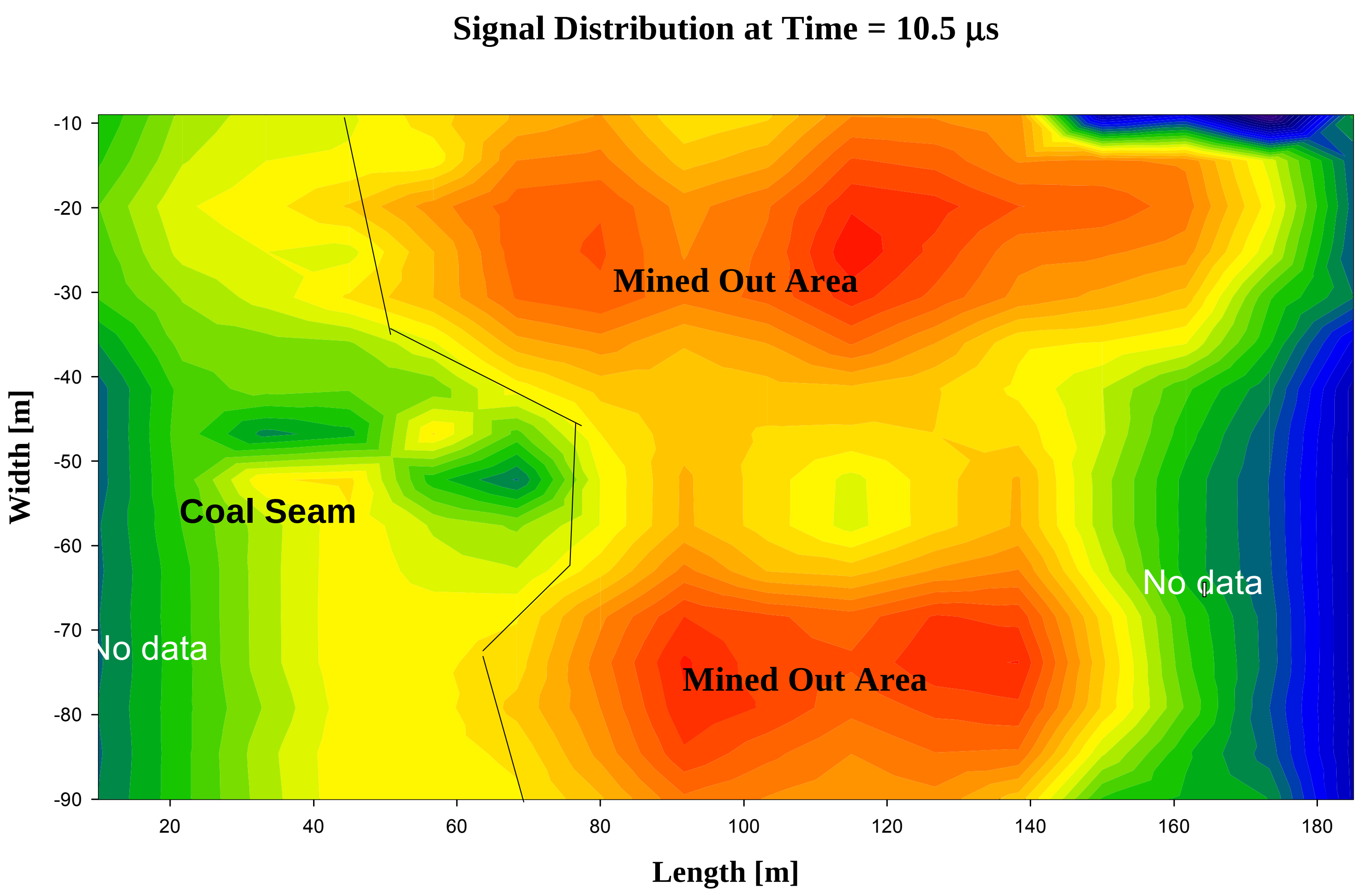

Figure 2: Contour map of the signal distribution at time t=10.5 µs showing the separation of un-mined and mined-out areas (black line) for the area investigated.

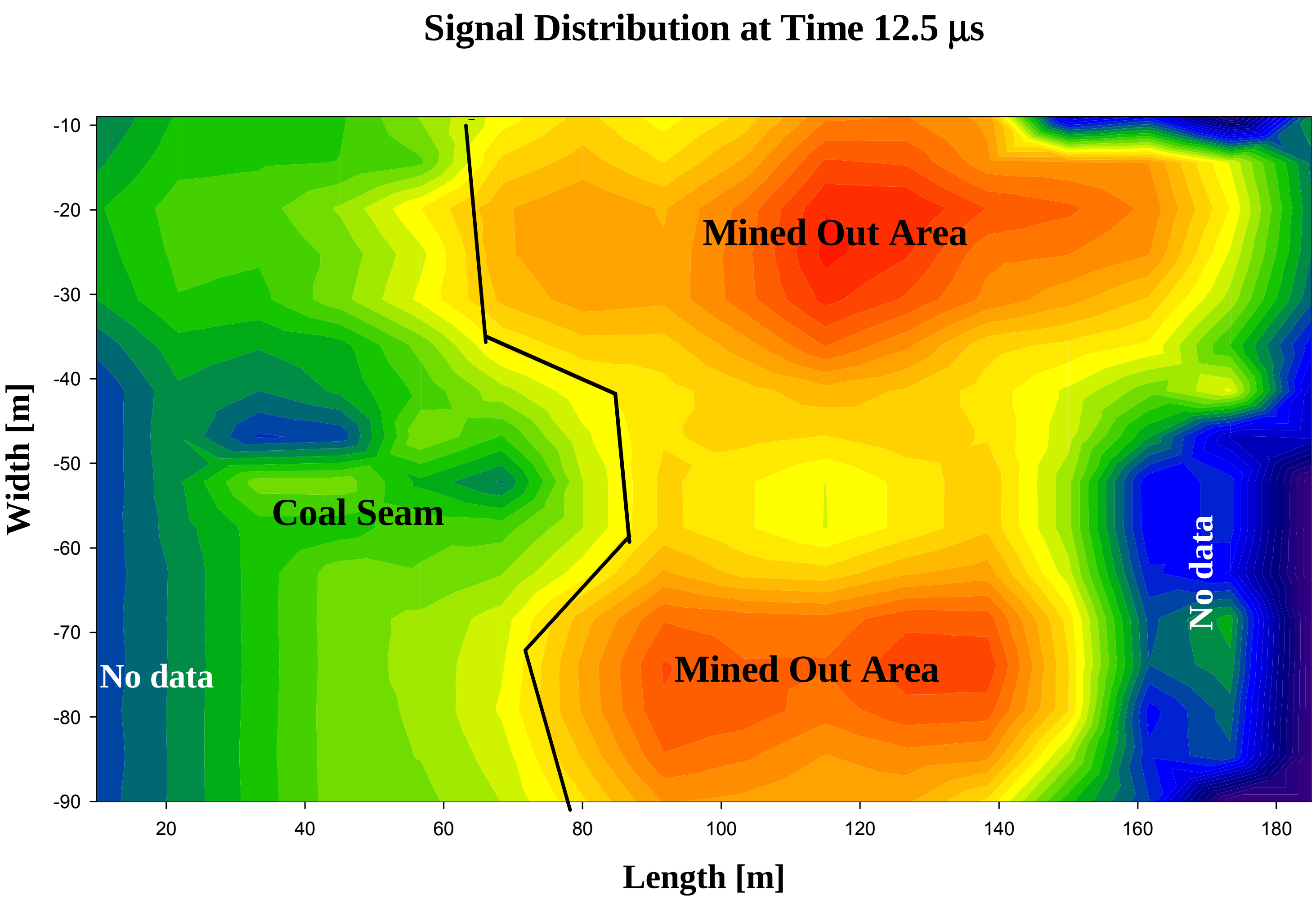

Figure 3: Contour map of the signal distribution at time t=12.5 µs showing the separation of un-mined and mined-out areas (black line) for the area investigated.

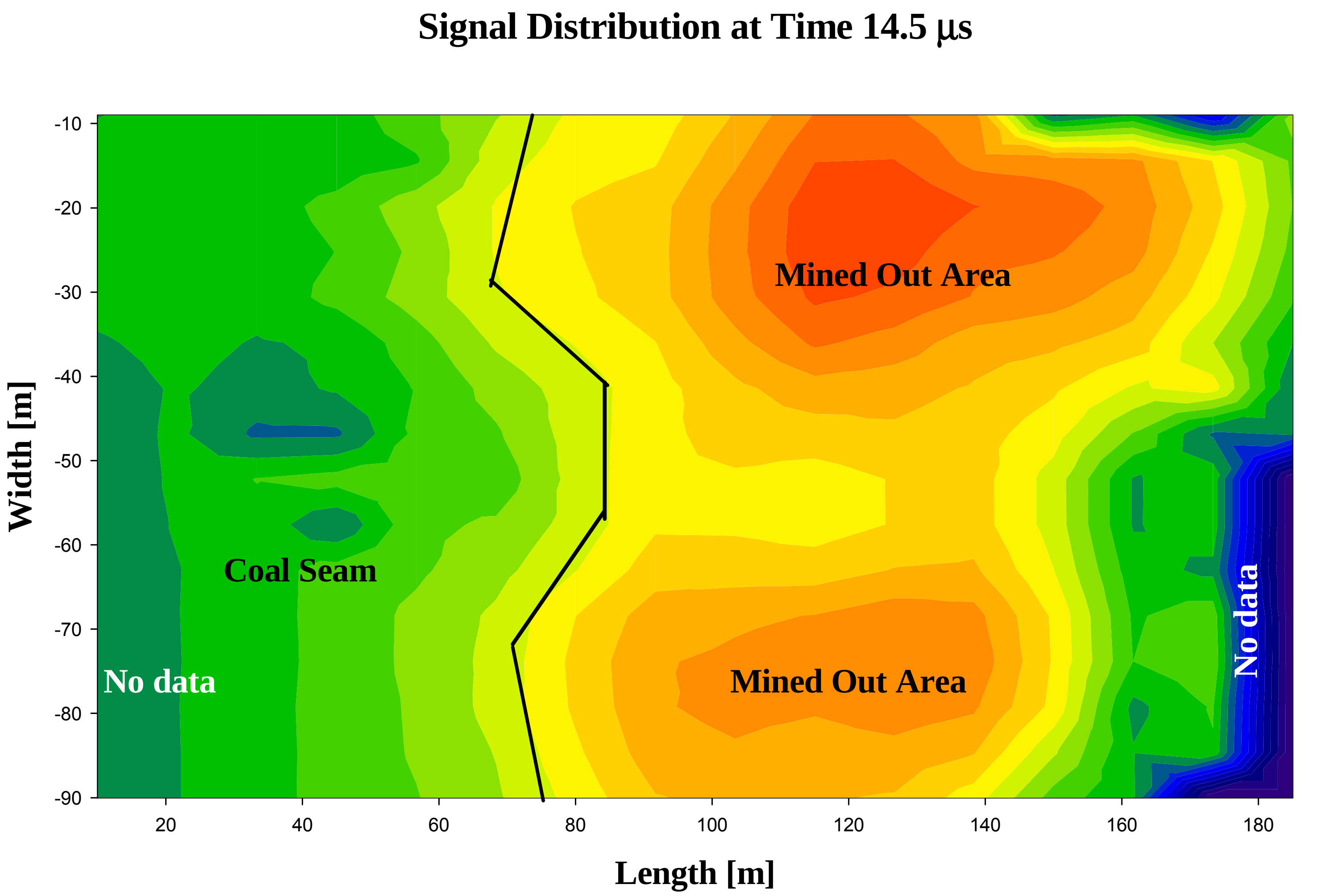

Figure 4: Contour map of the signal distribution at time t=14.5 µs showing the separation of un-mined and mined-out areas (black line) for the area investigated.

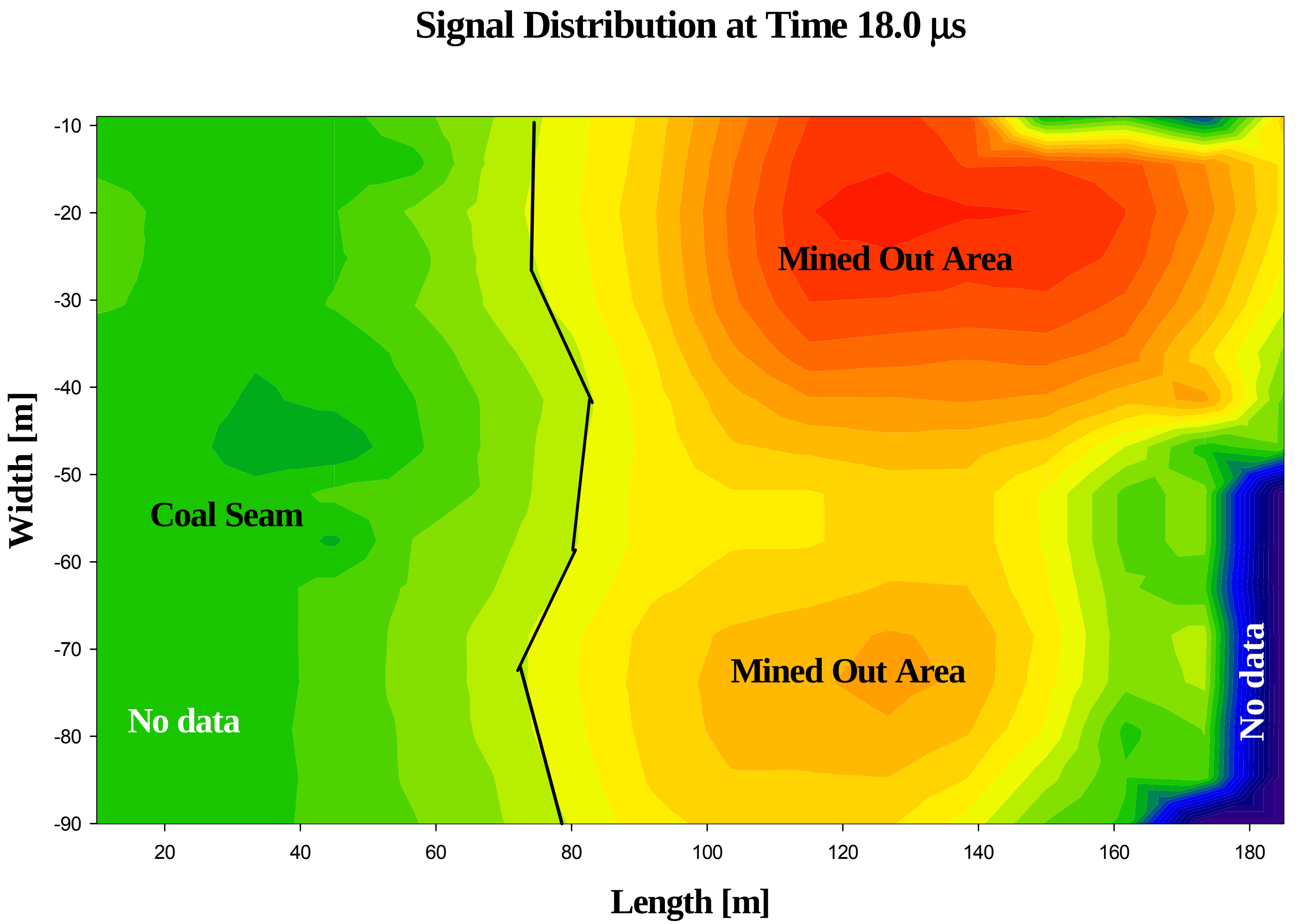

Figure 5: Contour map of the signal distribution at time t=18.0 µs showing the separation of un-mined and mined-out areas (black line) for the area investigated.

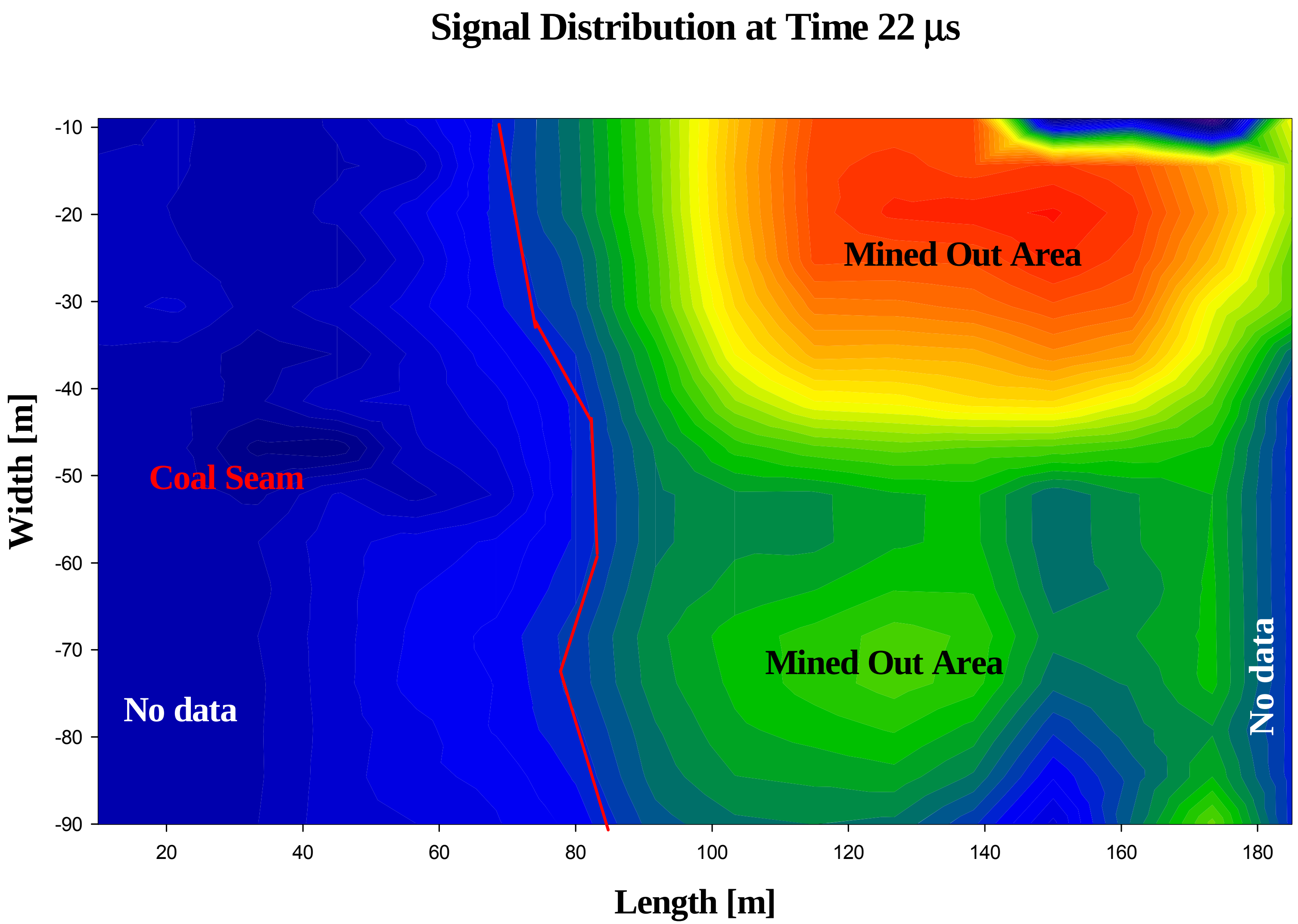

Figure 6: Contour map of the signal distribution at time t=22.0 µs showing the separation of un-mined and mined-out areas (red line) for the area investigated. Because of the low resistivity of the acid water in the mined-out area the electrical field is concentrated in that part of the area.

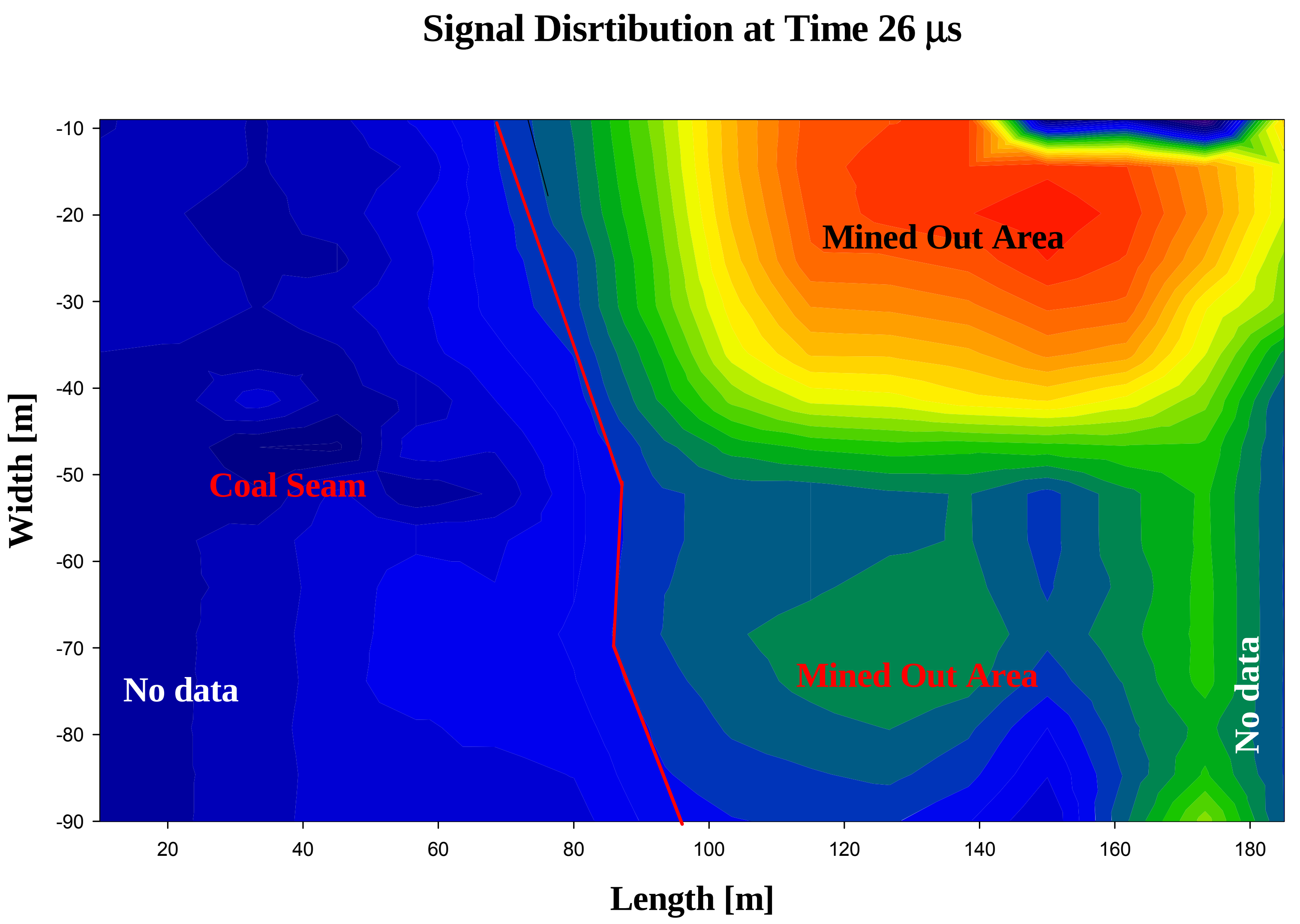

Figure 7: Contour map of the signal distribution at time t=26.0 µs showing the separation of un-mined and mined-out areas (red line) for the area investigated. Because of the low resistivity of the acid water in the mined-out area the electrical field is concentrated in that part of the area.

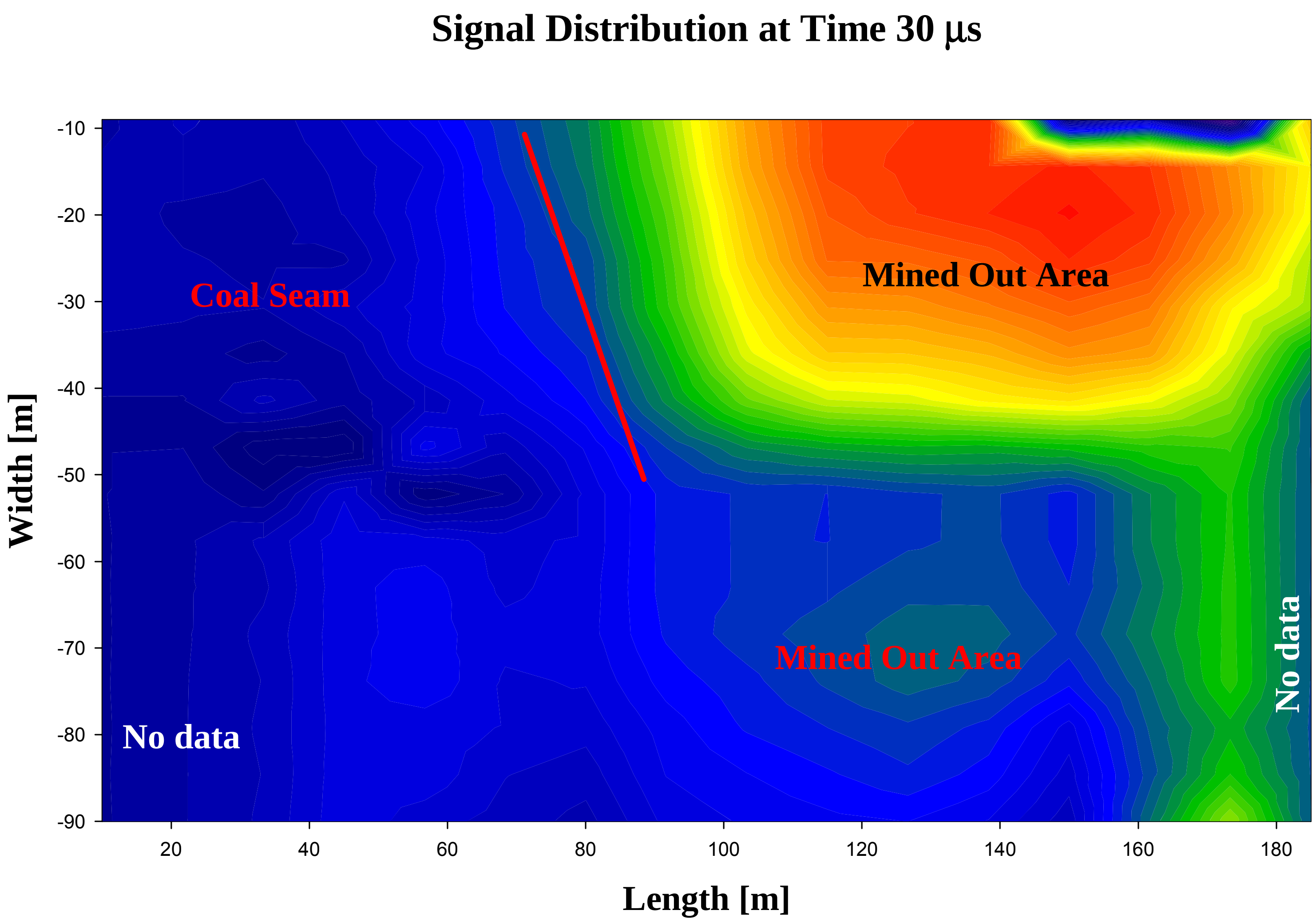

Figure 8: Contour map of the signal distribution at time t=30.0 µs showing the separation of un-mined and mined-out areas (red line) for the area investigated. Because of the low resistivity of the acid water in the mined-out area the electrical field is concentrated in that part of the area.

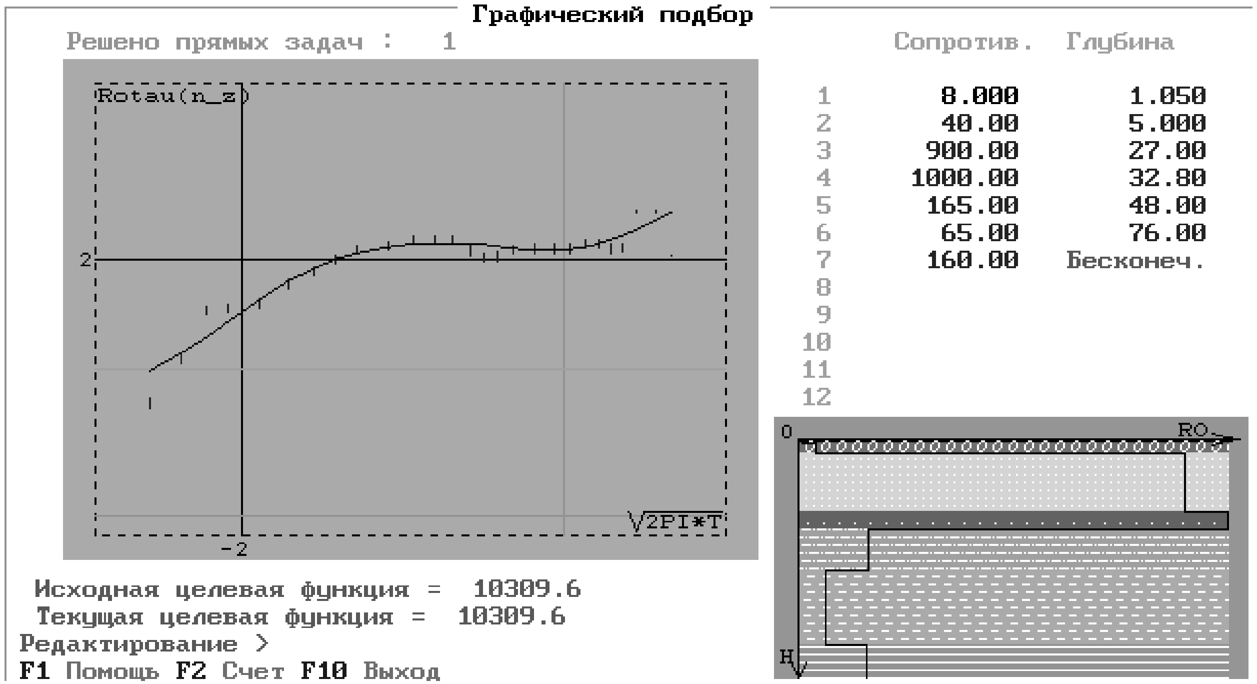

Figure 9: Mathematical modelling of TDEM data (upper left) for station 11. On the upper right hand corner the two columns show depth [m] (right) and resistivity [Ωm]. Below is a schematic diagram of resistivity changes as a function of depth and unspecified lithology. This station was situated within the coal seam area. The resistivity of the coal, according to TDEM data, was found to be approximately 1000 Ωm. The depth of the upper contact was determined at 27.0 m with a thickness of the opening of approximately 5.0 m.

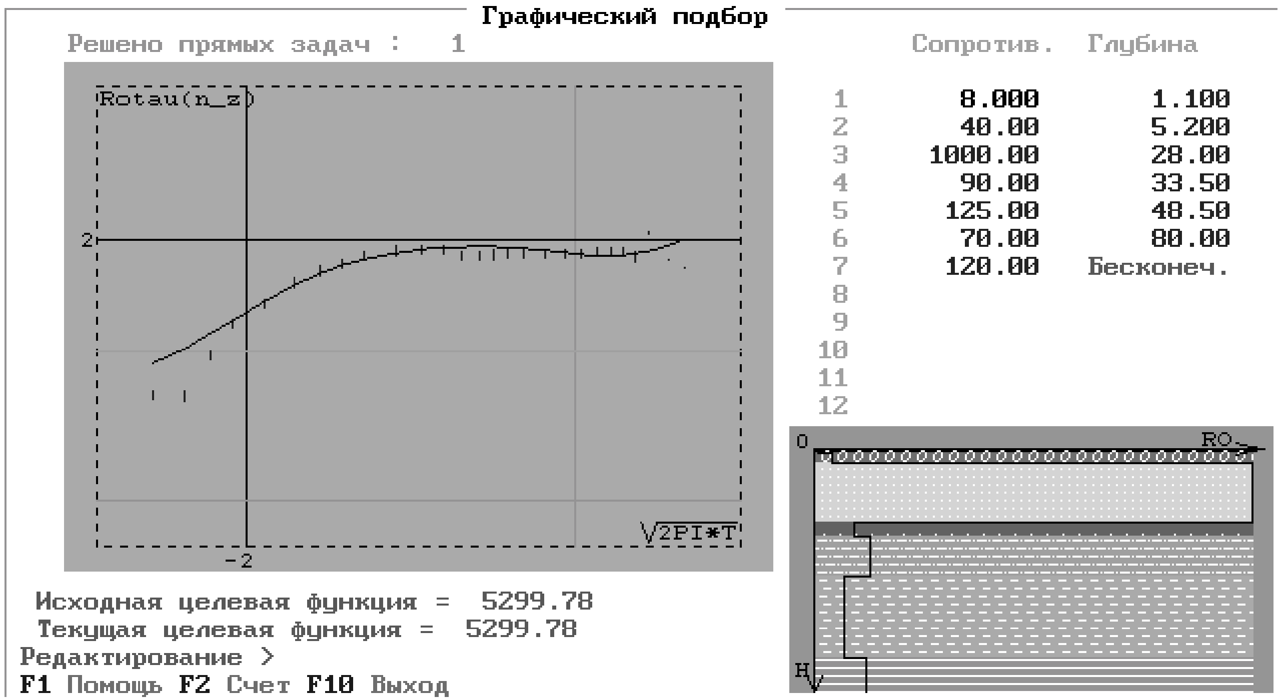

Figure 10: Mathematical modelling of TDEM data (upper left) for station 25. On the upper right hand corner the two columns show depth [m] (right) and resistivity [Ωm]. Below is a schematic diagram of resistivity changes as a function of depth and unspecified lithology. This station was situated on the boundary between mined and un-mined areas. The resistivity of coal, according to TDEM data, was found to be 90 Ωm. The depth of the upper contact of the coal seam was determined at 28 m with a thickness of approximately 5.5 m.

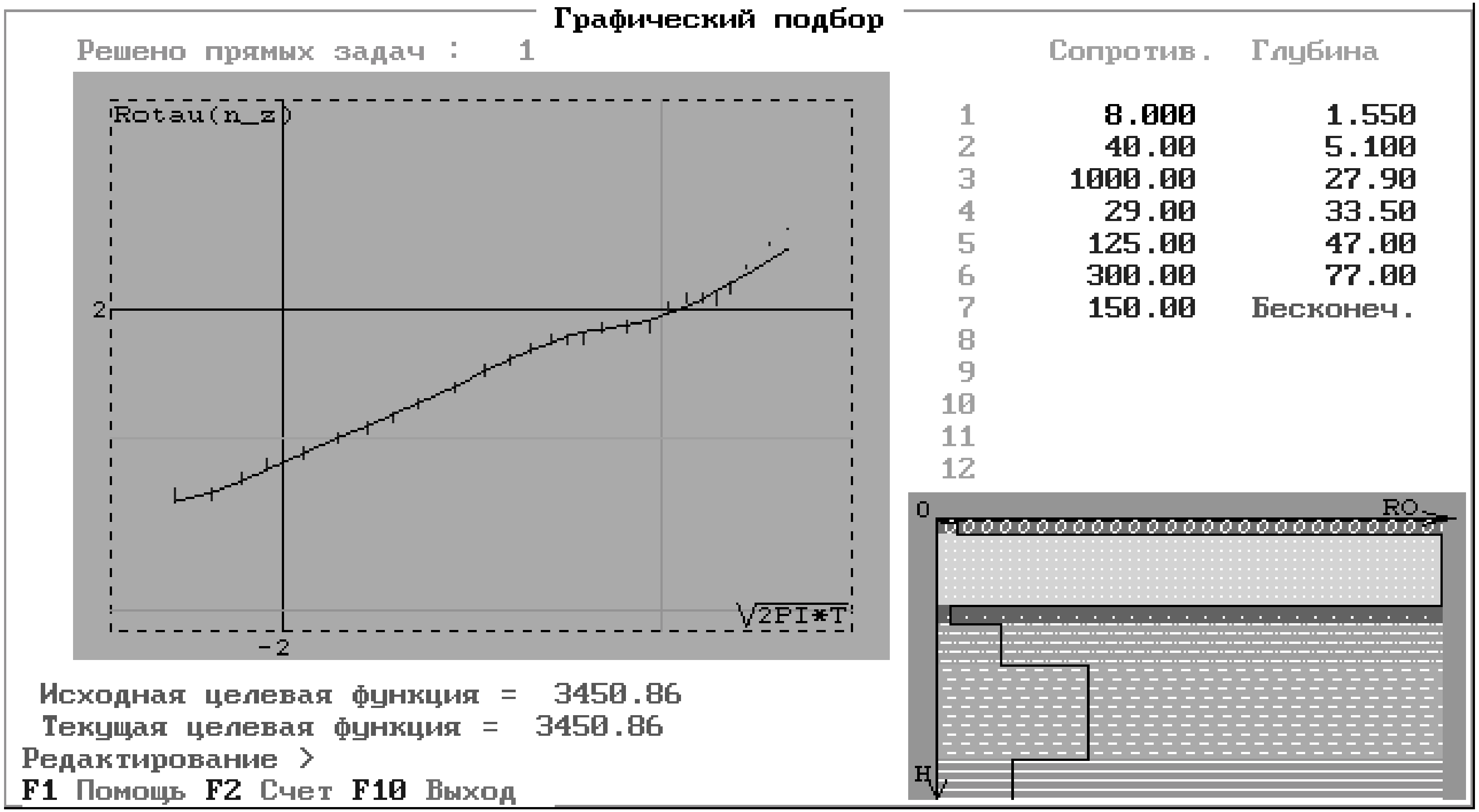

Figure 11: Mathematical modelling of TDEM data (upper left) for station 59. On the upper right hand corner the two columns show depth [m] (right) and resistivity [Ωm]. Below is a schematic diagram of resistivity changes as a function of depth and unspecified lithology. This station was situated within the mined-out area. The resistivity of water-filled area, according to TDEM data, was found to be 29 Ωm. The depth of the upper contact was determined at 27.9 m with a thickness of the opening of approximately 5.6 m.

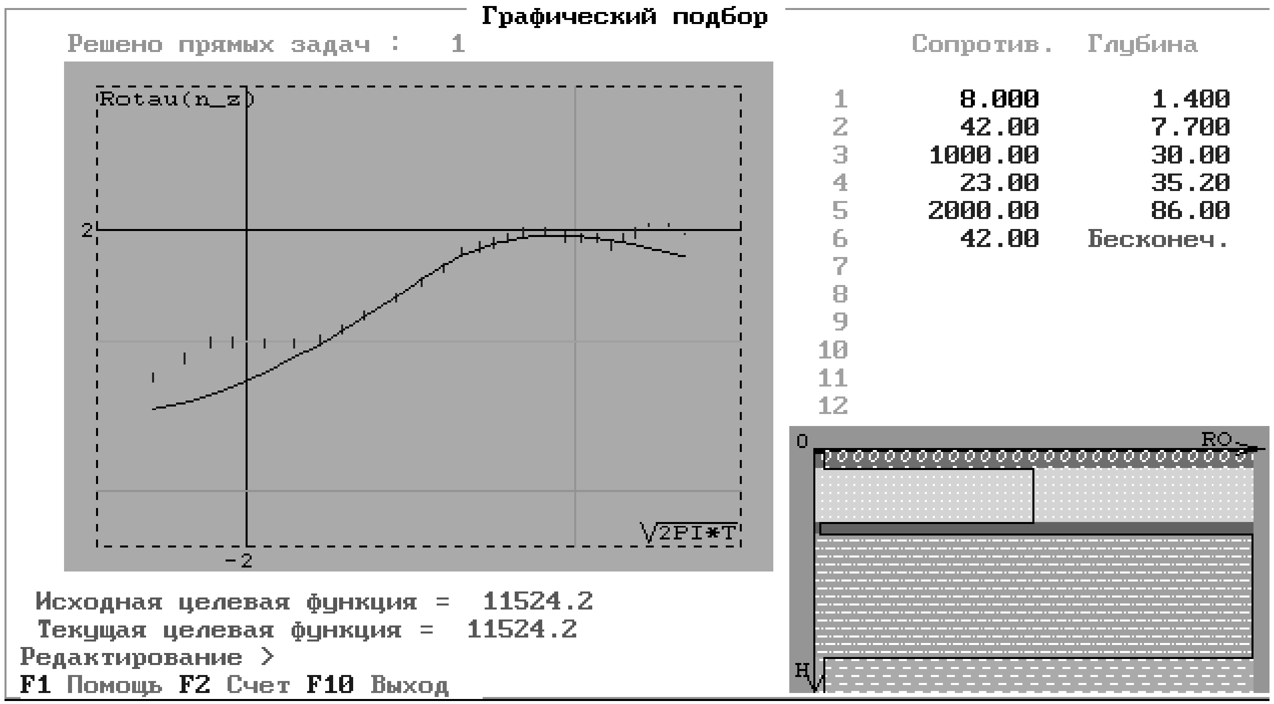

Figure 12: Mathematical modelling of TDEM data (upper left) for station 86. On the upper right hand corner the two columns show depth [m] (right) and resistivity [Ωm]. Below is a schematic diagram of resistivity changes as a function of depth and unspecified lithology. This station was situated within the mined-out area. The resistivity of water-filled area, according to TDEM data, was found to be 23 Ωm. The depth of the upper contact was determined at 30.0 m with a thickness of the opening of approximately 5.2 m.

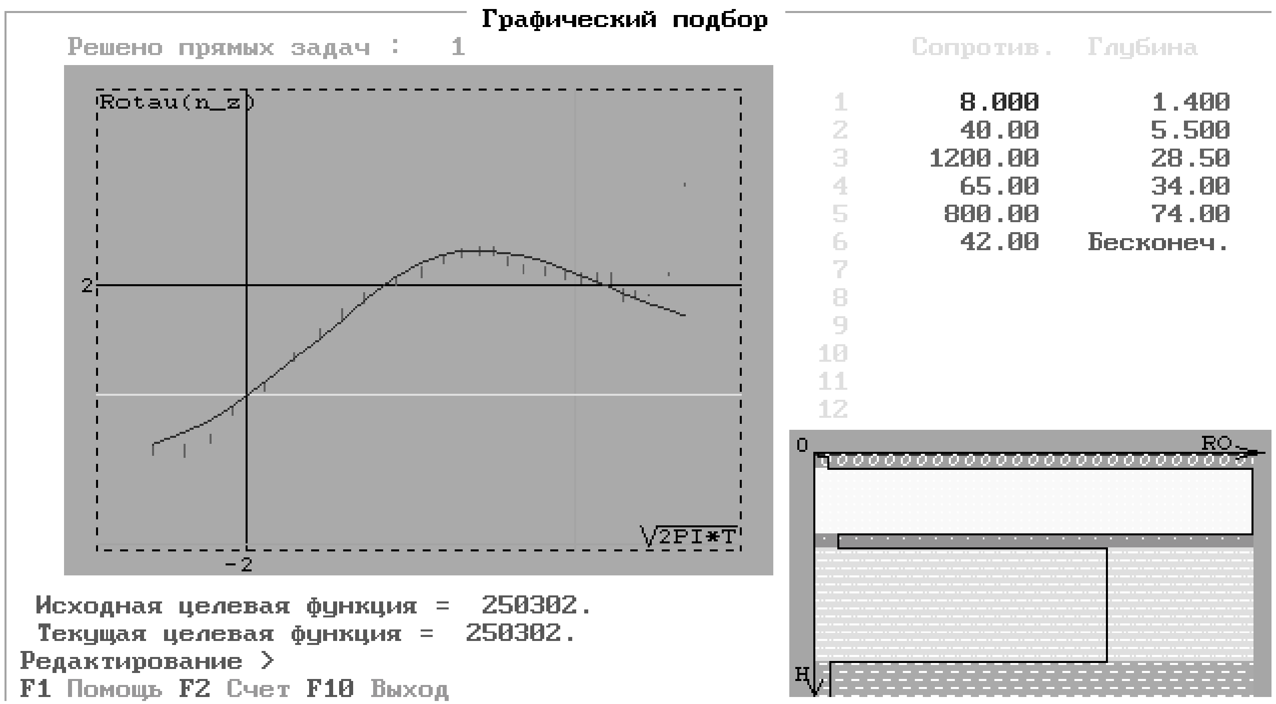

Figure 13: Mathematical modelling of TDEM data (upper left) for station 133. On the upper right hand corner the two columns show depth [m] (right) and resistivity [Ωm]. Below is a schematic diagram of resistivity changes as a function of depth and unspecified lithology. This station was situated within the mined-out area. The resistivity of water-filled area, according to TDEM data, was found to be 65 Ωm. The depth of the upper contact was determined at 28.5 m with a thickness of the opening of approximately 5.5 m.

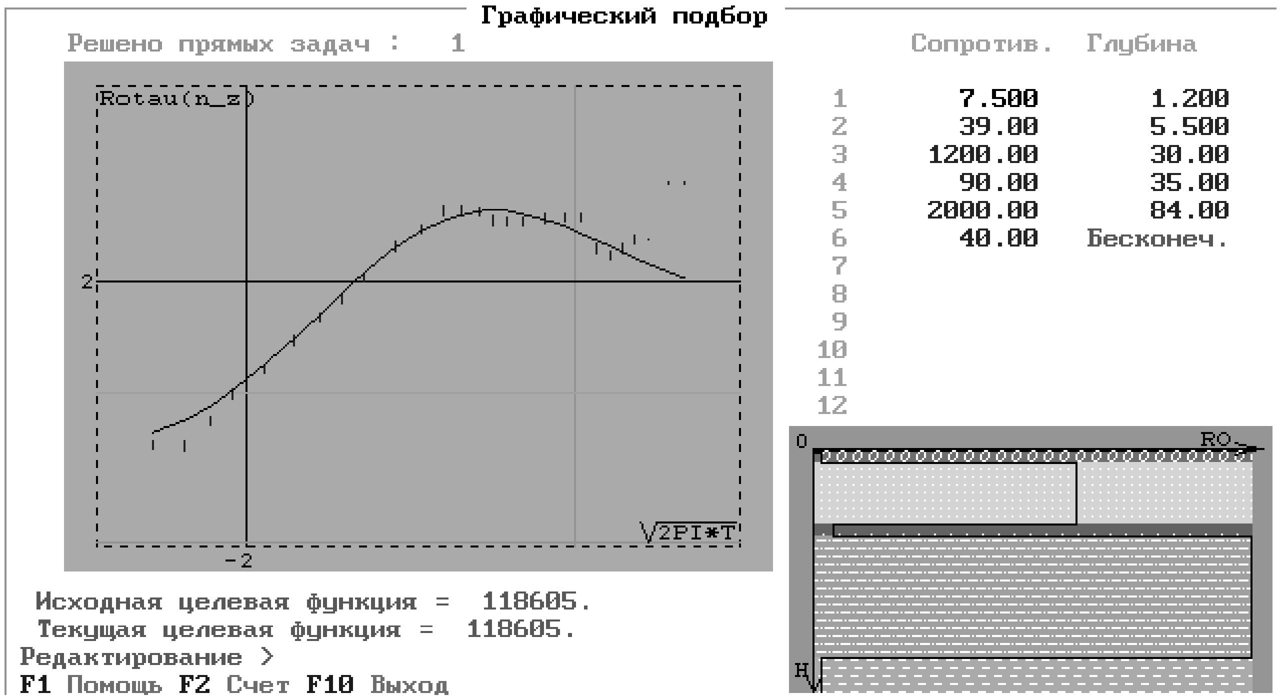

Figure 14: Mathematical modelling of TDEM data (upper left) for station 159. On the upper right hand corner the two columns show depth [m] (right) and resistivity [Ωm]. Below is a schematic diagram of resistivity changes as a function of depth and unspecified lithology. This station was situated in the mined-out area close to the coal seam. The resistivity of water-filled area, according to TDEM data, was found to be 90 Ωm. The depth of the upper contact was determined at 30.0 m with a thickness of the opening of approximately 5.0 m.

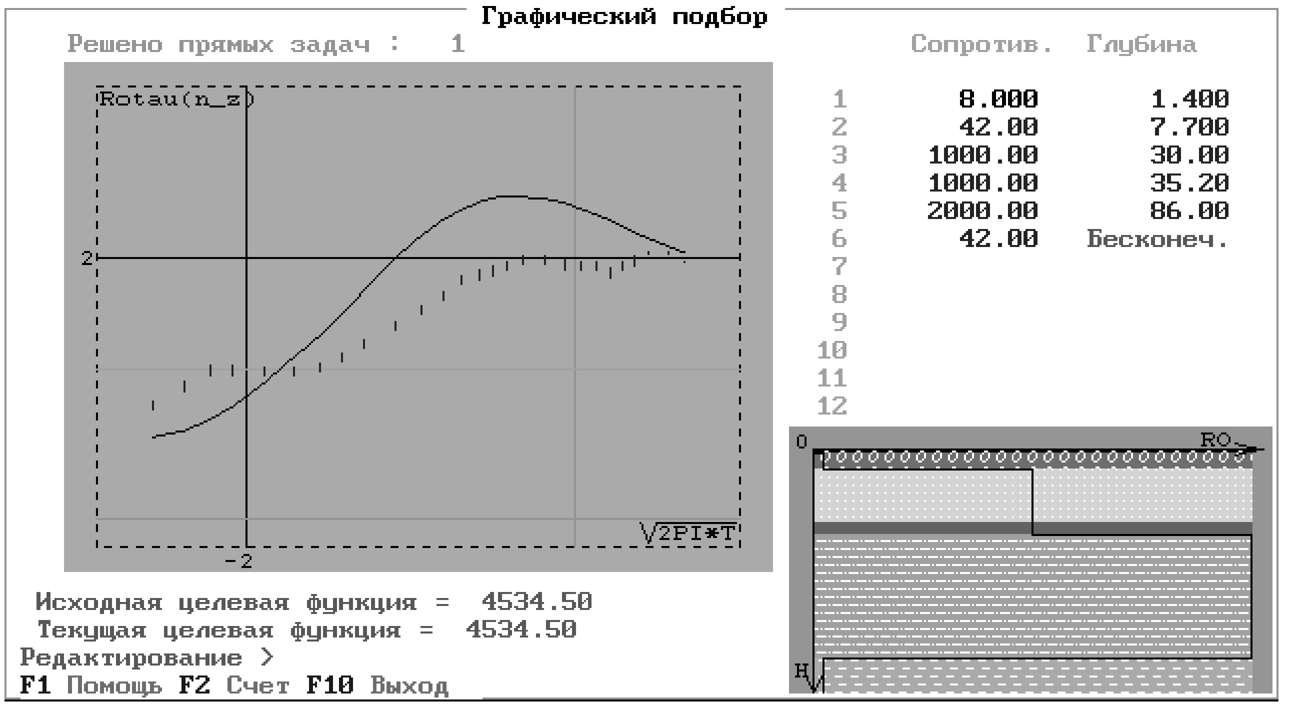

Figure A1: Modelling the cavity using a conductivity of 1000 Ωm.

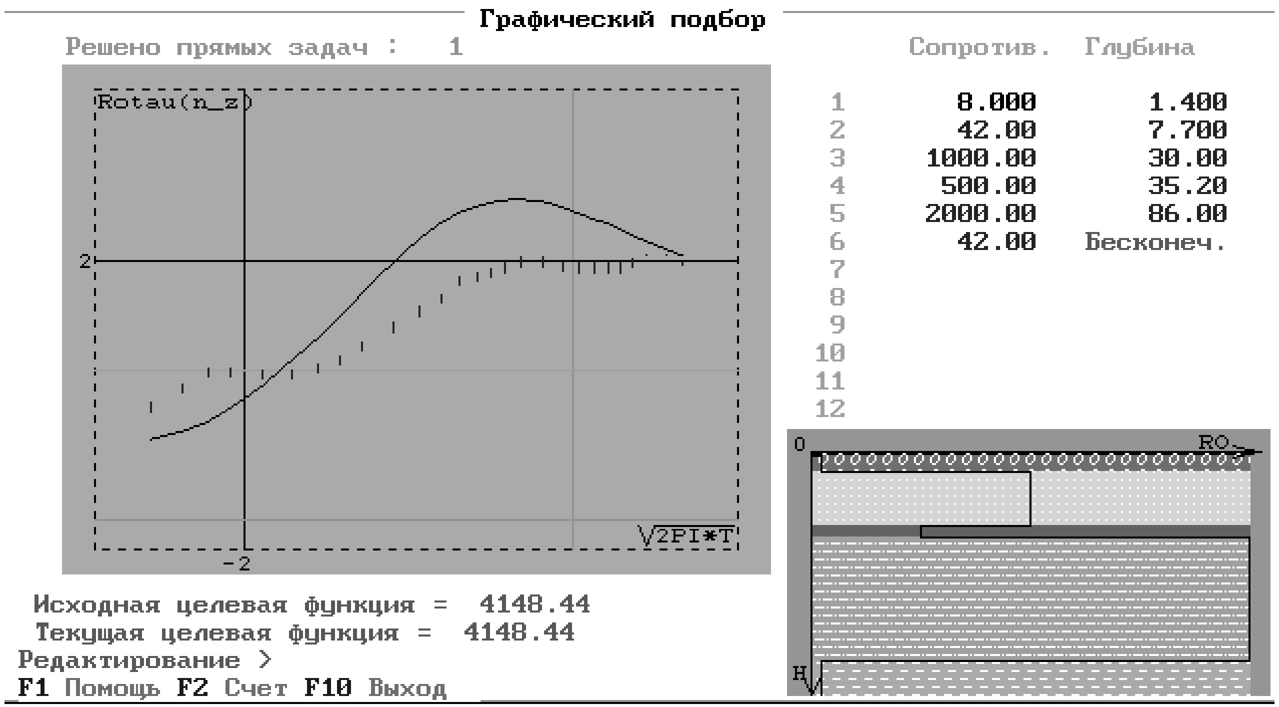

Figure A2: Model with conductivity 500 Ωm.

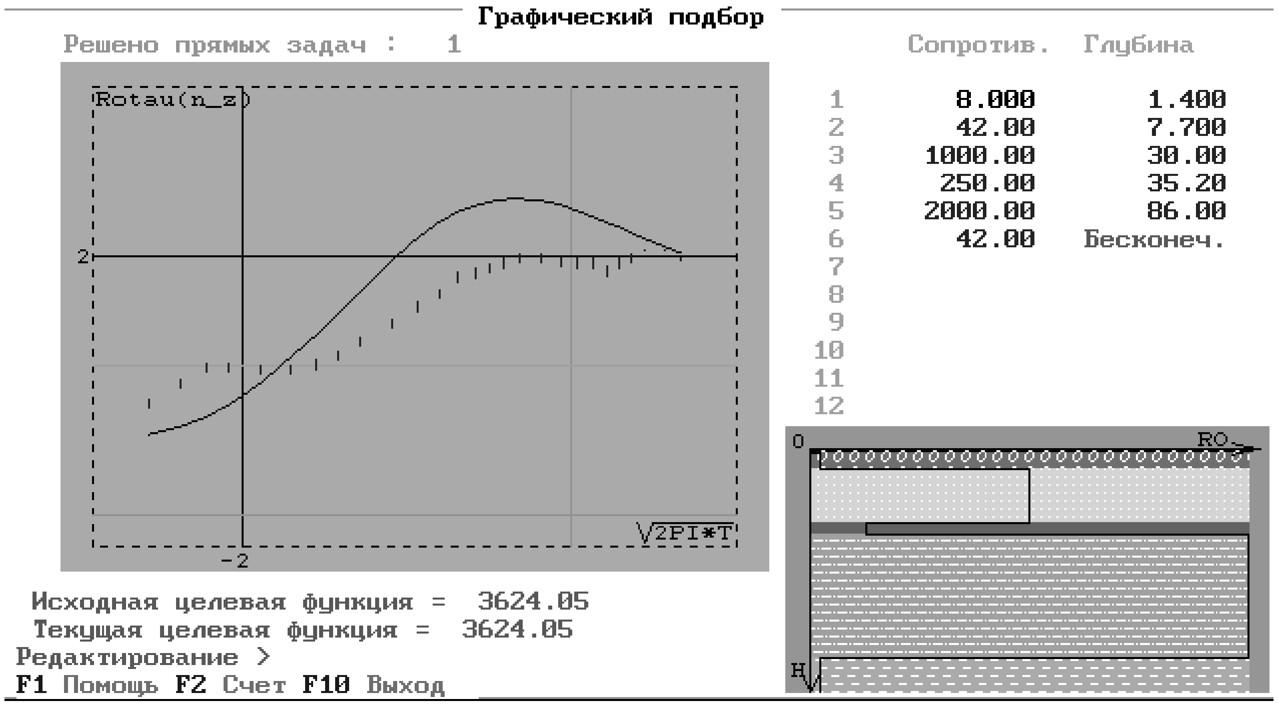

Figure A3: Model with conductivity 250 Ωm.

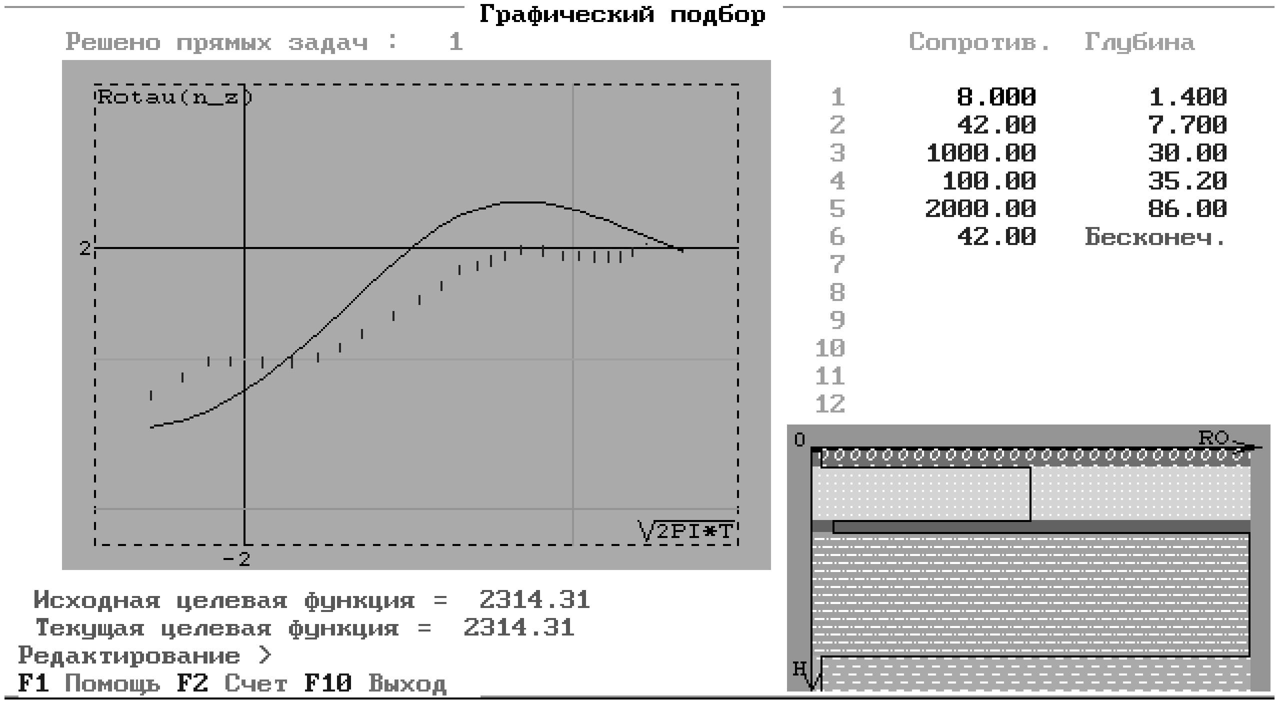

Figure A4: Model with conductivity 100 Ωm.

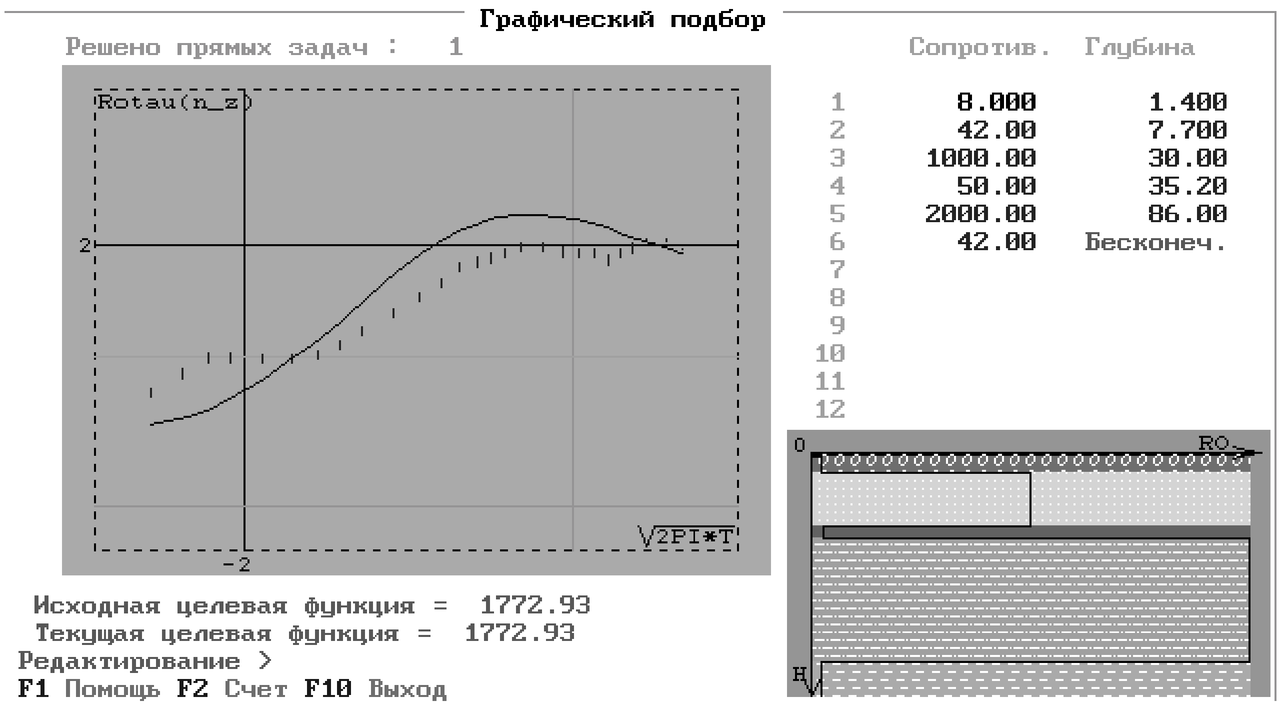

Figure A5: Model with conductivity 50 Ωm.

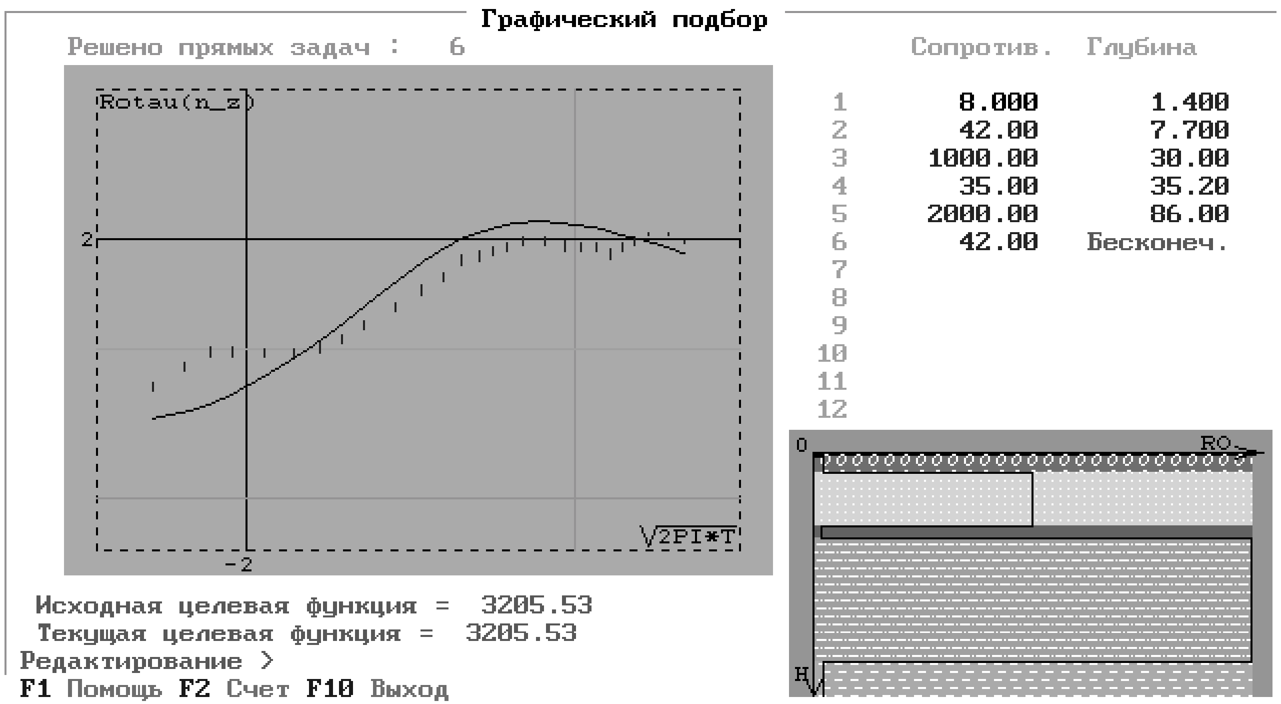

Figure A6: Model with conductivity 35 Ωm.

APPENDIX IV

COALTECH 2020

Interim Report

Detection of old workings, sinkholes, underground fires and acid mine pollution using geophysics and airborne thermal infrared imagery

Sub-task 4

Technology audit of other techniques that may be applicable to the detection of old workings

V.A. Kononov

M.J. Maccelari

Research Agency	**:**	**CSIR Division of Mining Technology**
Task Number	**:**	**1.3.1b**
Report Number	**:**	**2002-0139**
Date	**:**	**March 2002**

EXECUTIVE SUMMARY

The timeous detection and accurate mapping of old workings in the Witbank Coalfield is critical both town planning and mine planning. Of the technologies considered in this report it has been concluded that laser surveying and the tracking of a randomly orientated, self-propelled electromagnetic tag are potentially applicable in the Witbank Coalfield. It is thus recommended that the performance and suitability from a logistical point of view of both technologies be investigated further.

TABLE OF CONTENTS

1 INTRODUCTION

Reliable information as to the location* of old workings is critical in an area where building or mining activities are planned. Such information needs to be accurate and timeously available.

When considering shallow features, conventional reflection seismic methods are not cost effective under the geological conditions prevailing in the Witbank Coalfield (Maccelari, 2001,). This is a result of the negative influence of the weathered layer on the performance of the source and geophones. In order to improve acoustic matching, the top layer should be removed or boreholes drilled for an explosive-type energy source, rendering the method economically unsuitable. It was thus decided to investigate novel and other acoustic-type technologies applicable to the problem of detecting and locating old workings.

2 ACOUSTIC AND SEISMIC REFRACTION METHODS

The standard acoustic method employed by organisations such as municipalities to locate leakages in underground pipes was considered as a potential technology for the location of old workings. However, this method is impractical for the following reasons:

- If the energy source is positioned in a cavity, the energy transferred to the cavity walls will be negligible due to the poor load matching of the acoustic signal source.
- Providing a good acoustic contact with the cavity wall will be extremely difficult.

Consequently, no acoustic signal will be registered on the surface and, thus, it will not be possible to detect a transmitted signal.

The possibility of employing the refraction seismic method has also been investigated aunder sub-task 3a of Coaltech 2020 Task 1.3.1b. Prof. Cedric Wright (pers. com. 2002) conducted a technology audit of reported theoretical and practical work where refraction seismics have been used to located and delineate sub-terrain cavities. From this audit it was concluded that, the absence of readily available published examples suggests that such applications of seismology have not been particularly successful, or that the methodology has not been adequately developed. A series of discussions with BMA GeoServices, a natural resources engineering company based in Ireland, confirmed this. The possibility of Mr. Chris van Dam (pers. com. 2002) believes that, through the use of a fan array of geophones, it may be possible map old workings, however, a series of trials would need to be conducted.

At this juncture it can thus be concluded that, acoustic techniques are not applicable to the detection and location of old workings.

* In this document "location" implies accurate determination of true position, whereas "detection" means only the presence of old workings.

3 OTHER PROSPECTIVE TECHNOLOGIES

Continued monitoring of published material over many years has revealed the following techniques may be applicable to the mapping of old workings:

3.1 High spatial and temperature resolution infrared thermography

In countries with a continental-type climate, infrared thermography provides the required information provided measurements are taken during autumn when there are rapid changes in atmospheric temperature. Experiments were conducted 15 to18 years ago (Kononov, pers. com. 2002). The depth of penetration obtained was 20 to 30 m. It is proposed that through the use of contemporary IR technology, superior results will be obtainable in South Africa. This is one of the technologies currently being investigated under Coaltech 2020 Task 1.3.1b.

3.2 Time domain electromagnetic method (TDEM).

In 2001 the TDEM method was tested at the Arthur Taylor Colliery and proved applicable (Hallbauer-Zadarozhnaya, 2001). This was a preliminary application of the TDEM method and further trials are recommended in order to fully evaluate the method.

3.3 Laser surveying

MDL Rock Lasers Ltd (Stuttle, 1998, Appendix A), a leading supplier of underground surveying systems to the mining and quarrying industry has undertaken successful mapping trials of abandoned mine workings for Kalgoorlie Consolidated Gold Mines Pty Ltd, Australia's largest gold producer. For the trial the C-ALS, cavity laser scanning system, was inserted in the drilled borehole and lowered by means of a winch on a tripod to an operating depth of 76 m below the surface. From here an initial survey of the stope was conducted taking measurements every 5 degrees in the horizontal and vertical planes. Once the initial stope survey data had been processed using KCGM's in-house software an area of the stope floor was identified as being of further interest. Another survey was carried out using the same horizontal increment as before but with a 1 degree vertical increment between 160 degrees and 165 degrees from vertical, thus providing a further six sets of data. Processing and visualization of this data provided the mine with a plan of the cavity of interest.

It is recommended that this technology be investigated further and assessed for its applicability in the South African coal environment.

3.4 Tracking of a random oriented, self-propelled electromagnetic tag

This proposed method is only applicable in flooded underground workings. The method requires at least one borehole intercepting an old, flooded underground roadway.

A disposable, submersible, self-propelled, randomly oriented electromagnetic (EM) tag and surface location receiver could be developed in order to implement the method. The tag would consist of a low frequency (LF) transmitter that radiates an EM signal via an inductive loop, an electrical motor with a propeller, and a battery to power the propeller and transmitter. All components would need to be housed in a sealed, zero gravity cylindrical enclosure that enables the tag to be suspended in water and move freely in any direction.

To conduct a survey, the tag would be lowered into the borehole, followed by a 100 g weight to ensure that it sinks. Upon entering the water filled cavity, the tag will assume a horizontal position and start moving. On the surface, a person equipped with a searching receiver and a loop antenna would follow and track the tag movement. Each time the tag is deflected off the sidewall the position is recorded using either a GPS or by placing a marker in the ground corresponding to the position of the sidewall.

Through the random movement of the tag, it will be possible to map old workings. The anticipated location accuracy for old workings located at a depth of 40 m is approximately 10 cm. Results will be dependent on the operator training. The principal of this technique is illustrated in Figures 1 and 2.

There are, however, three drawbacks to this novel method:

- An access borehole is required.
- The method is only applicable in flooded workings.
- The method is time consuming.

Surveying time could be reduced by the use of multiple tags, but additional personnel would then be involved in the location process.

4 CONCLUSIONS AND RECOMMENDATIONS

For reasons presented in Section 2, it is concluded that acoustic techniques, including conventional reflection and refraction methods, are inappropriate technologies for the detection and location of old workings in the Witbank Coalfield.

Through other sub-tasks conducted under Coaltech 2020 Task 1.3.1b, the time domain electromagnetic method and infrared thermography have proved applicable to the mapping of old workings. However, further trials using these methods are recommended.

The laser surveying technique of MDL Rock Lasers Ltd. needs to be investigated further to determine if the technology can be readily applied in the South African environment. It amy transpire that this technology is applicable to the mapping of old workings that are not flooded.

Finally, employment of a randomly orientated, self-propelled electromagnetic tag appears to be an applicable technology. As this technology has yet to be tested in the field it is recommended that a simple prototype system be built and tested in the field.

REFERENCES

Maccelari, M.J., 2001. The optimum methodology for conducting high resolution, shallow reflection seismic surveys on South African collieries. *Coaltech 2020 Interim Report Number 2001-0329*. CSIR Division of Mining Technology.

Stuttle M.C., 1998. Probe drilling & laser surveying in old mine workings. Geodrilling International, 6/9, p.12-13.

Hallbauer-Zadarozhnaya, V., 2001. Report on a TDEM survey at the Arthur Taylor Colliery Terra Sounding and Analytical (Pty) Ltd. *Coaltech 2020 Interim Report Number 2001-0649*. CSIR Division of Mining Technology.

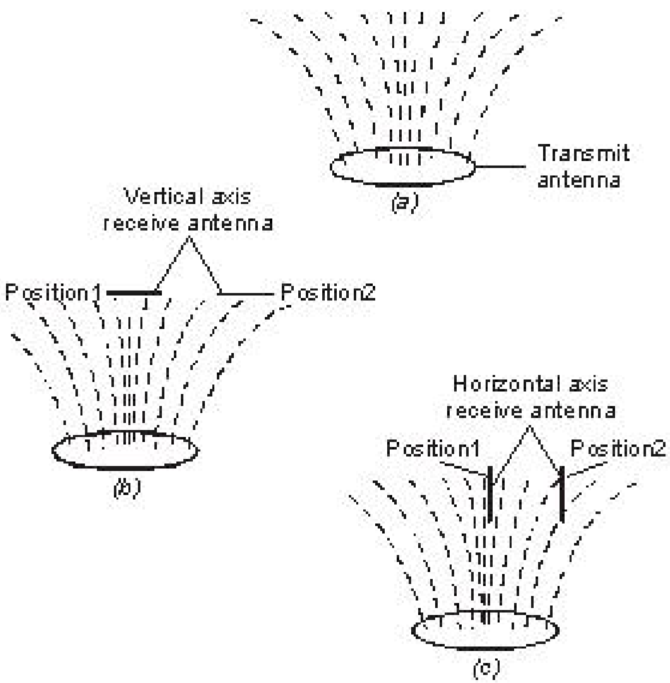

FIGURE 1. Tag's flux lines and antenna position

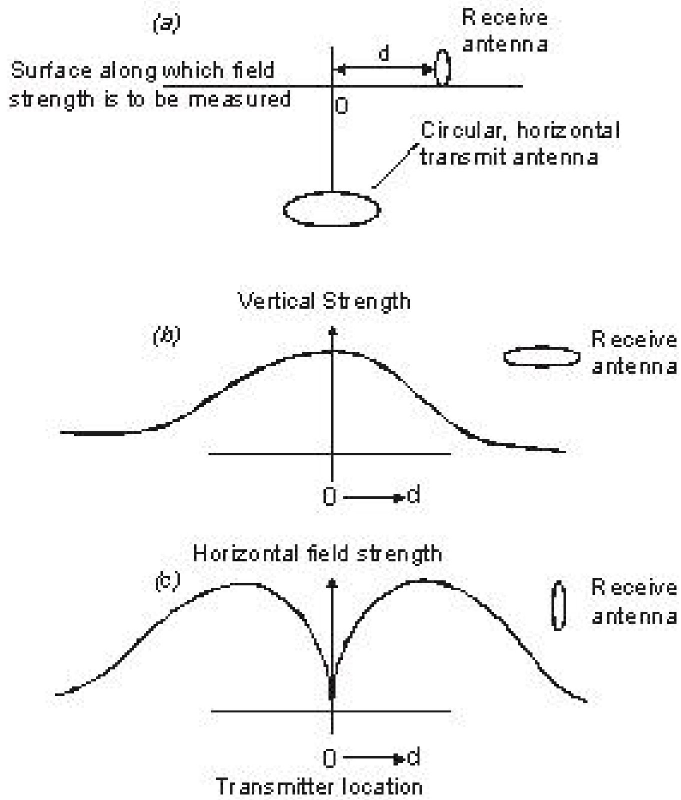

FIGURE 2. Horizontal and vertical EM fields

APPENDIX A

Probe drilling & laser surveying in old mine workings

MDL Rock Lasers' new underground cavity laser scanning system aided surveying of abandoned gold mine workings in Australia

By M.C. Stuttle*

MDL Rock Lasers Ltd, a leading supplier of underground surveying systems to the mining and quarrying industry has undertaken successful mapping trials of abandoned mine workings for Kalgoorlie Consolidated Gold Mines Pty Ltd (KCGM), Australia's largest gold producer.

KCGM's Fimiston Super Pit located in Kalgoorlie, Western Australia, is the largest open pit gold operation in the country. The final pit design at Fimiston is expected to be 3.7 km in length, 1.5 km in width and to reach a depth of 540 m. The open pit operation is located on Kalgoorlie's famous Golden Mile, and underground mining has been carried out in the area since 1893, since when an estimated 45 Moz of gold has been recovered.

During the early days of Australian mining, underground operations were labour intensive, mining was selective and generally narrow stopes were mostly back-filled. Improved processing technology and mine mechanisation during the 1970s and 80s has permitted larger scale operations to adopt less selective underground stoping operations. The 'super pit' concept was a logical step for mining companies working towards economies of scale. However, the industry recognised that there was no precedent for excavating a 500 m deep open pit through ground previously affected by extensive old workings.

In order to appreciate the geotechnical challenge facing KCGM, it is necessary to consider that under the proposed area of the open pit, stoping reached a level of 1 km and was supported by over 2,000 km of development headings.

KCGM was very fortunate in that plans were available for the Golden Mile underground operations. The existing plans were interpreted by the mine's geotechnical teams and computer models of the underground workings were constructed. These models can be imported into 3D mine planning packages such as Vulcan's UNIX based software, Envisage, to assist analysis and design.

This prior knowledge of the workings provides the focus for investigating/confirming ground conditions using probe drilling. After repeated drilling, followed by detailed analysis a number of decisions relating to the nature of the ground and the mining approach to be taken were finalised.

For the obvious reasons of human error, lack of original survey information and the progressive deterioration in ground conditions it is recognised that the stope models are not perfect. It also became apparent that sole reliance on probe drilling as a means of investigation is inefficient in terms of time and quality of information. This is particularly the case in complex areas where stopes are in close proximity. A major concern is the presence of open stopes (voids). In many cases stopes will consist of combinations of filled and void sections. The condition of pillars within these underground workings is extremely important. In time pillars collapse and as a result voids will propagate in upward and lateral directions, hence the need to develop systems that allow rapid and accurate verification of ground conditions.

KCGM, after much investigation into technology for underground mining was introduced to MDL Rock Lasers Ltd and the company's new underground laser cavity scanning system, the C-ALS. KCGM concluded after initial discussions with MDL Rock Lasers that a combined probe drilling and void mapping approach using the C-ALS would greatly improve the management of mining through affected ground. A recent field trial in one particular area of the mine has verified the capability of the C-ALS system to rapidly and efficiently assist in this process.

The C-ALS scanner features lightweight, carbon fibre alignment rods from Measurement Devices Ltd's (MDL) Boretrak MKII, a borehole deviation system to stop the two axis measurement head rotating, and to lower the system down a borehole. Once the device is deployed via a 110 mm borehole, up, down or sideways, the operator can carry out vertical and horizontal plan section scans at any user specified ARC or CHORD increments. The C-ALS is claimed to be the only

MDL Rock Lasers Ltd's cavity laser scanning system, the C-ALS.

Below: Surface deployment of the C-ALS using a winch system and MDL's Boretrak® MKII rods.

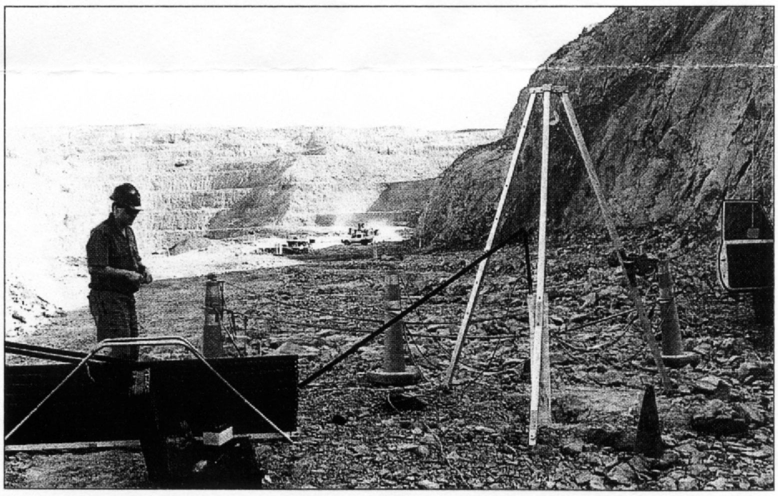

* *Director, MDL Rock Lasers Ltd.*

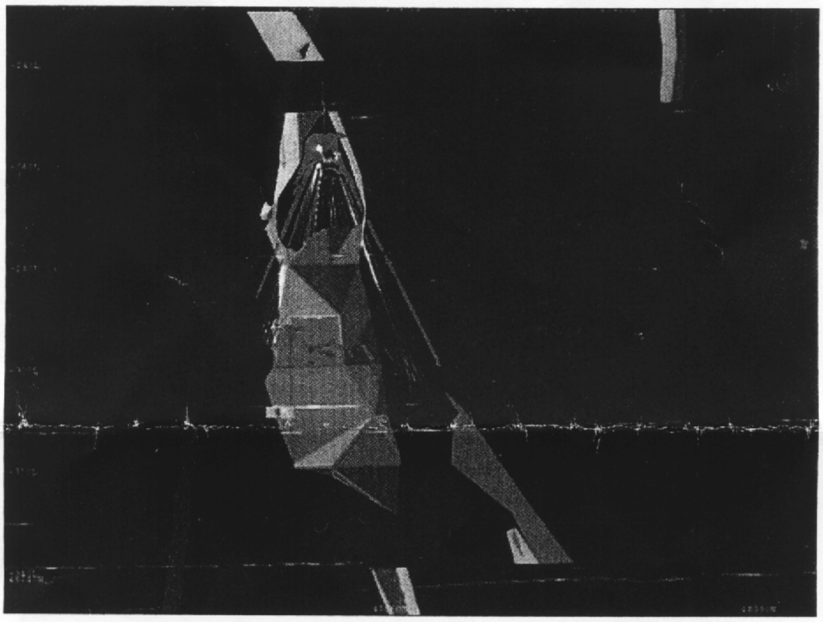

Maptek screen showing the survey sets (pink) and the second survey sets (yellow). The screen also shows a geological fault (red), and the assumed position of the Tetley Stope (brown).

instrument small and sophisticated enough to be able to do this.

Windows 95 software enables the operator to control the cavity scanner remotely, surveying the area in real time. The system makes accumulation of data extremely speedy and convenient. The C-ALS allows the operator to survey areas such as underground cavities in safety, scanning the entire cavity without operator intervention.

The area in which the field trial was conducted is located on the East wall of the Office Pit. In this area a number of ore-bearing lodes intersect and stopes centred on these lodes come together to form what is termed a 'ballroom'. This is known as the Tetley Stope. From the existing records a 3D model of the Tetley Stope was constructed. A 165 mm vertical borehole was drilled, the hole intersecting the stope at a depth of 71.5 m. This borehole was lined with 74 m of 125 mm plastic casing: around 1 m of the installed casing was above ground, giving a clearance of 1.5 m from the roof crown to the end of the casing.

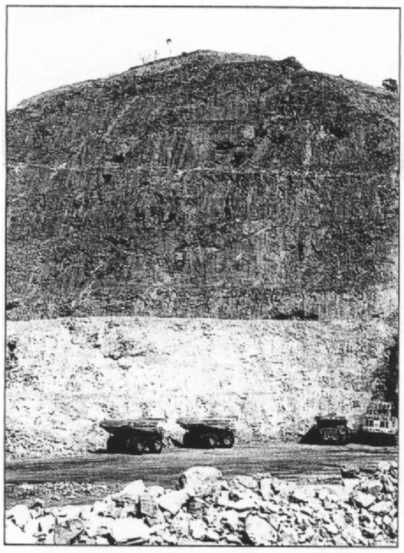

East wall of the Office Pit clearly showing abandoned workings. The Office Pit is part of Kalgoorlie's Fimiston Super Pit.

For the trial the C-ALS was inserted in the drilled borehole and lowered by means of a winch, on a tripod, to an operating depth of 76 m below the surface. From here an initial survey of the stope taking measurements every 5° in the horizontal and vertical planes was conducted. Once this initial stope survey data had been processed using KCGM's own bespoke software an area of the stope floor was identified as being of further interest. Another survey was carried out using the same horizontal increment as before but a 1° vertical increment between 160° and 165° from vertical was chosen. This gave a further six sets of data.

The completed data from the two surveys were fed into KCGM's software and a rendered view produced. Furthermore, it confirmed that the eastern hanging wall was formed by a steep east dipping fault at which point the mineralisation would have ceased abruptly.

MDL Rock Lasers Ltd, based in Northampton, England, is part of Measurement Devices Ltd (MDL), which provides a comprehensive range of underground surveying systems around the world. Internationally, MDL operates as MDL Technologies Inc., Measurement Devices (Africa) C.C. and Measurement Devices (Shenzhen) Co. Ltd.

Measurement Devices Ltd, Silverburn Crescent, Aberdeen AB23 8EW Scotland. Tel: (+ 44 1224) 246700. Fax: 824987. Website: http://www.mdl.co.uk

RES No. 207

APPENDIX V

COALTECH 2020

The Microgravity Method for Underground Cavity Detection in the Coal Mine Environment

S. J. Lowe & M. Muller
Geophysical Services Department
Anglo American

C. Pretorius
Quantitative Mineral Exploration

CSIR, Division of Mining Technology
Report number: 2001-0120

Task 1.3.1b

Detection of old workings, sinkholes, underground fires and acid mine pollution using geophysics and airborne thermal infrared imagery

20 March 2001

EXECUTIVE SUMMARY

The traditional approach to underground cavity detection involves the expensive and time-consuming process of drilling a regular grid of closely-spaced boreholes with the hope of intersecting the expected cavities. Geophysical surveys represent a more efficient alternative to this traditional approach.

Coal mines present difficult geophysical targets as surface and underground infrastructure such as pipes, buildings, drill rigs, railway lines etc. will result in high frequency, large amplitude noise in magnetic, electric or electromagnetic data which may overpower the geological response. Also, conductive overburden limits the subsurface depth of penetration of electromagnetic methods. Gravity is not affected by metal or electrical mining infrastructure and can 'see through' conductive overburden.

Microgravity surveys measure small changes in the Earth's gravitational field caused by density variations in the subsurface material. Underground cavities create a relative low density (or mass deficient) volume that corresponds to a negative gravity anomaly, relative to the measured background gravity field. Microgravity differs from conventional gravity primarily in terms of the sensitivity of the measurement instrument and the field procedure during the data acquisition phase. A microgravimeter (1 μGal sensitivity) is an order of magnitude more sensitive than a conventional instrument (10 μGal sensitivity) and more measurements are repeated to ensure data reliability. 30-50% of the measurements are repeated for microgravity surveys compared to the 10-20% repeat statistic of conventional gravity. The root-mean-square error of the repeat measurements of microgravity surveys is typically 4-6 μGal, depending on local conditions and represents the detection limit possible for microgravity surveys. The station elevations are measured with a high accuracy (better than 1 cm) in microgravimetric surveys to improve the accuracy of the elevation correction applied during the data reduction phase.

A desktop modelling exercise was undertaken, using three-dimensional gravity forward modelling software, to quantify the limits of detection of the microgravity method. Three different scenario's were investigated:

Model 1: Bord and Pillar Detection

The objective of this model was to determine whether the individual bords and pillars of old workings are resolved by the microgravity method. It was found that it is possible to map individual bords and pillars of ultra-shallow (<6m deep) old workings in ultra-high resolution (<5m station intervals) surveys. Standard microgravity surveys (at 5m grid intervals) over coal seams at depths below 6m only yield the average or bulk response of the bords and pillars in old workings.

Model 2: Edge of Workings Detection

The aim of Model 2 was to ascertain the *maximum depth* at which the edge of old workings can be reliably resolved by the microgravity method. It was shown that it is possible to detect the edge of water- or air-filled old workings to maximum depths of 50m and 150m, respectively.

A secondary objective of Model 2 was to establish the *minimum horizontal distance* between two separate coal seams (at different depths) for which their respective edges of workings will be resolved apart from each other in the gravity response. It was found that it is possible to resolve the edges of old workings on two different coal seams to a minimum horizontal separation of 30m for shallow seams (< 25m deep) or 90m for deeper seams (< 70m deep).

The edge of the old workings is located directly under the inflection point of the gravity response curve (to an accuracy of about half a station interval), between the gravity high over the unmined coal seam and the gravity low over the old workings. The inflection point in the gravity field corresponds to a peak or a trough in the horizontal gravity gradient response.

Model 3: 'Rathole' Detection

The objective of Model 3 was to determine the *minimum size* of ratholes and the *maximum depth* at which they can still be resolved using the microgravity method.

In the case of a few isolated, scattered ratholes the following was concluded:

- Air-filled large (6m diameter) ratholes will be observed by microgravity to a maximum depth of 12m.
- Air-filled small (3m diameter) ratholes will be observed by microgravity to a maximum depth of 9m.
- Water-filled large (6m diameter) ratholes will be observed to a maximum depth of 9m.
- Water-filled small (3m diameter) ratholes will be observed to a maximum depth of 6m.

Extensive surface weathering may produce lower amplitude gravity anomalies over ratholes than would otherwise be expected as the density contrast between the ratholes and the surrounding host rock is lower.

In the case of a cluster of ratholes, which would form a particularly high-risk area to mining activities, the following was concluded:

- A cluster of ratholes produces a large negative anomaly of the order of tens of µGals which would easily be observed by microgravity surveys.
- The individual ratholes in the cluster produce low amplitude anomalies (at the limit of detection by microgravity instruments), which are superimposed on the main low over the cluster. The high amplitude anomalies produced by single isolated ratholes are not observed when the ratholes exist in a cluster as all their individual responses interfere with each other, due to their close proximity, to form a set of low amplitude anomalies.

Microgravity surveys were conducted at Arthur Taylor (Duiker) and Kromdraai (Anglocoal) Collieries in order to detect the edge of the old workings and the possible occurrence of ratholes, respectively. These surveys were not carried out as part of the Coaltech2020 initiative, but are presented here with the permission of Duiker Mining and Anglocoal. The results of these surveys are presented as Case Histories in this report and the results of the forward modelling exercise are discussed within the framework of the results of these surveys.

At Arthur Taylor Colliery the edges of the old water-filled #2 seam workings, located at depths in the range 23-40m, were successfully detected with a predicted accuracy of about ±7m (one station interval) on all five of the microgravity profiles that were carried out during the test survey. The observed gravity anomalies compare well with the forward models (for water-filled workings) presented in this report (Figure 10).

At Kromdraai Colliery, where the objective was rathole detection, a number of roughly circular anomalies were detected in the microgravity data but none with an amplitude larger than 14 µGals. Therefore it was inferred that there are no ratholes with a diameter greater than 6 m at a depth shallower than about 6 m, and none with a diameter greater than 3 m shallower than about 3 m, anywhere in the survey area. The observed anomalies may instead be the result of local variations in overburden weathering and density. The results for both of the case histories are yet to be confirmed by drilling.

Based on the results of the gravity forward modelling and field results, the microgravity method is highly recommended for use in underground cavity detection in the coal mine environment. **It should always be borne in mind that real data is susceptible to noise and the detectability of targets would be poorer in a real field environment than predicted by**

numerical modelling.

The forward modelling discussed in this report involved the best-case detection scenarios. The effect of a less dense overburden and local variations within the overburden was not considered for any of the models. Also, only reasonably large areas of old workings were modelled. Smaller volumes of old workings may yield lower amplitude gravity responses. Specific densities were assumed for the coal and host rock in the forward models calculated in this report. Although these densities are typical of coal mine environments, different density contrasts will yield slightly different responses. Therefore, it is recommended that forward modelling be performed prior to all field surveys, using the specific geologic parameters of the survey area to provide an understanding of the responses which are likely to be obtained within that environment and to aid in the interpretation of the data acquired.

ACKNOWLEDGEMENTS

The authors of this report would like to thank Duiker Mining for granting us permission to present the microgravity data collected at Arthur Taylor Colliery in our Case History 1.

We also wish to thank Anglocoal for granting permission for us to discuss the microgravity survey performed at Kromdraai Colliery in Case History 2.

TABLE OF CONTENTS

LIST OF FIGURES

.

LIST OF TABLES

1 INTRODUCTION

Coal seams are traditionally mined using the 'Bord and Pillar' Method. Old workings thus contain a regular arrangement of coal pillars, usually 6 x 6m wide and 3m high, dispersed throughout an air or water-filled underground cavity. If the old workings are water-filled and its boundaries are not accurately known then modern mining activities near to the old areas could become flooded by accidentally 'holing into' the old workings. Therefore, it is necessary to find an economical, reliable method to check the position of the edge of the old workings, as mapped on old mine plans, before commencing new mining activities near old areas.

Coal seams are usually relatively shallow and when the depth of overburden weathering is similar to the depth of the roof of the old workings 'ratholes' or sinkholes may develop as the hanging wall sediment collapses into the old workings. These ratholes present a safety hazard to surface mining activities due to the instability of the ground above them. Again, a reliable method is necessary to detect these ratholes ahead of the planned mining activities.

A traditional approach to cavity detection is to drill a regular grid of closely-spaced boreholes which hopefully intersect and delineate the old workings and ratholes. However, this method can become extremely expensive and time consuming and offers no guarantee of success. Geophysical surveys represent a more efficient alternative to this traditional approach as larger areas can be mapped relatively quickly and cost-effectively to identify problem areas for follow up drilling.

A number of geophysical methods exist for potentially tackling the above problems, each exploiting different physical properties of the rocks and sediments comprising the subsurface.

- The *magnetic method* responds to different magnetic susceptibilities of the rocks constituting the subsurface. An air- or water-filled cavity generally has zero susceptibility and is therefore not directly detected by the magnetic method.

- *Electric methods* measure changes in the conductivity/ resistivity within the subsurface. Air-filled cavities represent resistive targets since the resistance of air is infinitely high while water-filled cavities are quite conductive targets, depending on the amount of dissolved solids in the water compared to the surrounding country rock. Sediment-filled or back-filled cavities have less predictable responses. This method has been successfully used to detect buried cavities in different environments (Bristow, 1966; Butler and Murphy, 1980; Friedel and Hanson, 1990; Lowry and Shive, 1990).

- The *electromagnetic method* also measures contrasts in the conductivity of different rock types using the principle of electromagnetic induction. The technique is most effectively utilised for the detection of good electrical conductors, such as massive sulphide deposits, at relatively shallow depths. This technique has not been extensively employed for cavity detection.

- *Ground penetrating radar*, a high-resolution, shallow electromagnetic wave technique, has been employed for cavity detection with varying success (Frankenhauser *et al*., 1995). A major problem for electromagnetic techniques is the presence of a conductive clay overburden which severely restricts the effective depth of penetration.

- The *microgravity method* is consistently quoted in literature as being one of the most effective geophysical methods for underground cavity detection. In particular, the U.S. Army Engineer Waterways Experiment Station initiated a research program in 1976 to investigate different geophysical methods for the detection and delineation of subsurface cavities in hard rock terrain (Butler and Murphey, 1980; Butler, 1980, 1983; Ballard, 1983; Curro, 1983; Cooper, 1983; Butler *et al*., 1983). Microgravity was found to be the most promising surface method for investigations of shallow cavities. They found that the maximum depth of investigation is approximately equal to 4 to 6 times the cavity diameter.

Coal mines present difficult geophysical targets as surface and underground infrastructure such as pipes, buildings, drill rigs, railway lines etc. will result in high frequency, large amplitude noise in magnetic, electric or electromagnetic data which effectively overpowers the geological response.

Gravity is not affected by metal or electrical mining infrastructure and can 'see through' conductive overburden. This report investigates the usefulness of microgravity and its limits of detection related specifically to the coal mine environment. Firstly, a short description of the microgravity method in terms of data acquisition, processing and interpretation procedures is provided and microgravity is compared to the conventional gravity method. Then a series of forward models are presented to characterise the gravity responses that would be obtained for specific problems in coal mines such as edge of old workings and rathole detection and the effect on the gravity data of the residual coal pillars in the old workings. Lastly, two case histories are presented which discuss the results of microgravity field surveys conducted to determine the edge of old workings and to detect ratholes at Arthur Taylor and Kromdraai Collieries, respectively.

2 THE MICROGRAVITY METHOD

2.1 Introduction

The gravity method measures very small differences in the Earth's gravitational field that result from density variations in the rock material that make up the subsurface. In practice, gravimeters measure relative changes in the vertical component of the Earth's gravitational acceleration at discrete stations on a survey grid or line.

Underground cavities create a relative low density (or mass deficient) volume that corresponds to a negative gravity anomaly, relative to the measured background gravity field. The amplitude of the anomaly will depend on the contrast in density between the material filling the cavity and the surrounding host rock. The maximum density contrast is achieved when underground cavities are air-filled, as air has zero density. This represents the best detection scenario. Water-filled cavities represent poorer targets as water has a density of 1 g/cm^3 (compared to a typical coal density of 1.5 g/cm^3). Cavities filled with sediment can produce a variety of responses depending on the amount of compaction of the sediment. Loose, unconsolidated sand (such as collapsed roof material) will have a low density and will therefore produce a larger gravity anomaly than more compacted sediments (such as back-fill).

The bulk effect of the individual bords and pillars of an underground coal mine will be evident in the gravitational response, but the individual structures will most likely not be imaged, unless the workings are extremely shallow and the gravity measurement interval is of the order of the dimensions of the bords and pillars.

The gravity response over old mine workings will generally be lower than the response over unmined areas due to the bulk effect of the lower density cavities in the workings which produce a negative density contrast with respect to the undisturbed coal seam of the unmined areas. Thus, the edge of workings will correspond to a step in the gravity response from a higher value (over the unmined areas) to a lower value (over the old workings).

A desktop modelling exercise was undertaken (Section 3) to quantify the limits of detection of the microgravity method. This section reviews the microgravity method in terms of data acquisition procedures and data processing methods. The microgravity method is also compared with the conventional gravity method.

2.2 Gravity Data Acquisition

Practically, a gravity survey consists of taking measurements of the gravity field, with a gravimeter (or microgravimeter), at discrete points (stations) within a grid or along survey lines laid out on the ground perpendicular to the anticipated trend of the target. The station positions must be accurately known for use in the gravity corrections applied to the data following the acquisition stage. Station elevations are used in the elevation corrections to remove the gravitational effect of the relative elevation differences between the station locations, which may obscure the target gravity anomaly. One measurement location is selected as a base station at which repeat readings are collected regularly (every hour or so for microgravity) in order to estimate drift in the readings due to the Moon's gravitational pull and instrument drift. Table 1 summarises the steps involved in the data acquisition phase.

Table 1: Steps involved in the microgravity data acquisition process.

1	Pegging of station positions.
2	Surveying of station X and Y coordinates.
3	Tagging and labelling of station pegs.
4	Clearing and smoothing of a small circle of ground at measurement stations on which microgravimeter will be placed.
5	Accurate levelling of station elevations with dumpy level.
6	Gravity field measurement with a microgravimeter

2.3 Microgravity Versus Conventional Gravity Methods

In comparison with ordinary gravimeters used to measure the Earth's gravity signal, a microgravimeter is an order of magnitude more sensitive. The Lacoste and Romberg microgravimeter shown in Figure 1 has a sensitivity of 1 μGal (microGal), compared to the 10 μGal sensitivity of a typical conventional instrument. In terms of survey procedure, a microgravity survey is characterised by a high percentage of repeat readings (between 30 to 50% of the measurement stations are repeated) to ensure high data reliability, compared to conventional surveys with lower repeat statistics (typically 10 to 20%). A further requirement of microgravity surveys is very high accuracy (better than 1 cm) in measuring the relative elevations of the stations for the elevation correction. The typical root-mean-square (RMS) error of the repeat measurements of microgravity surveys is about 4 - 6 μGal, depending on local conditions (e.g. weather and ground surface conditions). Ground vibrations caused by plants rustling in the wind and variable near-surface densities (resulting from ploughed lands for instance) may negatively affect the repeat statistic. This means that features associated with gravity anomalies that are smaller than about 6 μGal cannot be reliably detected. A typical production rate for microgravity surveys is about 30 stations per day. The major differences between conventional and microgravity surveys are summarised in Table 2.

Table 2: Comparison between conventional gravity and microgravity surveys.

	Conventional Gravimeter	**Microgravimeter**
Typical Sensitivity:	10 μGal	1 μGal
Percentage Repeat Readings:	10 to 20% measurement stations repeated	30 to 50% measurement stations repeated
Required Accuracy of Elevation Measurements:	A few cm's	Better than 1cm
Typical RMS Error of Repeat Measurements:	30 μGal	4 – 6 μGal

2.4 Gravity Data Reduction

A number of standard gravity corrections are applied to the microgravity data during the processing phase. Using repeat measurements at a base station an instrument drift and Earth tide correction is calculated. A latitude correction is applied to counteract the increase of gravity with latitude due to the combined effects of the rotation of the Earth and its equatorial bulge. Since gravity varies inversely with the square of distance, it is necessary to correct for the changes in elevation between measurement stations. The free-air correction effectively reduces the field readings to a datum surface (of constant elevation), but does not take the contribution of the rock between the station and the datum plane into account. The Bouguer correction is applied to account for the attraction of the material between the station and datum plane, assuming a slab of material of infinite length and a constant density and thickness. A terrain correction is sometimes calculated for survey areas of rugged topography to take into account the gravitational effect of local hills and valley's which bias individual station measurements.

2.5 Gravity Data Processing and Interpretation

Additional products may be derived from the corrected gravity data using Fourier techniques and image processing methods in order to aid the interpretation.

A regional gravity field, arising from deep-seated density contrasts, may be estimated from the measured Bouguer gravity and subtracted from it to reveal residual gravity anomalies arising from shallow variations in density. This process is automated by calculating the polynomial surface that best fits the regional field (Figures 30 and 31). Successively higher order polynomial surfaces account for the gravity effects of successively smaller and shallower subsurface features.

Vertical and horizontal derivatives may be calculated from the measured gravity data to enhance the edges of different subsurface geological structures (Figure 31). The edge of old workings produces a transition in the gravity response from a high over the unmined area to a low over the old workings. The edge of workings is located at the inflection point between this high and low. An anomalous positive or negative anomaly in the horizontal derivative results from an inflection point in the original gravity profile (Figure 31). Thus the horizontal derivative often locates the position of the edge of old workings quite definitively. The vertical derivative resembles the gravity field in shape but enhances the short-wavelength anomalies and degrades the longer wavelength features. As the derivatives generally enhance shallow features in the gravity anomalies, they will also enhance any noise in the data.

3 DESKTOP MODELLING

3.1 Introduction

Desktop modelling was performed using three-dimensional gravity forward modelling software developed by C. Pretorius (of Quantitative Mineral Exploration), with the objective of determining the limits of detection of the microgravity method for a coal mine environment. Three different scenarios were investigated to answer several different questions:

Model 1: Can the individual bords and pillars of old coal workings be resolved or does the gravity field yield the bulk (average) response of all the bords and pillars?

Model 2: What is the maximum depth at which the edge of old workings can be reliably determined? What is the minimum horizontal separation at which the edge of workings (of two different coal seams) can be reliably resolved from each other?

Model 3: What is the maximum depth and minimum size of underground cavities (or 'ratholes') that may be detected using the microgravity method?

In all three models the following density values were used:

Table 3: Densities used in all gravity forward models.

Lithology	Density (g/cm^3)
Shale Host Rock	2.4
Coal Seam	1.5
Air-Filled Cavity/ Tunnel	0.0
Water-Filled Cavity/ Tunnel	1.0
Unconsolidated Sediment-Filled Cavity/ Tunnel	1.0

The gravity field was calculated on a regular 5 x 5m grid of stations for all the models as this is the sampling interval typically used for the collection of microgravity data in the field.

A horizontal difference was calculated from the gravity response, using MATLAB software, as follows: [X(2)-X(1) X(3)-X(2) ... X(n)-X(n-1)], where X(1), X(2) … etc are successive stations along the survey line. The resulting field is an approximation to the horizontal derivative in units of μGals per station interval (simply labelled μGals in all the figures presented in this report).

3.2 Gravity Forward Modelling Algorithm

The algorithm employed to model the gravitational effects of synthetic density distributions in this desktop study is based on the methods developed by Nagy (1966) and Plouff (1976). A density distribution in the form of a collection of 3D cubes is created. The response at any given point is the sum of the response of all the sources (3D cubes) in the density distribution. Nagy (1966) and Plouff (1976) provide equivalent formulae for the response of a rectangular cube. These formulae are closed expressions found by integrating the vertical derivative of the gravity potential over the boundary of the cube.

The density distribution was created using Matlab software. The forward modelling algorithm was devised and coded into C++ and runs as a separate executable module. A 3D visualisation application was created to visualise the density distribution and the resultant gravitational response. All illustrations of the desktop models presented in this report were generated using Matlab software.

3.3 *Model 1:* Bord and Pillar Detection

The objective of this model is to determine whether the individual bords and pillars of old workings can be resolved by the microgravity method or if the gravity field represents only the bulk (average) response of all the bords and pillars.

A suitable density distribution was constructed as shown in Figure 2. A 3m wide coal seam occurs in a shale host rock. Half of the modelled area consists of unmined coal while the other half contains a regular arrangement of bords and pillars, typical of old coal workings. Each coal pillar is 6x6x3m in size. The edge of the workings is straight except for an exploratory tunnel (6m wide and 3m high) into the unmined area. The workings are air-filled representing the best detection case for the microgravity method. In order to determine the depth at which the bords and pillars are no longer individually resolved from each other, the coal seam was buried at three different depths, namely 3m (Model 1a), 6m (Model 1b) and 9m (Model 1c) below the surface. The gravity response was calculated on a 5m grid of measurement stations (Figure 3). Selected gravity profiles and their horizontal gradients have been displayed in Figures 4 and 5. The results of the investigation are summarised in Table 4 below:

Table 4: Summary of the gravity response of Model 1 (peak-to-peak amplitudes are quoted).

Structure	Model 1a	Model 1b	Model 1c
Depth to Top of Coal Seam	3m	6m	9m
Mined/ Unmined Transition	130 μGals	130 μGals	126 μGals
Exploratory Tongue ***(Full Width of Anomaly)***	63 μGals *(Width = 50m)*	42 μGals *(Width = 60m)*	30 μGals *(Width = 70m)*
Bords &Pillars	21 μGals	7 μGals	6 μGals

The following may be concluded from the results of the gravity forward modelling:

- A large step change in the gravity response (of the order of 130 μGals) is obtained over the edge of the old workings from a high over the unmined area to a low over the workings (Figures 3 & 4a). In the horizontal gradient (Figure 4b), a high is produced at the position of the inflection point between the high and low in the gravity profile. This inflection point (gradient high) is not situated directly over the edge of workings but is shifted by less than 2m towards the workings. The reason for this effect is not clear but it may be due to the positions of the measurement stations with respect to the edge of the workings.

- The amplitude of the step change in the gravity does not vary much with increasing depth to the top of the coal seam from 3m to 9m (Table 4). The edge of workings at these shallow depths is easily detectable by microgravity methods.

- A negative anomaly, relative to the background gravity response, is obtained over the exploratory tunnel into the unmined coal area (Figures 3 & 5a). The gradient response (Figure 5b) shows a low and a high over the western and eastern edges of the tunnel, respectively. While the high is directly above the eastern edge of the tunnel, the low is about 2m west of the tunnel's western edge. This may be a factor of the 5m sampling interval which was used to detect the 6m-wide tunnel.

- The gravity anomaly over the tunnel broadens and decreases in amplitude fairly rapidly as the coal seam is buried at successively greater depths (Table 4). Practically, the anomaly is detectable by microgravity methods but is at the limit of detection by conventional gravity surveys when buried at a depth greater than 6-9m. In all cases, the anomaly is broader than the actual width of the tunnel, but the anomaly inflection points map the edges of the tunnel well.

- The individual bords and pillars are detected quite convincingly in Model 1a, where the depth to the top of the coal seam is the shallowest at 3m, as they produce anomalies of amplitude 21 μGals (Figures 3 & 4a). However, the sampling interval of 5m is too large to enable accurate delineation of the *edges* of the pillars. There is generally only one measurement station above a bord or a pillar. Where this station is located at the centre of the bord or pillar (rather than on its edge), the response is the highest (Figure 4a). The gradient response is shown in Figure 4b. The gradient enhances the gravity response but the edges of the bords and pillars are still not resolved due to the large sampling interval with respect to the size of the pillars. Model 1b, with a depth to the top of the workings of 6m, represents the limit of detection of the bords and pillars using microgravity as anomalies of only 6 μGals are obtained over the workings.

- In practise, typical microgravity surveys will generally yield the average or bulk response of the bords and pillars in old workings unless the coal seam is ultra-shallow (less than 6m below surface) and the survey is conducted at a station interval of 5m or less.

3.4 *Model 2:* Edge of Workings Detection

The aim of Model 2 is to ascertain the *maximum depth* at which the edge of old workings can still be reliably resolved by microgravity (Model 2a). A secondary objective was to establish the *minimum horizontal distance* between two separate old workings (at different depths) for which their respective edges of workings will still be resolved apart from each other (Model 2b).

Model 2a:

A simple model of a square-shaped area (210x210m in size) of old workings, surrounded by unmined coal, was produced for Model 2a and the gravity response calculated at depths to the top of the coal seam of 12m down to 234m. The resultant gravity anomaly amplitudes are summarised in Table 5 for both water-filled and air-filled workings.

Table 5: Gravity response over the edge of old workings located at increasing depths below the surface (Figure 10).

Depth of Workings (m)	Gravity Response (μGals)	
	Air-Filled Workings	Water-Filled Workings
12	124	41
24	109	36
32	100	33
48	83	27
96	47	15
156	24	7
234	10	-

At shallow depths (less than 24m) a large gravity low, greater than 100 μGals in amplitude, is obtained over air-filled workings (Figures 6a and 7a). The horizontal gradient of the gravity response was calculated and is shown in Figures 6b and 7b. The inflection point in the gravity response between the high over the unmined area and the low over the old workings corresponds to a positive or negative anomaly in the gradient data. In this model, a negative and a positive gradient anomaly are positioned within about 2m of the northern and southern edges of the old workings, respectively. The small (less than 2m) shift of the gradient anomalies towards the workings may be attributed to the discrete 5m intervals at which the response was calculated.

As the depth to the coal seam increases, the gravity response broadens and flattens. That is, the amplitude of the gravity low decreases and the slope (gradient) of the curve at the inflection point decreases (Figure 8a and 9a). In plan view (Figure 8a), the gravity anomaly is circular in shape even though the workings are square-shaped. At a depth of 96m, a gravity low of 47 μGals is obtained over the workings. This amplitude is still well above the detection limit of the microgravity instrument **but the position of the edge of the workings is harder to interpret than for the shallower case**. This is because the slope at the inflection point is quite shallow resulting in low amplitude, broad gradient anomalies (Figures 8b and 9b).

The greatest depth of air-filled workings which still yield a measurable gravity anomaly (10 μGals) is 234m (Table 5, model not shown). However, at this depth the gravity response is so broad and the gradient response so weak that it is extremely difficult to accurately deduce the position of the edge of the workings. The greatest *practical* depth of detection of the edge of air-filled workings is about 150m.

Water-filled old workings present a more difficult target as the density contrast between the cavities and the surrounding host rock is reduced. Figure 10 presents a graph of the decrease in the amplitude of the gravity anomaly over the edge of workings with increasing depth to the top of the coal seam for air- and water-filled old workings. **Water-filled workings consistently**

produce anomalies about one third of the amplitude of the corresponding air-filled model. The greatest depth of water-filled workings which still yields a measurable gravity anomaly (7 μGals) is 156m (Table 5, model not shown) but the maximum *practical* depth is closer to about 50m. Also shown on Figure 10 is the gravity response observed over water-filled workings as described in Case History 1 and 2 (Sections 4.1 and 4.2). The observed results correspond well with the forward models but the Arthur Taylor Colliery results seem to show a greater decrease with increasing depth than observed for the models.

Summary:

- Although a measurable response over the old workings is obtained to great depths, the position of the edge of the workings can only be delineated from the gravity data to a *practical* depth of about 150m (for air-filled workings) and 50m (for water-filled workings), to an accuracy of within ± half a station interval.
- Water-filled workings produce a response equivalent to about one third of the amplitude of the corresponding air-filled model.
- The narrower the workings the lower the response. The amplitude of the gravity response and hence the maximum depth of detection of the edge of old workings is very reliant on the extent of the old workings.

Model 2b:

In Model 2b, two coal seams were created. One seam is buried 10m below the other seam. Each seam has been 'mined' by the bord and pillar method to different extents. The two coal seams share a common position for the western edge of their workings (at x=5000m). However, the shallowest coal seam has been mined less extensively than the deeper seam in the model. Hence the edge of the deeper workings occur further east than the edge of the shallow seam (Figure 11). The edge of workings of the two different coal seams are separated by a horizontal distance of first 30m and then 90m and the model was calculated three times as both coal seams were buried at successively greater depths. Table 6 summarises the results:

Table 6: Results of Model 2b (peak-to-peak amplitudes shown).

Horiz. Distance between Edge of Workings (m)	Depth To top of Seam #1 (m)	Depth To top of Seam #2 (m)	Gravity Response (μGals)	Gradient Response over Eastern Edge of Workings	Figures
30	12	22	238	Asymmetric high	12 & 13
90	27	37	198	Two distinct, broad highs	14 &15
90	56	66	142	Two distinct, very broad highs	16 & 17

In all cases a large gravity low is produced over the area in which both seams have been mined out. The peak-to-peak amplitudes of these lows are almost double the amplitudes of the corresponding anomalies obtained over the air-filled workings in Model 2a (Table 5). This is because there is double the volume of low density material in Model 2b since there are two mined coal seams instead of just one. In each case the gravity low is asymmetrical in shape. The eastern slope is always more gentle than the western slope of the anomaly due to the different positions of the edge of the workings of the two coal seams in the east (Figures12a, 13a, 14a, 15a, 16a and 17a). The slope of the gravity curve depends on the horizontal separation of the two edges and the depths of the seams. In the horizontal gradient, a symmetrical negative anomaly occurs at the position of the inflection point in the gravity curve, directly above the common western boundary of the workings. But in the east an asymmetrical positive anomaly (Figures 12b and 13b) or two distinct positive anomalies (Figures 14b, 15b, 16b and 17b) are produced over the two edges of workings.

In the first case, the coal seams are fairly shallow occurring at depths of 12 and 22m, respectively. Their edges of workings are separated by a horizontal distance of just 30m. In the gradient response, the deeper seam produces an anomaly which forms a shoulder to the high over the eastern edge of the shallow seam (Figure 13b). Two distinct anomalies are not produced but you can still deduce the position of the edges from the gradient response. *Thus, 30m represents the minimum horizontal distance at which the edges of the workings of two shallow coal seams may be resolved separately*. When the seams are buried at greater depths (27m and 37m, respectively) and are separated by 90m, their eastern edges produce two distinct gradient anomalies (Figure 15b). In this case, the two edges of workings are easily resolved separately. However, at still greater depths (56 and 66m, respectively), the two edges may only just be distinguished in the gradient response as two separate, very broad highs (Figure 17b). *Thus, 90m represents the minimum horizontal distance at which the edges of the workings of two deep coal seams may be resolved separately.*

3.5 *Model 3*: 'Rathole' Detection

'Ratholes' or sinkholes develop in the hanging wall of underground workings particularly when the depth of overburden weathering is similar to the depth of the roof of the old workings. Cavities develop as the hanging wall sediment collapses into the old workings These ratholes present a safety hazard to surface mining activities due to the instability of the ground above them. The bigger and shallower the ratholes the more dangerous they are. The objective of Model 3 is to determine the *minimum size* of ratholes and the *maximum depth* at which they can still be resolved using the microgravity method.

Two different scenario's were considered, firstly the response of a few isolated ratholes (Models 3c and 3d) and secondly the response of a cluster of ratholes which would form a particularly high-risk area to mining activities (Models 3a and 3b).

A density model was created with the depth to the top of the old workings varying from 6m to 15m. Individual ratholes or a cluster of air- or water/ sediment-filled large (6m diameter) and small (3m diameter) ratholes were placed above tunnels in the old workings and extended from the workings up to various depths below the surface (Figures 18 and 22).

Models 3c and 3d: Isolated ratholes

Model 3c shows a few individual 6m diameter ratholes with varying depths below surface, density and height scattered throughout the overburden above the old workings. They each produce 'bull's eye' gravity anomalies of different intensities varying from 6 μGals to 33 μGals in amplitude (Figure 18). A north-south profile at x=180m crosses four different ratholes (Figure 19). The water/ sediment-filled rathole at a 9m depth produces an anomaly of only 6 μGals. Since this is the typical rms error of microgravity surveys, 9m represents the maximum depth at which water or sediment-filled 6m diameter ratholes can be detected. The air-filled 6m diameter rathole at a depth of 9m produces a response of 12 μGals suggesting that deeper ratholes of this size may still be detected using microgravity.

Model 3d is similar to Model 3c but smaller 3m diameter ratholes are modelled at depths of between 3m below the surface and 0m (i.e. exposed or nearly exposed at surface). Again, 'bull's eye' gravity anomalies are produced over the ratholes (Figure 20). The water-filled and air-filled, 3m diameter ratholes at a depth of 3m produce anomalies of amplitude 10 μGal and 19 μGals, respectively, suggesting that they may still produce observable anomalies at greater depths (Figure 21).

The ratholes were buried at successively greater depths until they produced responses which were similar to the rms error of microgravity surveys, 6 μGals (models not shown). Table 7 summarises the results.

Table 7: ***Summary of the gravity response over individual ratholes. (The results shown for ratholes which have a greater height than others are shaded grey. Responses close to the detection level of microgravity surveys are shown in red).***

Model	Material Filling Rathole	Depth to top of Rathole (m)	Rathole Width by Height (m)	Gravity Response (µGals)
3c (Figures 18 & 19)	Air	6	6 x 3	17 (not shown)
	Air	9	6 x 3	12
	Air	12	6 x 3	6 (Not shown)
	Air	6	6 x 6	33
	Water	6	6 x 3	9 (not shown)
	Water	9	6 x 3	6
	Water	6	6 x 6	18
3d (Figures 20 & 21)	Air	3	3 x 3	19
	Air	0	3 x 6	30
	Water	3	3 x 3	10
	Water	0	3 x 6	56

Previous forward modelling completed before the data acquisition phase of Case History 2 (discussed in Section 4.2 of this report), resulted in anomalies of lower amplitude than those discussed here. This is because the previous forward modelling assumed that the ratholes penetrated a fairly thick layer of low density, weathered overburden whereas this model does not incorporate any overburden but assumes dense shales exist right up to the surface. Therefore the density contrast of the ratholes with respect to the host rock is higher in this model yielding larger responses than that obtained for the previous modelling exercise. Thus, extensive weathering may result in lower amplitude gravity anomalies than would otherwise be expected. This should be kept in mind when interpreting gravity data for ratholes.

In summary:

- Air-filled large (6m diameter) ratholes will be observed by microgravity to a maximum depth of 12m.
- Water-filled large (6m diameter) ratholes will be observed to a maximum depth of 9m.
- Air-filled small (3m diameter) ratholes will be observed by microgravity to a maximum depth of 9m.
- Water-filled small (3m diameter) ratholes will be observed to a maximum depth of 6m.
- Extensive weathering may result in lower amplitude gravity anomalies over ratholes than would otherwise be expected.

The U.S. Army Engineer Waterways Experiment Station initiated a research program in 1976 to investigate different geophysical methods for the detection and delineation of subsurface cavities in hard rock terrain (Butler and Murphey, 1980; Butler, 1980, 1983; Ballard, 1983; Curro, 1983; Cooper, 1983; Butler *et al*., 1983). For the microgravity method, they found that the maximum depth of investigation is approximately equal to 4 to 6 times the cavity diameter. This forward modelling exercise predicts that ratholes will be detectable to depths of 2 to 3 times the cavity diameter (as summarised above). This is considerably less than the depths predicted by the Waterways Experiment. This discrepancy exists mainly because the Waterways Experiment was designed to detect large irregular-shaped underground solution cavities in dense dolomite rock while the forward modelling in this report investigates the gravity response of small ratholes in a less dense shale host rock.

Models 3a and 3b: Cluster of Ratholes

In Model 3a, a cluster of 6m diameter ratholes have developed, to a depth of 6m below surface, above old workings at a depth of 9m (Figure 22 and 23). A broad negative gravity response is obtained over the cluster of ratholes (Figure 24a). The amplitude of this anomaly is 60 μGals. Low amplitude, asymmetric anomalies are superimposed on the broad low in response to the individual ratholes (Figure 25a). These anomalies are very similar to the anomalies obtained over the bords and pillars of Model 1. In the gradient response (Figures 24b and 25b), a large low and a high occur over the northern and southern edges of the cluster of ratholes, respectively. Smaller amplitude high/ low pairs demarcate the edges of the individual ratholes within the cluster.

Figures 26 and 27 show how the gravity response changes with a change in density and depth to the top of the cluster of ratholes. The deeper the ratholes the lower the amplitude of the broad gravity low over the cluster. Also, the individual ratholes no longer produce measurable smaller anomalies superimposed on the broad low. If the ratholes are water- or sediment-filled so that the density contrast between them and the surrounding host rock is reduced then the gravity response is also decreased.

Note that the individual ratholes in the cluster do not produce anomalies with the sort of amplitudes produced by single isolated ratholes (as discussed in Models 3c and 3d). This is because all their individual responses interfere with each other, due to their close proximity, forming fairly uniform low amplitude anomalies as a net effect. In fact, the amplitudes of the individual ratholes in the cluster are at the limit of detection by current microgravity instruments.

For Model 3b, a cluster of 3m diameter ratholes were modelled (instead of 6m diameter as for Model 3a) at a depth of 3m below the surface, above old workings at a depth of 6m. A broad gravity low of amplitude 15 μGals is observed over the cluster of ratholes (Figure 28a). Again the individual ratholes produce smaller amplitude anomalies which are superimposed on the broad low, but this time, due to the shallow depth of the coal seam, the individual bords and pillars also produce small anomalies which are superimposed on the gravity response over the whole mined out area (Figure 29a). In the gradient response (Figures 28b and 29b), it can be seen that a high/low pair demarcates the edges of the individual ratholes within the cluster. These anomalies are larger than the gradient anomalies produced over the bords and pillars.

The results of Models 3a and 3b are summarised in Table 8.

Table 8: ***Summary of the gravity response over a cluster of ratholes. (The results for water-filled ratholes are shaded in grey for clarity).***

Model	Material Filling Rathole	Depth to top of Rathole (m)	Rathole Width by Height (m)	Rathole Cluster (μGals)	Individual Ratholes (μGals)
3a (Figures 23 to 27)	Air	6	6 x 3	60	< 7
	Air	9	6 x 3	53	< 5
	Water	6	6 x 3	33	< 4
3b (Figures 28 & 29)	Air	3	3 x 3	15	< 9

In summary:

- A cluster of ratholes produces a large negative anomaly of the order of tens of μGals which can easily be observed by microgravity surveys.
- The individual ratholes in the cluster produce low amplitude anomalies (at the limit of detection by microgravity instruments) which are superimposed on the main low over the

cluster. The high amplitude anomalies produced by single isolated ratholes are not observed when the ratholes exist in a cluster as all their individual responses interfere with each other, due to their close proximity, to form a set of low amplitude anomalies.

4 CASE HISTORIES

4.1 CASE HISTORY 1 - Edge of Workings Detection at Arthur Taylor Colliery

(Data reproduced courtesy of Duiker Mining)

Introduction

AATS (Anglo American Technical Services) was commissioned to carry out a microgravity test survey over old #2 seam workings at Arthur Taylor Colliery in January 2000. Future underground mining of #2 seam is planned, and the safety of these operations requires that an adequate buffer be maintained around the old workings to avoid flooding by groundwater that has inundated the old workings. The objective of the microgravity survey was to determine whether the method can be used to accurately and reliably identify the position of the edge of the workings as a cheaper alternative to surface or underground drilling. Compagnie Generale de Geophysique (CGG) were subcontracted by AATS to perform the microgravity survey, including both data acquisition and data processing.

Data Acquisition

An eight-day data acquisition program was carried out during which five 250m long lines were surveyed at 7m measurement intervals. Four of the lines (101 -104) crossed the edges of old workings where the #2 seam depth varies between approximately 23-33m (based on the available borehole data), while the fifth line (109) crossed a narrow 30m wide tongue of workings at a #2 seam depth of approximately 40m. Table 1 (Section 2.2) summarises the steps involved in the microgravity data acquisition process. A total of 184 gravity stations were measured, with a 46% repeat statistic. A standard deviation for the reoccupied stations of 6.4 μGals was achieved.

Data Processing

The following standard corrections were applied to the data during processing: latitude, tidal correction, elevation correction and Bouguer correction (assuming a density of 2 g/cm^3). The final Bouguer gravity profiles have a strong regional gradient, resulting from relatively deep-seated geological structures, that obscures the small gravity anomalies associated with the old mine workings (blue line, Figure 30). This regional gradient was effectively removed by subtracting a first-order polynomial from the data of Lines 101 to 104 and a sixth order polynomial from the data of Line 109, to produce a residual gravity anomaly that isolates the signal of the old mine workings (red line, Figure 30; blue line, upper panel, Figures 31 and 32). In addition to subtracting the regional gravity field, a five point smoothing filter has also been applied to the residual gravity data to remove the local station-to-station noise. The signal of the old workings is significantly enhanced in the resulting gravity profile (red line, upper panel, Figures 31 and 32).

Desktop modelling completed prior to the data acquisition phase showed that the edge of workings is located in the residual gravity data at the inflection point between the gravity low of the old workings and the gravity high of the unmined area. The inflection point produces a peak (or trough) in the horizontal gradient of the residual gravity data (red line, lower panel, Figures 31 and 32). This gradient anomaly may sometimes be quite broad and ambiguous. The half amplitude point of the gravity anomaly, that is the point midway between the minimum amplitude of the gravity low and the maximum amplitude of the gravity high also corresponds to the position of the inflection point of the gravity profile (green arrows, upper panel, Figures 31 and

32). Both the gradients and the half amplitude points were used to locate the position of the edge of workings from the residual gravity profiles.

Results

With the exception of two cases, the discrepancy between the microgravity predicted edges of workings and the mapped edges is less than one measurement station interval (Table 9; Figure 33 and 34). In the remaining two cases, 19m of extra development on #2 seam is predicted towards the west on Line 101, and 24 m of extra development towards the west on Line 109. In the case of Line 101, the depth of the workings is relatively shallow and the gravity prediction should be reliable. Therefore it is probable that the true edge of workings is located west of its presently mapped position, consistent with the microgravity prediction, but this theory should be tested by drilling. In the case of Line 109, where only a deep, narrow tongue of #2 workings is present, the discrepancy may be the result of the target being below the resolution limit of the microgravity method.

Table 9: Results of the microgravity survey, showing the peak-to-peak amplitudes of the gravity anomalies and the differences between the position of the edge of workings as predicted by microgravity and as indicated in old mine plans.

Line	Workings	Depth to Workings (m)	Peak-to-Peak Anomaly Amplitude (μGals)	Distance (m) (Along gravity survey lines)
101	Old #2 Seam	23-25	40	19
102	Old #2 Seam	23-25	36	4
103	Old #2 Seam	31-33	26	6
104	Old #2 Seam	31-33	23	4
109	Old #4 Seam	Unknown	6	3 (Western Edge)
109	Old #2 Seam	39-40	10	24 (Western Edge 1 (Eastern Edge)
109	Modern #2 Seam (Modern #2 Seam)	39-40	15 (30*)	

** Unsmoothed Data*

The survey results indicate a clear decrease in the amplitudes of the gravity anomalies with increasing depth of the workings, from survey line to survey line (Table 9). However the detection limit of the microgravity method, in terms of the depth to workings that may be reliably detected has not been reached by this test survey. The narrow tongue of workings on Line 109, estimated to be present at about 40m depth beneath the survey line, has produced a measurable gravity anomaly, despite its limited width. On Line 109, the modern workings on #2 seam have a higher amplitude gravity response than the old workings, despite the similar depths to both workings as the modern workings are air-filled rather than water-filled.

Discussion

The edges of the old #2 seam workings, located at depths in the range 23-40m, have been successfully detected with a predicted accuracy of about ±7m (one station interval), on all five of the microgravity profiles that were carried out during the test survey. The individual bords and pillars of the old workings at these depths are not directly imaged and the inflection point in the gravity data maps the average or bulk position of the edge of workings. Microgravity is not capability of imaging very narrow, deep, isolated fingers of underground development but could provide a good basis for optimising and planning other complimentary methods for detecting the edges of these workings.

Recommendations

At the time of completion of the survey a recommendation was made that a drilling program, consisting of several closely spaced boreholes on each line (particularly lines 101, 104 and

109), be initiated to test the predictions of the microgravity survey. This test is critical in establishing the accuracy and reliability of the microgravity method for edge of workings detection, and the extent of the 'averaging' effect inherent in the method. At the time of writing this case history, the recommended drilling program has yet to be carried out, so the results are as yet untested.

4.2 CASE HISTORY 2: 'Rathole' and Edge of Workings Detection at Kromdraai Colliery

(Data reproduced courtesy of AngloCoal)

Introduction

Kromdraai Open-Cast Colliery commissioned AATS (Anglo American Technical Services) to carry out a microgravity test survey over their old #1 seam workings. The primary objective of the test was to determine whether the microgravity method can be used to detect near-surface sinkholes ('ratholes') developed above the old workings. A significant proportion of planned future mining activity at Kromdraai will take place within areas identified as high risk in terms of sinkhole development and safe mining operations require that the positions of potentially dangerous, concealed near-surface sinkholes be identified. Previous ground penetrating radar and electrical resistivity surveys, aimed at imaging subsurface cavities at Kromdraai, have proven unsuccessful. A secondary objective was to establish whether microgravity might be successfully employed to identify and map out the edge of the old workings as for the previous case history. Again, Compagnie Generale de Geophysique (CGG) were subcontracted by AATS to perform the microgravity survey.

Data Acquistion

An eleven-day data acquisition program was carried out in January 2000 by CGG (managed by AATS), during which a 50 $\times$ 105 m grid and an additional 80 m long profile (Line 100) were surveyed at 5 x 5m station spacings. The depth to the roof of the #1 seam workings beneath the survey area is estimated to be about 12 - 15 m, and the depth of weathering about 10 m, as indicated in the mine model. As the depth of weathering penetrates very close to the roof of the old workings, there is a high probability of rathole/sinkhole development upwards from the old workings into the soft overburden. There is no surface expression to suggest the presence of sinkholes. The old workings are not known to be water-filled. The steps involved in the data acquisition process were very similar to the procedures used for Case History 1 (Table 1: Section 2.2). A total of 258 gravity stations were measured, with 40% of the stations being occupied for repeat readings. A standard deviation of 3.9 μGals was achieved for the reoccupied stations, which is a very good repeat statistic, and the data quality is therefore regarded as very good.

Data Processing

The following standard corrections were applied to the data by CGG during processing: latitude correction, tidal correction, elevation correction and Bouguer correction (assuming a density of 2.0 g/cm^3). As before, the observed Bouguer gravity field contains a strong regional field. This regional gradient was removed by subtracting a 2nd order polynomial surface from the data leaving residual gravity anomalies that could be interpreted for possible sinkhole positions. A three-point smoothing filter has been applied to the Bouguer gravity data recorded along Line 100 extending across the edge of workings, to remove the local station-to-station noise.

Results of 'Rathole' Detection

The map of relative ground elevation derived from the accurate levelling of the stations prior to the gravity measurements can often provide an indirect indication of subsurface sinkholes through the occurrence of subtle surface depressions. However, in the case of this survey, there is a regular 3m decrease in elevation towards the southwest, with no obvious surface expression that might relate to a subsurface cavity (Figure 35).

Figure 36 shows how the residual gravity data relates to the positions of the bords and pillars of the old mine workings. The broad region of elevated positive anomalies observed in the gravity field towards the west of the survey area (Region X in Figure 37) may be related to the fact that larger pillars have been left unmined in this area of workings.

The highest risk anomalies that have been identified in the gravity data (Table 10, Figure 37) represent those anomalies that have the highest negative amplitude and are spatially located over several measurement stations. The anomalies are categorised according to risk, with Priority 1 representing the highest risk.

Table 10: Summary of the most significant negative anomalies observed in the residual gravity data, ranked in order of significance and interpreted risk-potential for sinkhole development (anomaly A has the highest risk potential and anomalies F and G the lowest).

Priority	Anomaly	Anomaly Amplitude (µGals)	Anomaly Dimensions (m)
1	A	14	16 x 16
	B	7	16 x 9
	C	9	20
2	D	10	10
	E	8	13 x 9
3	F	7	13 x 9
	G	9	12 x 9

A desktop study, completed prior to the data acquisition phase, showed that significant ratholes, 'growing' into low density overburden, would produce anomalies of the order of 25 – 50 µGals. Therefore, even the Priority 1 anomalies (maximum amplitude of about 14 µGals) in this survey do not represent potentially large and problematic sinkholes. Also, from the results of the forward modelling of Section 3.5 of this report, it may be inferred that there are no sinkholes with a diameter greater than 6 m at a depth shallower than about 6 m, and none with a diameter greater than 3 m shallower than about 3 m, anywhere in the survey area (Table 7, Section 3.5). This prediction should be tested with drilling.

Results of Edge of Workings Detection

As discussed in Case History 1, theoretical modelling prior to the data acquisition phase indicates that the edge of workings can be located in the gravity data at the inflection-point between the gravity low of the old workings and the gravity high of the unmined area. The position of this inflection point may be determined from the half amplitude position (a point midway between the minimum and maximum amplitudes of the gravity low and high, respectively) or from the position of the peak (or trough) of the horizontal gradient of the gravity profile (Figure 38).

In comparison with the #1 seam edge of workings shown in old mine plans (also shown in Figure 39), the microgravity prediction is located some 5m to the northeast. This distance is within the estimated accuracy of ± 5m (one station interval) of the microgravity method. The peak-to-trough amplitude of the gravity anomaly is 49 µGal in the unsmoothed gravity anomaly of Figure 38 (41 µGal in the three-point smoothed data). This result compares well with the curve predicted by forward modelling for water-filled workings (Figure 10). The Kromdraai workings are not known to be water-filled but this has not yet been tested by drilling. If the Kromdraai workings are air-filled rather than water-filled, the lower than expected gravity response may be due to a lower coal and overburden density at Kromdraai than what has been modelled, which results in a lower density contrast between the unmined area and the workings.

Discussion

There are no anomalies in the observed gravity field that represent significant sinkholes. The maximum observed anomaly is about 14 μGals, which is significantly less than the 25-50 μGals typically associated with large near-surface sinkholes. The anomalies may instead be the result of local variations in overburden weathering and density. The edge of the old #1 seam workings has been successfully identified on Line 100 with a predicted accuracy of about ± 5m (one station interval). These findings still need to be tested by drilling.

Recommendations

At the time of completion of the survey a recommendation was made that boreholes be drilled at the positions of the gravity anomalies, starting with the Priority 1 anomalies, and if possible extending to Priority 2. The Priority 3 gravity lows are possible extensions to anomaly B. Thus they should only be drilled if anomaly B is found to represent a sinkhole. It was recommended that triple tube boreholes be drilled to provide the necessary ground truth on the origin of the anomalies and to allow the characteristics of the overburden to be determined. The borehole core should be submitted for laboratory density measurements. If possible geotechnical parameters, such as boring velocity and pressure on the tool, should also be recorded while drilling. Another microgravity test survey should be conducted over an area where a definite large subsurface sinkhole actually exists to compare the response obtained for this survey with the response over known cavities. It was also recommended that several suitably placed shallow boreholes be drilled along the gravity profile of Line 100 to determine the true position of the edge of the workings and the reliability of the microgravity prediction. At the time of writing this case history, the recommended drilling program has yet to commence so the results are presently untested.

5 CONCLUSIONS

Model 1: Bord and Pillar Detection

The objective of this model was to determine whether the individual bords and pillars of old workings are resolved by the microgravity method. It was found that the bords and pillars will only be observed over ultra-shallow (less than 6m deep) workings and the edges of the pillars will only be accurately delineated in ultra-high resolution (less than 5m station intervals) microgravity surveys. Standard microgravity surveys (at 5m grid intervals) over coal seams at depths below 6m will only yield the average or bulk response of the bords and pillars in old workings.

Model 2: Edge of Workings Detection

The aim of Model 2 was to ascertain the *maximum depth* at which the edge of old workings can be reliably resolved by the microgravity method. The following was concluded:

- Although a measurable response over the old workings is obtained to great depths, the position of the edge of the workings can only be reliably delineated from the gravity data to a depth of about 150m for air-filled workings and 50m for water-filled workings.
- The edge of the old workings is located directly under the inflection point of the gravity response curve (± half a station interval), between the high over the unmined coal seam and the low over the old workings. The inflection point in the gravity corresponds to a high or a low in the horizontal gradient response.
- Water-filled workings produce a response equivalent to about one third of the amplitude of the corresponding air-filled model.

- The narrower the workings the lower the response. The amplitude of the gravity response and hence the maximum depth of detection of the edge of old workings is very reliant on the extent of the old workings.

Case history 1 discusses the results of a microgravity survey which was conducted to detect the edge of old workings at the Arthur Taylor Colliery. The edges of the old water-filled #2 seam workings, located at depths in the range 23-40m, were successfully detected with a predicted accuracy of about ±7m (one station interval), on all five of the microgravity profiles that were carried out during the test survey. The gravity anomalies compare well with the forward models for water-filled workings as illustrated in Figure 10.

A secondary objective of Model 2 was to establish the *minimum horizontal distance* between two separate old workings (at different depths) for which their respective edges of workings will be resolved apart from each other in the gravity response. It was found that:

- The minimum horizontal distance at which the edges of the workings of two shallow coal seams (at 12m and 22m depth, respectively) may be resolved apart is 30m, and
- The minimum horizontal distance at which the edges of the workings of two deep coal seams (at 56 and 66m depth, respectively) may be resolved apart is 90m.

<u>Model 3: 'Rathole' Detection</u>

The objective of Model 3 was to determine the *minimum size* of ratholes and the *maximum depth* at which they can still be resolved using the microgravity method.

In the case of a few isolated, scattered ratholes the following conclusions were drawn:

- Air-filled large (6m diameter) ratholes will be observed by microgravity to a maximum depth of 12m.
- Water-filled large (6m diameter) ratholes will be observed to a maximum depth of 9m.
- Air-filled small (3m diameter) ratholes will be observed by microgravity to a maximum depth of 9m.
- Water-filled small (3m diameter) ratholes will be observed to a maximum depth of 6m.
- Extensive surface weathering may produce lower amplitude gravity anomalies over ratholes than would otherwise be expected as the density contrast between the ratholes and the surrounding host rock is diminished.

In the case of a cluster of ratholes, which would form a particularly high-risk area to mining activities, the following conclusions were made:

- A cluster of ratholes produces a large negative anomaly of the order of tens of µGals which would easily be observed by microgravity surveys.
- The individual ratholes in the cluster produce low amplitude anomalies (at the limit of detection by microgravity instruments) which are superimposed on the main low over the cluster. The high amplitude anomalies produced by single isolated ratholes are not observed when the ratholes exist in a cluster as all their individual responses interfere with each other, due to their close proximity, to form a set of low amplitude anomalies.

Case history 2 discusses the results of a microgravity survey which was conducted to detect ratholes at the Kromdraai Colliery above old #1 seam workings which lies at depths (to the roof) of about 12-15m. A number of isolated roughly circular anomalies were detected in the Kromdraai microgravity data but none with amplitudes larger than 14 µGals. Therefore, it was inferred that there are no significant clusters of ratholes in the survey area. Also, there are no individual air-filled ratholes with a diameter greater than 6 m at a depth shallower than about 6 m, and none with a diameter greater than 3 m shallower than about 3 m, anywhere in the survey area. The observed anomalies may instead be the result of local variations in overburden weathering and density. These conclusions still need to be tested by drilling.

6 RECOMMENDATIONS

Based on the results of the gravity forward modelling and field results, the microgravity method is highly recommended for use in underground cavity detection in the coal mine environment. The modelling proves that microgravity may be successfully applied to solve the following problems:

- Mapping the bords and pillars of ultra-shallow (<6m deep) old workings in ultra-high resolution (<5m station intervals) surveys.
- Detecting the edge of water- or air-filled old workings to maximum depths of 50m and 150m, respectively.
- Resolving the edges of old workings on two different coal seams to a minimum horizontal separation of 30m for shallow seams or 90m for deeper seams.
- Detecting large (6m diameter), air-filled ratholes to a maximum depth of 12m.
- Detecting large (6m diameter), water- or sediment-filled ratholes to a maximum depth of 9m.
- Detecting small (3m diameter), air-filled ratholes to a maximum depth of 9m.
- Detecting small (3m diameter), water- or sediment-filled ratholes to a maximum depth of 6m.
- Detecting a cluster of ratholes to great depths depending on the size of the cluster and its density contrast with the host rock.

The forward modelling discussed in this report usually involved the best case scenario. The effect of a less dense overburden and local variations within the overburden was not considered here. Also, only reasonably large areas of old workings were modelled. Smaller volumes of old workings may yield lower amplitude gravity responses. Specific densities were assumed for the coal and host rock in the forward models calculated in this report. Although these densities are typical of coal mine environments, different density contrasts will yield slightly different responses. Therefore, it is recommended that forward modelling be performed prior to all microgravity field surveys, using the specific geologic parameters of the survey area to provide an understanding of the responses which are likely to be obtained in that environment and to aid in the interpretation of the data acquired.

It should always be borne in mind that real data is susceptible to noise and the detectability of targets would be poorer in a real field environment than predicted by numerical modelling.

The conclusions of the two case histories discussed in this report have not yet been tested by drilling. It is essential to obtain geological information over these survey areas to confirm the interpretations so that the results can aid the interpretation of microgravity data collected in future surveys.

7 REFERENCES

Ballard, R. F. 1983. Cavity detection and delineation research, Report 5, Electromagnetic (radar) techniques applied to cavity detection. Tech. Rept. GL-83-1, *U. S. Army Engineer Waterways Experiment Station*, CE, Vicksburg, MS.

Bristow, C. M, 1966. A new graphical resistivity technique for detecting air-filled cavities. *Studies in Speleology*, V. 1, Part 4, 204-227.

Butler, D. K. 1980. Microgravimetric techniques for geotechnical applications. Miscellaneous Paper GL-80-13, *U. S. Army Engineer Waterways Experiment Station*, CE, Vicksburg, MS.

----- . 1983. Cavity detection research, Report 1, Microgravimetric and magnetic surveys, Medford Cave Site, Florida. Tech. Rept. GL-83-1, *U. S. Army Engineer Waterways Experiment Station*, CE, Vicksburg, MS.

Butler, D. K. and Murphy, W. L. 1980. Evaluation of geophysical methods for cavity detection at the WES Cavity Detection Facility. Tech. Rep. GL-80-4, *U.S. Army Engineer Waterways Experiment Station.*

Butler, D. K., Whitten, C. B., and Smith, F. L. 1983. Cavity detection research, Report 4, Microgravimetric survey, Manatee Springs Site, Florida. Tech. Rept. GL-83-1, *U. S. Army Engineer Waterways Experiment Station*, CE, Vicksburg, MS.

Cooper, S. S. 1983. Cavity detection and delineation research, Report 3, Acoustic resonance and self-potential applications – Medford Cave and Manatee Springs Sites, Florida. Tech. Rept. GL-83-1, *U. S. Army Engineer Waterways Experiment Station*, CE, Vicksburg, MS.

Curro, J. R. 1983. Cavity detection and delineation research, Report 2, Seismic methodology – Medford Cave Site, Florida. Tech. Rept. GL-83-1, *U. S. Army Engineer Waterways Experiment Station*, CE, Vicksburg, MS.

Frankenhauser, R. M., Kelly, A. M., and Budd, D. K. 1995. Ground penetrating radar: Application guidelines for the South African mining industry. 1st Ed, *CSIR Mining Technology Publication*, 89p.

Friedel, M. J., and Hanson, J. C. 1990. Integrated geophysical approach to abandoned mine detection. *Proceedings of the 12th Annual National Association of Abandoned Mine Land Programs (NAAMLP) Conference*, 16-20 September, Breckenridge, Colorado.

Lowry, T. and Shive, P. N. 1990. An evaluation of Bristow's method for the detection of subsurface cavities. *Geophysics*, v. 55, No. 5, 514-520.

Nagy D. 1966. The gravitational attraction of a right rectangular prism. *Geophysics* vol. 31 p362-p371.

Plouff D. 1976. Gravity and magnetic fields of polygonal prisms and Application to magnetic terrain corrections. *Geophysics* vol. 41 p727-p741

APPENDIX A

FIGURES

Figure 1: Close up view of the Lacoste and Romberg microgravimeter, in position at a measurement station

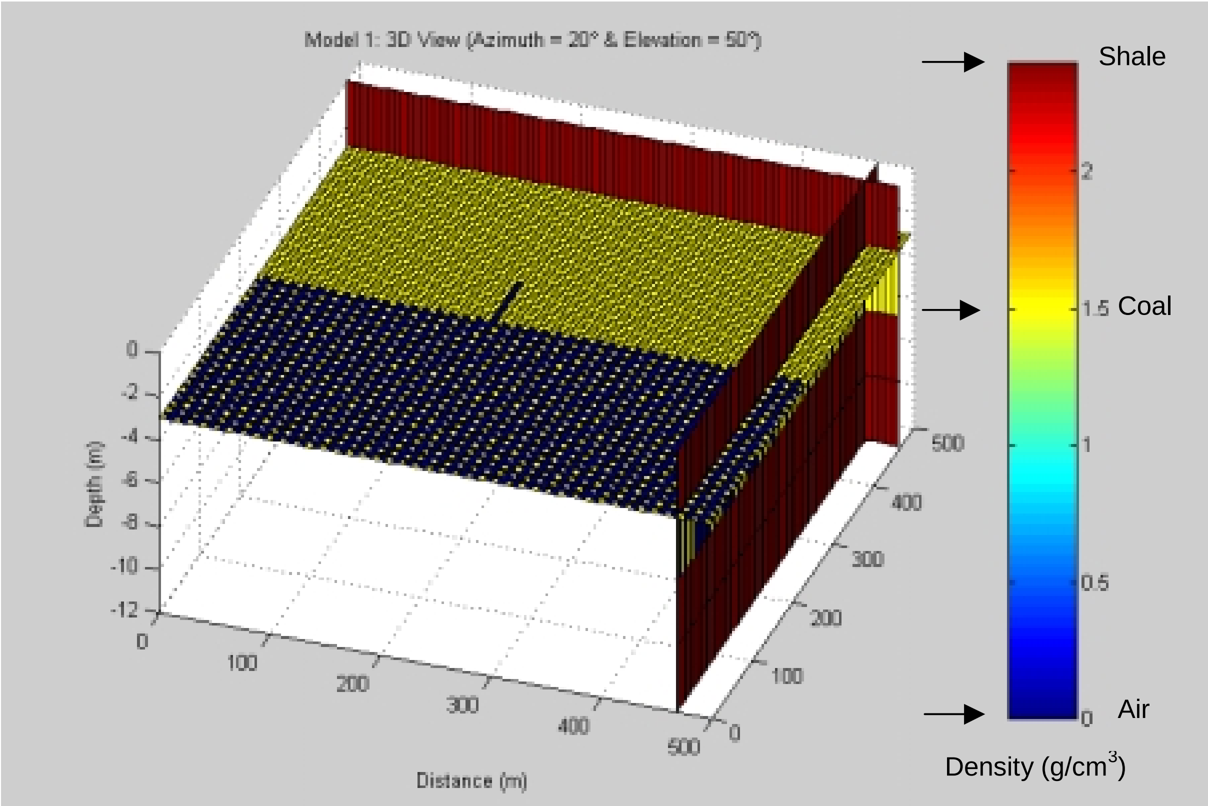

Figure 2: 3D view of the density distribution of Model 1. A partially mined-out coal seam (with density 1.5 g/cm^3) is placed in a shale host rock (of density 2.4 g/cm^3). The depth to the top of the seam is varied from 3m (Model 1a) to 9m (Model 1c) to determine if the individual bords and pillars (each 6x6x3m in size) of shallow mined-out areas may be resolved with the microgravity method. The mine workings are air-filled representing the best detection case.

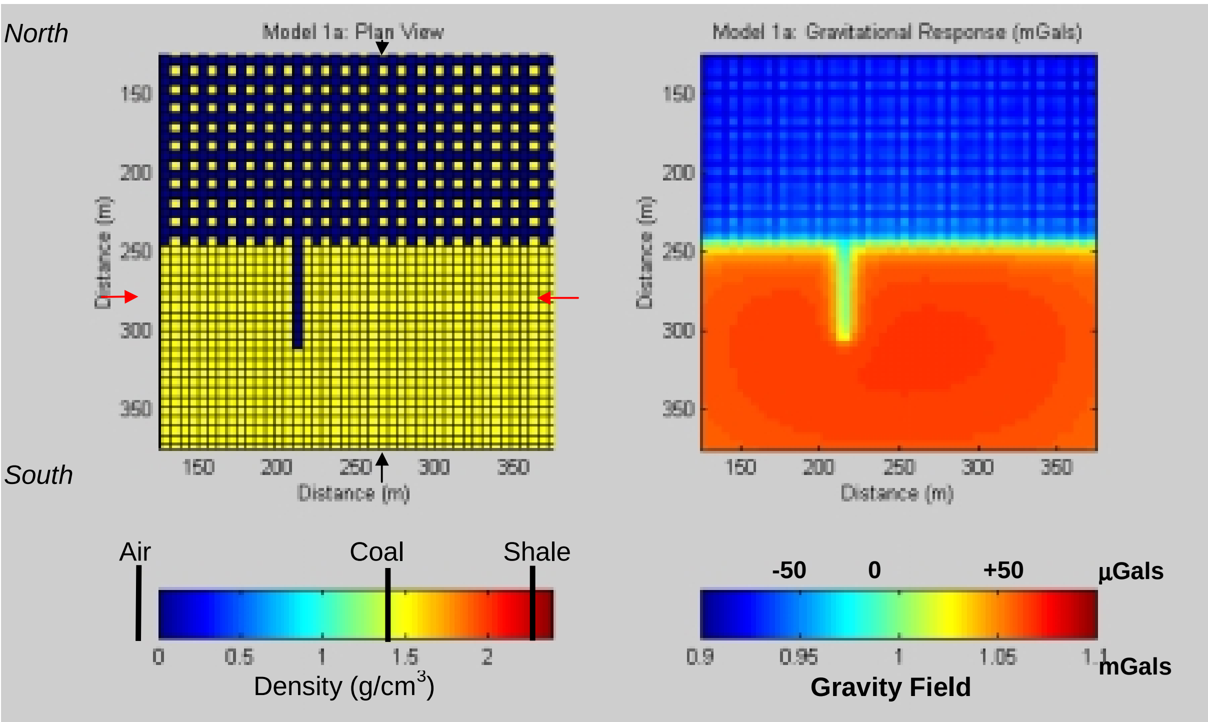

Figure 3: Plan view of Model 1a on the left with the gravitational response on the right. The depth to the top of the coal seam is 3m. In the south the coal is undisturbed while in the north it has been mined out leaving 6x6x3m residual coal pillars. An exploratory tongue extends into the unmined region at x=212m. Black and red arrows indicate approximate positions of profiles shown in Figures 4 and 5. Individual bords and pillars are observed in the gravity response. Some pillars produce a higher amplitude gravity response than others due to the spatial sampling provided by the grid.

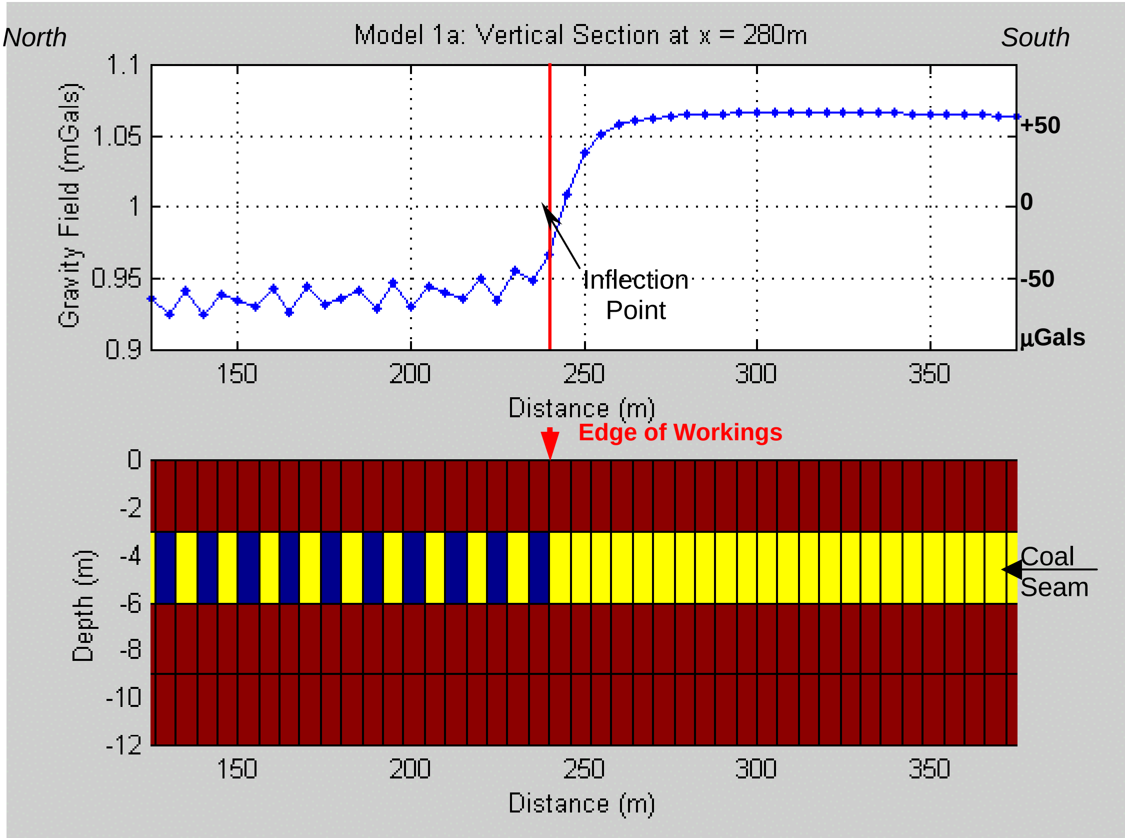

Figure 4a: North-South profile over Model 1a at x=280m, showing the gravitational response at 5m station intervals. A step decrease of 130 µGals occurs at the transition from unmined coal (south) to the mined-out workings (north). The edge of workings (red line and red arrow) occurs just south of the inflection point between the high and low of the gravity response. The coal pillars form irregular anomalies with a maximum peak-to-peak amplitude of 21 µGals. Where the measurement station is located near the centre of a pillar or air-filled tunnel a larger anomaly is obtained than when the station is located over the edge of a pillar.

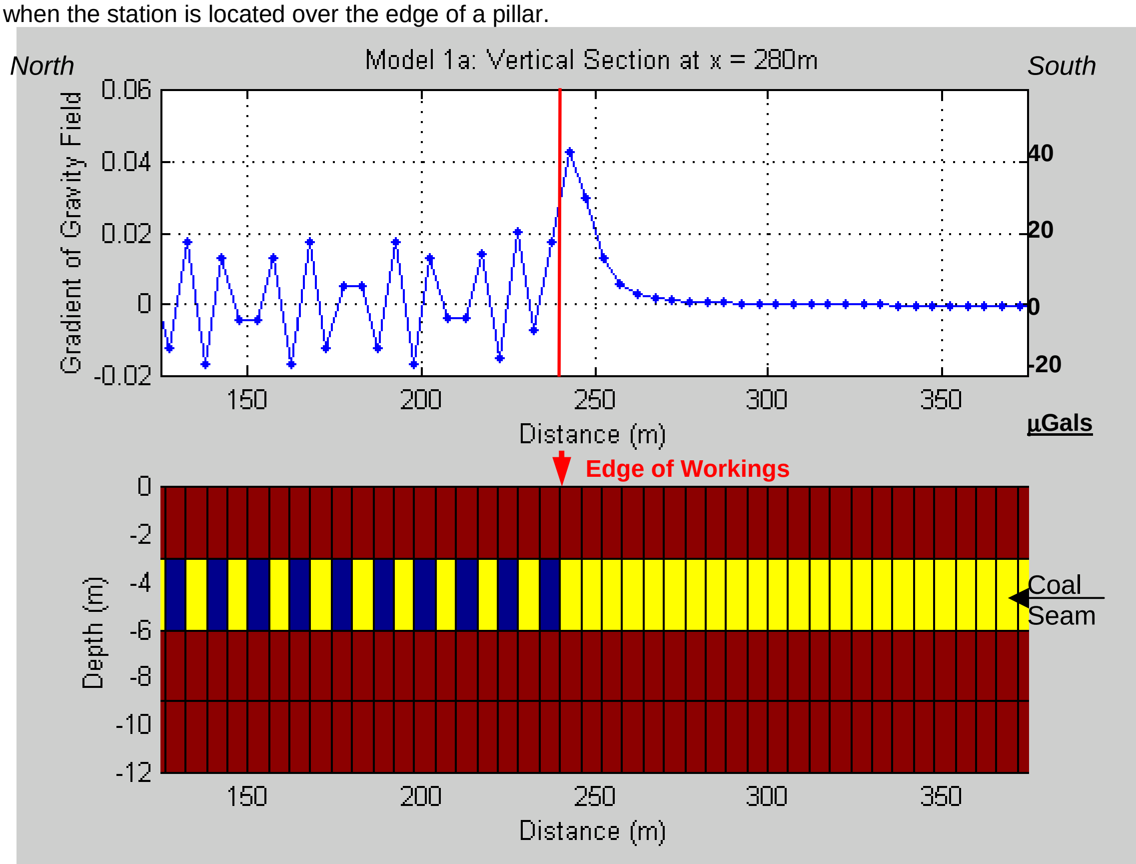

Figure 4b: Horizontal gradient (in µGals/ sampling interval) of the gravity response in Figure 4a. A high, corresponding to the position of the inflection point in the gravity response, is obtained in the gradient. This high is shifted by about 2m towards the workings. The red line and arrow shows the position of the edge of workings.

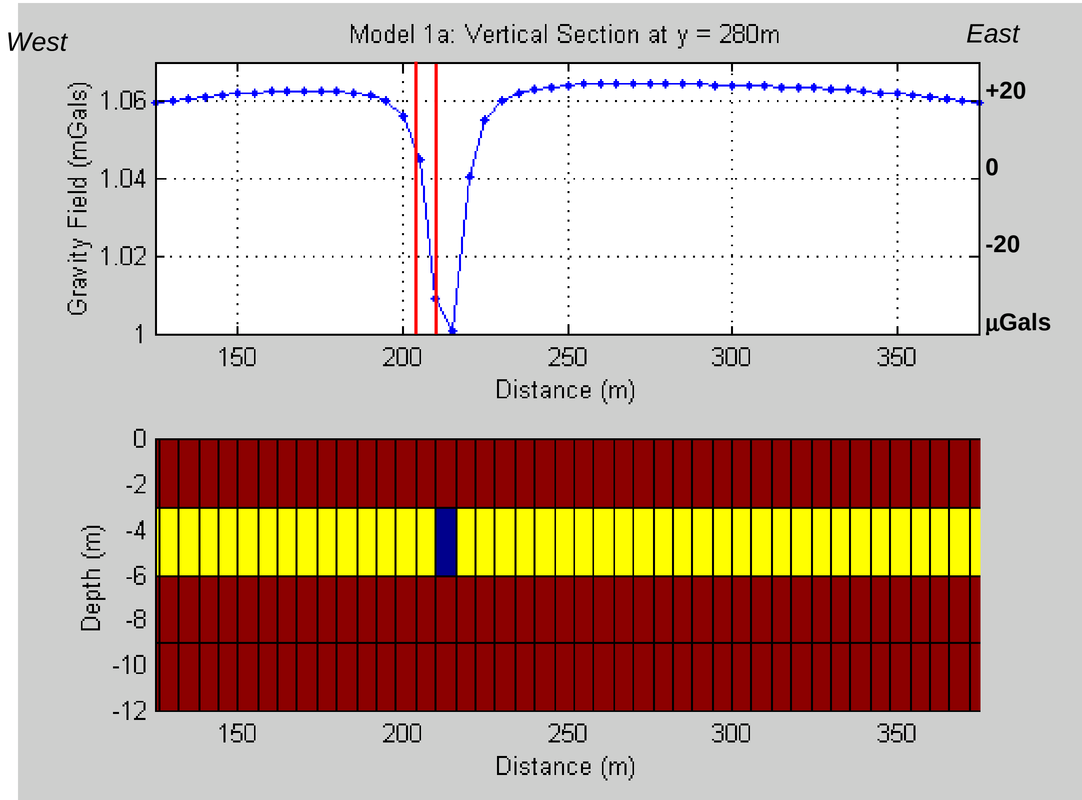

Figure 5a: West-east profile over Model 1a at y=280m, showing the gravitational response at 5m station intervals over the exploratory tongue extending into the unmined area. A gravity anomaly of 63 µGals occurs over the air-filled tongue when the depth to the top of the coal seam is only 3m. Red lines indicate tongue edges.

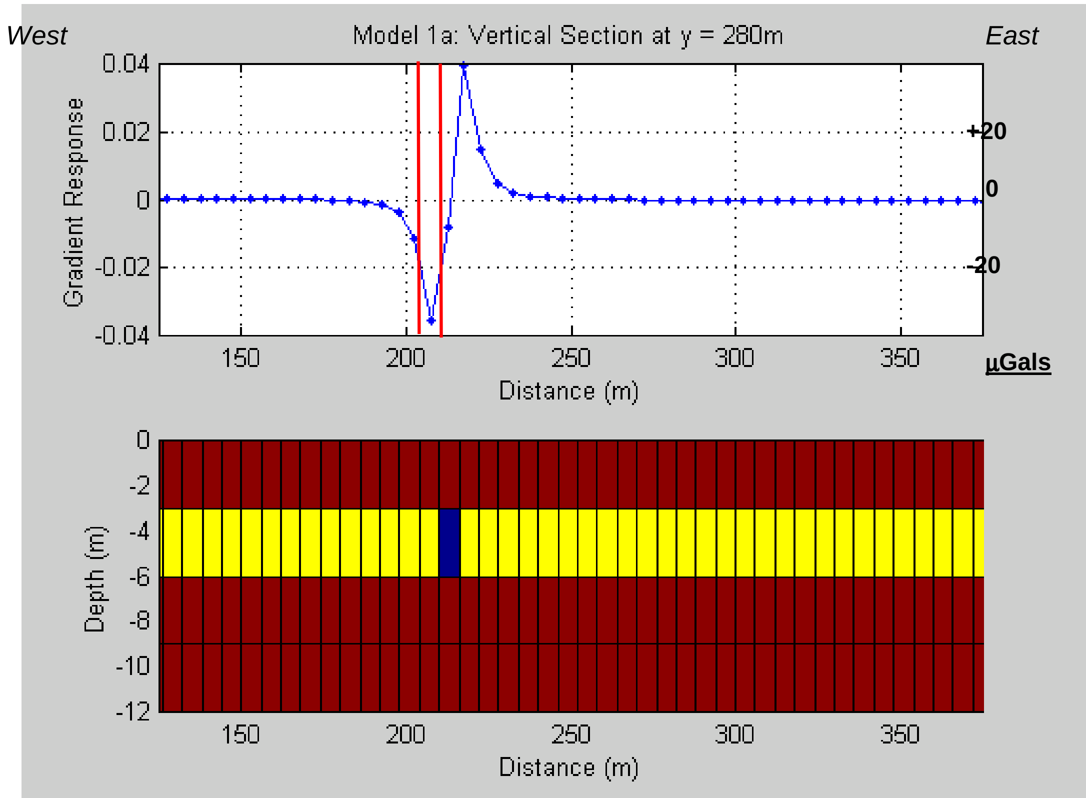

Figure 5b: Horizontal gradient of the gravity response in Figure 5a. A high/ low pair occurs over the tunnel in the gradient response. The high is positioned directly above the eastern edge of the tunnel but the low occurs about 2m west of the western edge. Red lines indicate tongue edges.

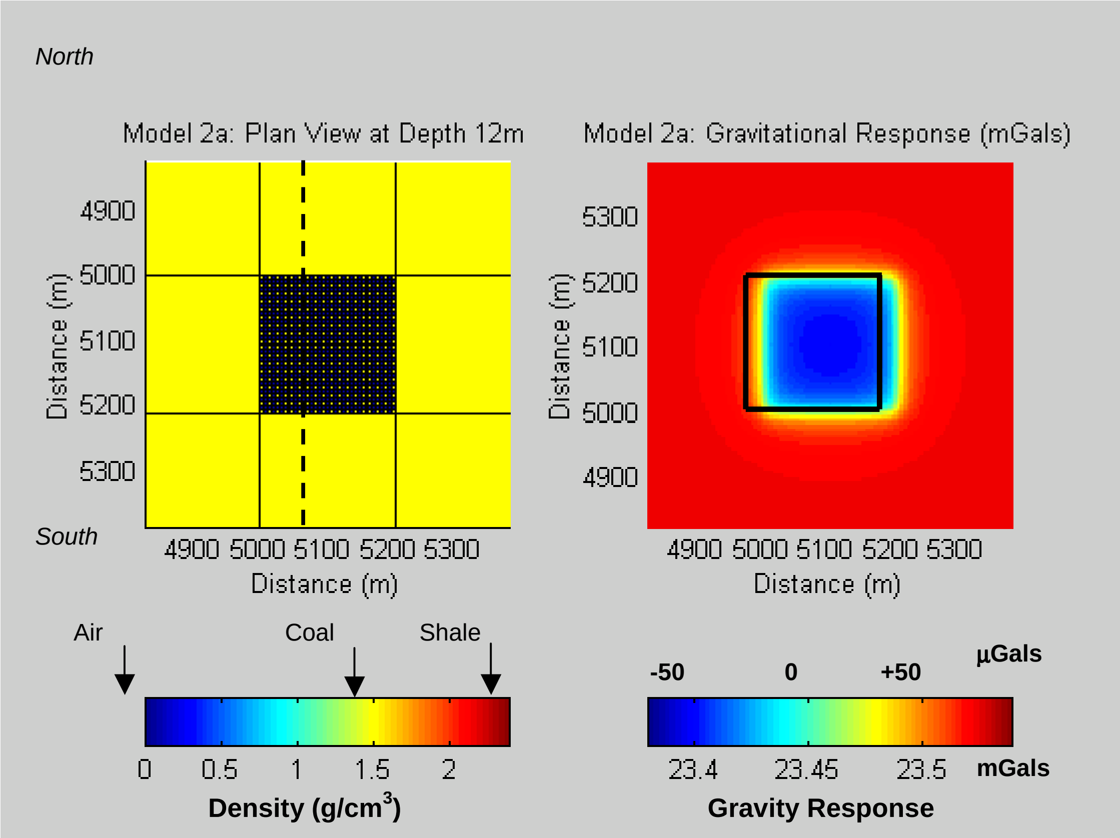

Figure 6a: Plan view of Model 2a at a depth level of 12m (left), showing air-filled old workings (210x210m) surrounded by unmined coal and its gravity response (right). A gravity low occurs over the workings. The edge of the workings are quite accurately defined by the gravity response. The dashed line in the left figure shows the position of the vertical section shown in Figure 7.

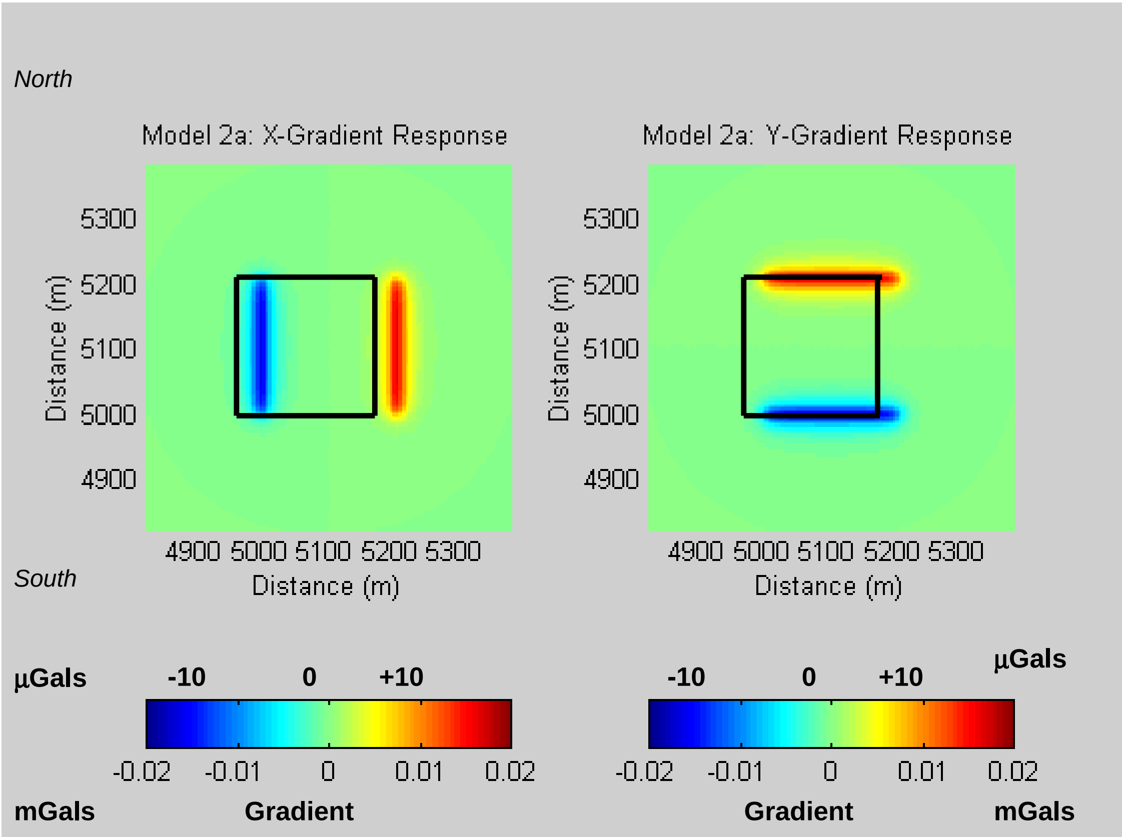

Figure 6b: Horizontal gradient of the gravity response in Figure 6a in the x (left figure) and y (right figure) directions respectively with the edge of the workings superimposed above the grid (black square outline).

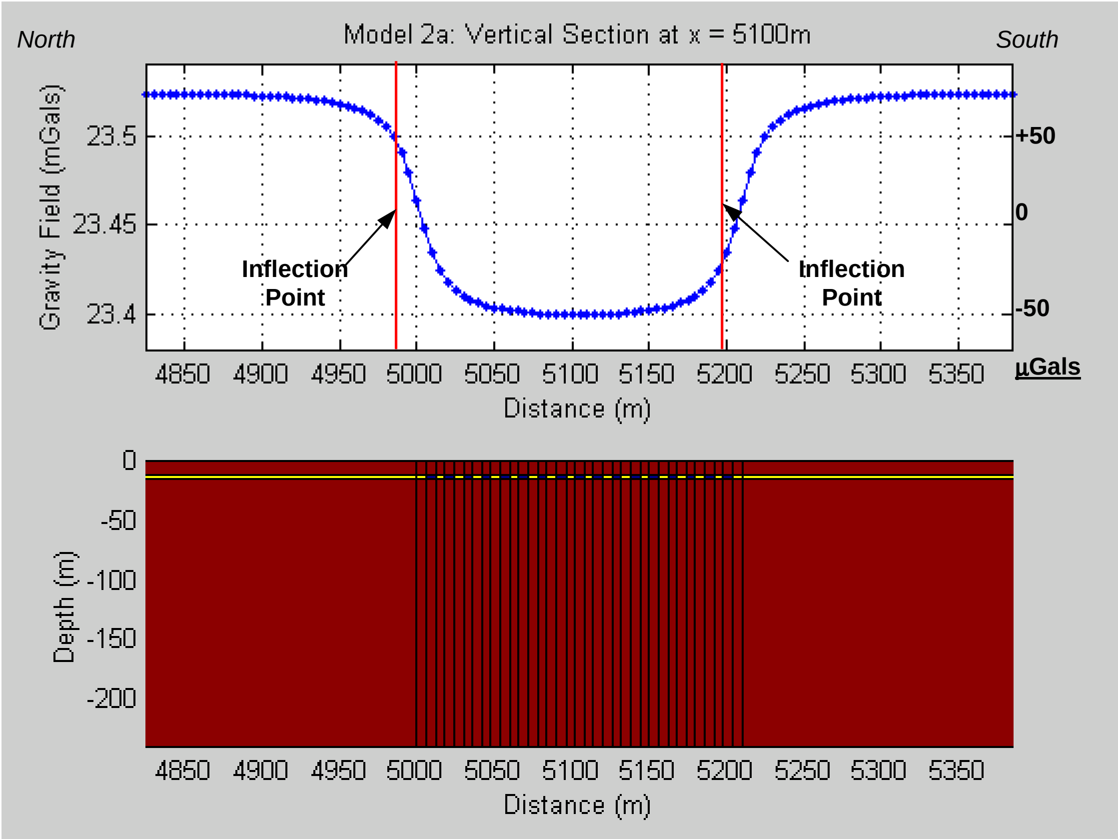

Figure 7a: North-South profile across Model 2a at x = 5100m. The coal seam occurs at a depth of 12m. A symmetrical gravity low of amplitude 124 µGal occurs over the workings. The position of the inflection points between the high and the low (black arrows) correspond to the position of the northern and southern edge of the workings (red lines).

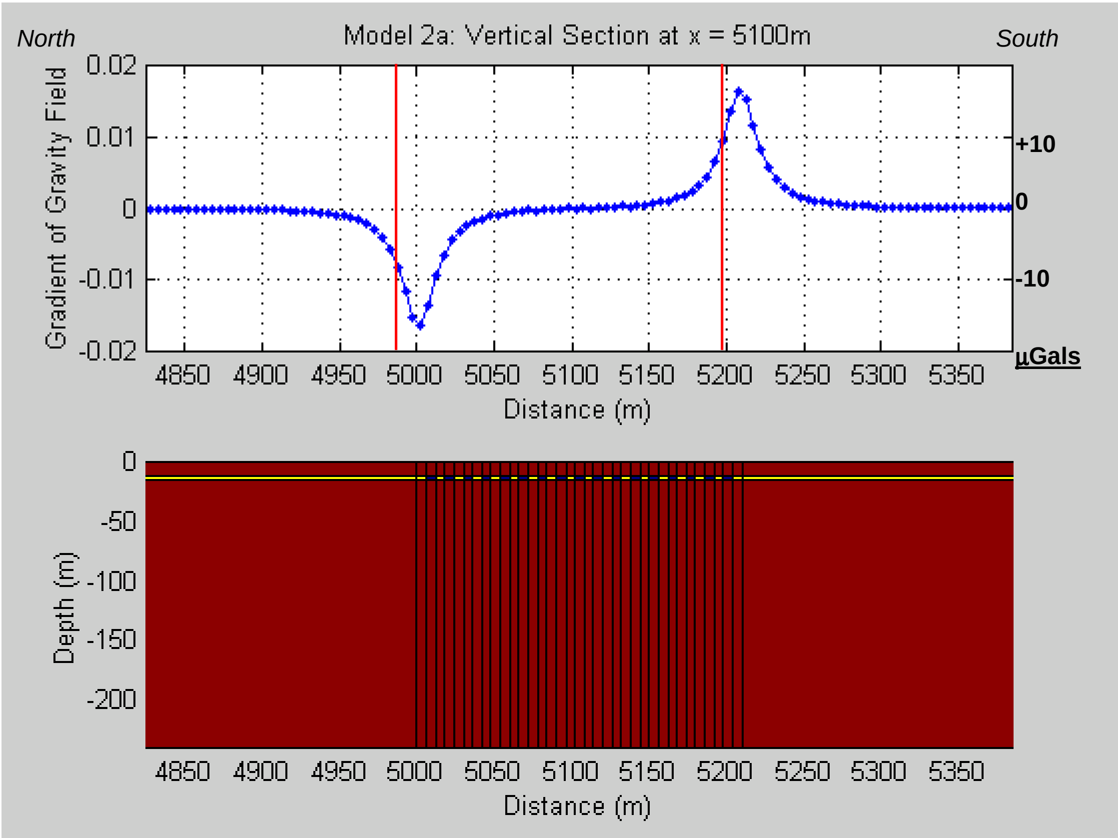

Figure 7b: Horizontal gradient of the gravity response in Figure 7a. A low and a high, corresponding to the position of the inflection points in the gravity response, is obtained in the gradient over the northern and southern edges of the old workings (solid red line), respectively.

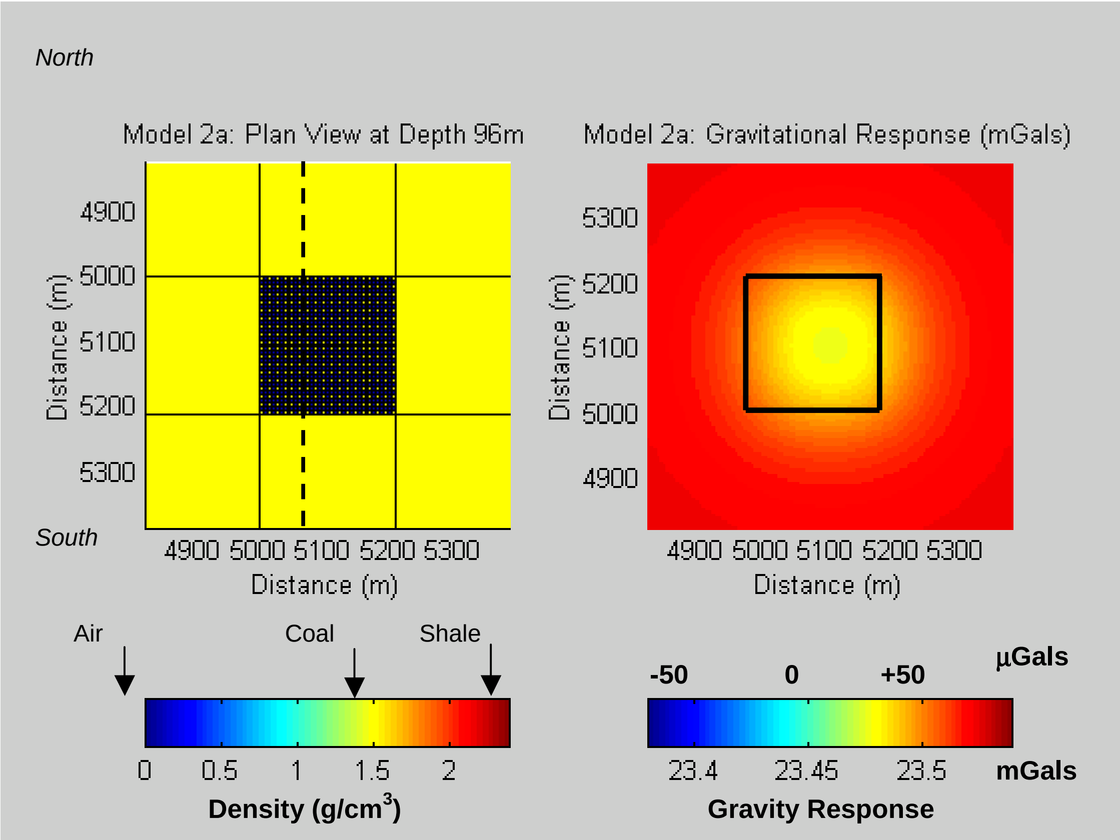

Figure 8a: Plan view of Model 2a at a depth level of 96m (left), showing old workings surrounded by unmined coal and its gravity response (right). A gravity low occurs over the workings but the edge of the workings are not very accurately defined. The dashed line in the left figure shows the position of the vertical section shown in Figure 9.

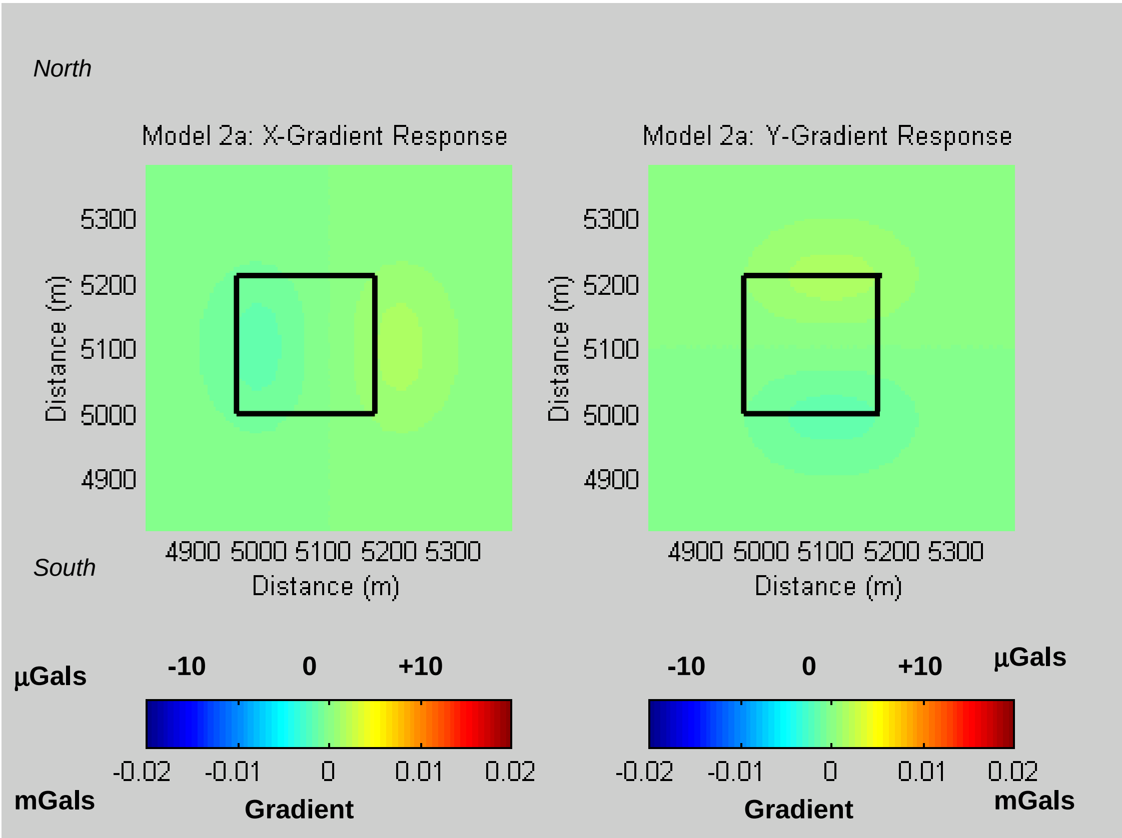

Figure 8b: Horizontal gradient of the gravity response in Figure 8a in the x (left figure) and y (right figure) directions respectively with the edge of the workings superimposed above the grid (black square outline).

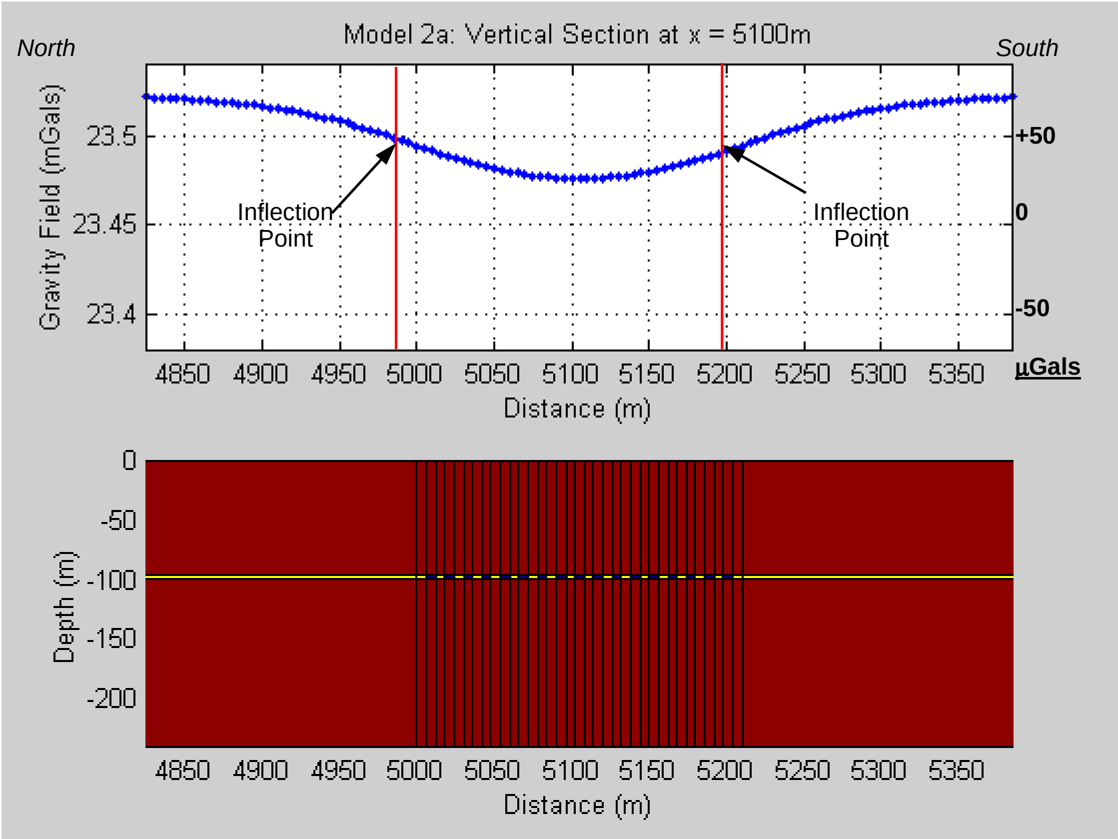

Figure 9a: North-South profile across Model 2a at x = 5100m. The coal seam occurs at a depth of 96m. A symmetrical gravity low of amplitude 47 µGal occurs over the workings The position of the inflection points between the high and the low (black arrows) correspond to the position of the northern and southern edge of the workings (red lines).

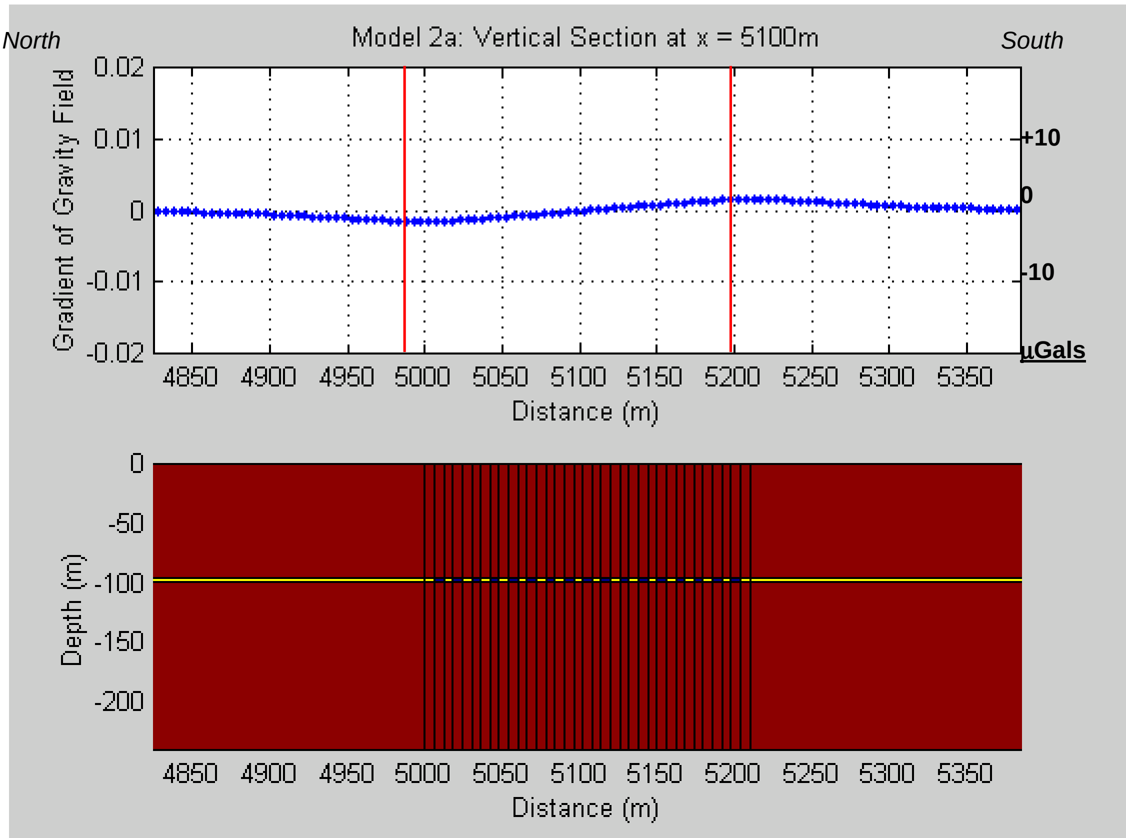

Figure 9b: Horizontal gradient of the gravity response in Figure 9a. A low and a high, corresponding to the position of the inflection points in the gravity response, is obtained in the gradient over the northern and southern edges of the old workings (solid red line), respectively.

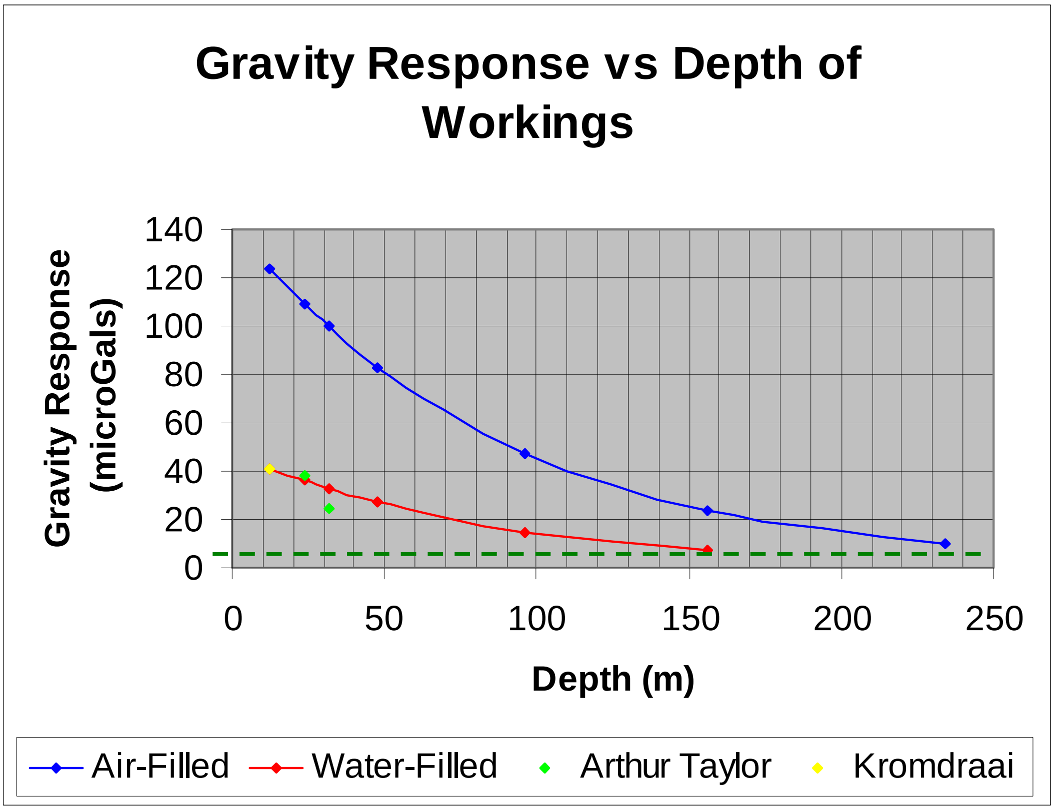

Figure 10: Plot of the gravity response of the edge of old workings versus increasing depth to the top of the coal seam (using the values of Table 5). The limit of detection of the microgravity method (6 µGals) is shown as a green dashed horizontal line. The results of the two Case Studies at Arthur Taylor and Kromdraai Collieries, to be discussed in later sections, are plotted for comparison.

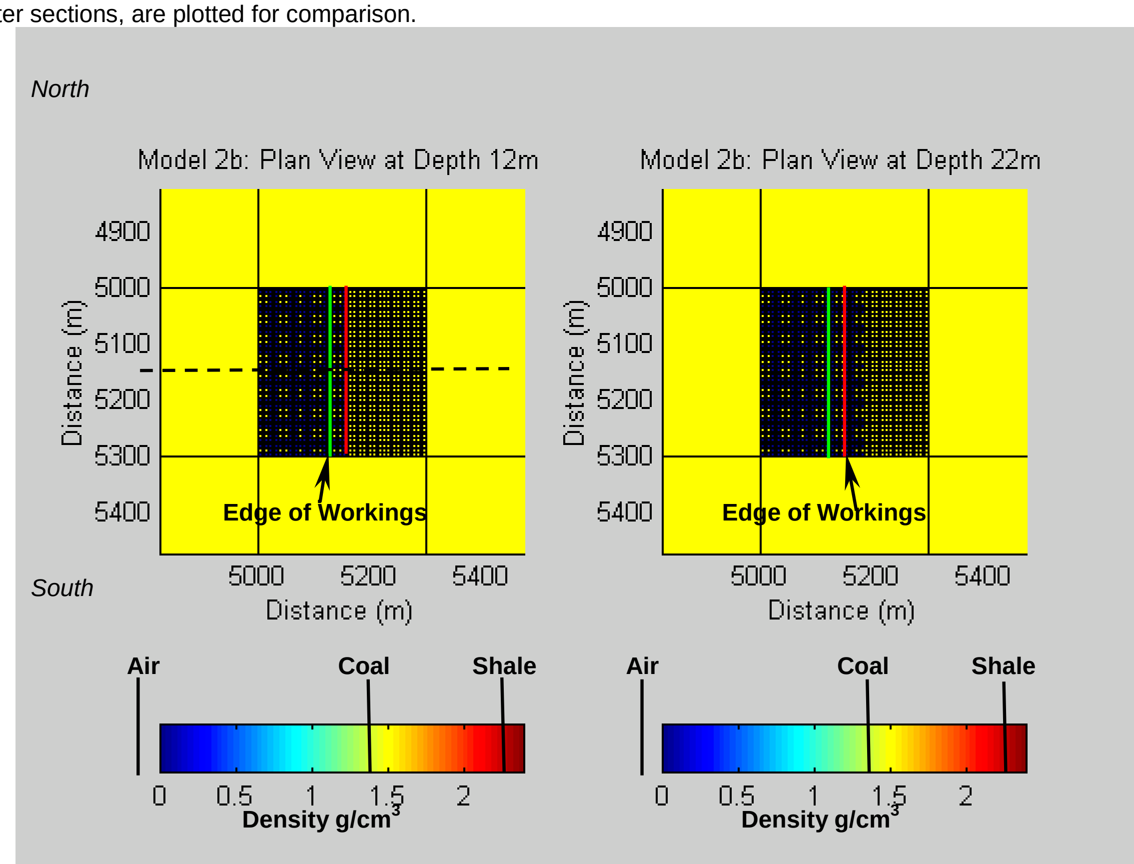

Figure 11: Plan view of Model 2b showing old workings at two different depths (12m and 22m). The edge of workings for the shallow seam is shown in green and for the deeper seam in red. There is a 30 m horizontal distance between the two edges. Variations of this model involve changes in the depths to the coal seams and the horizontal distances between the edge of workings. The black dashed line indicates the approximate position of the profile shown in Figures 13, 15 and 17.

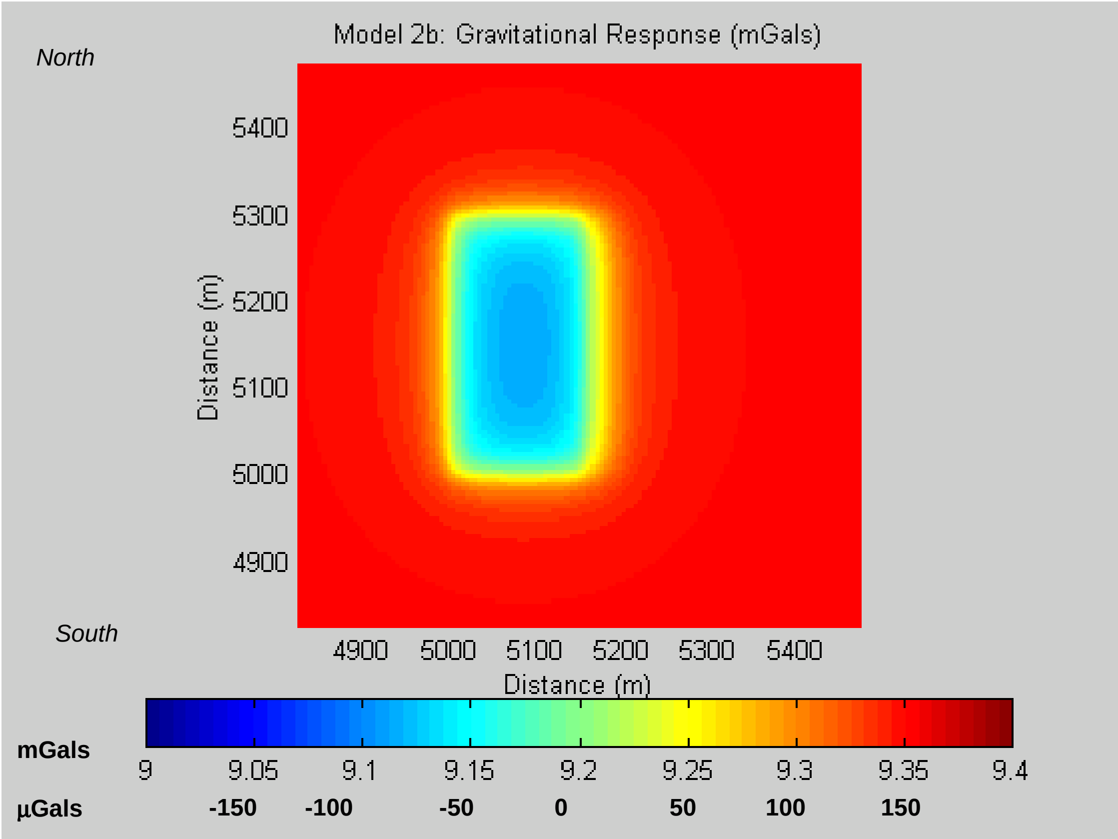

Figure 12a: Gravity Response of Model 2b, for seams buried at 12m and 22m, with a horizontal distance between the workings of 30m. A large negative response occurs over the area where both seams have been mined. The eastern edge of this anomaly is not as sharp as the western edge due to interference from the response over the edge of the deeper workings.

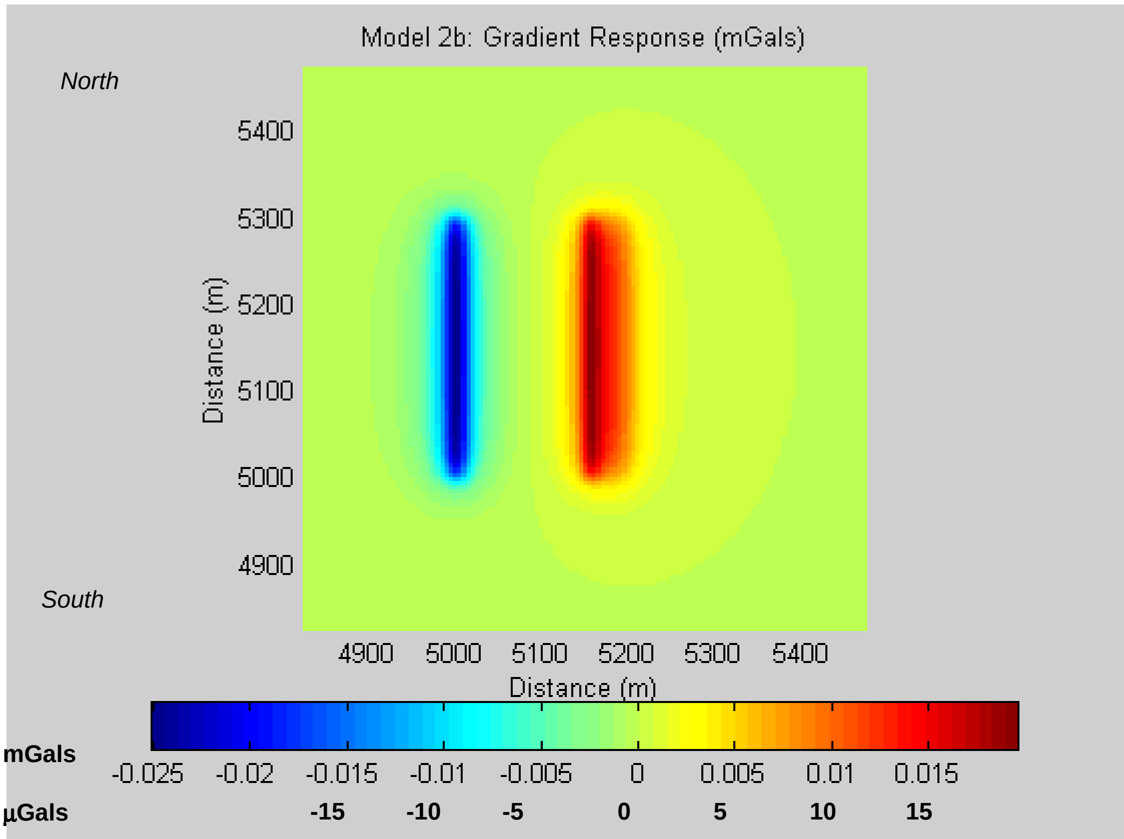

Figure 12b: Horizontal gradient of the gravity response in Figure 12a. The edge of workings on the upper seam is clearly delineated by high and low anomalies. The high is asymmetric suggesting the presence of another edge in the east but not quite resolving the position of this second edge.

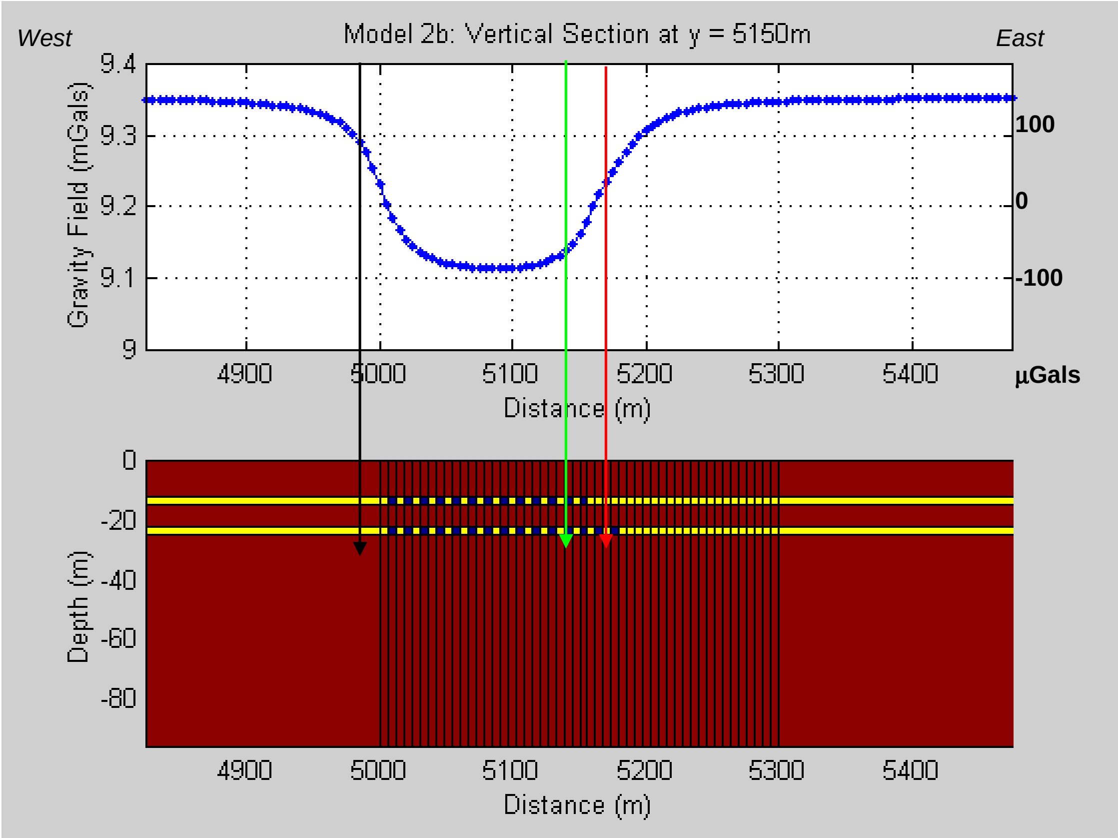

Figure 13a: West-East gravity profile across Model 2b (at y=5150m) in which two coal seams are buried at 12m and 22m and their edges are separated by a 30m horizontal distance. A large gravity low (238 µGals) occurs over the area in which both seams have been mined. The anomaly is asymmetric with a more gradual slope in the east due to the contributions from the shallow (green line) and deeper (red line) edges of the old workings. The black line indicates the western edge of both seams.

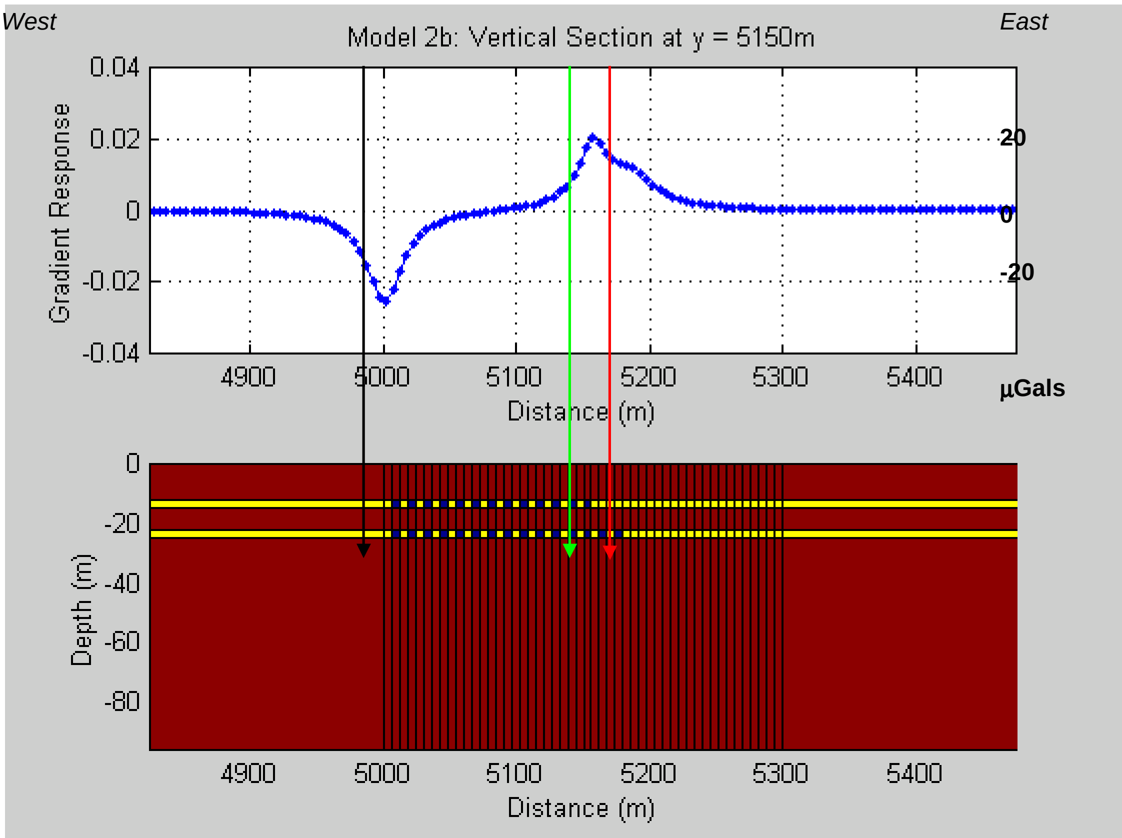

Figure 13b: The horizontal gradient of the gravity response in Figure 13a. A low occurs over the common western edge of both workings (black line). An asymmetric high occurs over the eastern edge of the shallow workings (green line) with a shoulder which indicates the position of the edge of the deeper seam (red line).

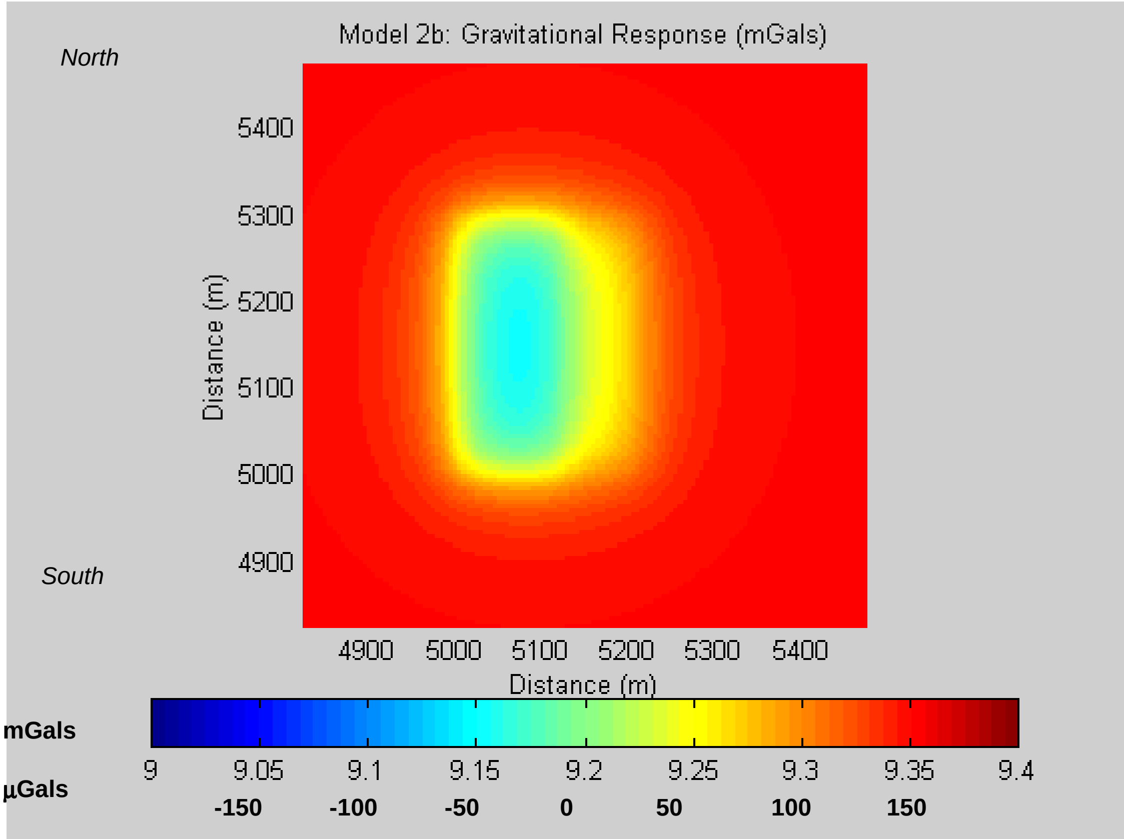

Figure 14a: Gravity Response of Model 2b, for seams buried at 27m and 37m, with a horizontal distance between the workings of 90m. A large negative response occurs over the area where both seams have been mined. The eastern edge of this anomaly has a more gradual slope than the western edge due to the deeper workings.

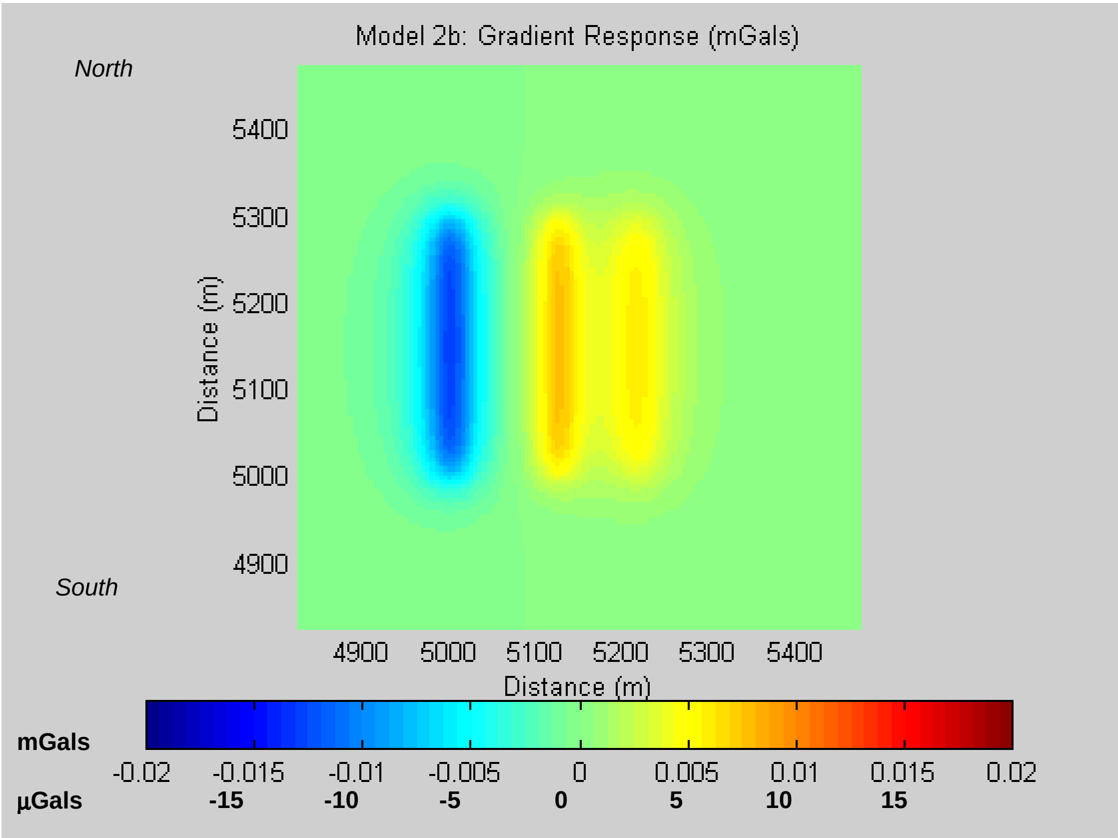

Figure 14b: Horizontal gradient of the gravity response in Figure 14a. The edge of workings on the upper seam is clearly delineated by a low (in the west) and a high (in the east). The eastern-most, weakest high represents the eastern edge of the deeper workings.

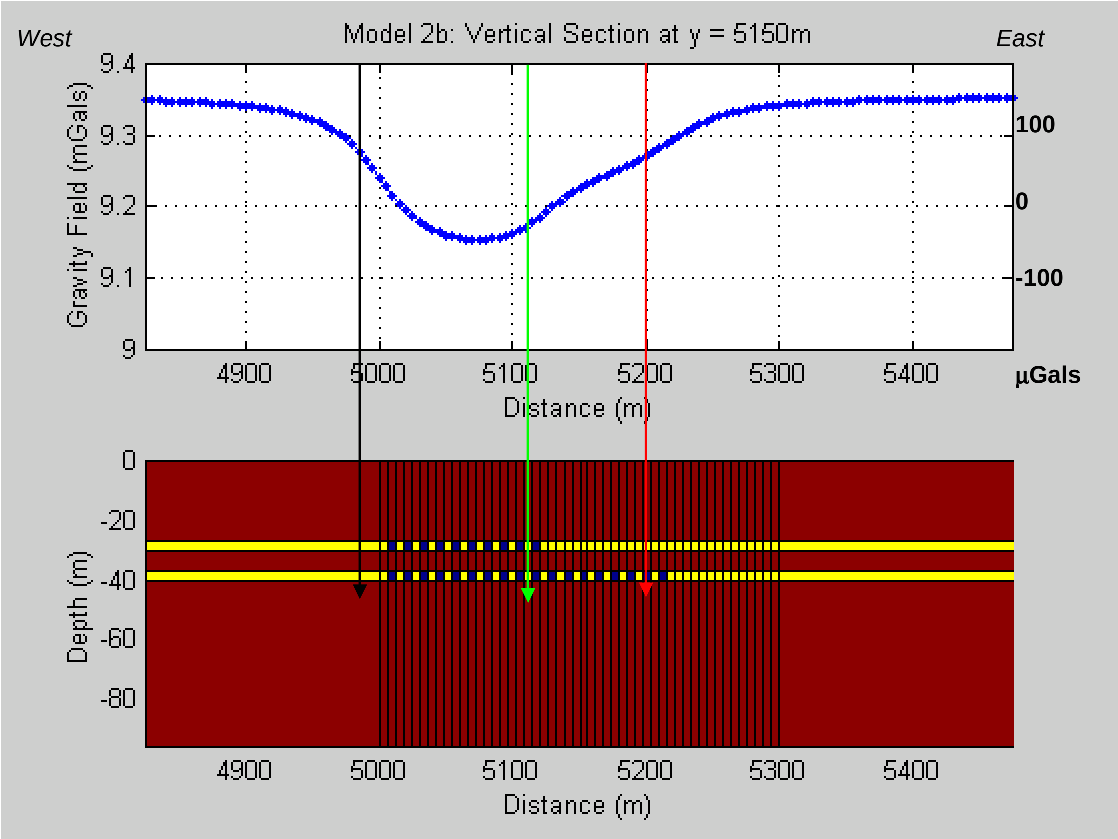

Figure 15a: West-East gravity profile across Model 2b (at y=5150m) in which two coal seams are buried at 27m and 37m and are separated by a 90m horizontal distance. A large gravity low (198 µGals) occurs over the area in which both seams have been mined. The more extensive workings of the deeper seam cause this low to be very asymmetric with a more gradual slope on its eastern side. (Annotations as for Figure 13)

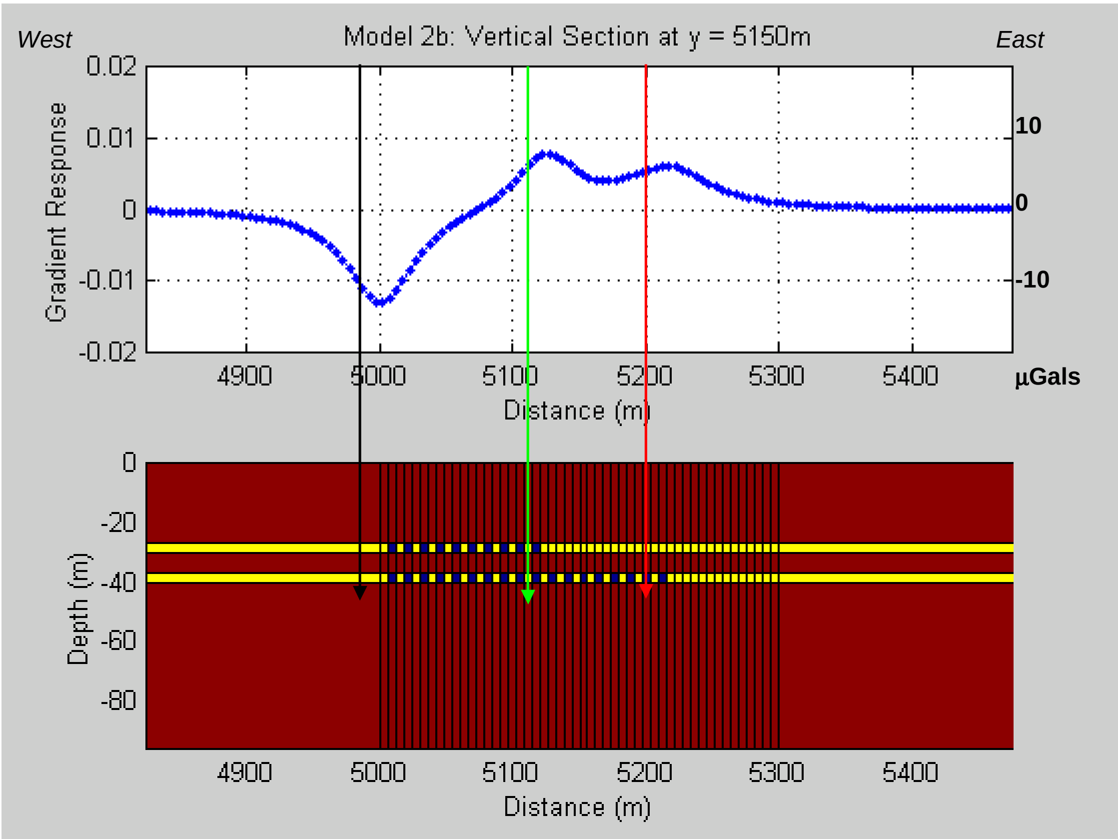

Figure 15b: Horizontal gradient of the gravity response in Figure 15a. The western edge of workings is clearly delineated by a low while the eastern edges of both coal seams produce distinct highs. The amplitude of the anomaly of the deeper seam is lower than that of the upper seam. (Annotations as for Figure 13).

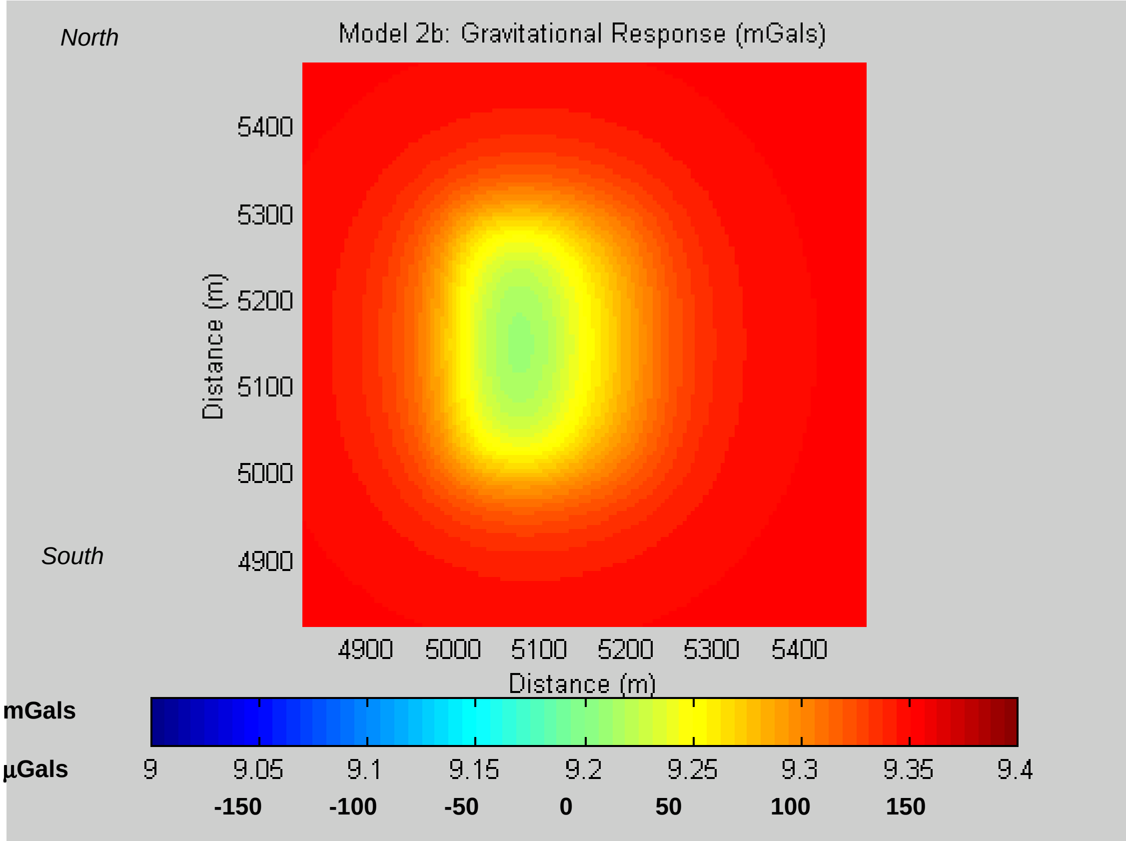

Figure 16a: Gravity Response of Model 2b, for seams buried at 56m and 66m, with a horizontal distance between the workings of 90m. A negative response occurs over the area where both seams have been mined. The eastern edge of this anomaly has a slightly more gradual slope than the western edge due to the deeper workings.

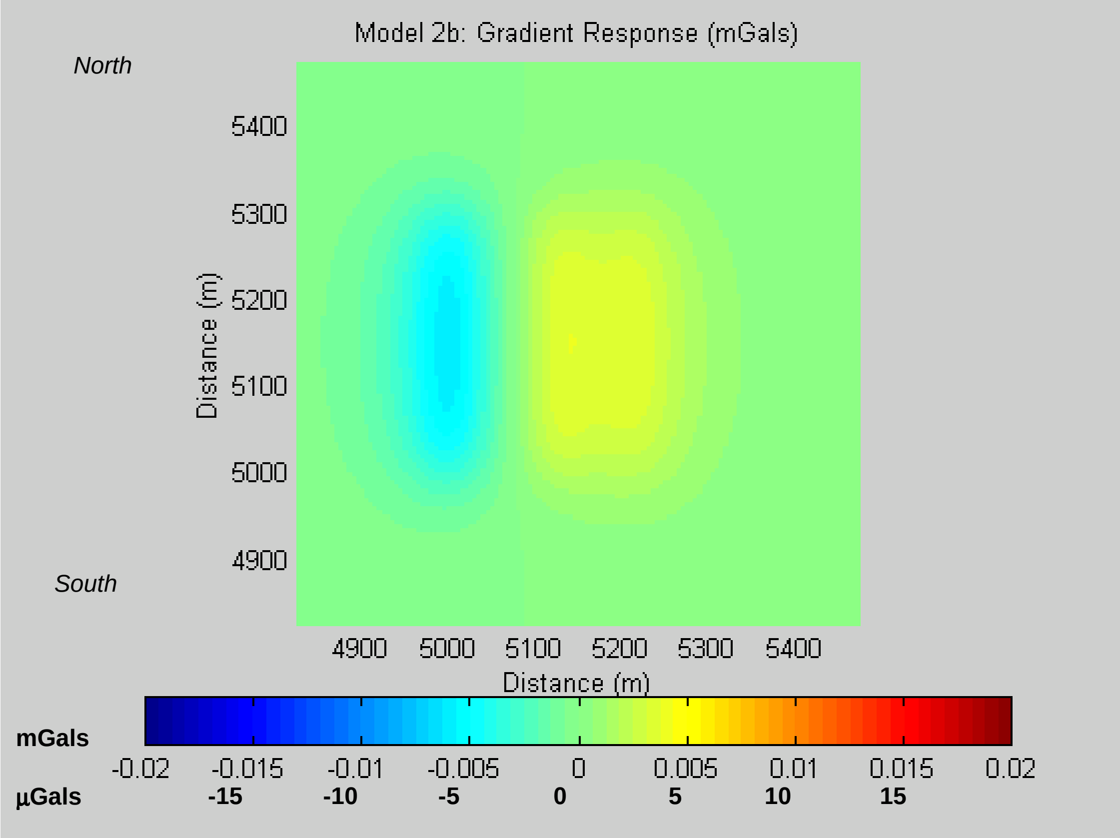

Figure 16b: Horizontal gradient of the gravity response in Figure 16a. The edge of workings is delineated by a broad low in the west and a very broad, double-lobed high in the east. The eastern-most lobe of this high represents the eastern edge of the deeper coal seam.

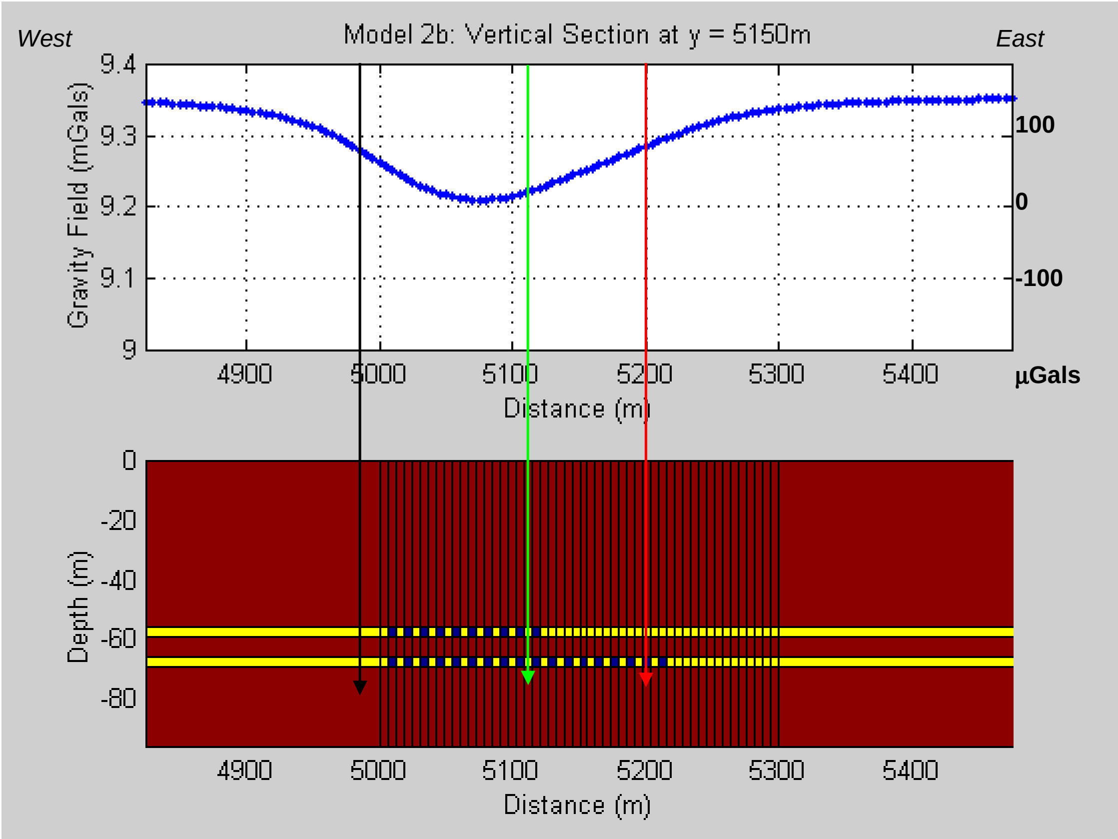

Figure 17a: West-East gravity profile across Model 2b (at y=5150m) in which two coal seams are buried at 56m and 66m and are separated by a 90m horizontal distance. A large gravity low (142 µGals) occurs over the area in which both seams have been mined. The response is asymmetrical with a more gradual slope in the east due to the presence of the deeper seam.

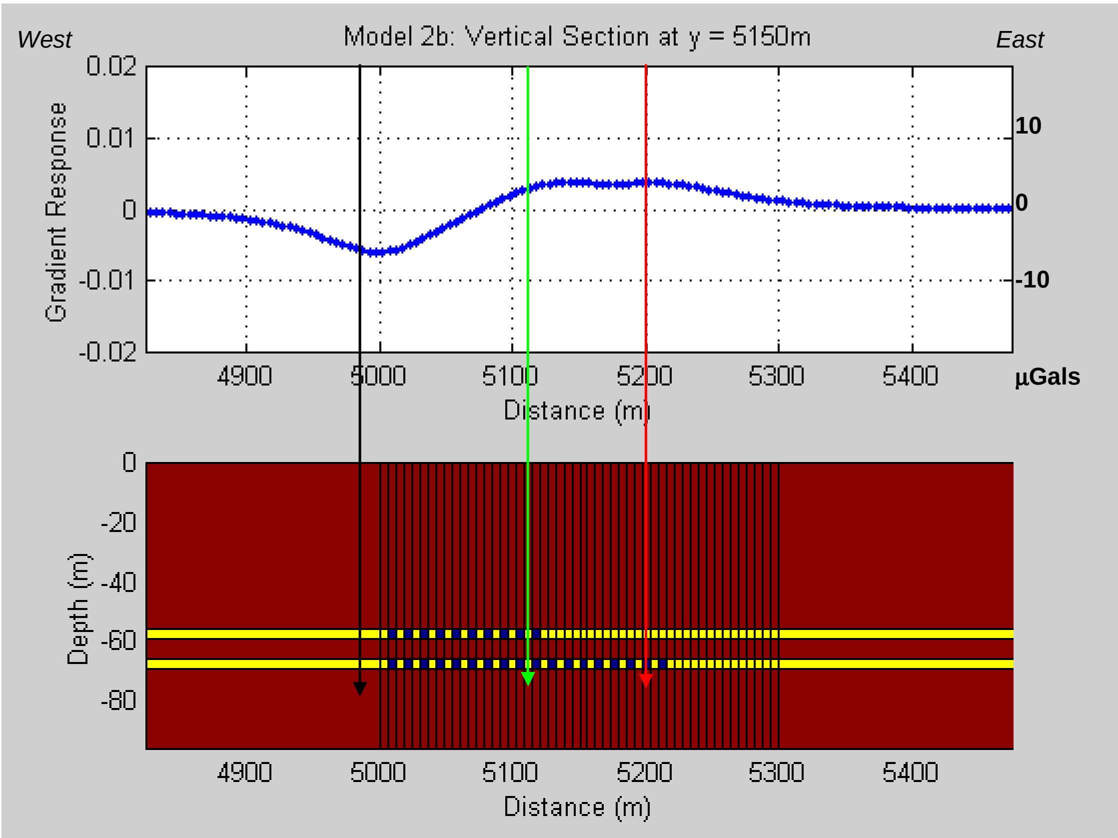

Figure 17b: Horizontal gradient of the gravity response in Figure 17a. The western edge of workings is clearly delineated by a broad low while the eastern edges of both coal seams produce broad, low amplitude highs, just distinguishable from each other.

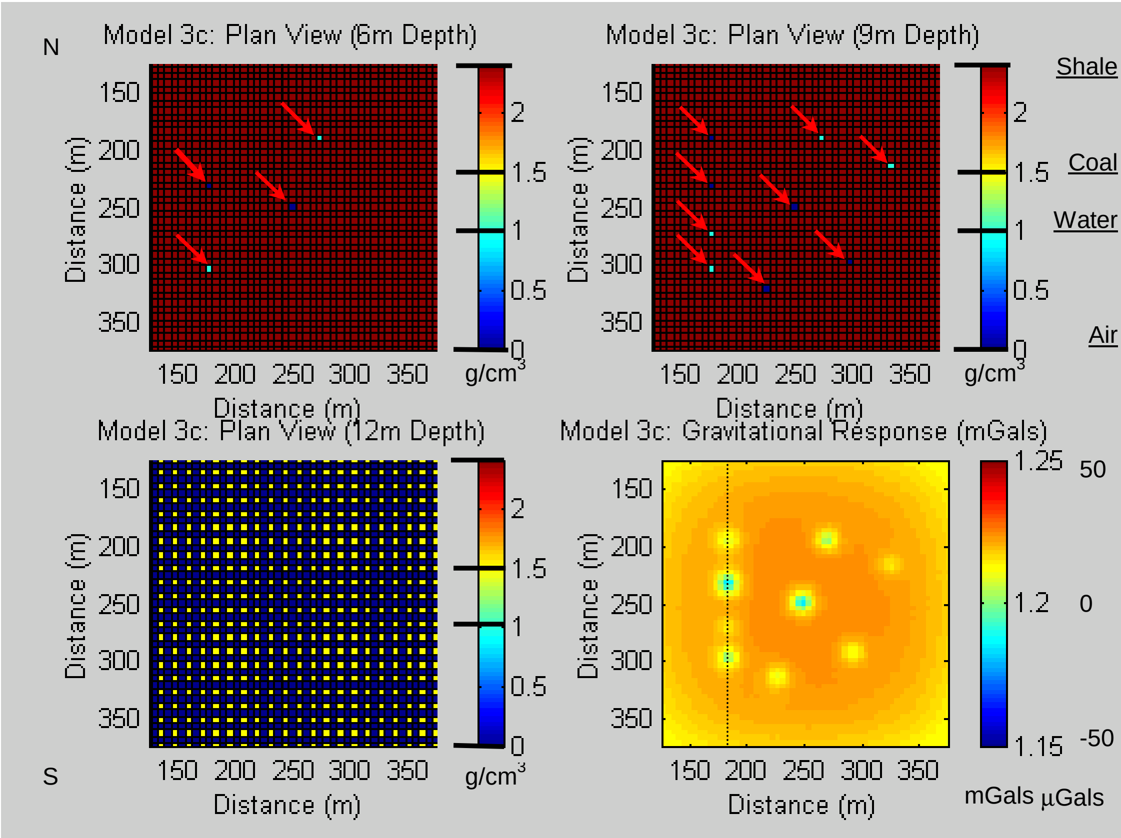

Figure 18: Plan views of Model 3c at depths of 6, 9 and 12 m. The depth to the top of the old workings is 12m. A scattered set of 6m diameter air or water/ sediment filled ratholes extend up from the mined tunnels to various depths below the surface (indicated by red arrows). Some of the ratholes extend up to 6m below the surface, while others only extend to 9m below the surface (see Figure 19a). The gravitational response shows negative 'bulls-eye' anomalies of varying intensity over each isolated rathole. The 4 shallowest ratholes have the highest amplitude response. A North-South profile at x=180m (shown by the dotted line) is presented in Figure 19a.

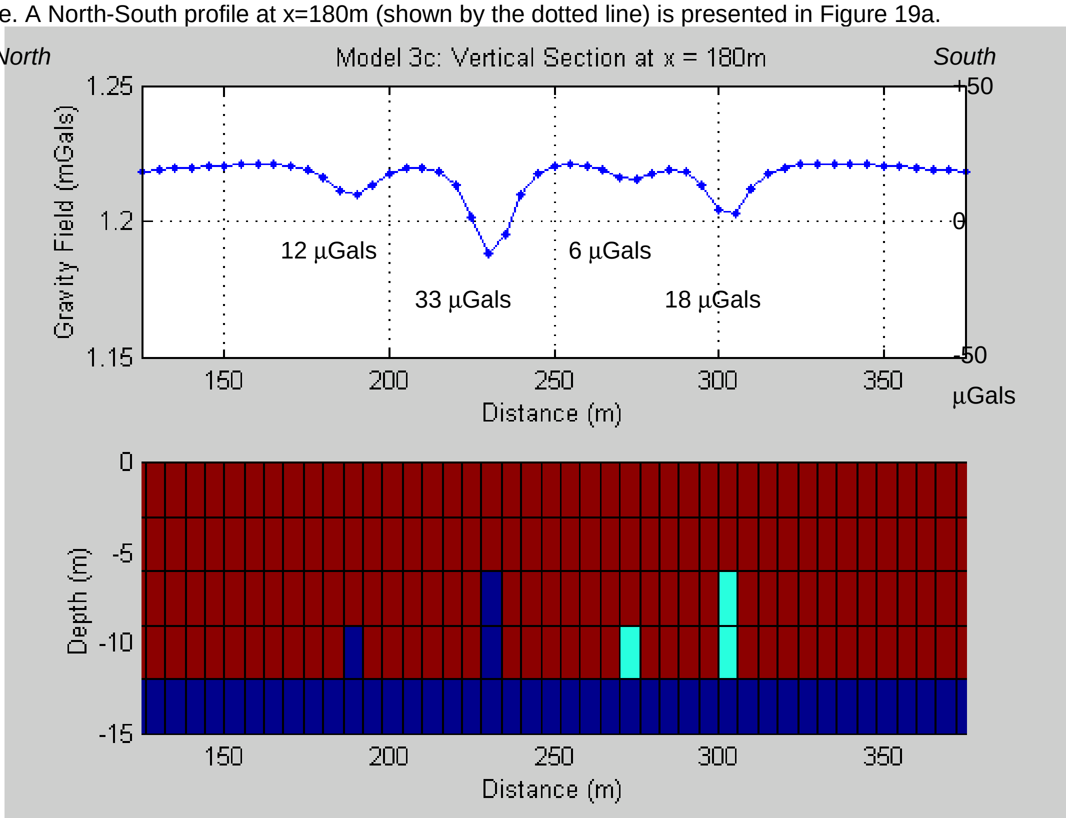

Figure 19a: Vertical North-South section through Model 3c at x=180m, directly over 'ratholes' developing into the roof of the air-filled tunnel of the old workings (dotted line in Figure 18). The individual ratholes produce anomalies of variable amplitude depending on their size, depth below surface and density as shown on the profile. Water-filled ratholes are light blue.

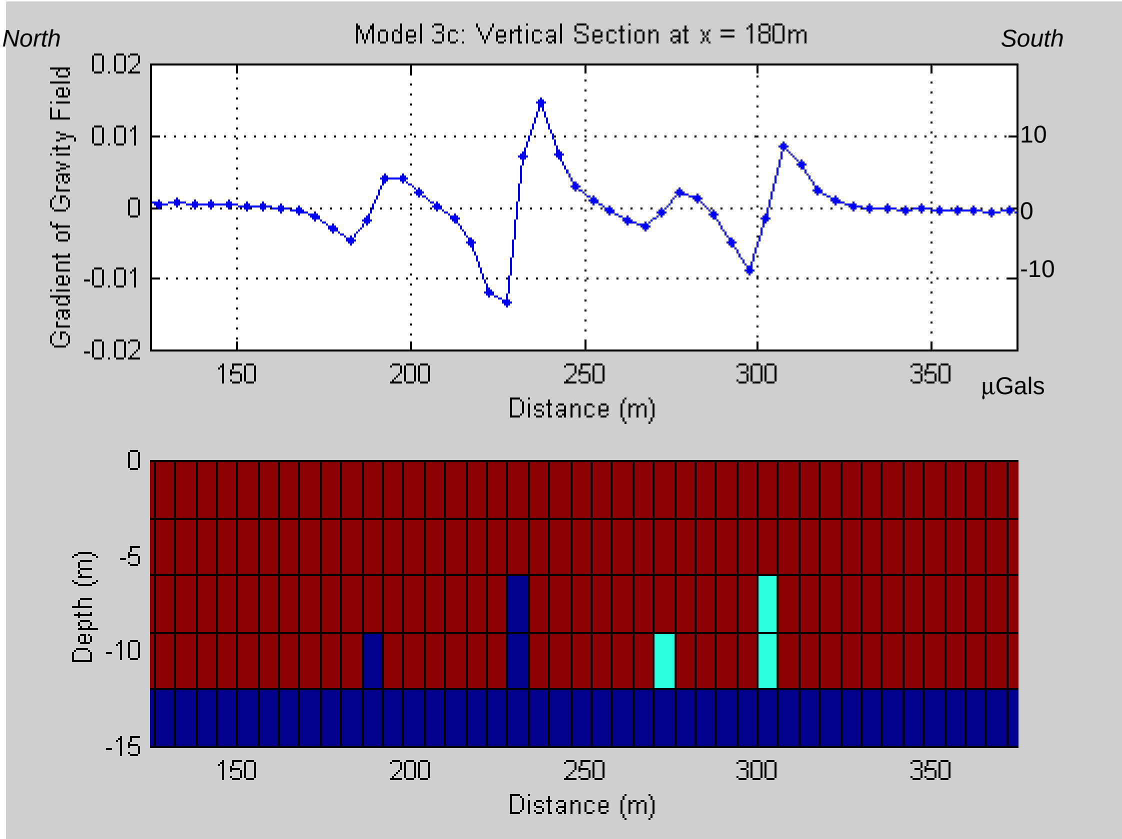

Figure 19b: Horizontal gradient of the gravity response of Figure 19a. A high/ low pair of anomalies is positioned over each rathole. The peak of the highs and lows generally occur within one station interval of the southern and northern edges, respectively, of each rathole.

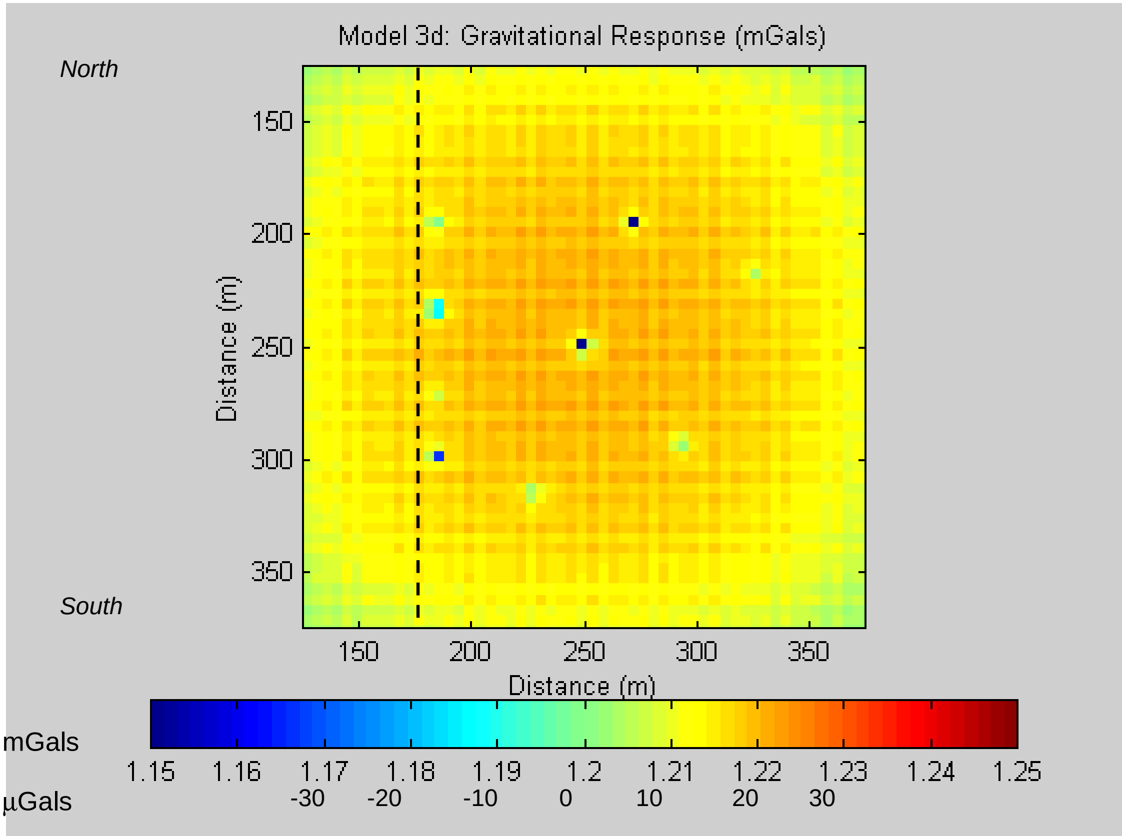

Figure 20: Gravitational response of Model 3d. A plan view of the model is not shown but the ratholes are positioned in the same locations as for Model 3c. The depth to the top of the old workings is 6m. 3m diameter, air or water/ sediment filled ratholes extend upwards from the mined tunnels to a depth below surface of 3m or are exposed on the surface. A North-South profile at x=180m (black dashed line) is presented in Fig.21.

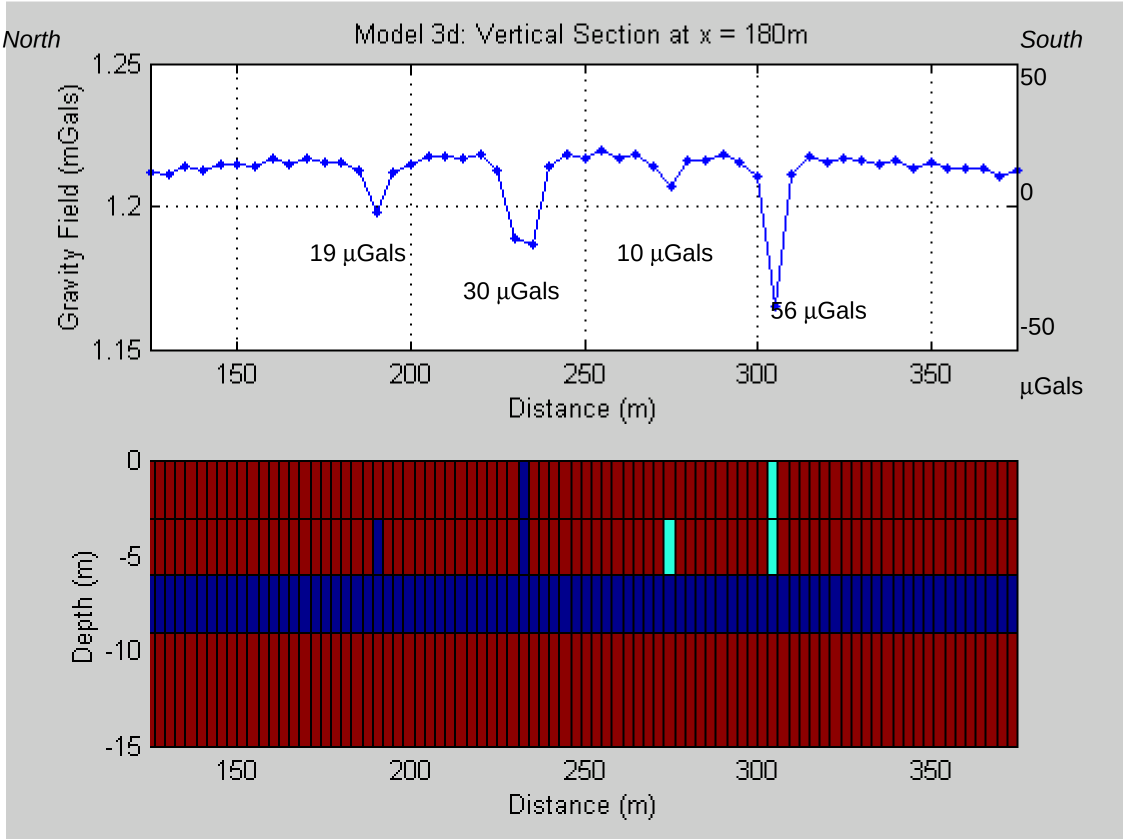

Figure 21a: North-South section through Model 3d at x=180m, directly over 3m diameter 'ratholes' developing into the roof of the air-filled tunnel of the old workings. The individual ratholes produce anomalies of variable amplitude depending on their size, depth below surface and density as shown on the profile.

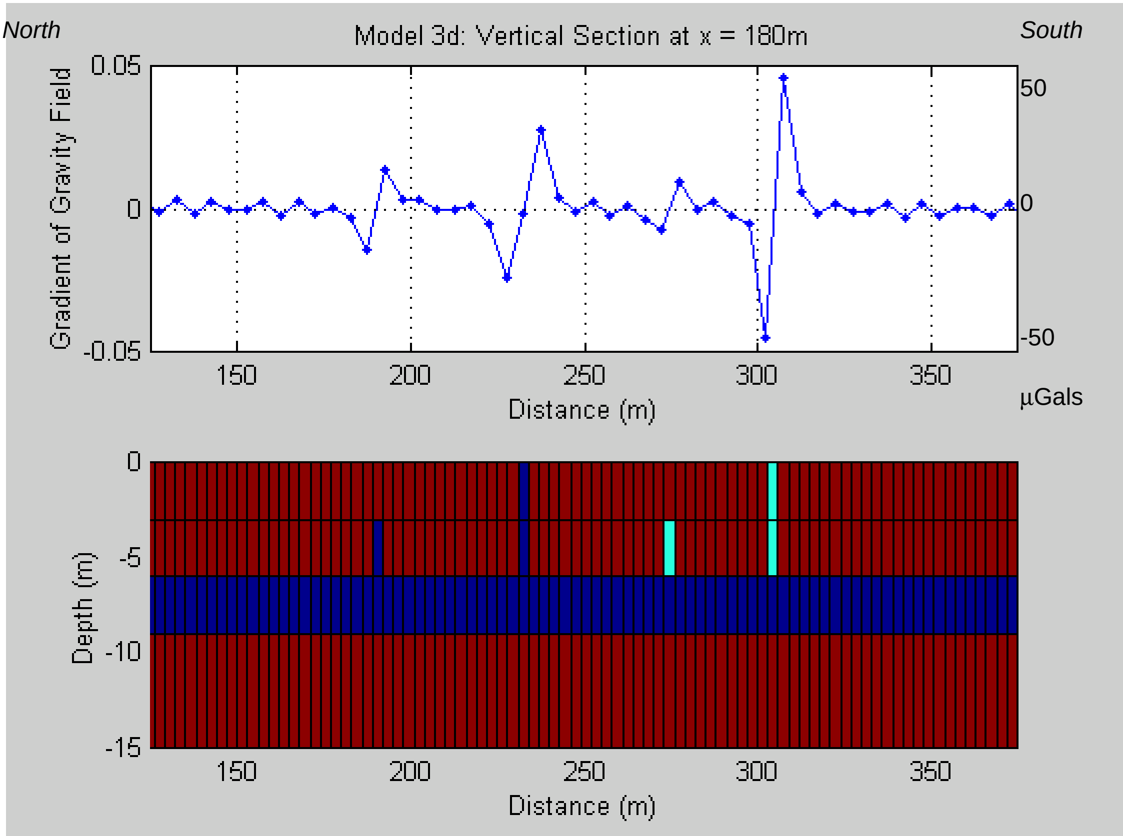

Figure 21b: Horizontal gradient of the gravity response of Figure 21a. A high/ low pair of anomalies is positioned over each rathole. The peak of the highs and lows generally occur within one station interval of the southern and northern edges, respectively, of each rathole.

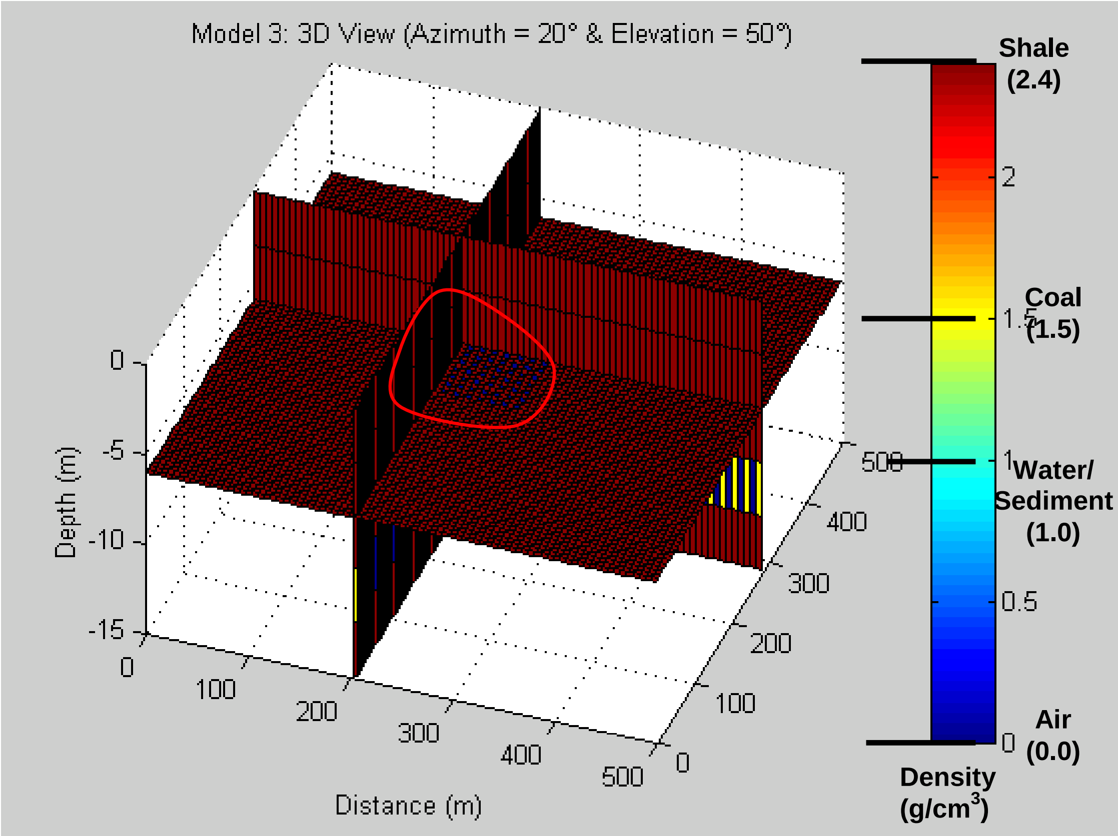

Figure 22: 3D view of the density distribution of Model 3a and 3b. Old coal workings are placed in a shale host rock. The depth to the top of the seam is varied from 6m to 12m. A cluster of ratholes (outlined by the red circle) of various sizes, developing upwards from the tunnels, are modelled at various depths to determine the minimum size and the maximum depth of the ratholes that can be resolved using microgravity.

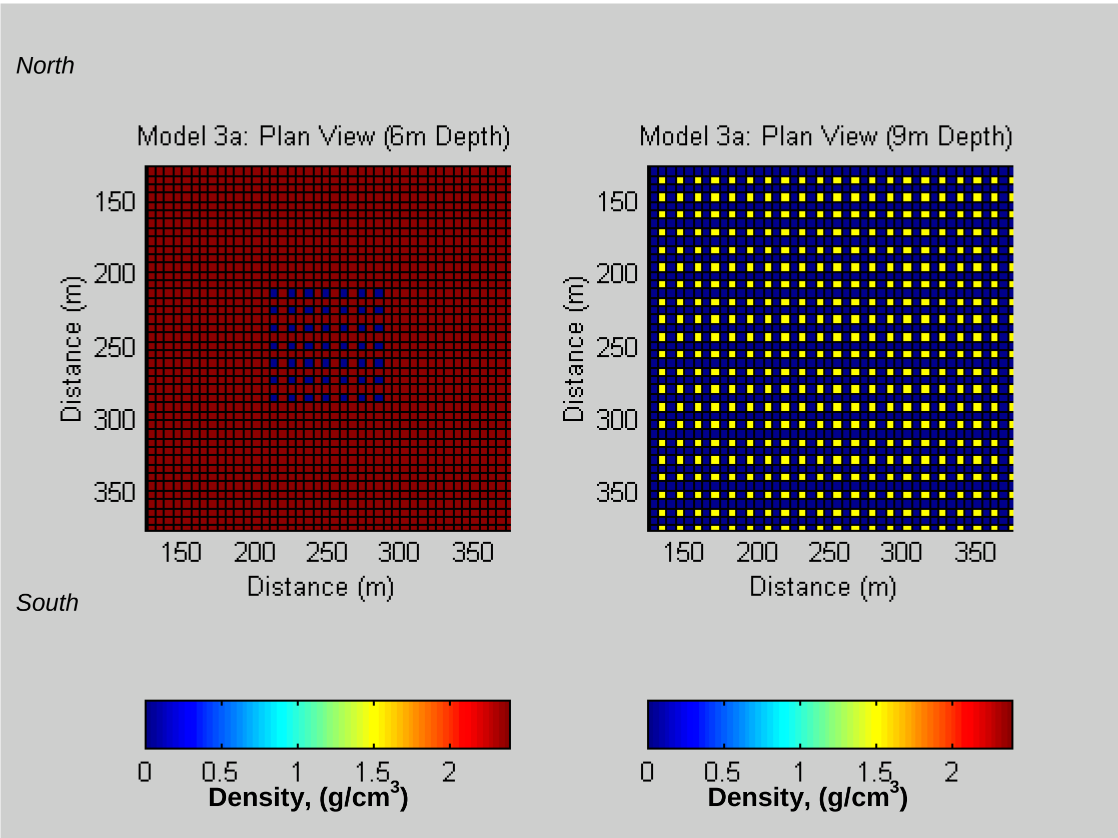

Figure 23: Plan views of Model 3a at a 6m and 9m depth level. The depth to the top of the bords and pillars of old workings is 9m. The depth to the top of a cluster of 6m diameter 'Ratholes', growing upwards from air-filled tunnels between the bords, is 6m.

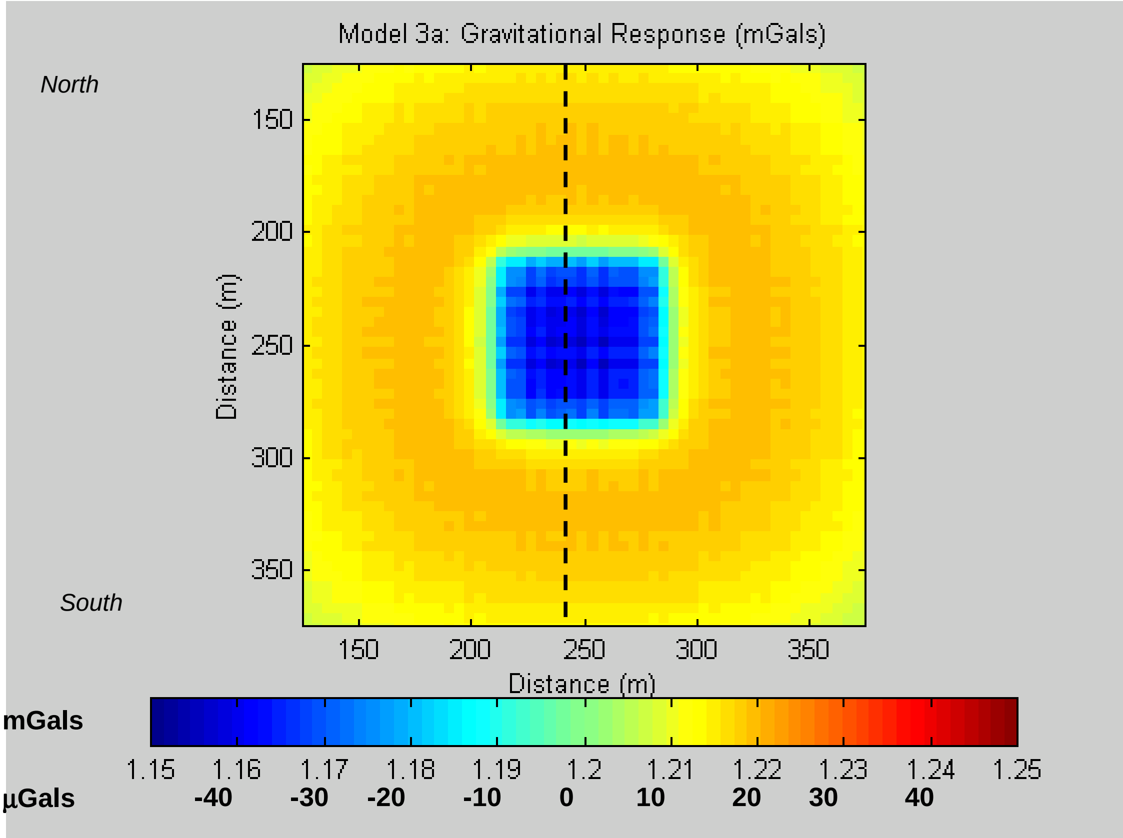

Figure 24a: The gravity response of Model 3a (illustrated in Figure 23) clearly shows a broad negative anomaly over the cluster of 'ratholes'. Superimposed on the broad negative anomaly are lower amplitude anomalies in response to individual ratholes. The position of the profile of Figure 25 is shown by the dashed line.

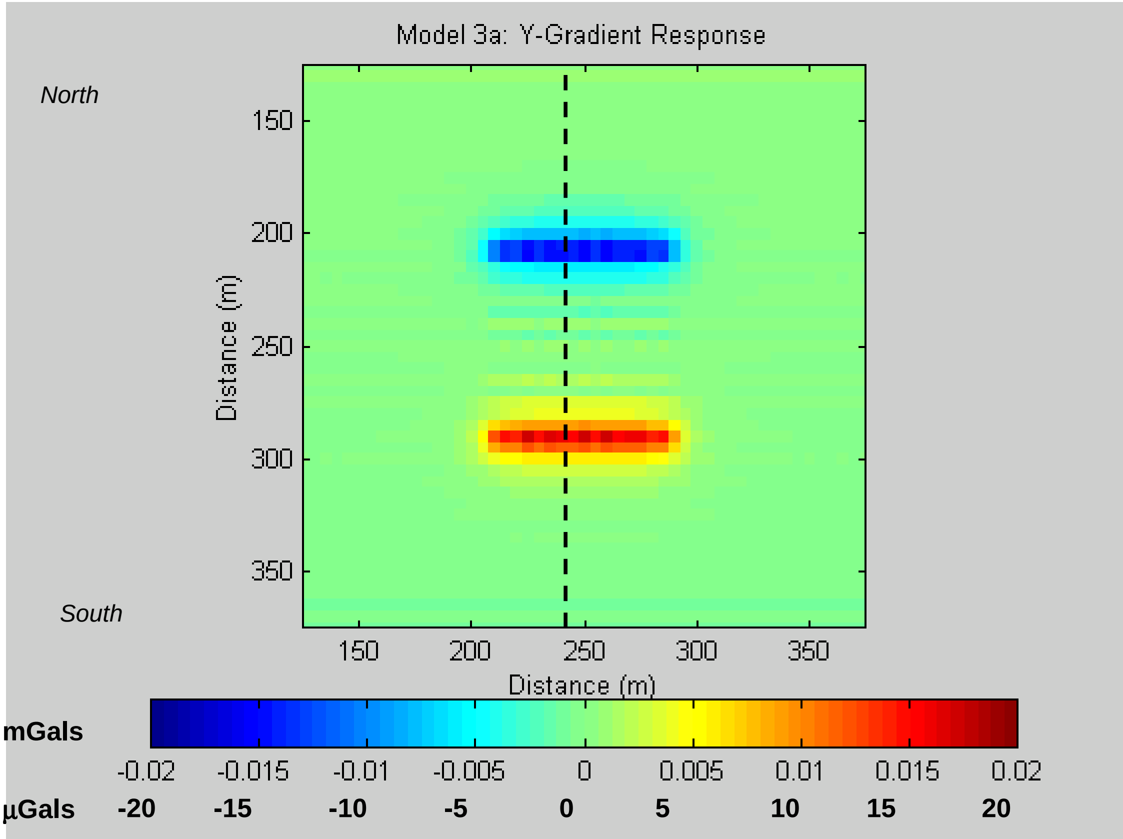

Figure 24b: Horizontal gradient (in the Y-Direction) of the gravity response of Figure 24a. The northern and southern edges of the cluster of ratholes are clearly observed as a low and a high in the gradient response. The regular arrangement of individual ratholes produce lower amplitude lows and highs creating a horizontal striped pattern in the image.

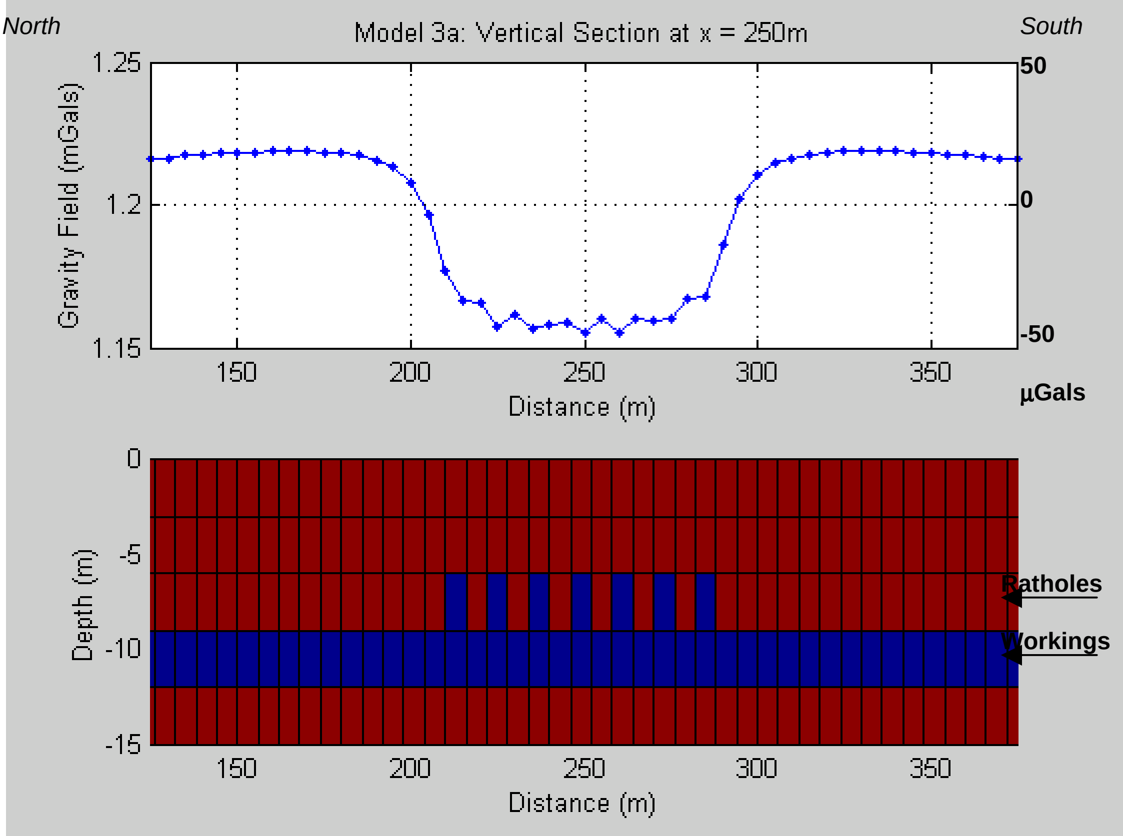

Figure 25a: North South section through Model 3a at x=250m (dashed line, Figure 24), directly over 'ratholes' developing into the roof of the **air-filled** tunnel of old workings. The 6m diameter ratholes are 3m high and occur **6m below the surface**. The combined response of all the ratholes is a gravitational low of amplitude 60 µGals. The individual ratholes produce anomalies of variable amplitude (maximum 7 µGals), superimposed on the broad negative of the combined response.

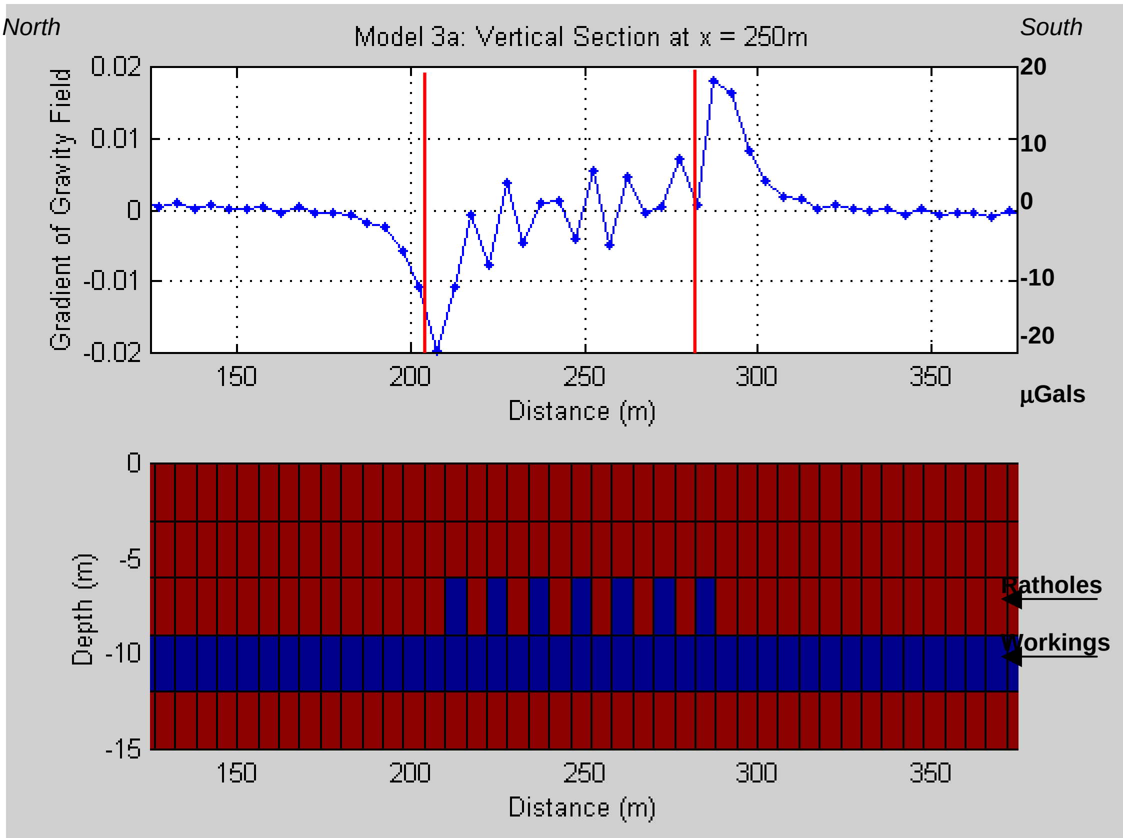

Figure 25b: Horizontal gradient of the gravity response in Figure 25a. A large low and high occur over the northern and southern edges of the cluster of ratholes, respectively (red lines) while lower amplitude high/ low pairs occur over individual ratholes in the cluster.

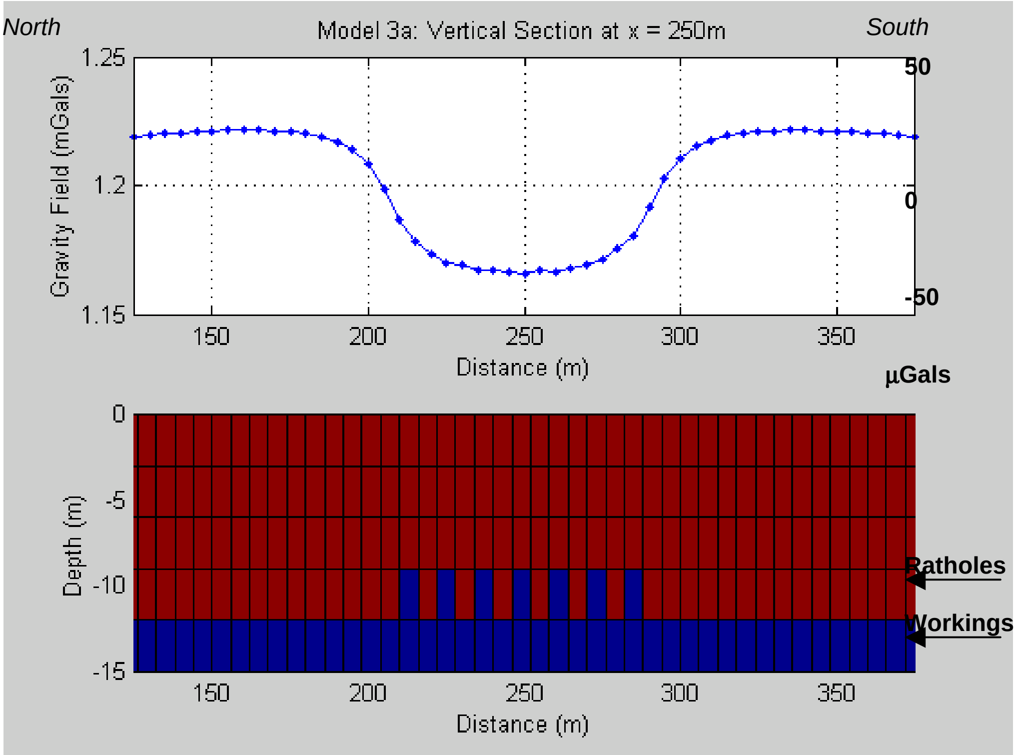

Figure 26: North-South section through Model 3a at x=250m, directly over 'ratholes' developing into the roof of the **air-filled** tunnel of old workings. The 6m diameter ratholes are 3m high and occur **9m below the surface**. The combined response of all the ratholes is a gravitational low of amplitude 53 µGals. The individual ratholes produce anomalies of variable amplitude (maximum 5 µGals), superimposed on the broad negative of the combined response.

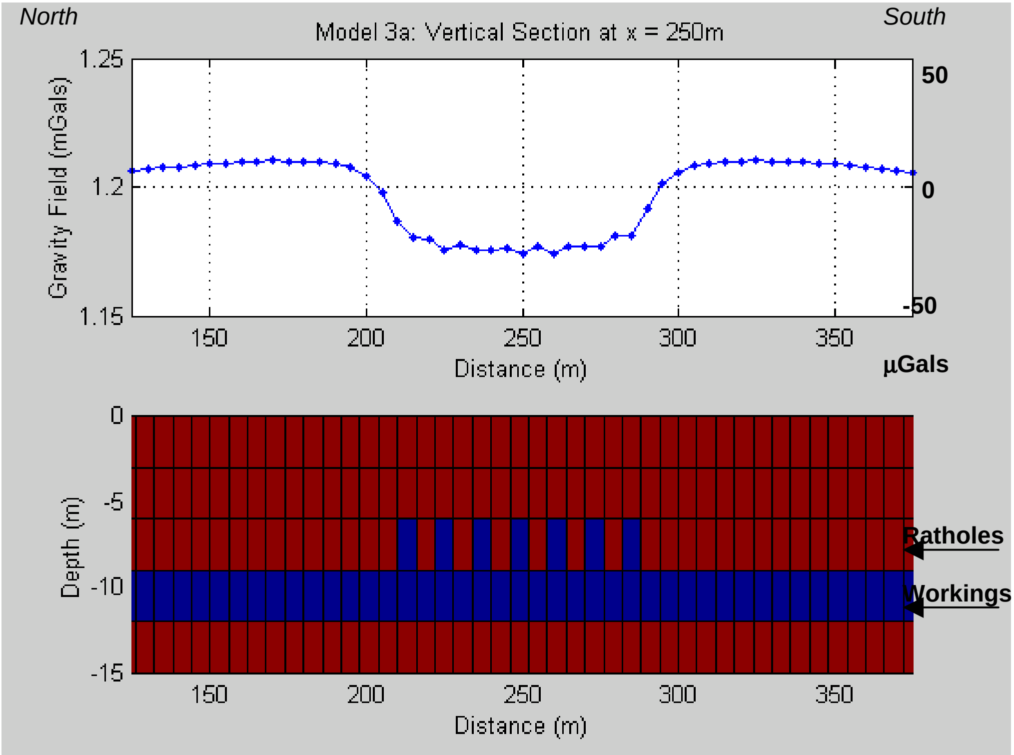

Figure 27: North-South section through Model 3a at x=250m, directly over 'ratholes' developing into the roof of the **water-filled** tunnel of the old coal workings. The 6m diameter ratholes are 3m high and occur **6m below the surface**. The combined response of all the ratholes is a gravitational low of amplitude 33 µGals. The individual ratholes produce anomalies of variable amplitude (maximum 4 µGals), superimposed on the broad negative of the combined response.

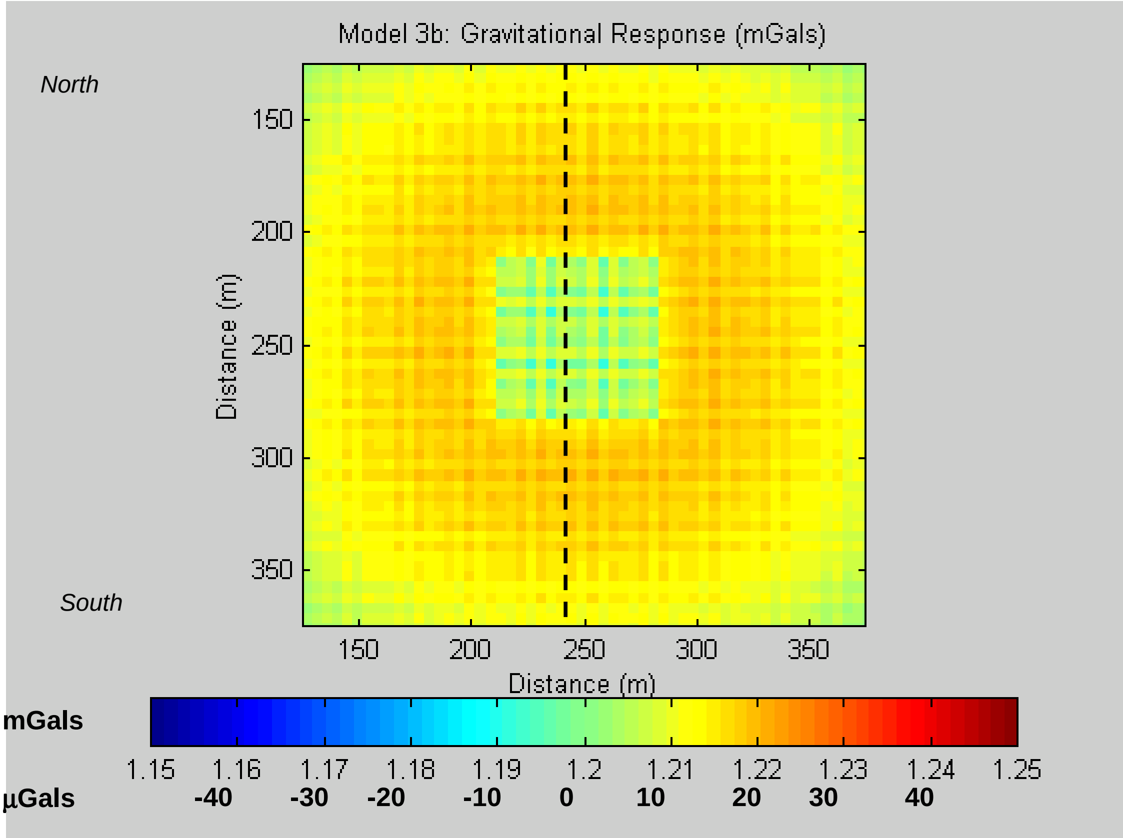

Figure 28a: The gravitational response of Model 3b clearly shows a broad negative anomaly over the cluster of 3m diameter 'ratholes' (at a depth of 3m below surface). Superimposed on the broad negative anomaly are lower amplitude anomalies in response to individual ratholes. The bords and pillars of the workings can also be identified in the gravity response. The dashed line shows the position of the section shown in Figure 29.

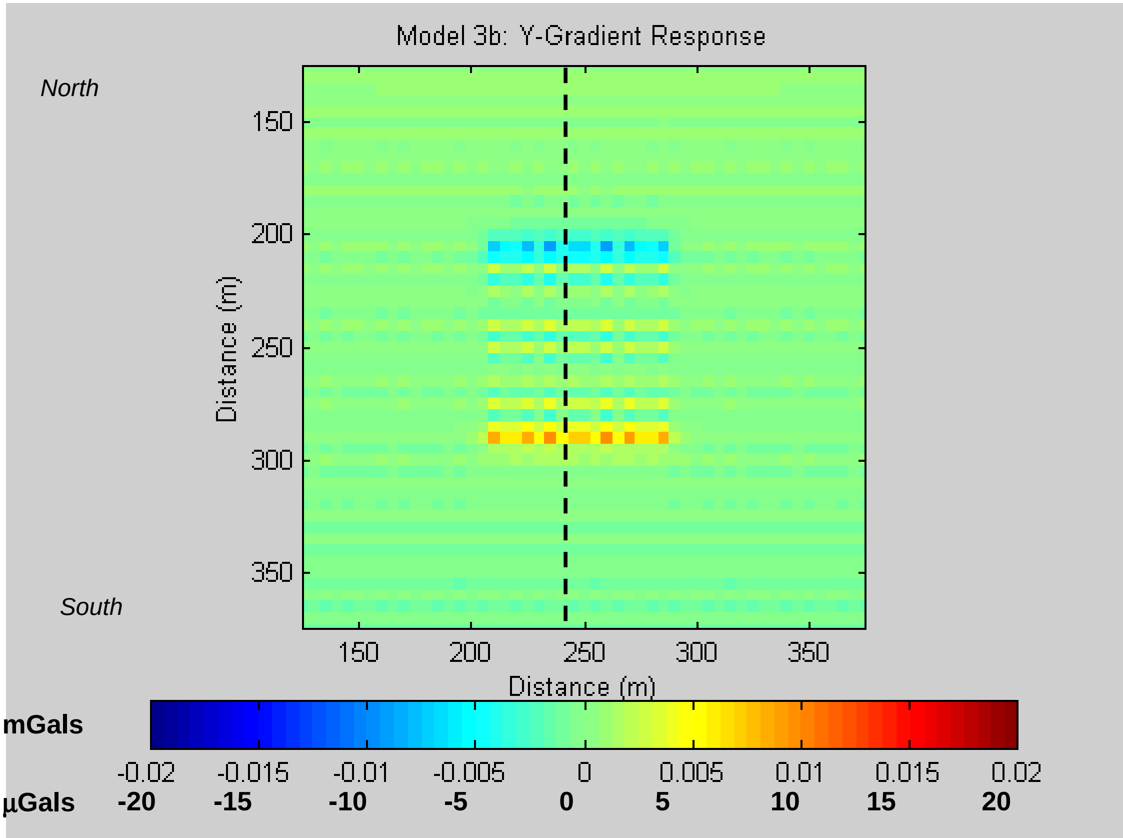

Figure 28b: Horizontal gradient (in the Y-Direction) of the gravity response of Figure 28a. The northern and southern edges of the cluster of ratholes are clearly observed as a low and a high in the gradient response. The regular arrangement of individual ratholes produce lower amplitude lows and highs. The edges of individual ratholes can be observed.

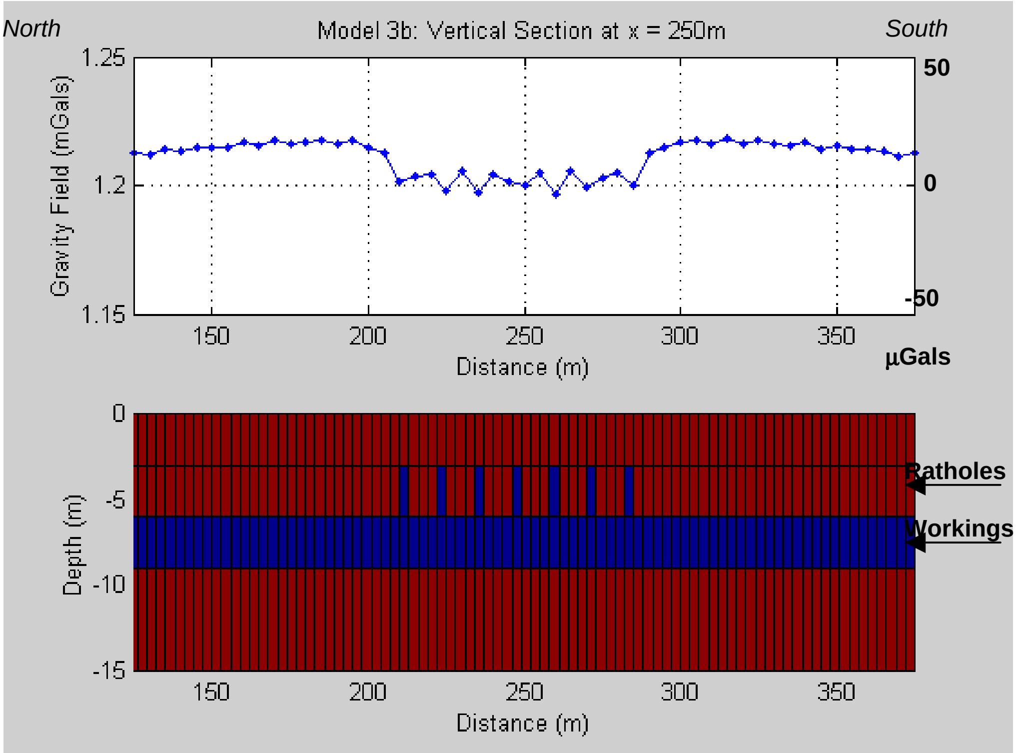

Figure 29a: North-South section through Model 3b at x=250m (dashed line in Figure 28), directly over 'ratholes' developing into the roof of the **air-filled** tunnel of the old workings. The ratholes have a diameter of 3m, are 3m high and occur at a depth of **3m below the surface**. The combined response of all the ratholes is a negative gravity anomaly (relative to the background response) of amplitude 15 µGals. The individual ratholes produce anomalies of variable amplitude (with a maximum amplitude 9 µGals) superimposed on the broad negative of the combined response.

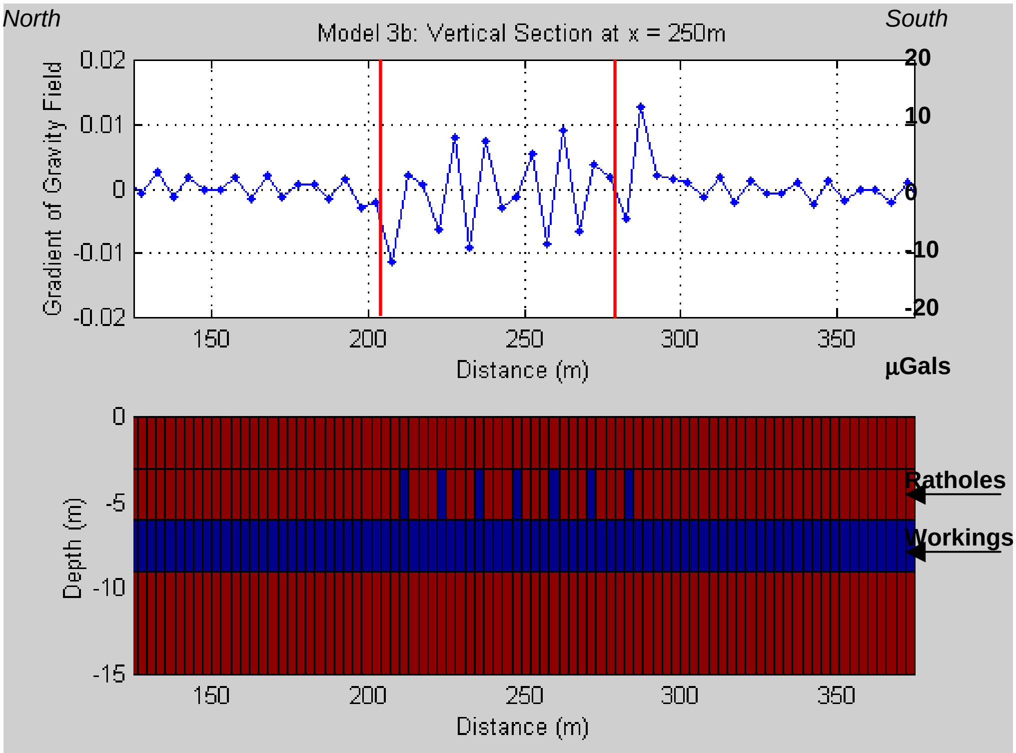

Figure 29b: Horizontal gradient of the gravity response in Figure 29a. A low and high occur over the northern and southern edges of the cluster of ratholes, respectively (red lines) while lower amplitude high/ low pairs occur over individual ratholes in the cluster. The rathole anomalies are larger than the high/ low pairs observed over the coal pillars (which occur adjacent to the tunnel illustrated in this section).

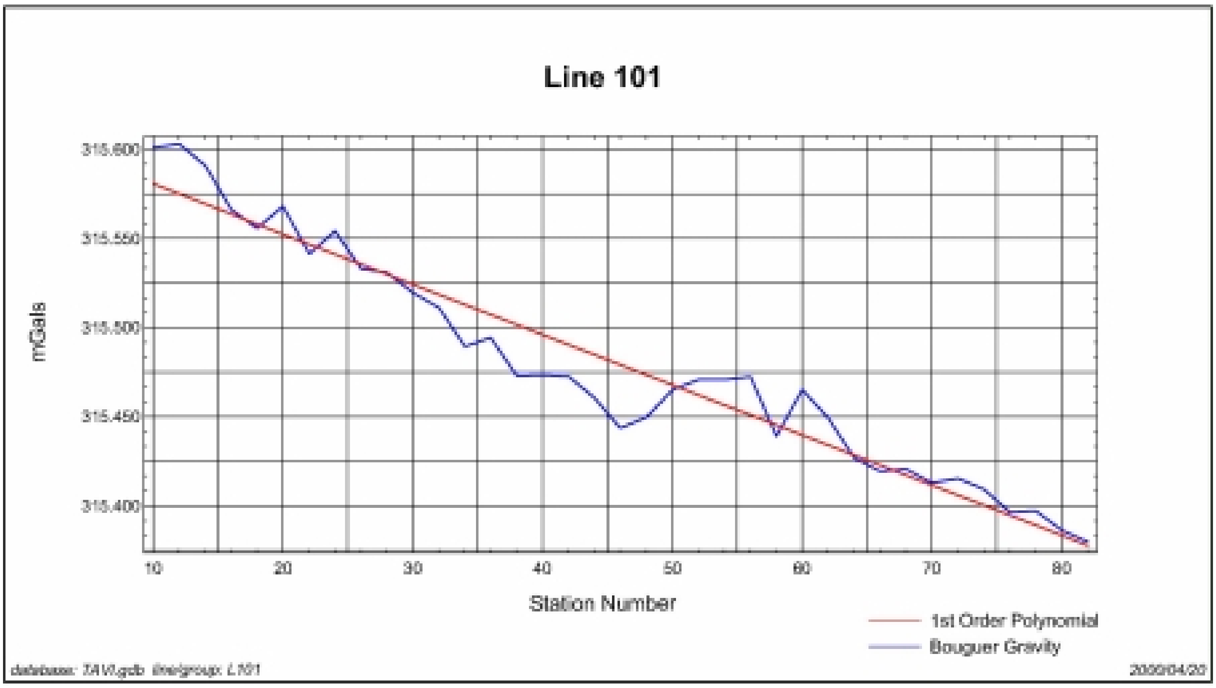

Figure 30: Bouguer gravity anomaly data on Line 101 (blue line), showing first order polynomial regional field (red line) which is subtracted from the Bouguer data to yield the residual gravity field.

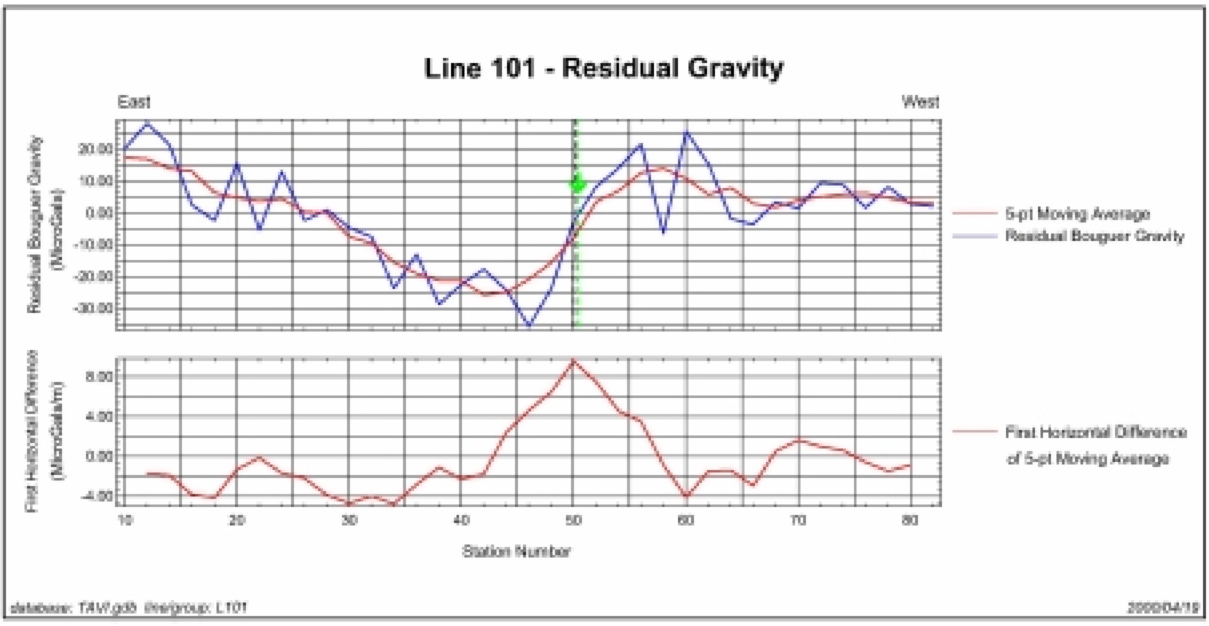

Figure 31: Residual gravity anomaly on Line 101. The residual gravity data (blue line in upper figure) is smoothed with a five point moving average filter (red line in upper figure) to show more clearly the signal resulting from the old workings. The edge of the old workings, interpreted using the half amplitude method, is indicated by the green arrow, and corresponds to the inflection point between the gravity low of the old workings (to the southeast) and the gravity high of the unmined seam (to the northwest). In the lower figure the horizontal gradient of the smoothed residual anomaly is shown, derived using a first difference operator. The peak of the horizontal gradient (black dashed lines) provides an alternative method for identifying the inflection point that corresponds to the edge of the workings.

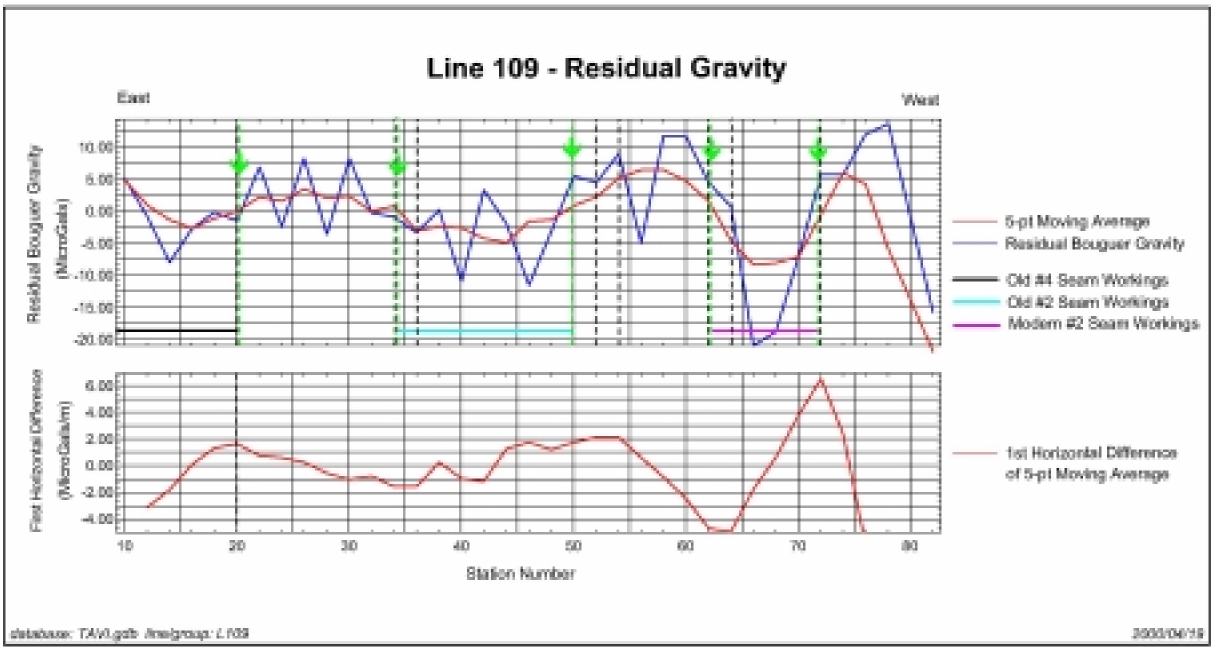

Figure 32: Residual gravity anomaly on Line 109. Details as for Figure 31. In addition to the edge of old #2 seam workings identified towards the centre of the line, the edge of the old #4 seam workings is identified towards the east of the line, and the interpreted edges of modern #2 seam workings towards the west of the line.

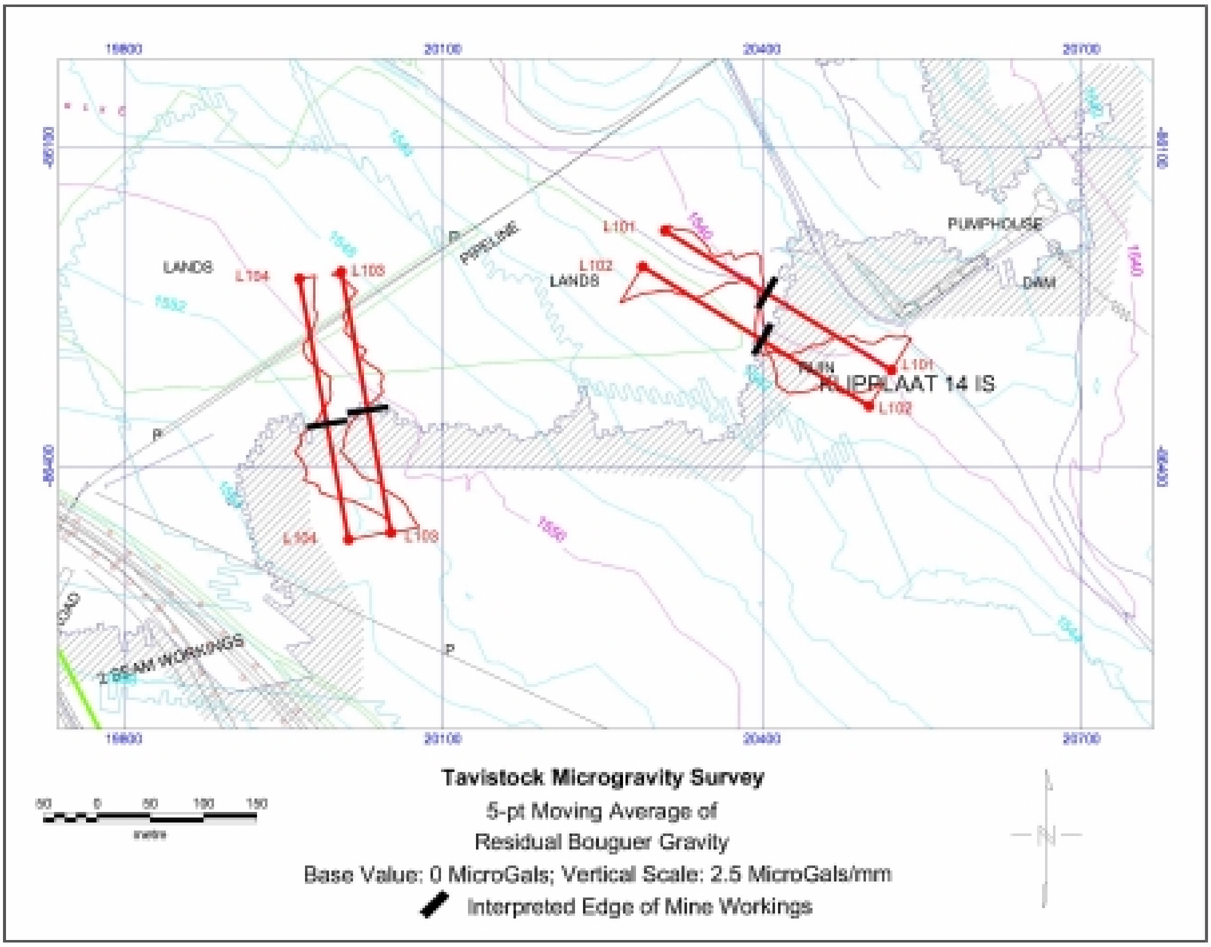

Figure 33: Base map detail showing mine infrastructure and the predicted edges of workings (shown as short bars) on microgravity Lines 101 - 104. Smoothed residual gravity profiles are also shown along each line in red. The hashed grey line and dark blue border demarcates the edge of #2 seam workings as known from the old mine plans and the light blue line demarcates the edge of # 4 seam workings.

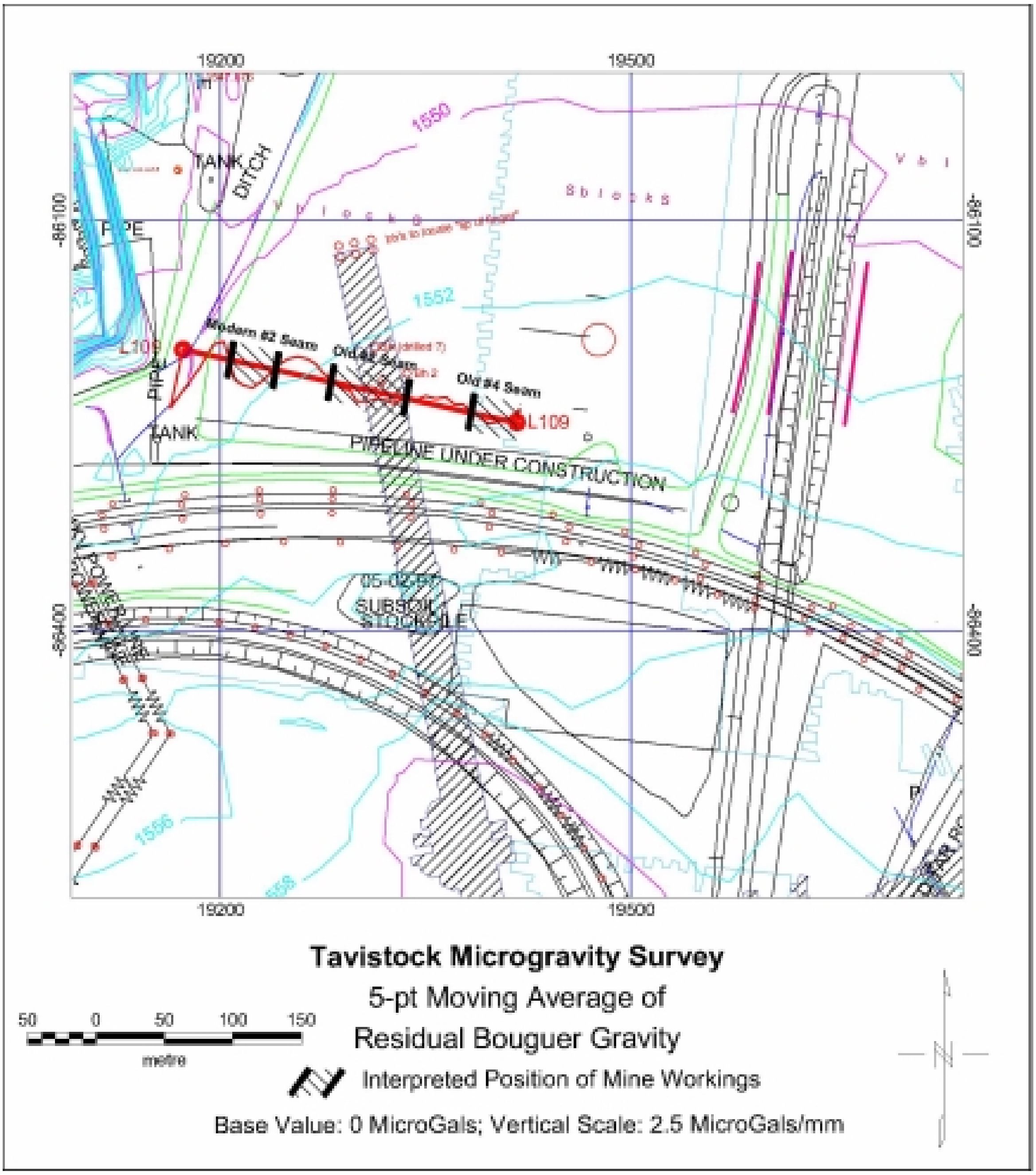

Figure 34: Base map detail showing mine infrastructure and the predicted edges of workings on microgravity Line 109. Details as for Figure 33.

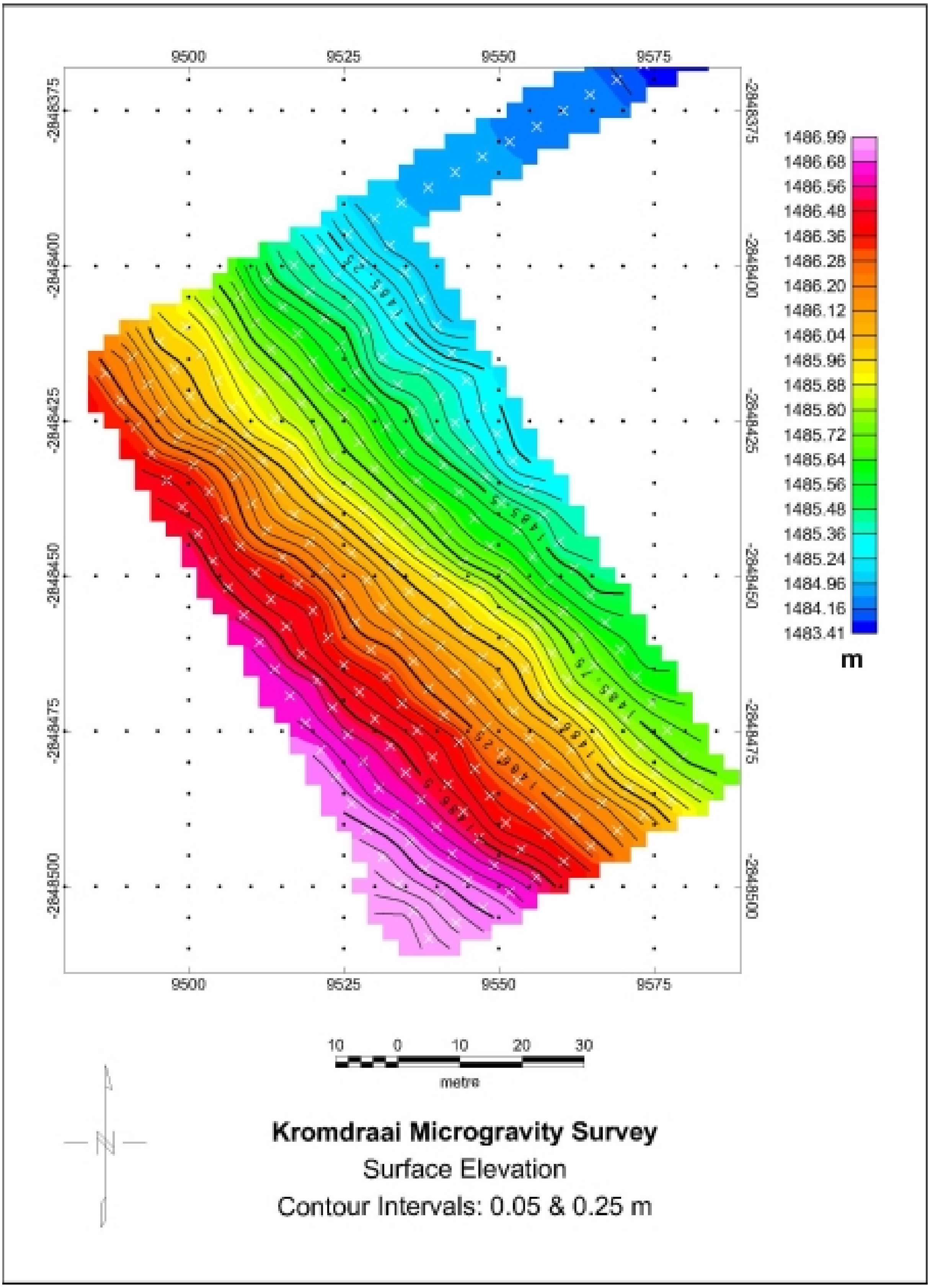

Figure 35: Relative surface elevation map over the survey area, derived from the accurate levelling of the gravity measurement stations. Station positions are indicated by small white crosses.

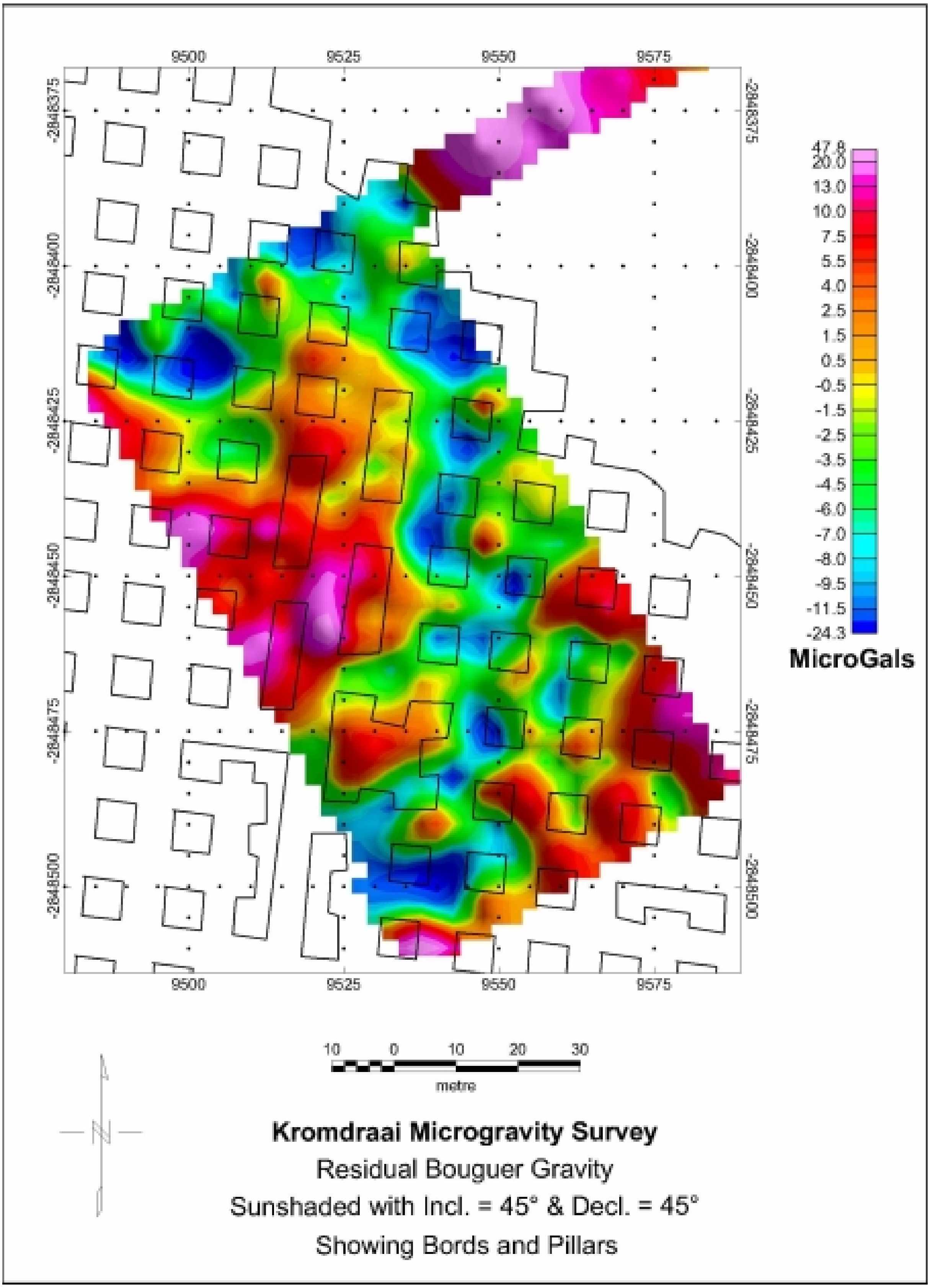

Figure 36: Residual Bouguer anomaly field with old underground mine workings (bords and pillars) shown. In general, a higher gravity response is obtained over an area in which larger than average pillar sizes occur. Individual bords and pillars are not resolved.

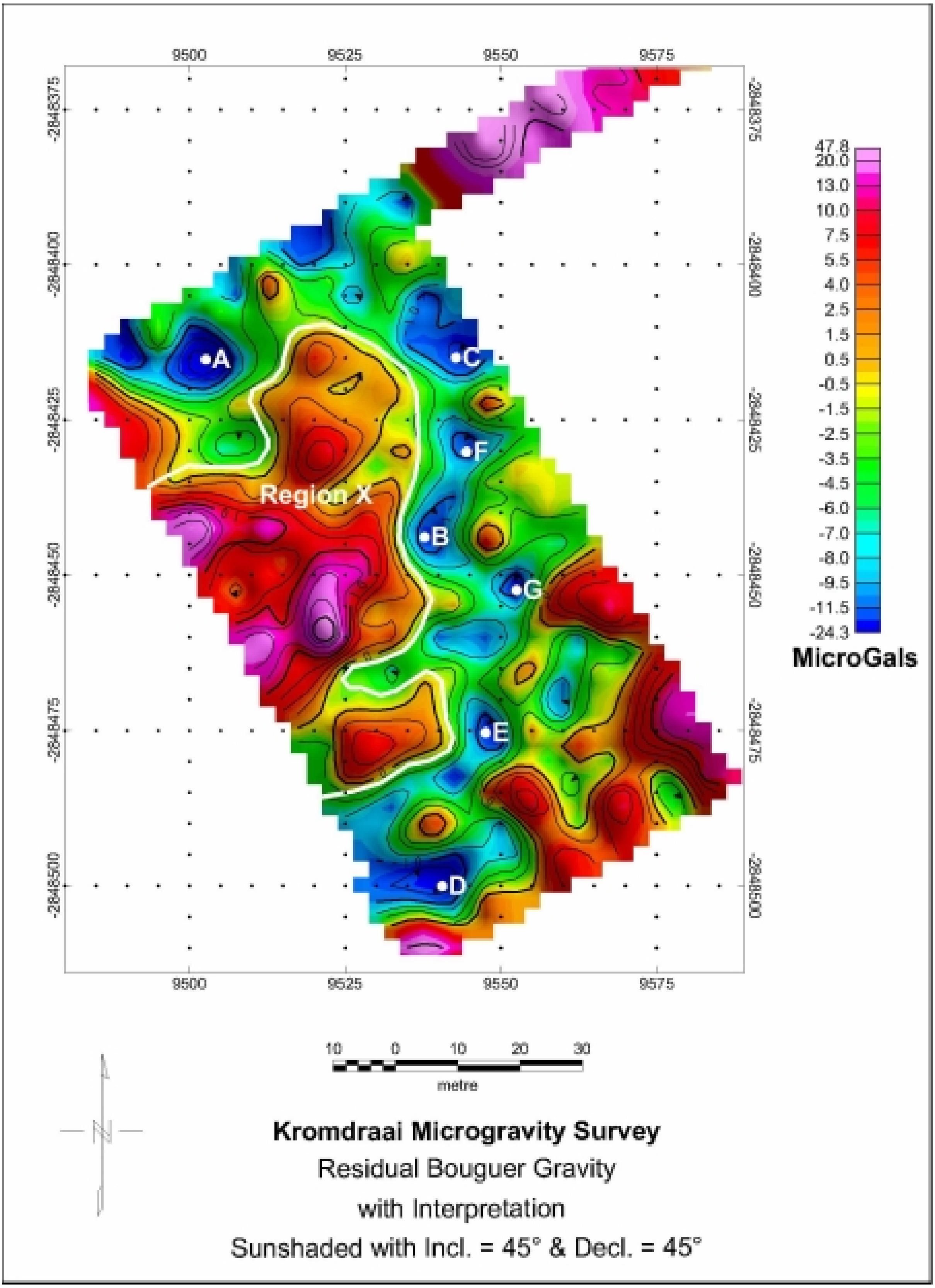

Figure 37: Residual Bouguer anomaly field over the survey area, with interpretation. Negative gravity anomalies, labelled in order of decreasing significance from A to G, are shown. The maximum anomaly amplitude is about 14 μGal, and none of the anomalies are large enough to indicate significant subsurface sinkholes – the anomalies may instead be the result of local variations in overburden weathering and density. The labelled anomalies are also the proposed sites of ground truth drilling, again in order of decreasing priority, A to G. The white line encloses an area of elevated gravity response (Region X), interpreted to correspond with an area of larger subsurface pillars in the old workings (see Figure 36).

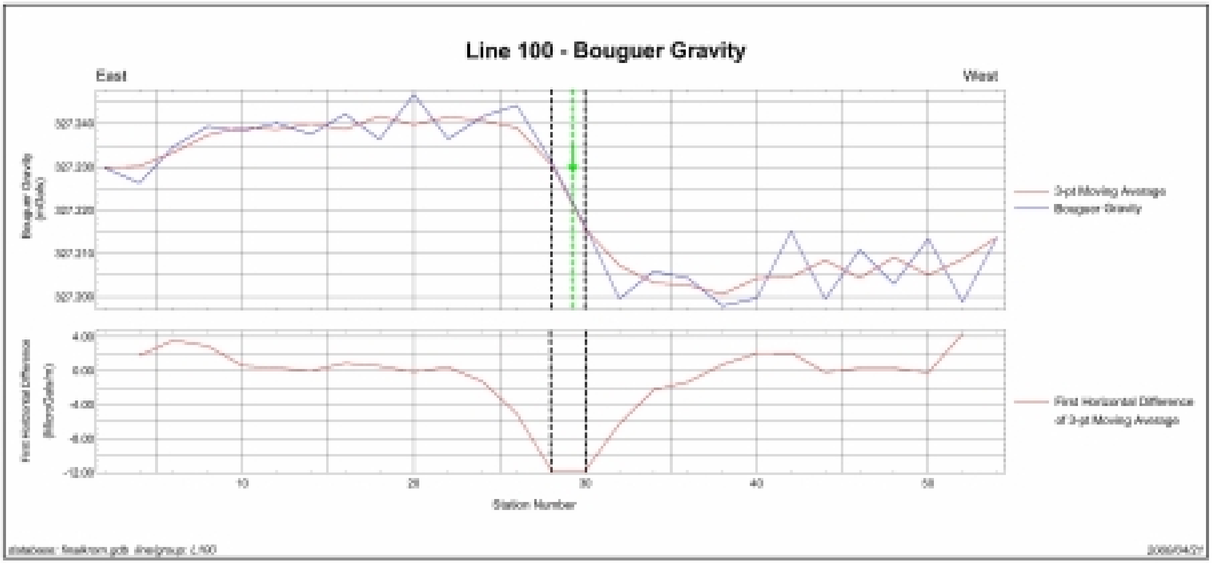

Figure 38: Gravity anomaly on Line 100. Smoothing the data with a three-point moving average filter (red line in upper figure) shows most clearly the signal resulting from the old workings. The interpreted edge of the old workings is indicated by the green arrow, and corresponds to the inflection point between the gravity low of the old workings (to the southwest) and the gravity high of the unmined seam (to the northeast) found by means of the half-amplitude method. In the lower figure the horizontal gradient of the smoothed anomaly is shown, derived using a 1st difference operator. The trough of the horizontal gradient (indicated by the dashed lines) provides an alternative method for identifying the inflection-point that corresponds to the edge of the workings.

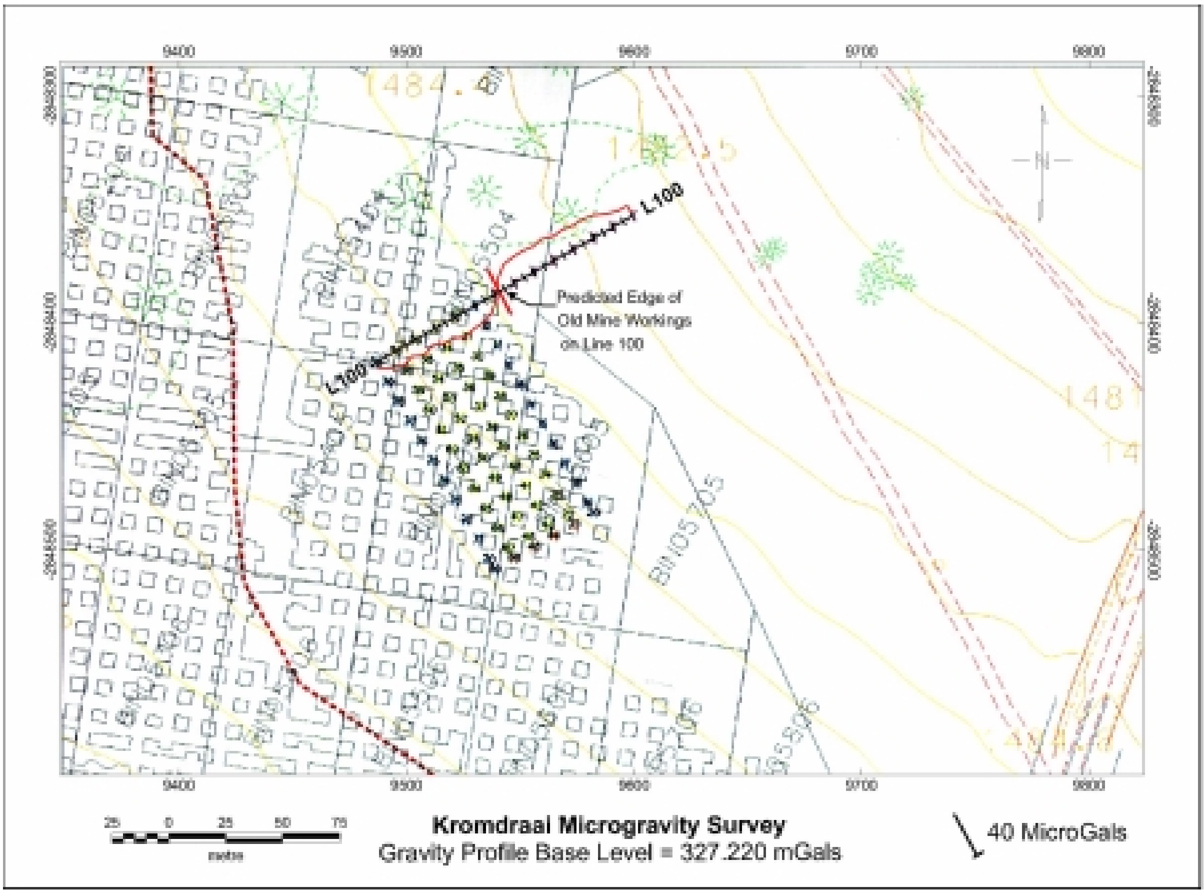

Figure 39: Base map detail showing the old #1 seam workings and the predicted edge of workings (short red bar) on microgravity Line 100. The smoothed gravity profile is also shown along the line in red.

APPENDIX VI

Chris van Dam
GEOPHYSICS & SEISMIC CONSULTANT
63 VAN RIEBEECK AVE.
LYTTELTON
CENTURION 0157
SOUTH AFRICA
E-mail: chrisvd@pop.co.za
Fax: +27 12 6643430
Tel: +27 12 6643430

FAN SHOOTING-A POSSIBLE LOW COST HAMMER REFRACTION SEISMIC METHOD TO MAP NEAR SURFACE MINING INDUCED CAVING

In his report "An Assessment of the use of Seismic Methodologies to Detect Buried Cavities or Tunnels" Prof. Cedric Wright of the University of the Witwatersrand reviewed available technical literature and concluded that very few practical examples are published in this field and what was published did not suggest any successful applications. He regarded the theoretical studies as largely unrealistic but model studies (Pant and Greenhalgh, 1989) making use of diffracted (not refracted) or scattered P waves, were regarded as promising provided the masking effect of the Raleigh waves could be suppressed.

Blocking the Raleigh waves was to be accomplished by digging a trench between the source and the receivers, not a very practical or a realistic solution. He subsequently further suggested that the Raleigh waves themselves can be used to detect shallow cavities, this I found confusing. Any way, instead of using a trench to block the Raleigh waves, surely a near surface caved roof situation may have the equivalent effect. Wright's most important conclusion is that seismic wavelengths are normally much longer than the dimension of mine cavities thereby excluding the use of seismic P wave reflection of any kind in mapping old mine workings and subsidence.

Geophysicists are often at a disadvantage in that problems needing to be resolved are not always clearly specified. Mapping in-tact mining tunnels at 30 m depth is a completely different problem to mapping a 20 m deep mine tunnel with roof caving up to close to surface. (The latter being of potential or eminent danger to industrial and domestic surface users.) In the latter case it also stands to reason that such caving will start and be at it's severest, at the intersection of two tunnels forming a dome-shaped rubble filled cavity. The top of such a cavity will in all likelihood be partially collapsed and ring cracks or joints will have developed, i.e. the bedrock refraction horizon will be locally seismically disturbed.

In my opinion what was overlooked in Prof. Wright's study is the slowing down, amplitude annihilation and/or severe frequency attenuation of the refracted wave when passing disturbed ground (bedrock) as described above. In such an admittedly selective case, I wish to recommend that Coaltech 2020 experiment with a revival of a 1923 seismic refraction technique, called Fan shooting.

The WW1 military were the first to developed (the inverse) Fan shooting technique to pinpoint the location of heavy artillery. Petroleum engineers later reversed the military method to map the location of salt domes, salt having a much higher density and P wave velocity than sedimentary rocks. I propose that the same approach is used but with the reciprocal outcome, mapping areas of slowness.

The method is simple; receivers are placed on the circumference of a semi circle, the seismic source at the loci, on the other side of the suspected caved area as shown on Figure 1. Those ray paths that miss the subsidised or caved area, should arrive first at full amplitude and peak frequency. Those that travel through the effected area will arrive later and be attenuated, or they may not arrive at all. Repeating the exercise from a new locus on the previous circumference (Figure 1), a cross fan pattern is obtained suitable for what we now call, tomographic reconstruction. Only the refracted waves are initially to be considered. As the radius of the circle will be relatively small, hammer seismic sources can be used. Twenty-four or forty-eight channel recording equipment will suffice.

Such work is an ideal student project and with Prof. Wright's first-class knowledge of the refraction method, the University of the Witwatersrand is a logical participant. Students can do the initial modelling, survey parameter design, the initial first break arrival time picking and the initial interpretations. Prof. Wright may want to use the data for more esoteric type of analysis on the other waves present in the shot record.

I have made no attempt at actually modelling the above scenario and cognisance must be taken of realistic potential dimensions of subsurface collapsed zones however, I believe this technique will provide useful results.

Chris van Dam
Geophysics & Seismic Consultant

Rererences

Pant, D.R. and Greenhalgh, S.A., 1989. Blocking surface waves by a cut – physical seismic model results, Geophysical Prospecting, 37, 589-605.

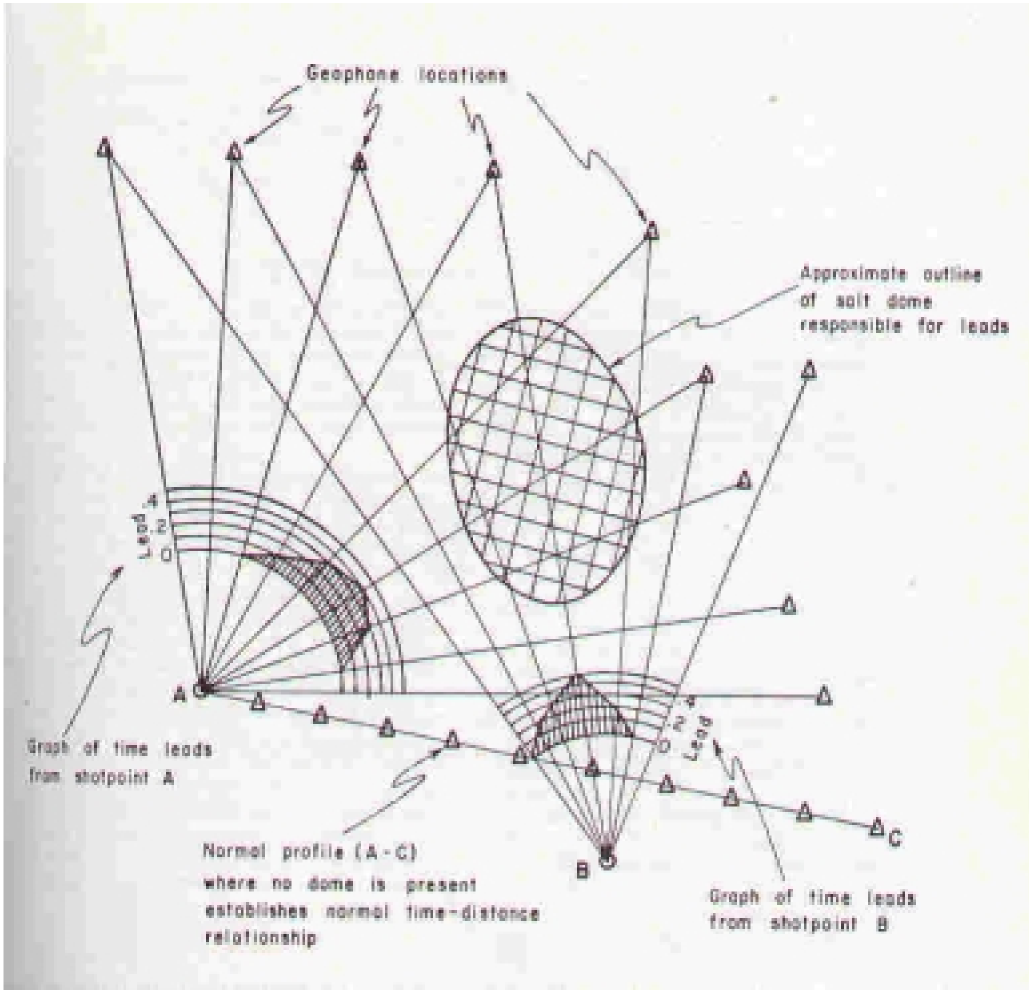

Figure 1. *Source and receiver configuration used for seismic refraction fan shooting.*

APPENDIX VII

COALTECH 2020

Final Report

Detection of old workings, sinkholes, underground fires and acid mine pollution using geophysics and airborne thermal infrared imagery

M. van Schoor

CSIR, Division of Mining Technology

Report number: 2001-0124

Task 1.3.1b

20 March 2001

EXECUTIVE SUMMARY

Task 1.3.1b focuses on the use of geophysical techniques for the detection and mapping of the following features:

1) pillars and voids of old mine workings,
2) shallow sinkholes developed in overburden above mining voids,
3) underground fires, and
4) acid mine pollution in previously mined, but currently inaccessible areas.

The overall aim of this task is to map the above features with an accuracy of 1 to 2 metres. The features of interest typically occur between surface and approximately 25-30 m below surface. In some cases old workings may be located between 30 and 60 m.

The issue of site specificity has been emphasized. The potential of any given geophysical technique should not be concluded from one or two successful or unsuccessful surveys. Valuable information can still be gathered from an unsuccessful survey thereby enriching the collection of case histories.

Various geophysical techniques were evaluated on a theoretical level during Year 1 of this task. This report provides feedback about the technology audits that were conducted, which were aimed at predicting the applicability of the different geophysical techniques. A performance prediction analysis of the different techniques is presented in Tables 2-4 in Section 7. The most promising techniques, of those considered to date were Thermal Infrared Imagery (TIR), micro-gravity and electrical resistivity. These three techniques will be tested at selected sites early in Year 2. To date three test sites have been identified.

TABLE OF CONTENTS

LIST OF TABLES

1 INTRODUCTION

This report summarises the results of Year 1 (of 2) of Task 1.3.1b. As has been stated in earlier progress reports the emphasis of this project is on the detection and delineation of secondary features. These are features which are either man-made or a result of mining related activities such as old mine workings, sinkholes, underground fires and pollution plumes.

A variety of potential geophysical solutions have been considered. The proposed focus of Task 1.3.1b is on a mine-scale, rather than on a regional scale, consequently the decision was made to concentrate on surface geophysical methods. The one exception is an airborne Thermal Infrared Imagery (TIR) survey proposed by Anglo American's Geophysical Services Division. There are basically three reasons for incorporating the TIR technique into this project:

1) Despite TIR being an airborne technique, it has the potential to provide high-resolution (possibly sub-metre) images over reasonably large areas.
2) There are examples in the literature where TIR has been used successfully to map old bord-and-pillar workings.
3) Representatives from various coal mines participating in Coaltech 2020 recommended to have a TIR survey flown as soon as possible, thus it was incorporated into Year 1.

A further decision was made to exclude seismic methods from the first Year of Task 1.3.1b even though a literature search has shown that seismics may be applicable to some of the problems listed above. The reason for this is that Coaltech 2020 Task 1.3.1a deals with the seismic technique. The output of Task 1.3.1a will be integrated into the 1.3.1b results towards the end of Year 2 (2001/2002).

Furthermore, this project does consider in-mine geophysics – this may form the focus of future Coaltech 2020 research. A new Coaltech project starting in April 2001 (Task 1.3.5) will assess the applicability of airborne and other remote sensing techniques to the coal environment. This new project, which can be viewed as a follow-on of Task 1.3.1b, will be aimed at assessing and monitoring on a regional scale.

A number of potential obstacles to the successful application of ground geophysics and TIR were evident at the outset of the project. These included:

i) The diversity of the four types of target mentioned above regarding their differing geometries and physical characteristics.
ii) The different depths and rock types in which they may occur.
iii) The sometimes complex geological structure, for example, the presence of alternating sedimentary layers in the overburden, varying overburden characteristics, and intrusions
iv) Cultural interference such as surface developments, current mining and farming activities, vegetation etc.

Since no single, ideal geophysical solution exists and similar problem scenarios have to be dealt with in a site-specific manner, the requirement for a “toolbox” approach has been acknowledged. It was decided to consider as many of the key parameters and factors that may influence the applicability of the various techniques, to test a variety of techniques in different environments and to learn from past experiences (e.g., literature reviews and interviews with the industry). Computer simulations also play an important role. The need for a cost-benefit analysis of all the various techniques tested in the course of this study has been recognized. The ultimate goal of Task 1.3.1b is to compile a semi-quantitative applications guideline for deciding which geophysical approach to use for a given problem scenario. In some cases the integrated use of more than one technique may be required.

Based on the results obtained in Year 1, a strategy for the final year of Task 1.3.1b has been formulated. This strategy is discussed in the Conclusions and Recommendations Section.

2 SUMMARY OF PROGRESS AT THE END OF YEAR 1.

Appendix A contains a table showing the various subtasks and deliverables planned for Year 1 of Task 1.3.1b. The first three subtasks include a technology audit of previous, similar research and of potential technological solutions. During this phase a performance prediction analysis was done on a number of promising geophysical techniques. A refined version of the analysis, incorporating new and up-to-date information, is presented in this report.

The TIR survey, originally planned for August 2000, was postponed until mid-2001, due to poor weather conditions and the onset of the rainy season. Dry, cloudless, night-time conditions (i.e., typical highveld winter conditions) are prerequisites for a successful TIR survey for the scanner that is to be used. Despite this setback, a brief desktop study of the TIR technique, which included details of the planned (TIR) survey over the Witbank coal field area, was completed. This contribution on the TIR technique fulfilled the requirements of Subtask 3.

Further geophysical desktop studies were conducted on some of the promising geophysical techniques identified in the technology audit (Subtask 2). The three techniques that were studied in more detail in Subtask 4 were:

a) ground penetrating radar (GPR),
b) controlled source audio magnetotelluric technique (CSAMT), and
c) electrical resistivity techniques.

The results and conclusions of these studies are discussed in this report.

At the start of Task 1.3.1b it was proposed to conduct field trials using the more promising techniques identified in subtasks 2 and 4. Although these surveys were projected to take place early in 2001, no field data had been acquired at the time of writing this report. Various reasons, including the relatively late postponement of the TIR surveys and unexpected difficulty in locating a suitable test site, contributed to the delay. However, field trials (Subtask 5) are to be conducted during April. Three test sites have been identified, namely on the Kromdraai, Tavistock and New Largo properties. At the first two of these sites micro-gravity survey data is already available from previous surveys. Additional, conventional geophysical techniques such as the magnetic and frequency domain electromagnetic methods may also be tested at the same sites, even though these techniques were not considered at a theoretical level in the desktop studies.

Subtask 6 involved a desktop study of the micro-gravity technique, including some 3D computer simulations. This study has been completed recently and is discussed in this report.

3 THE VARIOUS PROBLEM SCENARIOS

For the sake of completeness and continuity of this report, the discussion on the various problem scenarios that formed part of the Subtask 2 & 3 progress report and of the desktop study on electrical resistivity methods, is included here.

3.1 Old bord-and-pillar workings

By the mid 1980's approximately 70% of South Africa's coal production came from bord-and-pillar workings (Brink, 1983). Today, a major engineering problem linked to this mining method is that of surface subsidence. This problem is predominantly associated with the older mines – some dating back to the early 1900's. In the past irrational pillar design and pillar-robbing were commonplace and the results – often many years down the line – include the collapse of pillars, subsidence and even complete caving through to surface.

Subsidence associated with old bord-and-pillar workings is unpredictable and difficult to monitor. Caving can take place at any time (even after decades) as a result of one of the following:

- Gradual deterioration of pillars and bords.
- Changes in the seam conditions, such as the introduction or removal of water.
- Gradual punching of pillars into a weak floor.
- Deterioration of pillars as a result of waterlogged workings or underground fires.
- Collapse of bords with excessive spans.

Monitoring or inspection of old workings is very difficult because of limited access and inaccurate old mine plans; pillar robbing commonly took place in the last stages of the mining operations. Inspection of old workings was also done through the drilling of closely spaced boreholes (often in conjunction with downhole cameras). However, this was usually too costly. Development over old bord-and-pillar workings typically required a very accurate knowledge of the exact location of pillars. Rehabilitation of old workings, for example by construction of concrete pillars to provide additional support, is often necessary before development can take place.

The typical geometry of the pillars is approximately 6 m x 6 m horizontally, representing the remains of a 1-5 m thick mined out coal seam. The mined out bords separating these pillars have approximately the same horizontal dimensions as that of the pillars; however, they are sometimes slightly narrower. The bord height is usually slightly less than the seam height, leaving a thin coal roof and/or floor. These old working occur at an average depth of 30-40 m, but in extreme cases may be as shallow as 15 m or as deep as 80-100 m.

One of the key problems related to geophysically mapping bords and pillars is the unpredictable geoelectric structure. Coal is almost always electrically highly resistive (several thousand ohm metres). However, the cavities left by old mining operations may have a resistivity ranging from infinitely resistive to highly conductive. When air-filled a cavity is infinitely resistive and when it is filled with highly acidic mine water it can be highly conductive (resistivity of a few ohm metres). Any value between these two extremes is possible and one should expect such variations from site to site. For example, if a cavity is filled with relatively clean water, it may still be very resistive, but less so than in the air-filled case. For electrical techniques to be successful at mapping old workings a sufficient contrast in resistivity between the coal pillars and the mined-out cavities is needed. The fact that there may be little or no contrast between the electrical properties of the coal and the cavity filling material electrical properties should be taken into account.

The geoelectric character of the overburden can also have a major impact on the results of electrical resistivity survey. A thin surface layer with a highly contrasting resistivity can dominate a response and suppress any deeper, subtle anomalies. Near surface layers may vary from very conductive to very resistive, depending on factors such as climate and degree of weathering.

3.2 Sinkholes, cavities and underground fires

The occurrence of sinkholes and subsurface cavities in the Witbank area is a direct consequence of mining induced surface subsidence. Under the heading of sinkholes and cavities, two phenomena are considered, potholes and sinkholes.

As a result of subsidence, surface cracks appear, which extend down to the upper rock layers. The cracks in the soil may close up, but the extensions downward into the rock eventually form cavities as a result of subsurface soil erosion. Once these cavities attain a critical size they collapse resulting in potholes on the surface. The diameter of these potholes may vary from approximately 30 cm up to several metres. Potholes typically occur at relatively shallow depths – just below 6-10 m of overburden. The geophysical challenge is to detect potential cavities before they collapse. Once the first signs of early subsurface erosion potholes appear, the extent of the erosion needs to be determined. At times, the only evidence is a small surface hole a few centimeters in diameter.

The appearance of sinkholes above old bord-and-pillar workings is linked to the underground collapse of bords (mainly intersections). The width of such sinkholes is typically of the same order as the width of the underground bords, i.e., approximately six metres. The depth extent of sinkholes may be several metres (van der Merwe *et al*., 2000).

Typically, sinkholes occur at depths shallower than 50 m. A problem related to sinkhole formation is that of underground fires. Fires in old workings are usually a result of spontaneous combustion. Sinkholes allow fresh air into the old workings, supplying oxygen to the fires – this can, in turn, result in pillar failure and further subsidence.

The comments made in Section 3.1 regarding the unpredictability of the subsurface and near-surface geoelectric structure also applies to the detection of sinkholes and fires. Care must be taken when interpreting geoelectric data from any site, and it must be remembered that the nature of a specific type of problem may vary from site to site.

3.3 Acid mine drainage / pollution

High sulphate levels in excess mine water is the main cause of local acidification and regional salination of surface water resources in the Upper Olifants River Catchment in Mpumalanga. Sulphate levels varying between 120 and 160 mg/l are routinely recorded in the Witbank and Middelburg Dams, mainly as a result of coal mining and related activities. It is estimated that excess mine water currently amounts, volume wise, to only 4.6% of the total water usage, but contributes 78.4% to the sulphate load (Van Zyl *et al.*, 2000).

During mining operations the water table is often artificially lowered. The introduction of oxygen into the workings and the resulting oxidation of pyrites causes in-mine water quality to deteriorate (very low pH – acidic). After workings are abandoned, the water level may rise and the acidic water affects the surrounding groundwater system. Acid mine water is often pumped into massive evaporation/treatment dams. Leakage from such dams may also contribute to the contamination of groundwater resources.

The sulphate contaminants typically migrate as plumes from the source, which could be old workings or evaporation/treatment dams. A further concern regarding pollution associated with acid mine drainage is that, although acidic water is often treated to restore the pH to acceptable levels before it is introduced back into the water system, it may also contain dangerous heavy metals (Pers. Comm., R. Meyer, 2000).

4 GEOPHYSICAL PARAMETERS

For any geophysical method to be effective the fundamental criteria required is a contrast in the physical properties between the target and the surrounding rocks. The different classes of physical parameters where contrasts may be exploited, and the applicable geophysical methods are summarized in Table 1:

Table 1: Physical parameters that may be exploited with different geophysical techniques.

Physical parameters	Geophysical technique
magnetic susceptibility	magnetic method
density	Conventional or micro-gravity
electrical resistivity	direct current resistivity methods
electromagnetic resistivity and dielectric	electromagnetic methods
density and seismic wave velocity	seismic methods
thermal properties	thermal infrared imaging

The first step in solving a given geophysical problem is to determine which of the above parameters can best be exploited to discriminate the target from the host rock. This will determine the geophysical technique to select. There may be more than one applicable technique, allowing for the adoption of an integrated approach. The combined interpretation of two or more different data sets often results in a reduction in the ambiguity associated with interpreting the results derived from a single technique.

What follows is a brief discussion of some of the important physical and geometrical parameters of the various targets and other important features (e.g., overburden, interburden and intrusions) to be taken into account during this study.

As was stated previously, **coal** generally has a lower density, a higher electrical resistivity, a lower seismic wave velocity and a lower magnetic susceptibility than the surrounding rock (Jackson, 1981). Coal deposits usually occur as near-horizontal, planar seams with a thickness varying between tens of centimetres and a few metres. In a typical succession, several (4-6) coal seams occur at depths between 70-100 m and surface.

The primary geophysical target of Task 1.3.1b is old, abandoned bord-and-pillar workings. These **cavities** are either unfilled, or usually filled with water or mud. Other secondary cavities include sinkholes, potholes and cracks between the mined seam and surface. These may also be unfilled, or filled with water or unconsolidated rock and soil.

The physical properties of the **filling material** of cavities can vary depending on the type of filling. An air-filled cavity would have a lower density, lower magnetic susceptibility, lower seismic wave velocity and a higher electrical resistivity than the surrounding rock. A water or mud filled cavity will have a lower density compared to the surrounding rock, but a higher density compared to an air-filled cavity. If the water filling the cavity is relatively fresh it may also be resistive, although it will not be as resistive as in the air-filled case. However, the higher the sulphate content of the water, the more conductive the water will be. In the extreme case it might have a dc resistivity of only a few ohm metres.

The electromagnetic properties of such cavities will depend largely on the dissolved content of the water/mud, but will in all likelihood have relatively high conductivity (low resistivity) and high dielectric values.

Underground fires are confined to coal seams and their geometry and extent is principally dictated by the mine design/layout and geological structures, such as intrusions. Existing fires exhibit a significant thermal contrast with the environment. There is evidence in the literature that an underground fire may have a significant effect on the seismic and magnetic properties of the rock formations. The physical property differences between burning / burnt zones and the environment could be exploited.

The physical properties of **pollution plumes** are determined by the type or source of contamination. For example, sulphate, nitrate, chloride and hydrocarbon contamination typically causes an increase in electrical conductivity, while dense, non-aqueous phase liquid (DNAPL) contamination results in a decrease in electrical conductivity. The most common type of groundwater contamination expected on coal mines are high levels of sulphates and/or heavy metals.

The physical properties of the **overburden** are likely to constitute the most influential parameters in determining the applicability and performance of the various geophysical techniques. Layered sediments, which are notoriously conductive, cover most of the Coaltech 2020 study area. Traditionally this has been a significant obstacle to the application of electromagnetic techniques (Pers. Comm., E. Stettler, 2000, C. van Dam, 2001). The overburden is typically 10-20 m thick, rendering EM penetration to coal seams extremely difficult. The sedimentary rocks occurring between the various coal seams **(interburden)** are also relatively conductive and contribute further to the generally poor penetration achieved using EM methods.
The relatively large depth-to-size ratio of old coal pillars (up to and exceeding 5:1) makes the achievement of high mapping accuracies (1-2 m resolution) extremely difficult. This is particularly pertinent to potential field methods such as gravity, magnetic and electrical.

Dolerite **intrusions** (dykes and sills) are often mapped through exploiting their magnetic character. Dolerites intrusions tend to be very resistive and in some cases can be detected using electrical or electromagnetic techniques.

5 GEOPHYSICAL TRACK RECORD

In this section the potential applicability of various techniques is illustrated through relevant examples taken from the literature.

5.1 Detection of old workings and other cavities

A number of geophysical tools have the potential to detect old bord-and-pillar workings and the cavities associated with sinkholes and potholes:

Electrical methods are often used to detect various types of sub-surface cavities and some examples are mentioned below. Jackson (1981) reports on the successful use of electrical methods to detect sub-surface cavities in the coal environment. It is therefore beneficial to further investigate its applicability to the detection of old bords, sinkholes and potholes.

Spiegel *et al.* (1980) used theoretical calculations and model (tank) studies to illustrate how the resistivity method (surface profiling) can be used to detect subsurface voids. They also considered the problem of uneven surface topography and how to correct the measured data using a numerical transformation process. The pole-dipole electrode configuration was used to successfully detect elongated tunnels with a depth:size ratio of up to approximately 4:1.

Peters and Burdick (1983) report on the use of an automatic resistivity system to detect both air- and water-filled cavities in old coal mine workings. The detection of cavities with a depth-to-size ratio of up to, and exceeding, 10:1 is possible. The authors present the results of a number of field trials. The pole-dipole electrode array was used in preference to the more commonly used arrays like the Wenner array. The pole-dipole array provides a better response to deeper anomalies. This advantage of the pole-dipole array is related to the relatively small increase in the effective measurement volume as the depth of investigation increases (compared to the other electrode configurations mentioned above).

Sretonovic *et al.* (1992) reported on how shallow underground mine workings can be detected using electrical methods. The Wenner array was used with various electrode spacings and a depth of investigation in the range of 30-50 m was reported. Detected anomalies were correlated with disturbed zones (collapses and cavities) in the vicinity of old mine workings.

Ogilvy *et al.* (1991) applied the Very Low Frequency Resistivity **(VLF-R)** method successfully to map air-filled drainage galleries embedded in conductive clay and superficial gravels. The cavities were approximately 1 x 2 m and 4-5 m deep. A deviation and concentration of current flow lines above and below the voids (current gathering) resulted in an abnormally high primary electric field (higher apparent resistivities). A decrease in phase was also associated with a resistive structure below the uppermost layer. Ogilvy *et al.* (1991) confirmed the field results through numerical simulations.

The **magnetic method** may prove to be be a useful tool in detecting near surface cavities. Unfilled cavities produce a negative magnetic anomaly, however, a cavity filled with material of a higher susceptibility will produce a positive anomaly (Jackson, 1981).

Micro-gravity measurements - measured at much higher accuracies compared to conventional gravity surveys – may be applicable to the detection of sub-surface cavities and sinkholes and will be investigated in a separate study to be conducted by Anglo American Geophysical Services Division.

Conventional Frequency-Domain - **(FDEM)** and Time-Domain Electromagnetic **(TDEM)** profiling techniques are unlikely to be applicable to the detection of old workings because of the relatively thick, electrically conductive overburden. However, some EM techniques, for example, FDEM and Ground Penetrating Radar **(GPR)**, may prove useful in detecting near surface sinkholes and potholes. Jackson (1981) reports on the successful use of GPR to map the thickness of relatively shallow coal pillars (15 m deep). The presence of layered sediments and thick, conductive overburden however, are expected to pose major obstacles for the EM methods in a South African context.

The use of the Controlled Source Audiomagnetotellurics (**CSAMT**) technique for the location of abandoned mine voids was reported on at the 1983 Society of Exploration Geophysicists (SEG) Annual Meeting (Lepper, 1983). Unfortunately, a copy of the abstract could not be obtained. It is therefore not possible to comment on the success of the survey, or to assess the applicability of CSAMT to detecting/mapping subsurface voids based on the literature search.

The ability of the Thermal Infrared Imaging technique (**TIR**) to map old bord-and-pillar workings is presented in Appendix B. This technique has however, not been evaluated or benchmarked to determine its limitations in terms of spatial and depth resolution etc. In Appendix B, compiled by AATS, the principles and applicability of TIR are discussed.

5.2 Detection of fires

Although the focus of this Coaltech project is on non-seismic techniques, the technology audit did not exclude references to seismic studies. Bregman *et al.* (1989) conducted a cross-borehole **seismic** tomography experiment to locate and characterize a fire front at an enhanced oil recovery pilot project. The significant result from this study was that the high temperatures associated with underground fires can cause a significant reduction in P-wave velocity. This is attributed to the presence of combustion, the injection of gasses, and permanent alteration of the formations by high temperatures. The authors emphasized that the interpretation of the tomographic data is not straightforward – the presence of fracture systems, complex geology etc. complicate the interpretation process. The effect of heat on seismic parameters may have an important implication for Coaltech Project 1.3.1a and 1.3.1b.

In the United States **magnetic** susceptibility measurements are used to locate the edges of burnt zones (Jackson, 1981). The burning that results from the spontaneous combustion of coal seams bakes the surrounding rocks thus altering the magnetic properties of these rocks.

Laboratory tests have shown that temperatures as low as 200°C are sufficient to change the magnetic susceptibility of some sediments (Jackson, 1981).

TIR, for obvious reasons, appears to be the most applicable geophysical technique to detect/map underground fires. The principles and applicability of TIR are presented in Appendix B of this report.

The use of **CSAMT** for the evaluation of abandoned coal mine fires was reported on at the 1982 Society of Exploration Geophysicists (SEG) Annual Meeting (Bartel, 1982). This document could also not be traced at the time of conducting the literature review.

5.3 Detection of acid mine drainage/pollution

The use of geophysics to detect contaminant sources and to map (in space) and monitor (over time) groundwater contamination has been practiced for some time. **Electrical** and **electromagnetic** techniques have been in use for several decades to address contaminant problems. Inorganic pollutants tend to raise the groundwater conductivity, giving rise to measurable apparent conductivity anomalies at the surface. Geophysical techniques, such as four electrode resistivity methods, inductive methods, **VLF** methods and **GPR**, have been used effectively to exploit the relatively conductive signatures of such contaminant plumes (Greenhouse *et al.*, 1989).

The presence of conductive clays and the temporal variations in surface moisture and groundwater levels are factors that may have an adverse effect on the mapping of contaminant plumes in space and over time. The challenge here is to discriminate between the anomalous behaviour of the contaminant and that of other conductive features. **TIR** may also be applicable to the mapping of polluted areas (Franzen, 2000).

A literature search indicated that both **magnetic** and **gravity** methods have been applied to the detection of acid mine drainage in Northern Ontario, Canada (Gamey, 1998). The potential of the magnetic and gravity methods will be examined in more detail during Year 2 of Task 1.3.1b.

6 DESKTOP STUDIES

Geophysical techniques identified as having a potential application to at least one of the problem scenarios associated with Task 1.3.1b include:

Microgravity (M-GRAV)
Thermal Infrared imagery (TIR)
Electrical resistivity (RES)
Ground penetrating radar (GPR)
Controlled source audio magnetotellurics (CSAMT)
Very Low Frequency Resistivity (VLF)
Magnetics (MAG)
Frequency Domain Electromagnetics (FDEM)
Other geophysics?

During the course of Year 1 a qualitative performance prediction analysis was conducted and the above techniques were rated in terms of ability to *detect* the different targets under ideal conditions. The techniques were also rated in terms of their applicability as a function of depth. The intention is to refine these ratings over time, and eventually produce a geophysical applicability guide for the coal industry. However, before presenting the current analysis, the various desktop study results will be summarized. The individual desktop studies have been published as separate Coaltech subtask reports.

6.1 The controlled source audio magnetotelluric (CSAMT) method

The pertinent conclusions of this study (Cole, 2000) can be summarised as follows:

• The numerical modeling results suggested that the CSAMT method is not well suited to the investigation of old mine workings.

• The resolution of the technique is not high enough for the relatively small features that are targeted in Task 1.3.1b. For example, the technique is not able to separate two horizontal coal seams at 15 m and 30 m, respectively; these appear as a single resistive horizon on output mages.

• Air-filled cavities within a coal seam cannot be detected due to the poor discrimination between resistors. This is a general problem with electromagnetic techniques.

• A cavity filled with relatively conductive material does have an effect on the CSAMT output, but the resolution is too low for accurate location. This result, however, implies that the CSAMT method may still be useful to discriminate mined out areas that have been flooded with conductive material from unflooded areas or unmined areas.

6.2 Ground Penetrating Radar (GPR)

Relevant conclusions of this study (Vogt, 2001) are as follows:

• Geological materials in the coalfields are not suitable for GPR propagation.

• A potential application of interest is that of looking into the side walls of the seam, rather than up or down within the seam. This application is a result of electrical anisotropy.

• It is not possible to use GPR to image a coal seam from surface due to the range-resolution trade-of. A range of 30 m is unlikely and even if it is possible, the estimated resolution will be no better than 5 m to 7.5 m. For some materials studied, however, the loss tangent increases as frequency decreases, thus for frequencies low enough to penetrate 30 m, the resolution may be as poor as 15 m.

• Electrical properties are also a function of water content. In general, if there is water in the rock, it increases the resolution, while substantially decreasing the range. Near surface water will therefore contribute to poor GPR performance.

• In general, GPR is not expected to be a viable technique in the coal environment. There is, however, one exception: stress-induced cracks or voids located above beams over old workings, provided they are very close to surface.

• Theoretically, the electrical properties of burnt coal are sufficiently different to those of competent coal to make the change visible in the GPR record. In practise, the poor penetration of GPR in coal makes long-range prediction of burnt coal unfeasible.

6.3 Electrical resistivity methods

The most important conclusions from the study (Van Schoor, 2001) follow:

• Although the electrical resistivity method has good detecting capabilities, the resolution achieved is too low to solve the primary problem of resolving individual gaps / pillars within old bord-and-pillar workings.

• The detection of the boundary between un-mined and mined-out areas using resistivity profiling appears to be a promising application of the technique.

• A reasonable degree of confidence can be placed in the technique for mapping anomalous (conductive and resitive) features in the upper 15-20 m. This applies to the detection and mapping of potholes and sinkholes.

• Overburden may have an adverse effect on resistivity surveys. If a highly contrasting (resistivity) surface layer is present, variations in the thickness or resistivity of this layer (due to varying degrees of weathering) may result in unwanted anomalies that mask the deeper, less prominent anomalies of interest.

• It may be possible to delineate pollution plumes occurring close to surface using this technique. Dynamic monitoring may also prove useful in areas where known or potential pollution problems occur.

• It is uncertain whether the resistivity technique is applicable to the mapping of underground fires.

6.4 Micro-gravity

A 3D modelling exercise was undertaken to quantify the limits of detection of the microgravity method (Lowe and Muller, 2001). The conclusions of this study can be summarised as follows:

• Standard microgravity surveys (at 5m grid intervals) over coal seams at depths below 6m only yield the average or bulk response of the bords and pillars in old workings.

• It is only possible to map individual bords and pillars of ultra-shallow (<6m deep) old workings in ultra-high resolution (<5m station intervals) surveys.

• It is possible to detect the edge of water- or air-filled old workings to maximum depths of 50m and 150m, respectively.

• It is possible to resolve the edges of old workings on two different coal seams to a minimum horizontal separation of 30m for shallow seams (< 25m deep) or 90m for deeper seams (< 70m deep).

• Air-filled large (6m diameter) ratholes will be observed by microgravity to a maximum depth of 12m.

• Air-filled small (3m diameter) ratholes will be observed by microgravity to a maximum depth of 9m.

• Water-filled large (6m diameter) ratholes will be observed to a maximum depth of 9m.

• Water-filled small (3m diameter) ratholes will be observed to a maximum depth of 6m.

• Extensive surface weathering may produce lower amplitude gravity anomalies over ratholes than would otherwise be expected as the density contrast between the ratholes and the surrounding host rock is lower.

• A cluster of ratholes produces a large negative anomaly of the order of tens of μGals which would easily be observed by microgravity surveys.

Microgravity surveys were conducted at Arthur Taylor and Kromdraai Collieries in order to detect the edge of the old workings and the possible occurrence of ratholes. The edges of the old water-filled #2 seam workings, located at depths in the range 23-40m, were successfully detected with an accuracy of about ±7m (one station interval), on all five of the microgravity profiles that were carried out during the test survey at Arthur Taylor Colliery. The observed gravity anomalies compare well with the forward models (for water-filled workings).

At Kromdraai Colliery, a number of roughly circular anomalies were detected in the microgravity data but none with an amplitude larger than 14 μGals. Therefore it was inferred that there are no ratholes with a diameter greater than 6 m at a depth shallower than about 6 m, and none with a diameter greater than 3 m shallower than about 3 m, anywhere in the survey area. The observed anomalies may instead be the result of local variations in overburden weathering and density. The results for both of the case histories are yet to be confirmed by drilling.

6.5 Thermal Infrared Imagery (TIR)

The TIR report (Franzsen, 2000) is primarily a literature review does not include any numerical modeling or simulations. This report does, however, include some case studies and references to past surveys that suggest the following:

• TIR can be used to delineate, underground fires, sinkholes and pollution plumes.

• TIR can also be used for the high-resolution mapping of old bord-and-pillar workings.
However, the range of the instrument, and how it will respond in non-ideal conditions, have not yet been established. These issues should be resolved during the surveys planned for 2001.

• A resolution of ~ 5 m can be obtained with the TIR instrumentation to be used during the Coaltech 2020 programme.

7 PERFORMANCE PREDICTION ANALYSIS

On the basis of all the available information an applicability/performance assessment was carried out. The following simple rating system was used:

1 Unlikely to be useful or unsatisfactory results obtained in past - **Low potential.**

2 Survey(s) recorded in literature, but degree of success/potential uncertain or untested. Technique may have **some potential.**

3 Moderate/high success rate - **medium-high potential.**

The various problem scenarios relating to Task 1.3.1b were subdivided into the following categories:

• Delineation of old workings (flooded vs. unflooded)
• Mapping individual pillars within old working
• Mapping of cracks, potholes and sinkholes
• Delineation of pollution plumes
• Delineation of burning zones, and
• Delineation of burnt zones

Table 2: Applicability/performance prediction rating versus target type

	Target Type				
Technique	**Delineation of old workings: void / flooded**	**Pillar delineation**	**Cracks, potholes & Sinkholes**	**Underground fires and burnt zones**	**Pollution plumes**
Electrical	**3 / 3**	**1**	**3**	**1**	**3**
Magnetic	**2 / 2**	**1**	**2**	**2**	**2**
Micro-gravity	**3 / 2**	**1**	**3**	**1**	**2**
VLF	**2 / 2**	**1**	**2**	**1**	**2**
FDEM	**2 / 2**	**1**	**2**	**1**	**2**
GPR	**1 / 1**	**1**	**3**	**1**	**1**
CSAMT	**1 / 2**	**1**	**1**	**2**	**2**
TIR	**3 / 3**	**3**	**3**	**3**	**3**

Note that the principle variables considered in the above analysis are the expected target physical properties and geometry rather than the absolute depth of the target.

Table 3: Applicability/performance prediction rating versus depth of investigation

	Target Depth			
Technique	**0-15 m**	**15-30 m**	**30–45 m**	**>45 m**
Electrical	**3**	**2**	**2**	**1**
Magnetic	**2**	**2**	**1**	**1**
Micro-gravity	**3**	**3**	**2**	**1**
VLF	**2**	**2**	**1**	**1**
FDEM	**2**	**1**	**1**	**1**
GPR	**3**	**1**	**1**	**1**
CSAMT	**1**	**1**	**2**	**3**
TIR	**3**	**3**	**2**	**1**

The analysis in Table 3 is simply a qualitative indication of the comparative depth ranges for the various techniques considered in this study.

Table 4 Estimated relative surveys costs (assuming a 5 m station spacing and including mobilization / demobilization and data processing / interpretation)

Technique	*Relative* Cost per line km / ha	Is equipment/skills available locally?
Electrical	3	YES
Magnetic	1	YES
Micro-Gravity	10	NO
VLF	2	YES
FDEM	2	YES
GPR	1.5	YES
CSAMT	7	YES
TIR	2	NO

The following points relating to the above assessment (tables 2-4) must be highlighted:

• It is important to emphasise that the above analysis is not comprehensive, as some important factors have not yet been incorporated into the assessment. These factors include dykes and sills, overburden characteristics and surface activities, e.g., cultural, mining, vegetation etc. Note that these tend to be site specific factors that need to be dealt with on a site-by-site basis.

• Of all the techniques considered, the TIR and electrical methods appear to have the widest range of potential applicability (Table 2). Micro-gravity also shows good potential.

• The performance of most techniques is expected to deteriorate rapidly with increasing depth (Table 3). For targets beyond approximately 30 m depth only techniques such as electrical resistivity, micro-gravity, CSAMT, and possibly TIR are expected to produce useful data. It is highly likely that this data will provide qualitative information. Some techniques, like GPR, are only expected to provide useful data for very shallow (< 15 m) targets.

• The CSAMT technique is better suited to imaging deeper features than near surface features. Due to the underlying physics of the technique, the upper 20 m or so is effectively a “blind zone”, i.e., no resolution capability above a specific depth is possible. The CSAMT desktop study indicated that the resolution capabilities of CSAMT are not expected to be high enough for it to be used. However, the CSAMT technique should not be ignored as it is still considered to have potential in terms of delineating mined-out areas, mapping underground fires and pollution plumes.

• Other techniques such as FDEM, Magnetics, and VLF did not receive a medium-to-high potential (3) rating in any of the categories. These techniques may, however, still be useful tools when solving certain near surface problems. If new evidence suggests that one or more of these techniques should receive further attention, research efforts will be directed accordingly. The same holds for techniques that have up to now been overlooked. Such techniques include time-domain electromagnetics (TDEM) and Induced Polarization (IP).

• The degree of confidence in obtaining geophysical solutions for targets buried deeper than approximately 30 m is low. This is a cause for concern, as the average depth of old bord-and-pillar workings, the primary target of this project, is approximately 30 m. It is also appears that none of the techniques considered, with the exception of TIR, is capable of accurately imaging the precise location of individual pillars. However, the limitations of TIR will only be known once the planned Year 2 surveys have been completed.

• At present, appears to be the only technique capable of detecting underground fires directly. Available information suggests that seismics, magnetics and CSAMT may also be applicable to this problem (see Section 5.2).

• In terms of cost two of the techniques, namely micro-gravity and CSAMT, are very expensive to apply. The high cost is mainly dictated by the unavailability of appropriate instrumentation and skills locally, and by the fact that these techniques are extremely time-consuming. However, if micro-gravity and CSAMT prove to be valuable tools, ways of reducing their operating costs will be investigated. Applying the TIR technique is relatively inexpensive, provided a large enough area is targeted as the mobilization and flying costs are high. Promising TIR survey results may generate sufficient interest in the technique making routine application feasible.

8 CONCLUSIONS AND RECOMMENDATIONS FOR YEAR 2

Even though theoretical performance prediction analyses provide a useful guideline for deciding which technique(s) are best suited to a given problem, the proposed analysis must be tested against reality. In reality problems experienced by mines are more complex than many of the 2-D and 3-D models used in the desktop studies. Furthermore the issue of site specifics comes into play: Mine A and Mine B may have the same type of problem, for example, the need to delineate 30 m deep flooded workings, however, even subtle differences can result in two very different problems. Factors that can change the nature of the problem include the presence and characteristics of the overburden and interburden material, the physical properties of the material filling the workings, the presence of dolerite intrusions and cultural activity on surface etc.

Currently no new or existing field data has been acquired or evaluated. Field trials were planned for the latter part of Year 1, but a number of factors caused a delay. Site visits and field trials are now scheduled for the period March-June 2001. As was mentioned earlier, at least three test sites, (Kromdraai, Tavistock and New Largo) will be targeted during this period.

It is recommended that, at every test site, as many different techniques as is practically possible be tested. This may include techniques that have not been considered to date. Good geological control, for example, accurate mine plans, drilling reports etc. will be needed at the test sites for verification of geophysical interpretations. Although a large number of surveys are desirable, money needs to be invested in ground truthing existing geophysical interpretations.

It is recommended that the work programme for Year 2 include the following components:

• Continuation of site visit and field survey programme
• TIR surveys and data processing
• Ongoing evaluation of geophysical data, comparing of different data sets, and ground truthing, and
• Final assessment of all geophysical techniques investigated.

The anticipated end result is a user-friendly applications guideline for geophysical solutions applicable to the problems related to old bord-and-pillar workings. This document will be supported by a collection case histories.

9 REFERENCES

Bartel, L.C. 1982. Evaluation of the CSAMT geophysical technique to map abandoned coal mine fires: Annual Meeting Abstracts, Society Of Exploration Geophysicists, Session: C1.1.

Bregman, N.D., Hurley, P.A., and West, G.F. 1989. Seismic Tomography at a fire-flood site: *Geophysics*, 54 no. 09, 1082-1090.

Brink, A.B.A. 1983. Engineering Geology of Southern Africa, Volume 3 (Karoo Sequence).

Cole, J., 2000. CSAMT numerical modelling of coal seams: COALTECH 2020 Report (part of Subtask 4, Task 1.3.1b).

Gamey, T.J., 1998. Acid Mine Drainage in Northern Ontario, in Gibson, R.I. and Millegan, P.S., Ed., Geologic Applications of Gravity and Magnetics: Case Histories: Society of Exploration Geophysicists, 112-113.

Franzsen, A.J. 2000. Detection of old workings, sinkholes, underground fires and acid mine pollution using geophysics and airborne thermal imagery. Coaltech 2020 Report (part of Subtask 3, Task 1.3.1b).

Greenhouse, J.P., Monier-Williams, M.E., Ellert, N., and Slaine, D.D. 1989. Geophysical methods in Groundwater contaminant studies. *Proceedings of Exploration '87* held in Toronto, Canada, September-October, 1987, Ontario Geological Survey, p 666-677.

Jackson, L.J. 1981. Geophysical examination of coal deposits, IEA Coal Research Report ICTIS/TR 13.

Lepper, C.M. 1983. The controlled source audiomagnetotellurics (CSAMT) method for locating abandoned mine voids: Annual Meeting Abstracts, Society of Exploration Geophysicists, Session:C1.1.

Lowe, S.J. and Muller, M. The Microgravity Method for Underground Cavity Detection: Coaltech 2020 Report (part of Subtask 4, Task 1.3.1b).

Meyer, R. 2000. Personal communication on issue of ground water quality in the Witbank coal areas. CSIR: Environmentek, Pretoria.

Ogilvy, R.D., Cuadra, A., Jackson, P.D., and Monte, J.L., 1991. Detection of an air-filled drainage gallery by the VLF resistivity method: *Geophysical Prospecting*, 39, no. 06, 845-860.

Peters, W. R. and Burdick, R. G. 1983. Use of an automatic resistivity system for detecting abandoned mine workings. *Mining Engineering*, January 1983, 55-59.

Spiegel, R.J., Sturdivant, V.R., and Owen, T.E. 1980. Modeling resistivity anomalies from localized voids under irregular terrain: *Geophysics*, 45 no. 07, 1164-1183.

Sretonovic, B.B., Milicevic, B.A., and Marcetic, D.D. 1992. Detection of disturbed zones over old mine workings using electrical tomography: Technical Programme and Abstracts of Papers, 54th Meeting and Technical Exhibition of the European Association of Exploration Geophysicists, Paris France, 1992.

Stettler, E.R. 2000. Personal communication on the application of electromagnetic techniques. Council for Geoscience, Pretoria.

Van Dam, C. 2001. Personal communication on the application of electromagnetic techniques.

Van der Merwe, J. N., van Zyl, M. and Daehnke, A. 2000. The development of techniques to predict and manage the impact of surface subsidence. *COALTECH 2020 Interim Report (Task 6.9.1)*.

Van Schoor, A.M. 2001, Application of electrical resistivity in the coal environment: Coaltech 2020 Report (part of Subtask 4, Task 1.3.1b).

Van Zyl, H.C., Maree, J.P., van Niekerk, A.M., van Tonder, G.J., and Naidoo, C. 2000. Collection, treatment and re-use of mine water in the Olifants River catchment pp 93-98: Coal – The Future, 12th International Conference on Coal Research, 12-15 September 2000.

Vogt, D.R. 2001. Application of GPR in coal: Coaltech 2020 Report (part of Subtask 4, Task 1.3.1b).

APPENDIX A: Year 1 task plan (Task 1.3.1b)

Table 3: Sub-task information for Task 1.3.1b:

Sub-task No:	Sub-task Description	Expected Result	Deliverable	Start Date	Due Date	Cost KR
1)	Establish research team and define responsibilities.	Detailed project definition.	Interim Report	01/04/2000	30/09/2000	30
2)	Technology audit.	Identify most promising techniques, potential pitfalls etc.	Interim Report	01/07/2000	15/10/2000	20
3)	TIR survey planning	Detailed survey plans for at least 2 Witbank sites.	Interim Report	01/07/2000	15/10/2000	15
4)	Geophysical desktop studies Part I.	Applicability and performance prediction studies for electrical, electromagnetic and other techniques.	Interim Report	01/08/2000	30/11/2000	82
5)	Field trials	Trial data sets over parts of at least 2 of the sites where airborne TIR surveys were planned/conducted.	Interim Report	01/10/2000	30/12/2000	113
6)	Desktop studies Part II: Micro-gravity	Applicability and performance prediction study	Interim Report	01/10/2000	15/02/2001	25
7)	Project Final report	Conclusions and recommendation, Budget for Year 2	Final Report	01/01/2001	15/03/2001	70
			TOTAL (Excl. VAT)			**355**

APPENDIX VIII

COALTECH 2020

Interim Report

Geophysical trials at Kromdraai & New Largo Collieries.

Preliminary results

M. van Schoor

CSIR, Division of Mining Technology

Report number: 2001-0122

Task 1.3.1b

Detection of old workings, sinkholes, underground fires and acid mine pollution using geophysics and airborne thermal infrared imagery

1 September 2001

EXECUTIVE SUMMARY

Ground geophysical trials were conducted at Kromdraai and New Largo collieries during the winter months of 2001. The aim of these surveys was to build up a collection of case studies that form part of a geophysical applications guideline for the Witbank-Highveld collieries.

This report provides an overview of the preliminary results as at the end of August 2001. To date, all the ground geophysical trial surveys have focussed on the detection of old workings (mapping individual bords and pillars as well as mapping the edge of workings) and on the mapping of near surface sinkholes.

The micro-gravity and electrical resistivity methods show the most promise in terms of locating the edge of old workings and cavity detection. The accurate mapping of individual bords and pillars, however, does not seem possible with any of the conventional techniques tested thus far.

TABLE OF CONTENTS

LIST OF FIGURES AND TABLES

1 BACKGROUND

Coaltech 2020 Task 1.3.1b focuses on the use of geophysical techniques for the detection and mapping of the following features:

1) pillars and voids of old mine workings,
2) shallow sinkholes developed in overburden above old mine workings,
3) underground fires, and
4) acid mine pollution plumes.

During Year 1 of Task 1.3.1b various geophysical techniques were evaluated on a theoretical level and the applicability of the different techniques was predicted. Of those considered, a performance prediction analysis indicated that the most promising techniques were Thermal Infrared Imagery (TIR), micro-gravity and electrical resistivity (Van Schoor, 2001). It was recommended to test these, and a few other techniques at selected sites during Year 2 (2001/2002).

To date, geophysical trials have been conducted at the following sites (with the primary geophysical targets indicated in brackets):

- Kromdraai (individual bord-and-pillars, edge of workings and near surface cavities)
- New Largo (near surface cavities)

Further trials are planned for September/October 2001 at Arthur Taylor Colliery, where the target will be the edge of old 2 Seam workings.

The planned airborne TIR surveys were conducted during July and the data is currently being processed. It is anticipated that the method will have a high degree of success for mapping all the targets mentioned above. Processing of the data is currently underway and results can be expected towards the end of the current year. Further follow-up ground geophysical surveys may be conducted targeting interesting anomalies identified with the TIR method.

In this report only the results of the ground geophysical surveys conducted to date are presented and discussed. A cost analysis of the techniques employed is included.

2 KROMDRAAI FIELD SURVEYS

The test site at Kromdraai was selected on the basis that a small-scale micro-gravity survey had already been conducted on the property, shortly before Task 1.3.1b started in April 2000. The purpose of the micro-gravity survey was to map the boundary between old #1 Seam workings and unmined areas, and to detect subsurface sinkholes. As this survey fitted well into the project definition of Task 1.3.1b, it was decided to target the same survey area with other ground geophysical techniques. Unfortunately, when the site was revisited to conduct these follow-up surveys, the overburden removal for the next phase of surface mining had already commenced and this affected part of the planned survey area. Consequently, it was decided to focus the follow-up surveys on the south-eastern side of the grid and mainly on the problem of detecting the edge of old workings. A schematic of the Kromdraai test site, showing the micro-gravity survey grid and the area affected by current surface mining operations, is presented in Figure K1. Although the location of the edge of workings is not a problem for the geologists at Kromdraai, it is sometimes a problem at other collieries, especially when the accuracy of historic mine plans is uncertain. Furthermore, Kromdraai is the ideal test site as the old #1 Seam workings are relatively shallow (~12-15 m) compared to other Witbank-Highveld collieries. The Kromdraai site can therefore be regarded as an example of a “best-case-scenario” for evaluating the applicability of geophysical techniques to mapping the edge of old workings.

2.1 Micro-gravity survey

Compagnie Generale de Geophysique (CGG), a French company, was subcontracted by Anglo American's Geophysical Services Division (GSD) to conduct the micro-gravity survey at Kromdraai during January 2000. The 50 m x 105 m grid was surveyed at 5 m station and line intervals. An additional 80 m long profile was surveyed on the western side of the grid (see Figure K1). The total survey time was 11 days. A detailed discussion of the data acquisition and processing procedures is presented in Lowe et al. (2001). The results of the Kromdraai micro-gravity survey are presented in Figures K2 to K6.

2.2 Total field magnetics (TFM)

Two parallel magnetic profiles were acquired along the south-eastern edge of the original micro-gravity grid using an EDA OMNI-IV magnetometer. The profiles extended from 10 m south-west of S70 to approximately 76 m north-east of S19 (Figure K7). A total of 8 further profiles, spaced 5 m apart, were subsequently acquired to cover the 50 m x 35 m area indicated in Figure K7. A station spacing of 2.5 m was used. The placement of this grid is such that the known edge of workings traverses through the grid in a north-south direction, approximately midway along the long axis of the grid. The results of the two single SW-NE profiles are shown in Figure K8, while the contoured TFM data for the rectangular grid is presented in Figures K9 to K11. In Figure K9 the result of contouring all the data is shown. The effect of the prominent positive-negative anomaly is then suppressed and the trend in the data (Figure K10) is removed to produce the residual TFM map in Figure K11.

2.3 Frequency domain electromagnetics (FDEM)

The FDEM system of Des Barlow was used in this survey. This instrument is similar to the Geonics EM-34, but can measure up to 8 different frequencies simultaneously (compared to the single frequency EM-34). Two horizontal loop (vertical dipole) FDEM profiles were acquired. The first profile started on the area where the overburden had already been removed and extended in a NE direction for 96 m, crossing over onto unscraped terrain at 50 m, as is indicated in Figure K12. The second profile extended from 10 m west of S19 to approximately 80 m NE of S19. This profile runs over an area where the overburden is still intact. The station spacing for FDEM1 and FDEM2 was 2 m and 4 m, respectively. The results of the FDEM survey are shown in Figures K13 and K14.

2.4 Ground penetrating radar (GPR)

GPR profiles were run over the known edge of workings as well as over the to be mined area where the overburden had been removed. Both GPR profiles were 50 m long and data was acquired using a GSSI SIR-2M radar system with 300 MHz antennas. The location of the two GPR profiles is the same as for the FDEM profiles, except that they were shorter (Figure K12). The results of the GPR survey are presented in Figure K15.

2.5 Resistivity Tomography survey (RESTOM)

A RESTOM survey, aimed at mapping the boundary between the old workings and the unmined area, was conducted. The RESTOM profile was also located along the southeastern side of the original micro-gravity grid extending from approximately x = -40 to x = 110. The in-line dipole-dipole configuration was used with current and potential dipole lengths and station spacing all equal to 4 m. A line of approximately 150 m was surveyed. The RESTOM output image is presented in Figure K16.

3 DISCUSSION OF KROMDRAAI RESULTS

3.1 Micro-gravity

Although a detailed discussion of the micro-gravity results can be found in Lowe et al. (2001), the most important points, including some of the key modelling results, are highlighted:

- The map of relative ground elevation provides no indication of subsurface sinkholes through the occurrence of subtle surface depressions (Figure K2).
- The residual gravity map with the old workings map overlain is presented in Figure K3. The region of broad positive anomalies towards the west of the surface area may be related to the fact that larger pillars have been left unmined in this area.
- High risk anomalies (high negatives) were categorised according to their dimensions and amplitudes. However, it was concluded that even the highest priority anomalies (amplitude ~ 14 μGal) did not represent potentially large and problematic sinkholes (amplitudes of 25-50 μGal). The observed anomalies may be the result of local variations in overburden weathering and density.
- The edge of workings was successfully identified and is located at the inflection-point between the gravity low of the old workings and the gravity high of the unmined area. The accuracy of the mapping is ± 5 m (one station interval).
- Modelling has shown that individual bords and pillars will only be observed over ultra-shallow (< 6 m) workings using ultra-high resolution surveys (station intervals < 5 m).
- Modelling further shows that it should be possible to map the edge of workings to a depth of 150 m and 50 m for air-filled and water-filled workings, respectively.

3.2 Total field magnetics (TFM)

There is a subtle trend evident in the two TFM profiles in Figure K8, with slightly higher field values measured on the northeastern side of the survey area. There is a prominent anomaly at approximately x = 35 m. On TFM1 this anomaly is predominantly negative, but on TFM2 it comprises a negative and a positive peak. This anomalous feature, which is also evident in the contour map in Figure K9, dominates most other features of potential interest. From the contour map it is clear that the anomaly is caused by an isolated source, as opposed to a linear feature. The 1D trend observed in the profiles of Figure K8 is also manifested in 2D in Figure K10. This trend may be caused by the mined-out area having a smaller bulk susceptibility (due to the presence of air-filed voids) than the un-mined ground. Figure K11 shows a residual magnetic contour map in which the trend in Figure K9 is removed from the data. The effect of the prominent anomalous feature in Figure K8 is suppressed by clipping the data range. Details previously suppressed are now more pronounced. The contour map shows one interesting feature, namely the zone of low field strength that runs from approximately x = 35, y = 35 down in a southerly direction and then turns west towards x = 0, y = 15. This band of low field strength correlates reasonably well with the edge of the old workings (see schematic map in Figure K7). Unfortunately the area covered in this small-scale survey is not big enough to confirm this correlation. It is recommended that airborne magnetic data of the site, or a similar site, be studied to investigate this issue further. It is also recommended that the effect of sub-surface voids on TFM responses be modelled to gain a better understanding of magnetic data over mined-out areas.

The source of the isolated anomaly at x = 35, y = 5 - 10, which dominates the contour map in Figure K9, is not clear, but it is most probably caused by buried metal or machinery.

There is a further low-amplitude positive anomaly at x = -30 on profiles TFM1 and TFM2. Unfortunately, insufficient data is available to make a judgement on the source or geometry of this anomaly.

It must be emphasised that the sections of the TFM profiles that extend over the old workings do not show any indication that it is possible to map individual bords and pillars using the magnetic method.

3.3 Frequency domain electromagnetics (FDEM)

The purpose of conducting profile FDEM1 was to assess whether the alternating bord-and-pillar pattern would manifest itself on the FDEM signature. It is for this reason that a relatively small station spacing of 2 m was used. However, no clear pattern is evident in the rather noisy data, also the coherency between frequencies is poor. FDEM2 was conducted over the known edge of workings. There is a very subtle trend in the data, which can be explained in terms of the expected higher bulk conductivity on the northeastern side of the edge, and hence the associated increase in measured values. However, it must be emphasised that this trend is not clear. It can be concluded that this site is not well suited to the FDEM technique. The air-filled (resistive) voids in the mined-out area are poor EM targets as they are effectively transparent to the EM technique.

3.4 Ground penetrating radar (GPR)

The environment is too conductive to allow good radar penetration beyond a few metres. In GPR1 some near surface radar returns can be seen in the early part of the record (A in Figure K15). The corresponding two-way travel-time of ~0-50 ns corresponds to a depth range of approximately 0-2.5 m[A]. The dipping reflector, marked B in Figure K15, extends down to a time of aproximately 180 ns, which corresponds to a maximum depth of approximately 9 m. GPR is therefore not applicable to the mapping of individual bords and pillars. The reflectors in the GPR1 record are probably the result of near surface variations in overburden properties. GPR2 shows poorer radar penetration, compared to GPR1, with no prominent reflectors beyond approximately 100-120 ns (4-6 m). The reason for this is that there is an additional metre or so of overburden to be penetrated (as opposed to the scraped area). This is a good illustration of how the relatively conductive Karoo overburden has an adverse effect on GPR penetration. In this type of environment the detection of targets beyond 8-10 m is highly unlikely and the only potential application for GPR is the detection of near surface voids such as shallow sinkholes.

3.5 Resistivity Tomography survey (RESTOM)

The RESTOM image shows two zones of contrasting resistivity. A relatively resistive (green) zone covers the upper ~12-15 m of the surveyed line and appears to extend deeper to the left of the image. A more conductive (blue) zone occurs below a depth of ~12-15 m to the right of the image. This blue zone is abruptly terminated at the estimated position where the contact between old workings and un-mined ground occurs. This result is consistent with what can be expected for the given scenario. Where there are no workings present (right of image) the two coloured zones represent a relatively resistive overburden with more conductive material below 12-15 m. Where there are workings present, the air-filled voids contribute to a higher average electrical resistivity. Thus, the boundary of the old workings can be mapped indirectly by knowing that the voids are air-filled (highly resistive) and monitoring the continuity of the more conductive host material. The mapping accuracy of RESTOM is typically 2-5 m.

The conductive zone near x=0, z=0 is likely to be the result of a variation in near surface overburden conductivity, but may also be a processing artefact.

[A] Assuming a permittivity of 9 and therefore a depth of 5 cm per ns (Vogt, 2001).

4 NEW LARGO FIELD SURVEYS

The New Largo test site served as a substitute for Middelburg Steam & Station, which was initially one of the preferred test sites for Task 1.3.1b. Unfortunately, the latter was considered to be an unsafe area and members of the Coaltech 2020 committee proposed New Largo as an alternative. The primary target at New Largo is, however, the same as at Middelburg Steam & Station, namely near-surface cavities. The depth to the old workings at the survey site is approximately 30 m below surface, which is not necessarily beyond the probing range of geophysics, however, it was decided to focus on the detection of sinkholes.

During a site visit to the New Largo property, a small area was selected to serve as a tests site for various ground geophysical techniques. The chosen site is located in area 8, which is a low safety factor (< 1.0) area (Figure NL1). Part of the area subsided in 1999 due to the collapse of old bord-and-pillar workings. A relatively large sinkhole is present in the area. A schematic plan of the survey area showing the position of the sinkhole and the survey area is presented in Figure NL2.

An area south of the known sinkhole structure was targeted. Part of this area shows signs of subsidence and a prominent cracked zone is visible on the surface. The width of the cracks varies from a few centimetres to tens of centimetres and the visible depth from a few centimetres to a few metres in places (see photographs in Figure NL3).

The survey area was considered to be a potential site for near surface cavities.

4.1 Total field magnetics

A small survey grid of approximately 65 m x 60 m was positioned so that the cracked zone runs through the centre of rectangular grid (Figure NL4).

The total field ground magnetic survey was conducted with an EDA OMNI-IV magnetometer. A station spacing (y-direction) of 3 m and a line spacing (x-direction) of 5 m were used. The data was corrected for diurnal effects and contoured. The results are presented in Figure NL4-NL6.

4.2 Electrical resistivity method (gradient array)

A gradient array electrical resistivity survey was conducted over approximately the same area as was covered with the magnetic survey. The gradient array involves using a fixed current electrode spacing, with a grid of potential lines being surveyed in the middle third of the current electrode line (see Figure NL2).

A more detailed discussion of the gradient array method can be found in van Zijl (1985). In this case a current electrode spacing of 192 m was used, with the corresponding measuring grid being approximately 60 m x 50 m. The current electrode spacing of 192 m implies that lateral changes in the resistivity of the upper 30 m can be monitored. Potential difference measurements were made using a 4 m in-line dipole with a station spacing of 4 m. A total of 14 lines spaced 4 m apart were acquired. The data was then converted to apparent resistivities and plotted at the mid-point of the measuring dipoles. The resulting map of apparent resistivity was subsequently contoured (Figure NL7).

Figure NL9 shows the resistivity map with the regional resistivity trend removed.

4.3 Frequency Domain electromagnetics (FDEM)

A FDEM survey was conducted over approximately the same area as was covered by the gradient array resistivity and magnetic surveys. A Geonics EM-34 was employed in both the vertical and horizontal dipole configurations, with a 10 m coil spacing. Ten N-S profiles, spaced 5 m apart, were conducted using a 3 m station spacing. A 150 m long W-E profile was also acquired as indicated in Figure NL10. The results of the FDEM survey are presented in Figures NL11 and NL12.

4.4 Ground penetrating radar (GPR)

A GPR survey was conducted at the New Largo test site. The preliminary results from the magnetic and gradient array resistivity surveys were used to select areas of interest. The location of the GPR profiles is shown in Figure NL13. A GSSI SIR-2M radar system with 300 MHz antennas was used. Although GPR penetration was not expected to be good, it was anticipated that the method would be able to detect very shallow cavities or buried man-made objects. The GPR results are presented in Figure NL14. The maximum range is approximately 100 ns or 5 m only.

4.5 Resistivity Tomography (RESTOM)

Based on the results of the gradient array resistivity and magnetic survey results, a single in-line dipole-dipole RESTOM survey was conducted. The location of the RESTOM profile is indicated in the map in Figure NL10. A current dipole of 8 m was used with potential dipoles of 4 m. The current and potential dipole spacings were both 4 m. The result of the RESTOM survey is shown in Figure NL15.

5 DISCUSSION OF NEW LARGO RESULTS

5.1 Total field magnetics

The contour map of the total field magnetics (Figure NL4) is dominated by a pair of prominent anomalies (positive and negative) at x = 0, y = 20. A further variation is a general trend showing higher susceptibility values measured in the western third of the survey area and lower susceptibilities on the eastern side.

In an attempt to mask the effect of the prominent anomalies and possibly enhance other, more subtle features, the extreme data values responsible for the major positive and negative anomalies were discarded (subjectively) and the remaining data was again contoured. The result is shown in Figure NL5.

Finally, the above-mentioned regional trend that is apparent in the data is removed to yield the contour map in Figure NL6. The regional trend may be due to the different responses over mined and un-mined areas or the topographic trend (there is a positive correlation between topography and measured susceptibility).

It is recommended that a regional aeromagnetic contour map and a topographic map of the study area be obtained to investigate the cause of the observed trends.

Apart from the trend and the above-mentioned anomalies near x = 0, y = 0, there are no further features of interest. The variations that do occur are relatively small (< 10 - 15 nT) and are probably the result of near surface variations in the overburden.

In order to better interpret TFM results over old workings it is necessary to quantify the expected responses over subsurface cavities through computer modelling. This will be done before the end of the project in March 2002.

5.2 Electrical resistivity method (gradient array)

The apparent resistivity contour map exhibits some interesting features. The cracked zone can clearly be identified as a narrow resistive zone extending southward from approximately x = 0 in the north and then towards the south-eastern corner of the map. There are a few localised conductive anomalies in the map: at x = 26, y = -12, at x = 6, y = 8, at x = 12, y = -2, at x = 3, y = 22, at x = 28, y = 2, and in the south-western corner of the map at x = -30, y = -22.

During a subsequent visit to the site it was discovered that a fire had burnt the grass cover at the survey site. During this visit a borehole collar was discovered in the same location as the conductive anomaly at x = 3, y = 22. There was also evidence of possible boreholes co-insiding with the other prominent conductive anomalies (at x = 6, y = 8 and at x = 12, y = -2). It is highly probable that all the isolated conductive anomalies on the map are the result of metal borehole casings or other buried metal objects in the subsurface.

Areas of potential subsurface cavities would manifest as prominent resistive anomalies on such a map. Apart from the cracked zone, another interesting (resistive) anomaly is the finger-shaped area that extends south from the north-eastern corner of the map.

5.3 Frequency Domain electromagnetics (FDEM)

The horizontal dipole (HD) configuration is more sensitive to relatively shallow features than the vertical dipole (VD) configuration. The depth of investigation when using a 10 m coil spacing is approximately 7 m for the HD configuration, and 15 m for the VD configuration (Geonics Limited).

There are no major anomalies evident on any of the individual FDEM profiles, except for Line 1 (see Figure NL11). These anomalies are evident on both the HD and VD contour maps (Figures NL12a & 12b). The only obvious correlation between the FDEM maps and the resistivity map (Figure NL9) is the anomaly at x = 30 - 35, y = -10 on Line 1. The gradual decrease in conductivity (increase in resistivity) from west to east that was evident in the gradient array resistivity data can also be seen in the FDEM profile AB (Figure NL11e).

The FDEM technique is not well suited to the mapping of near surface cavities as the technique is not sensitive enough to resistive features. If the cavities are, however, filled with conductive material the FDEM technique may be a useful detection tool.

5.4 Ground penetrating radar (GPR)

The GPR data had not yet been processed at the time of publishing this report. However, preliminary processing indicated that radar penetration was very poor and that the only prominent reflectors in the data are probably due to the borehole casings mentioned earlier. The GPR result will be included in the Project Final report.

5.5 Resistivity Tomography (RESTOM)

The RESTOM profile was located such that it traverses the cracked zone with the aim of determining the depth extent of the cracks and to probe for potential larger cavities at depth. The profile was also extended to include the more resistive zone to the east of x=20 on the resistivity map (Figure NL9).

The only indication of potential subsurface voids in the RESTOM image is the deeper (below 10 m) resistive zone at x = 0 - 8 m. The near surface resistivity shows a reasonable correlation with the resistivity values depicted on the gradient array contour map. The cracked zone is represented by a relatively small, red area (at x = 8, z=0) on the image.

To obtain more meaningful RESTOM results a pseudo 3D RESTOM survey is required. That is a grid of closely spaced lines needs to be acquired. This would ensure greater confidence in the data and would allow correlation and interpolation between adjacent profiles. However, as will be seen in the next section, RESTOM, like micro-gravity, is relatively expensive. Electrical resistivity surveys should thus be limited to methods such as the gradient array or conventional horizontal profiling.

6 COST ANALYSIS

The cost of applying the five ground geophysical techniques covered in this report is compared with that of airborne thermal infrared imagery surveys. The cost analysis is for data acquisition only and excludes the cost of data processing.

Technique	Local technology?	Estimated survey time (1 ha at 5 m line spacings, unless stated otherwise)	Estimated cost (per hectare)
Micro-gravity	NO	15-20 days	R 100 000
Resistivity (gradient array)	YES	1-2 days	R8000
Resistivity Tomography (RESTOM)	YES	10 days	R40000
Magnetics	YES	1 day	R4000
Frequency domain electromagnetics (FDEM)	YES	1 day	R4000
Ground Penetrating Radar (GPR)	YES	1-2 days	R8000
Airborne thermal infrared imaging (TIR)	NO	1 night = 330 km^2 (at 1 m pixels)	R2.50[B]

A more detailed and complete cost analysis will be presented in the final project report. The above table does, however, highlight a very important issue. That is, airborne geophysics, despite a relatively costly mobilization component, tends to be more cost effective than ground geophysics. It is therefore strongly recommended to first extract all possible information from existing airborne data, or alternatively, to conduct a reconnaissance airborne survey(s) and then to follow-up with ground surveys.

7 CONCLUSIONS AND RECOMMENDATIONS

[B] Note that although the cost per hectare is extremely low the minimum cost of a survey is in the order of R50000 – R100 000, because of the high mobilization component.

The practical evaluation of geophysical techniques that formed part of Task 1.3.1b was complicated by the problems of surveying 'blind' and the lack of sufficient 'groundtruthing' data. For example, although it is relatively easy to design a survey to cover an area of old workings or the edge of old workings, sinkholes are more difficult to target because their location is usually unknown. Furthermore, once a geophysical anomaly has been interpreted as the potential results of a specific target, sufficient groundtruthing data, for example through drilling, is often not possible unless the drilling can be motivated, for example, in the event of a safety risk posed by a possible sinkhole.

In future it is recommendation that test sites should be more carefully selected to enable evaluation of interpretations using existing boreholes or accurate mine plans. Provision should also be made for limited additional drilling.
A further solution would be to limit future ground geophysical surveys to investigating anomalies identified using airborne or satellite based sensors. This approach would eliminate unnecessary costs and is recommended for the remainder of Task 1.3.1b, as well as for Task 1.3.5 (Remote Sensing project).

Despite not having sufficient groundtruthing data, the geophysical surveys conducted to date have been reasonably successful. The integrated use of various techniques has been demonstrated, which highlighted some of the strengths and weaknesses of the techniques in the coal environment. In the process, a collection of case studies for coal is being compiled which, in the future, may help geological staff on the mines decide on the applicability of various geophysical techniques to their specific problem.

The results to date confirm that the electrical resistivity and micro-gravity techniques are well suited to mapping air-filled voids. Both techniques are capable of mapping the edge of air-filled workings. It is anticipated that the effective depth of investigation, as well as the detectability of flooded workings, will be better quantified towards the end of this project.

Applicability of the GPR technique is limited due to the conductive nature of the Karoo sediments. Generally, radar penetration is limited to a few metres thus GPR would only be applicable to the mapping of ultra-shallow (< 6 - 8 m) voids or workings.

FDEM is unsuitable for the mapping of voids, but may still be effective for delineating conductive water-filled workings and pollution plumes. The same applies to Time-Domain electromagnetics (TDEM), which is yet to be tested. It is recommended that the applicability of both FDEM and TDEM methods be demonstrated by targeting one of the anomalies identified in the TIR surveys or by surveying known flooded workings.

Ground geophysical techniques are incapable of mapping individual bords and pillars at depths of 15-30 m and deeper. It is yet to be seen if the TIR method succeeds where ground geophysics appears to have failed.

On a regional scale the application of ground geophysical techniques is relatively expensive compared with airborne methods such as TIR or airborne magnetics.

It can be concluded that ground geophysics is best suited to solving high-resolution, mine-scale problems where the area of interest is approximately 1 hectare or less. A key result expected from the integration of this project with Task 1.3.5 is that, wherever possible, geophysics should be applied in an integrated and site specific manner. It is often only through the joint use of different techniques that a given geological problem can be solved. Finally, it must be emphasised that geophysical techniques are site specific; a technique that proves successful on one mine will not necessarily work at another mine and vice versa.

8 REFERENCES

Geonics Limited. Technical Note TN-6: Electromagnetic terrain conductivity measurements at low induction numbers.

Lowe, S.J., Muller, M., and Pretorius, C., 2001. The microgravity method for underground cavity detection in the coal mine environment. Coaltech 2020 report, CSIR Report number 2001-0120.

Van Schoor, M., 2001. Detection of old workings, sinkholes, underground fires and acid mine pollution using geophysics and airborne thermal infrared imagery. Coaltech 2020 report, CSIR Report number 2001-0124.

Van Zijl, J. S. V., 1985. A practical manual on the resistivity method (Revised edition). CSIR Report K79. Geophysics Division National Physical Research Laboratory, CSIR.

Vogt, D.R., 2001. Application of GPR in coal. Coaltech 2020 Report (part of Subtask 4, Task 1.3.1b).

APPENDIX A

FIGURES

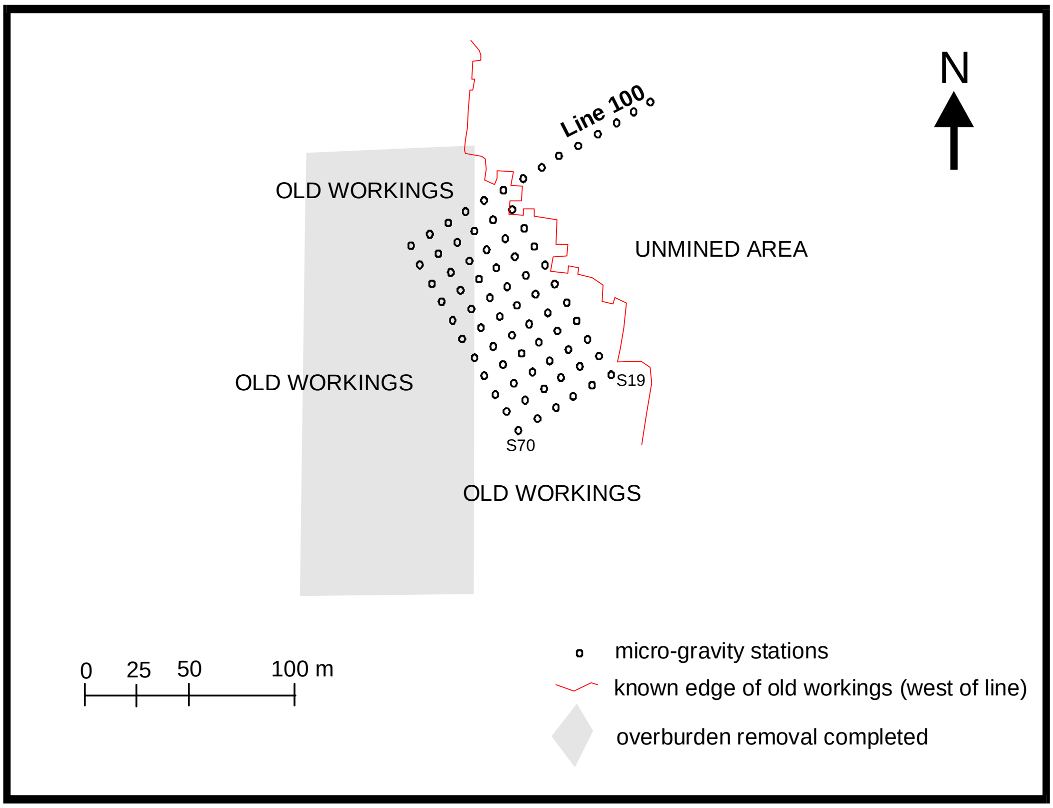

Figure K1: Schematic of the Kromdraai test site, showing the micro-gravity survey grid and the area affected by current surface mining operations.

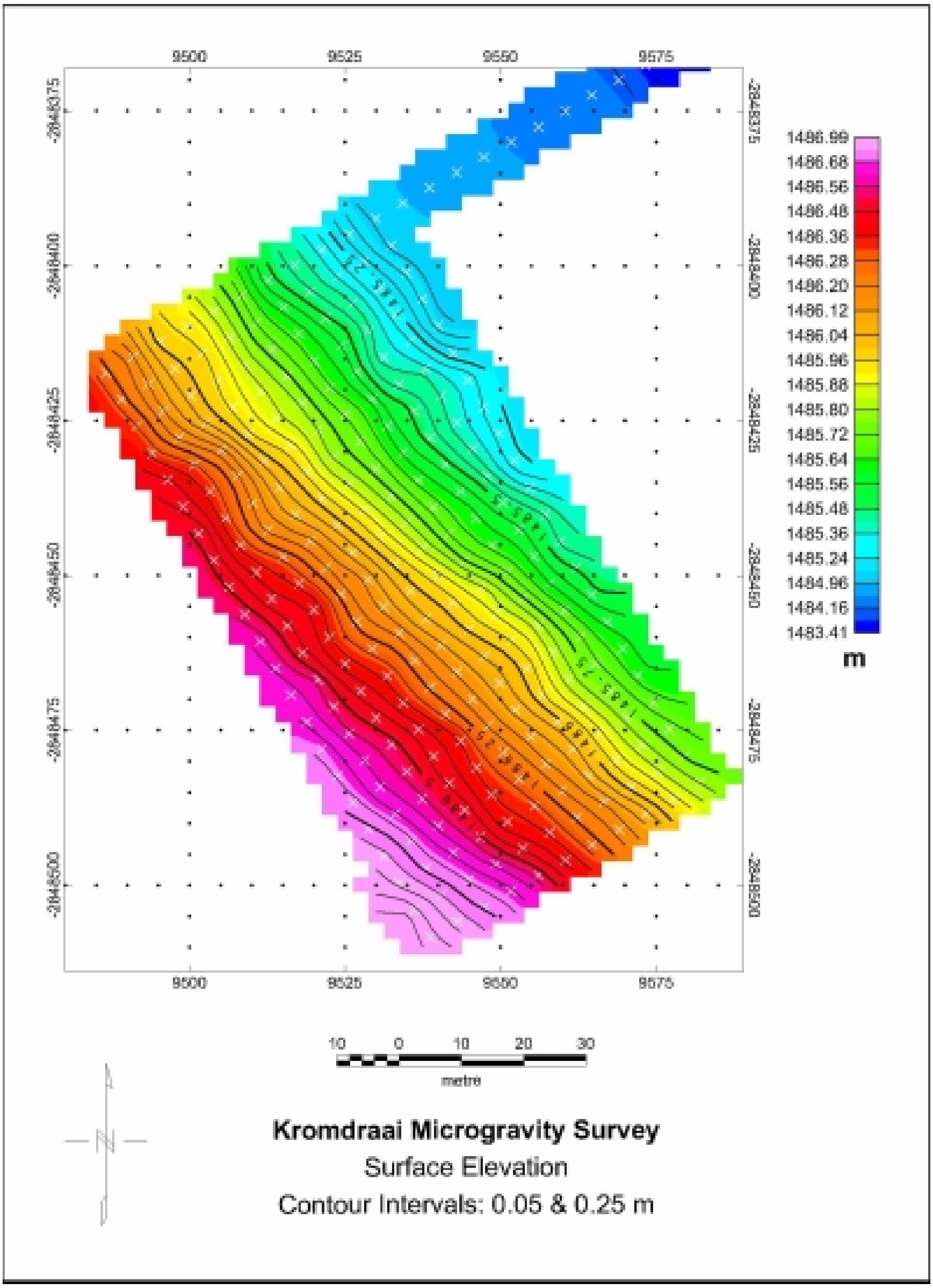

Figure K2: Relative surface elevation map over the survey area, derived from the accurate levelling of the gravity measurement stations. Station positions are indicated by small white crosses.

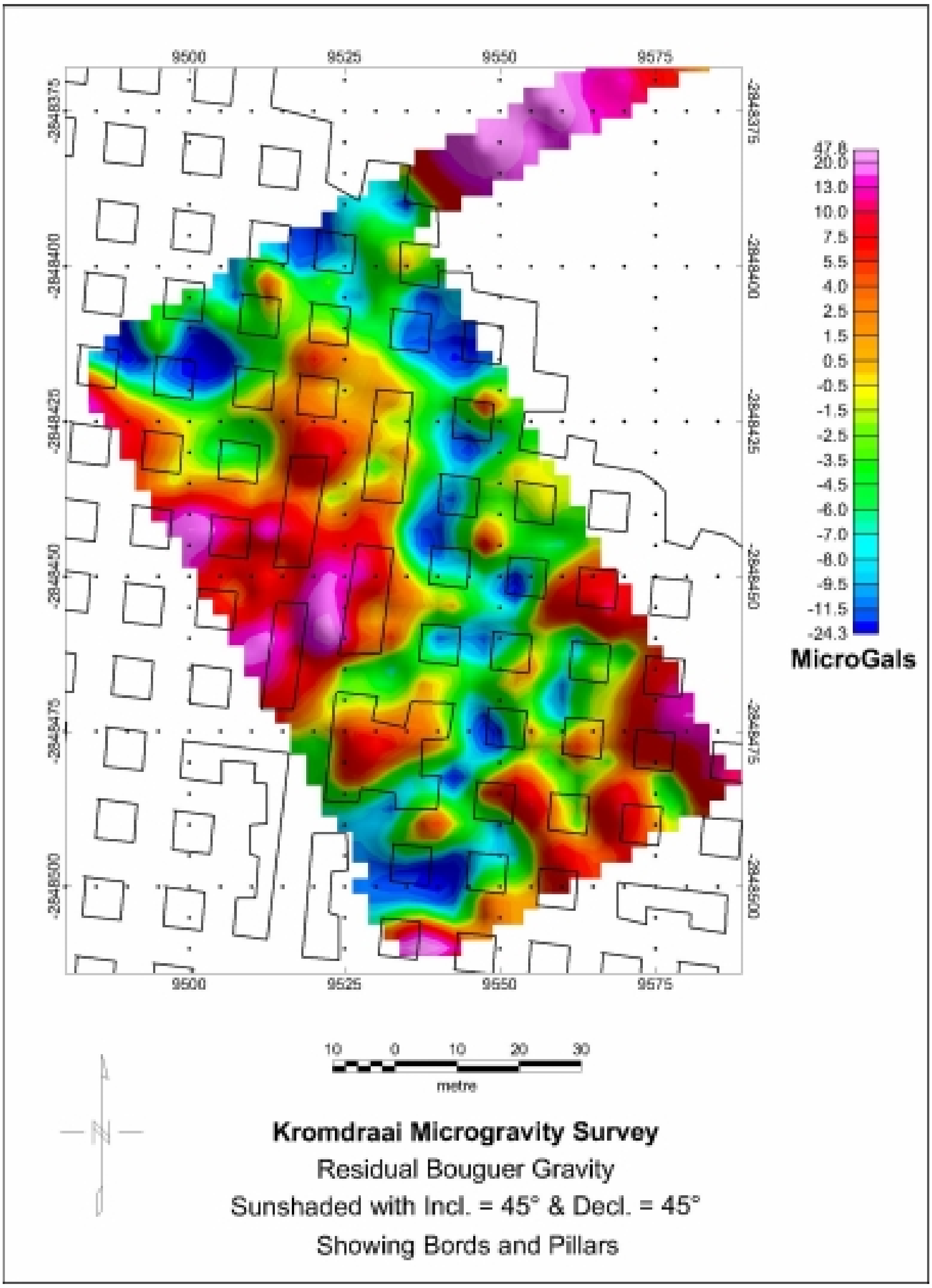

Figure K3: Residual Bouguer anomaly field over the survey area.

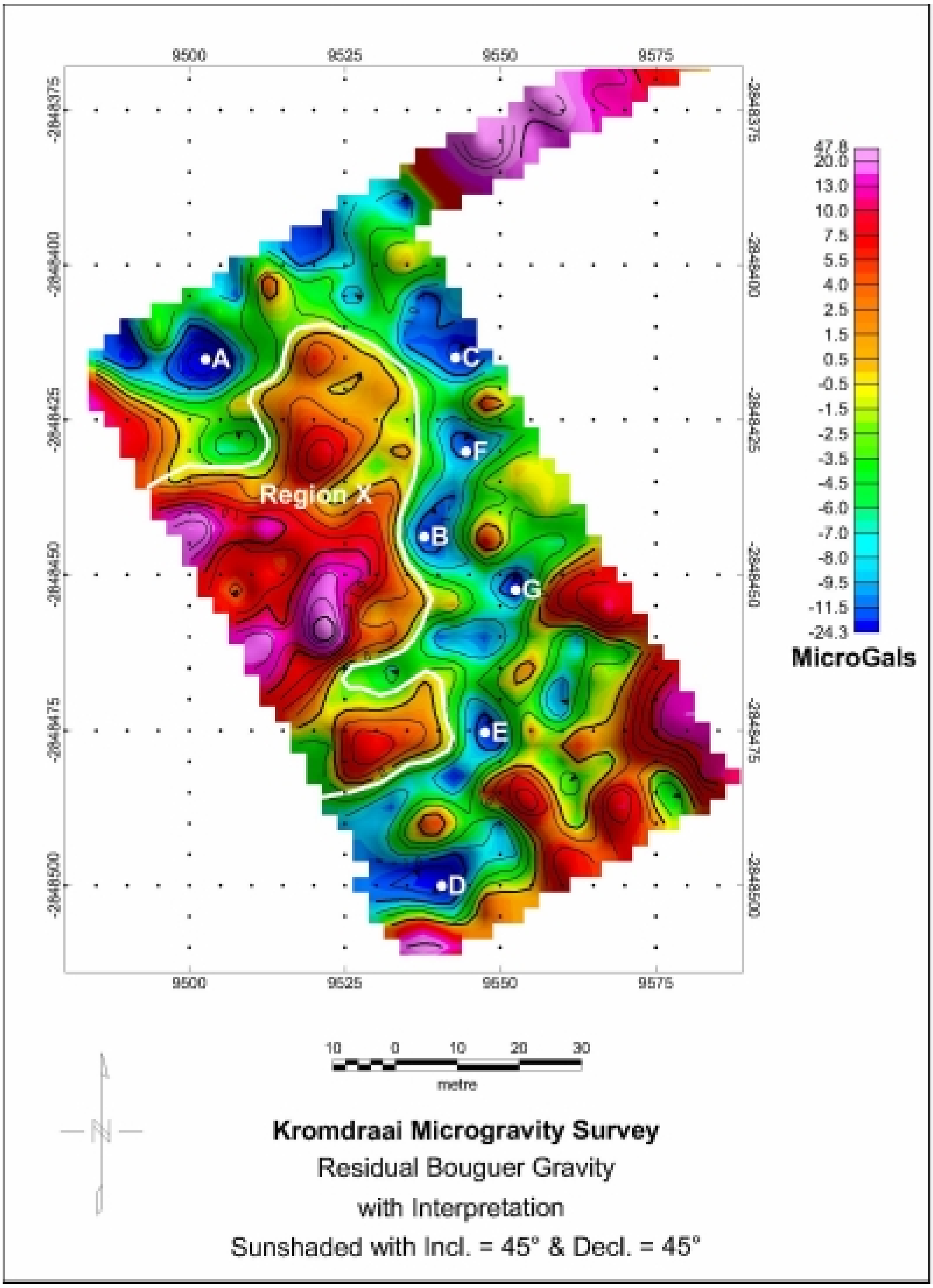

Figure K4: Residual Bouguer anomaly field over the survey area, with interpretation.

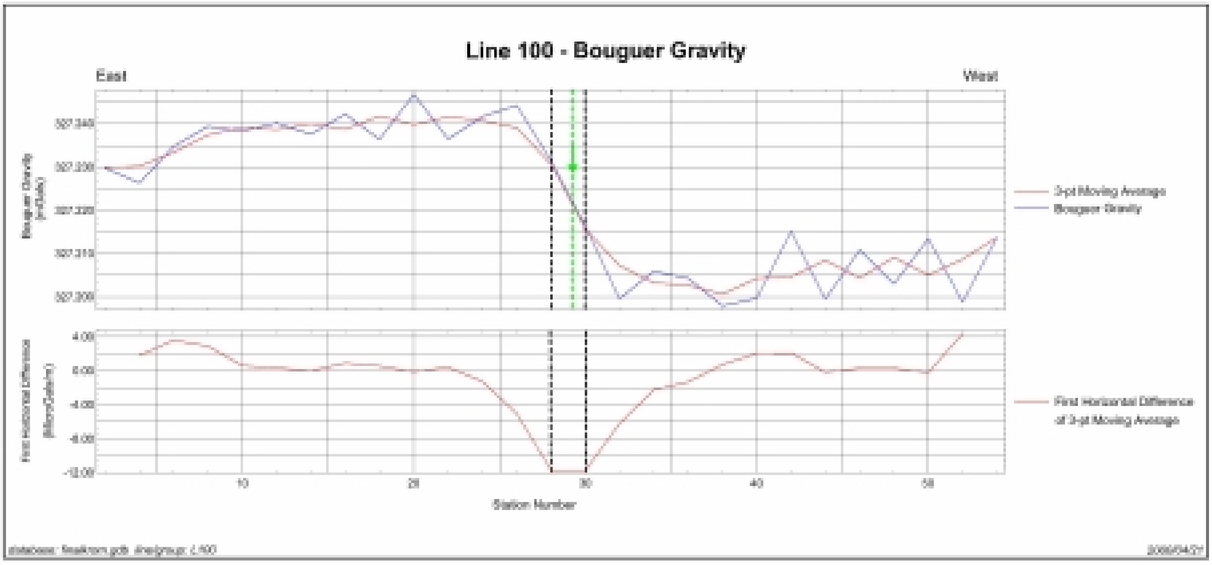

Figure K5: Gravity anomaly on Line 100. Smoothing the data with a three-point moving average filter (red line in upper figure) shows most clearly the signal resulting from the old workings. The interpreted edge of the old workings is indicated by the green arrow, and corresponds to the inflection point between the gravity low of the old workings (to the southwest) and the gravity high of the unmined seam (to the northeast) found by means of the half-amplitude method. In the lower figure the horizontal gradient of the smoothed anomaly is shown, derived using a 1st difference operator. The trough of the horizontal gradient (indicated by the dashed lines) provides an alternative method for identifying the inflection-point that corresponds to the edge of the workings.

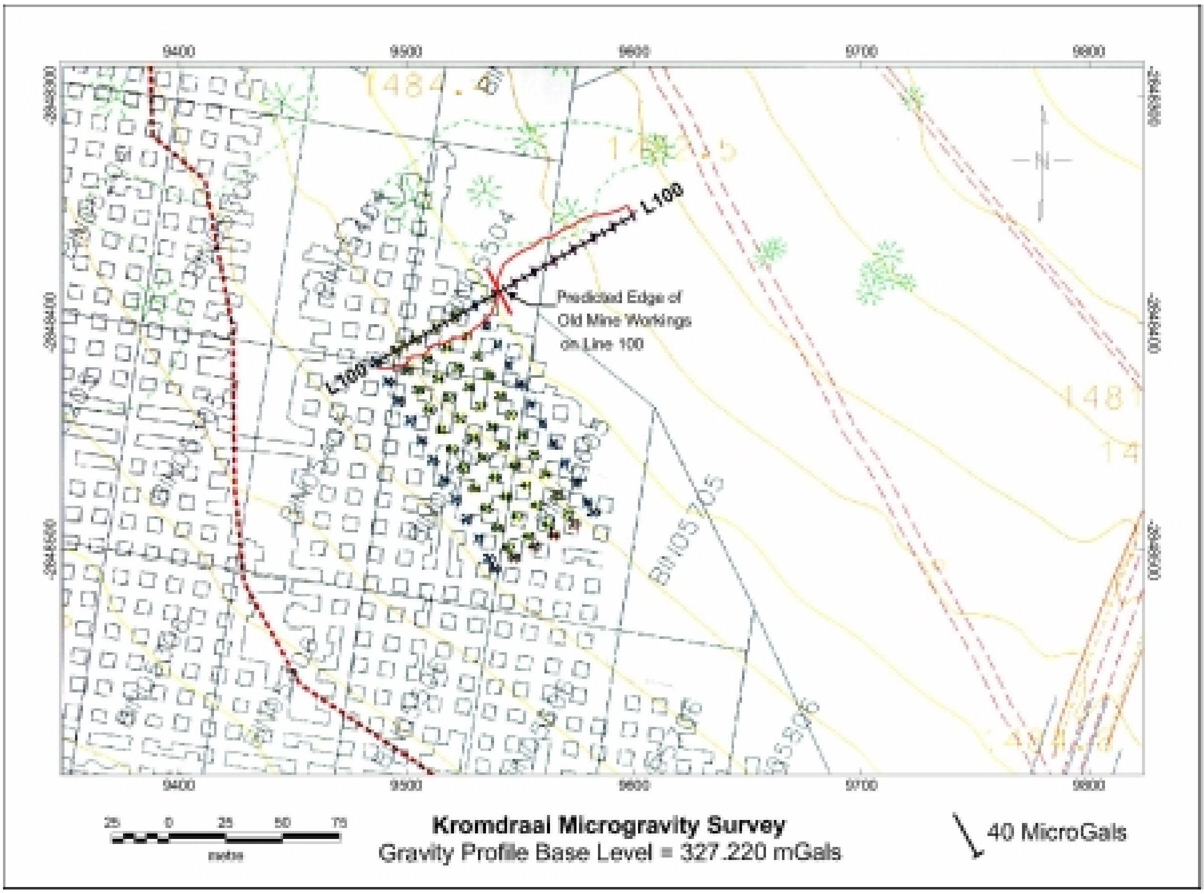

Figure K6: Base map detail showing the old #1 seam workings and the predicted edge of workings (short red bar) on microgravity Line 100. The smoothed gravity profile is also shown along the line in red.

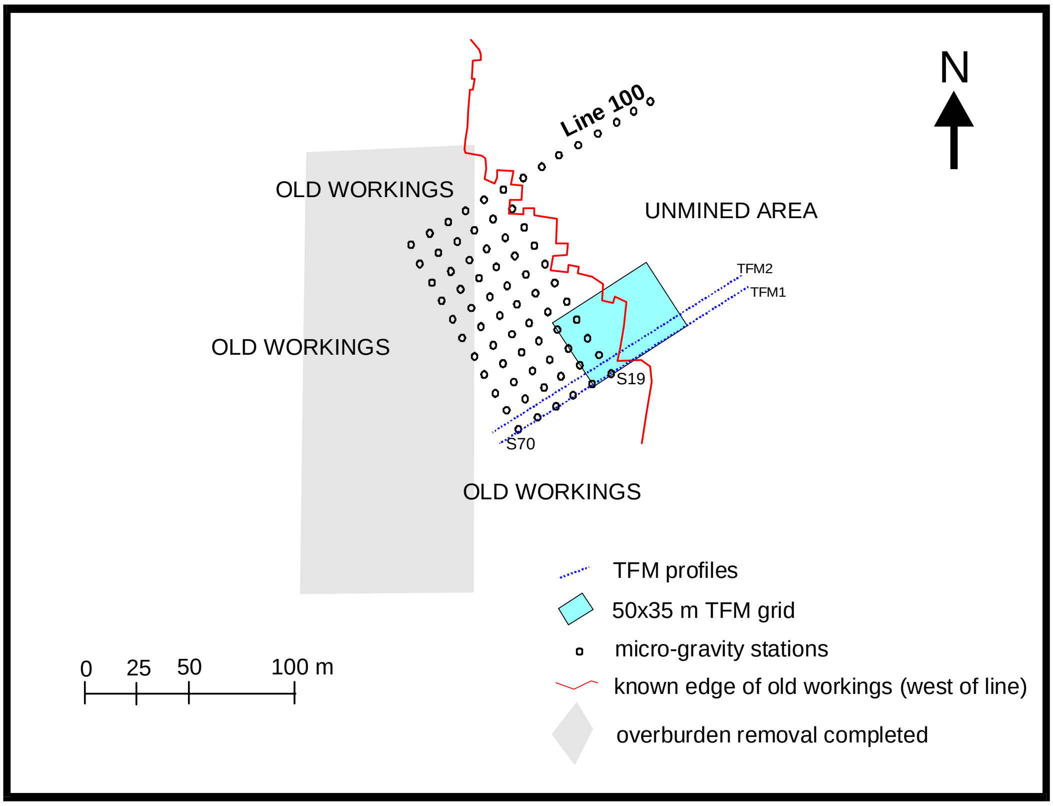

Figure K7: A schematic of the Kromdraai test site, showing the TFM survey grid and single TFM profiles.

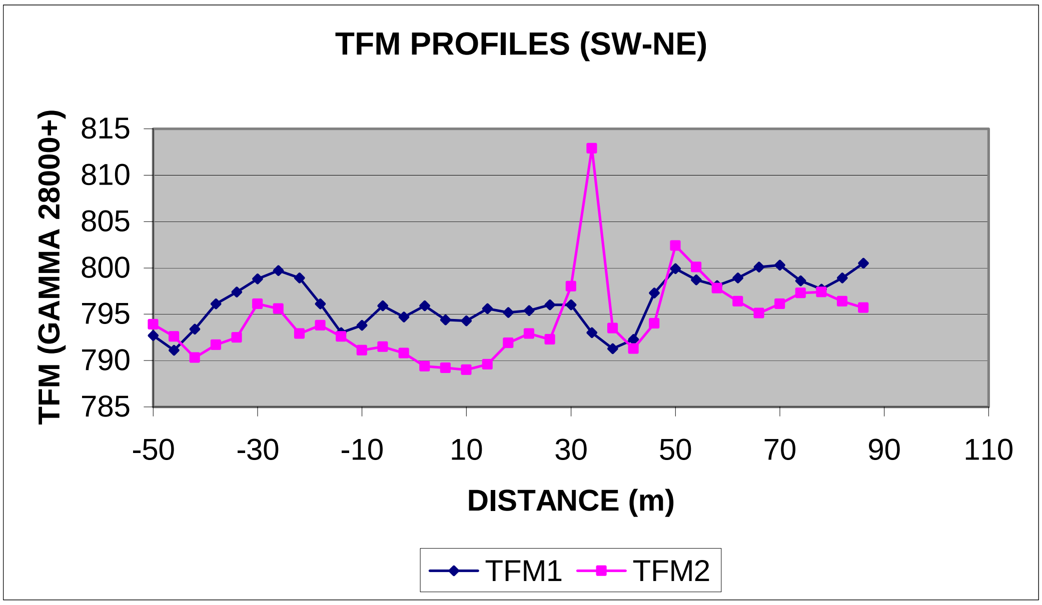

Figure K8: TFM profiles TFM1 and TFM2. The two corner pegs S70 and S19 are located at x = -40 and +10, respectively.

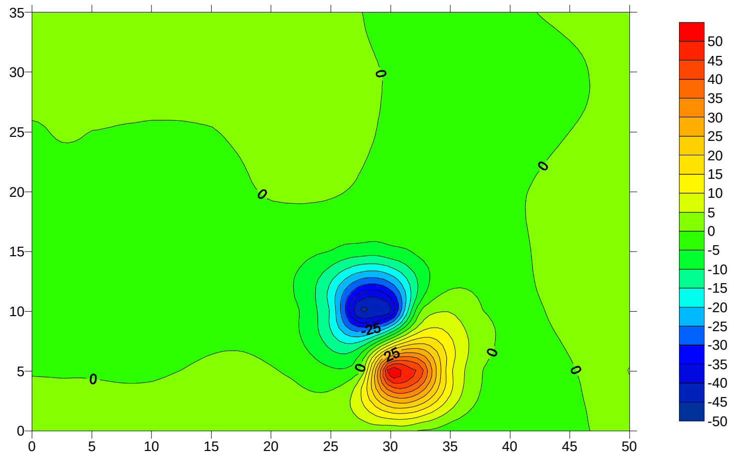

Figure K9: TFM contour map – all data.

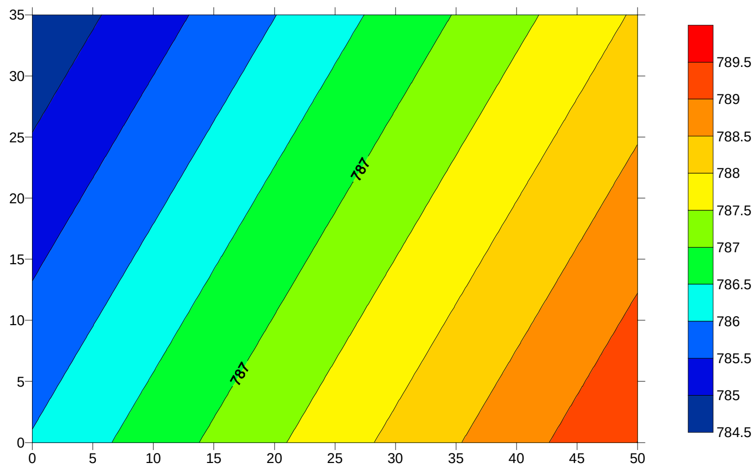

Figure K10: TFM contour map – trend only.

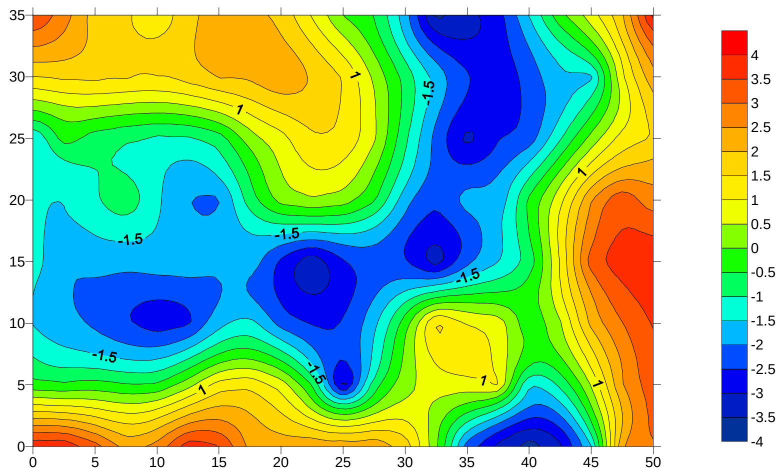

Figure K11: TFM contour map – trend removed and range reduced. S19 is located at x=10, y=0.

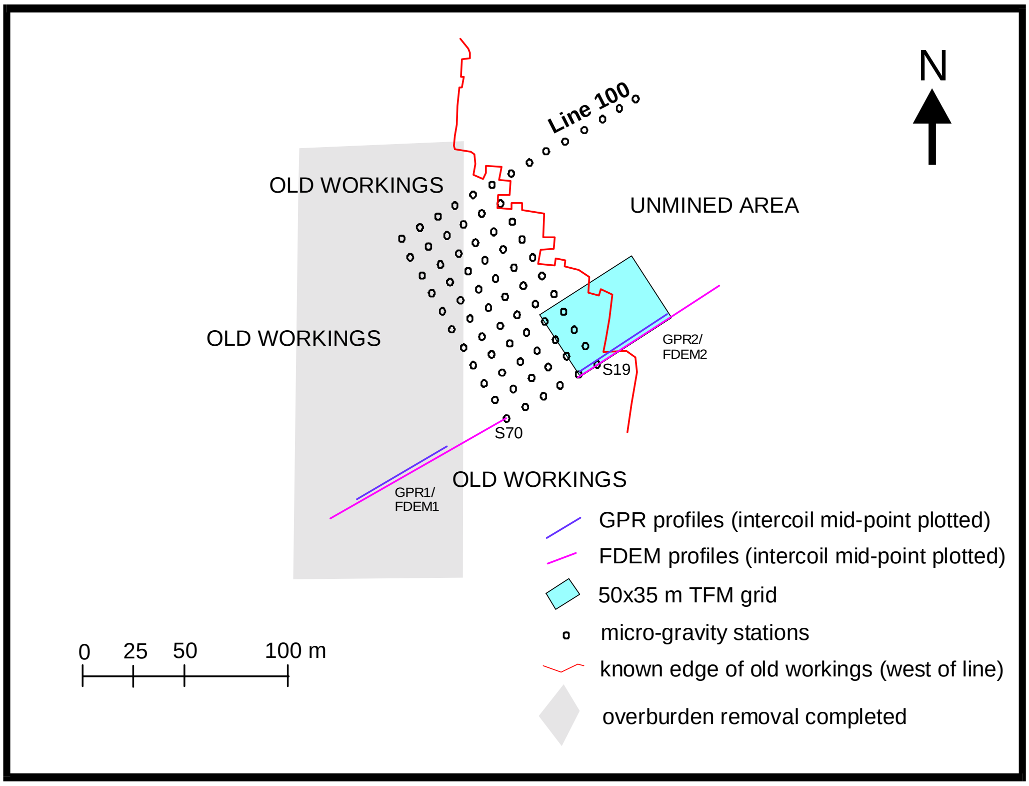

Figure K12: Map showing the location of the FDEM profiles.

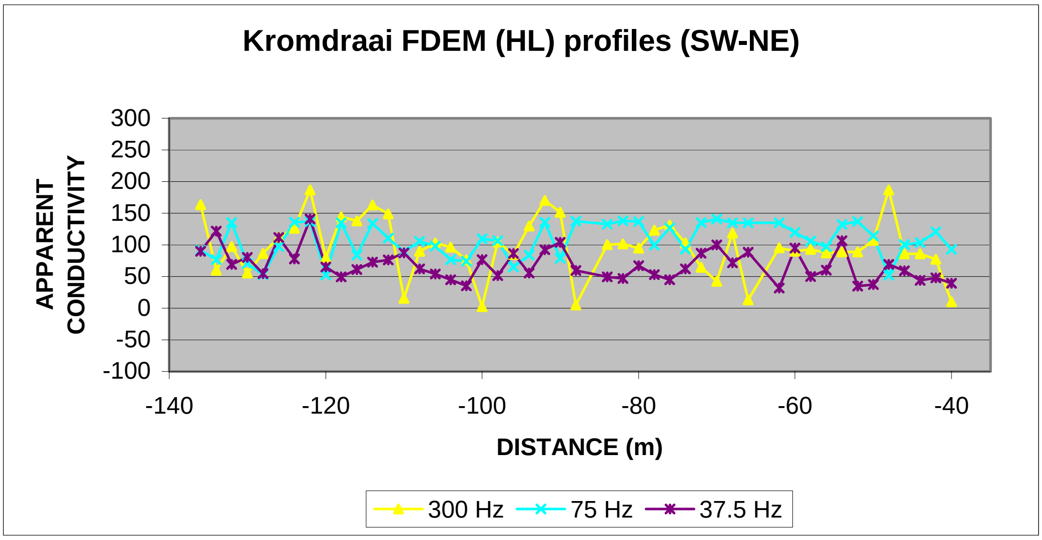

Figure K13: Kromdraai FDEM profile FDEM1. The values are plotted at the inter-coil mid-point. The last station coincides with S70.

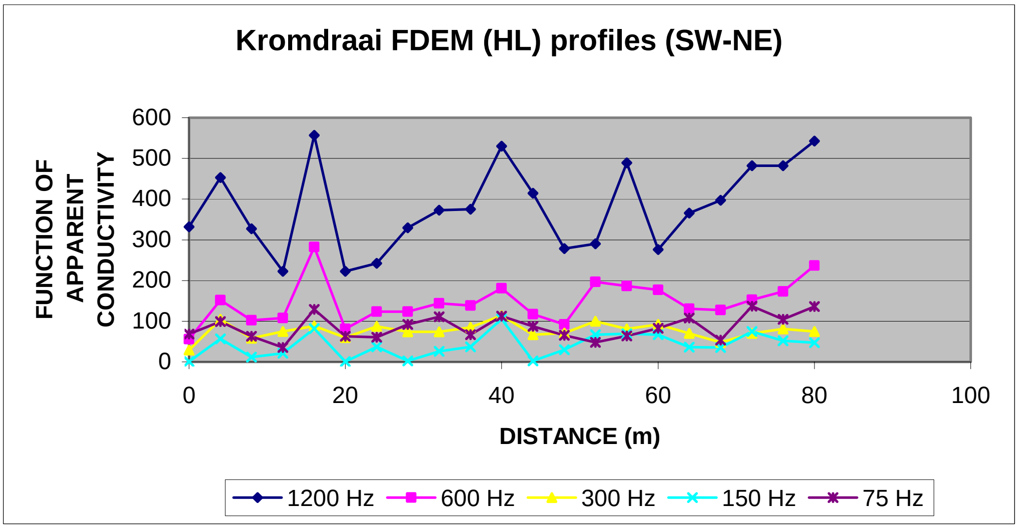

Figure K14: Kromdraai FDEM profile FDEM2. The values are plotted at the inter-coil mid-point. The first station is located 10 m SW of S19.

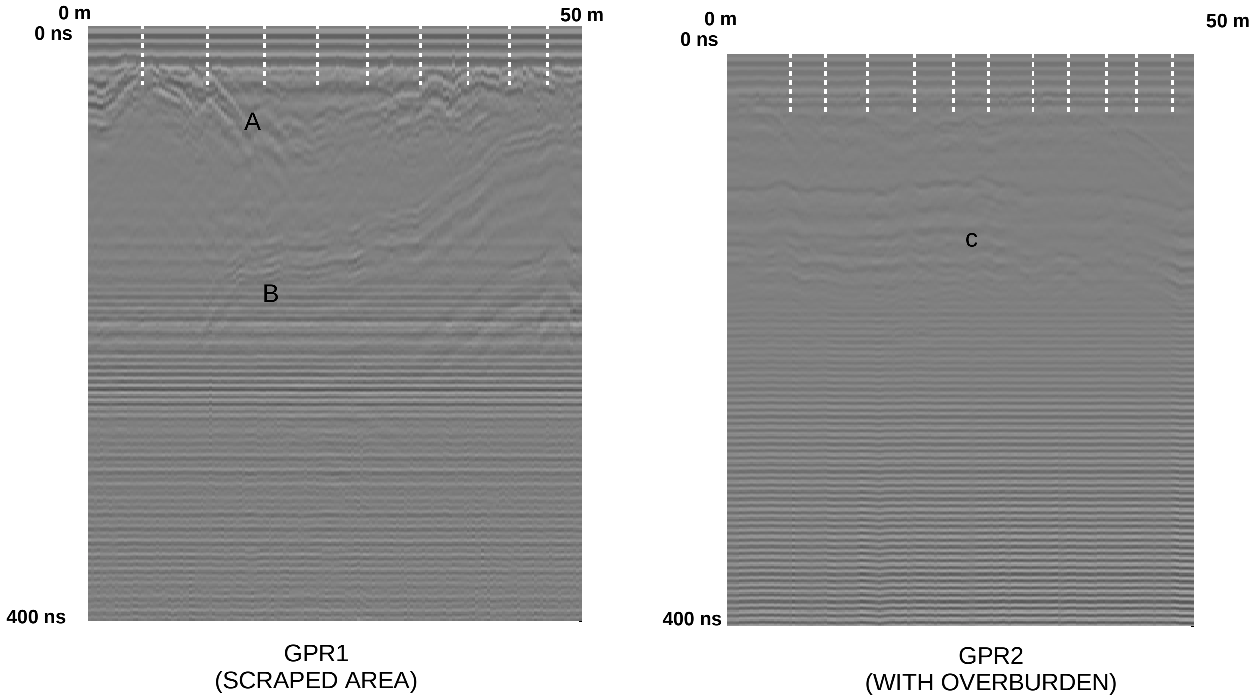

Figure K15: Kromdraai GPR results.

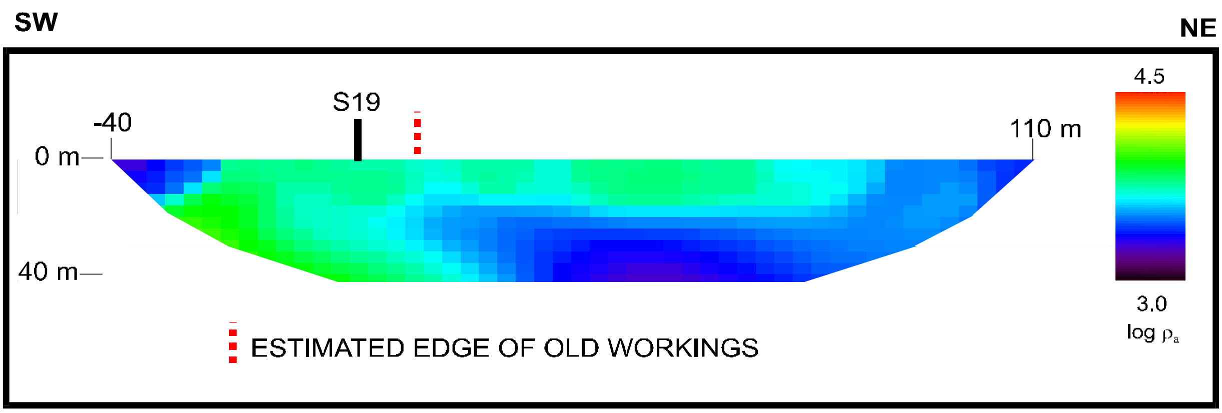

Figure K16: Kromdraai RESTOM result.

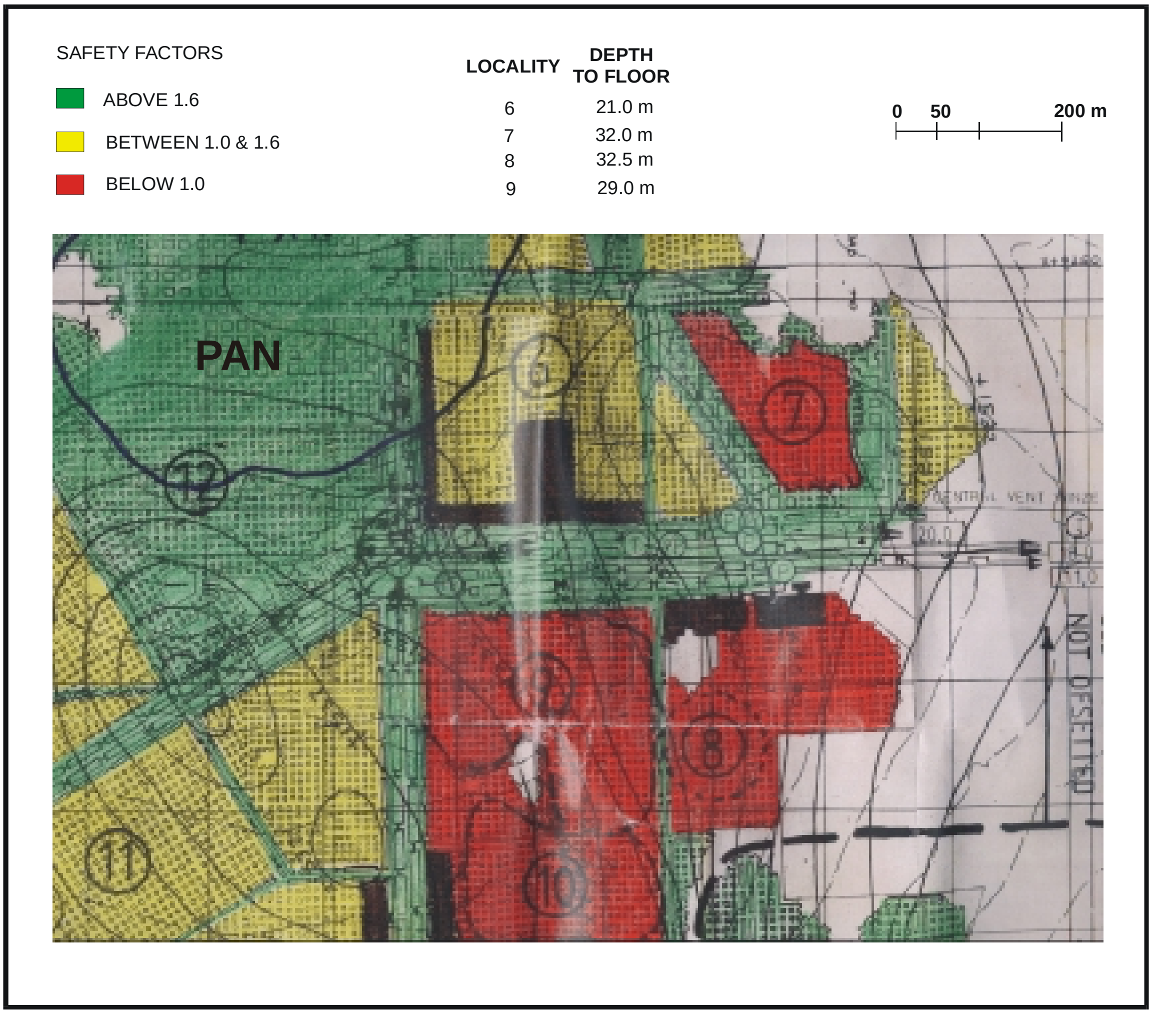

Figure NL1: Part of sinkhole and subsidence plan – New Largo Colliery.

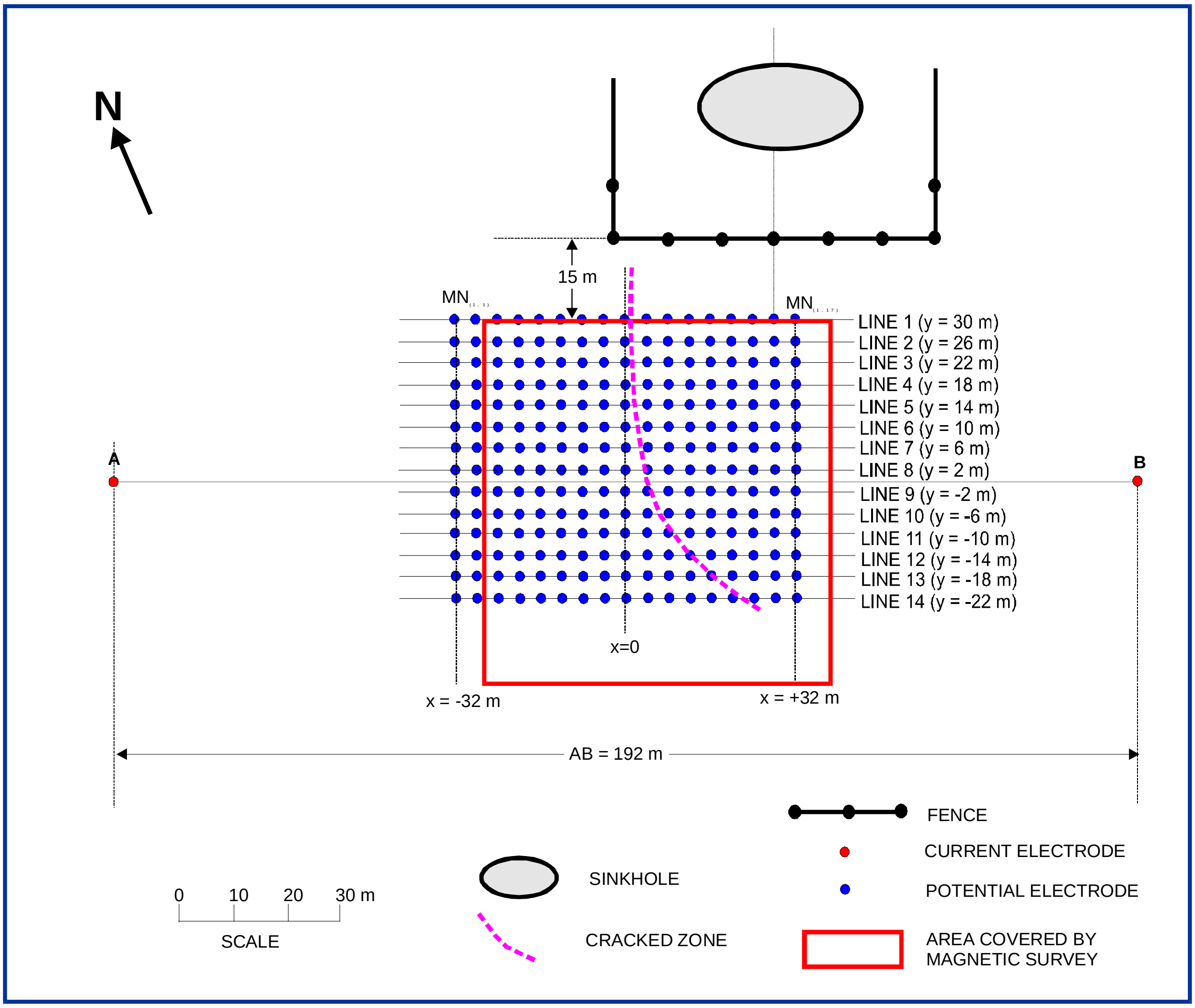

Figure NL2: A schematic plan of the New Largo survey area showing the layout of the gradient array resistivity and magnetic survey grids.

Figure NL3: Photographs showing the surface expressions of old bord-and-pilar collapses.

Top - looking north towards the pan, along the surface cracks indicated in Figure NL2
Bottom - looking north-northeast towards the fenced off sinkhole.

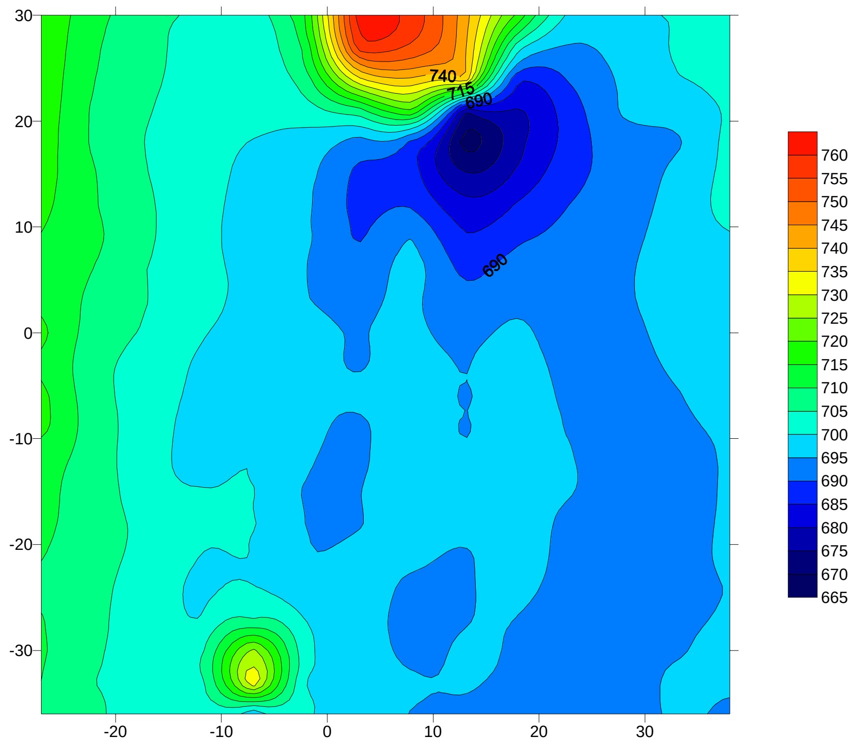

Figure NL4: Total field magnetic contour map of New Largo test site.

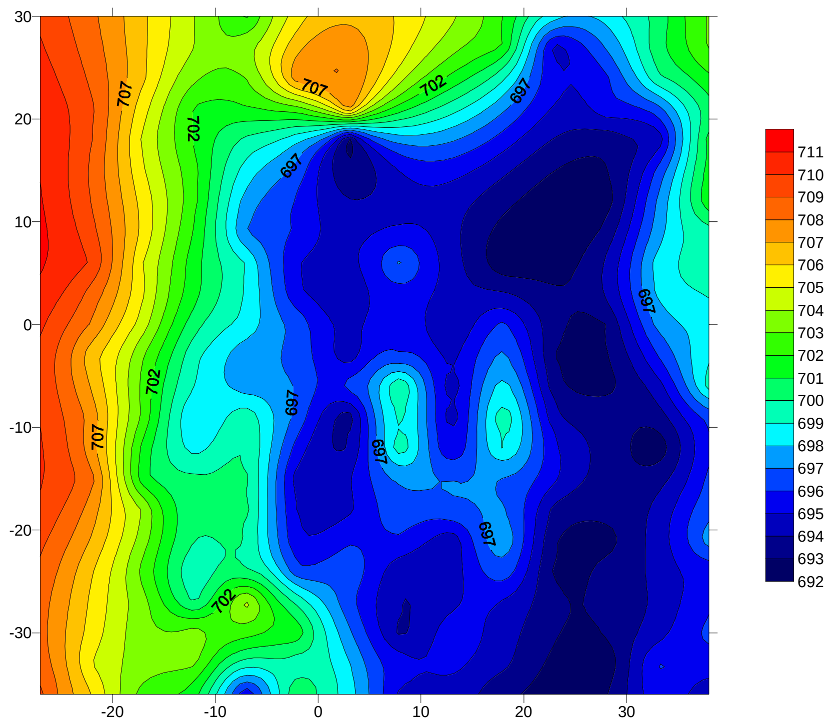

Figure NL5: New Largo total field magnetic contour map with the effect of the two most prominent anomalies in Figure NL4 suppressed.

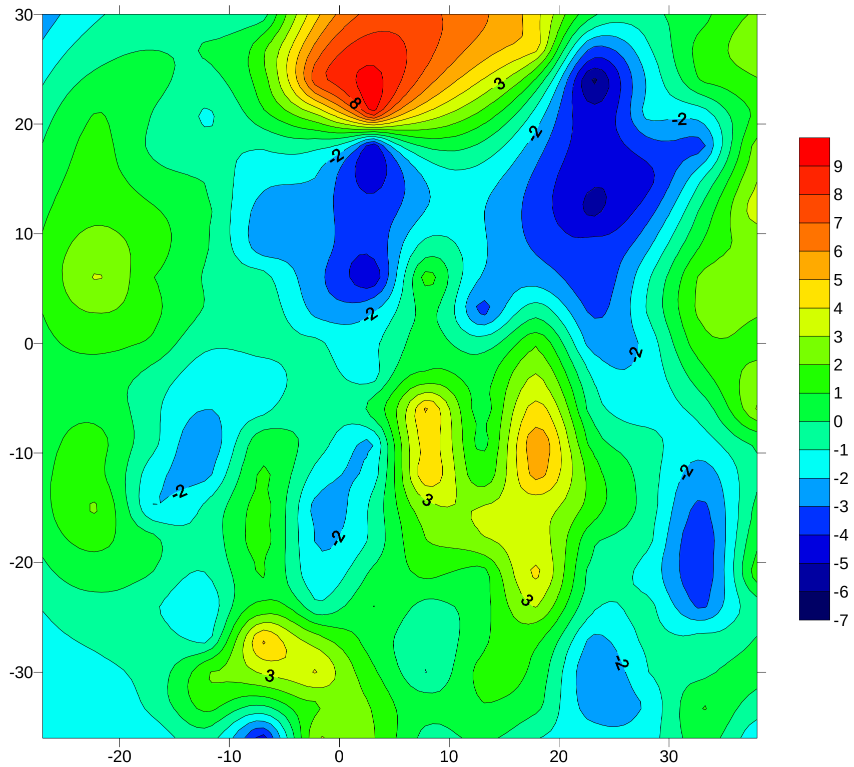

Figure NL6: New Largo total field magnetic contour map with regional trend removed and the effect of the two most prominent anomalies suppressed.

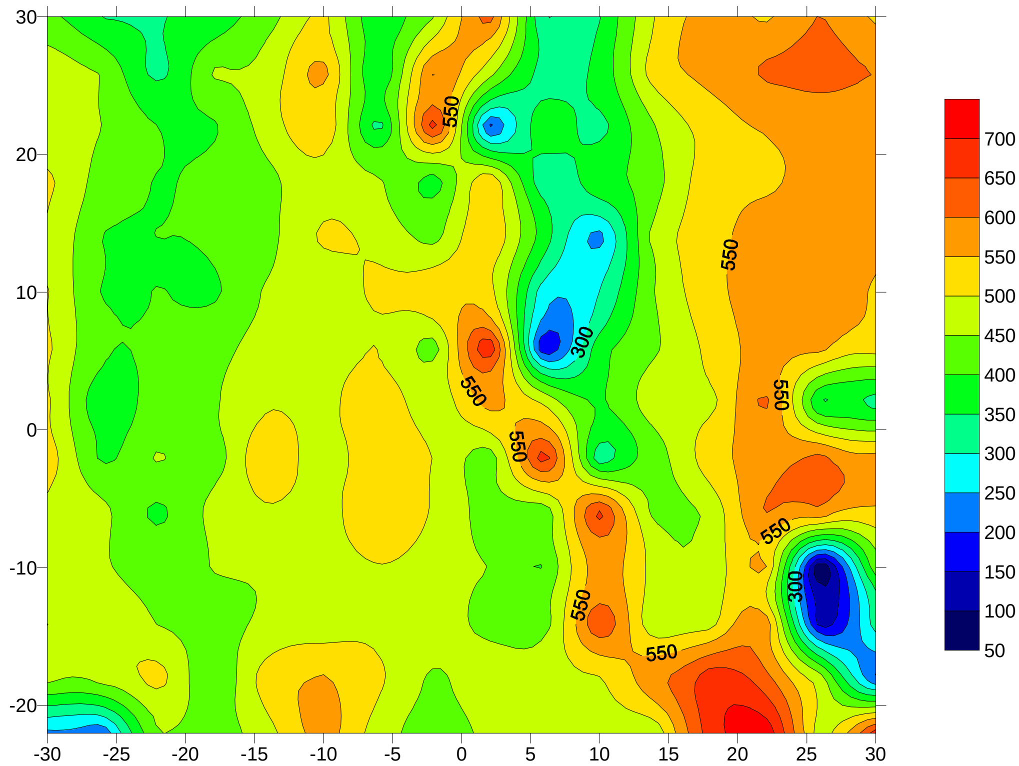

Figure NL7: Apparent resistivity contour map of the New Largo test site.

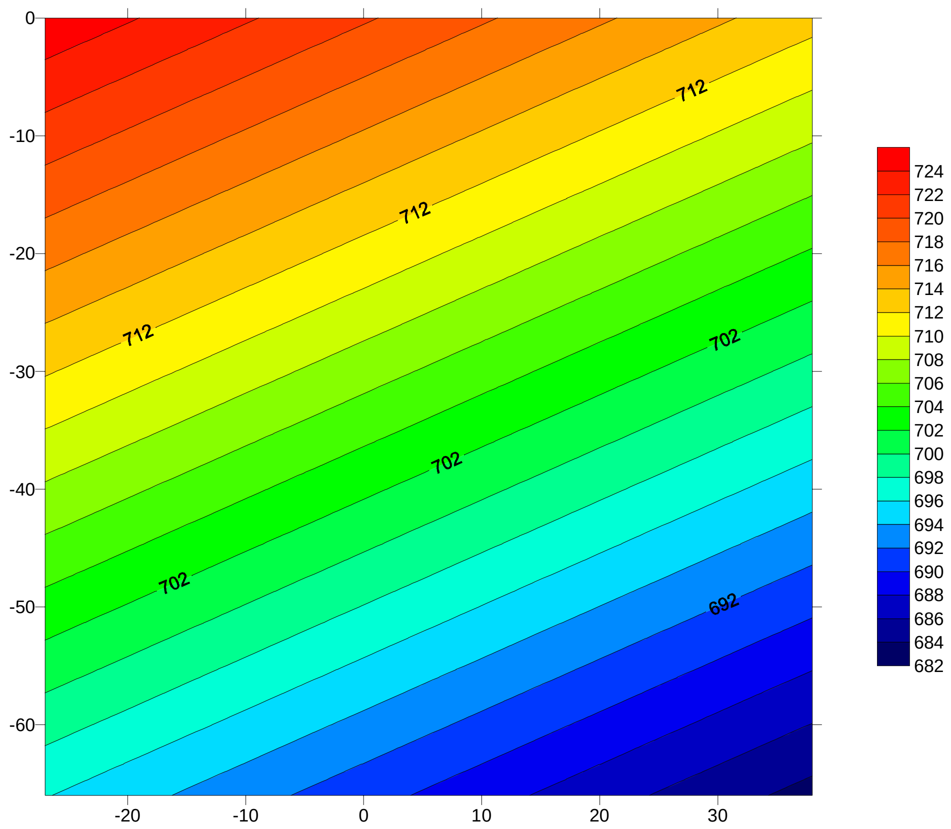

Figure NL8: Apparent resistivity trend contour map of the New Largo test site.

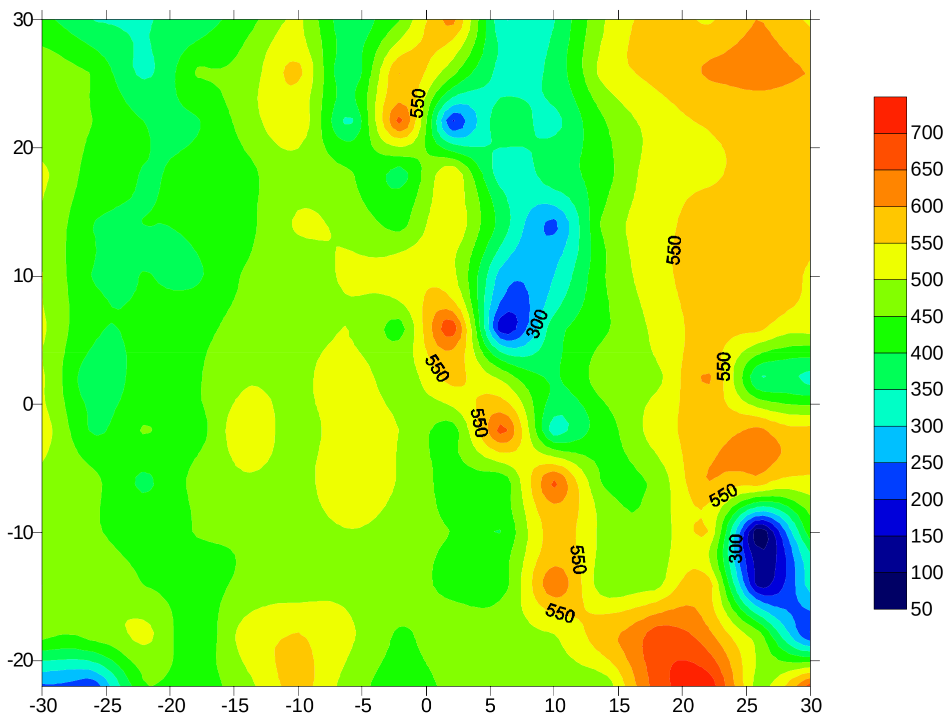

Figure NL9: Resistivity map with the regional resistivity trend removed.

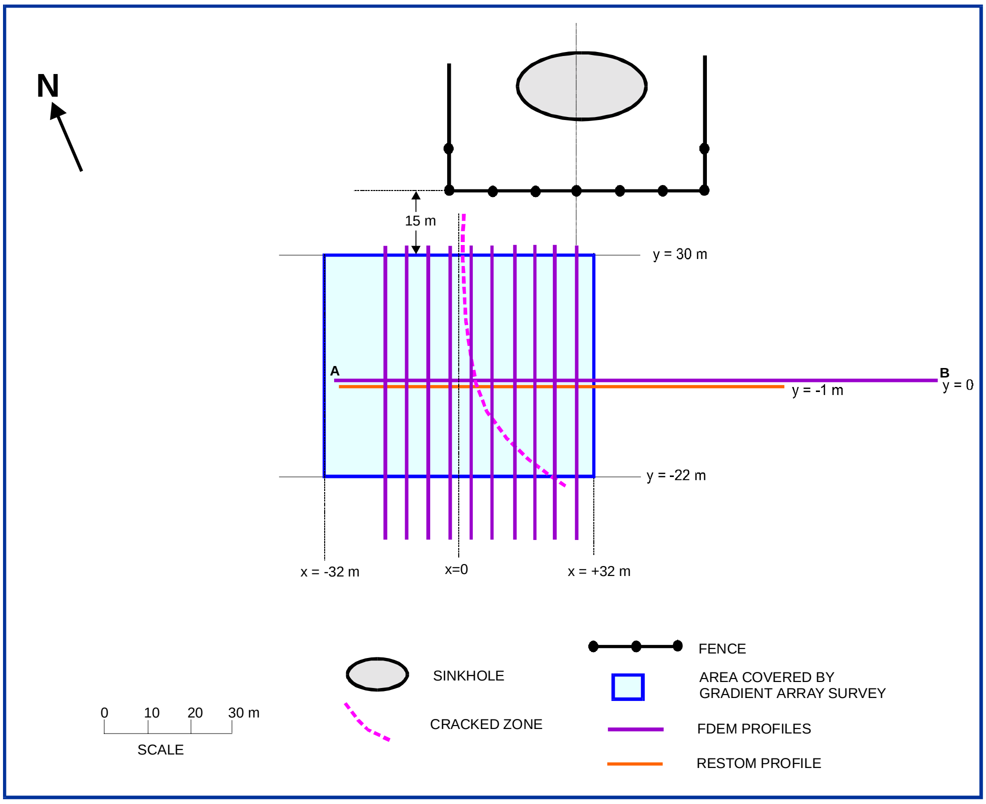

Figure NL10: Location of FDEM and RESTOM profiles.

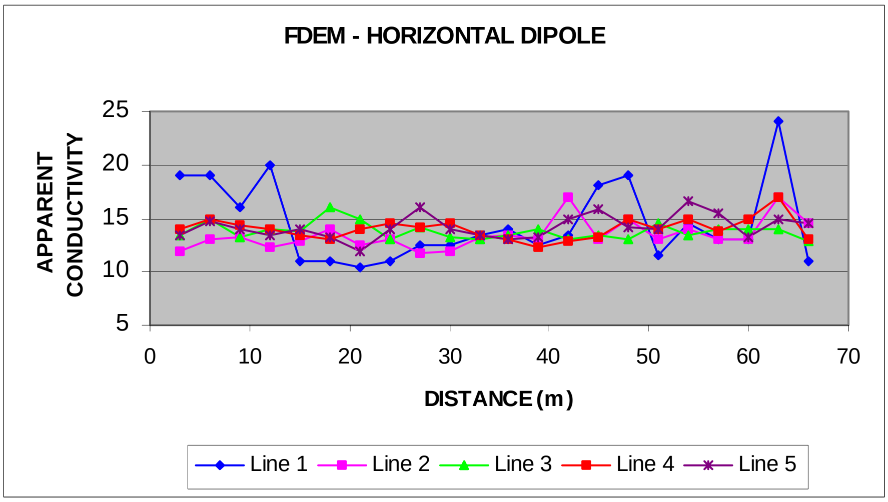

Figure NL11a: FDEM results – horizontal dipole, lines 1-5.

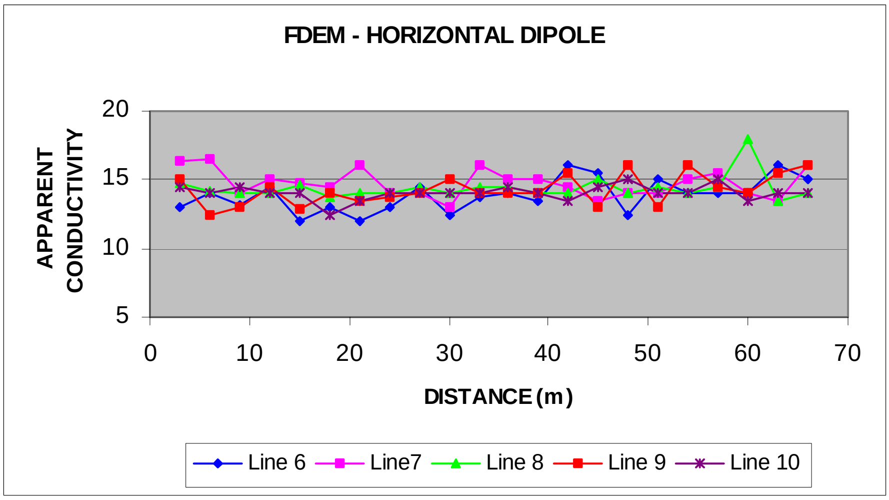

Figure NL11b: FDEM results – horizontal dipole lines 6-10.

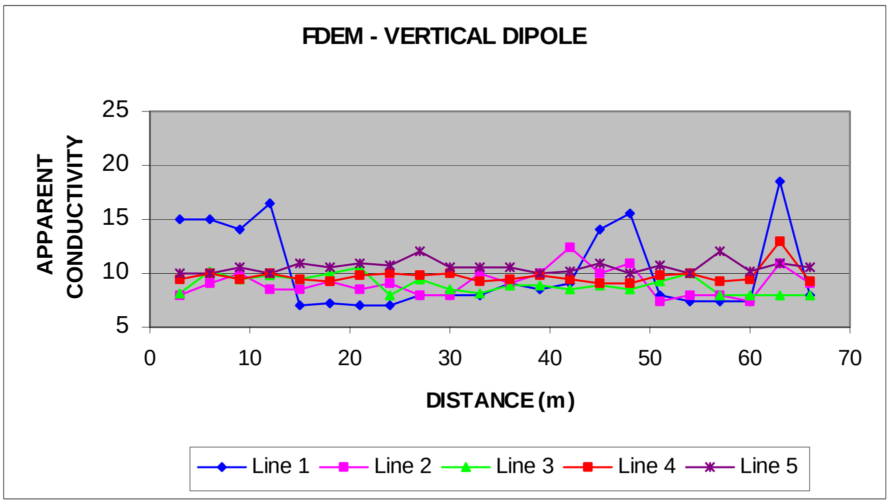

Figure NL11c: RESTOM results – vertical dipole, lines 1-5.

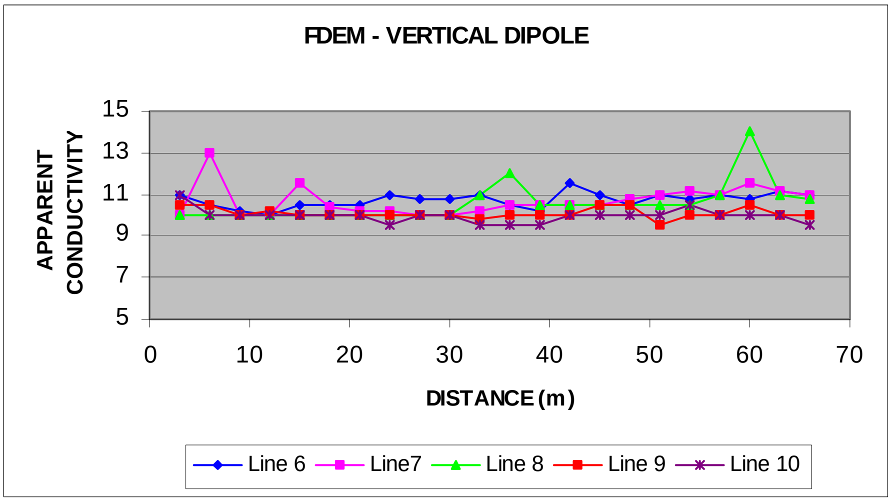

Figure NL11d: FDEM results – vertical dipole, lines 6-10.

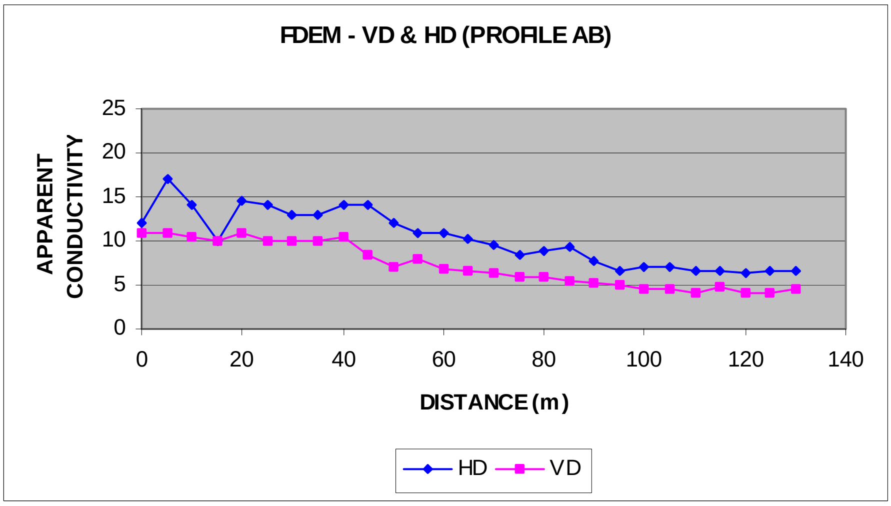

Figure NL11e: FDEM results – Profile AB, vertical and horizontal dipole.

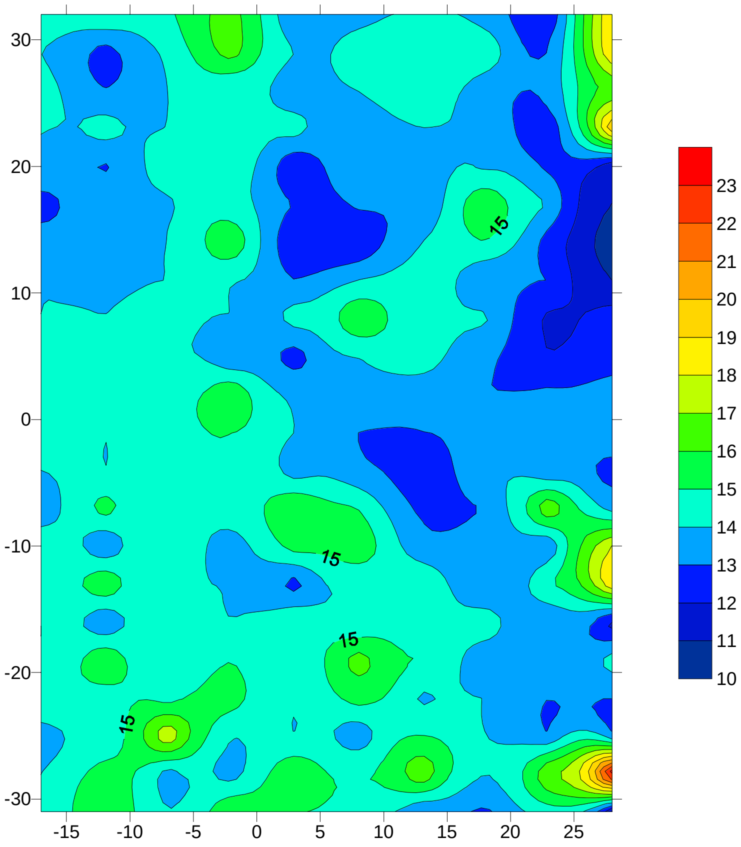

Figure NL12a: FDEM results - horizontal dipole contour map.

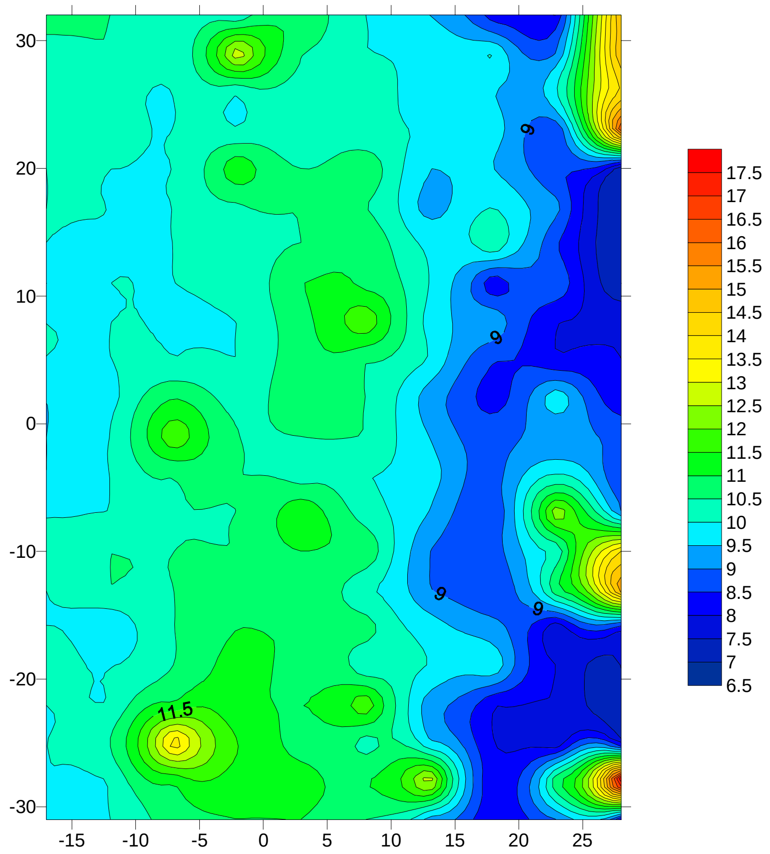

Figure NL12b: FDEM results – vertical dipole contour map.

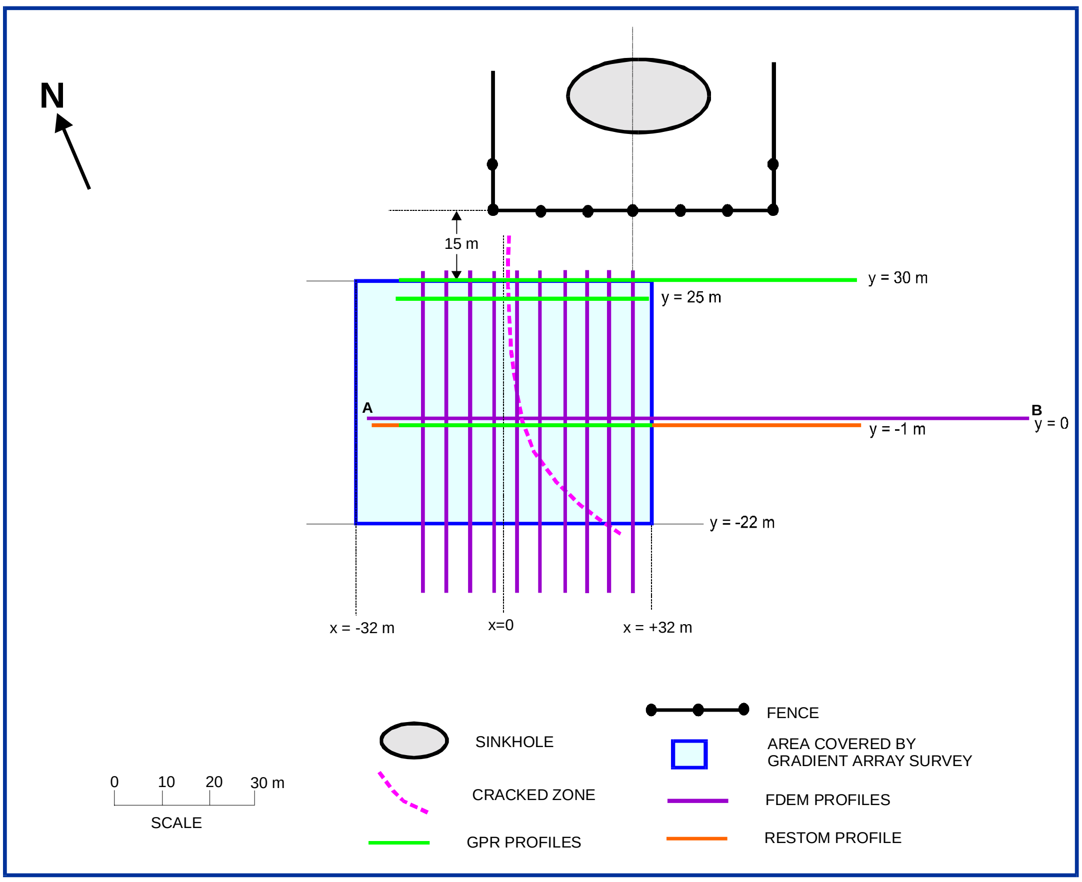

Figure NL13: New Largo – location of GPR profiles.

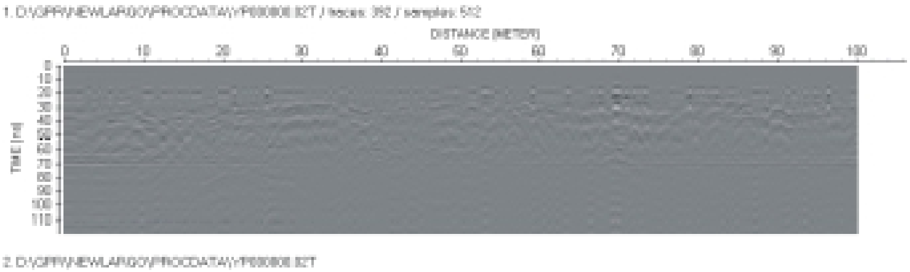

Figure NL14: New Largo – GPR results.

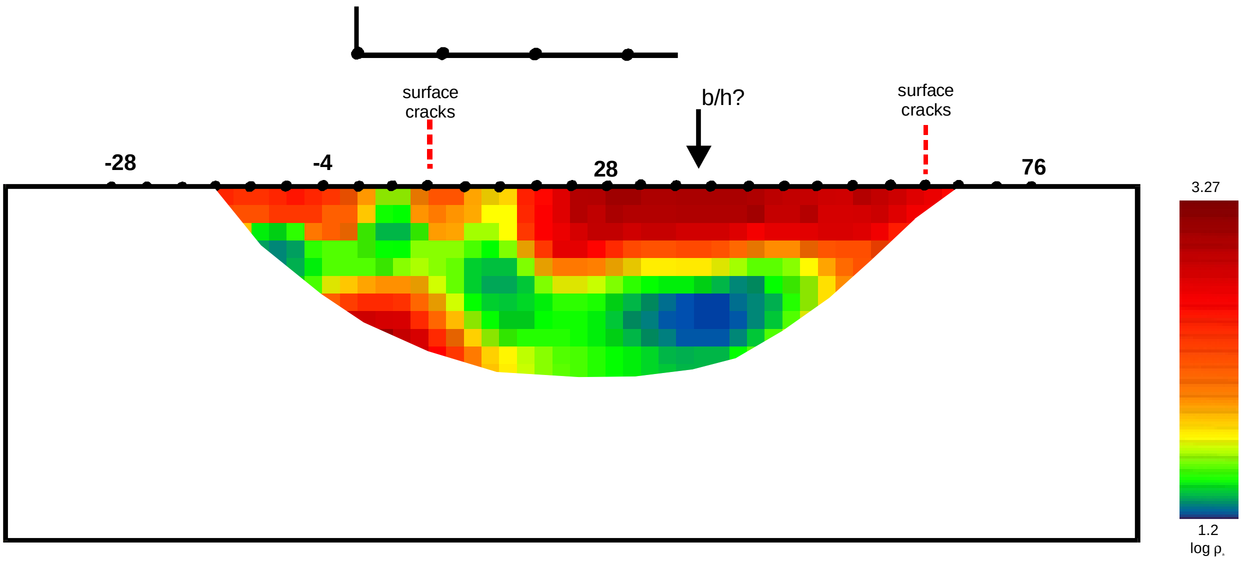

Figure NL15: New Largo - preliminary RESTOM image.

APPENDIX X

COALTECH 2020

Subtask Report
(part of Subtask 4)

Application of GPR in coal

D. Vogt

CSIR, Division of Mining Technology

Report number: 2001-0122

Task 1.3.1b

Detection of old workings, sinkholes, underground fires and acid mine pollution using geophysics and airborne thermal infrared imagery

20 February 2001

EXECUTIVE SUMMARY

Geological materials in the coalfields are not good for GPR propagation. The best material of those investigated is coal, but for coal there is a distinct difference in electrical properties parallel to bedding and perpendicular to bedding. The anisotropy, leads to better GPR performance looking into the side walls of the seam, rather than up or down within the seam.

It is not possible to use GPR to image a coal seam from surface. For a typical system, the GPR range in sandstone and siltstone is about 2 – 3 wavelengths. Resolution is about half a wavelength. For example, if the radar frequency is lowered sufficiently to be able to detect targets 30 m deep, the resolution will be 5 m – 7.5 m. However, for some materials studied the loss tangent goes up as frequency decreases, so for frequencies low enough to penetrate 30 m, the resolution could be as poor as 15 m.

Electrical properties are also a function of water content. In general, if there is water in the rock, it increases the resolution, but substantially decreases the range.

As far as the specific targets of Task 1.3.1b are concerned – for old workings, the problem is again one of range. In general, GPR is not expected to be a viable technique. There is one exception: stress-induced cracks or voids located above the beam over old working if they are very close to surface.

Theoretically, the electrical properties of burnt coal are sufficiently different to those of competent coal to make the change visible in the GPR record. In practise, the poor penetration of GPR in coal makes long-range prediction of burnt coal unfeasible.

TABLE OF CONTENTS

LIST OF FIGURES AND TABLES

1 BACKGROUND

Ground Penetrating Radar or GPR, is a high frequency electromagnetic technique for imaging in the earth. An antenna transmits pulses into the ground where the pulses are reflected from discontinuities. The reflections are detected and stored for later display and processing. An example of a time trace from a single antenna position is shown below:

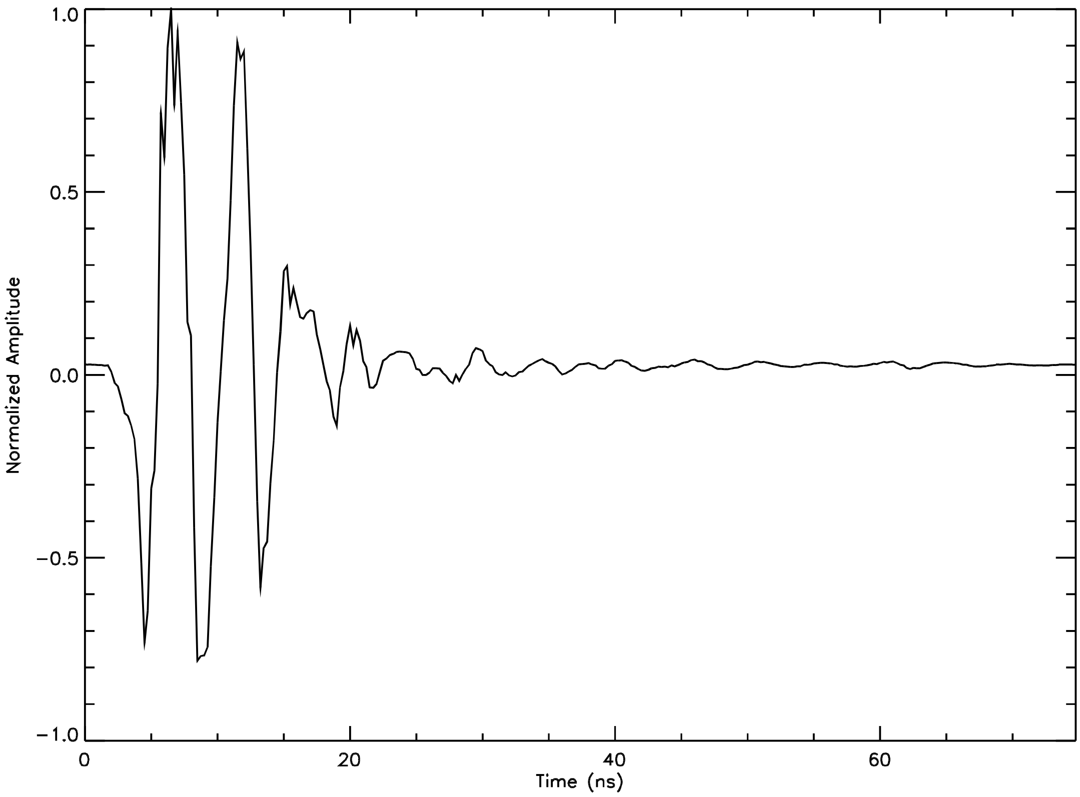

Figure 6.1: Time record of a single radar trace.

GPR data from a single trace is almost impossible to interpret. If data is collected from a number of antenna positions in a line, the resultant image provides a significant amount of additional information. An example of GPR data is shown below:

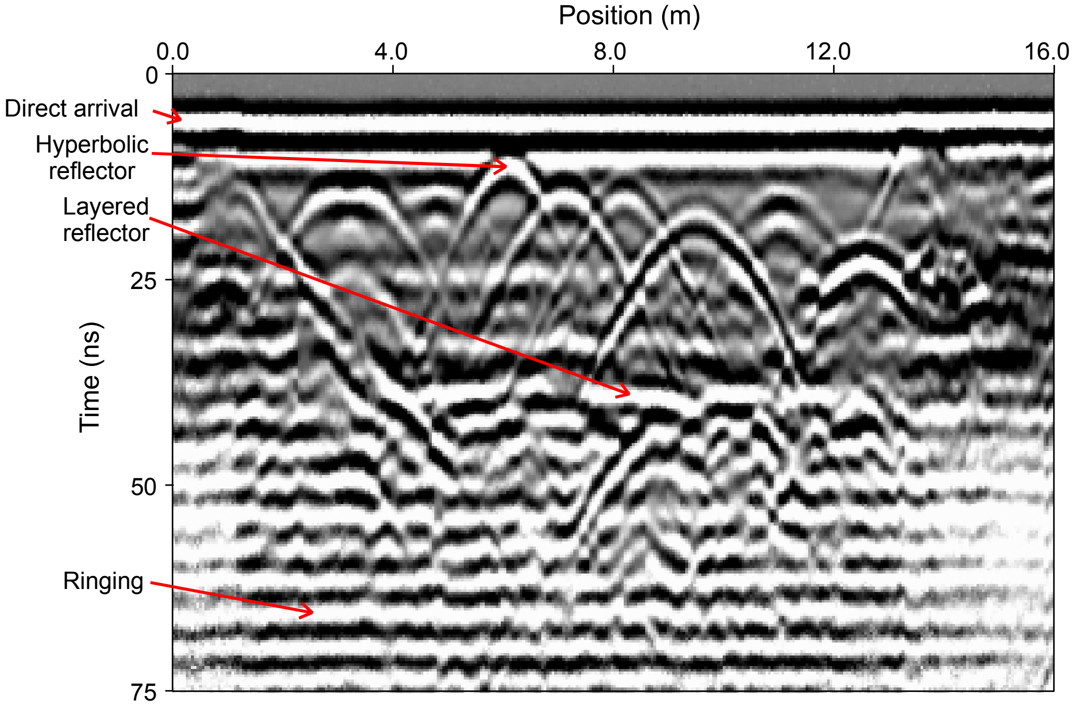

Figure 1.7: An example of a GPR image.

In the GPR image, position of the antenna is shown across the image and time is shown down the image. The response of the GPR at a particular antenna position and time leads to a shade of grey. If a large positive value is received, the response is black. If a large negative value is received, the response is white. The image in
Figure 1.7 contains a number of features characteristic to GPR data:

- The data late in time has been amplified. Because rock attenuates radio waves, it is necessary to amplify the data as a function of time to increase the strength of the signal from distant reflectors.
- The data has not been filtered. The most obvious symptom of unfiltered data is the ringing late in time across all the data. The ringing is evident as a series of horizontal bands across the image. Ringing occurs when the radar pulse resonates the radar antenna. As an analogy, a bell rings for a long time after being struck once. GPR antennas can be designed not to ring, but they are then less efficient.
- The direct arrival is present across the data. The direct arrival is the series of dark – light – dark bands at the top of the image. It occurs because some of the radar energy doesn't enter the rock, but travels directly from the transmit antenna to the receive antenna. The direct arrival is also present as the series of high amplitude oscillations early in time on the trace in *Figure 6*.
- Point reflectors appear in the radargram as hyperbole. The image in
- *Figure 1.7* shows clear point reflector hyperbole. The radar antennas do not radiate only directly down into the earth, but radiate with a hemispherical pattern. The hyperbole come about as a function of the geometry between the transmit and receive antennas and the target.
- There is a layer shown in the image. The layer is a prominent horizontal reflector at about

40 ns. In general layers on the GPR image do not have the true angle of the layers in the earth itself, but the change in angles can be calculated.

- The radar data is presented as a function of time, rather than as a function of depth. Conversion of time to depth is conceptually simple, because distance = speed x time, but in practice the velocity is usually not constant. Radargrams that are presented as a function of time should always be viewed with a small dose of doubt, particularly if no velocity information is given.

The two specifications of greatest interest are the range and the resolution of the radar.

2 ROCK ELECTRICAL PROPERTIES

The performance of a GPR is controlled by the electrical properties of the rock that it is operating in. The two performance parameters of greatest interest are the range and the resolution of the radar. Two rock electrical parameters largely control the behaviour of GPR propagation in rock: the rock conductivity and the dielectric constant or permittivity.

The dielectric constant, also called the permittivity, controls the velocity of propagation of radio waves in materials. The permittivity is normally measured relative to the permittivity of a vacuum. The relative permittivity, ε_r, is always greater than 1, so the velocity of propagation of radio waves in rock is always slower than the velocity of propagation in air. The relationship between the two is

$$v = \frac{c}{\sqrt{\varepsilon_r}} \qquad 1$$

where c is the velocity of light in free space, $\approx 3\text{x}10^8$ m/s.

Conductivity, σ, is measured in Siemens/metre (S/m), or more usually mS/m. Conductivity is the inverse of resistivity, measured in Ω.m, and controls the amplitude of the transmission of radio waves within materials. Metals have high conductivity, and pure insulators have very low conductivity. High conductivity is not conducive to the transmission of radio waves, because the waves are unable to penetrate the skin of the conductive object. For example, car radios stop working in tunnels, because the rock surrounding the tunnel is considerably more conductive than the air that normally separates the car radio antenna from the transmitter.

The actual decay in the amplitude of a radio wave as it travels through rock is called the attenuation, and is a function of conductivity, permittivity, permeability and frequency. For rocks that will support GPR propagation, the attenuation is given by

$$\alpha = \sqrt{\frac{\omega\mu\sigma}{2}} \qquad 2$$

where μ is the magnetic permeability of the rock, $1.25\text{x}10^{-7}$ H/m, and ω is the rotational frequency, ω=2πf. The unit of attenuation is Np.m^{-1}. If $10\log_{10}(\alpha)$ is taken, the attenuation can then be expressed in dB/m.

In general, the permittivity and conductivity of a rock vary as a function of frequency. GPR performance can be inferred from measurements made at DC, but accurate estimations of performance require measurements of rock electrical properties at radio frequencies, preferably within the frequency band that will be used. Another parameter used to describe how radio waves attenuate in rock is the loss tangent,

$$\tan\delta = \frac{\sigma}{\omega\varepsilon}. \qquad 3$$

Empirically, the loss tangent is constant over a wide frequency range for a wide variety of rock types. If the loss tangent is much less than 1, then the rock is considered to be an insulator, and is a good rock for GPR. As the loss tangent rises, the rock is more conductive, and ultimately the range falls to the point where GPR is useless.

3 RESOLUTION

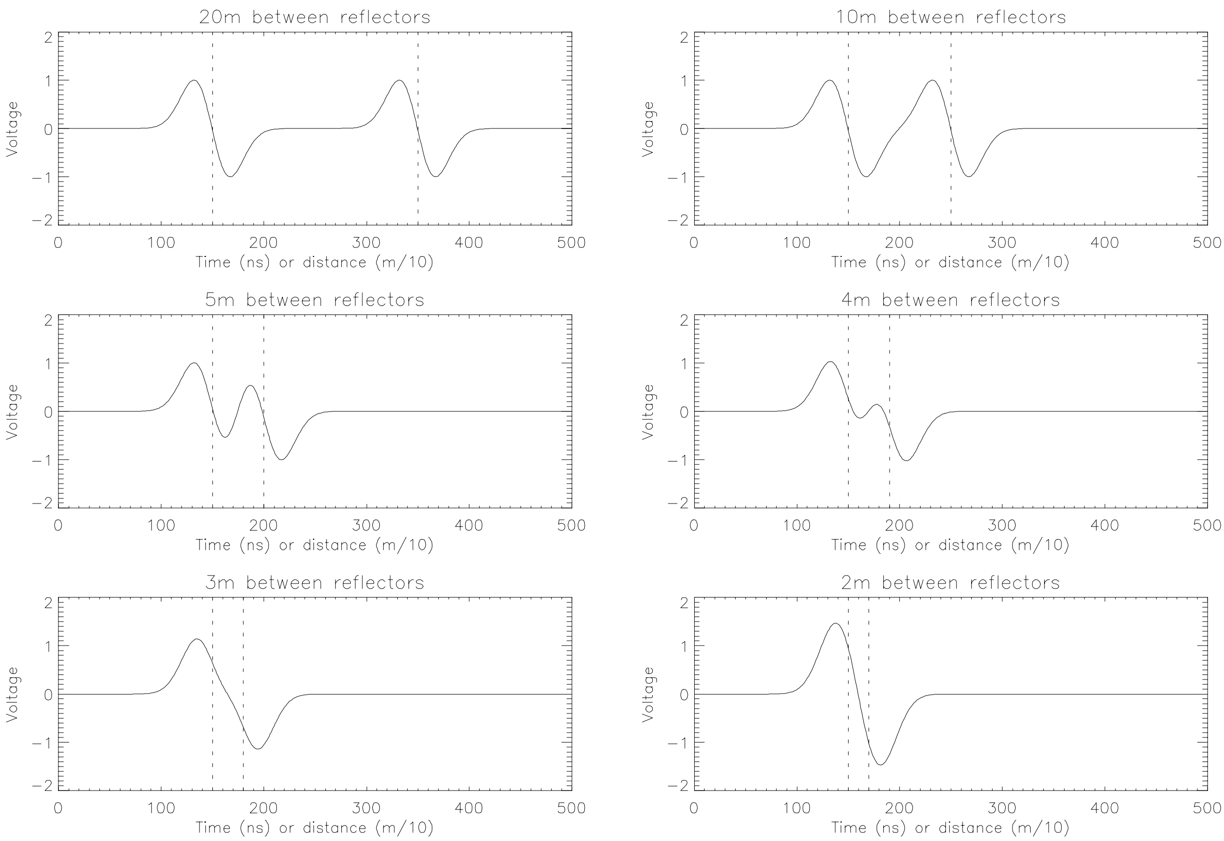

Figure 8.1: Resolving two closely spaced reflectors.

The resolution that can be achieved by a reflection technique is a fraction of the wavelength, typically half of the wavelength.

A simple situation is illustrated in
Figure 8.1: A GPR antenna is placed on a rock surface. Reflections are returned from two reflectors, the first at 150 ns from the radar antenna, the second some distance behind that. The reflections are shown as the received voltage at the GPR antenna as a function of time. If the velocity of propagation is 10 cm/ns, then the first reflector is at 15 m. The pulse shown has a bandwidth of about 40 MHz.

In

Figure 8.1a, the two reflectors each return discrete, easily discernable pulses. In *Figure 8.1b*, the two reflectors are separated by only 10 m, but the two returns are still distinguishable. As the reflectors now come closer together, the echo from the first interferes with the echo from the second. Between 10 and 4 m, the two reflectors can still be separated, although information about the magnitude of the reflections has become lost. When the reflectors are separated by less than 4 m, the individual reflections merge into a single event.

The example has been simplified greatly. In practice, additional information can be gained from adjacent traces, and it is not necessary to completely resolve the pulse waveforms to resolve closely spaced reflections. However, the example does illustrate that resolution is related to the wavelength of the radar pulse, which is related in turn to its bandwidth, or frequency content. One definition of resolution is $\lambda/2$, where λ is the wavelength. The wavelength can be determined from the rock electrical properties:

$$\lambda = \frac{v}{f} \qquad 4$$

where v is the velocity of propagation of the pulse in the rock, and f is the bandwidth of the radar pulse. Equation 4 can be rewritten as

$$\lambda = \frac{c}{\sqrt{\varepsilon_r}\, f}. \qquad 5$$

4 RANGE

The resolution of a GPR system is a function of frequency, and to a lesser extent the permittivity of the rock. What controls how far a GPR can image?

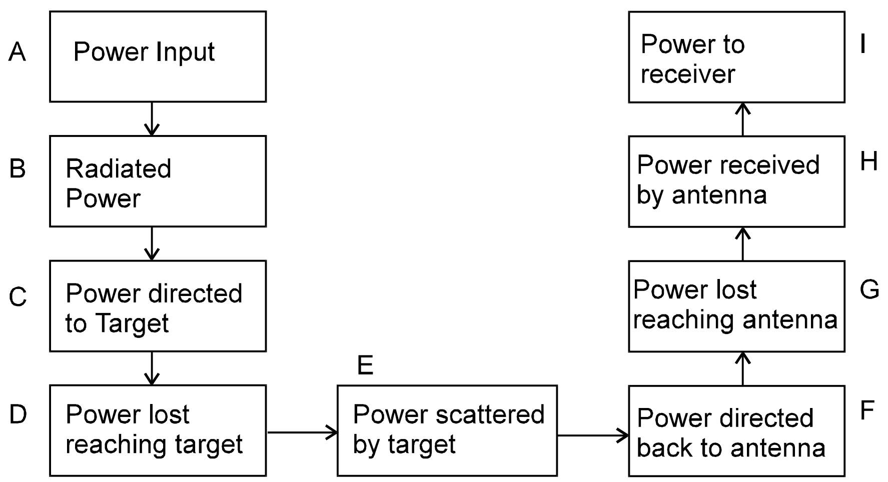

***Figure 9.1*: Block diagram of factors affecting radar return signal strength (after Turner, 1993).**

Ultimately, a GPR must be able to receive the echoes from the target that are produced by the transmitted pulse. The whole process is illustrated in *Figure 9.1*: A pulse is produced in the transmitter, with a certain power. That power is slowly dissipated on route to the target, where some of the power is reflected back towards the receive antenna. The power that is reflected is again dissipated in a variety of ways, until it arrives at the receiver detector electronics, where it is measured.

The process allows us to define the *System Performance Figure*, or SP. The SP is the ratio between the power transmitted, and the smallest signal that can be received, and is normally measured in dBs. The transmitted power is normally restricted by battery life and by the requirement not to interfere with other electronic equipment. The smallest signal that can be received is restricted by thermally generated noise in the rock. For typical GPR systems, the SP is between 80 and 150 dB.

The SP determines the range of the radar. The relationship between range and SP is expressed in highly simplified form as

$$-SP = 10\log_{10}\left[\frac{ke^{-4\alpha R_{\max}}}{R_{\max}{}^{4}}\right] \qquad 6$$

where $R_{\max}$ is the range, and k is a constant that incorporates the radar system characteristics, the target characteristics and the radar pulse frequency and velocity. Range depends critically on the attenuation rate, α. The relationship between range and system performance is non-linear and is best illustrated in graphical form. SP is possibly not the best measurement of GPR performance for two reasons: Firstly, the non-linear relationship between range and SP implies that a large increase in SP can result in a fairly small increase in range. Secondly, the constant, k, in the equation hides a multitude of sins, and can be used to obscure poor antenna efficiency.

5 THE RANGE-RESOLUTION TRADE OFF

As discussed earlier, resolution is a function of wavelength, and hence of frequency: resolution increases as frequency increases. Range is a function of attenuation, and attenuation is a function of frequency. Typically, attenuation increases as frequency increases, so range decreases with increasing frequency.

Noon (1996) describes GPR system performance in terms of two parameters, the loop gain, G_L, and the external loop loss, L_E. The loop gain contains all the terms that are open to the radar system designer, including the antenna gains and efficiencies, and the system performance figure. The external loop loss contains terms that dictate how the radar waves attenuate as they travel through the rock, and how much energy is reflected by the target. The maximum range that a GPR system can achieve occurs when $G_L = L_E$. If rock is assumed to have a constant loss tangent, the external loop loss can be expressed in terms of the loss tangent. Noon gives an equation for the maximum range in terms of the external loop loss,

$$L_{E_Q} = \left[\frac{e^{-4\pi \tan\delta R_{\max\lambda}}\sigma_{\lambda^2}}{(4\pi)^3 R^4_{\max\lambda}}\right]^{-1} \qquad 7$$

where $R_{max\lambda}$ is the maximum range in terms of wavelength, and σ_{λ^2} is the normalized radar cross section of the target, also in terms of wavelength. Note that here σ is the radar cross section, not the conductivity, as it was earlier. Equation 7 cannot be solved for $R_{max\lambda}$, but it can be plotted as a nomogram.

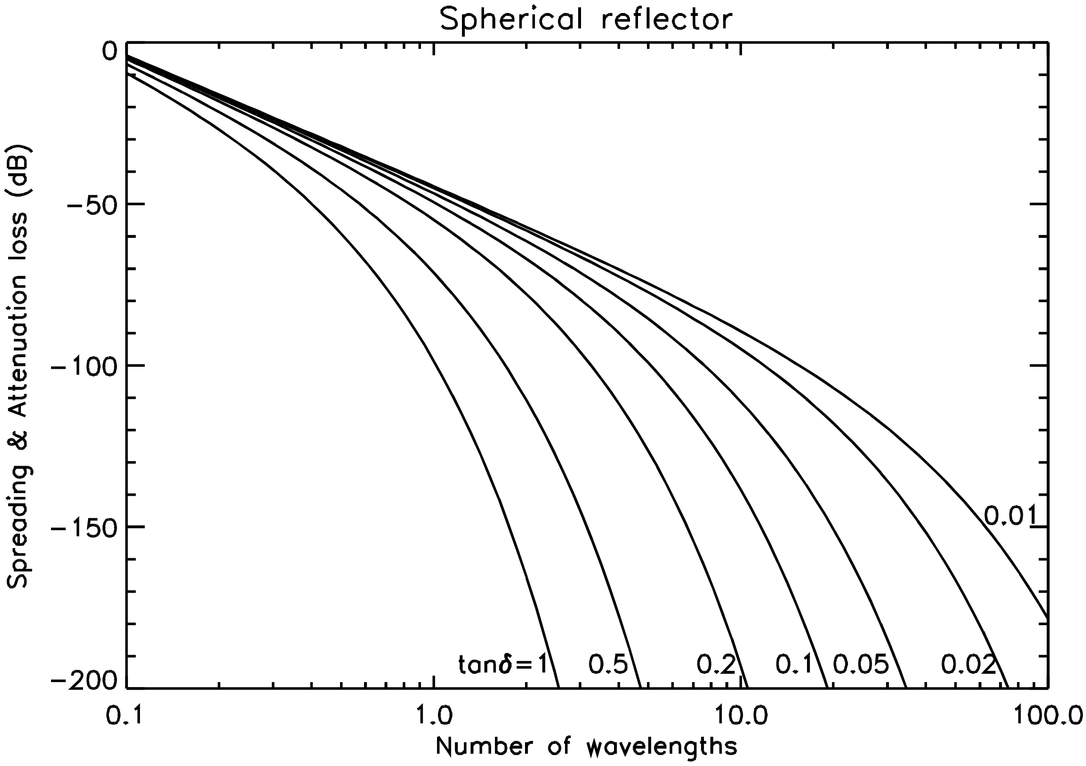

Figure 10.1: Nomogram of GPR maximum range in wavelengths as a function of loss tangent and system performance figure.

The nomogram in *Figure 10.1* is the key to understanding the performance of GPR systems. If a rock is assumed to have a constant loss tangent with frequency, then *Figure 10.1* applies regardless of frequency. From the figure, the range can be determined in terms of wavelengths. The absolute wavelength then depends on the frequency of the radar. In fact, the figure shows how resolution is a function of range in a particular rock type. The spreading and attenuation loss on the vertical axis is the system performance figure. For estimation, a value of 100 dB is reasonable.

- For loss tangents greater than about 0.1, no realistic radar system has a range of more than about 20 wavelengths. For this reason, any rock with a loss tangent of greater than 0.1 is unlikely to be suitable for GPR.
- Improvements in system performance figure offer better improvements in range in low loss rocks. For example, if the system performance is increased from 100 dB to 150 dB, the range in rocks with a loss tangent of 1 goes up from about 1 λ to about 1.8 λ. For the same improvement in performance in rock with a loss tangent of 0.01, range goes up from about 15 λ to about 50 λ. In other words, getting a better system is not a viable way of increasing GPR performance in lossy rocks.
- The nomogram in *Figure 10.1* applies for a conductive spherical target whose circumference is approximately one wavelength. If the target is a rough or smooth planar reflector, slightly better range can be expected.
- The reflection from an interface is determined by the radar reflection coefficient, Γ. The reflection coefficient is a function of the materials either side of the interface:

$$\Gamma = \frac{\sqrt{\varepsilon_{r1}} - \sqrt{\varepsilon_{r2}}}{\sqrt{\varepsilon_{r1}} + \sqrt{\varepsilon_{r2}}} \qquad 8$$

where ε_{r1} and ε_{r2} are the relative permittivities of the materials on either side of the interface. The rock – air interface always has a high reflection coefficient, as does the rock – water interface. Interfaces between two different rock types can be good reflectors, or very poor, depending on the specific rocks.

6 APPLICATION TO COAL

The range-resolution discussion in the previous section is general. For the coalfields of the Witbank area, range and resolution depend on the electrical properties of the coal and the surrounding sandstones, mudstones and silts. Some example properties are given in *Table 6.2*. As a general rule, materials containing clay minerals have higher loss tangents than those with high silicate content.

Table 6.2. Electrical properties for specific samples of coal and related lithologies, measured at 64 MHz. Note that no generalizations can be made from this data.

Rock type	Relative permittivity	Loss tangent
Sandstone	9.2	0.48
Siltstone	12.5	0.70
Shale	26.5	1.15
Coal, parallel to bedding	15	0.3
Coal, perpendicular to bedding	7.9	0.13

From the table, all the geological materials in the coalfields are not good for GPR propagation. The best material of those listed is coal, but for coal there is a distinct difference in electrical properties parallel to bedding and perpendicular to bedding. The difference, or anisotropy, leads to better GPR performance looking into the side walls of the seam, rather than up or down within the seam.

It is not possible to use GPR to image a coal seam from surface. For a system with a performance of about 100 dB, the GPR range in sandstone and siltstone is about 2 – 3 wavelengths. Resolution is about half a wavelength. For example, if the radar frequency is lowered sufficiently to be able to detect targets 30 m deep, the resolution will be 5 m – 7.5 m. In fact, for all the materials in *Table 6.2*, the loss tangent goes up as frequency decreases, so for frequencies low enough to penetrate 30 m, the resolution could be as poor as 15 m.

Electrical properties are also a function of water content. In general, if there is water in the rock, it carries conductive ions, and increases both the relative permittivity and the loss tangent of the rock. For radar, it increases the resolution, but substantially decreases the range.

Specific Targets

- Reef from surface: For the reasons discussed above, it is not feasible to use GPR to map the reef horizon from surface.
- Old mine workings in the coal: again, the problem is one of range. In general, GPR is not a viable technique. There is one exception: if the beam over the workings is stressed sufficiently, cracks can form in the corner of the beam, directly over the pillar – void interface. The cracks fill with soil from above, causing sub-surface voids. The voids themselves should be good GPR targets as they are very close to surface.
- Burnt coal: Theoretically, the electrical properties of burnt coal are sufficiently different to those of competent coal to make the change visible in the GPR record. In practise, the poor penetration of GPR in coal makes long range prediction of burnt coal unfeasible.
- In seam imaging: if the GPR could be placed within the seam, for example as a borehole radar, it stands a good chance of imaging the roof and floor, and other discontinuities within the coal. If the coal has a loss tangent of 0.13, from *Table 6.2*, then from *Figure 10.1*, for a 100 dB system, the range is about 7 wavelengths. In other words, the resolution is about 7% of the range. In a 2 m thick coal seam, imaged from the middle of the seam, a resolution of 7 cm can be achieved. *Figure 10.1* applies for a spherical target. Better results could be expected from a planar target, or from a system with higher performance.
- Roof beam thickness: in many mines, the beam supporting the roof becomes unsafe if it is

thinner than a given distance. If there are partings in the roof, the beam may be thinner than the safe thickness. The parting is an excellent radar reflector, the range required is small, so GPR should be able to determine whether there is a parting within a given distance.

7 RADIO TRANSMISSION TECHNIQUES

Radar relies on an echo from an interface to produce an image. Radio Transmission techniques transmit through an area of interest from one borehole to another. The underlying physics are the same as those that govern GPR. The wavelength required for penetration is plotted in *Figure 7.1* as a function of spacing between the transmitter and receiver, and the loss tangent of the medium. The result is broadly similar to that of *Figure 10.1*, for a fixed system performance: resolution decreases with increasing loss tangent down to a minimum resolution.
Figure 7.1 is from Vogt (2000). More information about the figure is available there.

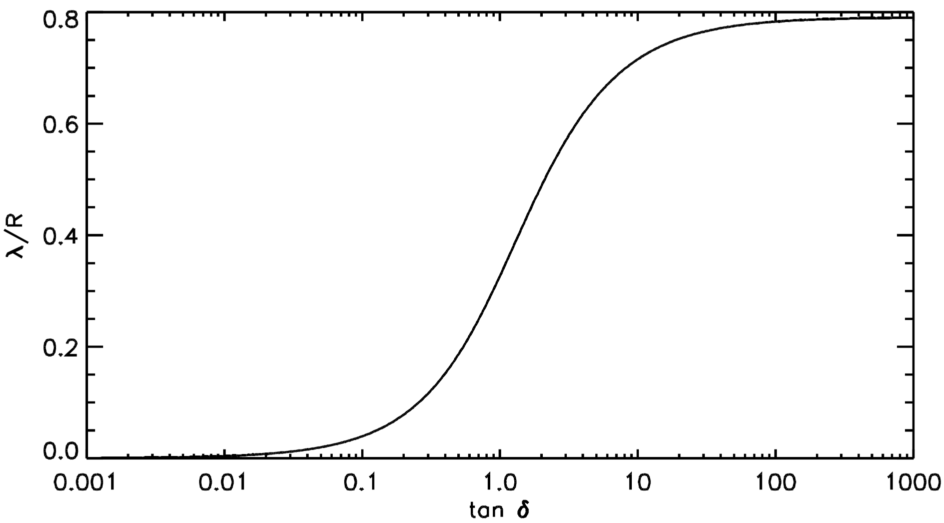

Figure 7.1: Radio transmission techniques: resolution as a function of range and loss tangent.

There are three transmission techniques of interest, from highest frequency to lowest:
1. Cross-hole borehole radar
2. Radio Tomography (RT)
3. Radio Imaging Method (RIM)

Note: The difference between RIM and RT is the type and frequency range of the antennas used. RT generally utilises E-field antennas with frequencies above 1 MHz, whereas B-field antennas with frequencies below 1 MHz are used in RIM surveys.

Coal requires low frequencies for two reasons: coal has a relatively poor loss tangent for radio techniques, as shown in Table 6.2, and the high production rate in coal dictates very long range techniques.

The most promising methods for coal are RIM and RT, both operated from within the coal, to map a block of coal. For example, once the two roads have been developed for a longwall, radio imaging can be undertaken between the two roads. Low radio frequencies would be used, to achieve the long range required in the coal. Resolution of about 5% of the range could be expected. A radio image between two roads would show the presence of any intrusions not intersected by the roads themselves, it would show the presence of burnt coal, and may give an indication of seam thickness.

Radio imaging is not likely to have any use in the strata above or below the coal. Miningtek undertook RT surveys between two vertical boreholes in a coal environment, and mapped the position and thickness of the coal seam. However, the range of 50 m means that the image is almost useless for production.

There is one potential use of radio from vertical boreholes. The attenuation through the coal can be measured by inserting a transmitter into one borehole and a receiver into another borehole, both within the coal seam. The expected attenuation is known: if higher attenuation is measured, then there is some disruption to the coal between the two boreholes. Ranges of greater than 100 m can be expected, and the technique would be very quick to apply. Once the coal between two boreholes had been determined as disrupted, other more expensive techniques could be applied to determine the cause of the disruption and its extent.

8 REFERENCES

Noon, D. A. 1996. Stepped-Frequency Radar Design and Signal Processing Enhances Ground Penetrating Radar Performance. PhD thesis, The University of Queensland.

Turner, G. 1993. The influence of Subsurface Properties on Ground Penetrating Radar Pulses. PHD thesis, Macquarie University.

Vogt, D. 2000. The Modelling and Design of Radio Tomography Antennas. Dphil Electronics, University of York

APPENDIX XI

An Assessment of The Use of Seismic Methodologies to Detect Buried Cavities or Tunnels

C. Wright

Work address:

Bernard Price Institute of Geophysical Research

The University of the Witwatersrand, Johannesburg,

Private Bag 3, Wits 2050, South Africa

Tel. 011-717-6623

Fax. 011-339-7367

E-mail: 006cwrig@cosmos.wits.ac.za

Home address:

83 West Park Road,

Montgomery Park 2195, South Africa

Tel. 011-888-6441

E-mail: cedric.wright@freemail.absa.co.za

Latest Update: 24 January, 2001

Executive Summary

An investigation of the feasibility of applying seismic methodologies to detect and locate old mine workings at depths of a few metres to about 50 m below the surface has uncovered no previous examples of the use of this approach. However, there are a few examples of related uses of seismology to detect cavities in limestones and in civil engineering problems, whose success is variable. The absence of good, readily available published examples suggests that such applications of seismology have not been particularly successful, or that the methodology has not been adequately developed.

In contrast, numerous theoretical studies of the effects on seismic body and surface waves of buried elastic inclusions or cavities in a homogeneous medium have been undertaken over the last fifty years. Two- and three-dimensional models with circular, cylindrical, spherical and arbitrarily-shaped inclusions have all been considered. However, the more complicated problem of generating exact synthetic seismograms for a source buried in a multilayered half-space containing a buried explosive source and an inclusion or cavity in one of the layers appears to have been investigated by just a single group of researchers in Sweden. The resulting synthetic seismograms for complicated models that simulate conditions in the Earth show direct and reflected waves, head waves and surface waves. Most exact modern methods of generating synthetic seismograms for complicated models make use of the finite difference approach, but are computationally time consuming. Many approximate methods that are computationally fast have been developed, but do not always give reliable results for models with structural complexity. Further work on the use of synthetic seismograms to test the feasibility of detecting old mine workings is therefore not recommended at present, because of the extreme complexity of reliable methods, and the availablity in the literature of theoretical results for simplified situations.

Laboratory models have also been developed as an alternative to synthetic seismograms for simulating the seismic response of a buried cavity, though only for the two-dimensional case. The detection of buried cavities by use of diffracted or scattered P waves is the most promising and cost-effective approach, provided that the masking effect of the Rayleigh waves can be suppressed by placing a trench between the source and geophones to block the Rayleigh waves. The Rayleigh waves themselves may be used to detect shallow cavities by measuring fluctuations in phase velocity as a function of frequency. A trial experiment is recommended in which seismic waves are recorded over a shallow cavity (< 10 m deep) and over a deeper one (10-30 m below the surface). The recording should be undertaken both with and without trenching, so that the Rayleigh waves can be used to detect the shallow cavity, and so that the body waves can be analysed to locate the deeper cavity without interference from the Rayleigh waves.

Literature Survey and Assessment of Available Work

Introduction

Old coal mine workings at depths between a few metres and about 50 m pose a serious hazard to overlying buildings and the development of open-cast or strip mining. The risk of damage to buildings, equipment used in mining operations, and injuries to persons in the area may be considerable, if locations of old tunnels are not accurately known, because of the possibility of sudden ground collapse. One approach to detecting buried tunnels or cavities is the use of seismic methods, of which seismic refraction has been suggested as the most useful. However, the use of refracted arrivals alone will not enable the detection of a single buried cavity, though the combined use of all kinds of body wave arrivals (refracted, reflected, diffracted and scattered) looks promising as a practicable and effective methodology. Surface waves or ground roll have also been used to detect shallow cavities (Ganji, Gucunski and Maher, 1997), but can effectively mask the body wave response produced by a cavity at moderate depths. It may be possible to suppress the surface waves using trenching to block them (Pant and Greenhalgh, 1989).

There are few experimental results available for the real Earth, and the reported studies are in rather obscure publications that are not readily available. This suggests that the results have not been particularly successful, or that appropriate methodologies have not yet been fully developed. In contrast, many relevant theoretical studies have been published over the last fifty years that calculate the response in both two and three dimensions of buried obstacles or cavities to incident P, S or surface waves. Most of these studies are concerned with the derivation of results for a particular type of wave (e.g. plane longitudinal) travelling through a medium that is homogeneous apart from the inclusion. Results are usually derived in closed form, which can then be used to provide results that are simplifications of the situations encountered in the Earth. These papers are widely distributed through the literature on acoustics, applied physics, civil and earthquake engineering, exploration geophysics, geotechnical investigations, seismology and soil mechanics. From the titles of many of the publications, it appears that researchers in some areas have derived results without knowledge of appropriate literature in related disciplines. This suggests an enormous duplication of effort that would be interesting to investigate further with a more rigorous assessment of the literature.

The calculation of synthetic seismograms for a buried cavity has been attempted by very few workers. Modern research into the methodologies of generating synthetic seismograms for realistic earth models is a very complex and highly developed area in which both approximate (and generally fast) methods and exact (computationally demanding) are still being improved and compared. However, most of these methodologies focus on calculating the response of sub-horizontally layered media with small inhomogeneities (variations in elastic constants or wavespeeds) that give rise to weak scattering; they are useful for simulating complex stratification that occurs on the scale of oil exploration or in studying earth structure on a crustal scale or greater. Furthermore, the development of complex methods and algorithms that deal with anisotropic materials has been a priority in both exploration and fundamental problems, because of the widespread occurrence of anisotropy in the Earth due to preferential alignments of cracks or fractures. However, the development of methods involving anisotropy are not important for the cavity detection problem. The main contribution to the development of realistic synthetic seismograms for the problem of the buried cavity has been contributed by Boström and his colleagues at Chalmers University of Technology in Sweden (Boström and Karlsson, 1984, 1987).

The objective of this report is to survey the literature relevant to the detection of underground cavities. This comprises theoretical work that includes the generation of synthetic seismograms, model simulations and practical field trials. The theoretical principles involved in this work are also reviewed, since critical considerations in determining the success of any experiment to locate buried cavities are the relationship between the wavelength of the seismic signals and the dimensions and depth of burial of the cavity, and the signal-to-noise ratio of the recorded response.

Search Methodology

Information on the detection of cavities by seismological means was sought through the computer search facilities of the library of the University of the Witwatersrand, and through the science and technology search engine 'Scirus' available through Internet. While a certain amount of relevant information was located, mainly by use of 'Scirus', most of it was in obscure publications or in journals not available either in the University library or in libraries in the Johannesburg area. Several of the most important publications have been ordered from overseas. Because the search was not commenced until 21 December, and because libraries have been working with few staff over the Christmas/New Year holiday period, these key publications have not yet been received.

Much of the useful or relevant literature that needs to be evaluated lies in journals that are not available in South Africa, including the following:

Bulletin of the Indian Society of Earthquake Technology

Earthquake Engineering and Engineering Vibration

European Earthquake Engineering

Seismic Methodologies – Principles

In using seismology to study the structure of the earth, there are four types of wave that might be used: two types of body waves, known as P and S, that penetrate the medium and whose propagation paths can be approximately represented by rays, and two types of surface waves, Rayleigh and Love waves. In an isotropic medium these waves have the following properties. P waves have particle motions in the direction of propagation of the waves, are analogous to sound waves in air, and are always the first to arrive at a location distant from the source. S or shear waves travel more slowly than P waves, have particle motions at right angles to the direction of propagation, and can only exist in a solid. Rayleigh waves travel along the surface of the Earth and have particle motions in a vertical plane in the direction of the wave; they travel with a speed slightly less than that of shallow S waves, and exhibit dispersion if the properties of the medium change with depth below the surface. Love waves have particle motions in a horizontal plane at right angles to the direction of propagation; they propagate with the same speed as shallow S waves, exhibit dispersion, and can only exist in a solid in which the elastic constants change with depth. Only P, S and Rayleigh waves have been considered for detecting buried cavities.

P waves are the easiest to use because they are the earliest arrivals, and are well recorded in surface seismic surveys by vertical-component geophones. The effective use of other wave types generally requires the recording of more than one direction of ground motion, making field operations much slower and comparatively expensive. An important consideration in the use of seismology is that P or S waves impinging on a boundary where there is a change in impedance (product of seismic wavespeed and density) will usually generate both transmitted and reflected P and S waves (or scattered waves in the case of irregular boundaries), making the mathematical treatment of the problem complicated compared with the scattering of acoustic or sound waves by obstacles. For this reason the theory of scattering of sound waves by obstacles is well developed compared with the seismological case, with key theoretical results derived long ago (e.g. Morse, 1948, pp. 346-360).

The Detection Problem

Figure 1 shows a horizontal plan of a seismic experiment that might be devised to detect a buried mine tunnel, represented schematically in section as a rectangle. The assumption is that the object to be detected is elongated. A surface or near-surface seismic source is shown with a linear array of geophones deployed on the surface on the far side of the buried cavity. In general, because the orientation, shape and dimensions of the buried cavity will not be known, three cases can be considered for the orientation of the seismic profile relative to the tunnel: (i) parallel, in which the profile lies parallel or sub-parallel to the long dimension of the tunnel, providing the largest seismic response compared with a parallel profile displaced well away from the tunnel; (ii) orthogonal, in which the profile is at or almost at right angles to the trend of the tunnel, providing the smallest seismic response compared with a parallel profile displaced well away from the tunnel; (iii) oblique, in which the profile crosses the longest dimension of the tunnel at an angle, providing a complicated seismic response intermediate between cases (i) and (ii). Most of the available theoretical treatments deal with case (ii) or the response of a spherical cavity. The real situation is therefore both geometrically complex and difficult to model mathematically, in which body or surface waves might be used for detection, the appropriate wave type depending on the depth and size of the tunnel.

The Effects of Fractures and Cavities on Seismic Wave Propagation

Both body waves and surface waves have been used to detect underground cavities in engineering-scale applications of seismological principles. The data analyses for evaluation have been based on travel-time or spectral analyses. Many mathematical studies of the effects of cavities of simple geometrical shapes on seismic wave propagation have been published and will be summarised in the next section. Theoretical studies of elastic wave propagation in both isotropic and anisotropic fractured or porous materials have also been made with applications to hydrocarbon exploration, earthquake monitoring, tectonics, and shallow environmental studies. However, such work is concerned with the computation of the seismic characteristics of large aggregates of inclusions or cavities that change the effective elastic constants of the material. To make the problem tractable, the assumption is made that the dimensions of the inclusions are small compared with the wavelengths of the seismic signals. Such work is considered here, since it may have relevance in the detection of partially collapsed or water-filled tunnels.

An important consideration in the detection of cavities using seismic waves is the size of the cavity or cavities in relation to the wavelengths of the seismic signals generated. Three cases must be considered:

(i) The wavelength λ of the signal is small compared with the dimensions d of the cavity or cavities ($\lambda \ll d$). In this case a cavity could be detected by reflection or scattering, or by diffraction around the cavity, if body waves are used, the approach depending on the depth of the cavity below the surface. Alternatively, for a near-surface cavity, spectral analysis of surface waves to identify reflections from the cavity may be used (Ganji et al., 1997). Estimation of the dimensions of the cavity is in principle possible.

(ii) The wavelength λ of the signal is comparable with the dimensions of the cavity or cavities (λ ~ d). This is a more difficult situation that cannot be modelled easily, in which detection using body waves may be possible, though reliable estimation of cavity size may not be obtainable. This is the situation where Mie scattering will occur in which the equivalent source for the scatterer is no longer a point source. The phase difference of the incident field at different points of the inclusion and the scattered field from different parts of the inclusion can no longer be ignored.

(iii) The wavelength λ of the signal is large compared with the dimensions of the cavity or cavities (λ >>d). In this case direct detection and location is difficult, since the effect of a cavity or cavities is expressed as the elastic constants of the equivalent elastic medium. Thus, all that may be observed under ideal conditions is a localised lowering of the seismic wavespeeds in the region containing the cavity or inclusions. This is the situation for Rayleigh scattering.

To obtain some idea of the conditions that might be encountered in searching for old mine tunnels in the sedimentary rocks that host coal seams in South Africa, assume that the average seismic P wavespeed is 3000 m/s (Maccelari et al., 2001). For explosive seismic sources detonated near the surface or in boreholes in areas of coal mining, P waves recorded by geophones on the surface have dominant frequencies of around 100 Hz, and may have significant energy up to 200 Hz (Maccelari et al., 2001). The wavelengths of the signals are therefore in the range 15 to 30 m. If a seismic survey is conducted along a line orthogonal to a mine tunnel of lateral dimensions d in the range 2 to 4 m, the situation corresponds to that of cases (ii) and (iii) above (λ (15-30 m) ~ d (2-4 m) or λ >> d). Thus the real situation does not correspond to the best conditions for seismic detection (λ << d or λ ~ d). Consideration of S and surface waves does not improve the situation, because both wave types usually have much lower frequencies on seismograms than P waves.

Results of Literature Survey on Mathematical Modelling and Field Trials

The measurement of both reflected and refracted travel times have been tried, and show some merit for cavity detection. Cooper and Ballard (1988) showed that the presence of voids close to the surface results in an increase in travel times. However, they found that refraction methods fail to detect water or soil-filled cavities, or a rigid obstacle, because the travel-time changes are too small. Lateral variations in local stratification can also influence the travel times as much as shallow cavities, resulting in ambiguity in interpretation (Belesky and Hardy, 1986; Cooper and Ballard, 1988). The reflection method has also been used successfully to detect deep cavities, but detection at moderate depths is problematic, since the reflected or scattered waves arrive at the receivers at about the same time as the surface wavetrain. It may be possible to overcome the problem of detection of cavities at relatively shallow depths by using trenches to bock the surface waves (Pant and Greenhalgh, 1989)

Surface waves have been used less extensively than body waves for obstacle or cavity detection. The effects on surface waves of anomalies close to the surface were discussed mathematically by Dravinski (1983) and experimentally by Curro (1983). For surface waves, the amplitudes are more sensitive to the presence of obstacles or cavities than travel times, so that spectral methods are more appropriate for data analysis. Ganji et al. (1997) examined the ability of spectral analysis of surface waves (SAWS) to detect underground obstacles of different shapes and depths (Figure 2) by using a finite element method to devise a simulation test. The obstacle, which can be rigid or a cavity, is detected through fluctuations in the phase velocity dispersion curve. The results from the finite element simulation were compared with experimental results and verified through mathematical modelling. The SAWS test was found to be an effective way of detecting underground obstacles, provided they are close to the surface.

A number of relevant papers have been published by Lee and coworkers in the Department of Civil Engineering in the University of Southern California, Los Angeles. Their work comprises the derivation of mathematical results for scattering and diffraction in an elastic half space, and the results are expressed in closed form, which can then be evaluated numerically. Lee, Chen and Hsu (1999) recently considered the problem of the 2D scattering and diffraction of plane SH waves by a circular canyon on top of an underground cavity in a homogeneous elastic half space. Similar 2D diffraction problems with only surface topography (canyons or alluvial valleys) or subsurface features (buried cavities or tunnels) have been solved mathematically by several workers (Figure 3). The diffraction of SH waves by an underground circular cavity was solved by Lee (1977) and extended to P and SV waves by Lee and Karl (1993a,b). The diffraction of elastic waves by shallow circular to semi-circular surface canyons was also investigated by Cao and Lee (1989, 1990) and Todorovska and Lee (1990, 1991a,b).

Extension of the theory to three dimensions has also been implemented for some forms of cavity. Lee (1988) used the integral representation of Hankel functions to investigate diffraction by an underground inclusion. Deformations near a long cylindrical inclusion at the surface and an underground cylindrical tunnel (Figure 4) were estimated by Ghosh and Lee (l995) and Lee, Ghosh and Sabban (l996).

Much earlier work for 3D cases than that of Lee and coworkers was published by Ying and Truell (1960) and Yamakawa (1962), who investigated the scattering of periodic plane P waves by spherical obstacles and cavities. Einspruch, Witterholt and Truell (1956) considered the equivalent problem for plane shear waves. Yamakawa (1962) obtained the following results for P waves:

(i) The amplitudes of both scattered P and S waves are proportional to the square of the frequency and to the volume of the obstacle or cavity.

(ii) There is more scattered S wave than P wave energy.

(iii) More energy is scattered in front of than behind the obstacle.

The scattering of elastic waves by a cavity was also considered by Varatharajulu and Pao (1975). Wu and Aki (1985) formulated the scattering of elastic eaves by a general elastic heterogeneity, using the Born approximation. In the low frequency range (Rayleigh scattering), the scattered field by an arbitrary heterogeneity having an arbitrary variation of density and elastic constants can be equated to: (i) a radiation field from a point source composed of a unidirectional force, which is proportional to the density change between the inclusion and he medium, and (ii) a force moment tensor proportional to the changes of elastic constants between matrix and inclusion. Both plane P and plane S waves were used, and the special cases of scattering by a uniform sphere and a Gaussian spherical inhomogeneity were also considered. Figure 5 summarises the features of available theoretical studies of the 3-D scattering problem.

Theoretical developments that parallel those in civil and earthquake engineering have been contributed by seismologists who have attempted the solution of more complicated problems specifically of relevance to geophysical research and exploration. The detection of a bounded inhomogeneity in a layer within a layered elastic half space is a problem of importance in several areas of geophysical exploration. Most methods that have been tried are approximate and often asymptotic. As an improvement on the simple method of computing travel times, methods that have been suggested include the exploitation of head waves (Cerveny and Ravindra, 1971), perturbation methods (Kennett, 1972), boundary methods (Sánchez-Sesma, Herrera and Alvilés, 1982), integral equations (Ahenbach and Brind, 1981) and matched asymptotic expansions (Datta and El-Akily, 1978). Datta and El-Akily’s work is of particular interest, because they consider diffraction from a cylindrical cavity. They derived the far-field asymptotic behaviour of the scattered displacement for a general wave incident on a cylindrical cavity in an elastic half space. The only numerical results provided were for surface displacements due to Rayleigh waves.

The exact solution for the full boundary problem is time-consuming, and was investigated by Boström and colleagues. The work of Boström and others in the Institute of Theoretical Physics, Chalmers University of Technology, Goteborg, Sweden, has some similarities to that of Lee and colleagues, but the more complicated theory is developed for layered media rather than a single elastic half-space, and, most importantly, synthetic seismograms are produced.

Boström and Karlsson (1984) considered the propagation of a pulse from an explosive source in an elastic half space with an overlying surface layer of different properties, and containing a bounded 3D inhomogeneity. The numerical limitations of the method is that the theory is applicable when the dimensions of the inhomogeneity are a few wavelengths ($\lambda \sim d$). The shape of the inhomogeneity, the location and depth of the source, and the material properties were all varied (Figure 6). Rayleigh waves, direct and reflected waves, and head waves were identified in the synthetic seismograms. Most importantly, their synthetic seismograms are for the vertical component of particle velocity, and therefore simulate the recording of seismic waves by vertical-component geophones. Boström and Karlsson (1987) extended their work to the generation of synthetic seismograms for a spherical inclusion in a multilayered half space.

There have been many different theoretical studies of the effects of cavities, fractures and cracks on the propagation of seismic waves through rocks. Approaches to estimating the elastic properties of fractured and porous media include the computation of static elastic moduli (Gassman, 1951, Walsh, 1965), the use of scattering theory for dynamic elastic moduli for high and low porosity materials (Kuster and Toksöz, 1974a,b), and the use of the self-consistent energy method for both static and dynamic elastic moduli of low-porosity materials (O'Connell and Budiansky, 1974, 1977; Henyey and Pomphrey, 1982).

When the wavelength of the seismic signal is large compared with the inclusion or inclusions, the strategy is to determine the properties of the composite medium, given the properties of the matrix and inclusions, and the concentrations and shapes of the inclusions. One approach developed by Kuster and Toksöz (1974a) is to consider the waves scattered by inclusions of regular shapes to develop a mathematical relationship between the elastic moduli of the effective medium, the matrix and the inclusions. The theory is valid for small concentrations of inclusions, and is developed from the results of Yamakawa (1962). Their results can be applied to media containing vugular pores or cracks of low aspect ratio. The difficulty of the problem for high concentrations of inclusions is in coping with multiple scattering (i.e. several different scattering surfaces) for which detailed theories have yet to be developed.

Another approach to the estimation of the effective elastic moduli of media containing cracks (i.e. inclusions of low aspect ratio) is the self-consistent energy approach which involves consideration of the change in energy upon introducing a crack into an elastic matrix. Results for static and dynamic elastic moduli are given by O'Connell and Budiansky (1974, 1977). However, their results are only applicable for dilute concentrations of cracks because they did not include the effects of crack interactions. A modified computational scheme that takes into account the crack interaction energy was developed by Henyey and Pomphrey (1981). Wright, Walls and Carneiro (2000) have provided an example of the application of Henyey and Pomphrey's methodology to the interpretation of seismic wavespeed variations in terms of variations in fracture density near the surface of a mine tunnel. The results for fractured low porosity rocks are discussed briefly here, because they may also have applications in interpreting seismic data close to collapsed or partially collapsed cavities.

Synthetic Seismograms: Notes on Physical Principles

The generation of synthetic seismograms is a widely-used approach to simulating the response of the earth to man-made or natural seismic sources. The synthetic seismograms themselves are then used as a guide in interpreting real seismological data. The methodologies are mathematically complicated and highly developed. Many methods focus on simulating the response of horizontally-layered systems or concentric spherical shells in which there are impedance contrasts (product of density and seismic wavespeed) that give rise to reflected and transmitted waves at a discontinuity in impedance. The complicating factor in seismology is that in general an incident P or SV wave will give rise to reflected and transmitted P and SV waves, so that waves are converted from one type to another. SH waves, however, do not result in conversions to P at a boundary.

For applications to cavity detection, the important methodologies are those that are able to accurately predict the response of model that contains complicated variations in seismic wavepseeds and densities in two or three dimensions, where diffraction and scattering from inhomogeneities are likely to occur. Kelly et al. (1976) examined the replacement of the two-dimensional wave equation by a finite difference representation for estimating the relative amplitudes of arrivals for laterally varying media, including diffraction effects around a corner. Their paper, although not the first to discuss finite-difference seismograms, was one of the earliest to examine the methodology in the context of petroleum exploration or the interpretation of seismic data on an exploration scale.

Finite-difference algorithms are accurate, but consume enormous amounts of computer time when used for realistic geological models. Consequently, faster approximate methods were developed, and attempts made to assess their accuracy by comparing the response with that of the finite difference approach. For example, Coates and Charrette (1993) compared the Born and Generalised Born approximations for dealing with scattered waves in 2-D elastic random media with the results from finite difference seismograms. Both the Born and Generalised Born methods are approximations and computationally faster, and involve single scattering processes. Two types of model were tested: those using impedance variations in which the P and S wavespeeds remain constant, and those in which the P and S wavespeeds vary while the impedances remain constant. Both forms of Born approximation performed satisfactorily for the impedance models in which the seismic wavepeeds did not vary. However, when the wavespeeds were varied, both approximate methods performed poorly in the situation in which scattering was strong, though the Generalised Born method was much better than the older Born method.

The finite element method suggests another approach to synthetic seismogram generation for complex geological models, which has not been extensively developed. Olson, Orcutt and Frazier (1994) described a discrete wavenumber/finite element method for producing synthetic seismograms in a vertically heterogeneous half space. The numerical solution involves the use of both the finite element and finite difference methods.

Model Seismology

An alternative approach to the use of synthetic seismograms to simulate the seismic response of buried obstacles or cavities is the use of laboratory-scale models and a piezo-electric source that generates seismic energy at ultrasonic frequencies, which is recorded by a probe attached to the surface of the model (Oliver, Press and Ewing, 1954; O'Brien and Symes, 1971; Behrens and Waniek, 1972). Pant and Greenhalgh (1989) used the ultrasonic pulse technique to study the effects of rectangular, circular and wedge-shaped saw cuts on the surface of a 2-D physical model on Rayleigh wave propagation. The objective was to simulate the blocking effect on Rayleigh waves of a trench placed between a surface source and an array of geophones. Rectangular cuts (Figure 7) were found to be the most effective; cuts of depths $\lambda/4$ and λ, where λ is the wavelength of the Rayleigh wave, produced 12 dB and 30 dB increases in signal-to-noise ratios for the scattered energy. In the field situation, this scales to the use of trenches a few metres deep. The significance of this result to the detection of old mine workings is the clear demonstration of the effectiveness of the saw cut in allowing the imaging of a small hole deeply buried in an aluminium plate. The Rayleigh wave masked the scattered P wave energy from the hole, but a rectangular saw cut of depth 3λ/4 blocked the Rayleigh wave sufficiently to permit detection of the presence of the hole. The results scale to a field experiment of imaging a tunnel of 6 m diameter at a depth of 400 m (Figure 7), using a surface trench of 2 m depth to suppress the ground roll.

Design of an Experiment to Detect Cavities in Areas of Coal Mining

Lee et al. (1999) considered the dimensionless wave number ka defined as 2π x (radius of cavity, a) / (wavelength of signal, λ), and showed that significant observable effects were obtained for k in the range 2 to 15. In the coal mining situation, a is in the range 2-4 m while λ would be in the range 15-30 m for P, with similar values for S waves. This gives ka in the range 0.4-1.7, showing that in the mine-tunnel detection problem, the ratio of the wavelengths of the signals to cavity size are much larger than in the situations discussed by Lee et al. (1999).

Boström and Karlsson (1984) used a dimensionless frequency range of $0.1 \leq \omega d/v_p \leq 12.8$ to generate their synthetic seismograms, where ω is the angular frequency, d the thickness of, and v_p the P wavespeed in the layer containing the inclusion. Scattering by an inclusion of radius a, where a/d = 0.3 was considered. This corresponds to a range of ka of 0.03 to 3.8, which lies nicely in the range 0.4-1.7 for the coal-mining situation. Boström and Karlsson's results, although for a spherical rather than a cylindrical cavity, cover the appropriate frequency range for the detection of buried mine workings.

The Recording of Shear Waves

To record interpretable shear waves, three components of recording (usually vertical and two orthogonal horizontal components) are required. This enables the rotation of components to detect vertically- and horizontally-polarised shear waves, SV and SH respectively. The experimental procedures for shear-wave analyses are more tedious and costly than for P waves, because of the need to accurately align horizontal-component sensors with an accuracy of about 2^o; P wave experiments on the Earth's surface require only the vertical component of ground motion or the use of a pressure-sensitive device (hydrophone). The use of shear waves is therefore not recommended in trial experiments for tunnel detection.

Anisotropy, Shear Wave Polarisation and Shear-Wave Splitting

The anisotropic propagation of both P and shear waves is influenced by stresses which may cause the preferential alignment of fractures and cracks, regular sequences of fine layers, or anisotropic minerals. Differences in the propagation times of the SV and SH components is known as shear-wave splitting. If the direction of polarisation (particle motion) of a propagating shear wave is parallel or sub-parallel to the plane of orientation of cracks or fractures, or the slow direction of aligned minerals, that component will travel more slowly than the orthogonal component, thereby giving rise to measurable differences in propagation times of the two observable shear waves. P wave anisotropy and shear-wave splitting are not considered important for the cavity detection problem. The theory of the propagation of seismic waves in anisotropic and cracked elastic media has been extensively developed, and a review of much of the early work was provided by Crampin (1981).

An old example of the use of P wavespeed anisotropy to infer the orientation and density of fractures in limestone was described by Cramplin, McGonigle and Bamford (1980). In a more recent experiment, Bates and Phillips (2000) used shear-wave splitting to study shallow structures in central Wyoming and in southern England.

Conclusions

Both reflected and refracted body waves (P and S) and surface (Rayleigh) waves have been used with varying degrees of success to detect buried cavities, although there is relatively little literature on the subject in readily available publications. Applications have been mainly in detecting cavities or sinkholes in limestone or in civil engineering/geotechnical problems. The field conditions encountered in areas of South Africa where there is the need to detect buried tunnels formerly used in coal mining are not ideal for detection and location, because the dimensions of the tunnels are often less than the wavelengths of the highest frequency seismic signals that can be generated by seismic sources near the surface or in boreholes.

Mathematical studies using two and three-dimensional models for elastic wave propagation of buried inclusions or cavities in homogeneous media provide insight into the detection problem, but generally consider plane body waves and Rayleigh waves separately. Thus, calculations based on the derived formulae will give results for just one wave type. The limitation of this approach is that the relative amplitudes of the different wave types generated by a seismic source cannot be determined. Only one research group in Sweden has made significant progress on the more difficult problem of deriving exact synthetic seismograms showing all wave types generated by an explosive source in a layered elastic medium containing an inclusion or cavity. However, the results require a formidable amount of computation. A survey of the methodologies of synthetic seismogram generation reveals that accurate and reliable results for geologically complicated models are often obtained using finite difference methods, which require a large amount of computation time. Approximate methods of calculating synthetic seismograms, although computationally relatively fast, do not always give accurate results for the strongly heterogeneous models that are required to simulate real geological situations.

P and Rayleigh waves are the appropriate wave types that can be used for cavity or tunnel detection. S waves require recording of two or preferably three components of ground motion to be used effectively, which entails more elaborate, time-consuming and expensive field procedures. P waves may be effective in detecting and locating mine workings to depths between a few metres and about 50 m through combined analysis of refracted, diffracted and scattered energy. The success of this approach requires the blocking of the surface (Rayleigh) waves by use of trenches between source and geophones. Alternatively, the Rayleigh waves themselves may be useful for detection of shallow cavities through detection of fluctuation of phase velocities in the computed phase velocity dispersion curves.

Finally, it is emphasized that the present study is incomplete. Critical evaluation of both relatively obscure publications and fairly recent articles in journals that are not available in South Africa has not been undertaken, because these publications ordered have still not been received.

Recommendations

Because of the complexity of the methodologies used to generate accurate synthetic seismograms, and the abundance of simplified theoretical calculations available in the literature, further simulation studies are not recommended. Instead, test experiments over a mapped mine tunnel or cavity are recommended, based on the results obtained from existing theoretical and numerical results, synthetic seismograms and laboratory-scale simulation experiments.

The first experiment (Figure 1) should be conducted over a shallow cavity less than 10 m deep, and the second over a deeper tunnel 10-30 m below the surface. In both cases the experiment should be recorded twice: with and without trenching. This would enable both the Rayleigh wave dispersion and P wave scattering approaches to be evaluated for a shallow tunnel. The recording of the experiment over the deeper tunnel would evaluate the effectiveness of the trenching in suppressing Rayleigh waves. Furthermore, if near-surface explosives are used, a barrier (e.g. bill board propped up against a vehicle) should be set up between the geophone array and source to minimize the effects of the sound wave in air on the recorded seismograms. Recording should be done, if possible, using very small, well-buried explosive sources to maximize the amount of high-frequency seismic energy while retaining a bandwidth of two octaves or greater. For the shallow tunnel, low-frequency vertical-component geophones (natural frequency 14 Hz, for example) can be used to provide a broad range of recorded frequencies of the Rayleigh waves. However, for the deeper tunnel, it is preferable to eliminate unwanted low-frequency energy in the field, rather than by subsequent processing, to emphasise the high-frequency scattered energy from the tunnel. High-frequency geophones (preferably with natural frequencies in the 40 to 50 Hz range) should be used in this situation. A 24 or 48-channel recording system would be adequate for both experiments.

Acknowledgments

S.N. Wright assisted with the computer searches for relevant information, particularly the downloading of information from 'Scirus'.

References

Ahenbach, J.D. and Brind, R.J., Scattering of surface waves by a sub-surface crack, Journal of Sound Vibration, 76, 43-46, 1981.

Bates, C.R. and Phillips, D.R., Multi-component surveying for near-surface investigations: examples from central Wyoming and southern England, Journal of Applied Geophysics, 44, 257-273, 2000.

Behrens, J. and Waniek, L., Modellseismik, Zeitschrift für Geophysik, 38, 1-44, 1972.

Belesky, R.M. and Hardy, H.R., Seismic and microseismic methods for cavity detection and stability monitoring of near-surface voids, in: Proc. 27th U.S. Symposium on Rock Mechanics, Rock Mechanics: Key to Energy Production, University of Alabama, Tuscaloosa, Alabama, 248-258, 1986.

Boström, A. and Karlsson, A., Exact synthetic seismograms for an inhomogeneity in a layered elastic half space, Geophysical Journal of the Royal Astronomical Society, 79, 835-862, 1984.

Boström, A. and Karlsson, A., Broad-band synthetic seismograms for a spherical inhomogeneity in a many-layered elastic half space, Geophysical Journal of the Royal Astronomical Society, 89, 527-547, 1987.

Cao, H. and Lee, V.W., Scattering of plane SH waves by circular cylindrical canyons with variable depth-to-width ratio, European Journal of Earthquake Engineering, 3, 29-37,1989.

Cao, H. and Lee, V.W., Scattering of plane P waves by circular cylindrical canyons with variable depth-to-width ratio, International Journal of Soil Dynamics and Earthquake Engineering, 9, 141-150,1990.

Cerveny, V. and Ravindra, R., Theory of Seismic Head Waves, University of Toronto Press, 312 pp., 1971.

Coates, R.T. and Charrette, E.E., A comparison of single scattering and finite difference synthetic seismograms in realizations of 2-D elastic random media, Geophysical Journal International, 113, 463-482, 1993.

Cooper, S.S. and Ballard, R.F., Geophysical exploration for cavity detection in Karst terrain, in: Proc., Symp. Geotech. Aspects of Karst terrains: Exploration, Found. Dec. and Perf., and Remedial Measures, Geotech Spec. Publ. No. 14, ASCE, New York, N.Y., 25-39, 1988.

Crampin, A review of wave motion in anisotropic and cracked elastic-media, Wave Motion, 3, 343-391, 1981.

Crampin, S., McGonigle, R. and Bamford, D., Estimating crack parameters from observations of P-wave velocity anisotropy, Geophysics, 45, 345-360, 1980.

Curro, J.R., Cavity detection and delineation research, Report 2, Seismic Methodology, Medford Cave Site, Florida, U.S. Army Wtrwy. Experiment Station, Tech. Repoert GL-83-1, U.S. Army Wtrwy. Experiment Station, Vicksburg, Missouri, 1983.

Datta, S.K. and El-Akily, N., Diffraction of elastic waves by a cylindrical cavity in a half space, Journal of the Acoustical Society of America, 64, 1692-1699, 1978.

Dravinski, M., Ground motion amplification due to elastic inclusions in a half-space, Earthquake Engineering and Structural Dynamics, 11, 313-335, 1983.

Einspruch, N.G., Witterholt, E.J., and Truell, R., Scattering of a plane transverse wave by a spherical obstacle in an elastic medium, Journal of Applied Physics, 31, 806-818, 1960.

Ganji, V., Gucunski, N. and Maher, A., Detection of underground obstacles by SAWS method, Journal of Geotechnical and Geoenvironmental Engineering, 123, 212-219, 1997.

Gassman, F., Elastic waves through a packing of spheres, Geophysics, 16, 673-685, 1951.

Ghosh, T. and Lee, V.W., Diffraction of plane and surface waves by three-dimensional cylindrical, sub-surface cavities in an elastic half-space, Civil Engineering Thesis Report No. CE 95-01, University of Southern California, Los Angeles, California, 1995.

Henyey, T. and Pomphrey, R.J., Self-consistent moduli of a cracked solid, Geophysical Research Letters, 9, 903-906, 1982.

Kelly, K.R., Ward, R.W., Treitel, S. and Alford, R.M., Synthetic seismograms: a finite-difference approach, Geophysics, 41, 2-27, 1976.

Kennett, B.L.N., Seismic waves in laterally inhomogeneous media, Geophysical Journal of the Royal Astronomical Society, 27, 301-325, 1972.

Kuster, G.T. and Toksöz, M.N., Velocity and attenuation of seismic waves in two-phase media: part 1. theoretical formulations, Geophysics, 39, 587-606, 1974a.

Kuster, G.T. and Toksöz, M.N., Velocity and attenuation of seismic waves in two-phase media: part 2. experimental results, Geophysics, 39, 607-618, 1974b.

Lee, V.W., On deformations near underground circular cavity subjected to incident plane SH waves, Proceedings Symposium on Applications of Computer Methods in Engineering, August 23-26, University of Southern California, Los Angeles, 951-961, 1977.

Lee, V.W., Three–dimensional scattering of elastic waves by a spherical cavity in an elastic half space. I: P closed-form solutions, International Journal of Soil Dynamics and Earthquake Engineering, 7(3), 149-161, 1988.

Lee, V.W., Ghosh, T. and Sabban, M.S., Scattering and diffraction of plane P waves by 3D cylindrical canals, European Journal of Earthquake Engineering, 9(3), 12-22, 1996.

Lee, V.W. and Karl, J., Diffraction of SV waves by underground, circular, cylindrical cavities, International Journal of Soil Dynamics and Earthquake Engineering, 11, 445-456, 1993a.

Lee, V.W. and Karl, J., Diffraction of elastic plane P waves by circular, underground, unlined tunnels, European Journal of Earthquake Engineering, 6(1), 29-36, 1993b.

Lee, V.W., Chen, S. and Hsu, I.R., Antiplane diffraction from canyon above subsurface unlined tunnel, Journal of Engineering Mechanics, 125, 668-675, 1999.

Maccelari, M.J., Higgs, R.M.A., Wright, C. and Vorster, A., Investigate the Applicability of Shallow, High Resolution Seismic Surveys on South African Collieries, Coaltech 2020 year-end report, Report No. 2001-0126, CSIR Division of Mining Technology, Johannesburg, 2001.

Morse, P.M., Vibration and Sound (second edition), McGraw-Hill, New York, 468 pp., 1948.

O'Brien, P.N.S. and Symes, M.P., Model seismology, Reports on Progress in Physics, 34, 697-764, 1971.

O'Connell, R.J. and Budiansky, B., Seismic velocities in dry and saturated cracked solids, Journal of Geophysical Research, 79, 5412-5426, 1974.

O'Connell, R.J. and Budiansky, B., Viscoelastic properties of a fluid-saturated cracked solid, Journal of Geophysical Research, 82, 5719-5735, 1977.

Oliver, J., Press, F. and Ewing, M.W., Two-dimensional model seismology, Geophysics, 19, 202-219, 1954.

Olson, A.H., Orcutt, J.A. and Frazier, G.A., The discrete wavenumber/finite element method for synthetic seismograms, Geophysical Journal of the Royal Astronomical Society, 77, 421-460, 1984.

Pant, D.R. and Greenhalgh, S.A., Blocking surface waves by a cut – physical seismic model results, Geophysical Prospecting, 37, 589-605, 1989.

Sánchez-Sesma, F.J., Herrera, I. and Alvilés, J., A boundary method for elastic wave diffraction: application to scattering of SH waves by surface irregularities, Bulletin of the Seismological Society of America, 72, 473-490,1982.

Todorovska, M.I. and Lee, V.W., A note on response of shallow circular valleys to Rayleigh waves: Analytical approach, Earthquake Engineering and Engineering Vibtration, 10, 21-34, 1990.

Todorovska, M.I. and Lee, V.W., Surface motion of shallow circular alluvial valleys for incident plane SH waves - Analytical solution, International Journal of Soil Dynamics and Earthquake Engineering, 10, 192-200, 1991a.

Todorovska, M.I. and Lee, V.W., A note on scattering of Rayleigh waves by shallow circular canyons: Analytical approach, Bulletin of the Indian Society of Earthquake Technology, 28, 1-16, 1991b.

Varatharajulu, V. and Pao, Y.-H., Scattering matrix for elastic waves, Journal of the Acoustical Society of America, 60, 556-566, 1975.

Walsh, The effect of cracks in rocks on Poisson's ratio, Journal of Geophysical Research, 70, 5249-5257, 1965.

Wright, C., Walls, E.J. and Carneiro, D. de J., The seismic velocity distribution in the vicinity of a mine tunnel at Thabazimbi, South Africa, Journal of Applied Geophysics, 44, 369-382, 2000.

Wu, R. and Aki, K., Scattering characteristics of elastic waves by an elastic heterogeneity, Geophysics, 50, 582-295, 1985.

Yamakawa, N., Scattering and attenuation of elastic waves: Part 1 Scattering of elastic waves by various kinds of obstacles, Geophysical Magazine (Tokyo), 31, 63-103, 1962.

Ying, C.F. and Truell, R., Scattering of a plane longitudinal wave by a spherical obstacle in an elastic medium, Journal of Applied Physics, 27, 1087-1097, 1960.

Appendix

1. Software Products.

The following finite element packages were used by Ganji et al. (1997):

- ABAQUS, Finite Element Software Package, Hibbitt, Karlsson and Sorenson Inc., 1994.
- ANSYS, Finite Element Software Package, Revision 5.0, Swanson Analysis Systems, Inc.

2. An Archaeological Problem.

Debates over the age and purpose of the Great Pyramid and the Sphinx contain references to seismic work undertaken to detect cavities or tunnels beneath the Sphinx by T.L. Dobecki of McBride-Ratcliff and Associates of Houston, Texas (Bauval and Hancock, 1996, pp. 19, 54, 98, 103). 'Anomalies and cavities were located in the bedrock between the paws and along the side of the Sphinx. One of these cavities was described as a fairly large feature about nine metres by twelve metres in dimension, and buried less than five metres in depth…. rectangular in shape' (modified slightly from Bauval and Hancock, 1996, p. 19). A recent Internet search located an article by Hancock entitled 'The Modern Riddle of the Sphinx' (http://www.dreamscape.com/morgana/hancock.htm). There is a section in that article which refers to the use of seismic techniques to detect several unexplored tunnels and cavities in the bedrock, including a large rectangular cavity about 25 feet below the front paws of the monument. However, an Internet address for either Dobecki or McBride-Ratcliff and Associates has not been found, and no references to the details of the seismological methodologies used have been located. The incomplete information on this archaeological application of seismology is certainly interesting, and requires careful evaluation in the future.

Reference

Bauval, R. and Hancock, G., Keeper of Genesis: A Quest for the Hidden Legacy of Mankind, Madarin Paperbacks, 396 pp., London, 1996.

List of Figures

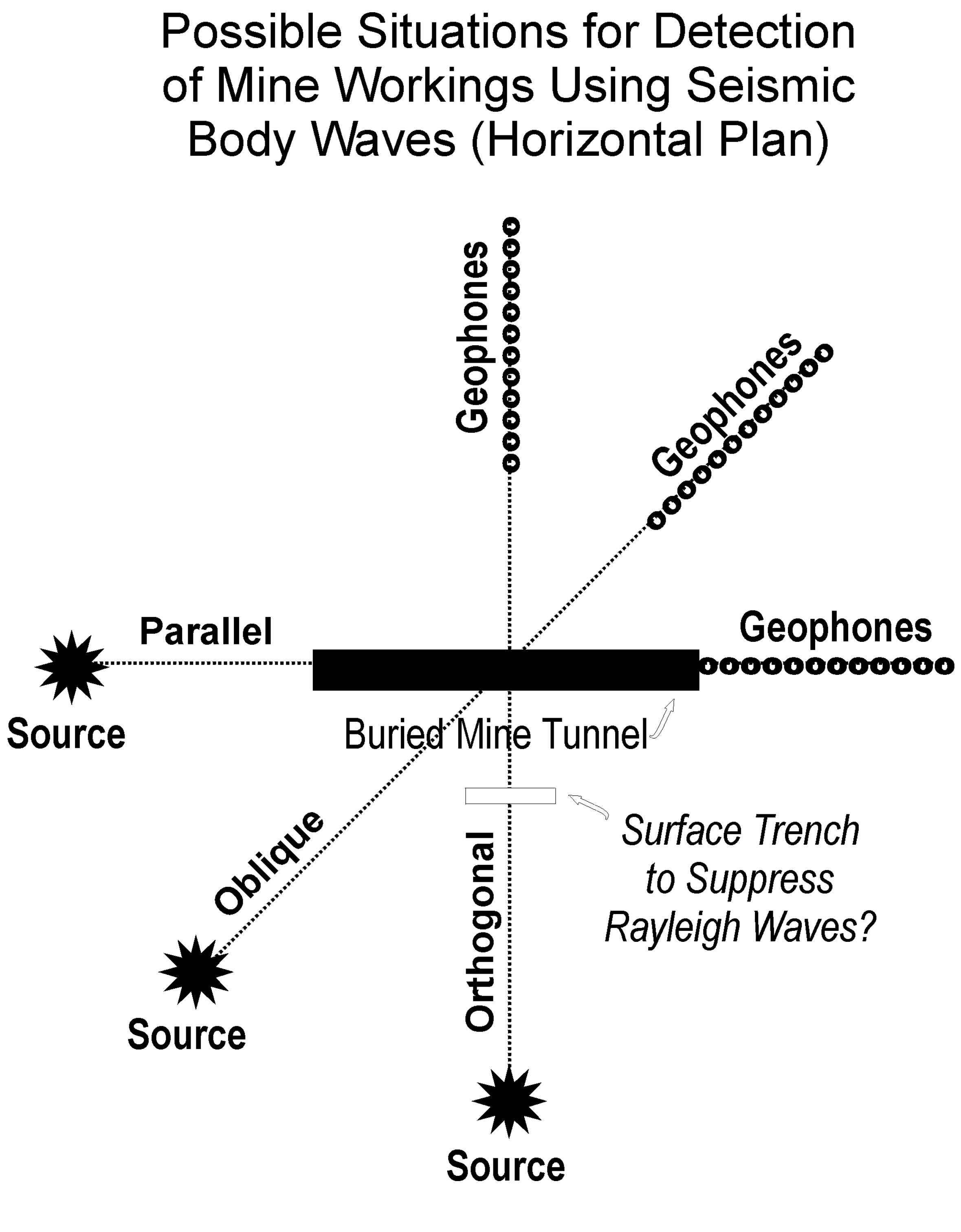

Fig. 1: Schematic representation of the possible source-to geophone configurations that occur in the design of an experiment to detect buried mine workings.

2-D Problem for Surface Waves Considered by Ganji et al. (1997) - SASW Method

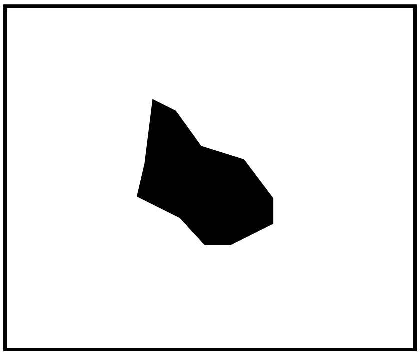

Shaded object represents an obstacle, inclusion or cavity, which is detected by fluctuations in phase velocity. Half-space is homogeneous.

Fig. 2: Illustration of type of body that might be detected by the SAWS method.

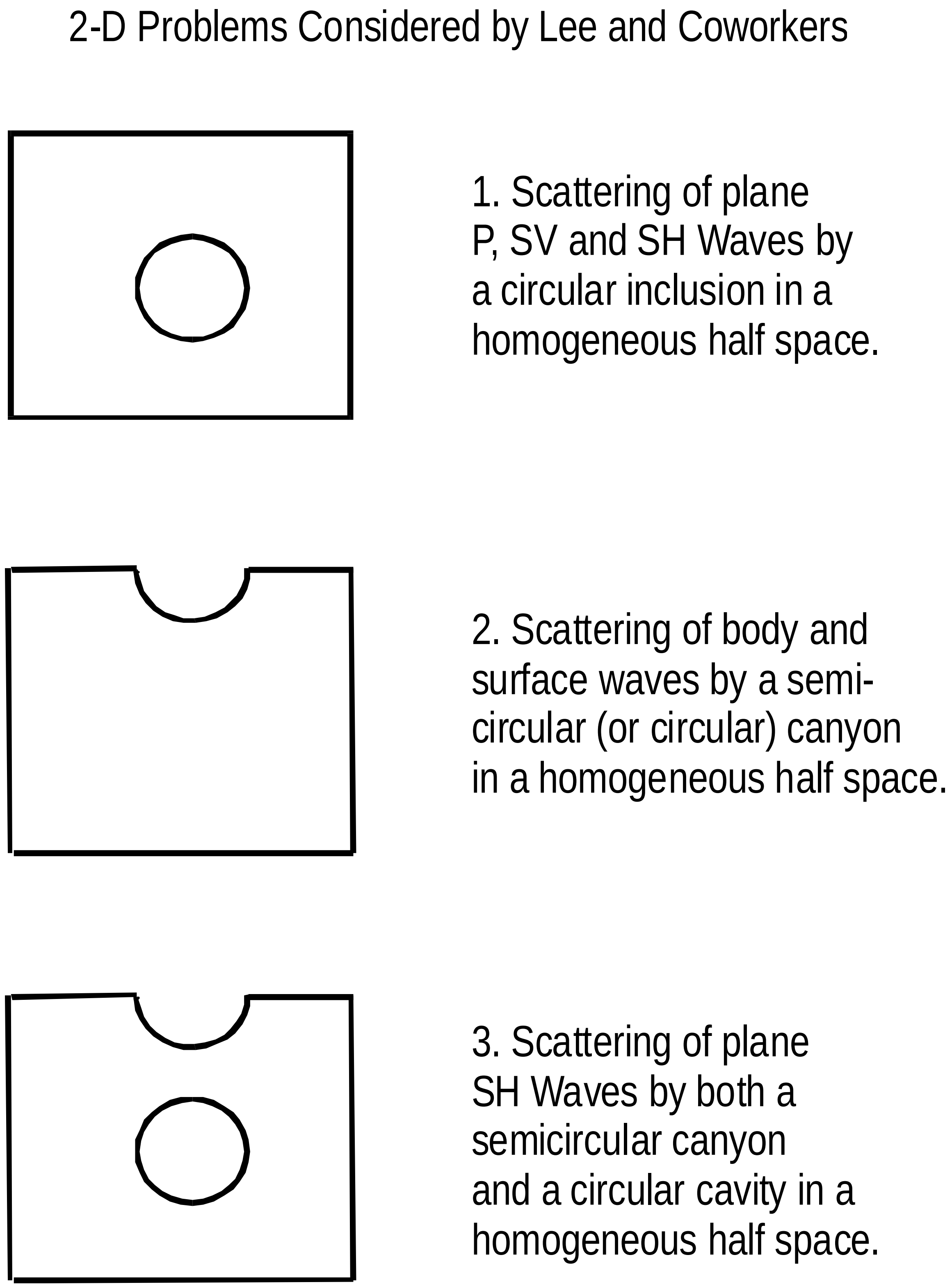

Fig. 3: Geometry of 2-D scattering problems for canyons and cavities, considered mainly by Lee and coworkers.

3-D Problem for Scattering by Cylindical Inclusions

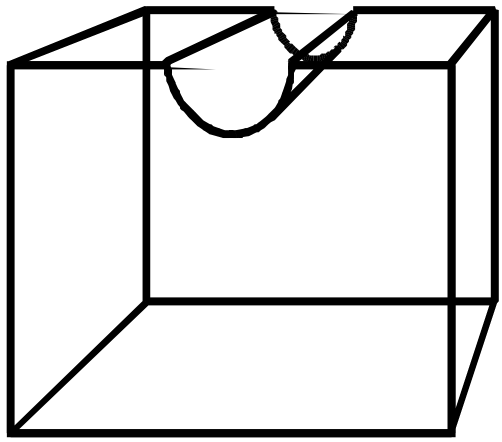

2. Scattering of plane body and surface waves by a cylindrical canyon in a homogeneous half space (Lee et al., 1996)

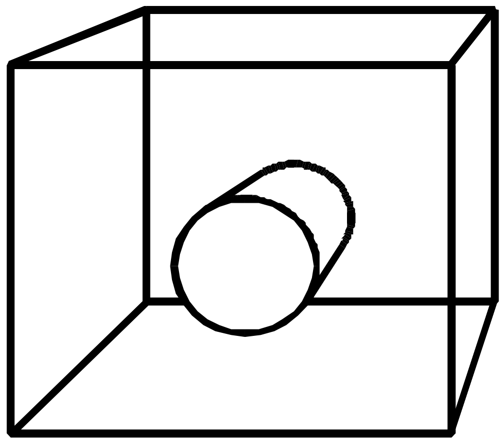

2. Scattering of plane body and surface waves by a cylindrical cavity in a homogeneous half space (Ghosh and Lee, 1995)

Fig. 4: Geometry of scattering of elastic waves by cylindrical troughs and tunnels in a homogeneous elastic half space.

3-D Problem for Elastic Waves Scattered by Spheres and Arbitrarily-Shaped Inclusions

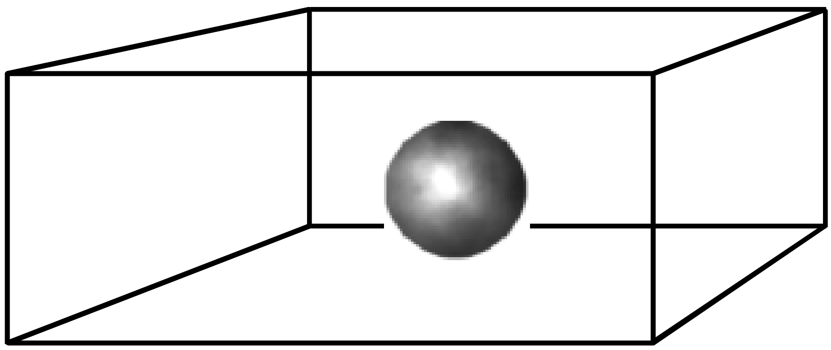

Spherical inclusion or cavity in a homogeneous half-space:
Ying and Truell (1956); Einspruch et al. (1960);
Yamakawa (1962);Varatharajulu and
Pao (1975); Lee (1988)

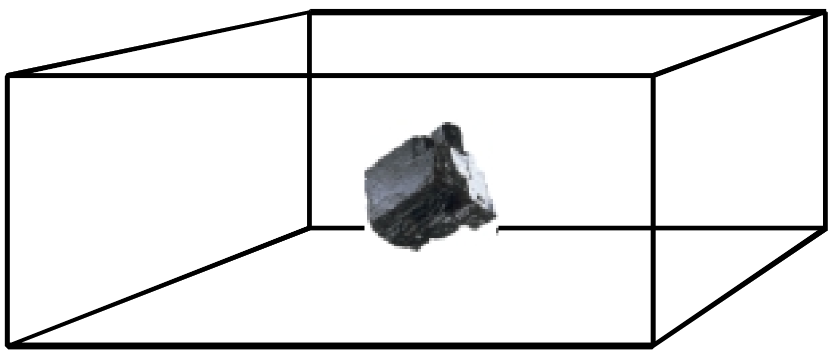

Cavity or inclusion of arbitrary
shape and a Gaussian spherical
inclusion in a homogeneous
half-space: Wu and Aki (1985)

Fig. 5: Summary of theoretical studies of scattering in 3 dimensions by a buried inclusion or cavity.

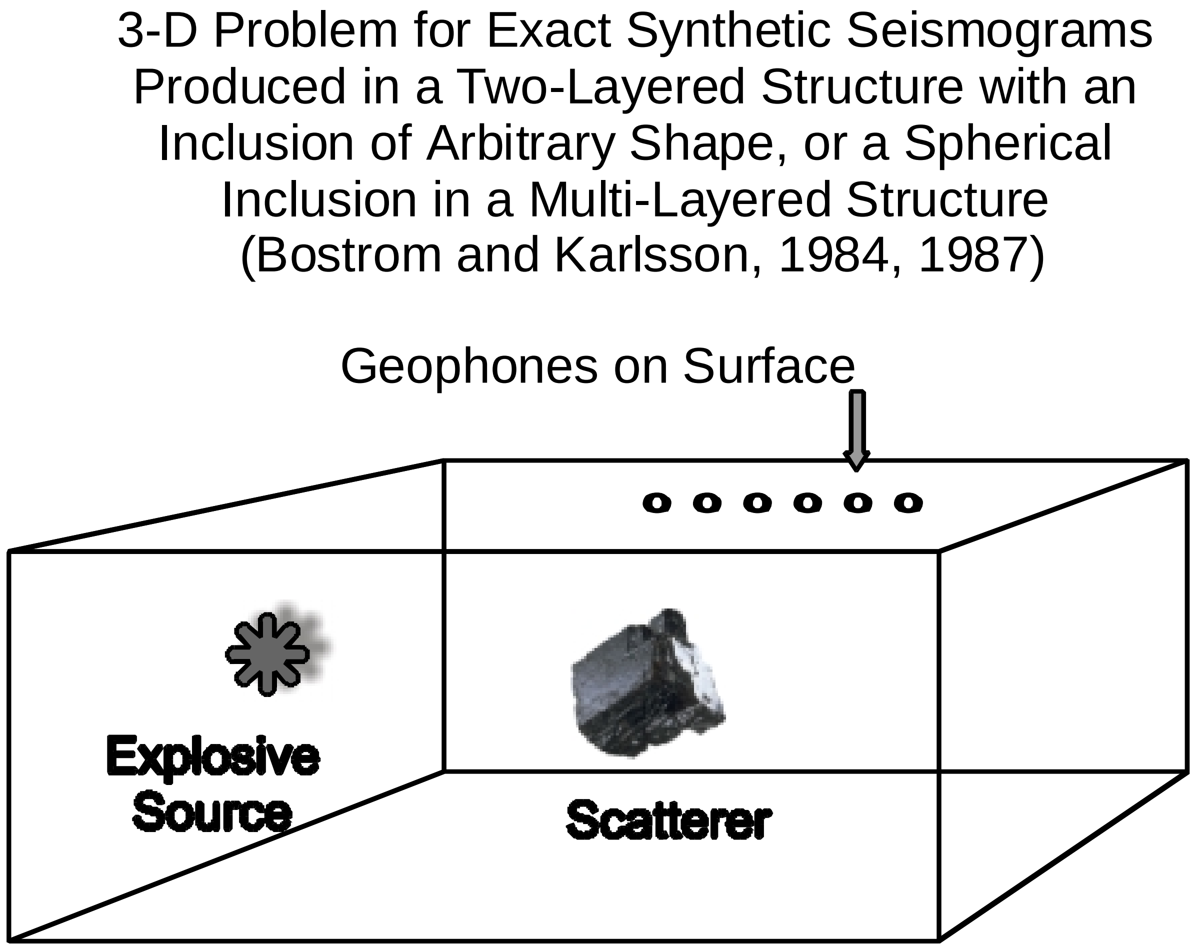

Fig. 6: Sketch of the type of model for producing synthetic seismograms by Boström and Karlsson (1984), and extended to the multilayered case for spherical inclusions by Boström and Karlsson (1987).

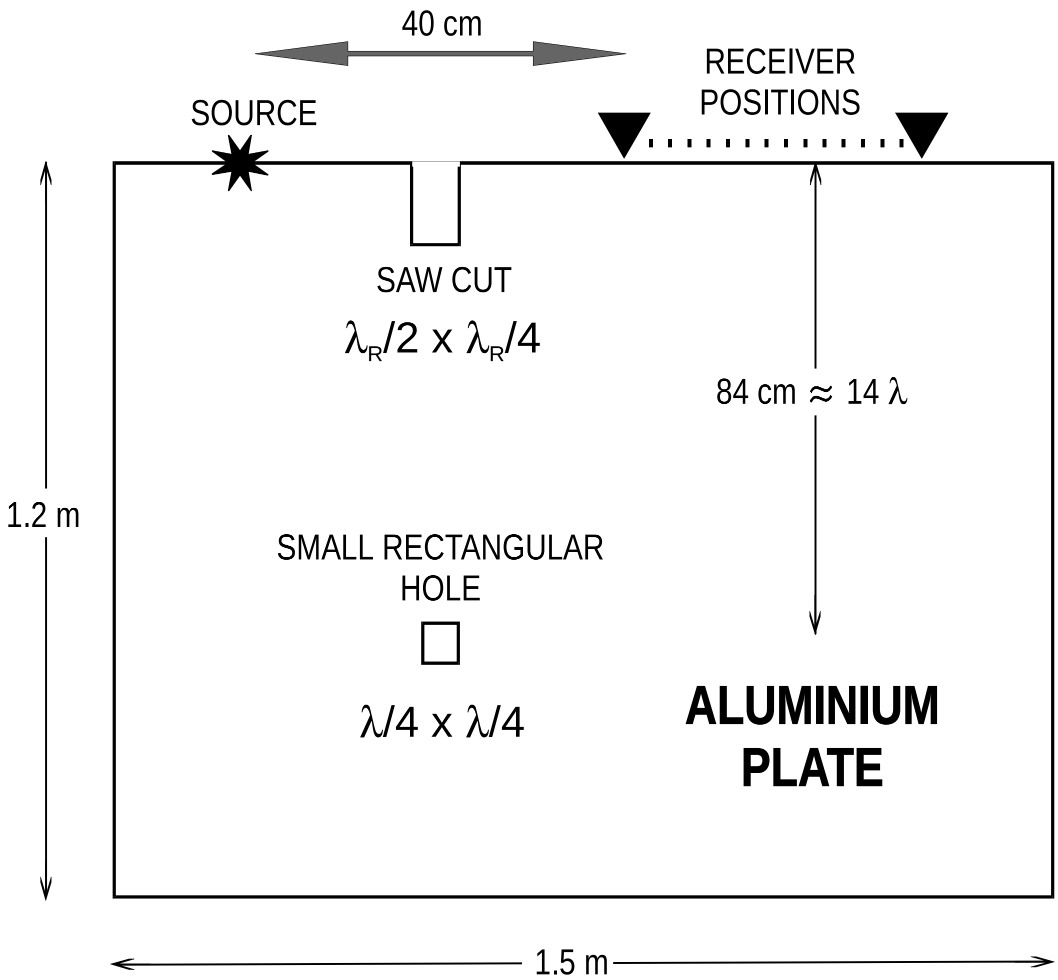

Fig. 7: Shot-receiver geometry (not accurately to scale) used in a physical model designed to simulate a 6 m square cavity at a depth of 400 m, using a 150 Hz signal (after Pant and Greenhalgh, 1989).

APPENDIX XII

COALTECH 2020

Subtask Report
(part of Subtask 4)

The application of electrical resistivity in the coal environment

M. Van Schoor

CSIR, Division of Mining Technology
Report number: 2001-0123

Task 1.3.1b

Detection of old workings, sinkholes, underground fires and acid mine pollution using geophysics and airborne thermal infrared imagery

20 March 2001

EXECUTIVE SUMMARY

A literature review, computer simulations and results of previously conducted field trials indicate that the electrical resistivity technique is applicable to the detection of isolated cavities close to surface, that is, depths less than 15-20 m. Such features can be air- or water filled. The technique is thus particularly useful for the detection and mapping of sinkholes associated with the subsidence or collapse of old workings. However, at these shallow depths, high-resolution mapping of the grid-like pattern associated with bord-and-pillar workings, is not possible. Areas where old workings occur can, however, be delineated and, it would be possible to discriminate between water-filled and air-filled cavities. This can probably be done successfully for workings down to a depth of 20-30 m.

It is highly likely that the type of pollution plumes anticipated in coal areas, that is, high levels of sulphate contamination, will be ideal targets for the electrical resistivity technique. Monitoring of the migration of such plumes should also be possible using dynamic monitoring techniques.

Finally, the applicability of the electrical resistivity technique to detection and mapping of underground fires is in doubt. However, a field trial is recommended to determine whether the technique is applicable to this specific problem.

TABLE OF CONTENTS

LIST OF FIGURES IN APPENDIX A:

1 INTRODUCTION

Generally, the detection of coal using applied geophysical methods is possible as the physical properties of coal contrast markedly with those of the host rock. For example, coal has a much lower density, a higher electrical resistivity, a lower seismic wave velocity and a lower magnetic susceptibility than the surrounding host rock (Jackson, 1981). Geophysical methods are also used in the coal mining environment to detect or delineate secondary features that are either man-made or a direct result of mining related activities. Such features include sinkholes and voids, flooding, underground fires, subsidence and roof falls, and pollution plumes. Knowledge of the location and extent of these features is often crucial to the planning of future mining activities or developments on surface. This study focuses on four specific secondary features that commonly result in problematic scenarios in the Witbank area:

1) Old bord and pillar mine workings.
2) Sinkholes – these typically develop above abandoned workings.
3) Underground fires.
4) Acid mine pollution.

The electrical resistivity method was one of a wide variety of potential geophysical solutions considered. This report deals with the electrical resistivity method and its potential applicability to solving problems discussed in the following section.

2 PROBLEM SCENARIOS

2.1 Old bord and pillar workings

By the mid 1980's approximately 70% of South Africa's coal production came from bord-and-pillar workings (Brink, 1983). Today, a major engineering problem linked to this mining method is that of surface subsidence. This problem is predominantly associated with the older mines – some dating back to the early 1900's. In the past irrational pillar design and pillar-robbing were commonplace and the results – often many years later – include the collapse of pillars, subsidence and complete caving through to surface.

Subsidence associated with old bord-and-pillar workings is unpredictable and difficult to monitor. Caving could take place at any time (even decades later) as a result of one of the following:

- Gradual deterioration of pillars and bords.
- Changes in the seam conditions, such as the introduction or removal of water.
- Gradual punching of pillars into a weak floor.
- Deterioration of pillars as a result of waterlogged workings or underground fires.
- Collapse of bords with excessive spans.

Monitoring or inspection of old workings are very difficult because of limited access and inaccurate old mine plans. Pillar robbing commonly took place in the last stages of mining operations. Inspection of old workings was also done through the drilling of closely spaced boreholes, often in conjunction with downhole cameras. However, this was usually too costly. Development over old bord-and-pillar workings typically requires knowledge of the exact location of pillars. Rehabilitation of old workings is sometimes necessary before development can take place.

Typically, pillars are of the order of 6 m x 6 m horizontally, representing the remains of a 1 m to 5 m thick mined-out coal seam. The mined-out bords separating these pillars have approximately the same horizontal dimensions as that of the pillars; however, occasionally they are narrower. The bord height is usually slightly less than the seam height, leaving a thin coal roof and/or floor behind. The old workings occur at an average depth of 30-40 m, but in extreme cases may be as shallow as 15 m or as deep as 80-100 m.

One of the key problems related to geophysically mapping these bords and pillars is not so much the geometry of the problem, but the unpredictable geoelectric structure. Coal is almost always electrically highly resistive (several thousand ohm metres), however, the cavities of old mining operations may have a resistivity ranging from infinitely resistive to highly conductive. When a cavity is air-filled it is effectively infinitely resistive, but when it is filled with highly acidic mine water it can be highly conductive (resistivity of a few ohm metres). Anything in between these two extremes is possible and one should expect such variations from site to site. For example, if a cavity is filled with relatively clean water, it may still be very resistive, but less so than in the air-filled case. For electrical techniques to be successful at mapping the old workings a sufficient contrast in resistivity is needed between the coal pillars and the mined-out cavities. The fact that there may be little or no contrast between the electrical properties of the coal and the material filling the mined-out cavities should be taken into account.

The geoelectric character of the overburden can also have a major impact on the results of electrical resistivity surveys. A thin surface layer with a highly contrasting resistivity can dominate the response and suppress any 'deeper', subtle anomalies. Near surface layers may vary from very conductive to very resistive, depending on factors such as climate and degree of weathering.

2.2 Sinkholes, cavities and underground fires

The occurrence of sinkholes and subsurface cavities in the Witbank area is a direct consequence of mining induced surface subsidence. Under the heading of sinkholes and cavities, two phenomena are considered, i.e., potholes and sinkholes.

As a result of subsidence, surface cracks appear that extend down to the upper rock layers. The cracks in the soil may close, but the extensions downward into the rock eventually form cavities as a result of subsurface soil erosion. Should these cavities attain a critical size, they collapse, resulting in potholes on the surface. The diameter of such potholes vary from 30 cm up to several metres. Potholes generally occur at relatively shallow depths – below approximately 6-10 m of overburden. The geophysical challenge is to detect potential cavities before they collapse. Once the first signs of early subsurface erosion potholes appear, the extent of the erosion needs to be determined. At times, the only evidence is a small surface hole a few centimeters in diameter.

The appearance of sinkholes above old bord-and-pillar workings is linked to the underground collapse of bords (mainly intersections). The width of these sinkholes is typically of the same order as the width of the underground bords, that is, approximately 6 metres. The depth extent of sinkholes may be several metres (Van der Merwe *et al*., 2000).

Sinkholes typically occur at a depth shallower than approximately 50 m. A problem related to sinkhole formation is that of underground fires. Fires in old workings are generally the result of spontaneous combustion. Sinkholes may allow fresh air into the old workings, supplying oxygen to the fires. This can result in pillar failure and further subsidence.

The comments made in paragraph 2.1 regarding the unpredictability of subsurface and near-surface geoelectric structure also applies to the detection of sinkholes and fires. Care must be taken when interpreting geoelectric data from any site and it must be remembered that the nature of a specific type of problem may vary from site to site.

2.3 Acid mine drainage

High sulphate levels in excess mine water is the main cause of local acidification and regional salination of surface water resources in the Upper Olifants River Catchment in Mpumalanga.

Sulphate levels varying between 120-160 mg/l are routinely recorded in the Witbank and Middelburg Dams, mainly as a result of coal mining and related activities. It is estimated that excess mine water currently amounts, volume wise, to only 4.6% of the total water usage, but contributes 78.4% to the sulphate load (Van Zyl *et al.*, 2000).

During mining operations the water table is often lowered temporarily. The introduction of oxygen into the workings and the subsequent oxidation of pyrites cause in-mine water quality to deteriorate. That is, the pH becomes very low, indicative of acidic water. When workings are abandoned, the water level may rise again causing the surrounding groundwater system to be affected by the acidic mine water. Acid mine water is often pumped into massive evaporation/treatment dams. Leakage from these dams also contributes to the contamination of groundwater resources.

The sulphate contaminants tend to migrate as plumes from their source. Another concern regarding pollution associated with acid mine drainage is that although acidic water is often treated to restore the pH to acceptable levels before it is introduced back into the water system, it can also contain dangerous heavy metals (Pers. Comm., R. Meyer, 2000).

3 BACKGROUND AND TERMINOLOGY FOR THE ELECTRICAL RESISTIVITY TECHNIQUE

In this section a brief overview of the electrical resistivity technique is presented.

Conventional DC resistivity measurements are conducted using four electrodes in galvanic contact with the earth (Figure 1a). A pair of electrodes (A and B) is employed to inject a constant DC current (I) into the earth, while a second pair (M and N) measure the resulting potential difference (ΔV). The relationship between the resistivity (ρ) of a uniform half-space and the measured quantities is given by:

$$\rho = K*\Delta V/I$$

where K, the *geometric factor*, is determined by the relative positioning of the electrodes.

In practice, in the above equation, the resistivity parameter (ρ) is replaced with the *apparent resistivity* parameter (ρ_a). This takes account of the fact that the subsurface is, by nature, not a uniform resistivity structure. The apparent resistivity is, however, a useful parameter for evaluating lateral and vertical variations in subsurface electrical resistivity.

There are numerous possible *electrode configurations* (relative positions of A, B, M and N for a single measurement), depending on the aim of the survey and, to a degree, the user's preference (see Figure 1b). The relative electrode positions from one measurement to the next, that is, the systematic way in which a data set is compiled, is also determined by the aim of the survey. Some commonly used electrode configurations are the dipole-dipole, the pole-dipole, pole-pole and Schlumberger configurations. These configurations are depicted in Figure 1b (Sheriff, 1989). For the dipole-dipole array the AB and MN dipole lengths are usually appreciably smaller than the AB-MN spacing. If one of the current electrodes (A) is moved to "infinity" (at least 5 times the B-M spacing) the dipole-dipole array is converted to a pole-dipole array. In the Schlumberger array, the two current electrodes constitute the outer electrodes of the array, while the potential pair (MN) are located in the central third portion of AB. The inter-electrode spacing ('na' in Figure 1b) is sometimes also referred to as 'm'.

4 PRICIPLES OF RESISTIVITY SOUNDINGS, PROFILING AND IMAGING

The depth of investigation for the DC resistivity method is largely determined by the relative spacing between the current electrodes and the measuring or potential electrodes. This concept is exploited when conducting resistivity *soundings*. By incrementally increasing the AB-MN spacing symmetrically about a fixed location a sounding curve is obtained that contains semi-quantitative information about the vertical variation in subsurface electrical resistivity. This approach is often used to estimate the thickness and resistivity of individual, near-horizontal layers.

Alternatively, one or more fixed electrode spacings, associated with specific depth ranges, may be selected and measurements are acquired at fixed intervals along profiles. This approach is referred to as resistivity *profiling* and is used to identify lateral changes in resistivity. Typically, profiling is used to map features such as faults and dykes, subsurface cavities, pollution plumes and variations in subsurface topography.

The sounding and profiling concepts are often integrated where high-resolution information is required: Large volumes of data are acquired along profiles or on grids from which resistivity pseudo-sections, tomographic images or 2-D contour maps are constructed. These approaches can collectively be termed *imaging* methods. The concept of resistivity imaging may also be extended to incorporate borehole measurements. Borehole-to-borehole and borehole-to-surface resistivity surveys can be used to detect subsurface resistivity anomalies at greater depths than is possible when surveying on surface only.

In this study, the conventional approach of gridding and contouring apparent resistivity values will be employed, as well as inversion based 2-D electrical imaging.

5 LITERATURE REVIEW

There are numerous references in the literature illustrating the applicability of resistivity techniques in the coal environment. A number of the more interesting / relevant references are listed below:

Spiegel *et al*. (1980) used theoretical calculations and model (tank) studies to illustrate how the resistivity method (surface profiling) can be used to detect subsurface voids. They also considered the difficulty of uneven surface topography and how to correct the measured data through a numerical transformation process. The pole-dipole electrode configuration was used to successfully detect elongated tunnels with a depth:size ratio of up to 4.

Noel and Xu (1992) used the pole-pole approach to successfully image a cavity with an estimated diameter of 11 m located at a depth of 10-20 m. Although the aim of this survey was proof-of-concept, it was concluded that, inversion based resistivity imaging yielded better spatial resolution and less ambiguous results than the conventional pseudosection approach.

Sretonovic *et al*. (1992) reported how shallow underground mine workings can be detected using electrical methods. They used the Wenner array (special case of dipole-dipole array where na = a – refer to Figure 1b) with various electrode spacings reporting a depth of investigation range of 30-50 m. Detected anomalies were correlated with disturbed zones (collapses and cavities) in the vicinity of old mine workings.

Owen (1983) also reported on the use of the electrical resistivity method for detecting subsurface cavities. A variety of electrode configurations were compared in terms of their ability to detect cavities relatively deep in comparison to their size. The dipole-dipole, pole-dipole and three-electrode arrays, including the three electrode difference technique (special case of pole-dipole array where the current pole is employed symmetrically on either side of the potential pair and the difference reading is taken), appeared to perform better than more conventional arrays like Wenner and Schlumberger. Owen reported on similar work conducted by Militzer *et al*. (1979) in which the direct use of surface potentials, rather than apparent resistivities, were advocated. The implication of this is that the target anomaly may be more pronounced in terms of its effect on potentials, compared to its influence on apparent resistivity. Furthermore, Militzer *et al*. also advocate the use of electrode arrays whereby the normal response of the host medium is reduced. The three-electrode difference technique, in which only the secondary fields from the target contribute to the response, is an example of such an array.

Peters and Burdick (1983) proved that the electrical resistivity method could be used to detect both air-filled and water-filled cavities at depth-to-diameter ratios of greater than 10:1. Successful tests were carried out at various sites, including the detection of abandoned coalmine workings in USA. Peters and Burdick used the pole-dipole technique in single profile mode. Resistivity sections of the subsurface were then generated through trial-and-error correlation with the predicted responses of assumed targets. The detection capability of the above technique is very promising in that it means that in theory a single 6 m x 6 m cavity is detectable at a depth of up to 60 m. Unfortunately, the resolution capability of the technique is not adequately quantified in the study. It appears, however, that the mapping accuracy of the technique is probably insufficient to resolve regions as small as 5 or 6 m between such cavities.

6 BASIC COMPUTER SIMULATIONS

A series of computer simulations were conducted with the aim of identifying strengths and limitations of the resistivity technique. Even though most of these simulations involved very simple geoelectric models, the intention was to highlight various aspects of the data acquisition, processing and interpretation stages. The results will be used in quantifying the applicability of the resistivity technique in terms of the geophysical problems stated in Section 2.

The majority of the synthetic data sets used in this study were generated using a 3-D finite difference modelling code (Loke, 1997). For the purposes of this study no 3-D inversions were done. Rather, the data sets were used to either generate plan contour maps (using SURFER software), or individual profiles were extracted from the main data sets to be displayed in the form of apparent resistivity graphs. In some cases several in-line profiles were extracted and combined to serve as input for a 2-D finite element resistivity inversion scheme (Kemna *et al*., 1996). Application of this 2-D inversion code yielded 2-D cross-sections, which estimate the resistivity distribution as a function of lateral position and depth.

Simulation A

Figure 2a and 2b shows what could be described as *ideal* resistivity survey results. These images were derived from simplified synthetic models or model responses and were chosen / designed for demonstration purposes only.

As was earlier stated, the main targets of interest in this project are subsurface cavities, in particular abandoned bord-and-pillar workings, as well as sinkholes that develop above current and abandoned workings. Figure 2a shows the result of a hypothetical resistivity survey over a 50 m x 50 m area in the form of a 2-D map of subsurface resistivity variations. The target cavities were assumed to be water-filled and relatively conductive compared to the host rock environment. Ideally, subsurface cavities would be mapped as accurately as this image suggests. This image is, in fact, a contour plan of the 3-D geolectric model. Alternatively, the relative location and depth of cavities along a specific profile need to be accurately determined. The processed data may then be presented in the form of a 2-D cross-section (Figure 2b). This image represents real 2-D inversion results.

Unfortunately, the cavity detection problem in the coal environment tends not to be as straightforward as the above example would suggest. During the course of the following simulations some of the problems anticipated are highlighted.

Simulation B

For this simulation the following 3-D geoelectric model was used: A thin (4 m), shallow (6-10 m), very resistive coal layer (5000 Ωm) was placed in a moderately resistive (500 Ωm) host rock environment. Two target blocks were placed in this coal layer at the following x, y-coordinates: x = 15-21 m, y = 22-28 m and x = 27-33 m, y = 22-28 m. These 6 m x 6 m x 4 m targets were assigned a resistivity of 10 Ωm and represent two water-filled (conductive) near-surface cavities.

Using the above geometry, a theoretical resistivity survey was modelled using Loke's 3-D finite difference modelling software. The survey area was covered by 676 (26 x 26) electrodes with an electrode and line spacing of 2 m. A complete in-line dipole-dipole data set was calculated. The measured potential values were then converted to apparent resistivity values and data sets for various dipole spacings extracted from the main data set. The resulting apparent resistivity values were then designated to grid positions equivalent to the centre of the dipole array for each meaurement. Finally, 2-D contour maps were generated using SURFER. In ***Figures 3a and 3b***, the n = 3 and n = 4 contour maps are shown. Note that, in both cases, the two conductive targets were detected, but that the resolution is improved for the n = 4 data set. This can be explained by the fact that a greater source-receiver separation implies deeper current penetration, and the measured voltages therefore contain more information about the target geometry. Also, note that the resolution of the blocks are not as sharp as was the case with the ideal results (Figure 2a).

Figure 3c shows the result of a single profile of in-line dipole-dipole, data (n=1- 8) inverted using a 2-D finite element inversion scheme, RESITOMO (Kemna *et al*. 1996). The data was extracted from the 3-D data set described above. The location and depth of the target was resolved with a high degree of accuracy.

Simulation C

This simulation illustrates how resolution deteriorates with increasing target depth. For this exercise the same target geometry was used as in the previous simulation, except that the coal layer and conductive blocks were moved down to a depth of 12-16 m. This provides a depth-to-diameter ratio of 2:1, compared to 1:1 in Simulation B. A similar approach to data processing and representation as in Simulation B was used. In this case the n = 5 (m = 10 m) data yielded the best result (***Figure 4***). Although evidence of the two target blocks can be seen on the image, it is difficult to resolve them. The contrast between target and surroundings on this image is not prominent. In other words, although the blocks were detected, they are not well resolved.

Simulation D

The geoelectric model used for this simulation was the same as that used in Simulation B, with the exception that the two blocks were infinitely resistive compared to their surroundings. This is the case for air-filled cavities. The target depth was 6-10 m yielding a depth-to-diameter ratio of 1:1. The resulting contour map (***Figure 5***) suggests that the targets were detected, but are not as well resolved as the relatively conductive blocks (Figure 2b). This simulation provides insight to the problem of relative resistivity contrast as was discussed in paragraph 2.1. The results of this simulation suggest that the resistivity technique is more sensitive to the contrast between electrically conductive features within a relatively resistive coal seam than it is to the contrast between the resistive coal and highly resistive air.

Simulation E

This simulation was similar to Simulation D. However, the resistive coal layer was removed from the model. That is, the two target blocks were isolated in a uniform background. The resulting contour map of apparent resistivity (***Figure 6***) displays an improved resolution of the blocks than when the coal seam was present. This confirms the earlier observation that, despite the relatively large resistivity contrast between the (air-filled) target blocks and the coal, the presence of a highly resistive coal layer suppresses the ability to resolve the region between the individual blocks.

Simulation F

In this exercise the focus was on isolated, single cavities. In the first of these simulations the target block was larger (12 x 12 x 8 m) than that previously used. The survey area and dipole spacing were increased to 100 m and 4 m, respectively. The target block was infinitely resistive and placed at a depth of 12-16 m in a uniform host rock of 500 Ωm. ***Figures 7a and 7b*** show the resulting contour maps for m = 8 m (n=2) and m =12 m (n=3), respectively. Note how the target anomaly increases in apparent size as the inter electrode spacing was increased, while using the same processing / contouring parameters. This is the result of the array sampling a larger portion of the earth and the associated resistivity averaging effect.

Simulation G

In this case the target size was reduced to a block of 6 x 6 x 4 m. The data set and processing was otherwise the same as in Simulation F. In ***Figure 8*** the target anomaly is clearly smaller than the anomaly displayed in Figure 7b. In both cases an inter-electrode spacing of m = 12 m was used. The electrode separation was then increased to m = 16 m and the result can be seen in ***Figure 9***. As was expected, the target anomaly is somewhat bigger than in Figure 9.

Simulation H

Using the same geoelectric model as above, the isolated cavity was moved down to a depth of 24 m, making it difficult to detect. The contour maps for the various inter-electrode spacings showed little convincing evidence of the target's presence. ***Figure 10*** shows a hint of a target anomaly, but it is not prominent and could only be extracted by specifying a contouring interval beyond the resolution capabilities of the average resistivity meter.

Simulation I

In this simulation exercise the focus was moved to a grid of target blocks similar to the coal pillars expected within old workings. ***Figure 11a*** shows several horizontal sections through a geoelectric model of this nature. In this case the pillars, located at a depth of 24-28 m, were surrounded by conductive material (10 Ωm), assumed to be acidic water. That is, a flooded area with a grid of coal pillars located in half of the survey area with the adjacent area unmined. Individual resistivity profiles were then compared to determine whether the boundary between the mined and un-mined areas can be identified.

In ***Figure 11b*** the profiles for y =12 m and y = 88 m (m = 16 m for both) were compared. For reference purposes the origin (x=0, y=0) is the top left corner of the grid. The response for the y = 12 m profile shows an increase in apparent resistivity earlier than y = 88 m response. This is explained by the fact that the contact between mined-out and unmined areas occurred at x = 30 m (for the y = 12 profile) and at x = 40 m (for the y = 88 profile). To the left of the contact the bulk resistivity of the subsurface is lower due to the presence of the conductive water. Those measurements taken to the right of the contact are therefore expected to yield higher apparent resistivity values. The position of the contact is not easily deduced from these responses and is located along the upward slopes, close to the start of the slope.

Simulation J

The previous bord-and-pillar model was modified for this simulation: The pillars were moved to a shallower level, between 8 and 12 m. The two profiles, y = 12 m and y = 88 m, were again considered (***Figure 12a and 12b***).

The same trend is again observed – with the y =12 m response increasing before the y = 88 m response. However, note the marked increase in relative apparent resistivity difference in the individual responses. With the targets located at a depth of 24-28 m (Simulation I) the relative difference in apparent resistivity in the individual responses is less than approximately 1 Ωm . With the targets at 8-12 m, this relative difference is now of the order of a few hundred Ωm. Again, the position of the contact is difficult to estimate using the individual responses. The accuracy of doing this estimation through a graphical interpretation is likely to result in an accuracy no better than 4-5 m.

Simulation K

The bord-and-pillar model of Simulation J was modified such that the conductive, flooded areas were simulated as being air-filled (10^6 Ωm) as is illustrated in ***Figure 13a.*** As with the previous simulations, the profiles y = 12 m and y = 88 m were interpreted. Ignoring the numerical edge effects, the contact between unmined and mined-out areas is associated with a sudden decrease in apparent resistivity, almost at the point where the centre of the measuring array crosses the contact (***Figure 13b*** and ***13c***).

Simulation L

In the final simulation using the grid of blocks, the target depth was changed to an intermediate depth of 14-18 m. The y = 12 m and y = 88 m profiles are shown for the unflooded case (***Figures 14a and 14b***) and the flooded or conductive case in (***Figures 15a and 15b***). As expected, the responses in Figures 14a and 14b are similar to those in Figure 13c, except that the relative apparent resistivity differences in the individual graphs are now of the order of 10-20 Ωm, compared to 40 Ωm (Figure 13c). The trends of the responses in Figures 15a and 15b are also similar in shape to the responses in Figure 13b, however, the relative apparent resistivity differences in the individual responses are more pronounced.

Simulation M

In this modelling exercise the two-block model used previously was considered with the following modification. A very conductive surface layer was present, 1 m thick and 50 Ωm. A 2-D model representing this scenario is depicted in ***Figure 16a***. The 2-D inversion result, using the synthetic dipole-dipole data set, is shown in ***Figure 16b***. Comparing these results with the image in Figure 2b it can be seen how the conductive surface layer dominates and masks the block anomalies. The geoelectric model in Figure 16a was then modified further such that the depth of surface layer varies (***Figure 17a***). These variations are manifested in the inversion output (***Figure 17b***). Even though this simulation represented a severe case of conductive overburden, it was designed to demonstrate how a highly contrasting surface layer or weathering profile can dominate an electrical resistivity responses. One should be careful of the pitfall of interpreting anomalies from near surface sources in terms of deeper targets.

7 FURTHER RELEVANT COMPUTER SIMULATIONS AND FIELD RESULTS

In this section a number of results, not directly linked to coal but which may be of future relevance to the project, are presented. These surveys / simulations were conducted by CSIR, Miningtek.

• 2-D imaging of sinkholes from surface

The aim of this survey was to test the applicability of the resistivity technique for mapping near surface sinkholes. Although this example is from a dolomitic environment it is still relevant as it illustrates how both electrically conductive sinkholes (principally comprising weathered material) as well as electrically resistive (air-filled) sinkholes can be imaged. The survey was conducted diagonally across an existing tarred road where two sinkholes had suddenly appeared. A small sinkhole, approximately 2-3 m in diameter and 2-3 m deep, was located on the eastern edge of the road, while a larger one, approximately 10 m across and 3-4 m deep, was located on the western side of the road (refer to ***Figure 18a***). Three noteworthy features were manifested on the output resistivity image (***Figure 18b***):

1) It appears that both sinkholes are probably part of the same system. This was deduced from the basin like conductive or weathered zone shown in magenta in image.
2) The two cavities are seen as relatively resistive areas (blue areas) compared to the weathered zone (magenta) and are located within this weathered zone.
3) The highly resistive feature further to the south (red-orange area) is most likely due to a near surface air-filled cavity. Unfortunately, no surface evidence or drilling was conducted to confirm this interpretation.

• **2-D imaging of pollution from surface**

The survey results discussed here are not from a coal environment, However, they are relevant as they illustrate how in-line resistivity imaging can be used to map electrically conductive pollution plumes. The occurrences of sulfate pollution in certain parts of the Witbank coalfield represent a similar target type.

A resistivity tomography (RESTOM) survey was conducted along a boundary of a waste disposal site, where the leakage and migration of a pollution plume into neighbouring land was a concern. As indicated in ***Figure 19***, there were four water-monitoring boreholes along this 400 m line, and a fifth approximately 50 m south of the southern-most edge of the profile. Water conductivity values measured in these boreholes prior to the RESTOM survey provided some information as to the location of the pollution plume. Relatively low values of water conductivity (blue numbers in Figure 19) indicate unpolluted areas, while high conductivity levels (red numbers) indicate polluted groundwater.

The RESTOM results were in agreement with the borehole monitoring measurements. The cold colours (blue-green) in the image correspond well with a known unpolluted area where unweathered norite outcrops. The warmer colours (red-yellow) in the image correlate with the polluted area extending north of B/H-23 through to beyond B/H 24.

Note that the unpolluted host rock in the typical coal environment is expected to have a significantly lower bulk resistivity compared with the unweathered norite environment of the above survey. However, it is anticipated that the contrast in electrical resistivity between sulfate polluted sediments in the Witbank Coalfield and the unpolluted sediments is sufficiently high to be able to discriminate between the two.

Unfortunately, insufficient borehole control was available to quantify the accuracy of the interpretation in terms of delineating this specific pollution plume. However, it must be said that the resistivity imaging method’s most suitable application is in environmental / pollution / groundwater related problems such as that presented here.

• **Simulation illustrating dynamic monitoring**

Dynamic monitoring involves the imaging of a specific site over time to detect changes in the subsurface resistivity. Such changes may be the result of migrating pollution plumes or increased weathering (e.g., a forming sinkhole).

The dynamic process simulated was a simple storage tank leakage situation (***Figures 20*** and ***Figure 21***). This example is representative of any hypothetical pollution plume migration. A pair of boreholes, one on either side of the target area was used for monitoring the leakage.

The first image (Figure 20a) is a reconstruction of a simple 2-layer earth (uppermost 40 m = 200 Ωm and basement = 65 Ωm). The contact between these two units, indicated by the dotted yellow line in the image, was mapped reasonably clearly. The apparently conductive features near the bottom of the boreholes are artifacts, presumably the result of a non-ideal electrode configuration. Figures 20b to 20d are reconstructions of the same model with slight modifications to the 2-layer resistivity distribution. The resistivity changes which were implemented were restricted to the magenta outline and represent a decrease in resistivity from 200 Ωm to 100 Ωm. A downward migrating 'plume' was thus simulated in progressive time steps.

The migration of the 'plume', downward and to the left, is clearly evident on the 'time stepped' images in Figure 20. It is possible to highlight the dynamic process more clearly by applying difference tomography. One way of doing this is to simply subtract one image from the next (difference between pixel values). The resulting image emphasises any changes in resistivity that occur between the two time steps while eliminating the static global resistivity distribution. This technique applied to the images in Figure 20 results in the difference images (Figure 21). The migration and growth of the plume is now much more evident; the violet-red colour bands define the pollution plume.

The dynamic process displayed in Figures 20 and 21 are easily detectable even without applying difference tomography. However, if the resistivity distribution of the survey area is more complex with subtle dynamic changes, they may be difficult to detect without applying difference tomography. For further information and field examples of difference tomography, refer to Daily and Ramirez, 1995.

8 CRITICAL EVALUATION OF THE APPLICABILITY OF THE RESISTIVITY TECHNIQUE

Although the detection capabilities of the electrical resistivity method are promising, the resolution may not be sufficient to solve the primary problem of resolving individual gaps / pillars within old bord-and-pillar workings. The difference between detection and resolution is of great significance. Detection refers to the ability to deduce from field data whether a given target manifests itself in the data or not. Resolution, or mapping accuracy, refers to the ability to 'see' the gaps between individual target features. For example, two small, closely spaced, air-filled cavities may be detectable, as a single resistive anomaly at depth-to-diameter ratio of 5:1 or more. However, in order to discriminate between the two cavities they may need to be shallower than a depth-to-diameter ratio of the order of 2:1.

Another, more fundamental problem for the applicability of resistivity techniques to mapping out old workings is that the average depth of these workings in the Witbank area is of the order of 30-40 m. This is beyond the range where the resistivity technique is capable of providing the desired resolution. The detection of boundaries between mined and unmined areas at these depths may be a worthwhile application of the resistivity profiling technique.

It is evident from the computer simulations that the technique is capable of imaging conductive and resistive features close to surface. It is not possible to assign a cut-off value to the investigation depth at which resistivity imaging becomes ineffective as the size and geometry of the target will influence this. However, the simulation results, together with past experience, indicate that a promising level of confidence can be placed in the technique for mapping anomalous features in the upper 15-20 m. This range applies to the detection and mapping of potholes and sinkholes as described in Section 2.2.

The very critical issue of the effect of the overburden on resistivity surveys needs to be emphasised. If a highly contrasting surface layer is present variations in the thickness or resistivity of this layer may result in unwanted anomalies that mask the deeper, less prominent anomalies that are desired.

Aside from the influence of the surface layer, the effect of other layers (e.g., alternating sandstone and shale layers) above the coal seam of interest must also be taken into account. There is often at least one other coal seam present between surface and the mined-out seam. The vertical and lateral resistivity variations associated with these layers will inevitably complicate the interpretation of resistivity data. It is difficult to account for all possible scenarios through simulation studies and thus the applicability of resistivity needs to be assessed on a site-by-site basis.

Pollution plumes occurring close to surface can be delineated in the manner described in the second case study in Section 7. Although it is not demonstrated here, data can also be acquired over a gridded area and presented as 2-D contour maps, as was done in Section 6. Furthermore, the dynamic monitoring process, which was demonstrated in Section 7, may also prove a useful tool in areas where known or potential pollution problems occur.

To date the applicability of the resistivity technique to the mapping of underground fires has not yet been determined. No recorded cases were found in the literature. It may be of value to conduct a test survey in an area where a known underground fire occurs. The successful application of the technique to this problem will require a marked contrast in electrical resistivity between the burning zones, burnt coal / rock, and unaffected areas.

9 RECOMMENDATIONS

It is recommended that alternative data acquisition and processing schemes, that may enhance subtler resistivity contrasts, be investigated. Improved lateral resolution and depth of investigation than suggested through the computer simulations are desired. Although a portion of this work can be achieved on a theoretical level, genuine case studies and field data are now required. This will enable confirmation of anticipated and predicted results in addition to applying new surveying and / or processing schemes.

On these grounds it is recommended that a variety of data sets be acquired at carefully selected sites. A comprehensive benchmarking of the resistivity technique will be possible if sites associated with a wide variety of issues are surveyed. That is, different targets at a range of depths in differing geoelectric settings.

Finally, a more creative approach to solving some of the typical problems is required. Issues that need to be investigated include:

- How boreholes can be utilised. Techniques such as mise-a-la-masse or borehole-to-borehole resistivity tomography should be considered in cases where the survey site and given problem lends itself towards this.
- What is the potential of in-seam work? Is there an effective way of utilising in-seam exploration boreholes?

The resistivity technique is one of the most promising geophysical techniques evaluated during Year 1 of Task 1.3.1b and every effort should be made to exploit its applicability on the coal mines of the Witbank-Highveld area.

10 ACKNOWLEDGEMENTS

The Geological and Geophysical Coaltech 2020 Working Group is thanked for their continuous guidance.

11 REFERENCES

Brink, A.B.A. 1983. Engineering Geology of Southern Africa, Volume 3 (Karoo Sequence), 320p.

Daily, W., and Ramirez, A., 1995. Environmental process tomography in the United States. *The Chemical Engineering Journal*, 56, p159-165.

Jackson, L. J. 1981. Geophysical examination of coal deposits. *IEA Coal Research Report ICTIS/TR 13*, 116p.

Kemna, A., Engels, O. G., and Martin, I. 1996. Resitomo Resistivity Tomography v 2.0 User Manual – Software package for 2.5D-modelling and 2D-inversion of DC-resistivity measurements, March 1996, 43p.

Loke, M. H. 1997. RES3DMOD - 3D Resistivity and IP forward modelling version 2.0.

Meyer, R. 2000. Personal communication on issue of ground water quality in the Witbank coal areas. CSIR: Environmentek, Pretoria.

Militzer, H., Rösler, R. and Lösch, W. 1979. Theoretical and experimental investigations for cavity research with geoelectrical resistivity methods. *Geophysical Prospecting* **27**(3), 640 – 652.

Noel, M., and Xu, B. 1992. Cave detection using electrical resistivity tomography. *Cave Science* Vol. 19, No. 3. Transactions of the British Cave Research Association, p 91-93.

Owen, T. E. 1983. Detection and mapping of tunnels and caves in Developments in Geophysical exploration methods – 5, Edited by A. A. Fitch, Applied Science Publishers Ltd, p 161 –204.

Peters, W. R. and Burdick, R. G. 1983. Use of an automatic resistivity system for detecting abandoned mine workings. *Mining Engineering*, January 1983, 55-59.

Sheriff, R. E. 1989. Encyclopedic Dictionary of Exploration Geophysics, Second Edition. Society of Exploration Geophysicists, 323p.

Spiegel, R. J., Sturdivant, V. R., and Owen, T.E. 1980. Modeling resistivity anomalies from localized voids under irregular terrain. *Geophysics*, **45** no. 07, 1164-1183.

Sretonovic, B. B., Milicevic, B. A., and Marcetic, D. D. 1992. Detection of disturbed zones over old mine workings using electrical tomography. *Technical Programme and Abstracts of Papers, 54th Meeting and Technical Exhibition of the European Association of Exploration Geophysicists*, Paris France, 1992.

Van der Merwe, J. N., van Zyl, M. and Daehnke, A. 2000. The development of techniques to predict and manage the impact of surface subsidence. *COALTECH 2020 Interim Report (Task 6.9.1)*.

Van Zyl, H. C., Maree, J. P., van Niekerk, A. M., van Tonder, G. J., and Naidoo, C. 2000. Collection, treatment and re-use of mine water in the Olifants River catchment pp 93-98. *Coal – The Future, 12th International Conference on Coal Research*, 12-15 September 2000.

Appendix A

Figures – Electrical resistivity computer simulations

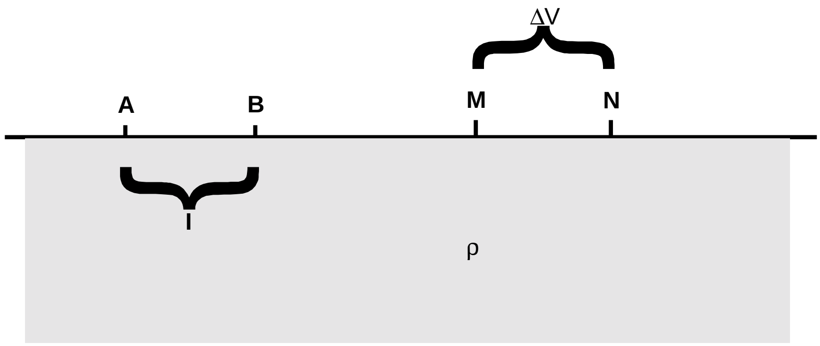

ρ = K*ΔV/I (for electrically homogeneous and isotropic earth)

Figure 1a: Relationship between the earth's resistivity (ρ), the injected current (I) and measured potential difference (ΔV), and the relative position of the electrodes, or geometric factor (K).

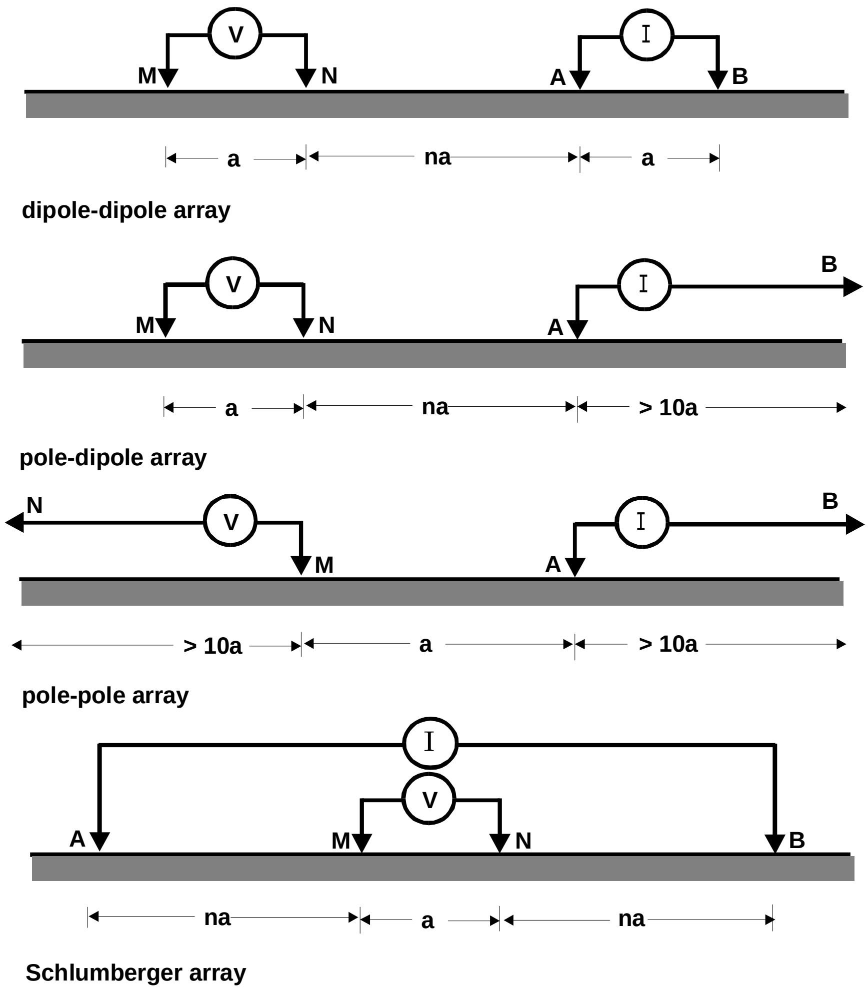

Figure 1b: Electrode arrays commonly used in resistivity surveying (after Sheriff, 1989).

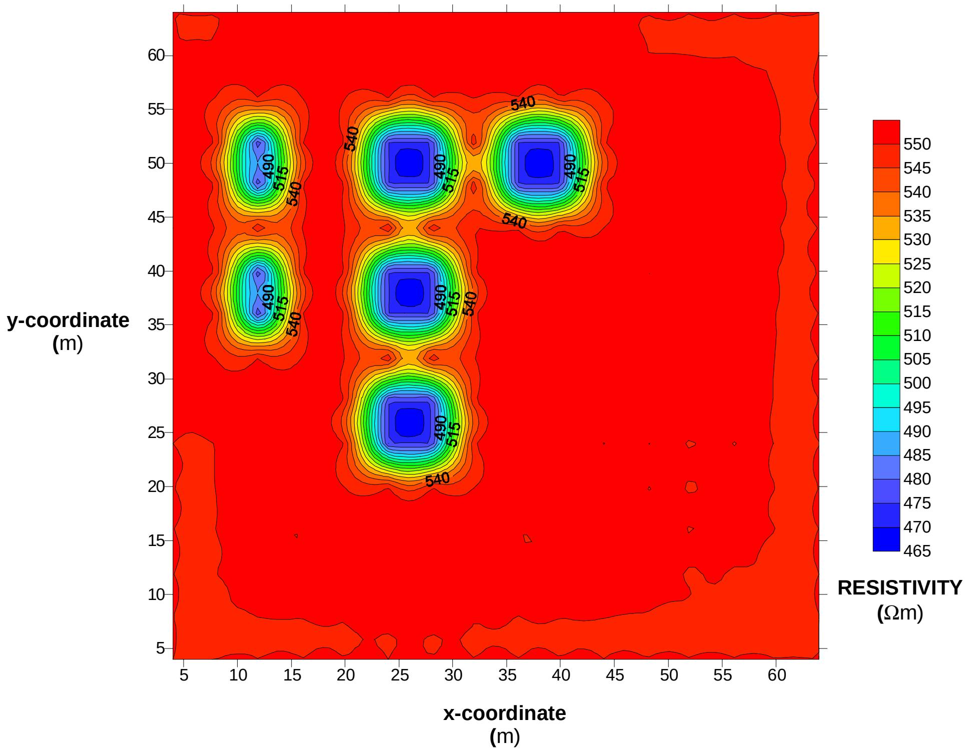

Figure 2a: Plan view of an ideal resistivity result. A 2-D contour (plan) map showing the location of water-filled (conductive), mined-out cavities.

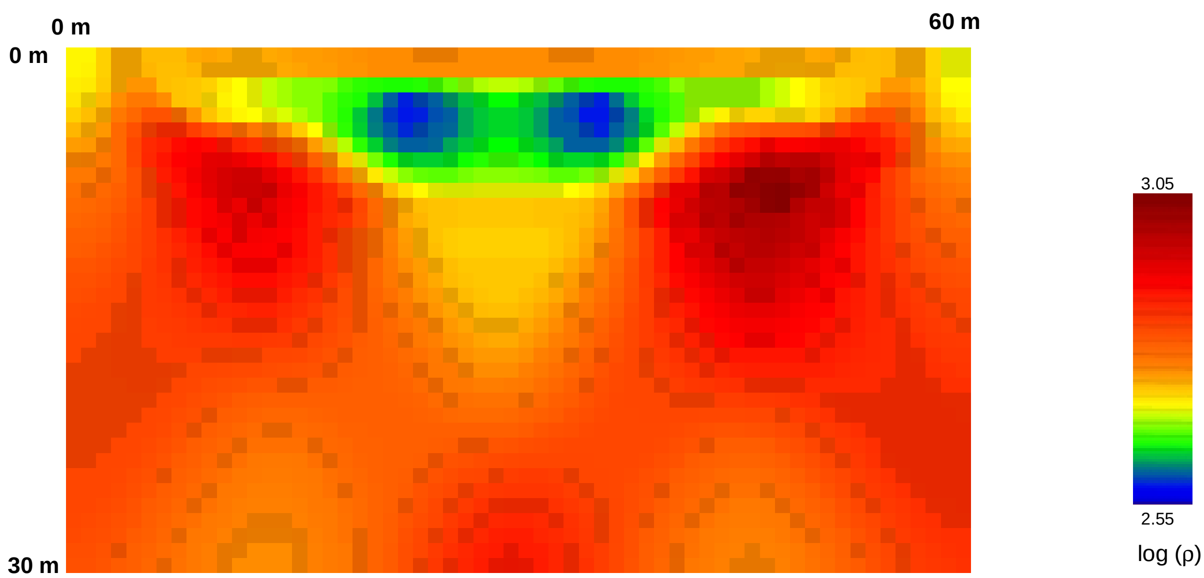

Figure 2b: An ideal cross-sectional resistivity result – a 2D resistivity section showing the location and depth of two mined-out, water-filled (conductive) cavities along a single survey profile.

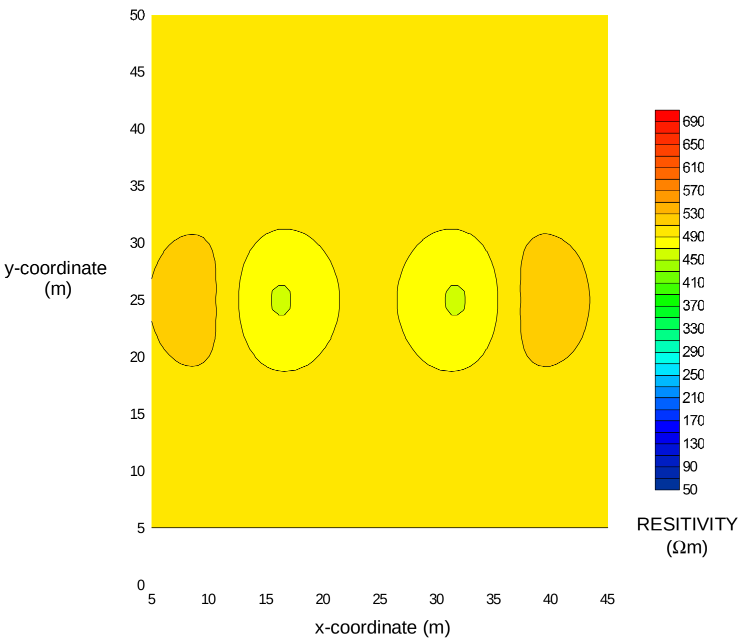

Figure 3a: Simulation B resistivity map for n=3.

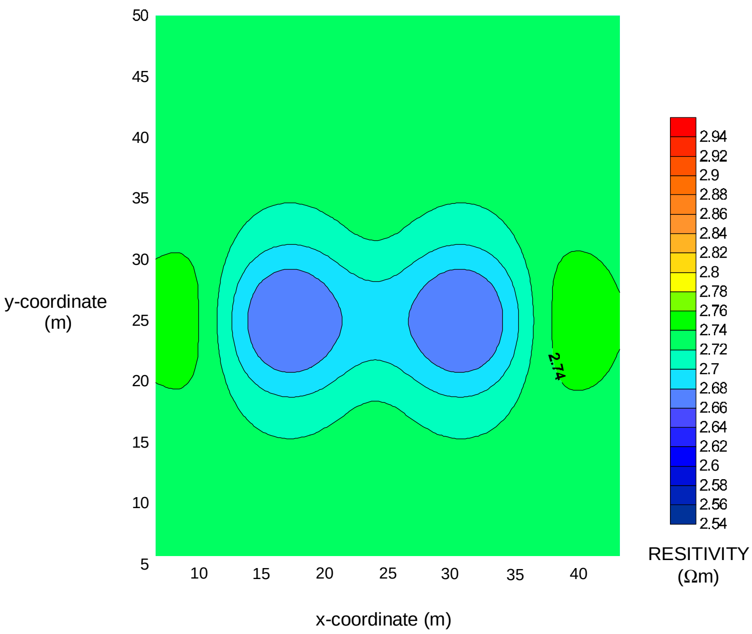

Figure 3b: Simulation B resistivity map for n=4.

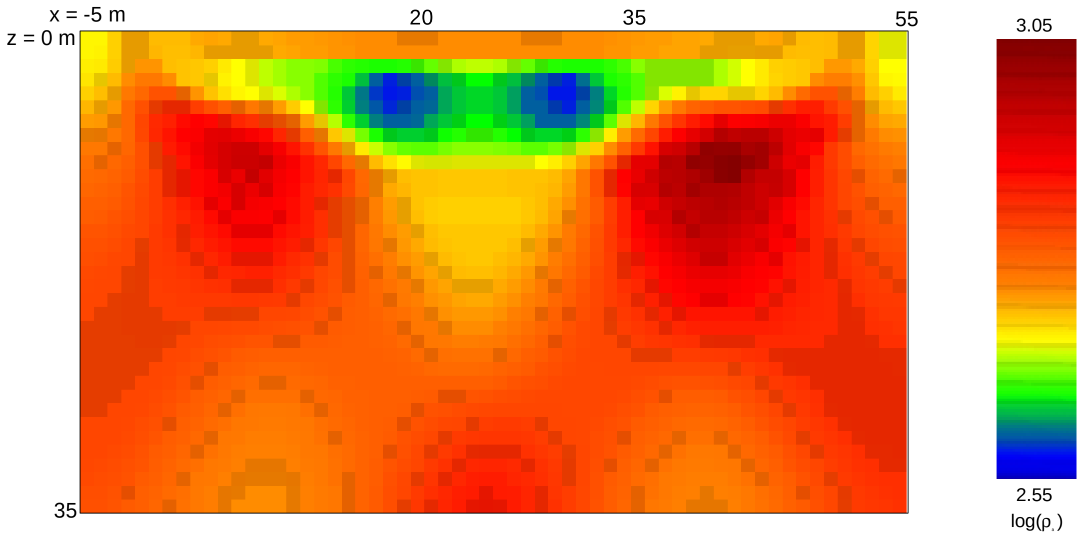

Figure 3c: 2D inversion result, Simulation B.

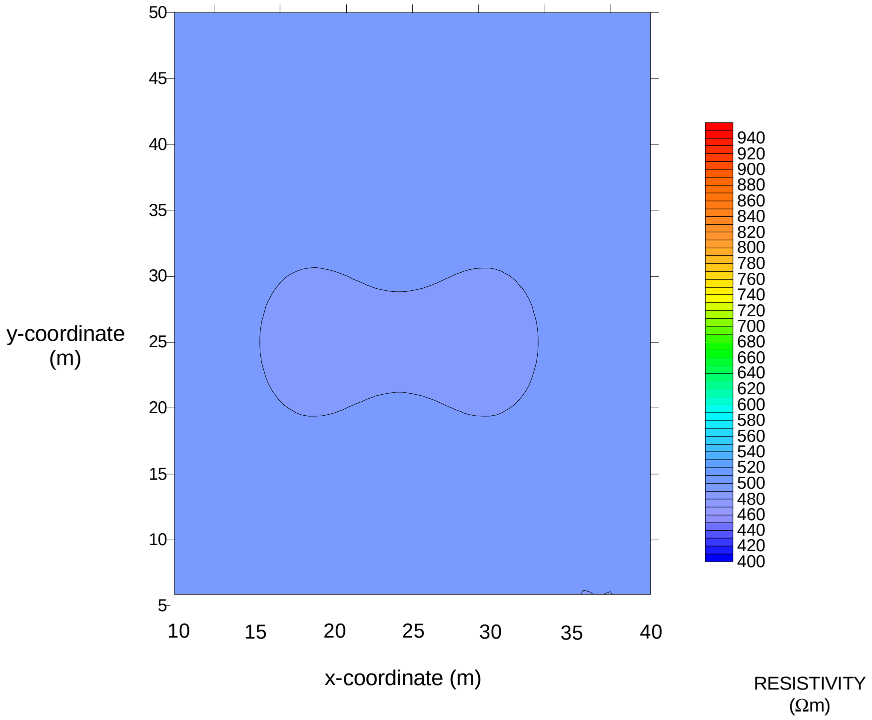

Figure 4: Simulation C resistivity map for n=5.

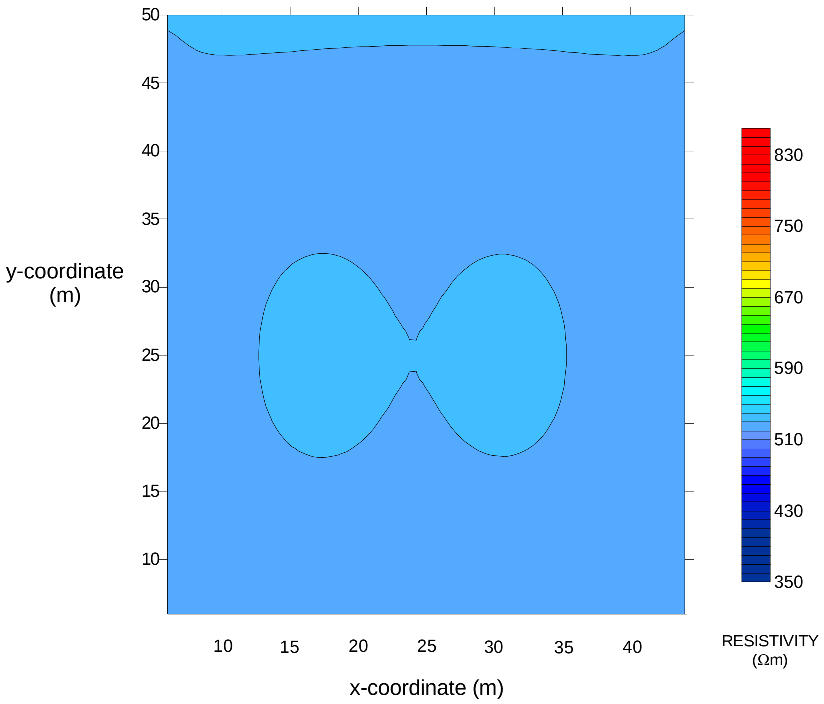

Figure 5: Simulation D resistivity map.

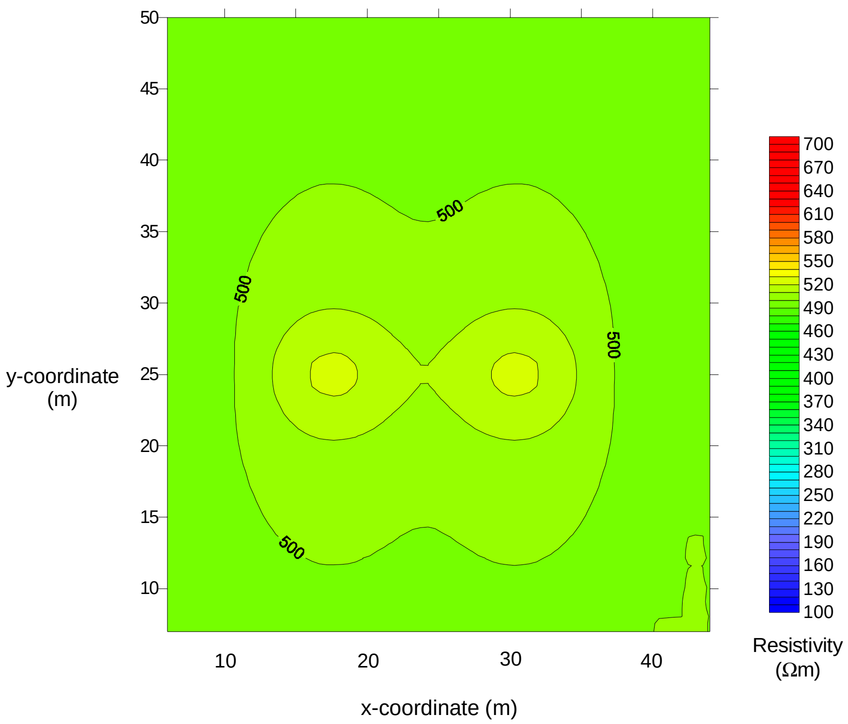

Figure 6: Simulation E resistivity map.

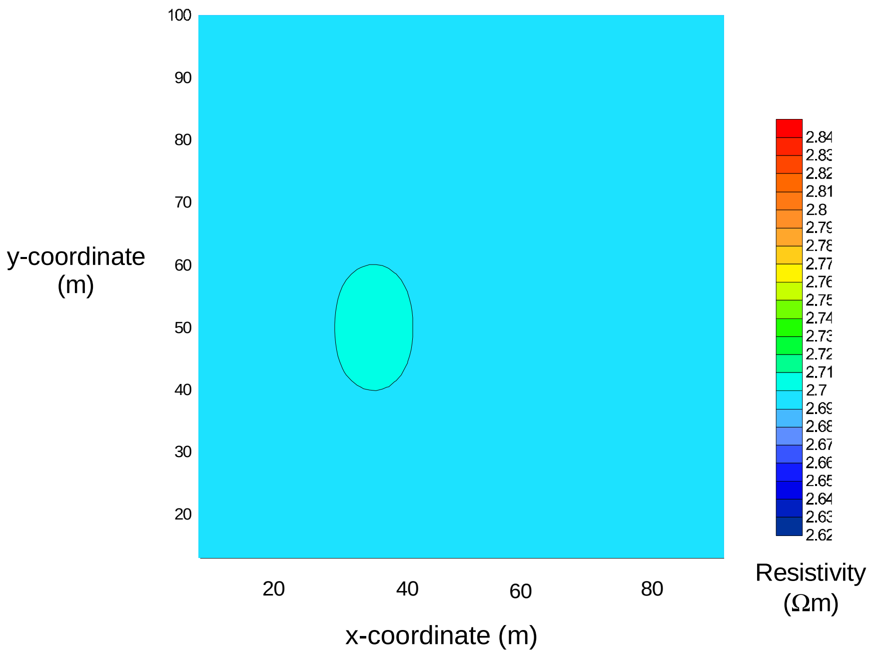

Figure 7a: Simulation F resistivity map for n=2.

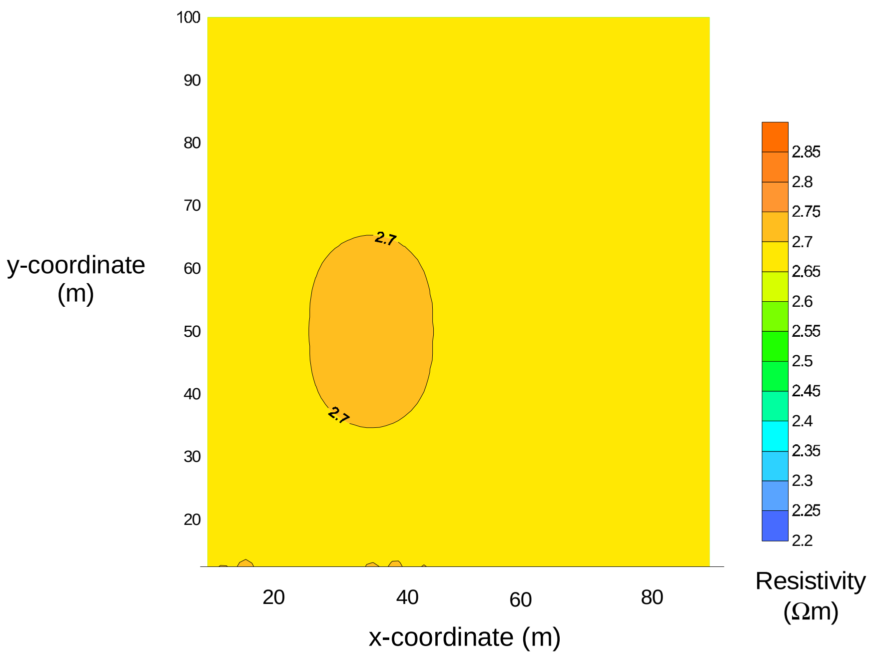

Figure 7b: Simulation F resistivity map for n=3.

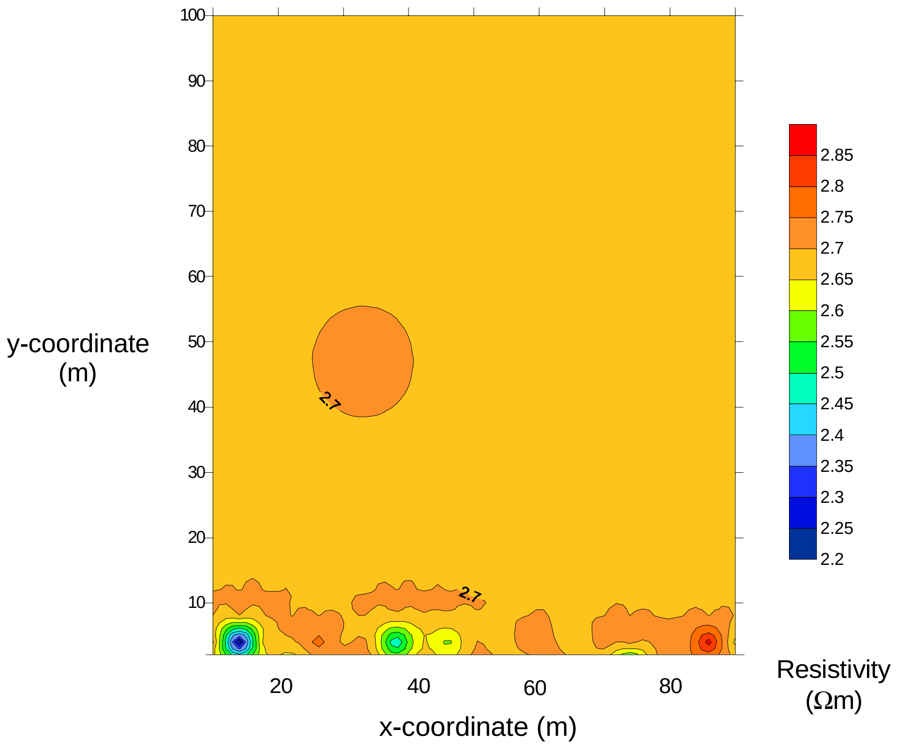

Figure 8: Simulation G resistivity map for m=12.

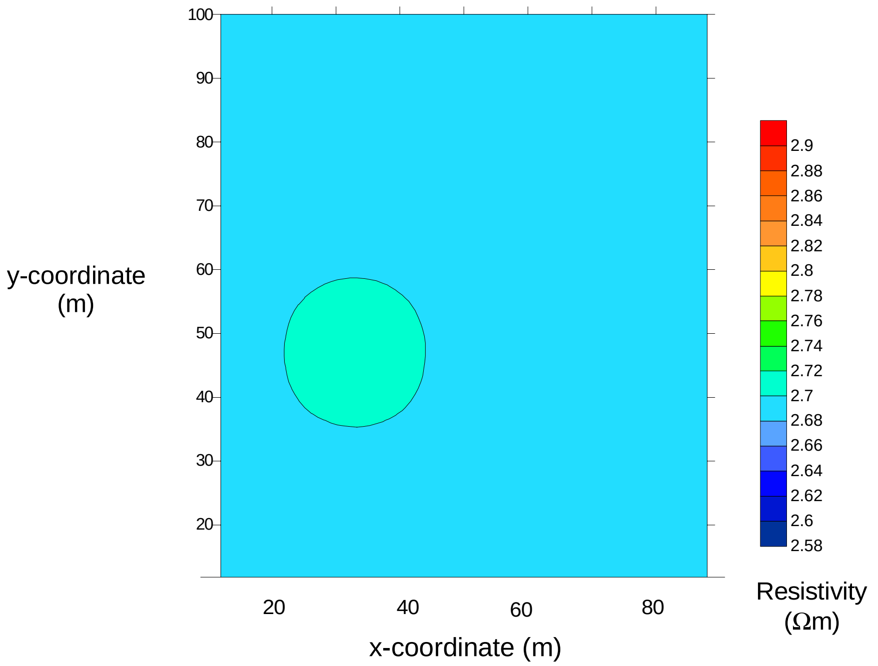

Figure 9: Simulation G resistivity map for m=16.

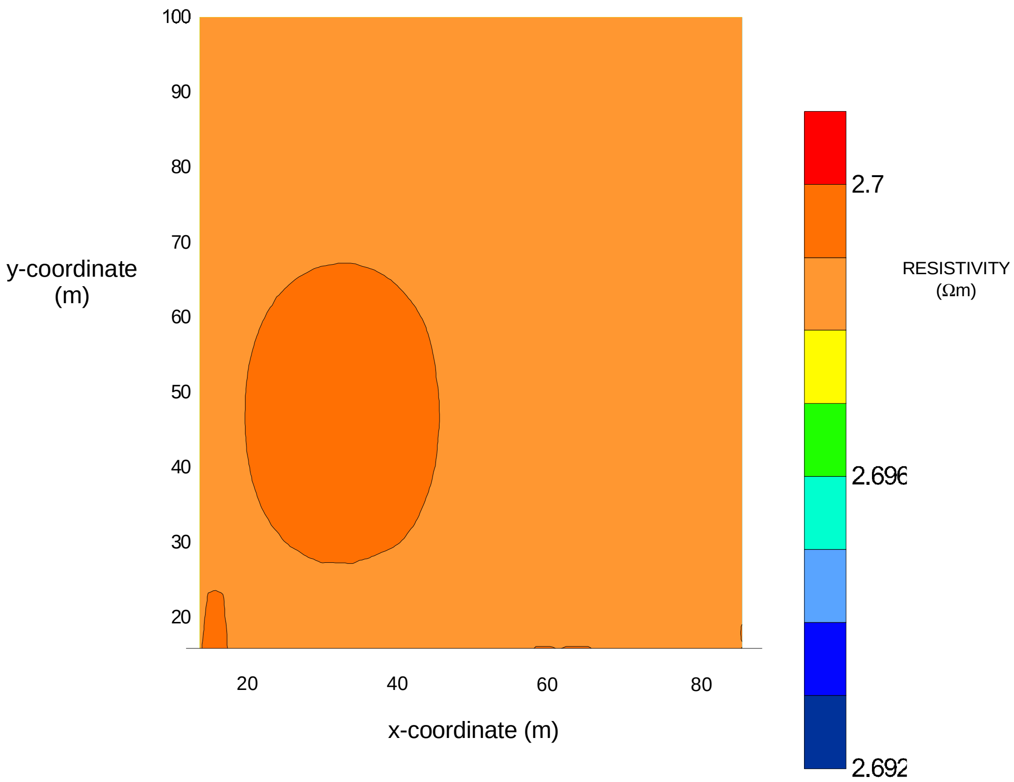

Figure 10: Simulation H resistivity map.

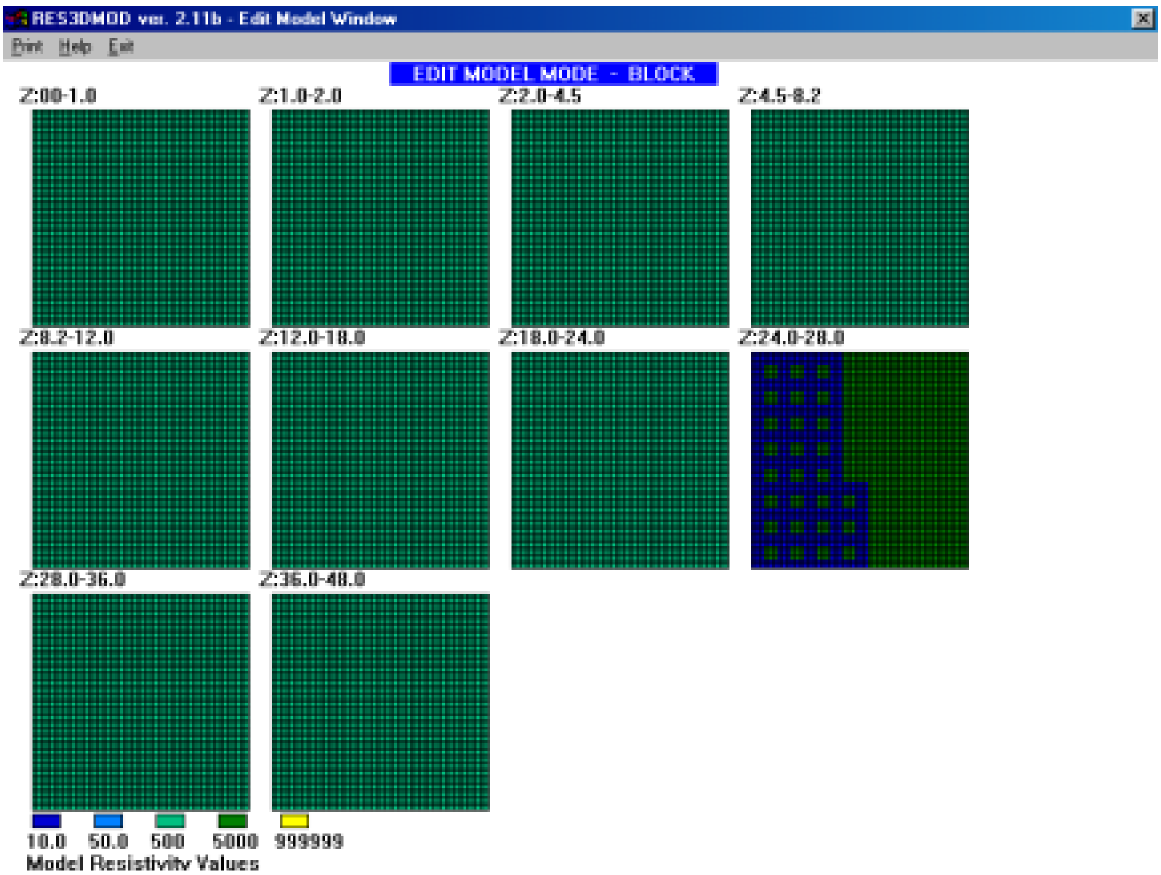

Figure 11a: Simulation I geoelectric model.

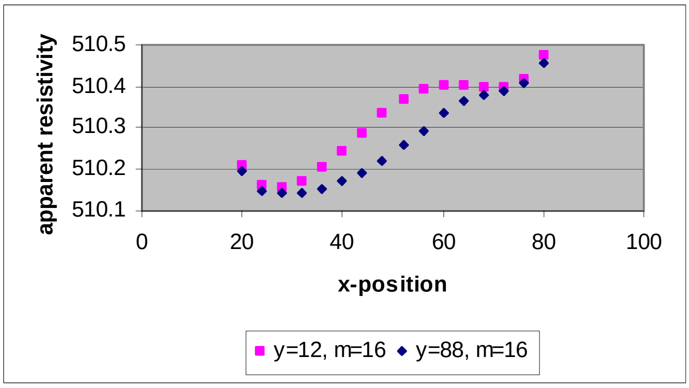

Figure 11b: Simulation I, y =12 m and y = 88 m profiles.

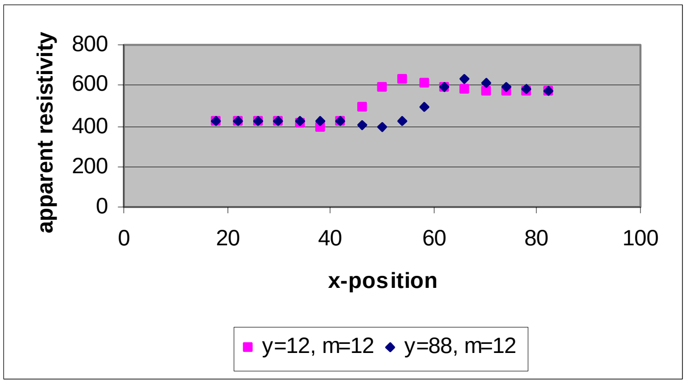

Figure 12a: Simulation J, y =12 m and y = 88 m profiles for m=12.

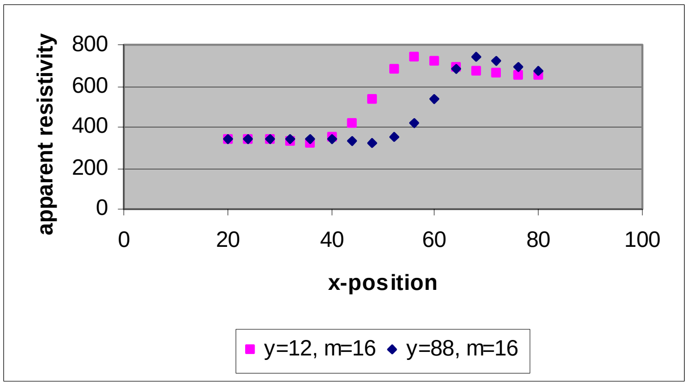

Figure 12b: Simulation J, y =12 m and y = 88 m profiles for m=16.

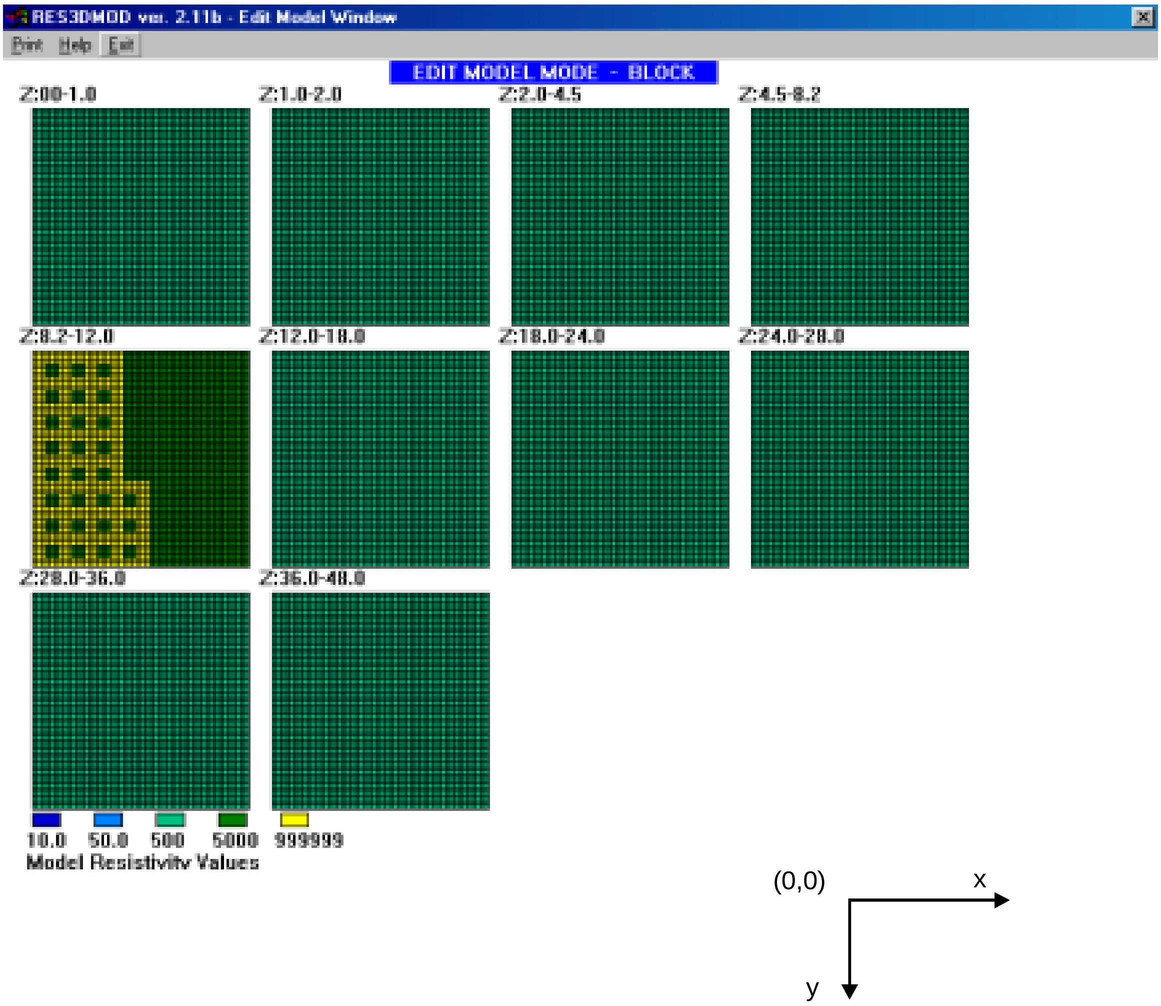

Figure 13a: Simulation K geoelectric model.

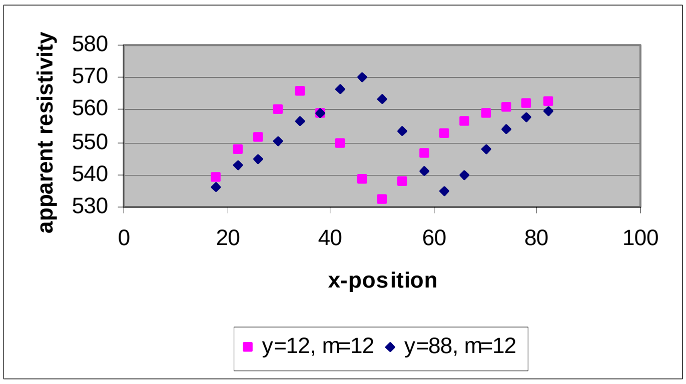

Figure 13b: Simulation K, y =12 m and y = 88 m profiles for m=12.

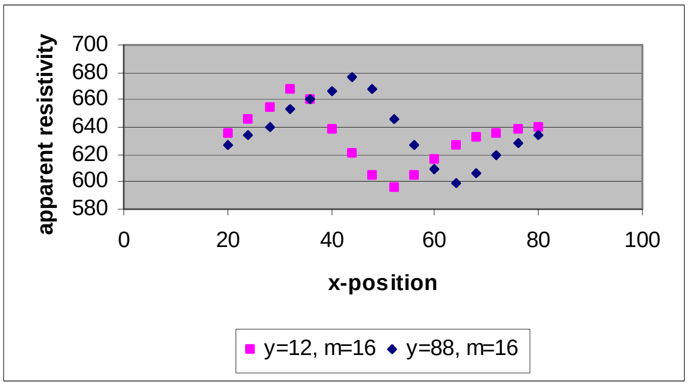

Figure 13c: Simulation K, y =12 m and y = 88 m profiles for m=16.

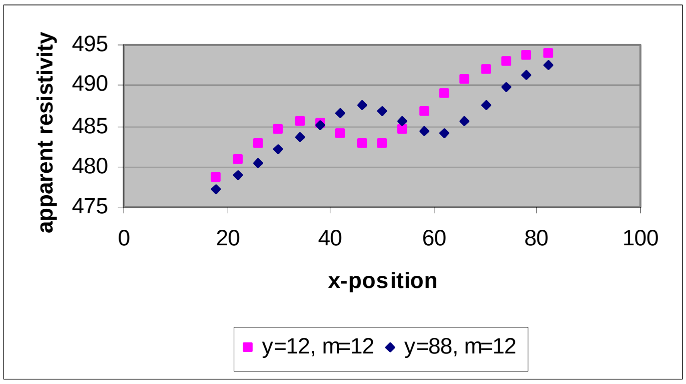

Figure 14a: Simulation L (unflooded case), y =12 m and y = 88 m profiles for m=12.

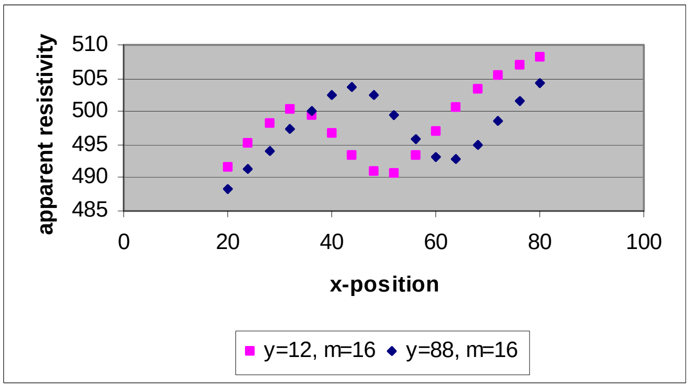

Figure 14b: Simulation L (unflooded case), y =12 m and y = 88 m profiles for m=16.

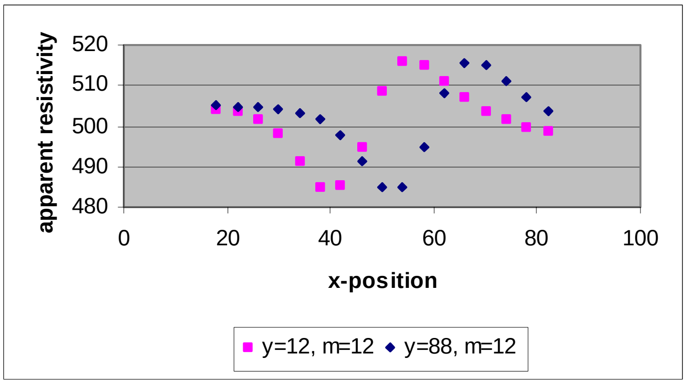

Figure 15a: Simulation L (flooded case), y =12 m and y = 88 m profiles for m=12.

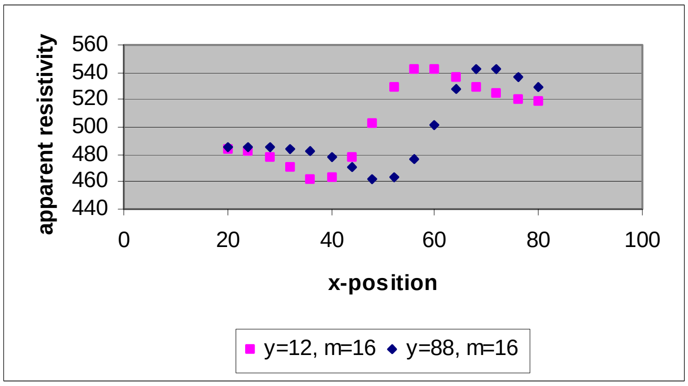

Figure 15b: Simulation L (flooded case), y =12 m and y = 88 m profiles for m=16.

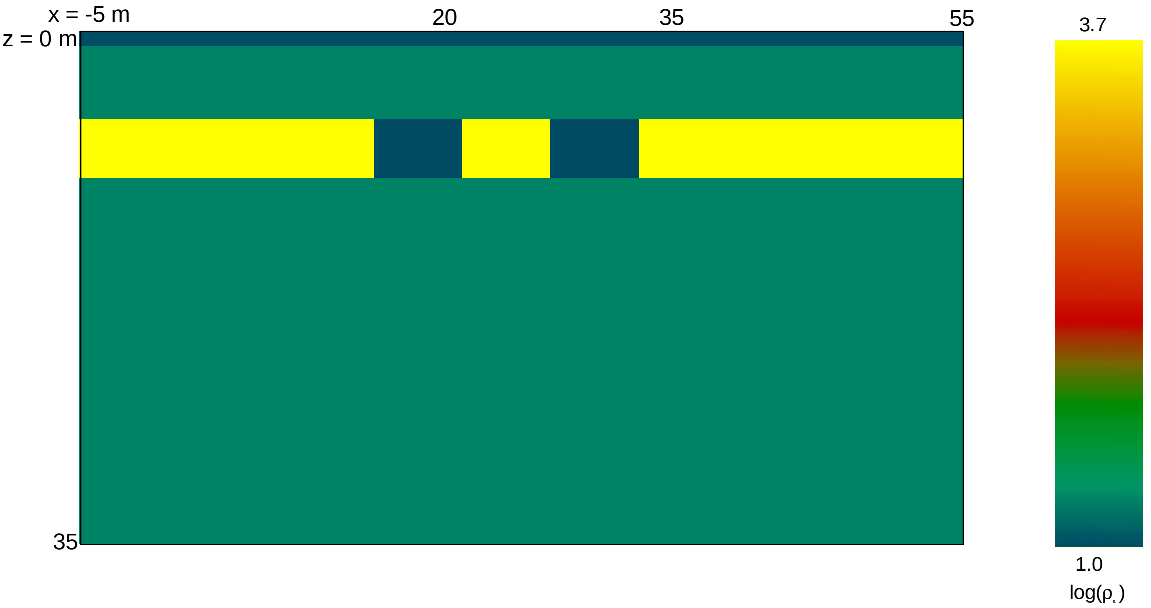

Figure 16a: Simulation M geoelectric model.

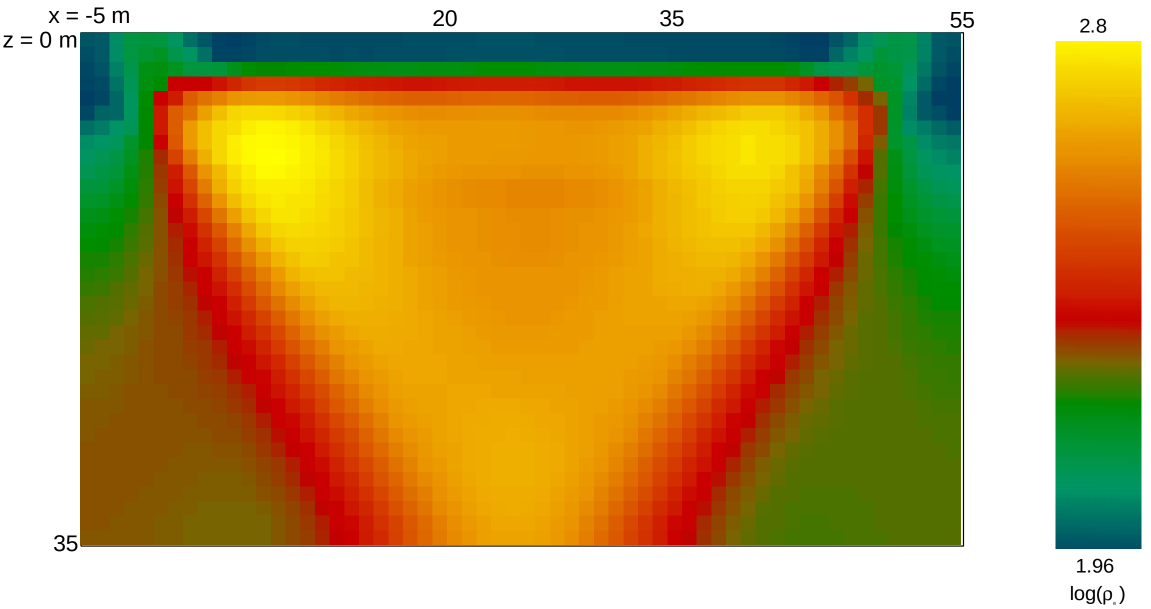

Figure 16b: 2D inversion result, Simulation M.

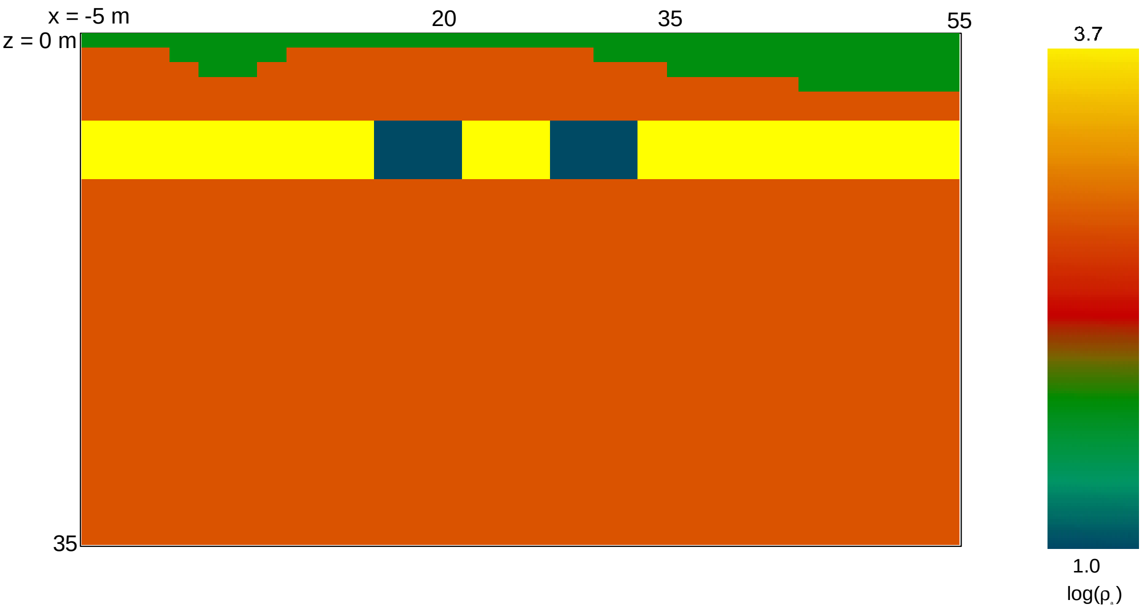

Figure 17a: Simulation M geoelectric model (varying overburden thickness).

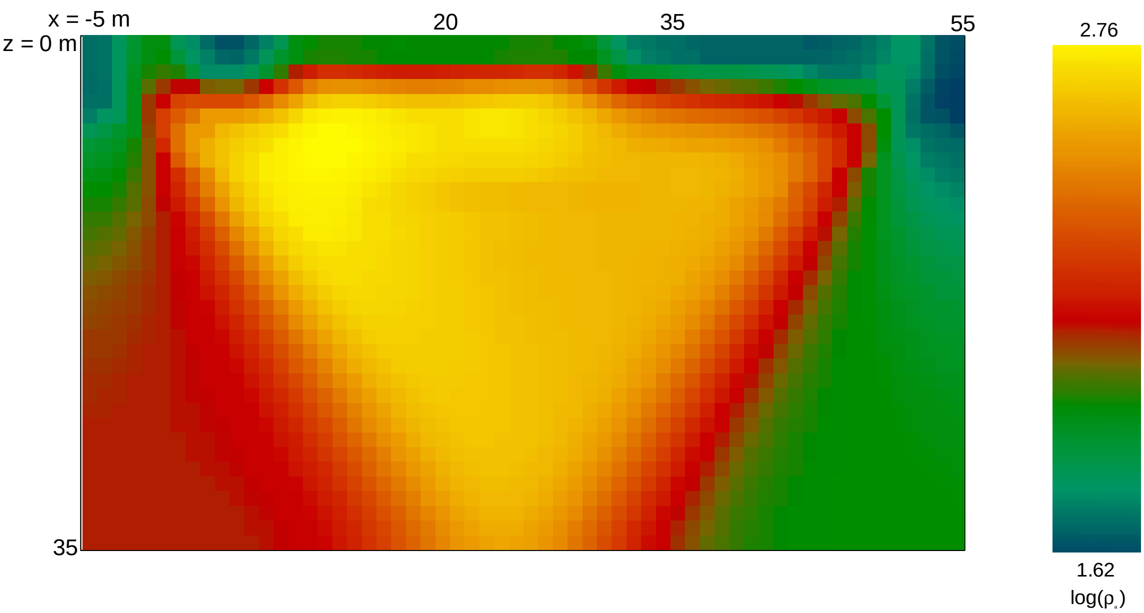

Figure 17b

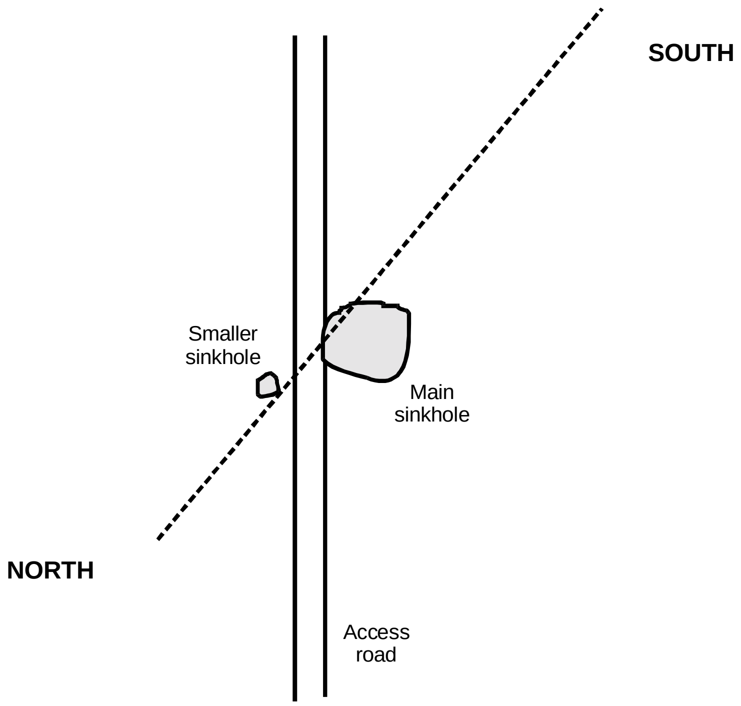

Figure 18a: Schematic plan view of Sinkhole survey.

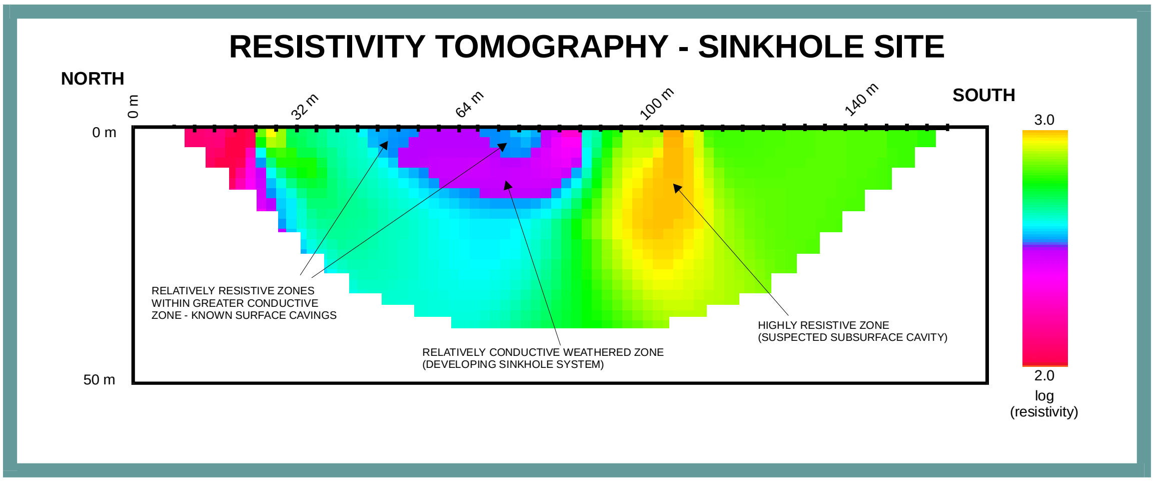

Figure 18b: RESTOM image resulting from the sinkhole survey.

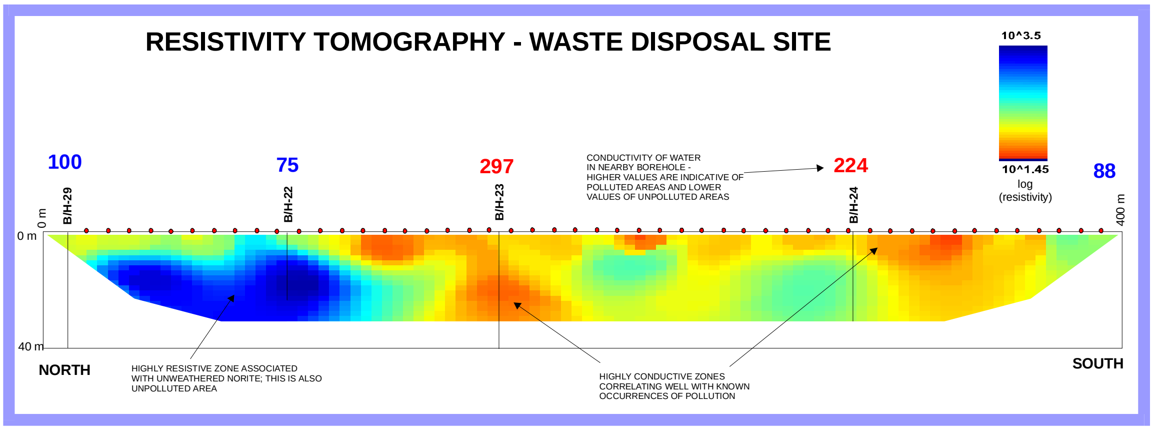

Figure 19: RESTOM survey at a waste disposal site.

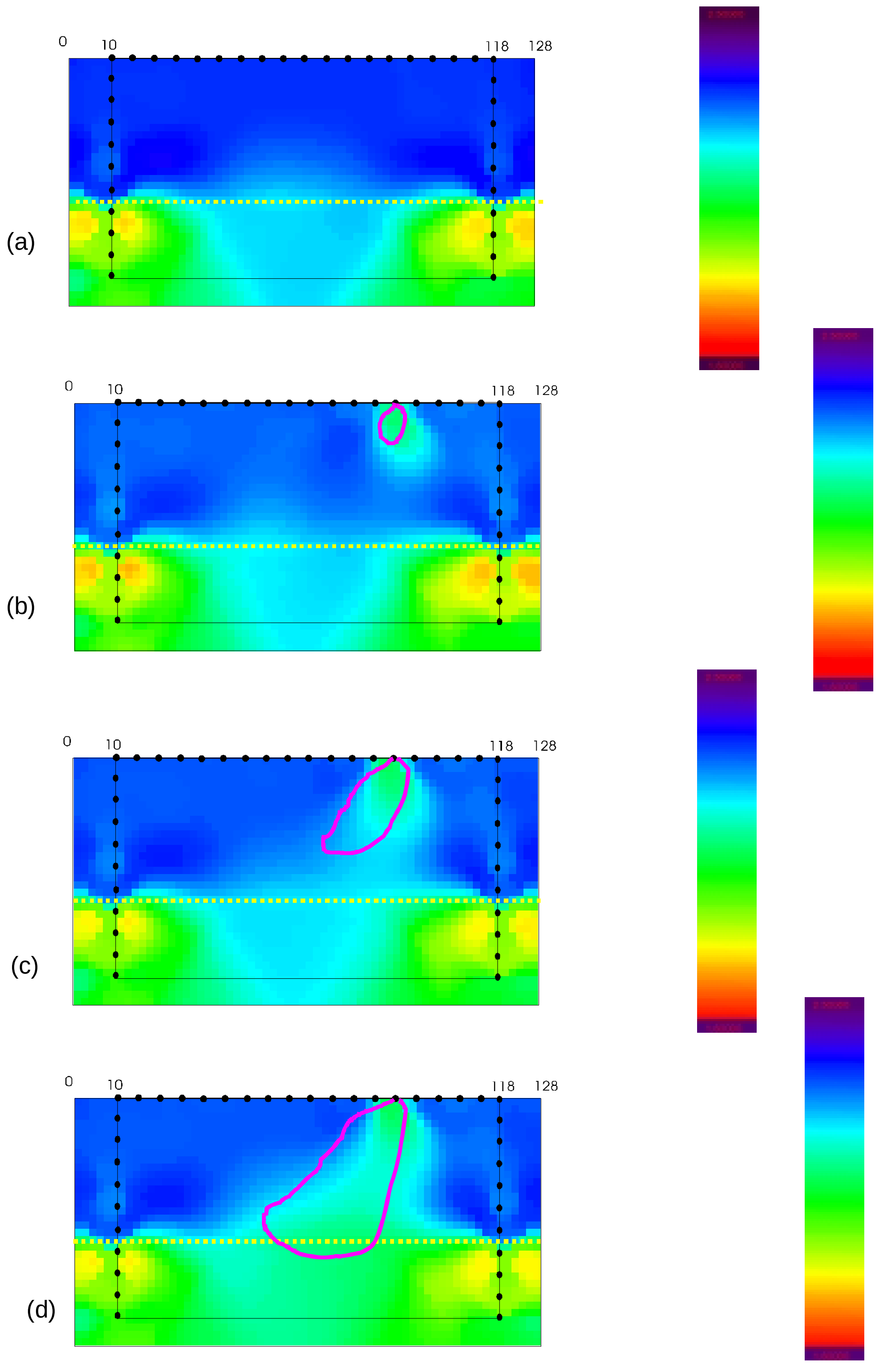

Figure 20: Model of dynamic pollution process.

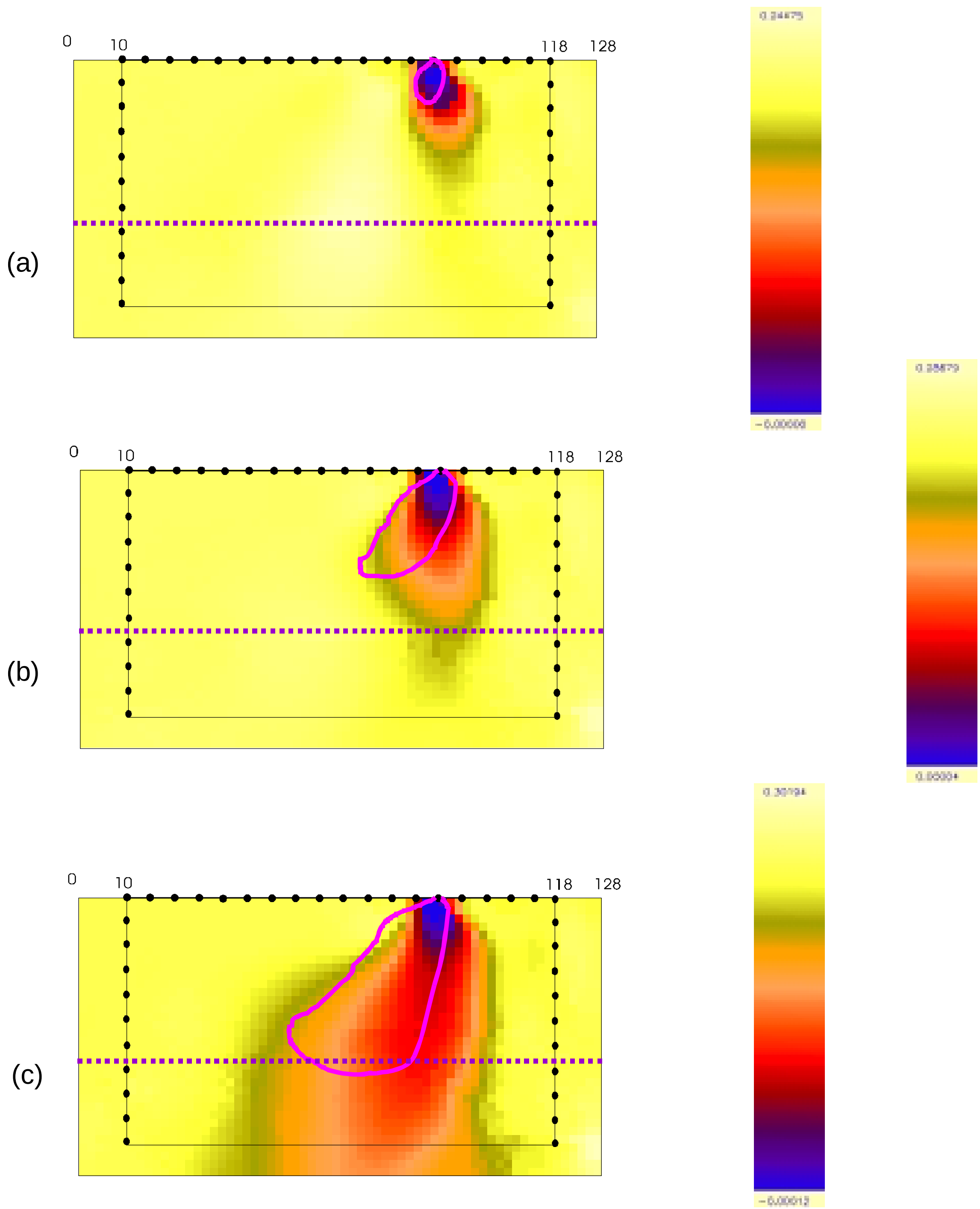

Figure 21: Results of RESTOM difference tomography.

APPENDIX XIII

COALTECH 2020

Subtask Report
(part of Subtask 4)

The application of airborne thermal imagery to the coal environment

A. J. Franzsen

Anglo Operations Limited

CSIR, Division of Mining Technology

Report number: 2001-0119

Task 1.3.1b

Detection of old workings, sinkholes, underground fires and acid mine pollution using geophysics and airborne thermal infrared imagery

October 2000

EXECUTIVE SUMMARY

Airborne Thermal Remote Sensing is a technique which was used in Southern Africa during the mid 1970's by a company called Spectral Africa, a subsiduary of JCI. Many successful surveys were flown during that time for a variety of applications, including the detection of old workings and of fires in the Witbank Area. Unfortunately, this technology fell by the wayside following management changes and restructuring at JCI. The Geophysical Services Department of Anglo Operations Limited revived interest in this technology in the late 1990's by bringing a thermal scanner out from Australia, all be it at considerable cost. During 1999, several commercial surveys were flown for a number of clients using the same instrument. It was intended to fly an instrument from the United Kingdom during 2000, however bad weather during the scheduled survey time precluded any airborne work.

This report describes some of the basic principles of thermal remote sensing, quotes some of the typical applications and concludes with the intended survey plan for the 2000 operations in the Witbank Area.

Long Wave Thermal Infrared (LWTIR) is the most suitable technique for sub-surface imaging since the wavelengths, from 8 to 14 µm fall in the region where the earth emits maximum thermal energy. Mid Wave Thermal Infrared (MWTIR), from 3 – 5 µm, is not suitable for earth science studies as the wavelength measured is too short.

Airborne LWTIR surveys have been used for a variety of applications including : geological and structural mapping, lithological mapping, detection of sub-surface palaeochannels, mapping of old workings, pollution detection, mapping coal fires and various hydrogeology applications. Satellite systems have been used for similar studies on a regional scale, but are not suitable in the South African context because of the relatively poor spatial resolution.

Three areas were planned for the Coaltech 2020 airborne surveys over the Witbank area. They were selected on the basis of existing ground geophysical work, old workings and the geographical spread of various mining companies.

TABLE OF CONTENTS

LIST OF FIGURES AND TABLES

1 INTRODUCTION

This report comprises two sections: An introduction to airborne thermal remote sensing and secondly, a survey plan for the intended 2000 Witbank Surveys.
Airborne Thermal Remote Sensing is a technique which was used in Southern Africa during the mid 1970's by a company called Spectral Africa, a subsiduary of JCI. Many successful surveys were flown during that time for a variety of applications, including the detection of old workings and of fires in the Witbank Area. Unfortunately, this technology fell by the wayside following management changes and restructuring at JCI. The Geophysical Services Department of Anglo Operations Limited revived interest in this technology in the late 1990's by bringing a thermal scanner out from Australia, all be it at considerable cost. During 1999, several commercial surveys were flown for a number of clients using the same instrument. It was intended to fly an instrument from the United Kingdom during 2000, however bad weather during the scheduled survey time precluded any airborne work.
Thermal imagery used for earth science applications comprises the 8 to 14 μm portion of the Electromagnetic Spectrum because it is in this spectral range where the earth radiates maximum thermal energy. This portion of the spectrum is known as Long Wave Thermal Infrared (LWTIR). In contrast, the Mid Wave Infrared (MWTIR), used in military applications to detect mainly the heat from engines, falls in the 3 – 5 μm portion of the Electromagnetic Spectrum. Most thermal camera systems use this spectral range, which is not suitable for earth science applications because of the short wavelength.

2 THE PHYSICS OF THERMAL REMOTE SENSING

The physics of thermal remote sensing relates to energy emitted from the earth, rather than reflected energy, as is the case in traditional remote sensing. Matter capable of absorbing and re-emitting all electromechanical energy that it receives is known as a blackbody. The total energy emitted by a blackbody (H) in $^{Wm-2}$ is proportional to the fourth power of its absolute temperature (T). This relationship is known as the Stefan-Boltzmann law.
$H = \sigma T^4$
Where $\sigma = 5.7 \times 10^{-8} Wm^{-2} K^{-4}$, the Stefan-Boltzmann constant.
Blackbodies also have the characteristic of emitting energy at different wavelengths, depending on their absolute temperature.This relationship is described by a function known as Wien's displacement law.
$\lambda = 2898/T$
As the temperature of the blackbody increases, total energy emitted rises very quickly and the wavelength which carries most of the energy becomes shorter. The sun, at an absolute temperature of 6000 K, does not emit radiation below 0.1 μm. It has an energy peak at 0.5 μm (in the visible portion of the spectrum), and emits wavelengths up to beyond 100 μm. By contrast, the earth has an absolute temperature of about 300 K and emits maximum energy at 9.7 μm. This is illustrated in *Figure 1,* below. *Drury (1993:4)*

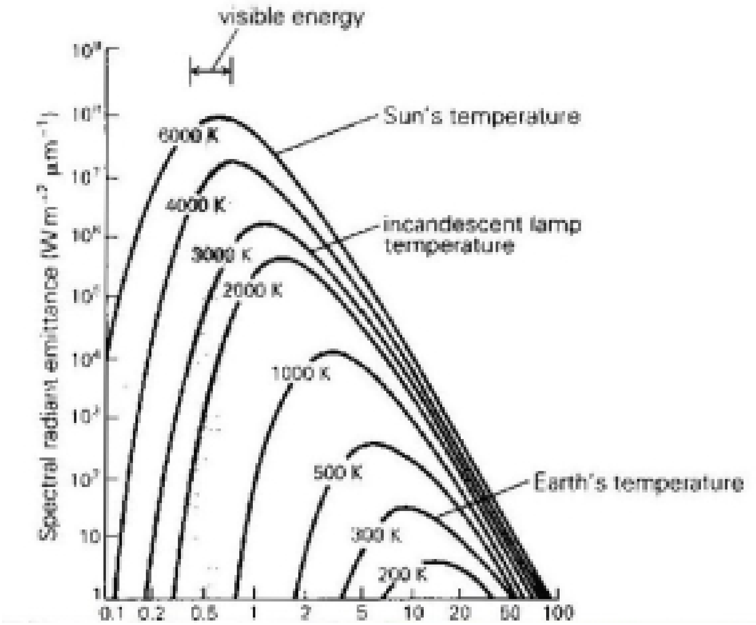

Figure 1: Wien's displacement law.

3 THERMAL IMAGERY

Imagery used in thermal remote sensing is generally collected by opto-mechanical radiometers flown on either airborne or satellite platforms. A typical airborne LWTIR detector images from 8 to 14 µm which coincides with the atmospheric window in that portion of the EMS. The instantaneous field of view is typically 2 to 3 milliradians, which corresponds to a ground pixel size of between 2 to 3 metres at an altitude of 1000 metres.

Diurnal temperature variations of the target materials need to be taken into account . During the day, water is generally cooler than the surrounding rock. At night the converse is true. Rocks and soils typically heat up quickly soon after sunrise. Green vegetation appears warm at night because of the high moisture content. During the day, transpiration from the leaves of green vegetation causes the plants to cool down while the soil and rocks heat up. Dry vegetation tends to appear warm at night as opposed to bare soil as it has an insulating effect.

Night time flying for earth science applications are therefore normally flown after midnight up to just before sunrise to minimise the daytime solar effects. In South Africa the best results are obtained during the dry months. In the gold and coal mining areas of Gauteng and Mpumalanga, June to August are the optimum months for obtaining thermal data. *Figure 2*, below, illustrates the static earth temperature during pre-dawn times. *Sabins (1980:275-295)*

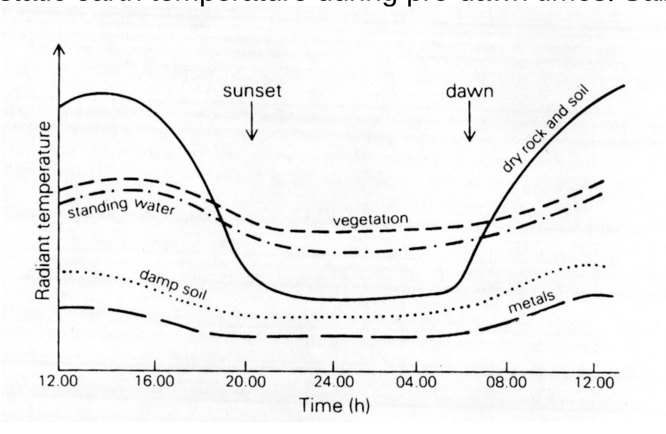

Figure 2: Static earth temperature during pre-dawn times.

4 APPLICATIONS OF LONG WAVELENGTH THERMAL REMOTE SENSING

Apart from synthetic aperture radar, no imaging technique, other than Long Wavelength Thermal Imaging is capable of depicting sub-surface features. *Brink (1979:218-219),* discusses the use of airborne LWTIR imagery to map sub-surface features in the Malmani dolomite in the Lichtenburg area. These images were used by diamond mining companies to detect potentially mineralised palaeochannels which were known to occur in the area. *Figure 3,* is a conventional aerial photograph of a mined out palaeochannel in the Lichtenburg area. *Figure 4,* is a LWTIR image of the same area illustrating how sub-surface features are detected by the thermal instrument. The darker features are water filled solution fractures in the dolomite which are not visible on the aerial photograph.

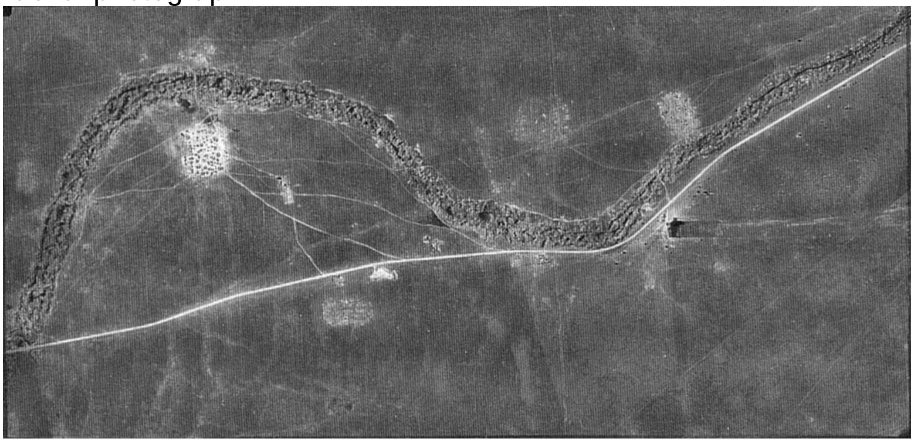

Figure 3: Conventional aerial photograph of a mined out palaeochannel in the Lichtenburg area.

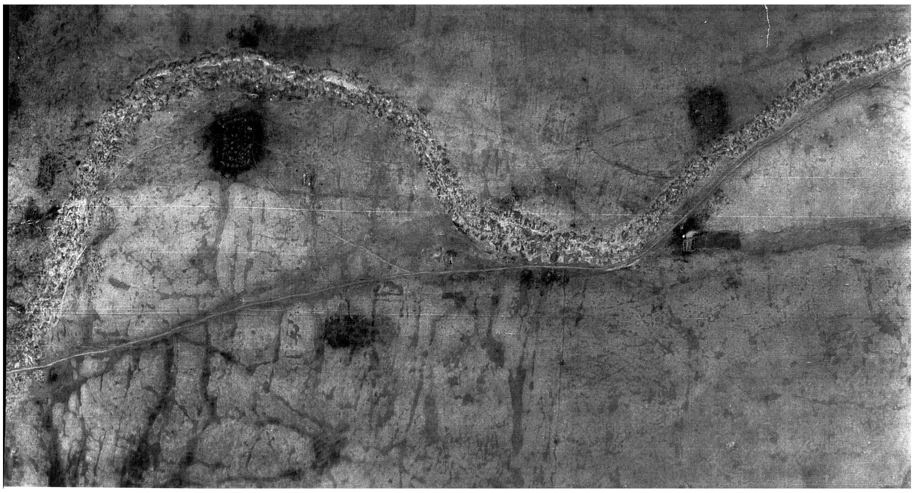

Figure 4: LWTIR image of the same area as in Figure 3.

Brink (1983:126), illustrated the use of LWTIR airborne work in the Witbank area to map subsidence and to detect old bord and pillar workings.

Longshaw (1977), documented a number of applications including, geological and structural mapping, lithological mapping and sub-surface water detection. Recent, undocumented surveys, have used LWTIR for pollution detection and geohydrology studies in the gold, diamond and platinum mining industry. In some cases, the data was used to plan the siting of slimes dams and other structures.

Prakash et al (1999), use satellite based thermal data, Landsat 4 and 5, to detect and monitor coal fires in China. The large size of these fires make the relatively poor resolution of between 60 and 120 metres of these systems feasible. In the South African context, the use of satellite thermal data is not feasible because of the relatively small size of the fires.

Figure 5: Airborne LWTIR image with 5 metre resolution, over the old T & DB Colliery west of Witbank taken in pre-dawn conditions in 1998.

Figure 5, is an airborne LWTIR image with 5 metre resolution, over the old T & DB Colliery west of Witbank taken in pre-dawn conditions in 1998. The N4 highway is on the bottom left, the KwaGuqa township covers most of the left of the image. Most of the lighter parts of the image to the right are heat from and underground fire in the now defunct colliery. In *Figure 6,* the same area is depicted as a Landsat 7 LWTIR, with 60 metre resolution, which is currently the best available from space. It is not possible to fully resolve the fires from the many cultural features which also occur in the area. The newly launched ASTER LWTIR satellite system has a spatial resolution of 90 metres, which is also only suitable for regional studies. *Barsi (1998).*

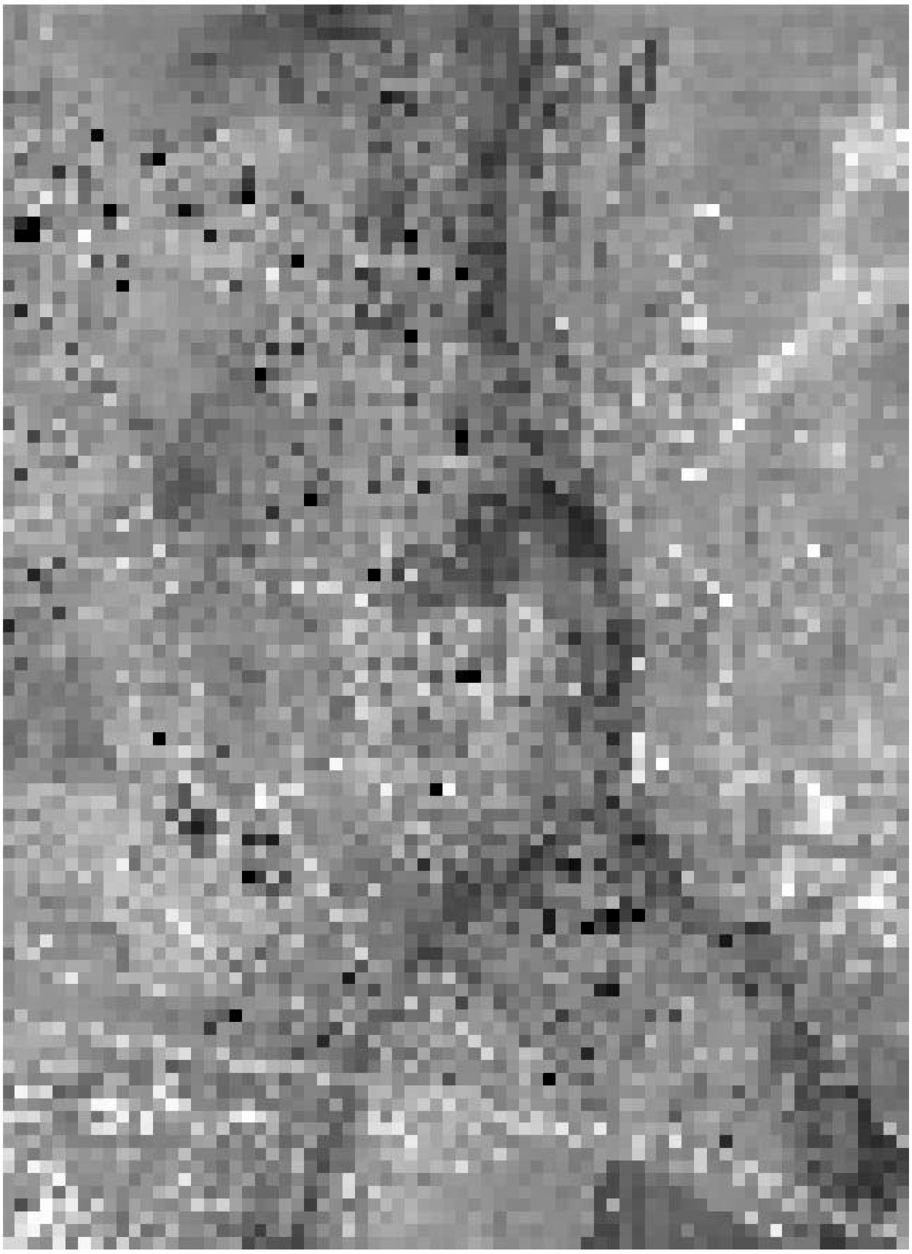

Figure 6: Landsat 7 LWTIR image of same aarea as in Figure 5.

The even coarser resolution obtained from the NOAA weather satellites of one kilometre has been used on a regional basis, *Catt (1992),* illustrated the usefulness of comparing day/night thermal images over the Mt. Isa region in Australia. *McCarthy et al (1998),* described the use of multi-temporal NOAA data to study the dynamics of the hydrology of the Okavango Delta in Botswana. Multi-temporal data allow for relatively easy change detection using digital techniques, and is a useful monitoring method. *Figure 7,* is a pre-dawn LWTIR image over the Okavango delta.

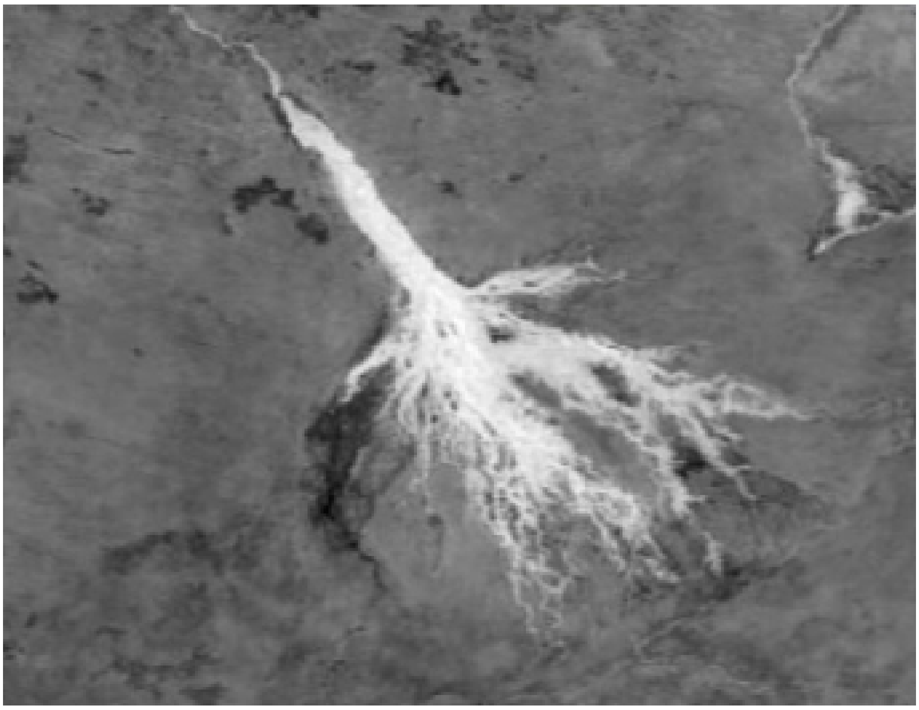

Figure 7: Pre-dawn LWTIR image over the Okavango delta.

5 PLANNING OF THE WITBANK AIRBORNE SURVEYS

It was intended to fly a LWTIR scanner over the Witbank coalfields during August 2000. Because of weather problems, the survey did not take place. However, the survey plans may well be used should a survey be undertaken during 2001.

All the surveys were planned to be flown with a ground pixel size of one metre so as to maximise the spatial informational content. At this resolution, the data strips would be about 860 metres wide, depending on undulations in the topography. All strips were planned with an intended overlap of 20% to allow for any undue yaw or roll of the aircraft. Post processing of the data would have compensated for roll as this would have been measured and recorded together with GPS information.

The survey plan provided for coverage of areas from all the major companies involved with coal mining in the Witbank area. At the same time, Anglo Coal and other interested parties had planned a separate survey over Witbank town and adjacent areas. The Coaltech survey, Area 3, was planned around the Anglo Coal area to avoid repetition. This is an area where old workings as well as dumps occur. Area 2, was planned to coincide with the ground geophysical work undertaken at Tavistock (Duiker) Colliery, as well as several dumps and active workings. This area also has both water filled and dry older bord and pillar workings. A different thermal response would be expected from these two sub-surface areas.

Area 3, near Delmas, was planned over the ISKOR colliery, mainly to detect possible pollution from dumps and current workings. *Figure 8,* illustrates the strips of the three planned survey areas.

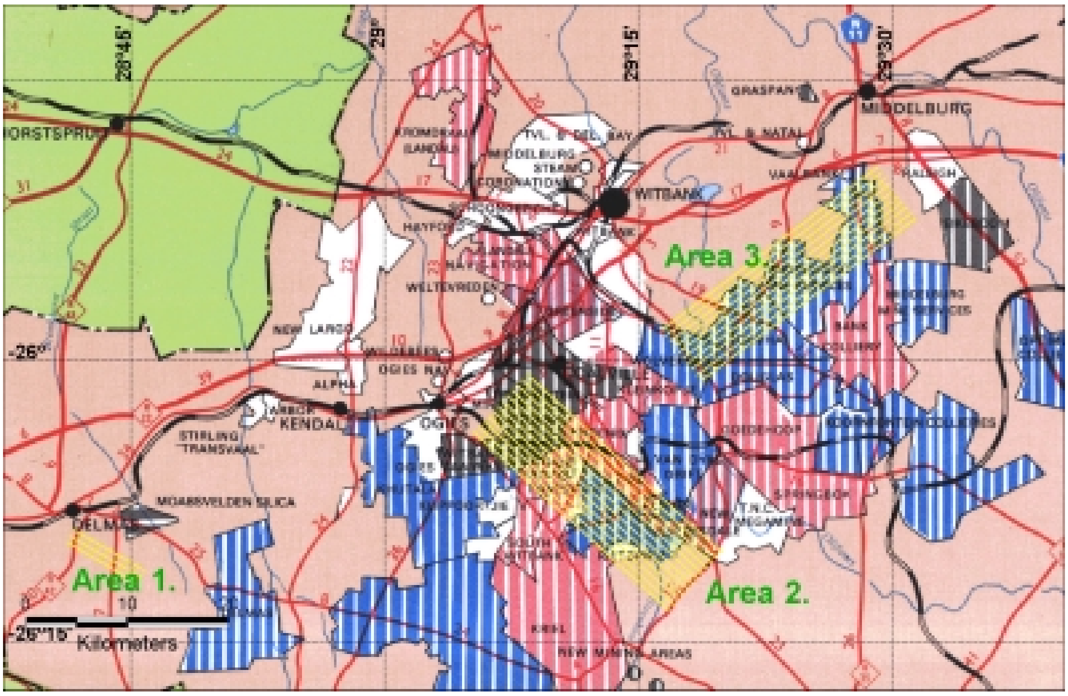

Figure 8: the strips of the three planned survey areas.

6 REFERENCES

Barsi, J. 1998. A Review of the Thermal Components on MODIS and ASTER. Internet Document from the Center for Imaging Science, Rochester Institute of Technology. http://www.cis.rit.edu/class/simg707/Web_Pages/barsi.htm.

Brink, A. B. A.,1983. Engineering Geology of Southern Africa Volume 3. Building Publications, Pretoria, 320p.

Catt, P. 1992. NOAA/AVHRR Day/Night Thermal Imagery for Geological Mapping in NW Queensland, Australia. Proceedings of the 6th Australasian Remote Sensing Conference, Wellington, New Zealand, 1992.

Drury, S. A. 1993. Image Interpretation in Geology, Vol 2, Chapman Hall, London, 283p.
Longshaw, G. 1977. Better Mapping through Remote Sensing. *Gold and Base Minerals of South Africa*. Volume 25, No.9.

Prakash, A., Gens. R. and Vekerdy. Z. 1999. Monitoring coal fires using multi-temporal night-time thermal images in a coalfield in north-west China. *International Journal of Remote Sensing*, Volume 20, no. 4, 2883-2888.

Sabins, F. F. 1980. Interpretation of Thermal Infrared Images, Chapter 9 in Remote Sensing in Geology, B. S. Siegal and A. R. Gillespie (eds), Wiley, New York, 525p.